Novel Photoswitchable and Dualsteric Ligands Acting on Muscarinic Acetylcholine Receptors for Receptor Function Investigation

Neue lichtschaltbare und dualstere Liganden für die muskarinischen Acetylcholin Rezeptoren zur Untersuchung der Rezeptorfunktion

Doctoral thesis for a doctoral degree
at the Graduate School of Life Sciences,
Julius-Maximilian-University Würzburg,
Section Neuroscience

submitted by

Dipl.-Chem. Luca Agnetta

from

Palermo

Würzburg 2019

The presented work has been carried out under the supervision of Professor Dr. Michael Decker at the Chair of Pharmaceutical and Medicinal Chemistry at the Institute of Pharmacy and Food Chemistry of the Julius Maximilian University Würzburg between April 2015 and March 2019. This thesis was funded by Elite Network of Bavaria within the framework of the International Graduate Program "Receptor Dynamics: Emerging Paradigms for Novel Drugs" and was supported by the Graduate School of Life Science.

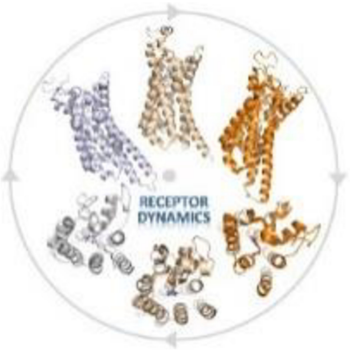

Submitted on:

……..……..

Office stamp

Members of the *Promotionskomitee*:

Chairperson: Prof. Dr. Peter Jakob

Primary Supervisor: Prof. Dr. Michael Decker

Supervisor (Second): Prof. Dr. Ulrike Holzgrabe

Supervisor (Third): Prof. Dr. Pau Gorostiza

Supervisor (Fourth): Prof. Dr. Marco de Amici

Date of Public Defence:

Date of Receipt of Certificates:

List of Publications

Schramm, S.†; **Agnetta, L.**†; Gerwe, H.; Bermudez, M.; Littmann, T.; Irmen, M.; Holze, J.; Wolber, G.; Tränkle, C.; Decker, M.* Novel Dualsteric M_1 Ligands from Carbachol and BQCA/TBPB Show Different Extents of Partial Agonism, submitted.

Agnetta, L.; Bermudez, M.; Riefolo, F.; Matera, C.; Claro, E.; Messerer, R.; Littmann, T.; Gorostiza, P.; Wolber, G.; Holzgrabe, U.; Decker, M.* Fluorination of Photoswitchable Muscarinic Agonists Tunes Receptor Pharmacology and Photochromic Properties. *J. Med. Chem.* **2019**, *62*, 3009-3020.

Riefolo, F.; Matera, C.; Garrido-Charles, A.; Gomila, A., **Agnetta L.**; Claro, E.; Masgrau, R.; Ulrike Holzgrabe, U.; Batlle, M.; Decker, M.; Guasch, E.; Gorostiza, P.* Control of cardiac function *in vivo* with a light-regulated drug. *J. Am. Chem. Soc.* **2019**, *141*, 7628-7636.

Agnetta, L.†; Kauk, M.†; Canizal, M. C. A.; Messerer, R.; Holzgrabe, U.; Hoffmann, C.; Decker, M.*, A Photoswitchable Dualsteric Ligand Controlling Receptor Efficacy. *Angew. Chem. Int. Ed.* **2017,** *56* (25), 7282-7287. Ein Photoschaltbarer Ligand Zur Regulierung Der Rezeptoraktivierung. *Angew. Chem.* **2017**, *129*, 7388-7393.

Agnetta, L.; Decker, M.* Photoresponsive Hybrid Compounds. In *Design of Hybrid Molecules in Drug Development*; Decker, M., Ed.; Elsevier: Oxford, **2017**.

† equally contributed

* corresponding author

Other scientific contributions

Agnetta, L., Photo-tuned compounds for the optical control of the muscarinic ACh Receptor, Poster and Presentation, 2nd International Symposium on Photopharmacology, Vic – Barcelona (Spain), November 1st, **2018**.

Agnetta, L., A Photoswitchable dualsteric M1 ligand, Poster, 253rd ACS National Meeting – American Chemical Society, San Francisco (USA), April 2nd–6th, **2017**.

Agnetta, L., Photoswitchable hybrid molecules to investigate dynamic ligand binding on M1 receptors, Poster, 1st International Symposium on Photopharmacology, Groningen (Netherlands), February 16th, **2017**. - awarded with poster prize -

Copyrights

Parts of this work have been published previously and are reproduced, adapted and/or modified with the permission of:

Agnetta, L.; Bermudez, M.; Riefolo, F.; Matera, C.; Claro, E.; Messerer, R.; Littmann, T.; Wolber, G.; Holzgrabe, U.; Decker, M. Fluorination of Photoswitchable Muscarinic Agonists Tunes Receptor Pharmacology and Photochromic Properties. *J. Med. Chem.* **2019**, *62*, 3009-3020.

https://pubs.acs.org/doi/10.1021/acs.jmedchem.8b01822

Agnetta, L.; Kauk, M.; Canizal, M. C. A.; Messerer, R.; Holzgrabe, U.; Hoffmann, C.; Decker, M., A Photoswitchable Dualsteric Ligand Controlling Receptor Efficacy. *Angew. Chem. Int. Ed.* **2017,** *56*, 7282-7287.

https://onlinelibrary.wiley.com/doi/abs/10.1002/anie.201701524

Agnetta, L.; Decker, M. Photoresponsive Hybrid Compounds. In *Design of Hybrid Molecules in Drug Development*; Decker, M., Ed.; Elsevier: Oxford, **2017**.

https://www.sciencedirect.com/science/article/pii/B9780081010112000118

Declaration of Authorship

Publication (complete reference): Schramm, S.; Agnetta, L.; Gerwe, H.; Bermudez, M.; Littmann, T.; Irmen, M.; Holze, J.; Wolber, G.; Tränkle, C.; Decker, M. Novel Dualsteric M1 Ligands from Carbachol and BQCA/TBPB Show Different Extents of Partial Agonism, submitted.					
Participated in	**Author Initials,** Responsibility decreasing from left to right				
Study Design Methods Development	SS/LA	TL/MB	MD/CT	GW	
Data Collection	SS/LA	HG/MB	MB	GW	
Data Analysis and Interpretation	SS/LA	MI/JH/HG/MB	MD	CT	GW
Manuscript Writing					
Writing of Introduction	SS/LA	MD			
Writing of Materials & Methods	SS/LA	MI/JH/HG/MB	MD/CT/GW		
Writing of Discussion	SS/LA	MI/JH	MD/CT		
Writing of First Draft	SS/LA	MD			

Explanations (if applicable): Shared first authorship

Publication (complete reference): Agnetta, L.; Bermudez, M.; Riefolo, F.; Matera, C.; Claro, E.; Messerer, R.; Littmann, T.; Wolber, G.; Holzgrabe, U.; Decker, M. Fluorination of Photoswitchable Muscarinic Agonists Tunes Receptor Pharmacology and Photochromic Properties. *J. Med. Chem.* **2019**, *62*, 3009-3020.					
Participated in	**Author Initials,** Responsibility decreasing from left to right				
Study Design Methods Development	LA/MD	MB	FR/CM	EC/TL	
Data Collection	LA	MB	FR/CM	EC/RM	
Data Analysis and Interpretation	LA	MB	FR/CM	EC/RM	
Manuscript Writing					
Writing of Introduction	LA	MD	UH		
Writing of Materials & Methods	LA	MB	FR/CM	EC/RM	
Writing of Discussion	LA	MB	MD/UH	FR/CM	EC
Writing of First Draft	LA	MD			

Explanations (if applicable): exclusive first authorship

Publication (complete reference): Agnetta, L.; Kauk, M.; Canizal, M. C. A.; Messerer, R.; Holzgrabe, U.; Hoffmann, C.; Decker, M., A Photoswitchable Dualsteric Ligand Controlling Receptor Efficacy. *Angew. Chem. Int. Ed.* **2017,** *56* (25), 7282-7287.					
Participated in	**Author Initials,** Responsibility decreasing from left to right				
Study Design Methods Development	LA	MK	MD	CH	UH
Data Collection	*Explanation*				
Data Analysis and Interpretation	*Explanation*				
Manuscript Writing Writing of Introduction Writing of Materials & Methods Writing of Discussion Writing of First Draft	LA *Explanation* MK LA	MK CH MK	 LA MD	 MD CH	 UH

Explanations (if applicable): shared first authorship

Referring to Data Collection:

Synthesis and chemical Characterization: LA, RM, MD, UH

Pharmacological Characterization: MK, MCAC, CH

Referring to Data Analysis and Interpretation:

Synthesis and chemical Characterization: LA, RM, MD, UH

Pharmacological Characterization: MK, MCAC, CH

Referring to Writing of Materials & Methods:

Synthesis and chemical Characterization: LA, RM, MD, UH

Pharmacological Characterization: MK, MCAC, CH

Publication (complete reference): Agnetta, L.; Decker, M. Photoresponsive Compounds. In *Design of Hybrid Molecules in Drug Development*; Decker, M., Ed.; Elsevier: Oxford, **2017**.					
Participated in	**Author Initials,** Responsibility decreasing from left to right				
Study Design Methods Development	LA	MD			
Data Collection	LA	MD			
Data Analysis and Interpretation	LA	MD			
Manuscript Writing Writing of Introduction Writing of Materials & Methods Writing of Discussion Writing of First Draft	LA	MD			

Explanations (if applicable): exclusive first authorship. This publication represents a book chapter of 37 pages. Study design, literature research and writing were conducted by LA. MD assisted, corrected and edited the manuscript.

Publication (complete reference): Schramm, S.; Agnetta, L.; Gerwe, H.; Bermudez, M.; Littmann, T.; Irmen, M.; Holze, J.; Wolber, G.; Tränkle, C.; Decker, M. Novel Dualsteric M1 Ligands from Carbachol and BQCA/TBPB Show Different Extents of Partial Agonism, submitted.					
Figure	**Author Initials,** Responsibility decreasing from left to right				
1	MB	GW			
2	SS/LA	MD			
3	LA	MD			
4	LA	MI/JH/HG	MD	CT	
Scheme					
1-9	SS/LA	MD			
Table					
1-2	LA	MD			

Explanations (if applicable): Shared first authorship

Publication (complete reference): Agnetta, L.; Bermudez, M.; Riefolo, F.; Matera, C.; Claro, E.; Messerer, R.; Littmann, T.; Wolber, G.; Holzgrabe, U.; Decker, M. Fluorination of Photoswitchable Muscarinic Agonists Tunes Receptor Pharmacology and Photochromic Properties. *J. Med. Chem.* **2019**, *62*, 3009-3020.					
Figure	**Author Initials,** Responsibility decreasing from left to right				
1	LA	MD			
2	LA	MD			
3	FR/CM	EC			
4	LA	MD			
5	MB	GW			
S1	MB	BW			
Table					
1-2	LA	MD			
Scheme					
1-2	LA	MD			

Explanations (if applicable): exclusive first authorship

Publication (complete reference): Agnetta, L.; Kauk, M.; Canizal, M. C. A.; Messerer, R.; Holzgrabe, U.; Hoffmann, C.; Decker, M., A Photoswitchable Dualsteric Ligand Controlling Receptor Efficacy. *Angew. Chem. Int. Ed.* **2017,** *56* (25), 7282-7287.					
Figure	**Author Initials,** Responsibility decreasing from left to right				
1	LA	MD			
2	LA	MD			
3	LA	MD			
4	MK	CH	MCAC		
S1	LA	MD			
S2	MK	CH			
S3	MCAC	MK	CH		

Explanations (if applicable): shared first authorship

Publication (complete reference): Agnetta, L.; Kauk, M.; Canizal, M. C. A.; Messerer, R.; Holzgrabe, U.; Hoffmann, C.; Decker, M., A Photoswitchable Dualsteric Ligand Controlling Receptor Efficacy. *Angew. Chem. Int. Ed.* **2017,** *56* (25), 7282-7287.					
Figure	**Author Initials,** Responsibility decreasing from left to right				
1-28	LA	MD			

Explanations (if applicable): exclusive first authorship

The doctoral researcher confirms that she/he has obtained permission from both the publishers and the co-authors for legal second publication.

The doctoral researcher and the primary supervisor confirm the correctness of the above-mentioned assessment.

Doctoral Researcher's Name Date Place Signature

Primary Supervisor's Name Date Place Signature

Affidavit

I hereby confirm that my thesis entitled *Novel Photoswitchable and Dualsteric Ligands Acting on Muscarinic Acetylcholine Receptors for Receptor Function Investigation* is the result of my own work. I did not receive any help or support from commercial consultants. All sources and / or materials applied are listed and specified in the thesis.

Furthermore, I confirm that this thesis has not yet been submitted as part of another examination process neither in identical nor in similar form.

Place, Date Signature

Eidesstattliche Erklärung

Hiermit erkläre ich an Eides statt, die Dissertation *Neue lichtschaltbare und dualstere Liganden für die muskarinischen Acetylcholin Rezeptoren zur Untersuchung der Rezeptorfunktion* eigenständig, d.h. insbesondere selbständig und ohne Hilfe eines kommerziellen Promotionsberaters, angefertigt und keine anderen als die von mir angegebenen Quellen und Hilfsmittel verwendet zu haben.

Ich erkläre außerdem, dass die Dissertation weder in gleicher noch in ähnlicher Form bereits in einem anderen Prüfungsverfahren vorgelegen hat.

Ort, Datum Unterschrift

Acknowledgments

I would like to thank my supervisor Professor Michael Decker for giving me the opportunity to start my doctoral studies in his group, to work on an exciting and highly competitive topic and for his constant incentive to push me and my research beyond its own borders. I am grateful for the confidence that he put in my work, which motivated me to perform the best way possible.
I also want to express gratitude to my additional supervisor Professor Ulrike Holzgrabe, who was always available for scientific suggestions during the course of my studies and especially for her constructive and extremely helpful support while writing publications.
I want to thank Professor Pau Gorostiza for accommodating me in his group during my research stay and for the fruitful collaboration that arose thenceforward. I had a wonderful and inspiring time in his group and am very grateful for the thrilling insights in his research field, which allowed me to think outside the box.
I thank Professor Marco de Amici who is one of the pillars upon which my research was built on, for his contributions to a successful doctoral study.

Furthermore, I want to thank all my internal and external collaboration partners without whose support it wouldn't have been possible to produce this work:
Professor Carsten Hoffmann, Michael Kauk and Maria Consuelo Alonso Canizal from the University of Jena for sharing their fluorescence-based techniques and the successful collaboration.
Professor Ulrike Holzgrabe and Regina Messerer from the University of Würzburg for the synthesis of reference compounds, which substantially enriched my research.
Professor Gerhard Wolber and Marcel Bermudez from the Freie Universität in Berlin for the molecular docking of the target compounds, which essentially contributed to the quality of my project.
I am deeply grateful to Professor Armin Buschauer and especially to Timo Littmann from the University of Regensburg who shared the split luciferase complementation assay with me and our research group and for all the detailed questions he was never tired to answer.
I want to thank Professor Pau Gorostiza, Fabio Riefolo, Dr. Carlo Matera and Dr. Enrique Claro from the University of Barcelona for providing binding data of the target compounds, which complemented my research very nicely and for the intellectual support during my research stay.

I want to thank Sebastian Schott from the physical chemistry department and Christoph Keßler from the technical support team for their help in the acquisition of the LED lamps
I want to thank Dr. Valerie Jahns, Claudia Schütz and Nadine Groß for the incredibly great help in establishing the IP-one accumulation assay and for a funny time in their lab.
Furthermore, I thank all the people in the research groups I have worked with, including Trainee, Bachelor and Master-students. They all substantially contributed to my personal and scientific growth: Xinyu, Sarah, Eddi, Dominik, Simon, Antonis, Sandra, Matthias S., Matthias H., Julian, Christian, Hubert, Anna, Thorge and Feng from the Decker group. Daniela, Antonio, Regina, Florian, Patrick, Lina from the Holzgrabe group. Rosalba, Fabio, Carlo, Rossella, Davia, and Nuria from the Gorostiza Lab. Lieselotte Möhler and Christine Ebner from the secretariat. Georg Walter, Matthias Völker and Karl Vollmuth from the technical service team. Curd, Jens and Lu. All the members of the Elite Network of Bavaria. A huge THANKS! I spent a great time with all of you!

Last but not least, I want to express my gratitude to my family and especially my parents from the bottom of my heart. They never stopped supporting and believing in me in every aspect of my personal and educational life.

Finally, I want to thank my wife Rahel, who always accompanied me in moments of doubts and weakness and pushed me to best performances. Thank you for your love, which carries me every day.

Table of Content

1. Introduction

1.1. G Protein-Coupled Receptors

The superfamily of G protein-coupled receptors (GPCRs), also called seven-transmembrane (7-TM) receptors represents the largest family of signaling proteins encoded in the mammalian genome.[1,2] Apart from being responsible for sensory perception (olfaction, vision and taste), GPCRs mediate intracellular signals across the membrane for a great variety of extracellular stimuli, such as neurotransmitters, lipids, hormones and even photons.[3] The high therapeutic relevance of GPCRs becomes evident considering that approximately one third of all pharmaceutical drugs approved by drug regulatory authorities target this class of receptors, even though they are not completely elucidated structurally and regarding their mode of action.[4-6] Depending on their structural features and topology, GPCRs are classified into five main subfamilies: rhodopsin (class A), secretin (class B), glutamate (class C), adhesion and frizzle/taste.[7,8] However, in direct relation to their conserved sequence motifs, all members were found to share similar mechanisms of action involving the activation of multiple heterotrimeric guanine nucleotide binding proteins (G proteins) and complex regulatory processes. All class A GPCRs are characterized by a transmembrane domain with a common structural organization, which is composed of seven α-helices (TM1-7) that are connected by alternating

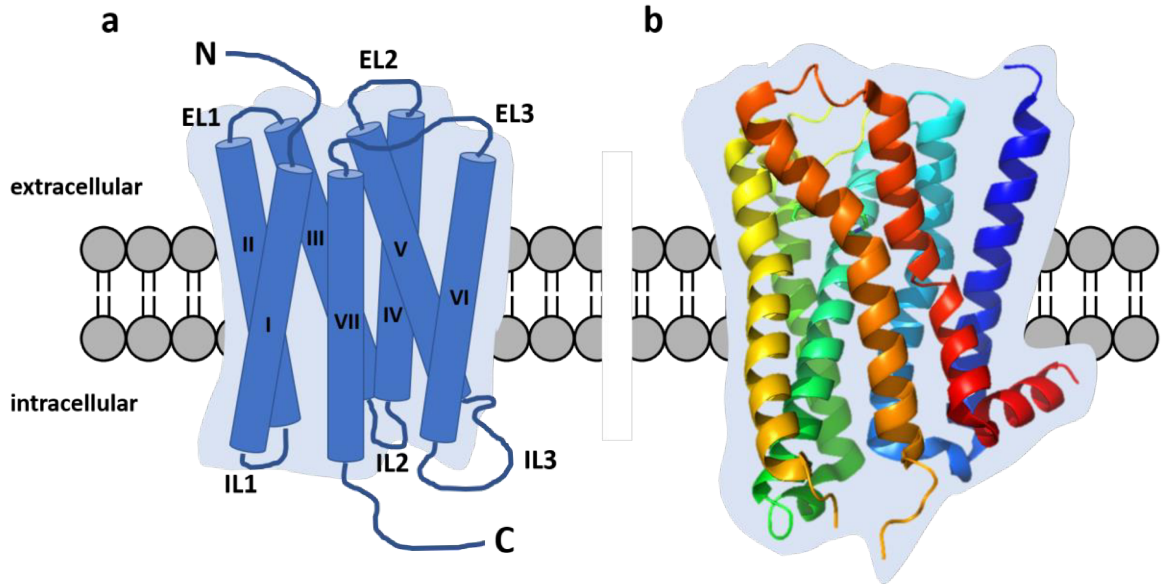

Fig. 1. a) Schematic structure of a G protein-coupled receptor showing seven transmembrane domains (7-TM), three extracellular (ECL1-3), intracellular loops (ICL1-3) and *N*- and *C*-termini. b) Crystal structure of the human muscarinic receptor M_1 highlighting the α-helical transmembrane domain.

extracellular (ECL1-3) and intracellular loops (ICL1-3, Fig.1). The extracellular *N*-terminus is responsible for ligand recognition and protein access while the *C*-terminus and the ICLs interact with the cytosolic proteins involved in the signal's transduction pathways.[3,9]

Starting from the successful crystallization of the rhodopsin and the β_2 adrenergic receptors, the breakthroughs in structural biology and crystallography significantly contributed to the understanding of the molecular basis of GPCR physiology, pharmacology and function. In addition, protein NMR spectroscopy experiments and computer-aided simulations are used to determine GPCR dynamics – i.e. the ability of the protein to change conformation over time.[10] Despite the challenges, the combination of these powerful cutting-edge methodologies helps to provide deeper understanding of GPCR function and promotes drug discovery towards the achievement of therapeutics based on rational, structural-based drug design.[11,12] This approach has already revolutionized the field of GPCR research.[13] Currently, approximately 65 new drugs are under investigation in clinical trials for this receptor family, highlighting the great potential as therapeutic targets for a broad spectrum of diseases, such as diabetes, obesity and neurological disorders.[14]

1.2. Muscarinic Acetylcholine Receptors

1.2.1. Classification

Muscarinic acetylcholine receptors (mAChRs or M receptors) are members of the rhodopsin (class A) GPCR family and are widely expressed throughout the central (CNS) and peripheral nervous system (PNS).[7] Together with the nicotinic ACh receptors, they mediate many of the diverse effects of the endogenous agonist acetylcholine (ACh). As such, they control a variety of neuronal, cardiac, and digestive functions, which endows them with a highly relevant role as therapeutic drug targets.[15]

The M receptor family consists of five distinct receptor subtypes (M_1-M_5), sharing the rhodopsin characteristic barrel-like organization and the strong sequence homology among each other. Depending on their primary coupling efficiency to different Gα proteins, they can further be sub-divided into two main groups. Upon activation with an agonist, the M_1, M_3 and M_5 receptors preferentially couple with the $G\alpha_{q/11}$ protein, while the M_2 and M_4 receptors bind to $G\alpha_{i/o}$, leading to different signaling cascades.[16,17].

1.2.2. Function

Binding of an agonist forces the M receptors to undergo a conformational change in their three-dimensional structure, which allows the G protein to bind to the receptor. The following exchange of guanosine diphosphate (GDP) with guanosine triphosphate (GTP) induces a physical dissociation of the Gα from the Gβ/γ-subunit mediating the intracellular response. According to the respective G protein, two different signal transduction pathways are determined: the phosphatidylinositol-4,5-bisphosphate (PIP_2) pathway for the $G\alpha_{q/11}$ and cyclic adenosine monophosphate (cAMP) pathway for $G\alpha_{i/o}$ protein.[18,19]

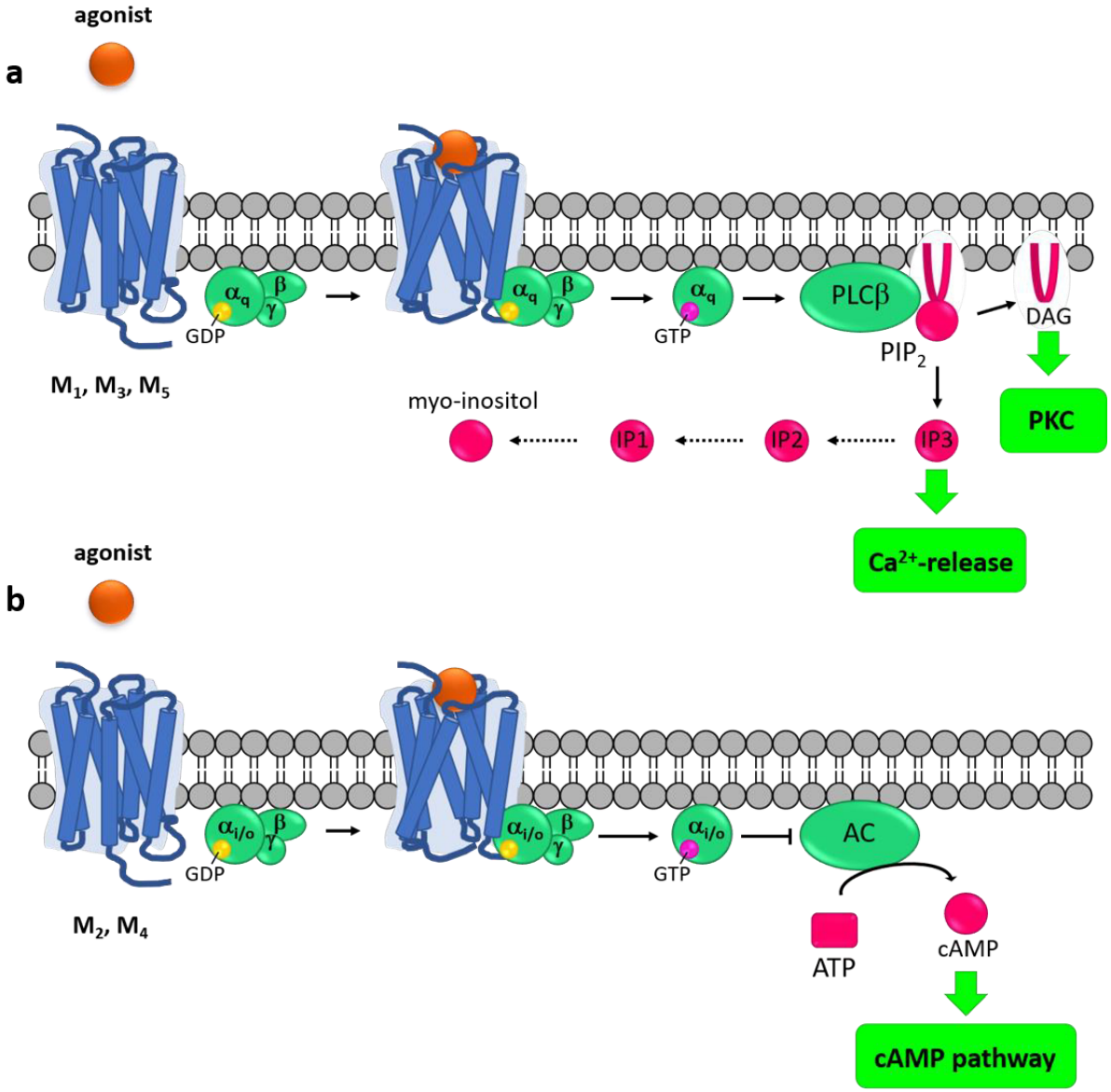

Fig. 2. a) Signaling specificity of the five M receptors. a) $G\alpha_q$-pathway leading mainly to cytosolic calcium efflux specific for odd-numbered receptors and b) even-numbered receptor specific $G\alpha_{i/o}$-pathway leading mainly to a reduction of cAMP and related cellular responses.

The $G\alpha_{q/11}$-pathway is characteristic for the M_1, M_3 and M_5 receptors and involves the activation of the membrane-bound phospholipase Cβ (PLCβ), which in turns initiates the PIP_2 hydrolysis to inositol-1,4,5-triphosphate (IP3) and diacylglycerol (DAG) as second messengers. DAG mediates protein kinase C (PKC) activation, while IP3 activates the IP3-receptors located in the membrane of the smooth endoplasmic reticulum (ER), promoting an increase in intracellular calcium ions (Ca^{2+}). This leads to cellular responses, such as muscle contraction, fusion and exocytosis of enzyme carrying vesicles and glycogen metabolism. As part of the self-regulating system, IP3 is gradually hydrolyzed to myo-inositol.

M_2 and M_4 receptors activate the $G\alpha_{i/o}$ pathway, mediating the inhibition of adenylyl cyclase (AC), responsible for the formation of cAMP from adenosine triphosphate (ATP). Consequently, the cAMP level in the cytosol is reduced, determining the activity of various ion channels as well as members of the protein kinase A (PKA).[20]

The range of Gβ/γ-signaling after dissociation from the Gα-subunit has not yet been elucidated completely, but it was found that this subunit performs its action as a dimer and interacts, depending on the location, with various effectors, such as G protein-gated inward rectifying potassium channels (GIRK), calcium channels and also ACs in an inhibitory or excitatory manner.

Although the metabotropic action of the M receptors induced by an agonist is coupled to the G protein, in many cases G protein-independent signaling pathways concomitantly occur, mainly as a result of a self-regulating or desensitization mechanism. This includes, for example, activation of G protein-coupled receptor kinases (GRKs) and β-arrestin recruitment for the internalization of activated GPCRs, eventually leading to secondary signaling responses.[21,22] Which downstream signaling is preferred is highly dependent on the conformation in which the receptor is stabilized and is dictated by the ligand-protein interaction. Biased signaling describes the ability of a receptor to differentiate between the different signaling pathways upon binding of a biased agonist. This well-established paradigm holds great potential for rational drug design of biased agonists as smart drugs, which could specifically target pathogenic signaling pathways and avoid pathways, which lead to undesired off-target effects.[23,24]

1.2.3. Physiology

The physiological role of muscarinic receptors is highly complex. All five subtypes assume defined functions in both the CNS and PNS. Being diffusely expressed throughout the body,

the physiological effects are based on the location and the specific identity of the distinct receptor.[25]

Among the five subtypes, the M_1 receptor is considered to be the most abundant subtype in the brain (50-60%), expressed both pre– and post-synaptically in neurons of the brain, predominantly in the cerebral cortex, striatum and hippocampus.[26] Therefore, the M_1 subtype has been identified as a key receptor for physiological brain functions such as neuronal excitability, synaptic plasticity, learning and memory and thus holds immense therapeutic relevance for cognitive and neurodegenerative diseases such as schizophrenia, Parkinson's Disease and Alzheimer's Disease (AD)[27-30]

M_2 receptors are expressed abundantly in both the CNS and PNS but are mainly found in the heart and are proven to regulate heart rate. Together with M_3 receptors, M_2 receptors are involved in muscle contraction due to their presence in smooth muscle and skin tissues. In the CNS, these receptors are associated with body temperature regulation, pain perception (M_2) and salivation (M_3).[16,17] The M_4 receptor, the second most frequent muscarinic receptor in the brain, especially in the striatum and cortex, is involved in the control of dopamine release. Therefore, it has been identified as a potential target for the therapeutic treatment of schizophrenia and Parkinson's disease.[31] The M_5 receptor is expressed in neurons of the brain and is also related to dopamine release. It has also been found in blood vessels, where it could be involved in vasoconstriction. However, the lack of differentiation methods between the other muscarinic receptors hampers a clear determination of the physiological profile of the M_5 receptor.[32]

1.2.4. Ligand Binding Sites

The crystal structures of the muscarinic receptors have been resolved by means of X-ray crystallography for the M_2 in 2012,[33] for M_3 in 2012[34] and for M_1/M_4 in 2016.[35] Efforts to crystallize the M_5 receptor have not been successful to this date. Radioligand binding experiments, mutagenesis and sequence analysis complemented this methodology, gaining fundamental insight into the molecular structure in their active as well as in their inactive conformation.

The crystal structures of the muscarinic receptors confirmed the high similarity in the tertiary structure and is demonstrated by a direct comparison of the respective transmembrane domains.[35] Within this domain, the muscarinic receptors show a cavity, presenting amino acids characteristic for agonist binding (Fig. 3a). In particular, the conserved aspartate residue in TM3 forms a charge interaction with the positive quaternary ammonium moiety, serving as a counter-

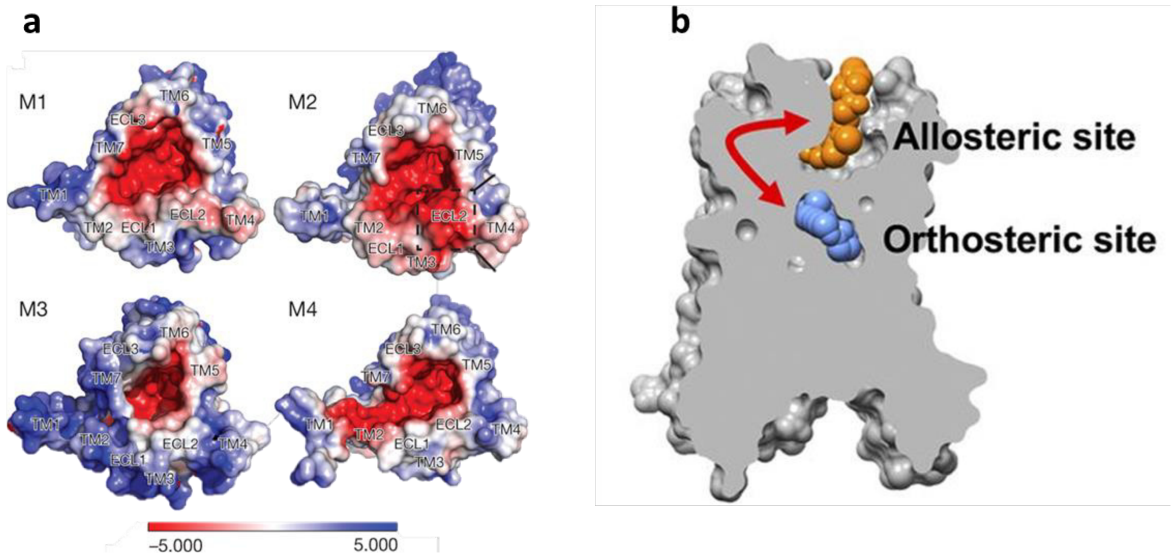

Fig. 3. a) Crystal structures of the muscarinic receptors M_1 to M_4 seen from above. All four receptors share a hydrophobic cavity (highlighted in red), which is able to bind ligands. Picture was adapted from Thal et al.[36] b) Topology of the orthosteric binding site compared to the allosteric binding site. The orthosteric site is located more towards the inner core of the receptor, while the allosteric site is oriented outside being part of the extracellular vestibule. In the active conformation, the orthosteric binding site is separated from the allosteric binding site by the tyrosine lid. Picture was adapted from Burger et al.[46]

ion for the endogenous ligand ACh. Further hydrogen bond interactions with threonine residues stabilize the ester function of the physiological agonist.[36] This amino acid sequence is highly conserved throughout the five subtypes and is reported as orthosteric binding site.[37] As a consequence, drugs that exclusively target the orthosteric site typically lead to unwanted side-effects due to their lack of subtype-selectivity. This orthosteric binding pocket is separated from extracellular vestibule (ECV) by a so-called tyrosine lid (Fig. 3b), consisting of three tyrosine residues, which form cation-π interactions with the ligand's ammonium group and a hydrogen bond network among themselves. Upon binding of an agonist, the tyrosine residues create an aromatic floor over the orthosteric site, hindering the ligand to dissociate from the receptor.[33,38] This is regarded as the cause for the high affinity observed for orthosteric ligands.

Above the tyrosine lid, the relatively large ECV is also accessible for small molecules, which represents a unique feature among the GPCRs (Fig. 3b). Importantly, the degree of amino acid sequence conservation in the ECV drops significantly within the subtypes compared to the orthosteric site, which makes this location suitable for differentiation between the subtypes by targeting the ECV, commonly labeled as allosteric site.[39,40] Targeting the allosteric binding site holds great potential for the discovery subtype-selective drugs, avoiding unwanted side-effects.[38]

1.2.5. Muscarinic Receptor Ligands

The ability of a GPCR to change its shape is crucial for the mediation of a distinct cellular response. Ligands, such as neurotransmitters, small molecules, hormones, and proteins are able to favor such a structural change by binding to the receptor.

To fully understand the structural basis that underlies receptor activation, one has to consider, that these GPCRs are highly dynamic structures rather than rigid entities.[10] They pass through several three-dimensional arrangements, potentially inducing a different cellular response. Even in absence of an external stimulus, GPCRs are constantly in motion, including different active and inactive states and produce a constitutive activity, which manifests in a basal level response. However, these conformational states can be characterized according to the signal they transmit and the ligand responsible for its stabilization. Shifting the receptor into its active conformation, agonists bind with high affinity and induce a cellular response. Partial agonists also favor the active state but mediate only a submaximal activation at the receptor. In contrast, inverse agonists bind to the inactive state reducing the constitutive basal response. Antagonists bind to the receptor but are not able to differentiate between an active or inactive conformation. Consequently, they do not change the basal level (Fig. 4).[41,42]

Despite the therapeutic relevance of muscarinic receptors, relatively few drugs target this receptor family typically due to their poor subtype selectivity as mentioned above, and hence leading to on- and off-target side effects[26]. For this reason, the agonist ACh, which plays a pivotal role as endogenous neurotransmitter is not administered therapeutically, (apart from

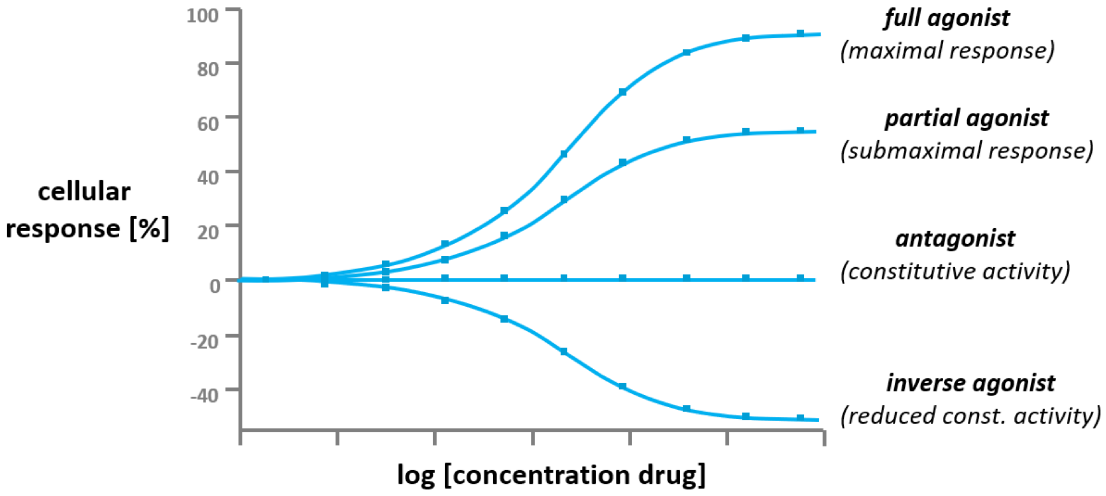

Fig. 4. Functional diversity of cellular response of a GPCR reflected by concentration-response-curves (CRCs). Upon increasing concentrations, full agonists induce a maximal response while partial agonists are only able to activate the receptor in a submaximal manner. Antagonists bind to the receptor but do not differentiate between active or inactive state leaving the basal level unchanged. Inverse agonists reduce the constitutive activity at the receptor.

being quickly degraded by cholinesterases). Same holds true for iperoxo, a synthetic high-affinity agonist, which is also known to perform super-agonistic efficacy at the M_2 receptor, i.e. higher than the maximal response of a full agonist.[43] Tiotropium bromide and ipratropium bromide are the most prominent drugs targeting muscarinic receptors and are used for chronic obstructive pulmonary disease (COPD),[44] but still show severe side effect, such as dry mouth, blurred vision, and incontinence, due to the deficiency in subtype selectivity.

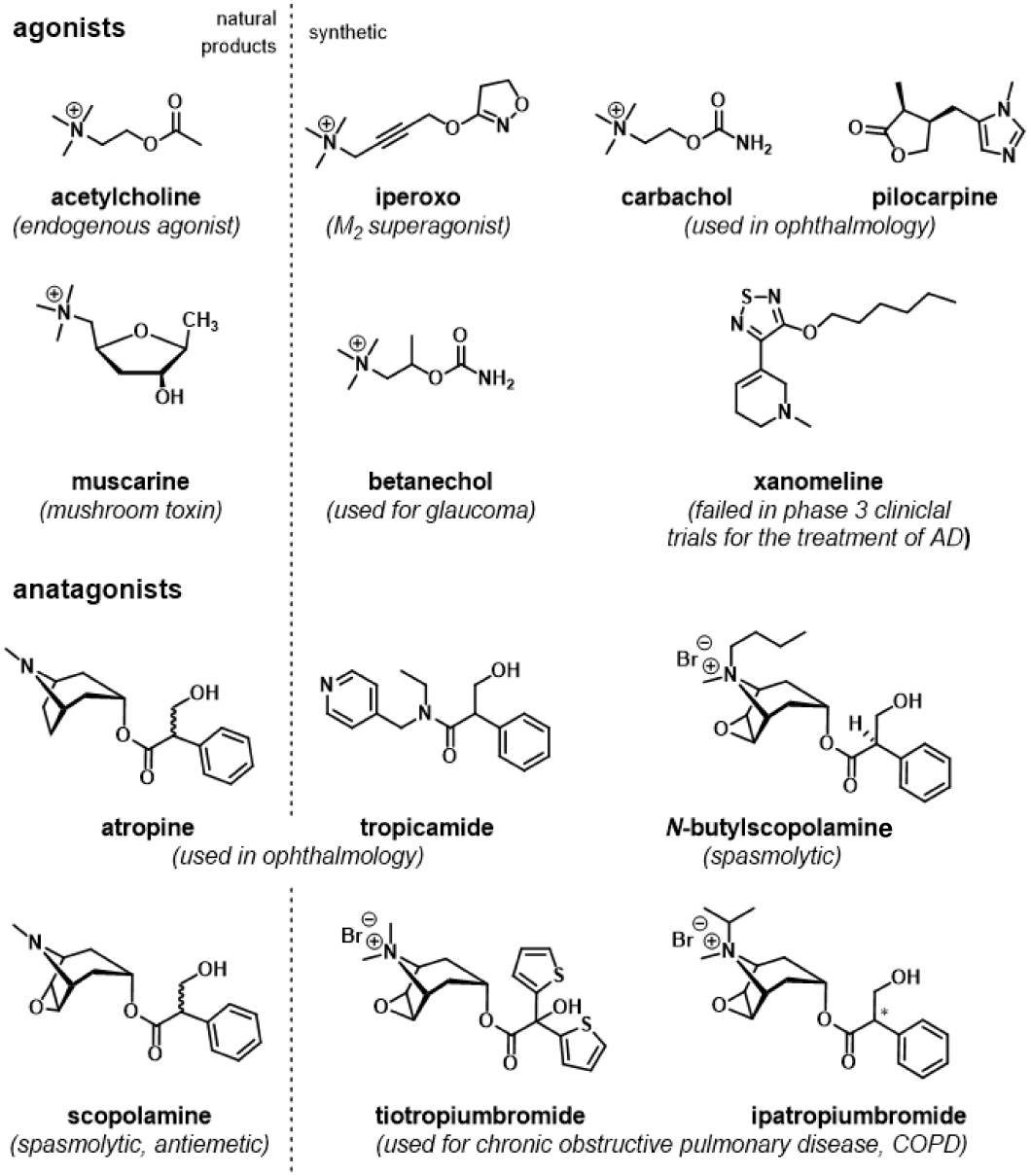

Fig. 5. A selection of the most important natural and synthetic agonists and antagonists of the muscarinic receptors and their main therapeutic relevance.

1.2.6. Allosteric Ligands

Extensive efforts have been undertaken to overcome the drawback of poor subtype-selectivity by investigating the less conserved allosteric binding sites, which are conformationally linked to the orthosteric binding site but are structurally different.[30,45] Allosteric modulation was firstly described and initially characterized for the M_2 receptor by Lüllmann and co-workers.[46] The bis-phthalimidyl-substituted bis-ammoniumalkyl derivative W84 (Fig. 7) was found to potentiate the antidote action of the antagonist atropine in an over-additive fashion.

A unique feature of allosterism is probe-dependency, meaning that allosteric ligands affect the binding affinity of concomitantly bound orthosteric ligands and vice versa. Making use of this cooperativity (α = cooperativity factor), allosteric modulators are able to influence the orthosteric ligand activity either by potentiating (positive allosteric modulator, PAM, $\alpha > 1$), diminish (negative allosteric modulator, NAM, $\alpha < 1$) or not affecting (neutral allosteric ligands, NAL) its affinity.[47] Particularly, these modulators perform their effect only in the presence of the orthoster. Exclusive binding of the allosteric modulators blocks the receptor without producing a signal, which is only transmitted when both the orthoster and the alloster are bound to the receptor forming a ternary complex. Therefore, the overall activity of the receptor is not only determined by the ternary complex, but also by the receptor bound solely to the allosteric modulator or orthosteric ligand, respectively (Fig. 6).[48,49] Thus, they provide

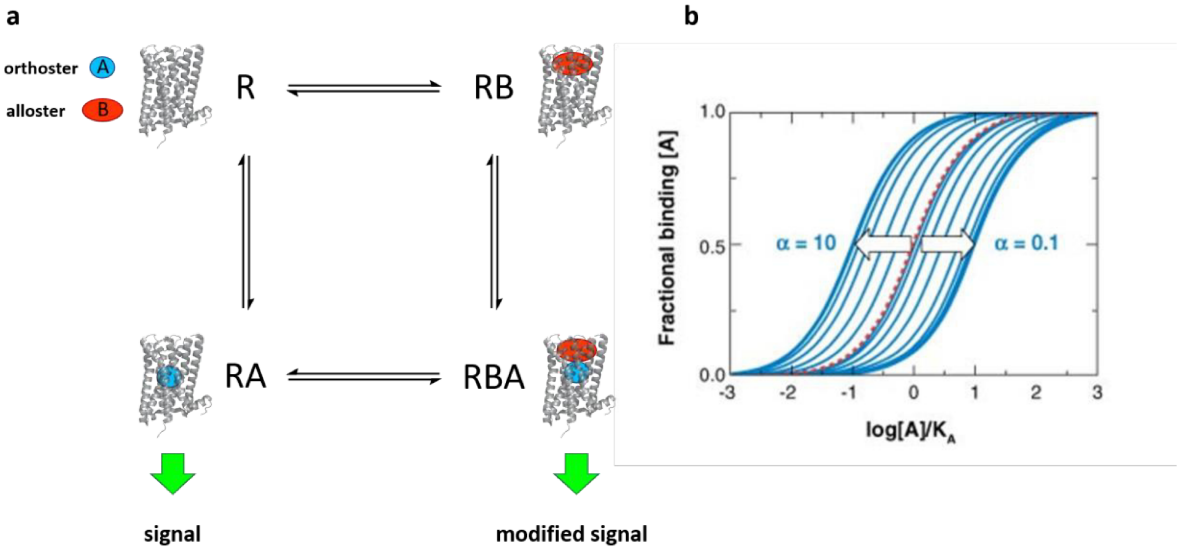

Fig. 6. a) Ternary complex model used to describe the interactions of GPCRs (R) with an orthosteric ligand (A) and allosteric modulator (B). Allosteric modulation results in a modified response compared to the response evoked only from the orthoster. b) Shifting of concentration-response-curves upon variation of the concentration of the allosteric modulator. Arrows indicate concentration increase or decrease. Positive cooperativity ($\alpha > 1$) results in left-shift, while negative cooperativity ($\alpha < 1$) is displayed by a right-shift of CRC (adapted from May et al.[49])

spatial and temporal specificity and are able to confine the activity to the location and time, where a physiological stimulus is set. Another hallmark of allosterism is the intrinsic ceiling effect of allosteric modulators. Contrary to orthosteric agonists, which often mediate a persisting "all-or-nothing" response causing side-effects, desensitization and overdose risks, the effect of allosteric ligands is dictated by the degree of cooperativity. Consequently, response intensity is limited. once all allosteric binding sites are occupied.[50]

Numerous allosteric modulators, either PAMs or NAMs, have been found, that exhibit pronounced selectivity upon a distinct subtype.[30] To name a few examples, benzyl quinolone carboxylic acid (BQCA) discovered by Merck shows absolute subtype selectivity and performs a high degree of cooperativity stabilizing the active receptor conformation favored by the

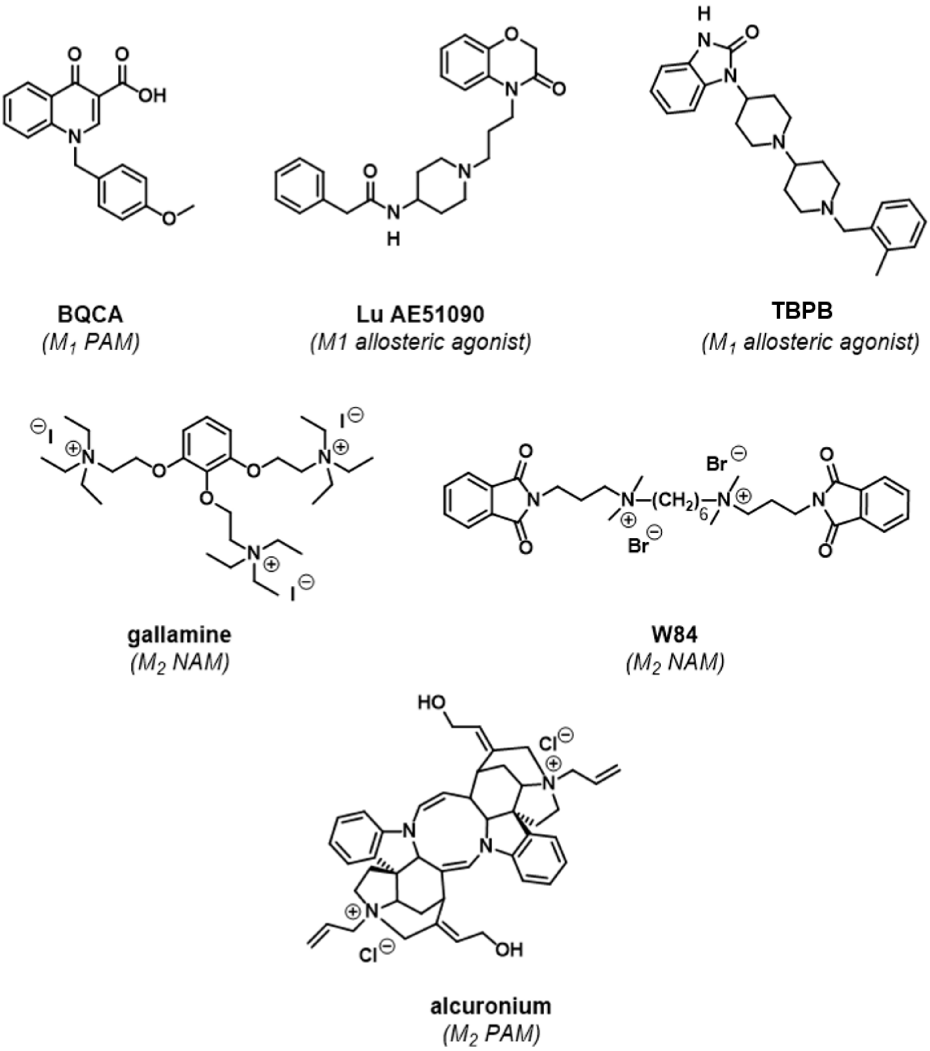

Fig. 7. Selection of allosteric modulators and allosteric agonists acting on muscarinic receptors.

orthosteric ligand at the M_1 receptor (PAM). At the M_2 receptor, negative allosteric modulation was found for alcuronium, gallamine and the archetypal phthalimido- and naphthalimido-derived ligands as examples (Fig. 7).[51,52]

However, some allosteric ligands show an intrinsic activity on its own, regardless of whether an orthoster is bound to the receptor or not. This is true for Lu AE51090, which is described as a M_1-preferring allosteric partial agonist.[53] Showing selectivity for the M_1 receptor even on a functional level, [1-(1′-(2-tolyl)-1,4′-bipiperidin-4-yl)-1*H* benzo[*d*]imidazol-2(3*H*)-one] (TBPB) was found to be an allosteric agonist. Both ligands show procognitive potential.[54]

Importantly, extending the knowledge on the mechanism underlying allosterism at the muscarinic receptors may lead to significant breakthroughs regarding subtype-selective and hence therapeutically relevant candidates, which can also be applied to other GPCRs.[47]

1.2.7. Dualsteric and Bivalent Ligands

A promising way for taking advantage of allosteric binding to achieve subtype selectivity while preserving high affinity at the receptor are dualsteric or bitopic ligands. As known as the address-message concept,[55] this class of ligands combines high affinity orthosteric moieties (message) with high selective allosteric building blocks (address) connected through appropriate linkers.[50,56-61] Dualsteric ligands, which have been investigated mostly for the M_1 and M_2 receptors,[62] show a notable preference for the receptor subtype respectively, while preserving (partial) agonistic activity. It was also shown that the length and nature of the linker must be taken under consideration, as these properties substantially contribute to the receptors binding mode.[63] For a complete list of allosteric modulators and dualsteric ligands, see Bock and co-workers.[30]

The binding mode of dualsteric ligands accounts for a unique pharmacology, which is characterized by multiple binding modes involving the orthosteric and the allosteric sites. It is, therefore, responsible for the overall functional activity of the receptor.

On the one hand, the ligand can bind concomitantly to both the orthosteric and allosteric site, referred to as dualsteric binding mode, and mediates receptor activation on G protein level. On the other hand, the dualsteric ligand can bind in a purely allosteric interaction stabilizing the receptor in the inactive state and, hence, blocking its activity.[63] Here, not only the allosteric pharmacophore but the whole dualsteric ligand resides in the allosteric vestibule, similar to the binding modes of the allosteric modulators W84 and gallamine. This ensemble of ligand binding poses, and its equilibrium which is achieved in-between, determines the efficacy at the

receptor and was extensively investigated for iperoxo-derived ligands iper-6/8-naph, iper-6/8-phthal and BQCAd hybrids (Fig. 9).[64,65] In addition to the improved subtype-selectivity, these ligands show additional interesting properties. Iper-6-phthal significantly prefers G_i activation over G_s recruitment, which is reported as biased signaling or functional selectivity.

All these ligands show, that by carefully designing dualsteric ligands, unique receptor conformations can be accessed, resulting in subtype-selective and functional-selective compounds.[66]

Another approach for allosteric modulation was suggested by Fronik and co-workers.[67] Based on in silico investigations, they postulated that homobivalent ligands composed of two identical orthosteric binding blocks connecting through a linker could be used to specifically target the

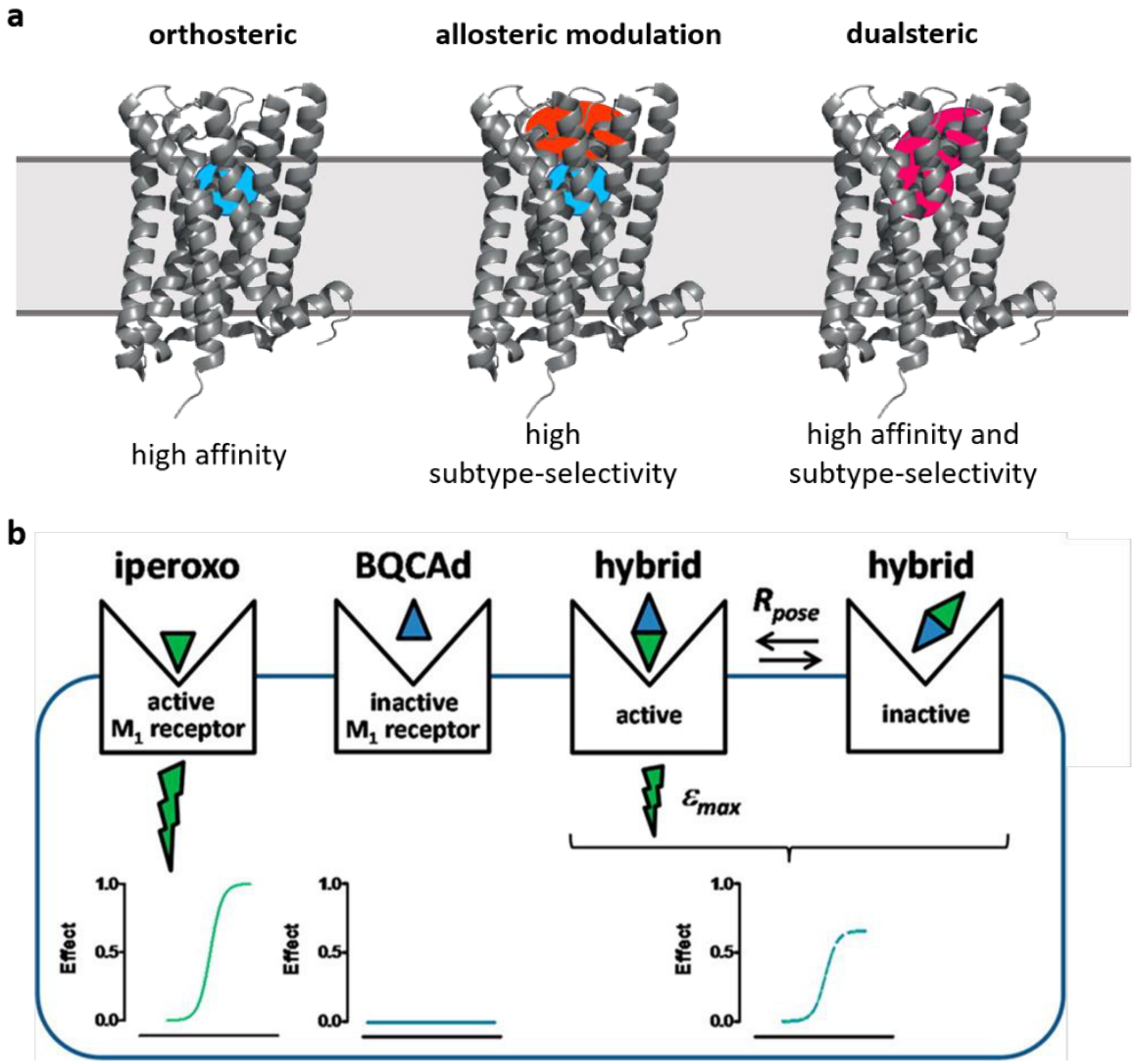

Fig. 8. a) Characteristic properties associated to the respective receptor targeting mode. Adapted from Kruse et al.[15] b) Concept of dynamic ligand binding can explain the partial agonism with graded efficacy at the M_1 receptor. Adapted from Chen et al.[65]

receptor in a dualsteric manner. This is due to another less conserved binding site at the extracellular vestibule of the receptor called metastable binding site, which is postulated by extensive molecular dynamics simulations. Such binding site holds great potential for investigations into receptor activation and may open possibilities for new dualsteric binding modes with homobivalent compounds. To date, no experimental data has been published, although there is considerable knowledge for the existence of a metastable binding site.

Until now, only few examples have confirmed the relevant therapeutic potential of dualsteric ligands for a therapeutic treatment. However, they are regarded as valuable pharmacological tool compounds for the investigation of receptor function and elucidation of receptor activation-induced dynamics.[59]

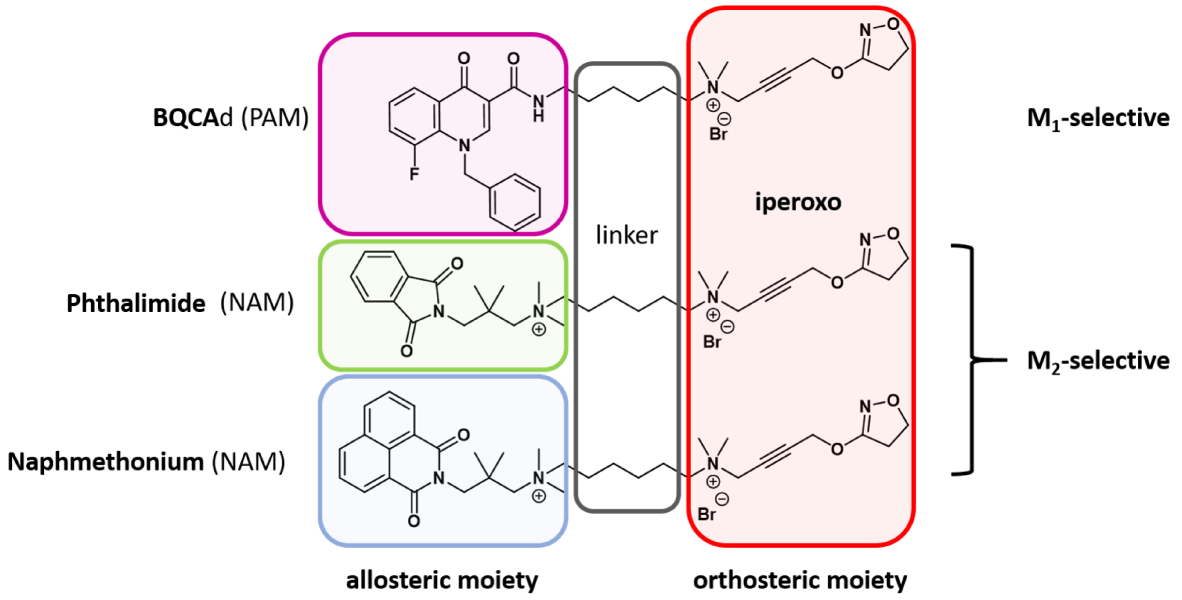

Fig. 9. Dualsteric ligands based on the "address/message" model with iperoxo as orthosteric and BQCAd, phthalimide and naphmethonium as allosteric building blocks for the selective targeting of the M_1 and M_2, respectively.

1.3. Photopharmacology

Light is a fascinating phenomenon that determines life on earth and is responsible for environmental interactions through photochemical reactions such as in vision, photosynthesis, and plant growth. Its bioorthogonality, unmatched spatiotemporal resolution, speed and easiness of modulation are only few of the advantages that render light a suitable external and non-invasive stimulus. Drugs that are designed in a way to respond to light have shown great impact for light-controlled regulation of biological processes related to a large number of diseases. In the last two decades, this emerging field, often called photopharmacology, attracted the attention of the research community and is still in its infancy.[68]

1.3.1. Photoresponsive Hybrid Compounds

Molecular photoswitches, such as azobenzenes, dithienylethenes, and spyropyrans, are the key elements, as they reversibly change their structures upon irradiation resulting in a change of the physicochemical properties (polarity, geometry). Hence, molecular hybridization of photoswitches with pharmacophores provides photochromic ligands (PCL) that can toggle between two distinct states depending on the wavelength of light. This photo-induced isomerization may be translated into a change in efficacy and/or activity of drugs, enabling remote control of the respective biological function (Fig 10).[69]

However, photopharmacology is still confined by significant factors. To date, with a few exceptions, high-energy UV light is required for isomerization, which can cause severe damage to tissue and penetrate only partially through most media, which limits its therapeutic applications as well.[70] Preferably molecular photoswitches are needed that may exhibit photoisomerization in a visible region of the electromagnetic spectrum and that increase the thermal stability of the less stable photoisomer. Obviously, photoisomerization should not be associated with toxicity. Another major concern is light delivery. Therapeutic targets, such as ion channels, receptors, and enzymes, can only be addressed with photoswitchable ligands if they are accessible by light. In contrast to exposed regions, i.e., skin and eyes, deeper organs are only accessible through more or less invasive incisions and operations.[71]

The design and development of novel light-sensitive compounds depends on the ability to render them photoresponsive, which is also called photodruggability. Based on a rational approach two main strategies have been developed. The “azologization approach” employs bioisosteres of the azobenzene chromophore (“azosteres”) and enables rational replacement of sterically and electronically similar moieties. On the other hand, azobenzenes can be attached

to certain substituents of the drug, i.e., phenyl rings and other aromatic systems without abrogating the pharmacological activity giving rise to the "azo-extension approach."[69] Currently, this field is rapidly expanding and is already featuring valuable breakthroughs especially in CNS research. With successes in cancer chemotherapy, diabetes, antimicrobial agents, and vision restoration in the first step, other applications will likely follow in the near future. It has to be kept in mind that *in vitro* studies in suitable assays can easily provide a proof-of-concept, but high affinity and selectivity plus easy switching with high spatiotemporal resolution in an *in vivo* setting is far more difficult to achieve.[72] Now as the foundations have been laid, researchers will need persistence in the evaluation of the right targets and the design of novel PCLs, but in the end photoswitchable hybrid compounds might find their way in clinical application. (For full review of the field see Agnetta and Decker[73] or appendix I)

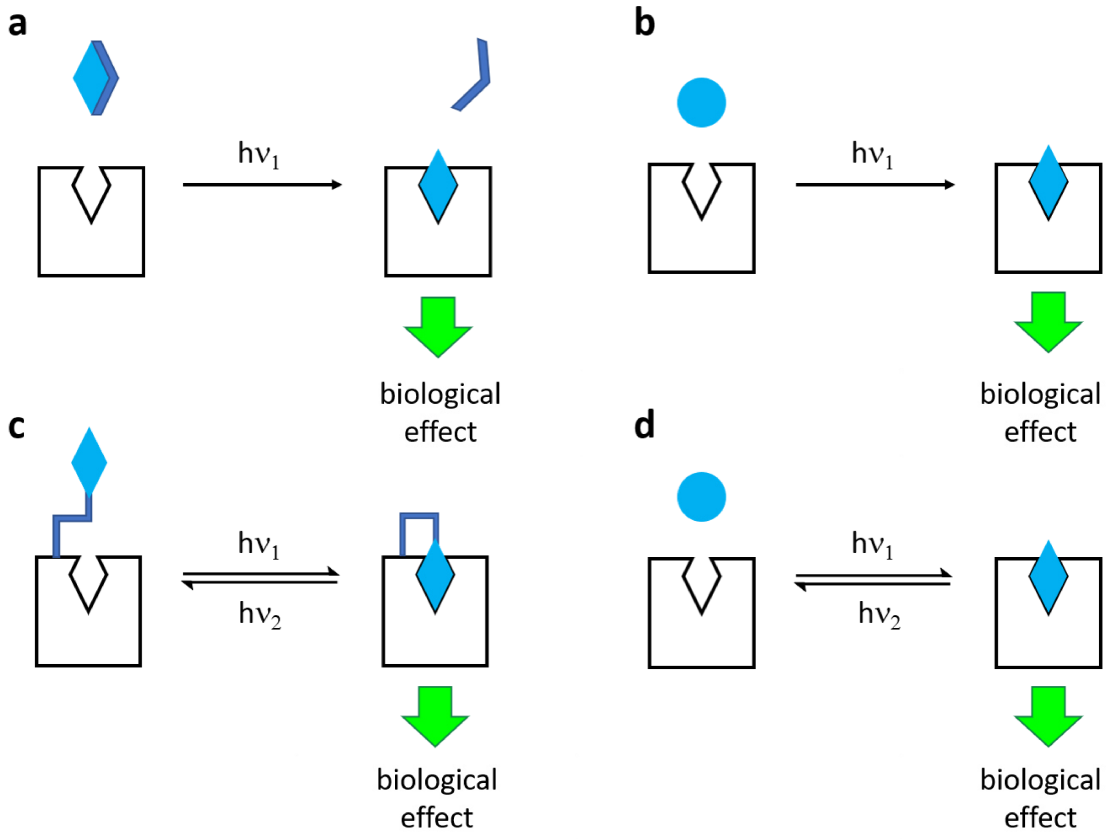

Fig. 10. Basic mechanisms of action of photopharmacology including irreversible a) (photo-) caged ligands (CL) b) photodynamic therapy (PDT). Reversible photoactivation or inactivation using c) photoswitchable tethered ligands (PTL) and photoswitchable orthogonal remotely tethered ligands (PORTL) or d) photochromic ligands (PCL).

1.3.2. Functional Assays for Photopharmacological Characterization

The development and implementation of reliable GPCR functional assays is a crucial aspect for the evaluation of the pharmacological profile and therapeutic potential of newly synthesized drug candidates. This is true not only for early stage drug-discovery processes but also for the characterization of target compounds on receptor level, which makes it possible, to a certain extent, to elucidate receptor dynamic mechanisms.

Typically, an ideal cell-based functional assay for GPCR should be easy in handling and preferentially be carried out in therapeutically relevant living cells. This excludes the use of radioactivity, which significantly complicates the testing conditions and requires high safety precautions. Furthermore, the readout should show a high signal-to-noise ratio, be homogenous and be amenable to microtiter formats. The expression pattern of the assessed GPCR and the multiplicity of signaling pathway also have to be considered. Their neglection can falsify the readout and cause incorrect interpretations. Importantly, signaling events proximal and hence, clear related to receptor activation should be observed preferentially.[74]

As mentioned earlier, GPCR signaling is provoked mainly by the movement of the receptor and its transition of conformations. Accordingly, novel fluorescence- and bioluminescence-based techniques have been developed, which are able to sensitively monitor these changes with spatiotemporal resolution by labeling suitable positions of the receptor. Depending on the location of fluorophore-labeling, these techniques can visualize a great span of processes, starting from the ligation of a small molecules up to further downstream signaling pathways.[75]

However, photopharmacology adds a new dimension to the already stringent requirements that have to be met by a biological assay. It is of prime importance that excitation of the fluorophores and photoisomerization reaction are independent of each other (orthogonal) and distinguishable in their operational wavelength.[69] This technical demand is a major concern in photopharmacology and limits the use of generally precise fluorescence imaging assays. That is why researchers, usually, find it more convenient to interface patch-clamp or electrophysiology techniques with the photoisomerization process. However, these methodologies measure signaling events distal from the receptor activation, which often produces false positives and makes it difficult to relate a signal to the exclusive activation of the given receptor.[76]

1.3.2.1. Resonance Energy Transfer Assays

Based on resonance energy transfer (RET), a variety of receptor sensors have been developed for GPCR recently, which have demonstrated to be highly suitable to determine the effect of ligands on a functional level in living cells.[75,77] These sensors consist of two chromophores, whereby the donor is able to transfer the energy to the acceptor through a non-radiative dipole-dipole-coupling, if they are in close proximity to each other. Depending on whether the acceptor is a fluorophore or a bioluminescencent probe, one can differentiate between fluorescence (FRET) and bioluminescence (BRET) resonance energy transfer. These sensors are reported as "molecular ruler" measuring the distance between the probe pairs by recording the change of FRET and BRET ratio, respectively. Advantages of these techniques include high efficiency due to the detection of very small changes in distance and the possibility of monitoring proximal signaling event, such as G protein or β-arrestin recruitment. However, the excitation and emission peaks of the respective biosensors dictate the wavelength for the optimal performance of the assay, which have to be matched for an orthogonal interface with photoisomerization processes.

1.3.2.2. Luciferase Complementation Assay

Most cellular responses on an external stimulus are mediated over protein-protein interactions into the cell, as visualized in Fig. 2. In living cells, the interaction between two proteins of interest can be examined with spatiotemporal resolution using protein complementation assays (PCA).[78] PCA is based on the reconstitution of a dissected reporter protein, in this case luciferase, which is responsible for the oxidation of luciferin with concomitant emission of light. For the investigation of the functional activity at the muscarinic receptor, the two catalytically inactive fragments of luciferase are fused to the $G\alpha_q$-subunit and the PLC-β3, respectively.[79] Upon activation of the receptor, the modified $G\alpha_q$-subunit interacts with the modified PLC-β3 bringing the biosensor fragments into close proximity and promoting its reconstitution, which results in emission of bioluminescence (Fig. 11). This strictly correlates with receptor activation and therefore, can be read out in a ligand concentration-dependent manner. Some major advantages characterize this assay: Firstly, receptors remain un-engineered contrary to RET-techniques, where often large constructs at the ILs may intrinsically effect receptor conformations. Secondly, it is amenable to microtiter formats enabling for high-throughput screening of target compounds. Lastly, this assay shows a high degree of robustness and reliability of data due to the monitoring of the $G\alpha_q$/PLC-β3 interaction

proximal to receptor activation reducing the incidence of false positives.[74] Importantly, no excitation with light, which potentially could interfere with the operational wavelengths of photoswitching is needed for the performance of this technique, which makes it highly suitable for photopharmacological investigations on GPCRs. However, this method is still in his childhood despite its strengths and was only developed for the human M_1, M_3 and M_5 receptors, the human histamine H_1 receptor and the human neurotensin NTS_1 receptor so far.[79] Currently, Littmann and co-workers are expanding split luciferase complementation (SLC) technique for other protein-protein interactions, such as in β-arrestin recruitment[80] and in the cAMP pathway, which may dramatically enhance the number of GPCRs exploitable with this method.

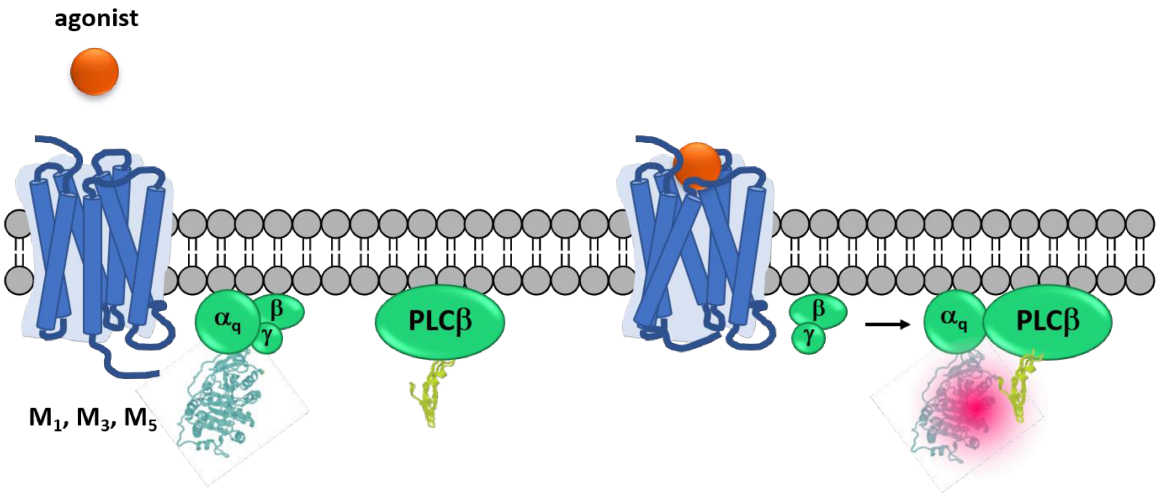

Fig. 11. Basic principle of the $G\alpha_q$/PLCβ3 complementation assay. Upon binding of an agonist, both fragments are brought in close proximity leading to a reconstitution of the functional luciferase protein and emission of bioluminescence, in the presence of the substrate luciferin.

2. Scope and Objective

Muscarinic receptors represent one of the most interesting G protein-coupled receptor families with high therapeutic relevance and potential especially related to the field of neurodegenerative diseases, such as Parkinson's Disease, Alzheimer's Disease and schizophrenia. In the past, researchers have mainly focused on overcoming the poor subtype-selectivity of muscarinic receptors by addressing allosteric binding sites and making use of the cooperativity between the binding sites. This gave birth to several ligands that are promising in terms of clinical application and are currently in different phases of clinical trials.[14] In contrast, dualsteric ligands have emerged as useful tools for the investigation of receptor function and signaling due to their unprecedented subtype-selectivity and specificity for signaling pathways, which can be beneficial for rational structure-based drug design. This includes the detailed examination of their binding sites, activation processes and mechanism of action dictated by the different receptor conformations and their transition dynamics.
However, spacial and temporal patterns of receptor activation and signaling are considered to be crucial factors for the determination of receptor function.[81] Making use of the unmatched properties of light, photopharmacology can add this additional dimension and provide the required spatiotemporal resolution with high precision.

The main scope of this study was the design and synthesis of ligands for the muscarinic acetylcholine receptors, which combine the benefits of the dualsteric approach with light-switchable configurational properties for the investigation of spatiotemporal receptor activation processes. The resulting bipharmacophoric and photoswitchable ligands were characterized regarding their pharmacological activity using FRET and split luciferase complementation techniques.

1. For this purpose, putatively dualsteric ligands consisting of different orthosteric and allosteric moieties were rationalized, into which the molecular photoswitch azobenzene was synthetically incorporated to introduce light-sensitivity. For subtype-selective interactions with the M_1 receptor, benzyl quinolone carboxylic acid (BQCA) was employed as the alloster, while iperoxo represented the orthosteric part. The resulting ligands named BQCAAI and BQCAAI-2 were characterized regarding to their photophysical properties. Furthermore, the ligands' applicability as a pharmacological research tool was investigated at the M_1 receptor using a set of FRET techniques. Following the same principle, two ligands containing phthalimido- (PAI) and

naphthalimido (NAI) moieties as allosteric building block were synthesized to address the M_2 receptor.

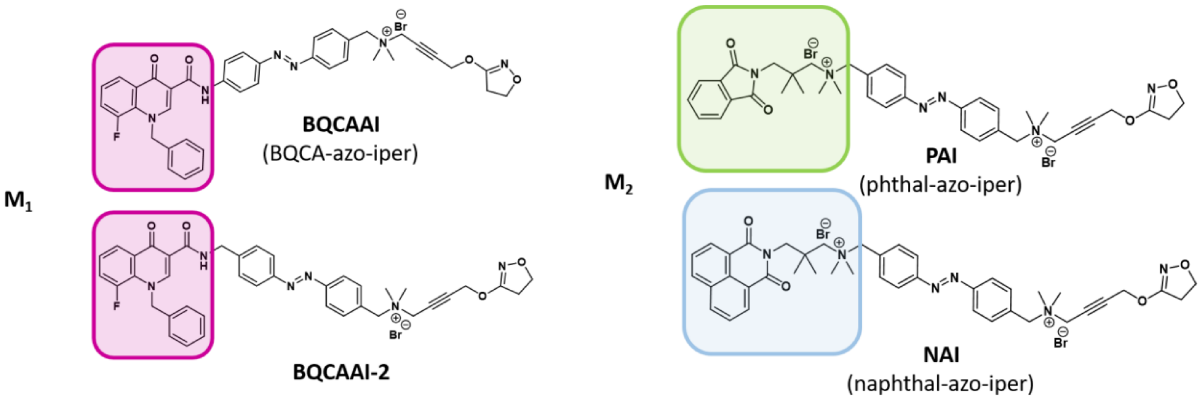

2. Despite this remarkable progress in the development of photopharmacological tool compounds, unsubstituted azobenzene-based systems often lack thermal stability and tissue compatibility. However, apart from overcoming these drawbacks, it is unclear how the replacement with red-shifted molecular photoswitches affects the ligands on a pharmacological level. In this context, a set of mono- (photoiperoxo and F_4 photoiperoxo) and bivalent photoswitchable compounds (iper-azo-iper and F_4-iper-azo-iper) based on the highly potent muscarinic acetylcholine receptor agonist iperoxo with both, an unsubstituted azobenzene core and redshifted tetra-*ortho*-fluorinated analogs were investigated in terms of photophysical properties binding and receptor activation.

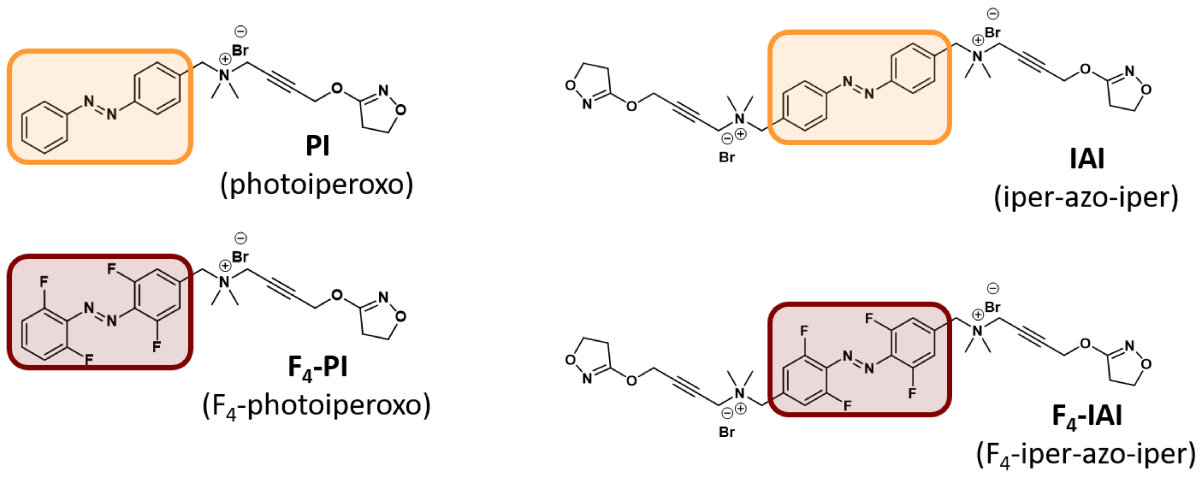

3. Furthermore, two sets of putatively dualsteric ligands containing either derivatives of BQCA or TBPB connected to the orthosteric agonist carbachol with varying linker-lengths were developed and evaluated biologically using a luciferase complementation assay. Ligands were synthesized by Dr. Simon Schramm (Decker group, Julius-Maximilian-University of Würzburg).

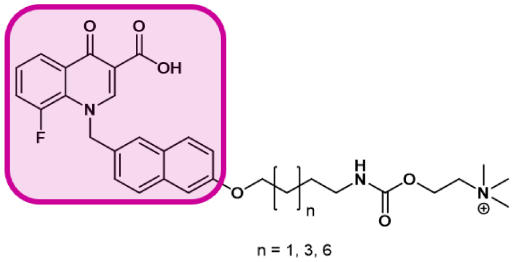

BQCAd-Cn-CCh

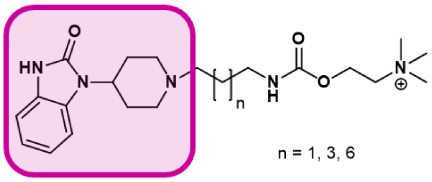

TBPBd-Cn-CCh

3. Published Artiles

3.1. A Photoswitchable Dualsteric Ligand Controlling Receptor Efficacy

GDCh Communications Angewandte International Edition Chemie

Photopharmacology

International Edition: DOI: 10.1002/anie.201701524
German Edition: DOI: 10.1002/ange.201701524

A Photoswitchable Dualsteric Ligand Controlling Receptor Efficacy

Luca Agnetta[+], Michael Kauk[+], Maria Consuelo Alonso Canizal, Regina Messerer, Ulrike Holzgrabe, Carsten Hoffmann,* and Michael Decker**

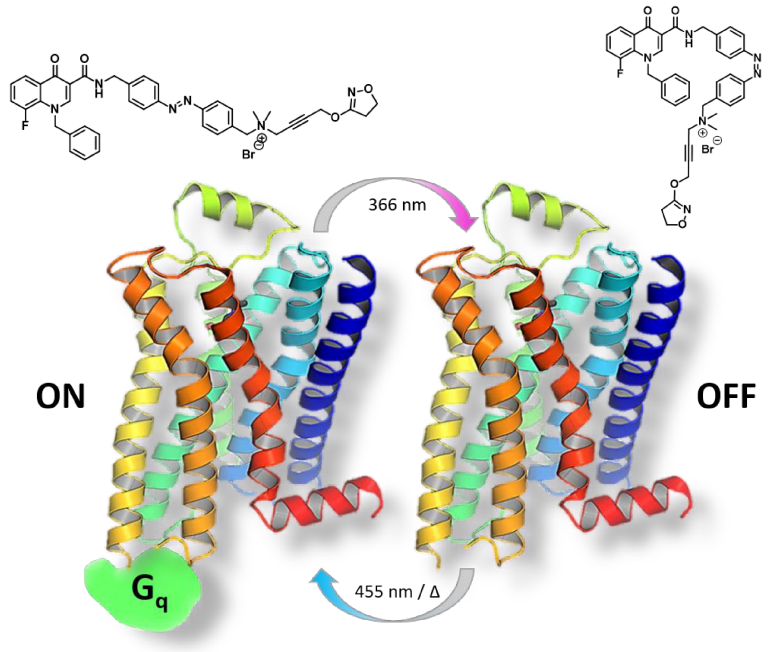

Author contributions

Luca Agnetta, under supervision of Prof. Dr. Michael Decker and Prof. Dr. Ulrike Holzgrabe, performed the design and synthesis of all target compounds and precursors as well as their photophysical characterization, including, UV/Vis-spectral analysis and determination of photostationary states using HPLC-methods.

Dr. Michael Kauk and Maria Consuelo Alonso Canizal, under supervision of Prof. Dr. Carsten Hoffmann, performed FRET-measurement for biological *in vitro* evaluation of target and reference compounds.

Dr. Regina Messerer, under supervision of Prof. Dr. Ulrike Holzgrabe, performed the design and synthesis of BQCA-rigid-iper reference compound.

Summary

The compound design was based on the findings that modification of the spacer length between the orthosteric and allosteric moieties of the iperoxo (orthosteric agonist)/BQCAd-type (positive allosteric modulator) hybrids controls its efficacy and leads to different degrees of partial agonism.[64,82] Synthetically incorporating a molecular photoswitchable azobenzene moiety as a linker between the agonist and the positive allosteric modulator has given rise to a BQCA-azobenzene-iperoxo (BQCAAI) hybrid compound (Fig. 12). Its photochromic behavior was investigated with UV/Vis-spectroscopical methods, showing that this ligand is truly responsive to light (Fig. 13).

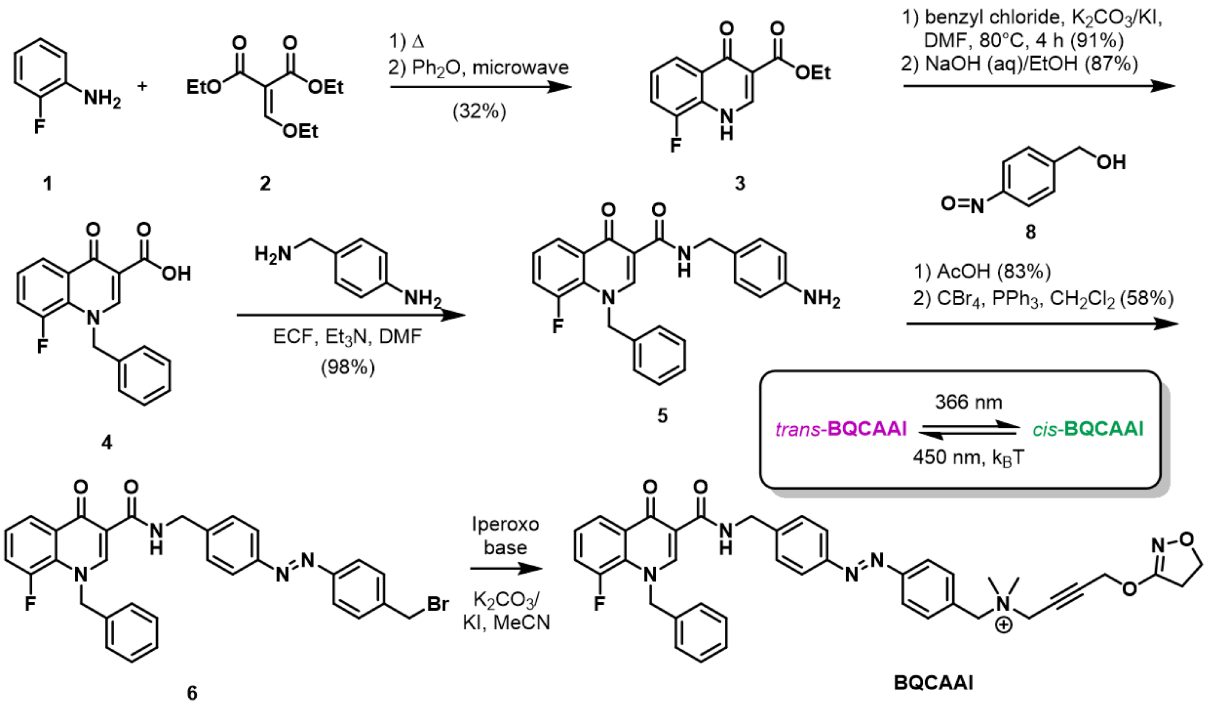

Fig. 12. Synthesis of photoswitchable hybrid BQCAAI employing Gould-Jacobs reaction followed by benzylation, saponification and amidation reactions and entailing a Mills reaction, bromination and attachment of iperoxo base.

Fluorescence-based studies, including FRET (Fig. 14 and 15), show that BQCAAI allows the change between an inactive purely allosteric and an active orthosteric/allosteric binding pose in a light-controlled fashion and offers the possibility to study the process of receptor activation at a molecular level. As such, BQCAAI provides not only spatiotemporal resolution, but also the ability to control the receptor efficacy remotely. (For full article see Agnetta et al.[76] or appendix II)

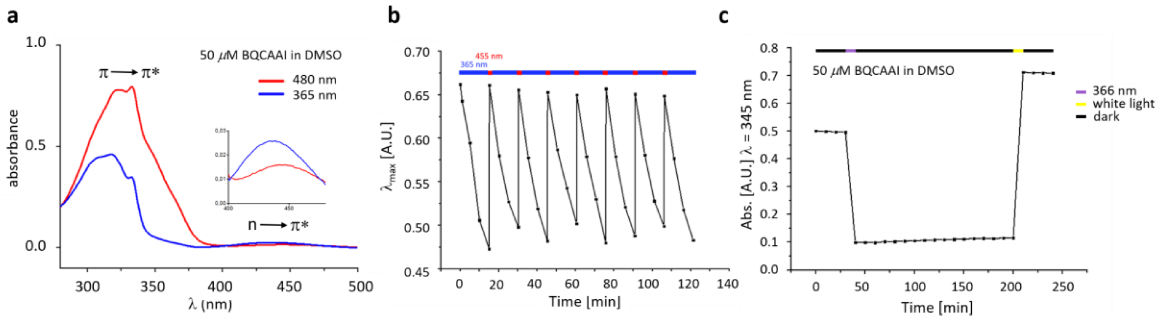

Fig. 13. a) Change of absorption spectrum upon irradiation with light proving photochromic behavior of BQCAAI. b) Isomerization process can be repeated over many cycles providing robust and reversible photoswitching ability. c) Thermal stability: Once switched to the *cis*-isomer, the achieved PSS is stable in the dark for more than 2.5 h. Upon irradiation with white light a PSS in favor of the *trans*-isomer is regained. This excellent thermal stability allows the investigation of BQCAAI on an hour's timescale, clearly distinguishing between the two PSSs.

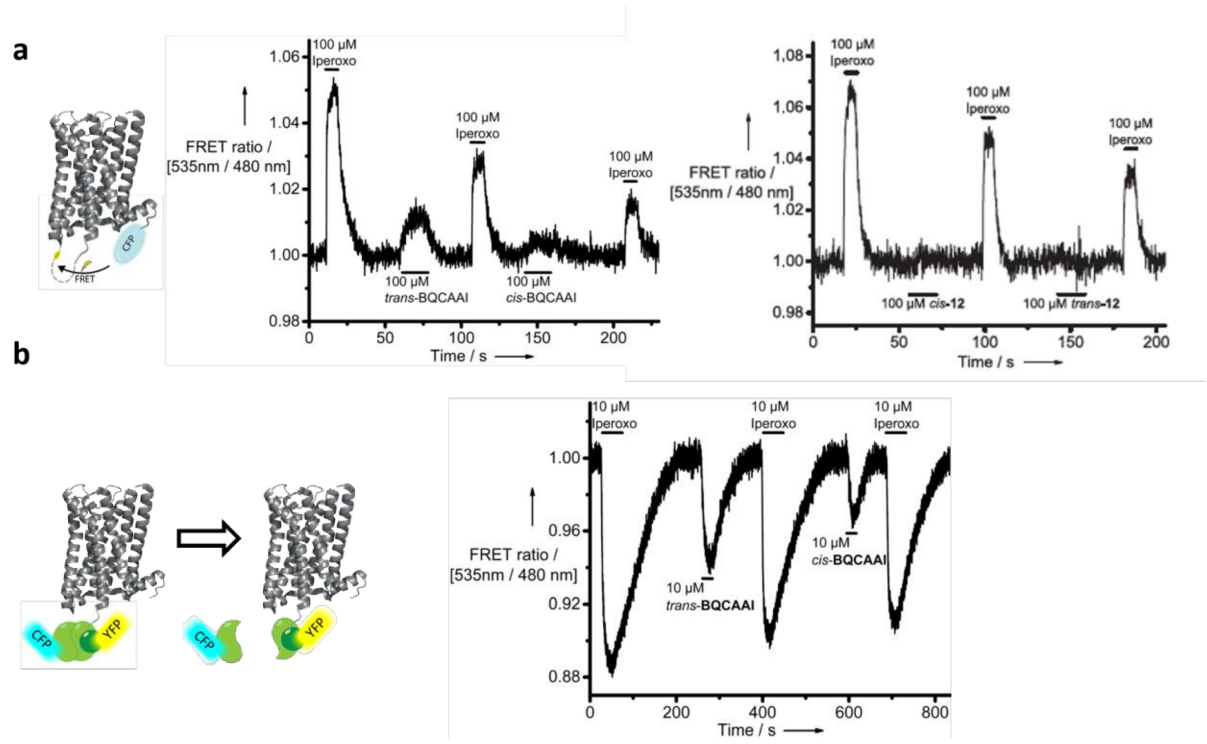

Fig. 14. a) FRET experiment for both conformations of BQCAAI and photoiperoxo at the M_1 receptor showing significantly reduced receptor response for the *cis*-conformer (14%) compared to the trans-conformer (25%) of BQCAAI while photoiperoxo is not able to induce any receptor response. b) FRET investigations of Gq protein activation for both BQCAAI isomers at the M_1 receptor. The cis-form induces a less pronounced effect also on Gq protein activation (40%) compared to the *trans*-form (58%).

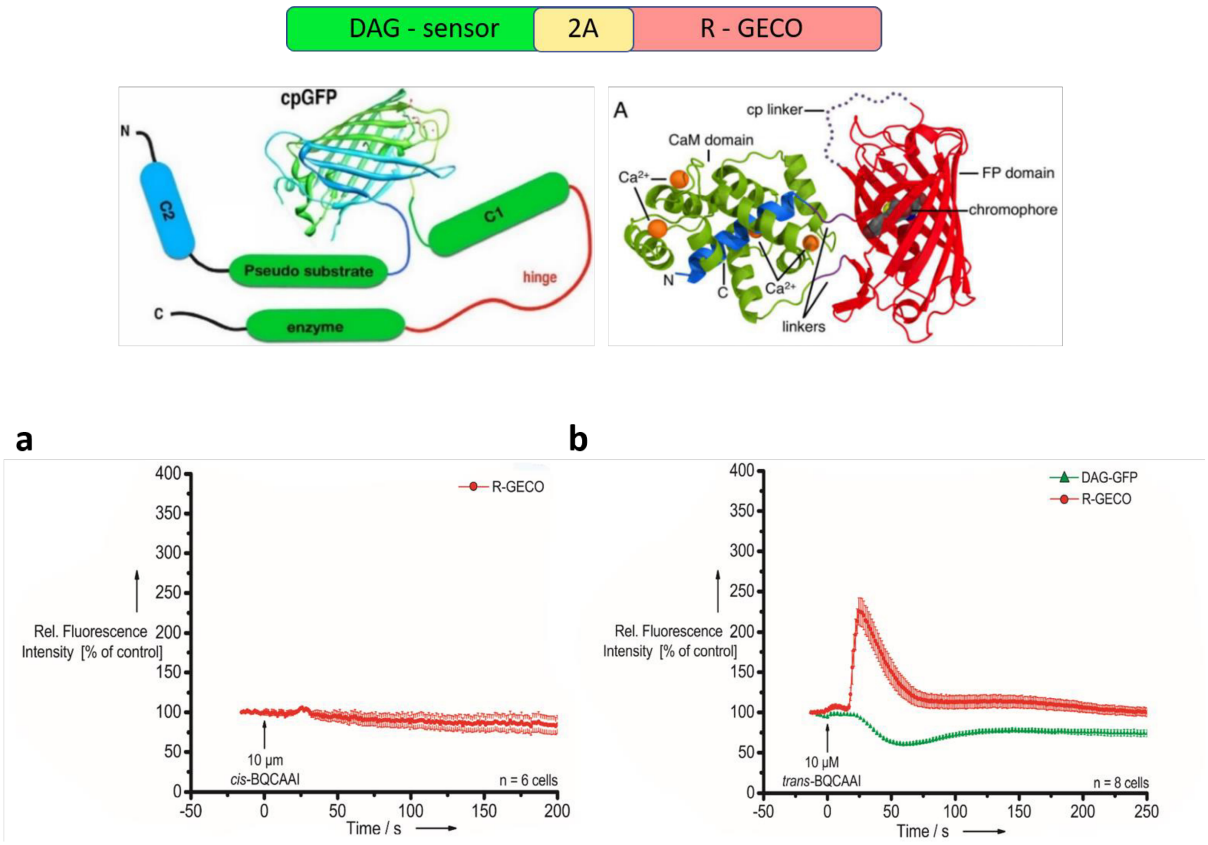

Fig. 15. Investigations of downstream signaling using a dual Ca2+/DAG sensor, which is excited at 488 nm (DAG) and 562 nm (Ca^{2+}) respectively. a) The *trans*-conformer induces a significant cellular response after 25 seconds. b) Using individual Ca^{2+} monitoring, the *cis*-conformer is not able to induce a cellular response.

3.2. Fluorination of Photoswitchable Muscarinic Agonists Tunes Receptor Pharmacology and Photochromic Properties

Journal of Medicinal Chemistry

Article

pubs.acs.org/jmc

Fluorination of Photoswitchable Muscarinic Agonists Tunes Receptor Pharmacology and Photochromic Properties

Luca Agnetta,[†] Marcel Bermudez,[‡] Fabio Riefolo,[§,∥] Carlo Matera,[§,∥] Enrique Claro,[⊥] Regina Messerer,[†] Timo Littmann,[#] Gerhard Wolber,[‡] Ulrike Holzgrabe,[†] and Michael Decker*[,†]

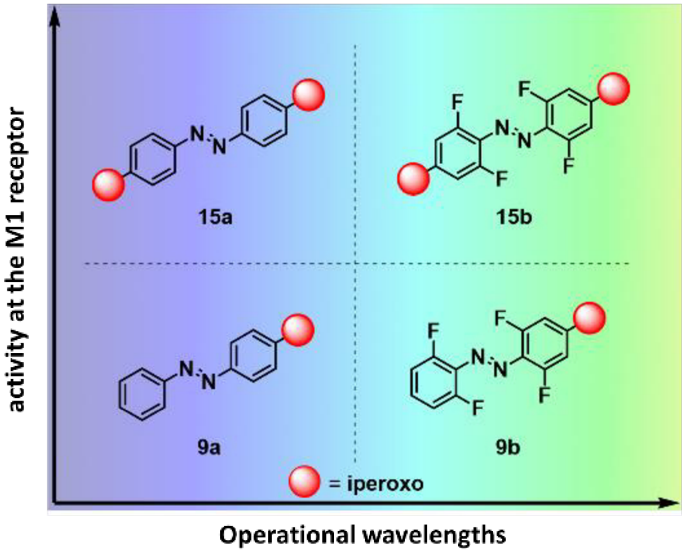

Author contributions

Luca Agnetta, under supervision of Prof. Dr. Michael Decker and Prof. Dr. Ulrike Holzgrabe, performed the design and synthesis of all target compounds and precursors as well as their photophysical and pharmacological characterization.

Dr. Marcel Bermudez and Prof. Dr. Gerhard Wolber provided receptor-ligand docking experiments for all target and reference compounds using a M_1 homology model.

Fabio Riefolo, Dr. Carlo Matera and Dr. Enrique Claro performed binding experiments for all target compounds and assisted in target compound characterization.

Dr. Timo Littmann provided the protocol and cell lines for pharmacological experiments.

Dr. Regina Messerer, under supervision of Prof. Dr. Ulrike Holzgrabe, performed the design and synthesis of iper-linker-iper reference compounds.

Summary

To expand the application of photopharmacological tool compounds to therapeutic applications, the need of redshifted azobenzenes for the design of light-responsive systems is frequently emphasized.[83] This is due to the tissue damaging and cell toxic properties of UV light, necessary to achieve the photoisomerization in unsubstituted azobenzenes.[70] In addition, low photostationary states (PSSs), poor thermal stability and potential interference with the commonly used optical readout methods, especially in GPCR research, are serious restrictions.[84] Generally, azobenzenes that can be switched with visible light are preferred over their blue shifted counterparts, as they overcome the above-mentioned drawbacks. We synthesized (Fig. 16 and 17) and investigated a set of mono- and bivalent photoswitchable compounds based on the highly potent M receptor agonist iperoxo with both, the unsubstituted azobenzene core and redshifted tetra-*ortho*-fluorinated analogs in a novel split luciferase assay in order to reflect Gq activation. Remarkably, tetra-*ortho*-fluorination does not only positively affect the photochromic behavior (Fig. 18), but also enhances efficacy and activity at the M_1 receptor: Uni- and bivalent iperoxo ligands act as “efficacy”-switches, whereas the tetra-*ortho*-fluorinated analogs act as potent “affinity”-switches (Fig. 20) with the desired PSS improvement and advantageous photophysical properties (redshift). These findings also demonstrate, that substituted azobenzenes in photopharmacological compounds not just represent analogs with other photophysical properties but can exhibit a considerably different biological profile that has to be investigated carefully. (For full article see Agnetta et al.[85] or appendix III)

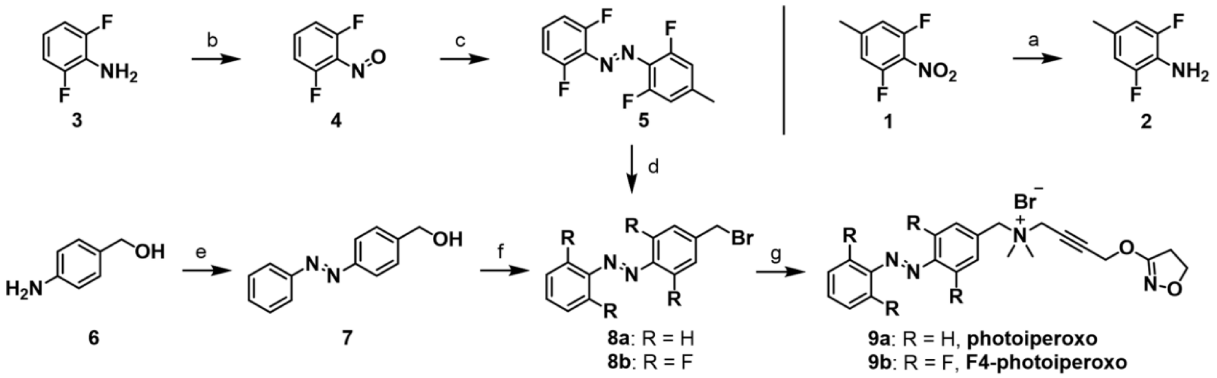

Fig 16. Synthesis of photoswitchable iperoxo derivatives photoiperoxo and F4-photoiperoxo. Reagents and conditions: (a) Pd/C, EtOH (87%); (b) Oxone, DCM, water; (c) **2**, AcOH/TFA, toluene (43%); (d) NBS, AIBN, CCl_4, 80 °C (50%); (e) nitrosobenzene, AcOH (75%); (f) CBr_4, PPh_3, DCM (60%); (g) 4((4,5-Dihydroisoxazol-3-yl)oxy)-N,N-dimethylbut-2-yn-1-amine, EtOAc/MeCN (39% for **9a**, 92% for **9b**).

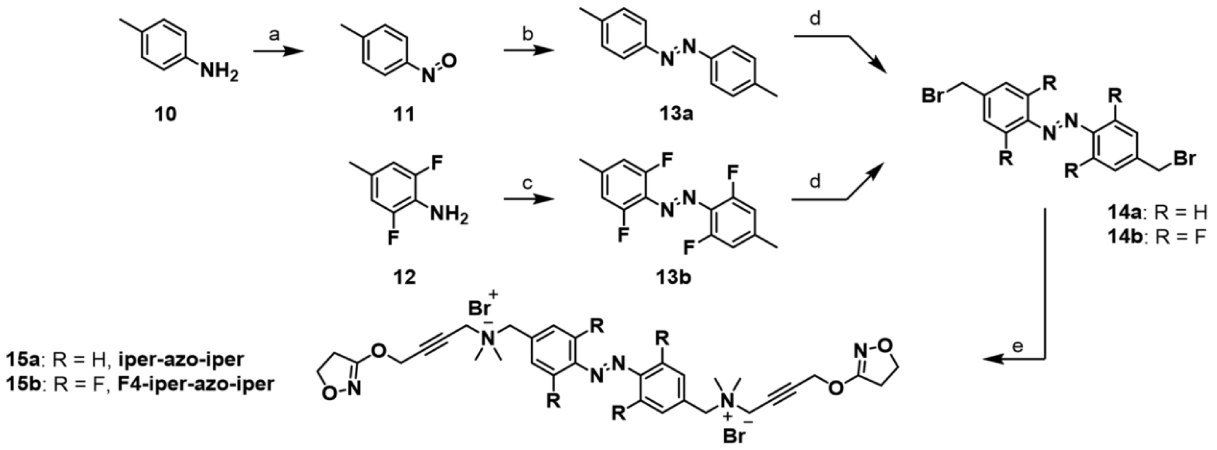

Fig 17. Synthesis of photoswitchable iperoxo homodimers **15a** and **15b**. Reagents and conditions: (a) Oxone, DCM, water; (b) **10**, AcOH (36%); (c) KMnO4, FeSO4.7H2O, DCM (29%); NBS, AIBN, CCl4, 80 °C (76% for 14a, 24% for 14b); 4((4,5-Dihydroisoxazol-3-yl)oxy)-N,N-dimethylbut-2-yn-1amine, EtOAc, 60 °C (83% for **15a**, 32% for **15b**).

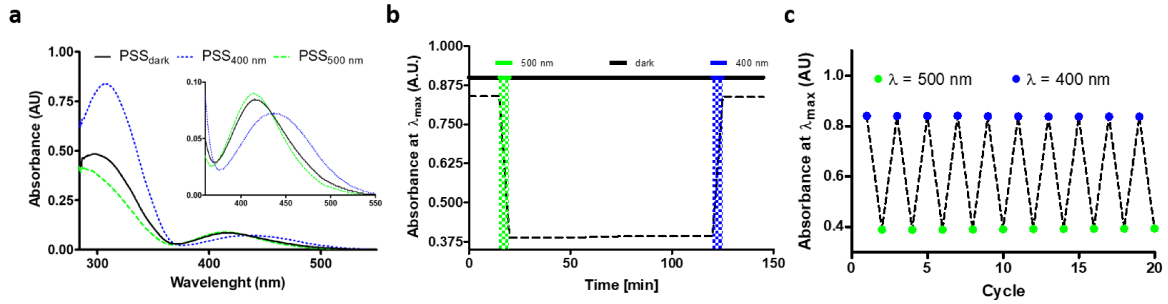

Fig. 18. 3 a) Absorption spectrum of **9b** upon irradiation with blue (400 nm) and green (500 nm) light showing good separation of n-π* transition bond b) Absorption at λ_{max} for determination of stability of the *cis* isomer c) Isomerization process can be repeated over many cycles providing robust and reversible photoswitching ability.

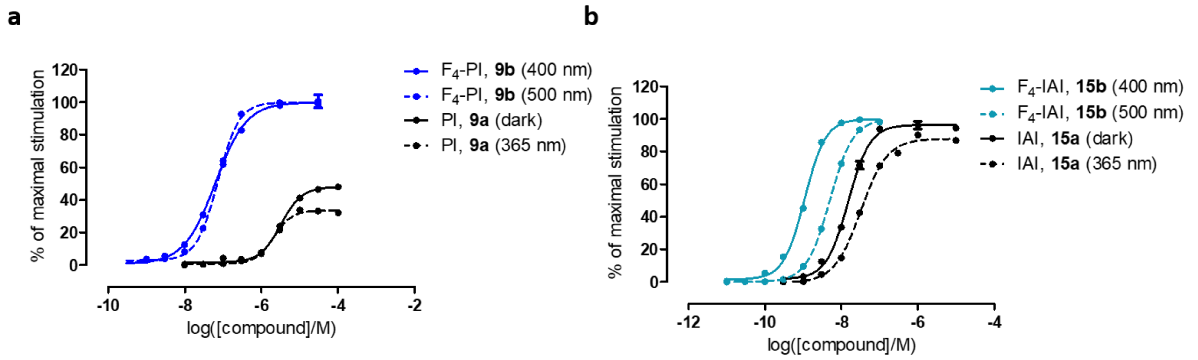

Fig. 19. a) Introduction of the tetra-*ortho*-fluoro scaffold causes a significant change in the pharmacological profile. While **9a** activates the receptor only weakly, **9b** shows full agonistic activity with remarkable gain of potency. b) Both iperoxo homodimers **15**a and **15b** are full agonists with significant potency enhancement for the tetra-*ortho*-fluorinated dimer and considerable difference in biological activity for the two photoforms.

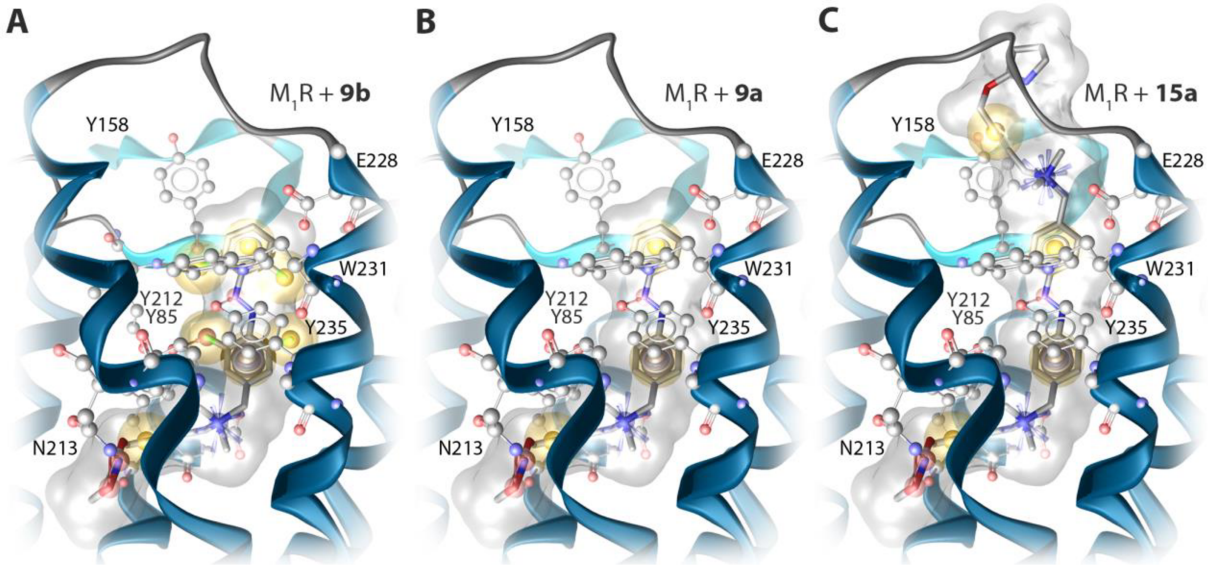

Fig. 20. Molecular docking: Pharmacological properties are mainly driven by binding of *trans* isomer. Due to the fluorination of azobenzene core, the aromatic ring adopts an optimal geometry for π-π interaction with the tyrosine lid. Additional charge interactions of the ammonium group of the dimers **15a** and **15b** in the extracellular receptor domain are responsible for the higher potencies, which were not observed with **9a** and **9b**.

4. Additional Research Work

4.1. Novel BQCA and TBPB Derived M_1 Receptor Hybrid-Ligands: Orthosteric Carbachol Differentially Regulates Partial Agonism

Simon Schramm, Luca Agnetta, Hubert Gerwe, Marcel Bermudez, Matthias Irmen, Janine Holze, Timo Littmann, Gerhard Wolber, Christian Tränkle, Michael Decker*

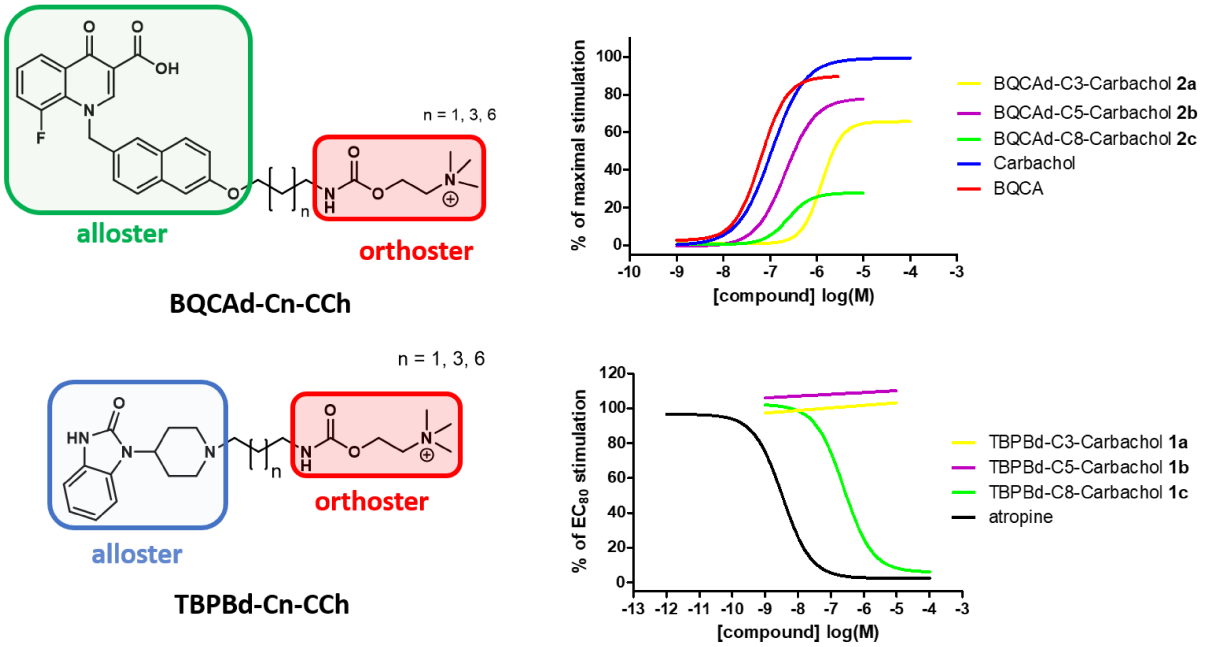

Author contribution

Dr. Simon Schramm, under supervision of Prof. Dr. Michael Decker performed the design and synthesis of all target compounds.

Luca Agnetta, under supervision of Prof. Dr. Michael Decker performed the pharmacological characterization of all target compounds.

Hubert Gerwe, under supervision of Prof. Dr. Michael Decker synthesized and characterized reference compounds.

Dr. Marcel Bermudez and Prof. Dr. Gerhard Wolber provided receptor-ligand docking experiments for all target and reference compounds using a M_1 homology model.

Matthias Irmen and Janine Holze under supervision of Prof. Dr. Christian Tränkle performed Schild and statistical analyses.

Dr. Timo Littmann provided the protocol and cell lines for pharmacological experiments.

Summary

In this work, we compare and discuss two sets of putatively dualsteric ligands, which were designed to connect the orthosteric ligand carbachol to different types of allosteric ligands. This is based on recent investigations of the complex mechanisms of allostery, providing a deeper understanding of GPCR activation and signaling processes. In this context, M receptors are highly relevant according to their exemplary role for the study of allosteric modulation. We chose a benzyl quinolone carboxylic acid derivative (BQCAd) as an M_1-selective positive allosteric modulator and derivatives of TBPB [1-(1‘-(2-tolyl)-1,4‘-bipiperidin-4-yl)-1*H*-benzo[*d*]imidazol-2(3*H*)-one] as an M_1-selective bitopic, i.e. orthosteric/allosteric agonist, i.e. TBPBds, varying the distance between the allosteric and orthosteric building blocks (Fig. 21). The pharmacological profile of these compounds, which was investigated using luciferase protein complementation techniques in both the agonist and antagonist mode. We could demonstrate that both alloster and linker length must be carefully chosen to obtain agonist or antagonist behavior, respectively. While BQCAd-carbachol derivatives show partial agonism, TBPBd-carbachol-derived compounds exhibit a formally competitive antagonism at the M_1 receptor (Fig. 22). These findings may provide detailed information about the relation between orthosteric and allosteric binding site and may help to design biased signaling and/or subtype selectivity in future studies. (For full manuscript and supporting information see appendix IV).

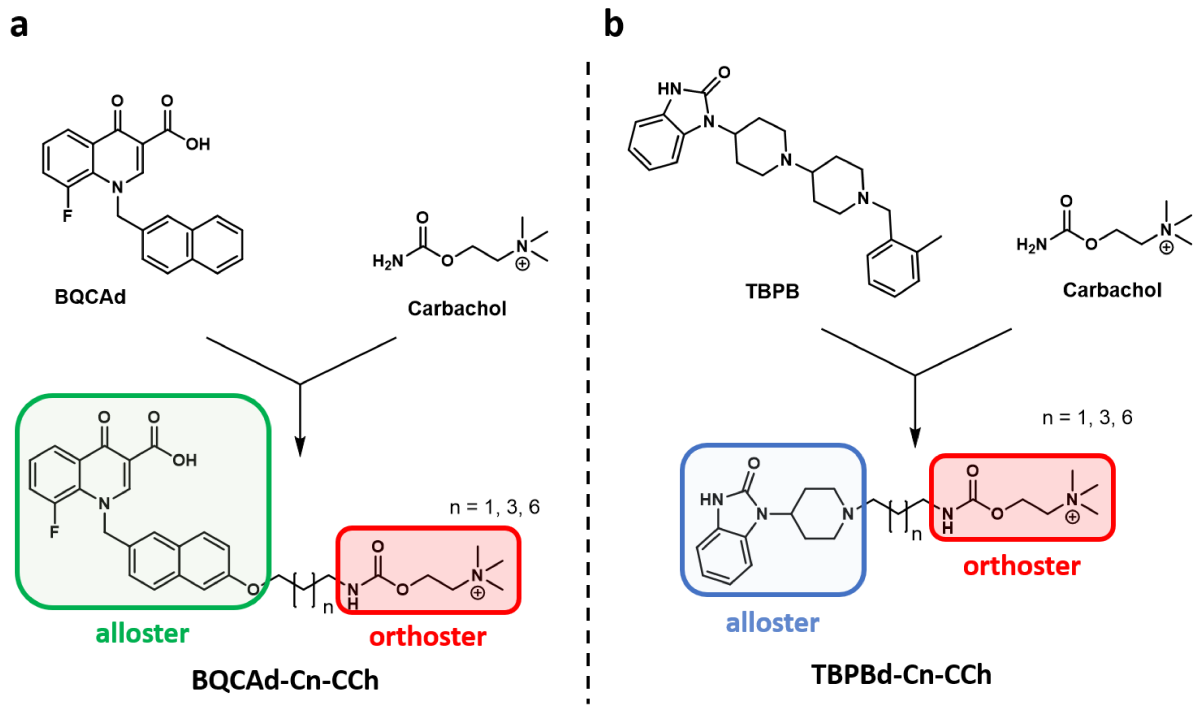

Fig. 21. Design strategy of putatively dualsteric compounds. The orthosteric moiety carbachol was connected to a) a derivative of BQCA and b) a TBPB derivative using aliphatic linker of different lengths (C3, C5, C8).

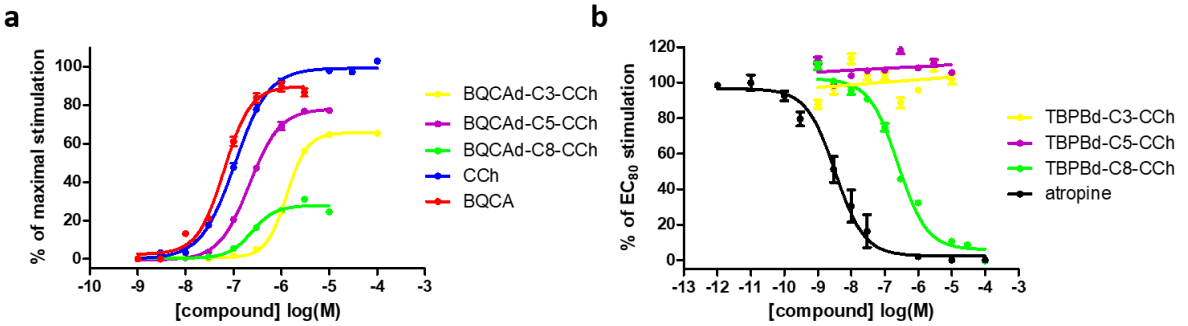

Fig. 22. Pharmacological characterization of BQCAd- and TBPB-derivatives by means of luciferase complementation assay in a) the agonist, showing the partial agonist nature of BQCAd-derivatives, and b) the antagonist mode, identifying the TBPBd-C8-CCh derivative as competitive antagonist.

4.2. Synthesis and Pharmacological Investigation of Photoswitchable and Dualsteric BQCA-based ligands

4.2.1. Design

It has been shown in previous studies that the length of the spacer connecting the orthosteric building block to the allosteric moiety can be crucial when designing dualsteric ligands with graded efficacy and partial agonism.[64] As shown for iperoxo/BQCAd hybrids, the aliphatic spacer length influenced the probability of a purely allosteric and a dualsteric binding mode. Following the previous design strategy for subtype-selective hybrid molecules preferring the M_1 receptor (cf. 3.1.), a photoswitchable iperoxo/BQCAd hybrid compound was investigated, which is one C-atom shorter than BQCAAI[76] and has been named BQCAAI-2.

4.2.2. Results

BQCAAI-2 was obtained according to the synthetic procedures mentioned before (cf. 3.1.) and included Gould-Jacobs and Mills reaction, followed by the substitution with the orthosteric moiety (Fig. 23.).

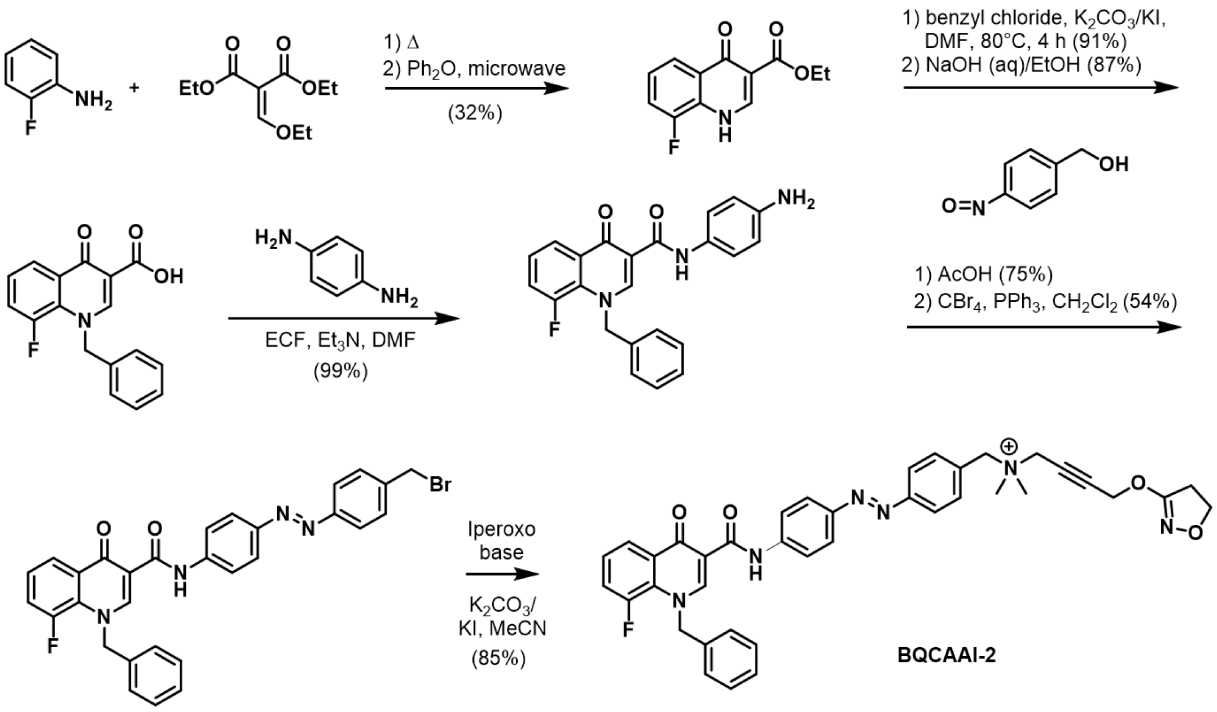

Fig. 23. Synthesis of photoswitchable hybrid BQCAAI-2 employing Gould-Jacobs reaction followed by benzylation, saponification and amidation reactions and entailing a Mills reaction, bromination and attachment of iperoxo base

To detect to which extent BQCAAI-2 responds to light, UV/Vis measurements were performed, evaluating for the ligands' robustness and sensitivity (Fig. 24). BQCAAI-2 clearly responds to the illumination with various wavelengths of the UV and visible regions of the spectrum. Moreover, it shows a great degree of stability and a good ability for multiple and reversible photoswitching. On a closer look, the absorption spectrum of BQCAAI shows a major

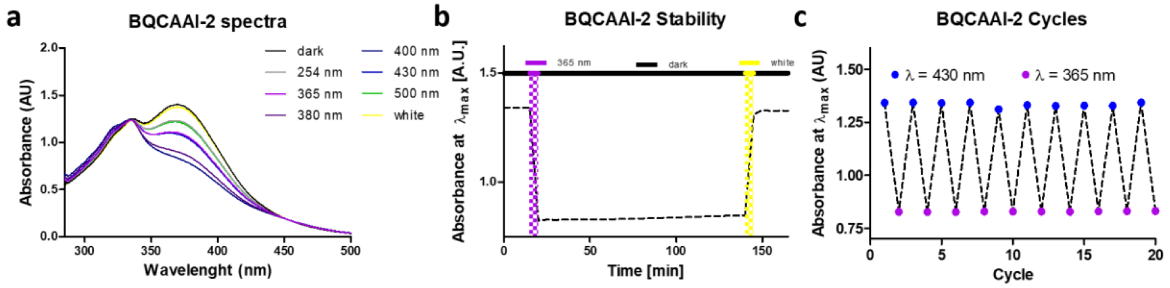

Fig. 24. a) Absorption spectrum of BQCAAI-2 upon irradiation with different wavelengths. b) Absorption at λ_{max} for determination of thermal stability of the *cis* isomer. c) Isomerization process can be repeated over many cycles providing robust and reversible photoswitching ability.

difference compared to BQCAAI. Usually, one strong π-π* and a weaker n-π* transition band is detected for azobenzene-based molecular photoswitches, which both change their absorption intensity upon irradiation. This is not the case for BQCAAI-2, which shows only the stronger transition π-π* transition band. This phenomenon is based on the attachment of the shorter azobenzene linker in BQCAAI-2 and therefore, represents a conjugated system. This causes the n-π* transition band to vanish and is in good accordance with literature. However, conjugation of the free electron pairs does not affect the photoswitching performance.

For the preliminary pharmacological characterization, a luciferase complementation assay was applied. The synthetic agonist carbachol was herein used as reference. BQCAAI-2 was tested on its functional activity in both the *trans* and *cis* photoforms and compared to the photopharmacological profile of BQCAAI. Both tool compounds are found to be "efficacy switches" (change of maximal effect upon irradiation) and only weak "potency switches" (change in EC_{50} value upon irradiation). The *trans* isomer in the dark-adapted state of both compounds shows a maximal efficacy of 57% for BQCAAI and 72% for BQCAAI-2 compared to 100% of CCh, evidencing a partial agonistic behavior at the M_1 receptor. The *cis* isomer decreases the efficacy further to 43% for BQCAAI and 50 % for BQCAAI-2 (Fig. 25). This is in accordance with our previous study, where BQCAAI was characterized as a partial agonist using FRET techniques. The shorter length of the photoswitchable linker seems to be beneficial

for a stabilization of the active conformation. BQCAAI-2 may fit slightly better to the receptor adopting a conformation, which makes it possible to interact with both the lipophilic core and the extracellular vestibule of the receptor to a higher degree. For a clear characterization of this compound, further experiments including selectivity studies using suitable fluorescent-based and molecular modeling techniques should complement the functional assay, which will identify the potential of BQCAAI-2 as suitable molecular tool for in-depth investigation of the molecular basis of M_1 receptor activation processes.

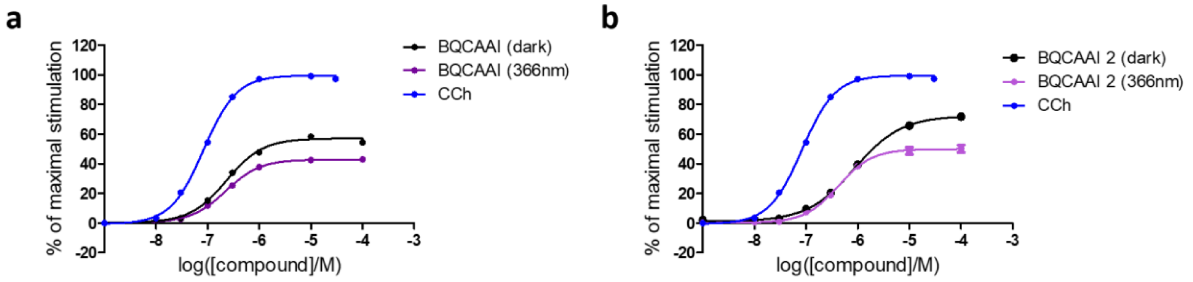

Cmpd	pEC_{50}	$\%E_{max}$
BQCAAI (dark)	6.64 ± 0.01	57 ± 0.1
BQCAAI (366nm)	6.65 ± 0.38	43 ± 0.3

Cmpd	pEC_{50}	$\%E_{max}$
BQCAAI-2 (dark)	6.07 ± 0.01	72 ± 0.5
BQCAAI-2 (366 nm)	6.37 ± 0.04	50 ± 1.0

Fig. 25. Gα/PLC-β3 split-luciferase interaction assay in HEK 293T cells for the preliminary photopharmacological characterization of light-sensitive iperoxo/BQCAd hybrid molecules a) BQCAAI and b) BQCAAI-2 in both the *cis* and *trans* photoforms. Data represent means ± SEM of 3-4 experiments conducted at least in triplicate observations.

4.2.3. Experimental Section

General Information. Common reagents and solvents were obtained from commercial suppliers (Aldrich, Steinheim, Germany; Merck, Darmstadt, Germany) and were used without any further purification. Tetrahydrofuran (THF) was distilled from sodium/benzophenone under an argon atmosphere. Microwave assisted reactions were carried out on a MLS-rotaPREP instrument (Milestone, Leutkirch, Germany) using 8-10 weflon disks. Thin-layer chromatography (TLC) was performed on silica gel 60 F254 plates (Macherey-Nagel, Düren, Germany) and spots were detected under UV light (λ=254 nm) or by staining with iodine. Merck silica gel 60 (Merck, Darmstadt, Germany) was used for chromatography (230-400 mesh) columns or performed on an Interchim Puri Flash 430 (Ultra Performance Flash Purification) instrument (Montluçon, France). Used columns are: Silica 25 g – 30 µm, Alox-B 40 g – 32/63 µm, Alox-B 25 g – 32/63 µm (Interchim, Montluçon, France). Nuclear magnetic

resonance spectra were performed with a Bruker AV-400 NMR instrument (Bruker, Karlsruhe, Germany) in [d_6]-DMSO, $CDCl_3$, $(CD_3)_2CO$. As internal standard, the signals of the deuterated solvents were used (DMSO-d_6: ^1H 2.50 ppm, ^{13}C 39.52 ppm; $CDCl_3$: ^1H 7.26 ppm, ^{13}C 77.16 ppm; $(CD_3)_2CO$: ^1H 2.05 ppm, ^{13}C 39.52 ppm). Abbreviation for data quoted are: s, singlet; d, doublet; t, triplet; q, quartet; m, multiplet; br, broad; dd, doublet of doublets; dt, doublet of triplets; tt, triplet of triplets; tq, triplet of quartets. Coupling constants (*J*) are given in Hz. For purity and reaction monitoring, analytical HPLC analysis was performed with a system from Shimadzu equipped with a DGU-20A3R controller, LC20AB liquid chromatograph, and a SPD-20A UV/Vis detector. Stationary phase was a Synergi 4 µm fusion-RP (150×4.6 mm) column (Phenomenex, Aschaffenburg, Germany). As mobile phase a gradient of MeOH/water with 0.1% formic acid was used. Parameters: A = water, B = methanol, V(B)/(V(A) + V(B)) = from 5% to 90% over 10 min, V(B)/(V(A) + V(B)) = 90% for 5 min, V(B)/(V(A) + V(B)) = from 90% to 5% over 3 min. The method was performed with a flow rate of 1.0 mL/min. Compounds were only used for biological evaluation if the purity was ≥ 95%. ESI mass spectral data were acquired with a Shimadzu LCMS-2020. Data are reported as mass-to-charge ratio (m/z) of the corresponding positively charged molecular ions.

***N*-(4-Aminophenyl)-1-benzyl-8-fluoro-4-oxo-1,4-dihydroquinoline-3-carboxamide.** *N*-Benzyl-8-fluoro-4-oxo-1,4-dihydroquinoline-3-carboxylic acid (0.79 g, 2.66 mmol) and triethylamine was dissolved in DMF and triethylamine (0.57 g, 0.77 mL, 5.59 mmol) and ethyl chloroformate (0.59 g, 0.52 mL, 5.45 mmol) were added at 0°C. The mixture was stirred for 1.5 h. After addition of *p*-phenyl diamine (0.69 g, 6.38 mmol) the mixture was stirred at 0°C and subsequently at room temperature overnight. The reaction mixture was poured into ice water and the precipitate was filtered off and washed with petroleum ether and water. After the drying under reduced pressure the product was obtained as a green solid (1.03 g, 2.66 mmol, 99%). ^1H-NMR (400 MHz, DMSO-d_6): δ [ppm] = 5.04 (s, 2 H), 5.86 (d, J = 2,7 Hz, 2 H), 6.58 (d, J = 8.7 Hz, 2 H), 7.13 (d, J = 7.3 Hz, 2 H), 7.33 (m, 5 H), 7.53 (m, 1 H), 7.65 (m, 1 H), 8.27 (d, J = 7.1 Hz, 1 H), 9.06 (s, 1 H), 11.80 (s, 1 H, NH) ppm. ^{13}C-NMR (101 MHz, DMSO-d_6): δ [ppm] = 54.8, 112.1, 114.8, 115.0, 121.6, 126.2, 126.5, 128.2, 128.4, 129.3, 130.3, 151.6, 153.7, 154.8 ppm. ESI: *m/z* calcd. for $C_{23}H_{18}FN_3O_2$ $[M+H]^+$: 388.15; found: 388.05.

1-Benzyl-8-fluoro-*N*-(4-((4-(hydroxymethyl)phenyl)diazenyl)phenyl)-4-oxo-1,4-dihydroquinoline-3-carboxamide. *N*-(4-aminophenyl)-1-benzyl-8-fluoro-4-oxo-1,4-dihydroquinoline-3-carboxamide (1.04 g, 2.66 mmol) was dissolved in acetic acid and nitrosobenzyl alcohol was added in portions. The reaction mixture was stirred at room temperature overnight. The mixture was poured into ice water and ethanol was added. The precipitate was filtered and

after drying under reduced pressure, the product was obtained as an olive coloured solid (1.00 g, 1.98 mmol, 75%). ^{1}H-NMR (400 MHz, DMSO-d_6): δ [ppm] = 4.60 (d, J = 5.6 Hz, 2 H), 5.38 (t, J = 5.7 Hz, 1 H, OH), 5.89 (s, 2 H), 7.16 (d, J = 7.3 Hz, 2 H), 7.25 – 7.40 (m, 3 H), 7.49 – 7.61 (m, 3 H), 7.68 (dd, J = 7.6, 15.1 Hz, 1 H), 7.85 (d, J = 8.3 Hz, 2 H), 7.96 (q, J = 9.1 Hz, 4 H), 8.30 (d, J = 7.8 Hz, 1 H), 9.15 (s, 1 H), 12.53 (s, 1 H, NH) ppm. ESI: *m/z* calcd. for $C_30H_{23}FN_4O_3$ $[M+H]^+$: 507.18 ; found: 507.20 .

1-Benzyl-*N*-(4-((4-(bromomethyl)phenyl)diazenyl)phenyl)-8-fluoro-4-oxo-1,4-dihydroquinoline-3-carboxamide. 1-benzyl-8-fluoro-N-(4-((4-(hydroxymethyl)phenyl) diazenyl)phenyl)-4-oxo-1,4-dihydroquinoline-3-carboxamide (1.00 g, 1.98 mmol) and tetra bromo methane (1.97 g, 5.94 mmol) were dissolved in dry dichloromethane. Triphenylphosphine (1.56 g, 5.94 mmol) was added at 0°C and the mixture was stirred at room temperature overnight. After the solvent was evaporated, ethanol was added. The precipitate was filtered off and dried under reduced pressure. The product was obtained as a orange solid (0.61 g, 1.07 mmol, 54%).^{1}H-NMR (400 MHz, DMSO-d_6): δ [ppm] = 4.56 (s, 2 H), 5.69 (s, 2 H), 7.17 (d, J = 6.5 Hz, 2 H), 7.40 (m, 6 H), 7.53 (d, J = 8.4 Hz, 2 H), 7.88 (d, J = 8.4 Hz, 2 H), 7.93 – 8.04 (s, 3 H), 8.40 (m, 1 H), 8.95 (s, 1 H), 12.41 (s, 1 H). ^{13}C-NMR (101 MHz, DMSO-d_6): δ [ppm] = 33.1, 61.7, 112.3, 120.5, 123.1, 124.2, 126.0, 126.2, 128.6, 129.1, 129.2, 129.9, 129.9, 135.3, 150.8, 178.7, 188.4. ESI-MS: *m/z* calc. for $C_{30}H_{22}BrFN_4O_2$ $[M+H]^+$: 591.08, found: 591.25.

***N*-(4-((4-((1-Benzyl-8-fluoro-4-oxo-1,4-dihydroquinoline-3-carboxamido)methyl) phenyl)diazenyl)benzyl)-4-((4,5-dihydroisoxazol-3-yl)oxy)-*N,N*-dimethylbut-2-yn-1-aminium bromide (BQCAAI-2).** 4-((4,5-dihydroisoxazol-3-yl)oxy)-*N,N*-dimethylbut-2-yn-1-amine was synthesized according to a literature procedure.[86] 4-((4,5-dihydroisoxazol-3-yl)oxy)-*N,N*-dimethylbut-2-yn-1-amine (0.13 g, 0.70 mmol) and 4-((4,5-dihydroisoxazol-3-yl)oxy)-*N,N*-dimethylbut-2-yn-1-amine (200.0 mg, 0.35 mmol) were dissolved in acetonitrile. A catalytic amount of a mixture of potassium iodide and potassium carbonate (1:1) was added. The mixture was treated in microwave at 80°C for 4 h. After the microwave vial was cooled to room temperature, the precipitate was filtered off and the solvent was evaporated in vacuo until 5 mL of acetonitrile. After the addition of diethyl ether, the precipitate was filtered off. The product was obtained as an orange solid (223.0 mg, 0.30 mmol, 85%). ^{1}H NMR (400 MHz, DMSO-d_6): δ [ppm] = 3.05 (t, J = 12 Hz, 2 H), 3.41 (s, 6 H), 4.44 (t, J = 12.8 Hz, 2 H), 4.76 (s, 2 H), 4.88 (s, 2 H), 5.14 (s, 2 H), 5.65 (s, 2 H), 7.16 (d, J = 6.5 Hz, 2 H), 7.28 – 7.47 (m, 5 H), 7.51 – 7.77 (m, 1 H), 7.83 (d, J = 8.5 Hz, 2 H), 7.87 – 8.01 (m, 5 H), 8.38 (m, 1 H), 8.90 (d, J = 17.3 Hz, 1 H), 12.41 (s, 1 H, NH) ppm. ^{13}C-NMR (101 MHz, DMSO-d_6): δ [ppm] = 33.1, 38.3,

50.2, 57.1, 57.5, 61.5, 70.3, 105.3, 112.2, 120.7, 123.5, 123.6, 124.7, 126.4, 128.2, 128.8, 128.9, 129.3, 130.7, 132.9, 134.2, 142.3, 148.7, 162.8, 168.6, 175.9 ppm. ESI-MS: *m/z* calc. for $C_{39}H_{36}FN_6O_4^+$ $[M]^+$: 671.28, found: 671.15.

Photochemical characterization. UV/Vis spectra and experiments were recorded on a Varian Cary 50 Bio UV/Vis Spectrophotometer using Hellma (Type 100-QS) cuvettes (10 mm light path). Data were plotted using GraphPad Prism 5.0. For irradiation, high performance LEDs (Mouser Electronics Inc. or Hartenstein) were used as light source. A concentration of 50 µM was prepared for each compound and measured in its dark-adapted state. Next, the probe was illuminated with LEDs of different wavelengths (254, 365, 380, 400, 430, 500 nm and white light) while gradually increasing the irradiation time until no change in the spectrum was detectable. Stability measurements were performed irradiating the probe with the light source, which provided the highest photoconversion to the *cis* isomer and kept in dark for at least 120 minutes at room temperature. During this time the absorbance at λ_{max} was recorded every 5 minutes. Lastly, the probe was irradiated with the light source, which provided the highest photoconversion to the *trans* isomer. Analysis was carried out with GraphPad Prism software (GraphPad Software Inc., San Diego CA, www.graphpad.com).

Pharmacology. *Cell culture.* All experiments were performed with HEK 293T cells stably expressing the novel split luciferase receptor sensor. Cells were incubated at 37 °C with 5% CO_2 and cultivated in DMED with 4500 mg/l glucose, 10% (v/v) FCS, 100 µg/mL penicillin, 100 µg/mL streptomycin sulfate and 2 mM L-glutamine and 600 µg/mL G-418. Every two to three days, the cell lines were routinely passaged. *Split Luciferase complementation assay.* The assay was performed as described previously,[79] except for the following modifications: A Berthold Mithras LB 940 plate reader was used to quantify the luminescence emitted by the cells, using white, flat bottomed nunc™ f96 microwell™ polystyrene plates.

4.3. Synthesis and Pharmacological Investigation of Dualsteric Ligands for Optical Control of the M_2 receptor

4.3.1. Design

The sympathetic and parasympathetic nervous systems play pivotal roles in controlling cardiac function mediated by GPCRs. Amongst them, the M_2 receptor is responsible for heart rate and atrio-ventricular conduction time regulation as well as for anti-inflammatory effects in the ventricle and therefore are, of high therapeutical relevance.[87] However, the afore-mentioned challenges of subtype-selectivity deficiency also holds true for the M_2 receptor. Following the allosteric/orthosteric hybrid design, ligands, which act in a dualsteric manner, are promising strategies for a selective stimulation of M_2 receptors. Starting from the known bis(ammonio)alkane-type allosteric fragments, such as the inhibitor W84 (phthalimide) and the enhancer naphmethonium, these ligands exhibit pronounced subtype-selectivity when

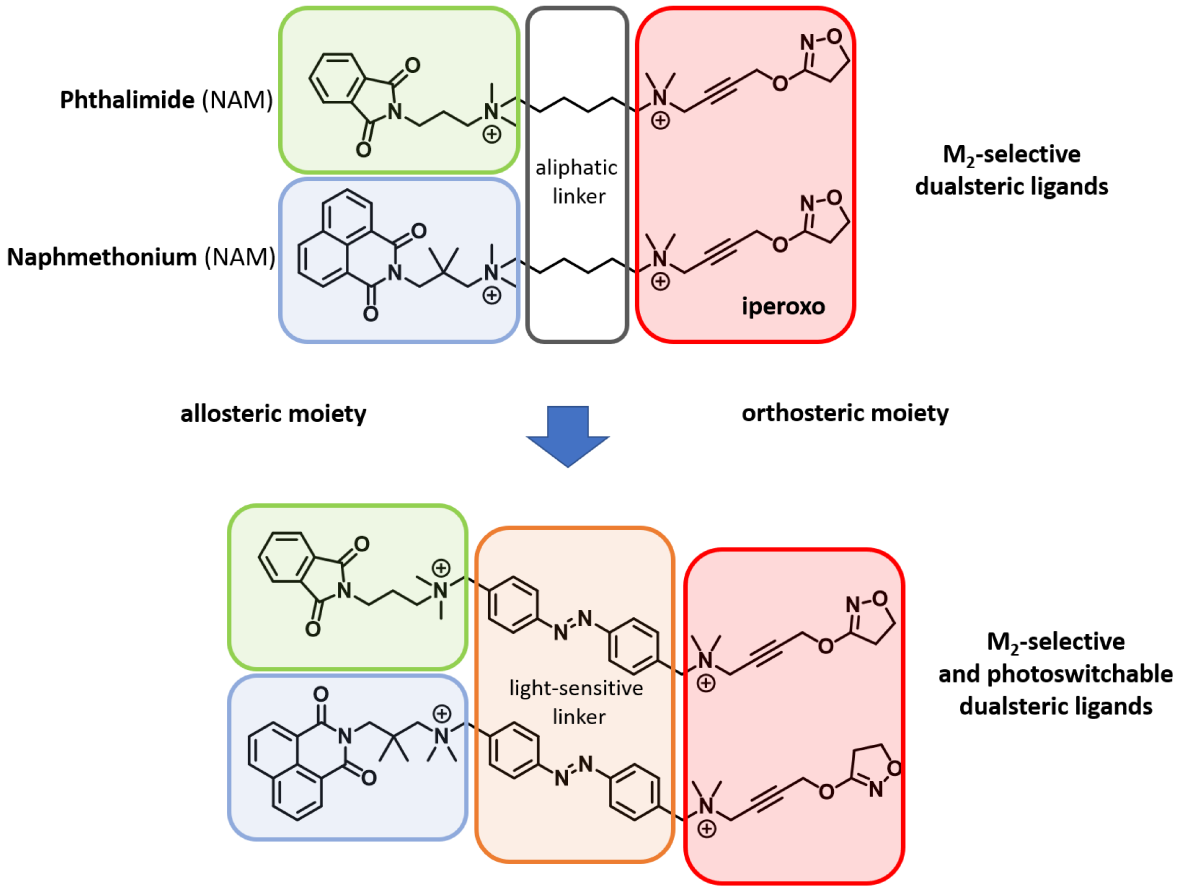

Fig. 26. Design strategy for the development of photoswitchable dualsteric ligands based on allosteric bis(ammonio)alkane-type fragments and orthosteric iperoxo connected through the molecular photoswitch azobenzene.

combined with the orthosteric high affinity agonist iperoxo building block through a polymethylene linker.[52,62]

For an efficient drug action targeting diseases related to the cardiovascular system, precision in space and time is indispensable. This is due to a complex interplay between electrophysiological and molecular processes occurring in different parts of the heart. Considerable efforts have been invested to use light with its spaciotemporal resolution as external regulator, leading to several breakthroughs in the field of optogenetics.[88-90] However, the need of genetical engineering limits the use of this strategy. Instead, we applied the photopharmacological approach, which was successfully developed for the M_1 receptor by introducing the photoswitchable azobenzene linker into the dualsteric M_2 ligands described previously. We aimed to pointedly design and synthesize dualsteric ligands for the investigation of receptor activation processes with high spatiotemporal precision for *in vitro* and *in vivo* purposes (Fig. 25).

4.3.2. Results

The synthesis of the two dualsteric and photoswitchable M_2 receptor ligands involves the nucleophilic substitution at both brominated benzylic carbon atoms of the 4,4'-bis(bromo-methyl)azobenzene moiety with the allosteric and the orthosteric building block, respectively

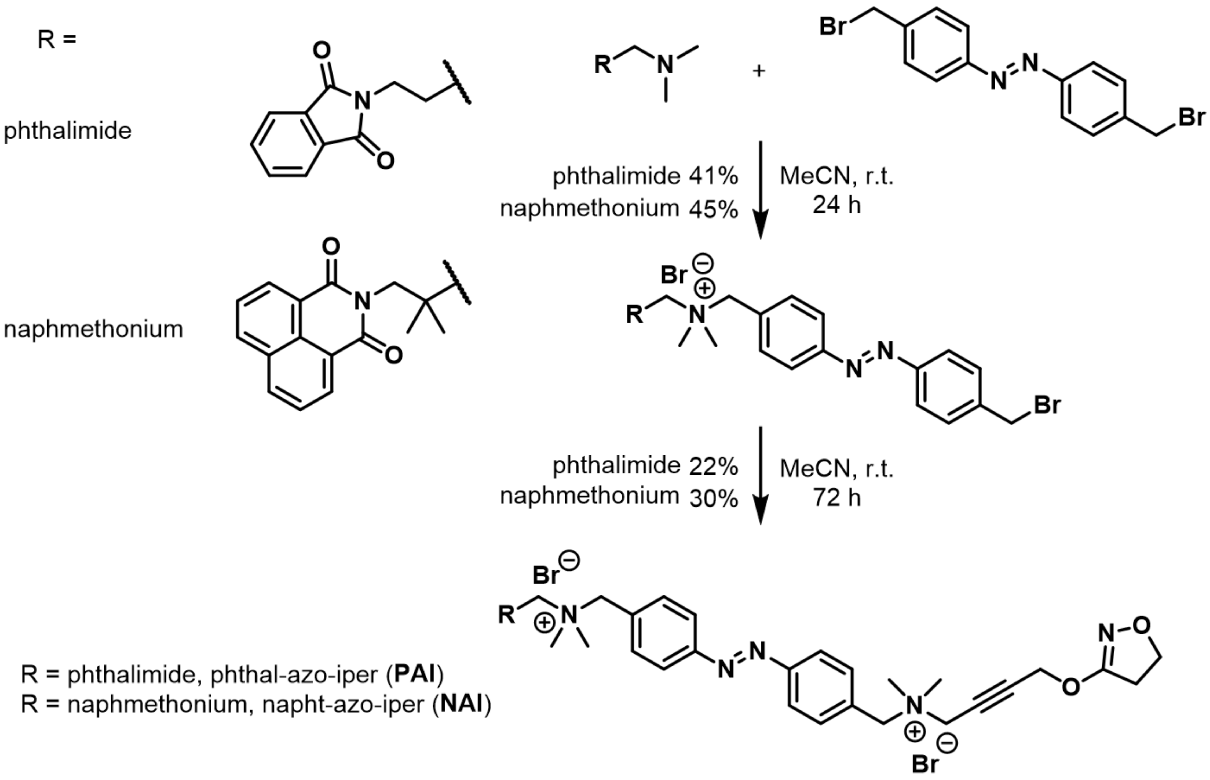

Fig. 27. Synthetic route of phthal-azo-iper (PAI) and naphth-azo-iper (NAI), which involves multiple substitutions at the azobenzene moiety with the allosteric and orthosteric building block, respectively.

(Fig. 26). As unsymmetrical azobenzene are not easy to access synthetically, double substitution can take place once the nucleophile is introduced. To avoid this, 4,4'-bis(bromo-methyl)azobenzene was firstly used in high excess and concentration and heated to reaction temperature. Subsequently, the phthalimide and naphmethonium building blocks were added dropwise. This procedure provided the mono-substituted products in optimized but still moderate yields.

The second substitution with 4-((4,5-dihydroisoxazol-3-yl)oxy)-*N,N*-dimethylbut-2-yn-1-amine, which was synthesized according to literature,[86] took place in equimolar amounts and conditions affording the target compounds phthal-azo-iper (PAI) and naphth-azo-iper (NAI).

PAI and NAI were investigated regarding to their photochemical behavior, showing characteristic transition bands in their absorption spectra (Fig. 28). Upon irradiation with light of different wavelengths, both PAI and NAI show a pronounced and reversible dependency on the specific wavelength used, which indicates photochromic behavior. However, PAI exhibits a higher degree in terms of photoswitching ability in comparison to the related NAI compound. From a thermal stability point of view, the target compounds meet the requirements for reliable photoswitching. In the dark, PAI and NAI are stable for over two hours and the process can be repeated over many cycles. Further pharmacological investigations with this tool compounds are currently done in collaboration with the group of Pau Gorostiza and were published as

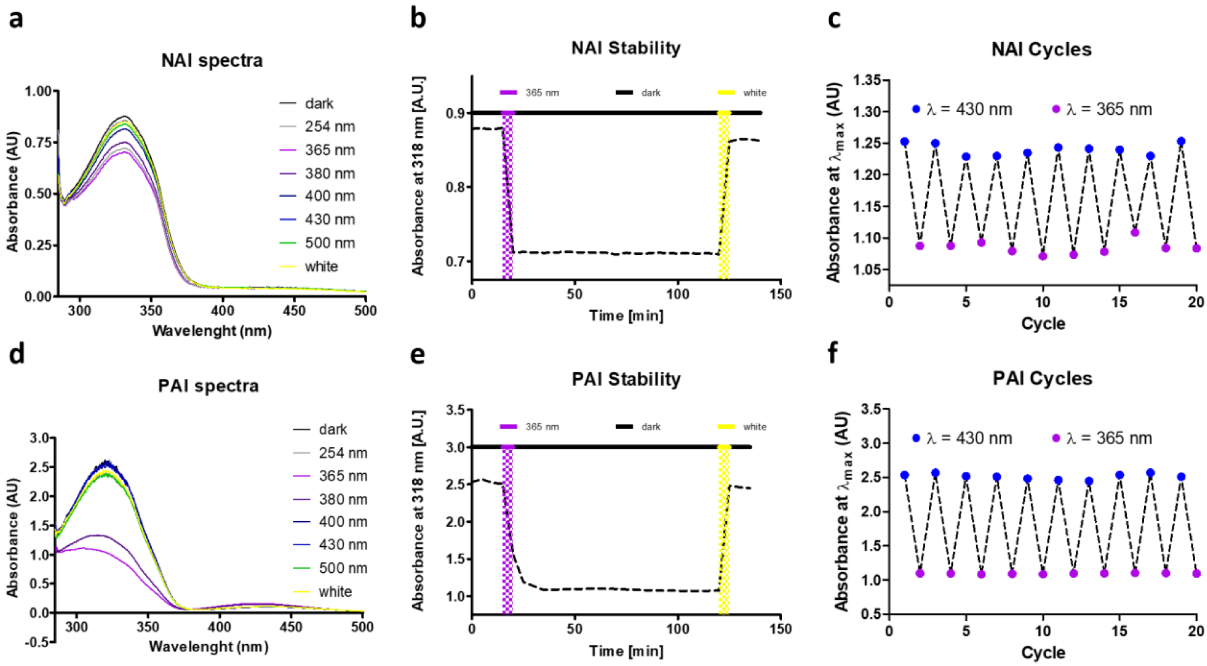

Fig. 28. Photocharacterization of PAI and NAI. a/d) Absorption spectra upon irradiation with different wavelengths. b/e) Absorption at λ_{max} for determination of stability of the *cis* isomer. c/f) Isomerization process can be repeated over many cycles providing robust and reversible photoswitching ability.

preprint.[91] Due to the higher photochromic performance, PAI was chosen for further investigations regarding binding and functional activity at the M_2 receptor, and its putative binding modes, which were studied *in silico*. Additionally, this tool compound has been proven to nicely control cardiac function in a light-dependent and reversible fashion *in vivo* using wildtype frog tadpoles and rats, which was shown for the first time in this scientific field.

4.3.3. Experimental Section

For general information see section 4.2.3.

***N*-(4-((4-(bromomethyl)phenyl)diazenyl)benzyl)-3-(1,3-dioxoisoindolin-2-yl)-*N*,*N*,2,2-tetramethylpropan-1-aminium bromide**. Previously synthesized 4,4'-bis(bromomethyl)azobenzene[85] (0.32 g, 0.86 mmol, 2 eq.) was dissolved in acetonitrile (50 mL) and heated to 50 °C and 2-(3-(dimethylamino)-2,2-dimethylpropyl)isoindoline-1,3-dione (100 mg, 0.43 mmol) was added and stirred for 24 h. After reaction was completed, the reaction mixture was cooled to room temperature and the product was precipitated with diethyl ether. The crude product was washed twice with diethyl ether to afford an orange solid (106 mg, 0.177 mmol, 41%). ^{1}H-NMR (400 MHz, $CDCl_3$): δ [ppm] = 7.92 -7.41 (m, 12H), 5.21 (s, 2H), 4.53 (s, 2H), 3.82 (t, J = 6.4 Hz, 2H), 3.75 – 3.58 (m, 6H), 2.40 – 2.29 (m, 2H). ^{13}C-NMR (101 MHz, $CDCl_3$): δ [ppm] = 168.3, 153.6, 152.1, 141.4, 134.4, 131.9, 130.0, 123.6, 99.2, 93.7, 77.2, 67.0, 61.4, 50.3, 35.0, 32.7, 22.8. ESI-MS: *m/z* calc. for $C_{27}H_{28}BrN_4O_2^+$ $[M]^+$: 519.14, 521.14, found 519.05 and 521.17.

4-((4,5-dihydroisoxazol-3-yl)oxy)-*N*-(4-((4-(((3-(1,3-dioxoisoindolin-2-yl)-2,2-dimethylpropyl)dimethylammonio)methyl)phenyl)diazenyl)benzyl)-*N*,*N*-dimethylbut-2-yn-1-aminium bromide (PAI). *N*-(4-((4-(bromomethyl)phenyl)diazenyl)-benzyl)-3-(1,3-dioxoisoindolin-2-yl)-*N*,*N*,2,2-tetramethylpropan-1-aminium bromide (106 mg, 0.177 mmol) and 4-((4,5-dihydroisoxazol-3-yl)oxy)-*N*,*N*-dimethylbut-2-yn-1-amine (63 mg, 0.353 mmol, 2 eq.) in acetonitrile (10 mL) were added into a sealed reaction vessel and stirred until the starting material was consumed. The crude is purified with reversed phase flash column chromatography to afford the desired product as an orange solid (30 mg, 38 µmol, 22%). ^{1}H-NMR (400 MHz, CD_3OD): δ [ppm] = 8.10 (d, J = 8.5 Hz, 2H), 8.01 (d, J = 8.5 Hz, 2H), 7.90 (dd, J = 5.4, 3.2 Hz, 2H), 7.85 (d, J = 8.6 Hz, 2H), 7.82 (dd, J = 5.4, 3.2 Hz, 2H), 7.75 (d, J = 8.5 Hz, 2H), 4.99 (s, 2H), 4.75 (s, 2H), 4.64 (s, 2H), 4.41 (t, J = 9.6 Hz, 2H), 4.36 (s, 2H), 3.84 (t, J = 6.4 Hz, 2H), 3.47 – 3.38 (m, 2H), 3.22 (s, 6H), 3.11 (s, 6H), 3.07 (t, J = 9.6 Hz, 6H), 2.38 – 2.25 (m, 2H). ^{13}C-NMR (101 MHz, CD_3OD): δ [ppm] = 169.9, 168.8, 163.4, 163.1, 162.7,

155.0, 154.8, 135.6, 135.3, 124.7, 124.5, 124.1, 88.8, 76.8, 71.2, 68.5, 67.4, 63.2, 58.3, 54.9, 50.9, 50.8, 35.7, 33.7, 23.5. ESI-MS: *m/z* calc. for $C_{38}H_{46}N_6O_4^{2+}$ $[M]^{2+}$: 325.18, found: 325.05.

2-(3-(Dimethylamino)-2,2-dimethylpropyl)-1*H*-benzo[*de*]isoquinoline-1,3(2*H*)-dione. 1H-Benzo[de]isoquinoline-1,3(2*H*)-dione (1.10 g, 5.58 mmol) and *N*1,*N*1,2,2-tetramethylpropane 1,3-diamine (0.73 mg, 5.58 mmol) were dissolved in toluene (120 ml). Catalytical amounts of *p*- toluene sulfonic acid (53.1 mg. 0.3 mmol) were added. The reaction mixture was refluxed under stirring and trapping the forming water for 48 h. The solvent was removed under vacuum yielding the crude product as a light brown solid, which was washed with ethanol (3 x 10 mL). The product was obtained as white solid (1.14 g, 3.68 mmol, 66%). ^{1}H-NMR (400 MHz, $CDCl_3$): δ [ppm] = 8.65 – 8.54 (m, 1H), 8.27 – 8.15 (m, 1H), 7.83 – 7.69 (m, 1H), 4.21 (s, 1H), 2.37 (s, 3H), 2.35 – 2.31 (m, 1H), 1.00 (s, 3H). ^{13}C-NMR (101 MHz, $CDCl_3$): 165.1, 133.9, 131.7, 131.5, 128.2, 127.1, 123.0, 70.2, 49.0, 47.9, 39.3, 25.1.

***N*-(4-((4-(Bromomethyl)phenyl)diazenyl)benzyl)-3-(1,3-dioxo-1*H* benzo[*de*]isoquino-line-2(3*H*)-yl)-*N*,*N*,2,2-tetramethylpropan-1-aminium.** Previously synthesized 4,4'-bis(bromomethyl)azobenzene[85] (0.24 g, 0.64 mmol) was dissolved in acetonitrile (40 mL) and heated to 50 °C and 2-(3-(dimethylamino)-2,2-dimethyl-propyl)-1*H*-benzo[*de*]isoquinoline-1,3(2*H*)-dione (40.2 mg, 0.13mmol) dissolved in acetonitrile (10 mL) was added dropwise. After reaction was completed, the reaction mixture was cooled to room temperature and the product was precipitated with diethyl ether. The crude product was washed twice with diethyl ether to afford an orange solid (41 mg, 0.057 mmol, 45%). ^{1}H-NMR (400 MHz, CD_3OD): δ [ppm] = 8.26 – 8.16 (m, 14H), 4.81 (s, 2H), 4.37 (s, 2H), 3.64 (s, 2H), 3.38 (s, 6H), 1.47 (s, 6H). ^{13}C-NMR (101 MHz, CD_3OD): δ [ppm] = 162.8, 150.6, 147.9, 146.8, 135.2, 134.0, 131.4, 131.0, 129.4, 128.6, 128.07, 127.9, 127.7, 123.4, 122.3, 78.1, 74.6, 56.2, 53.4, 30.8, 30.5, 26.3. ESI-MS: *m/z* calc. for $C_{33}H_{34}BrN_4O_2^+$ $[M]^+$: 597.19, 599.18, found: 597.02, 599.20.

4-((4,5-Dihydroisoxazol-3-yl)oxy)-*N*-(4-((4-(((3-(1,3-dioxo-1*H*-benzo[*de*]isoquinolin-2(3*H*)-yl)-2,2-dimethylpropyl)dimethylammonio)methyl)phenyl)diazenyl)benzyl)-*N*,*N*-dimethylbut-2-yn-1-aminium bromide (NAI). N-(4-((4-(Bromomethyl)-phenyl)diazenyl)benzyl)-3-(1,3-dioxo-1*H* benzo[*de*]isoquino-line-2(3*H*)-yl)-*N,N*,2,2-tetra-methylpropan-1-aminium bromide (41 mg, 0.057 mmol) and 4-((4,5-dihydroisoxazol-3-yl)oxy)-*N,N*-dimethylbut-2-yn-1-amine (21 mg, 0.11 mmol) were dissolved in acetonitrile (10 mL) and stirred at room temperature overnight. After reaction was completed, the crude product was precipitated with diethyl ether. The crude product was washed twice with diethyl ether to afford a dark orange foam (15 mg, 0.17 mmol, 30%). ^{1}H-NMR (400 MHz, $CDCl_3$): δ [ppm] = 8.56 – 8.47 (m, J = 23.1, 7.8 Hz, 2.5 H), 8.20 (t, J = 8.8 Hz, 2.5H), 8.03 – 7.62 (m, 8H),

7.49 (t, J = 8.8 Hz, 1H), 5.28 (s, 4H), 4.79 (t, J = 1.8 Hz, 2H), 4.40 (t, J = 9.6 Hz, 4H), 3.55 (s, 2H), 3.00 (s, 4H), 2.50 (s, 12H), 1.32 (s, 6H). ^{13}C-NMR (101 MHz, $CDCl_3$): δ [ppm] = 162.8, 159.3, 147.9, 135.2, 134.0, 131.4, 131.0, 129.4, 128.6, 127.9, 127.7, 123.4, 84.8, 78.1, 75.3, 74.6, 66.3, 65.3, 59.1, 56.2, 53.4, 50.0, 49.2, 30.5, 26.3, 24.6. ESI-MS: *m/z* calc. for $C_{42}H_{48}N_6O_{42}^+$ $[M]^{2+}$: 350.19, found: 350.05.

5. Discussion and Outlook

Most biological processes rely on chemical and biological events, which take place in stringent spacial confinements and in a defined temporal sequence.[81] As an example, a given GPCR can mediate different signaling pathways depending on its location (PNS or CNS, pre- or postsynaptically). At the same time, this GPCR can induce different signaling pathways after activation with a suitable ligand, according to the duration of activation and thus, in a temporal-dependent way. Short-term activation of a GPCR involves G proteins and their corresponding cellular response, while β-arrestin recruitment often takes place upon prolonged activation leading to a different response. To unravel the complex nature of the different processes, molecular basis and dynamics of a receptor in a space- and time-resolved manner, molecular tools are needed that allow their precise control without compromising their specific function.
Dualsteric ligands have been extensively used to characterize distinct orthosteric and allosteric binding sites of GPCRs giving essential information on the molecular basis of receptor function.[62] Photopharmacology, instead, adds the dimension of spatial as well as temporal resolution to the biological functions by introducing molecular photoswitches into the structure of the mediating ligand.[69] In this context, the aim of this work was the rational design, the synthesis, and the photochemical and pharmacological evaluation of such tool compounds for muscarinic receptors, by interfacing the dualsteric concept with photopharmacological methods. These photoswitchable dualsteric ligands were designed to remotely respond to light as external stimulus, hence triggering a change in activity at the receptor. Depending on the pharmacophores and the features of light-responsive unit, which are connected to each other, specific scientific questions can be pursued, including the nature of subtype-specific allosteric binding site, the dynamic of the receptor and the time course of activation.
On this basis, the first photoswitchable dualsteric ligand, BQCAAI (see cf. 3.1.), acting on the M_1 receptor, was developed, which allows controlling receptor efficacy upon irradiation.[76] In FRET experiments and using a dual Ca^{2+}/DAG sensor, the *trans* state BQCAAI was identified as a partial agonist, while *cis*-BQCAAI was found to be an antagonist. Using this light-sensitive tool compound, it was possible to quantify the kinetics of receptor activation without interfering with the system. While the reference agonist iperoxo induces an immediate calcium response, *trans*-BQCAAI activates the receptor after approximately 25 s suggesting that the ligand needs a specific amount of time to find the optimal binding geometry to stabilize the receptor in an active conformation. The delayed response was shown to be characteristic for partial agonists in comparison to conventional agonists.[82] However, whether the ligand shows partial or full

agonist activity essentially depends on the length of the linker, which connects the pharmacophores. Accordingly, BQCAAI-2, with a shorter photoswitchable linker, exhibits a higher efficacy compared to BQCAAI (cf. 4.2).

Photopharmacological tool compounds, such as BQCAAI and BQCAAI-2, which are designed to present subtype-selective pharmacophores and may prefer, in this case, M_1 receptors over the other muscarinic subtypes hold great potential for *in vivo* studies and therapeutic application. This was also shown for PAI, a photopharmacological tool compound, which was designed to present a M_2 subtype-selective allosteric modulator (a fragment of W84) connected to iperoxo through a photoswitchable azobenzene linker (cf. 4.3.). Results from the group of Pau Gorostiza clearly show that PAI is a useful tool for the regulation of cardiac function in a light-dependent fashion, which was demonstrated in wildtype frog tadpoles and rats.[91] The related compound NAI is still under investigation. Used in combination, photoswitchable tools with preference for the different subtypes may be even appropriate for "brain mapping", i.e. for studying the function of the brain and spinal cord with spatiotemporal resolution.

Moreover, we have shown that fluorescence-based techniques, which detect receptor conformational changes, have a major impact on the switching performance because of the current use of ~436 nm as excitation wavelength, which is also used for *cis*-to-*trans* isomerization. Apart from that, we realized that it is absolutely necessary that the operational wavelengths that trigger the isomerization of the photoswitch and hence, the change in activity at the receptor site, not only fit to the observed biological system but also to the conditions of the cellular assay and its readout. Ideally, the inserted molecular photoswitch should show superior photochemical properties, such as quantitative and stable bidirectional photoswitching, and be responsive to visible rather than high-energy UV-light, which can damage the cells used in functional assays. Ideally, the assay itself should be completely light-independent to obtain a clear correlation between the recorded activity and the observed photoisomer without influencing the photoswitching performance. [69,92]

In this regard, tetra-*ortho*-fluorination of the azobenzene scaffold was described and extensively investigated by the Woolley- and Hecht-groups.[83,84,93,94] The different substitution pattern changes the electronic environment of the system in such a way, that the operational wavelengths are shifted more into the visible region of the spectrum. This makes it possible to distinctively address each photoisomer by using green and blue light and to avoid cell-toxic UV-light.

Additionally, we utilized split luciferase complementation techniques instead of using fluorescence-based techniques. This assay is particularly suitable to detect protein-protein

interactions and associated signaling pathways, providing clear-cut and distinguishable concentration-response curves for each photoisomer, which makes it highly suitable for photopharmacological investigations into GPCRs.

These optimized methods allowed detailed investigation into the distinct effects of fluorination and bivalency on binding properties at the M_1 receptor, using a set of novel photoswitchable tool compounds based on the agonist iperoxo (cf. 3.2) .[85] We designed photoswitchable iperoxo (PI) and bivalent iperoxo (IAI) compounds, as well as the red-shifted congeners (F_4-PI, F_4-IAI) by introduction of the tetra-*ortho*-fluoro scaffold. The bivalent compounds show much higher affinity compared to the univalent compounds due to additional involvement of allosteric binding sites. Remarkably, the fluoro-substituted compounds not only showed improved optical properties, but also displayed increased potency at the M_1 receptor in the range of the reference agonist itself. Bivalent and fluorinated photoiperoxo act as pronounced affinity switches, whereas the univalent photoiperoxo acted as an efficacy switch. This is a remarkable observation, as the introduction of a molecular photoswitch generally causes an overall loss in activity at the receptor. A photoswitch-endowed compound, which shows an almost identical potency as the reference compound is often hard to achieve.

These results demonstrate for the first time, that fluorination of the azobenzene unit in receptor agonists dramatically alters the pharmacological profile of the compound. For the M_1 receptor this structural change turned out to be beneficial in terms of affinity, potency and efficacy. Therefore, using the tetra-*ortho*-fluorinated azobenzene scaffold represents a promising and convenient methods for the optimization of photoswitchable GPCR ligands. However, the pharmacological profile has to be investigated carefully for each application.

Based on the results of this work, further research issues are well worth being pursued in future projects.

1. The first generation of dualsteric photoswitchable tool compounds BQCAAI, BQCAAI-2, PAI and NAI still suffer from poor photochemical properties arising from their unsubstituted azobenzene core. Future studies should involve the development of the tetra-*ortho*-fluorinated analogs, which may well show an impact on the receptor affinity and functional activity.
2. To date, the herein presented ligands have been investigated exclusively on the receptor to which they have been designed for (BQCAAI and BQCAAI-2 for M_1 and, PAI and NAI for M_2 receptor). It will be interesting to evaluate to which extent these ligands truly hold their promise of subtype-selectivity. However, these studies depend on the

availability of suitable and light-independent assays. Further developments in split-luciferase complementation techniques, especially for the Gi/o signaling pathway will complement the photopharmacological characterization and will help to elucidate subtype-specificity.[79]

3. One major hallmark of dualsteric ligands is their ability to exhibit functional selectivity, preferentially activating one pathway over others (biased signaling). Further studies should investigate the functional specificity in detail in both the *trans*- and *cis*-state for the novel photochromic subtype-selective and -unselective ligands presented in this work. A promising approach may involve a recently published split luciferase-based assay for analyses of the ligand concentration- and time-dependent recruitment of β-arrestin. By doing this, it may be possible to investigate to which extent the photoswitching influences the receptors ability to mediate different signaling pathways.[80]
4. Albeit the fact that tetra-*ortho*-fluorinated azobenzenes stand out in their slow thermal *cis*-to-*trans* relaxation rate, representing a truly bistable molecular switch on the biological time scale,[94] they represent only one of many ways to improve the photochemical properties of photoswitchable compounds. As an example, *ortho*-methoxylation and *ortho*-chlorination have proven to provide similar influence on photophysics and have been successfully employed in biological applications. Additionally, substitution pattern can play a significant role in terms of regulation of relaxation time. Especially in neuroscience, it is not always beneficial to design slow-relaxing photoswitchable ligands. In fact, the scientific problem and the receptor in observation rather dictate the choice of the right photoswitch with the desired properties.[95] In this context, it is worth considering different substituents and substitution patterns at the azobenzene core after careful characterization of their properties before applying.

6. Summary

G protein-coupled receptor research looks out for new technologies to elucidate the complex processes of receptor activation, function and downstream signaling with spatiotemporal resolution, preferably in living cells and organisms. A thriving approach consists in making use of the unsurpassed properties of light, including its high precision in space and time, non-invasiveness and high degree of orthogonality regarding biological processes. This is realized by the incorporation of molecular photoswitches, which are able to effectively respond to light, such as azobenzene, into the structure of a ligand of a given receptor. The muscarinic acetylcholine receptors belong to class A GPCRs and have received special attention in this regard due to their role as a prototypic pharmacological system and their therapeutic potential. They mediate the excitatory and inhibitory effects of the neurotransmitter acetylcholine and thus regulate diverse important biological processes, especially many neurological functions in our brain.

In this work, the application of photopharmacological tool compounds to muscarinic receptors is presented, consisting of pharmacophores extended with azobenzene as light-responsive motif. Making use of the dualsteric concept, such photochromic ligands can be designed to bind concomitantly to the orthosteric and allosteric binding site of the receptor, which is demonstrated for BQCAAI (M_1) and PAI (M_2) and may lead to subtype- and functional-selective photoswitchable ligands, suitable for further *ex vivo* and *in vivo* studies.

Moreover, photoswitchable ligands based on the synthetic agonist iperoxo were investigated extensively with regard to their photochemical behavior and pharmacological profile, outlining the advantages and challenges of using red-shifted molecular photoswitches, such as tetra-*ortho*-fluoro azobenzene. For the first time on a GPCR it was examined, which impact the different substitution pattern has on both the binding and the activity on the M_1 receptor. Results show that substituted azobenzenes in photopharmacological compounds (F_4-photoiperoxo and F_4-iper-azo-iper) not just represent analogs with other photophysical properties but can exhibit a considerably different biological profile that has to be investigated carefully.

The achievements gained in this study can give important new insights into the binding mode and time course of activation processes, enabling precise spatial and temporal resolution of the complex signaling pathway of muscarinic receptors. Due to their role as exemplary model system, these findings may be useful for the investigation into other therapeutically relevant GPCRs.

7. Zusammenfassung

Die Forschung an G-Protein-gekoppelten Rezeptoren verlangt nach neuen Technologien zur Aufklärung der komplexen Prozesse der Rezeptoraktivierung, -funktion und ihrer nachgeschalteten Signalwege mit räumlicher und zeitlicher Auflösung, vorzugsweise in lebenden Zellen und Organismen. Ein erfolgreicher Ansatz besteht darin, die unübertroffenen Eigenschaften des Lichts zu nutzen, welche die hohe Präzision in Raum und Zeit, die Nicht-Invasivität und die hohe Orthogonalität in Bezug auf biologische Prozesse einschließt. Dies wird durch den Einbau von molekularen Photoschaltern, wie z. B. Azobenzolen, in die Struktur eines Liganden eines bestimmten Rezeptors realisiert, welche effektiv auf Licht reagieren. Die muskarinischen Acetylcholin Rezeptoren gehören zur Klasse A der GPCRs und haben aufgrund ihrer Rolle als prototypisches pharmakologisches System und ihres therapeutischen Potenzials diesbezüglich besondere Beachtung gefunden. Sie vermitteln die stimulierenden und hemmenden Wirkungen des Neurotransmitters Acetylcholin und regulieren somit verschiedene wichtige biologische Prozesse, insbesondere viele neurologische Funktionen in unserem Gehirn.

In dieser Arbeit wird die Anwendung photopharmakologischer „Tool"-Verbindungen auf die muskarinischen Rezeptoren vorgestellt, die aus Pharmakophoren bestehen, welche mit Azobenzol als lichtempfindlichem Motiv modifiziert wurden. Mit Hilfe des Konzepts der Dualsterie können solche photochromen Liganden so gestaltet werden, dass sie gleichzeitig an die orthosterische und allosterische Bindungsstelle des Rezeptors binden, was für BQCAAI (M_1) und PAI (M_2) gezeigt wurde und zu subtypen- und funktionsselektiven photoschaltbaren Liganden führen kann, die für weitere Ex- und In-Vivo-Studien geeignet sind.

Darüber hinaus wurden photoschaltbare Liganden auf Basis des synthetischen Agonisten Iperoxo hinsichtlich ihres photochemischen Verhaltens und ihres pharmakologischen Profils ausführlich untersucht, um die Vorteile und Herausforderungen der Verwendung rotverschobener molekularer Photoschalter wie tetra-*ortho*-Fluor-azobenzol zu erläutern. Es wurde erstmals an einem GPCR untersucht, welche Auswirkungen das unterschiedliche Substitutionsmuster sowohl auf die Bindung, als auch auf die Aktivität am M_1-Rezeptor hat. Diese Ergebnisse zeigen, dass substituierte Azobenzole in photopharmakologischen Verbindungen (F_4-Photoiperoxo und F_4-Iper-azo-iper) nicht nur Analoga mit anderen photophysikalischen Eigenschaften darstellen, sondern auch ein deutlich unterschiedliches biologisches Profil aufweisen können, das sorgfältig untersucht werden muss. Die in dieser Studie erzielten Ergebnisse geben neue und wichtige Einblicke in den Bindungsmodus und den

zeitlichen Verlauf von Aktivierungsprozessen und ermöglichen eine präzise räumliche und zeitliche Auflösung der komplexen Signalwege von muskarinischen Rezeptoren. Aufgrund ihrer Rolle als exemplarisches Modellsystem können diese Befunde für die Untersuchung anderer therapeutisch relevanter GPCRs sehr nützlich sein.

8. Abbreviations

AC	adenylate cyclase
ACh	acetylcholine
AD	Alzheimer's disease
ATP	adenosine triphosphate
BQCA	benzyl quinolone carboxylic acid
BRET	bioluminescence resonance energy transfer
Ca^{2+}	double positively charged calcium ions
cAMP	cyclic adenosine monophosphate
CCh	carbachol
CL	caged ligand
Cmpd	compound
CNS	central nervous system
COPD	chronic obstructive pulmonary disease
CRC	concentration response curve
DAG	diacyl glycerol
ECF	ethyl chloroformate
ECL	extracellular loop
ECV	extracellular vestibule
E_{max}	maximal efficacy
ER	endoplasmic reticulum
ESI	electrospray ionization
FRET	Fluorescence resonance energy transfer
G protein	guanine nucleotide binding protein
GDP	guanosine diphosphate
GIRK	G protein-gated inward rectifying potassium channel
GPCR	G protein-coupled receptor
GRK	G protein-coupled receptor kinase
GTP	guanosine triphosphate
HEK	human embryotic kidney
HPLC	high-performance liquid chromatography
ICL	intracellular loop
IP3	inositol-1,4,5-triphosphate

iper	iperoxo
LCMS	liquid chromatography mass specrometry
λ_{max}	wavelength at maximal absorption
M_1-M_5	muscarinic acetylcholine subtype 1-5
mAChR	muscarinic acetylcholine receptor
NAL	neutral allosteric ligand
NAM	negative allosteric modulator
NMR	nuclear magnetic resonance
NTS	neurotensin receptor
PAM	positive allosteric modulator
PCA	protein complementation assays
PCL	photochromic ligand
PDT	photodynamic therapy
EC_{50}	half maximal effective concentration
PIP2	phosphatidylinositol-4,5-bisphosphate
PKA	phosphokinase A
PKC	phosphokinase C
PLC	phospholipase C
PNS	peripheral nervous system
PORTL	photoswitchable orthogonal remotely tethered ligands
PSS	photostationary state
PTL	photoswitchable tethered ligand
RET	resonance energy transfer
SLC	split luciferase complementation
TBPB	[1-(1′-(2-tolyl)-1,4′-bipiperidin-4-yl)-1*H* benzo[*d*]imidazol-2(3*H*)-one]
TCM	ternary complex model
TLC	thin layer chromatography
TM	transmembrane
UV	ultraviolet
Vis	visual

8. References

(1) Vassilatis, D. K.; Hohmann, J. G.; Zeng, H.; Li, F.; Ranchalis, J. E.; Mortrud, M. T.; Brown, A.; Rodriguez, S. S.; Weller, J. R.; Wright, A. C.; Bergmann, J. E.; Gaitanaris, G. A. The G Protein-Coupled Receptor Repertoires of Human and Mouse. *Proc. Natl. Acad. Sci. U. S. A.* **2003**, *100*, 4903-4908.

(2) Insel, P. A.; Snead, A.; Murray, F.; Zhang, L.; Yokouchi, H.; Katakia, T.; Kwon, O.; Dimucci, D.; Wilderman, A. GPCR Expression in Tissues and Cells: Are the Optimal Receptors Being Used as Drug Targets? *Br. J. Pharmacol.* **2012**, *165*, 1613-1616.

(3) Rosenbaum, D. M.; Rasmussen, S. G. F.; Kobilka, B. K. The Structure and Function of G-Protein-Coupled Receptors. *Nature* **2009**, *459*, 356-363.

(4) Santos, R.; Ursu, O.; Gaulton, A.; Bento, A. P.; Donadi, R. S.; Bologa, C. G.; Karlsson, A.; Al-Lazikani, B.; Hersey, A.; Oprea, T. I.; Overington, J. P. A Comprehensive Map of Molecular Drug Targets. *Nat. Rev. Drug Discov.* **2017**, *16*, 19-34.

(5) Lagerström, M. C.; Schiöth, H. B. Structural Diversity of G Protein-Coupled Receptors and Significance for Drug Discovery. *Nat. Rev. Drug Discov.* **2008**, *7*, 339-357.

(6) Sriram, K.; Insel, P. A. G Protein-Coupled Receptors as Targets for Approved Drugs: How Many Targets and How Many Drugs? *Mol. Pharmacol.* **2018**, *93*, 251-258.

(7) Fredriksson, R.; Lagerstrom, M. C.; Lundin, L. G.; Schioth, H. B. The G-Protein-Coupled Receptors in the Human Genome Form Five Main Families. Phylogenetic Analysis, Paralogon Groups, and Fingerprints. *Mol. Pharmacol.* **2003**, *63*, 1256-1272.

(8) Insel, P. A.; Wilderman, A.; Zambon, A. C.; Snead, A. N.; Murray, F.; Aroonsakool, N.; McDonald, D. S.; Zhou, S.; McCann, T.; Zhang, L.; Sriram, K.; Chinn, A. M.; Michkov, A. V.; Lynch, R. M.; Overland, A. C.; Corriden, R. G Protein-Coupled Receptor (GPCR) Expression in Native Cells: "Novel" EndogGPCRs as Physiologic Regulators and Therapeutic Targets. *Mol. Pharmacol.* **2015**, *88*, 181-187.

(9) Venkatakrishnan, A. J.; Deupi, X.; Lebon, G.; Tate, C. G.; Schertler, G. F.; Babu, M. M. Molecular Signatures of G-Protein-Coupled Receptors. *Nature* **2013**, *494*, 185-194.

(10) Latorraca, N. R.; Venkatakrishnan, A. J.; Dror, R. O. GPCR Dynamics: Structures in Motion. *Chem. Rev.* **2016**, *117*, 139-155.

(11) Lee, Y.; Basith, S.; Choi, S. Recent Advances in Structure-Based Drug Design Targeting Class a G Protein-Coupled Receptors Utilizing Crystal Structures and Computational Simulations. *J. Med. Chem.* **2017**, *61*, 1-46.

(12) Erlandson, S. C.; McMahon, C.; Kruse, A. C. Structural Basis for G Protein–Coupled Receptor Signaling. *Annu. Rev. Biophys.* **2018**, *47*, 1-18.

(13) Tautermann, C. S. GPCR Structures in Drug Design, Emerging Opportunities with New Structures. *Bioorg. Med. Chem. Lett.* **2014**, *24*, 4073-4079.

(14) Hauser, A. S.; Attwood, M. M.; Rask-Andersen, M.; Schioth, H. B.; Gloriam, D. E. Trends in GPCR Drug Discovery: New Agents, Targets and Indications. *Nat. Rev. Drug Discov.* **2017**, *16*, 829-842.

(15) Kruse, A. C.; Kobilka, B. K.; Gautam, D.; Sexton, P. M.; Christopoulos, A.; Wess, J. Muscarinic Acetylcholine Receptors: Novel Opportunities for Drug Development. *Nat. Rev. Drug Discov.* **2014**, *13*, 549-560.

(16) Caulfield, M. P. Muscarinic Receptors - Characterization, Coupling and Function. *Pharmacol. Ther.* **1993**, *58*, 319-379.

(17) Caulfield, M. P.; Birdsall, N. J. International Union of Pharmacology. XVII. Classification of Muscarinic Acetylcholine Receptors. *Pharmacol. Rev.* **1998**, *50*, 279-290.

(18) Wess, J. Molecular Biology of Muscarinic Acetylcholine Receptors. *Crit. Rev. Neurobiol.* **1996**, *10*, 69-99.

(19) Simon, M.; Strathmann, M.; Gautam, N. Diversity of G Proteins in Signal Transduction. *Science* **1991**, *252*, 802-808.

(20) Wess, J.; Eglen, R. M.; Gautam, D. Muscarinic Acetylcholine Receptors: Mutant Mice Provide New Insights for Drug Development. *Nat. Rev. Drug Discov.* **2007**, *6*, 721-733.

(21) Heuss, C.; Gerber, U. G-Protein-Independent Signaling by G-Protein-Coupled Receptors. *Trends Neurosci.* **2000**, *23*, 469-475.

(22) Krasel, C.; Vilardaga, J. P.; Bunemann, M.; Lohse, M. J. Kinetics of G-Protein-Coupled Receptor Signalling and Desensitization. *Biochem. Soc. Trans.* **2004**, *32*, 1029-1031.

(23) Gundry, J.; Glenn, R.; Alagesan, P.; Rajagopal, S. A Practical Guide to Approaching Biased Agonism at G Protein Coupled Receptors. *Front. Neurosci.* **2017**, *11*, 17.

(24) Kenakin, T.; Christopoulos, A. Signalling Bias in New Drug Discovery: Detection, Quantification and Therapeutic Impact. *Nat. Rev. Drug Discov.* **2013**, *12*, 205-216.

(25) Eglen, R. M. Muscarinic Receptor Subtype Pharmacology and Physiology. *Prog. Med. Chem.* **2005**, *43*, 105-136.

(26) Svoboda, J.; Popelikova, A.; Stuchlik, A. Drugs Interfering with Muscarinic Acetylcholine Receptors and Their Effects on Place Navigation. *Front. Psychiatry* **2017**, *8*, 215.

(27) Fisher, A.; Pittel, Z.; Haring, R.; Bar-Ner, N.; Kliger-Spatz, M.; Natan, N.; Egozi, I.; Sonego, H.; Marcovitch, I.; Brandeis, R. M_1 Muscarinic Agonists Can Modulate Some of the Hallmarks in Alzheimer's Disease: Implications in Future Therapy. *J. Mol. Neurosci.* **2003**, *20*, 349-356.

(28) van Koppen, C. J.; Kaiser, B. Regulation of Muscarinic Acetylcholine Receptor Signaling. *Pharmacol. Ther.* **2003**, *98*, 197-220.

(29) Jiang, S.; Li, Y.; Zhang, C.; Zhao, Y.; Bu, G.; Xu, H.; Zhang, Y. W. M1 Muscarinic Acetylcholine Receptor in Alzheimer's Disease. *Neurosci. Bull.* **2014**, *30*, 295-307.

(30) Bock, A.; Schrage, R.; Mohr, K. Allosteric Modulators Targeting CNS Muscarinic Receptors. *Neuropharmacology* **2018**, *136*, 427-437.

(31) Volpicelli, L. A.; Levey, A. I. Muscarinic Acetylcholine Receptor Subtypes in Cerebral Cortex and Hippocampus. *Prog. Brain Res.* **2004**, *145*, 59-66.

(32) Eglen, R. M.; Nahorski, S. R. The Muscarinic M5receptor: A Silent or Emerging Subtype? *Br. J. Pharmacol.* **2000**, *130*, 13-21.

(33) Haga, K.; Kruse, A. C.; Asada, H.; Yurugi-Kobayashi, T.; Shiroishi, M.; Zhang, C.; Weis, W. I.; Okada, T.; Kobilka, B. K.; Haga, T.; Kobayashi, T. Structure of the Human M2 Muscarinic Acetylcholine Receptor Bound to an Antagonist. *Nature* **2012**, *482*, 547-551.

(34) Kruse, A. C.; Hu, J.; Pan, A. C.; Arlow, D. H.; Rosenbaum, D. M.; Rosemond, E.; Green, H. F.; Liu, T.; Chae, P. S.; Dror, R. O.; Shaw, D. E.; Weis, W. I.; Wess, J.; Kobilka, B. K. Structure and Dynamics of the M3 Muscarinic Acetylcholine Receptor. *Nature* **2012**, *482*, 552-556.

(35) Thal, D. M.; Sun, B.; Feng, D.; Nawaratne, V.; Leach, K.; Felder, C. C.; Bures, M. G.; Evans, D. A.; Weis, W. I.; Bachhawat, P.; Kobilka, T. S.; Sexton, P. M.; Kobilka, B. K.; Christopoulos, A. Crystal Structures of the M1 and M4 Muscarinic Acetylcholine Receptors. *Nature* **2016**, *531*, 335-340.

(36) Spalding, T. A.; Birdsall, N. J.; Curtis, C. A.; Hulme, E. C. Acetylcholine Mustard Labels the Binding Site Aspartate in Muscarinic Acetylcholine Receptors. *J. Biol. Chem.* **1994**, *269*, 4092-4097.

(37) Proska, J.; Tucek, S. Mechanisms of Steric and Cooperative Actions of Alcuronium on Cardiac Muscarinic Acetylcholine Receptors. *Mol. Pharmacol.* **1994**, *45*, 709-717.

(38) Kruse, A. C.; Ring, A. M.; Manglik, A.; Hu, J.; Hu, K.; Eitel, K.; Hubner, H.; Pardon, E.; Valant, C.; Sexton, P. M.; Christopoulos, A.; Felder, C. C.; Gmeiner, P.; Steyaert, J.; Weis, W. I.; Garcia, K. C.; Wess, J.; Kobilka, B. K. Activation and Allosteric Modulation of a Muscarinic Acetylcholine Receptor. *Nature* **2013**, *504*, 101-106.

(39) Christopoulos, A.; Kenakin, T. G Protein-Coupled Receptor Allosterism and Complexing. *Pharmacol. Rev.* **2002**, *54*, 323-374.

(40) Buller, S.; Zlotos, D. P.; Mohr, K.; Ellis, J. Allosteric Site on Muscarinic Acetylcholine Receptors: A Single Amino Acid in Transmembrane Region 7 Is Critical to the Subtype Selectivities of Caracurine V Derivatives and Alkane-Bisammonium Ligands. *Mol. Pharmacol.* **2002**, *61*, 160-168.

(41) Kenakin, T. Inverse, Protean, and Ligand-Selective Agonism: Matters of Receptor Conformation. *FASEB J.* **2001**, *15*, 598-611.

(42) De Amici, M.; Dallanoce, C.; Holzgrabe, U.; Trankle, C.; Mohr, K. Allosteric Ligands for G Protein-Coupled Receptors: A Novel Strategy with Attractive Therapeutic Opportunities. *Med. Res. Rev.* **2010**, *30*, 463-549.

(43) Schrage, R.; De Min, A.; Hochheiser, K.; Kostenis, E.; Mohr, K. Superagonism at G Protein-Coupled Receptors and Beyond. *Br. J. Pharmacol.* **2016**, *173*, 3018-3027.

(44) Singh, S.; Loke, Y. K.; Furberg, C. D. Inhaled Anticholinergics and Risk of Major Adverse Cardiovascular Events in Patients with Chronic Obstructive Pulmonary Disease: A Systematic Review and Meta-Analysis. *JAMA* **2008**, *300*, 1439-1450.

(45) Burger, W. A. C.; Sexton, P. M.; Christopoulos, A.; Thal, D. M. Toward an Understanding of the Structural Basis of Allostery in Muscarinic Acetylcholine Receptors. *J. Gen. Physiol.* **2018**, *150*, 1360-1372.

(46) Lüllmann, H.; Ohnesorge, F. K.; Schauwecker, G. C.; Wassermann, O. Inhibition of the Actions of Carbachol and DFP on Guinea Pig Isolated Atria by Alkane-Bis-Ammonium Compounds. *Eur. J. Pharmacol.* **1969**, *6*, 241-247.

(47) Keov, P.; Sexton, P. M.; Christopoulos, A. Allosteric Modulation of G Protein-Coupled Receptors: A Pharmacological Perspective. *Neuropharmacology* **2011**, *60*, 24-35.

(48) May, L. T.; Leach, K.; Sexton, P. M.; Christopoulos, A. Allosteric Modulation of G Protein-Coupled Receptors. *Annu. Rev. Pharmacol. Toxicol.* **2007**, *47*, 1-51.

(49) Stockton, J. M.; Birdsall, N. J.; Burgen, A. S.; Hulme, E. C. Modification of the Binding Properties of Muscarinic Receptors by Gallamine. *Mol. Pharmacol.* **1983**, *23*, 551-557.

(50) Davie, B. J.; Christopoulos, A.; Scammells, P. J. Development of M1 mAChR Allosteric and Bitopic Ligands: Prospective Therapeutics for the Treatment of Cognitive Deficits. *ACS Chem. Neurosci.* **2013**, *4*, 1026-1048.

(51) Muth, M.; Bender, W.; Scharfenstein, O.; Holzgrabe, U.; Balatkova, E.; Tränkle, C.; Mohr, K. Systematic Development of High Affinity Bis(ammonio)alkane-Type Allosteric Enhancers of Muscarinic Ligand Binding. *J. Med. Chem.* **2003**, *46*, 1031-1040.

(52) Matera, C.; Flammini, L.; Quadri, M.; Vivo, V.; Ballabeni, V.; Holzgrabe, U.; Mohr, K.; De Amici, M.; Barocelli, E.; Bertoni, S.; Dallanoce, C. Bis(ammonio)alkane-Type Agonists of Muscarinic Acetylcholine Receptors: Synthesis, in Vitro Functional Characterization, and in Vivo Evaluation of Their Analgesic Activity. *Eur. J. Med. Chem.* **2014**, *75*, 222-232.

(53) Sams, A. G.; Hentzer, M.; Mikkelsen, G. K.; Larsen, K.; Bundgaard, C.; Plath, N.; Christoffersen, C. T.; Bang-Andersen, B. Discovery OFN-{1-[3-(3-oxo-2,3-dihydrobenzo[1,4]oxazin-4-yl)propyl]piperidin-4-yl}-2-phenylacetamide (LU AE51090): An Allosteric Muscarinic M1receptor Agonist with Unprecedented Selectivity and Procognitive Potential. *J. Med. Chem.* **2010**, *53*, 6386-6397.

(54) Jones, C. K.; Brady, A. E.; Davis, A. A.; Xiang, Z.; Bubser, M.; Tantawy, M. N.; Kane, A. S.; Bridges, T. M.; Kennedy, J. P.; Bradley, S. R.; Peterson, T. E.; Ansari, M. S.; Baldwin, R. M.; Kessler, R. M.; Deutch, A. Y.; Lah, J. J.; Levey, A. I.; Lindsley, C. W.; Conn, P. J. Novel Selective Allosteric Activator of the M1 Muscarinic Acetylcholine Receptor Regulates Amyloid Processing and Produces Antipsychotic-Like Activity in Rats. *J. Neurosci.* **2008**, *28*, 10422-10433.

(55) Schwyzer, R. Acth: A Short Introductory Review. *Ann. N. Y. Acad. Sci.* **1977**, *297*, 3-26.

(56) Bock, A.; Mohr, K. Dualsteric GPCR Targeting and Functional Selectivity: The Paradigmatic M(2) Muscarinic Acetylcholine Receptor. *Drug Discov. Today Technol.* **2013**, *10*, 245-252.

(57) Lane, J. R.; Sexton, P. M.; Christopoulos, A. Bridging the Gap: Bitopic Ligands of G-Protein-Coupled Receptors. *Trends Pharmacol. Sci.* **2013**, *34*, 59-66.

(58) Mohr, K.; Schmitz, J.; Schrage, R.; Tränkle, C.; Holzgrabe, U. Molecular Alliance-from Orthosteric and Allosteric Ligands to Dualsteric/Bitopic Agonists at G Protein Coupled Receptors. *Angew. Chem. Int. Ed.* **2013**, *52*, 508-516.

(59) Mohr, K.; Tränkle, C.; Kostenis, E.; Barocelli, E.; De Amici, M.; Holzgrabe, U. Rational Design of Dualsteric GPCR Ligands: Quests and Promise. *Br. J. Pharmacol.* **2010**, *159*, 997-1008.

(60) Valant, C.; Robert Lane, J.; Sexton, P. M.; Christopoulos, A. The Best of Both Worlds? Bitopic Orthosteric/Allosteric Ligands of G Protein-Coupled Receptors. *Annu. Rev. Pharmacol. Toxicol.* **2012**, *52*, 153-178.

(61) Valant, C.; Sexton, P. M.; Christopoulos, A. Orthosteric/Allosteric Bitopic Ligands: Going Hybrid at GPCRs. *Mol. Interv.* **2009**, *9*, 125-135.

(62) Antony, J.; Kellershohn, K.; Mohr-Andrä, M.; Kebig, A.; Prilla, S.; Muth, M.; Heller, E.; Disingrini, T.; Dallanoce, C.; Bertoni, S.; Schrobang, J.; Tränkle, C.; Kostenis, E.; Christopoulos, A.; Höltje, H. D.; Barocelli, E.; De Amici, M.; Holzgrabe, U.; Mohr, K. Dualsteric GPCR Targeting: A Novel Route to Binding and Signaling Pathway Selectivity. *FASEB J.* **2009**, *23*, 442-450.

(63) Bock, A.; Bermudez, M.; Krebs, F.; Matera, C.; Chirinda, B.; Sydow, D.; Dallanoce, C.; Holzgrabe, U.; De Amici, M.; Lohse, M. J.; Wolber, G.; Mohr, K. Ligand Binding Ensembles Determine Graded Agonist Efficacies at a G Protein-Coupled Receptor. *J. Biol. Chem.* **2016**, *291*, 16375-16389.

(64) Chen, X.; Klöckner, J.; Holze, J.; Zimmermann, C.; Seemann, W. K.; Schrage, R.; Bock, A.; Mohr, K.; Tränkle, C.; Holzgrabe, U.; Decker, M. Rational Design of Partial Agonists for the Muscarinic M1 Acetylcholine Receptor. *J. Med. Chem.* **2015**, *58*, 560-576.

(65) Bock, A.; Merten, N.; Schrage, R.; Dallanoce, C.; Batz, J.; Klockner, J.; Schmitz, J.; Matera, C.; Simon, K.; Kebig, A.; Peters, L.; Muller, A.; Schrobang-Ley, J.; Trankle, C.; Hoffmann, C.; De Amici, M.; Holzgrabe, U.; Kostenis, E.; Mohr, K. The Allosteric Vestibule of a Seven Transmembrane Helical Receptor Controls G-Protein Coupling. *Nat Commun* **2012**, *3*, 1044.

(66) Bermudez, M.; Bock, A.; Krebs, F.; Holzgrabe, U.; Mohr, K.; Lohse, M. J.; Wolber, G. Ligand-Specific Restriction of Extracellular Conformational Dynamics Constrains Signaling of the M2 Muscarinic Receptor. *ACS Chem. Biol.* **2017**, *12*, 1743-1748.

(67) Fronik, P.; Gaiser, B. I.; Sejer Pedersen, D. Bitopic Ligands and Metastable Binding Sites: Opportunities for G Protein-Coupled Receptor (GPCR) Medicinal Chemistry. *J. Med. Chem.* **2017**, *60*, 4126-4134.

(68) Velema, W. A.; Szymanski, W.; Feringa, B. L. Photopharmacology: Beyond Proof of Principle. *J. Am. Chem. Soc.* **2014**, *136*, 2178-2191.

(69) Broichhagen, J.; Frank, J. A.; Trauner, D. A Roadmap to Success in Photopharmacology. *Acc. Chem. Res.* **2015**, *48*, 1947-1960.

(70) Matsumura, Y.; Ananthaswamy, H. N. Toxic Effects of Ultraviolet Radiation on the Skin. *Toxicol. Appl. Pharmacol.* **2004**, *195*, 298-308.

(71) Lerch, M. M.; Hansen, M. J.; van Dam, G. M.; Szymanski, W.; Feringa, B. L. Emerging Targets in Photopharmacology. *Angew. Chem. Int. Ed.* **2016**, *55*, 10978-10999.

(72) Hüll, K.; Morstein, J.; Trauner, D. In Vivo Photopharmacology. *Chem. Rev.* **2018**, *118*, 10710-10747.

(73) Agnetta, L.; Decker, M. Photoresponsive Hybrid Compounds. In *Design of Hybrid Molecules in Drug Development*, Decker, M., Ed. Elsevier: Oxford, **2017**.

(74) Thomsen, W.; Frazer, J.; Unett, D. Functional Assays for Screening GPCR Targets. *Curr. Opin. Biotechnol.* **2005**, *16*, 655-665.

(75) Lohse, M. J.; Nuber, S.; Hoffmann, C. Fluorescence/Bioluminescence Resonance Energy Transfer Techniques to Study G-Protein-Coupled Receptor Activation and Signaling. *Pharmacol. Rev.* **2012**, *64*, 299-336.

(76) Agnetta, L.; Kauk, M.; Canizal, M. C. A.; Messerer, R.; Holzgrabe, U.; Hoffmann, C.; Decker, M. A Photoswitchable Dualsteric Ligand Controlling Receptor Efficacy. *Angew. Chem. Int. Ed.* **2017**, *56*, 7282-7287.

(77) Kauk, M.; Hoffmann, C. Intramolecular and Intermolecular FRET Sensors for GPCRs - Monitoring Conformational Changes and Beyond. *Trends Pharmacol. Sci.* **2018**, *39*, 123-135.

(78) Hattori, M.; Ozawa, T. Split Luciferase Complementation for Analysis of Intracellular Signaling. *Anal. Sci.* **2014**, *30*, 539-544.

(79) Littmann, T.; Ozawa, T.; Hoffmann, C.; Buschauer, A.; Bernhardt, G. A Split Luciferase-Based Probe for Quantitative Proximal Determination of Gαq Signalling in Live Cells. *Sci. Rep.* **2018**, *8*, 17179.

(80) Littmann, T.; Buschauer, A.; Bernhardt, G. Split Luciferase-Based Assay for Simultaneous Analyses of the Ligand Concentration- and Time-Dependent Recruitment of Beta-Arrestin2. *Anal. Biochem.* **2019**, *573*, 8-16.

(81) Lohse, M. J.; Hofmann, K. P. Spatial and Temporal Aspects of Signaling by G-Protein-Coupled Receptors. *Mol. Pharmacol.* **2015**, *88*, 572-578.

(82) Messerer, R.; Kauk, M.; Volpato, D.; Alonso Canizal, M. C.; Klockner, J.; Zabel, U.; Nuber, S.; Hoffmann, C.; Holzgrabe, U. FRET Studies of Quinolone-Based Bitopic Ligands and Their Structural Analogues at the Muscarinic M1 Receptor. *ACS Chem. Biol.* **2017**, *12*, 833-843.

(83) Bléger, D.; Schwarz, J.; Brouwer, A. M.; Hecht, S. *O*-Fluoroazobenzenes as Readily Synthesized Photoswitches Offering Nearly Quantitative Two-Way Isomerization with Visible Light. *J. Am. Chem. Soc.* **2012**, *134*, 20597-20600.

(84) Bleger, D.; Hecht, S. Visible-Light-Activated Molecular Switches. *Angew. Chem. Int. Ed.* **2015**, *54*, 11338-11349.

(85) Agnetta, L.; Bermudez, M.; Riefolo, F.; Matera, C.; Claro, E.; Messerer, R.; Littmann, T.; Wolber, G.; Holzgrabe, U.; Decker, M. Fluorination of Photoswitchable Muscarinic Agonists Tunes Receptor Pharmacology and Photochromic Properties. *J. Med. Chem.* **2019**, *62*, 3009-3020.

(86) Kloeckner, J.; Schmitz, J.; Holzgrabe, U. Convergent, Short Synthesis of the Muscarinic Superagonist Iperoxo. *Tetrahedron Lett.* **2010**, *51*, 3470-3472.

(87) Brodde, O.-E.; Bruck, H.; Leineweber, K.; Seyfarth, T. Presence, Distribution and Physiological Function of Adrenergic and Muscarinic Receptor Subtypes in the Human Heart. *Basic Res. Cardiol.* **2001**, *96*, 528-538.

(88) Boyle, P. M.; Karathanos, T. V.; Trayanova, N. A. "Beauty Is a Light in the Heart": The Transformative Potential of Optogenetics for Clinical Applications in Cardiovascular Medicine1. *Trends Cardiovasc. Med.* **2015**, *25*, 73-81.

(89) Pianca, N.; Zaglia, T.; Mongillo, M. Will Cardiac Optogenetics Find the Way through the Obscure Angles of Heart Physiology? *Biochem. Biophys. Res. Commun.* **2017**, *482*, 515-523.

(90) Yu, L.; Zhou, L.; Cao, G.; Po, S. S.; Huang, B.; Zhou, X.; Wang, M.; Yuan, S.; Wang, Z.; Wang, S.; Jiang, H. Optogenetic Modulation of Cardiac Sympathetic Nerve Activity to Prevent Ventricular arrhythmias. *J. Am. Coll. Cardiol.* **2017**, *70*, 2778-2790.

(91) Riefolo, F.; Matera, C.; Garrido-Charles, A.; Gomila, A. M. J.; Agnetta, L.; Claro, E.; Masgrau, R.; Holzgrabe, U.; Batlle, M.; Decker, M.; Guasch, E.; Gorostiza, P. Control of Cardiac Function *in Vivo* with a Light-Regulated Drug. *J. Am. Chem. Soc.* **2019**, in press.

(92) Dong, M.; Babalhavaeji, A.; Samanta, S.; Beharry, A. A.; Woolley, G. A. Red-Shifting Azobenzene Photoswitches for in Vivo Use. *Acc. Chem. Res.* **2015**, *48*, 2662-2670.

(93) Beharry, A. A.; Sadovski, O.; Woolley, G. A. Azobenzene Photoswitching without Ultraviolet Light. *J. Am. Chem. Soc.* **2011**, *133*, 19684-19687.

(94) Samanta, S.; Beharry, A. A.; Sadovski, O.; McCormick, T. M.; Babalhavaeji, A.; Tropepe, V.; Woolley, G. A. Photoswitching Azo Compounds *in Vivo* with Red Light. *J. Am. Chem. Soc.* **2013**, *135*, 9777-9784.

(95) Rodríguez-Soacha, D. A.; Decker, M. Photopharmacology in Alzheimer's Disease. *Adv. Therap.* **2018**, *1*, 1800037.

9. Appendix

Appendix I:

Agnetta, L.†; Decker, M.* Photoresponsive Hybrid Compounds. In *Design of Hybrid Molecules in Drug Development*; Decker, M., Ed.; Elsevier: Oxford, **2017**.
https://www.sciencedirect.com/science/article/pii/B9780081010112000118

Appendix II:

Agnetta, L.; Kauk, M.; Canizal, M. C. A.; Messerer, R.; Holzgrabe, U.; Hoffmann, C.; Decker, M., A Photoswitchable Dualsteric Ligand Controlling Receptor Efficacy. *Angew. Chem. Int. Ed.* **2017,** *56*, 7282-7287.
https://onlinelibrary.wiley.com/doi/abs/10.1002/anie.201701524

Appendix III:

Agnetta, L.; Bermudez, M.; Riefolo, F.; Matera, C.; Claro, E.; Messerer, R.; Littmann, T.; Wolber, G.; Holzgrabe, U.; Decker, M. Fluorination of Photoswitchable Muscarinic Agonists Tunes Receptor Pharmacology and Photochromic Properties. *J. Med. Chem.* **2019**, *62*, 3009-3020.
https://pubs.acs.org/doi/10.1021/acs.jmedchem.8b01822

Appendix IV:

Schramm, S.; **Agnetta, L.**; Littmann, T.; Irmen, M.; Holze, J.; Tränkle, C.; Decker, M. Novel Dualsteric M_1 Ligands from Carbachol and BQCA/TBPB Show Different Extents of Partial Agonism. *ChemMedChem* **2019**, in revision.

Appendix V:

Curriculum Vitae

Appendix I:

Agnetta, L.†; Decker, M.* Photoresponsive Hybrid Compounds. In *Design of Hybrid Molecules in Drug Development*; Decker, M., Ed.; Elsevier: Oxford, **2017**.

https://www.sciencedirect.com/science/article/pii/B9780081010112000118

11 Photoresponsive Hybrid Compounds

Luca Agnetta, Michael Decker
JULIUS MAXIMILIAN UNIVERSITY OF WÜRZBURG, WÜRZBURG, GERMANY

11.1 Introduction

The ability of living organisms to adapt to a variety of natural environments is fundamental for life and is performed often through light-dependent biological phenomena such as vision, photosynthesis, phototaxis, or circadian timing (photoperiodism), allowing organisms to interact with environment. On the microscale most of these processes rely on chromophores absorbing light and responding with a physicochemical reaction, which then controls biological function. Putting pharmacological-relevant targets under light control offers great possibilities to investigate their dynamic behavior, complexity, and mode of action. Furthermore, such photocontrollable compounds help to develop powerful and selective drugs. However, most natural targets lack these moieties and accordingly cannot be externally photoregulated.

A first attempt to overcome this drawback was optogenetics, a technology that combines optical techniques with bioengineering to obtain genetically targeted photostimulation typical for neurons.[1,2] Based on the expression of inherent light-sensitive proteins neuronal control in living cells and even in living animals is achieved (Fig. 11-1). Naturally occurring microbial opsins are inserted into the neuron used to control action potential (AP) firing with millisecond precision. The introduced channelrhodopsins and halorhodopsins function as light-gated ion channels, which enable light to control electrical excitability. The former are permeable for calcium and sodium ions once activated by light, causing depolarization and AP firing. The latter is specific for chloride ions and is responsible for light-dependent inhibition of AP in neurons (Fig. 11-2).[3] This technology, the "Method of the Year" in 2010, significantly contributes to a greater understanding of the principles of neuronal control and has enabled numerous applications beyond basic research.[4] However, this method is confined by genetically defined neurons and by the limited numbers of opsins as optogenetic actuators that are introduced into neurons. At the same time, the cell itself expresses plenty of endogenous receptors on its surface, representing potential candidates for photosensitization.

Optogenetic pharmacology, in contrast, combines optics, genetics, and chemistry and is an approach to enable precise manipulation of individual receptors of all kinds, such as enzymes, ion channels, and G-protein coupled receptors (GPCRs) through photoswitchable tethered ligands (PTLs).[5] These proteins are genetically designed to present a cysteine group, near the binding site. The PTL, reported by Trauner and coworkers, features the maleimide

Design of Hybrid Molecules for Drug Development. DOI: http://dx.doi.org/10.1016/B978-0-08-101011-2.00011-8

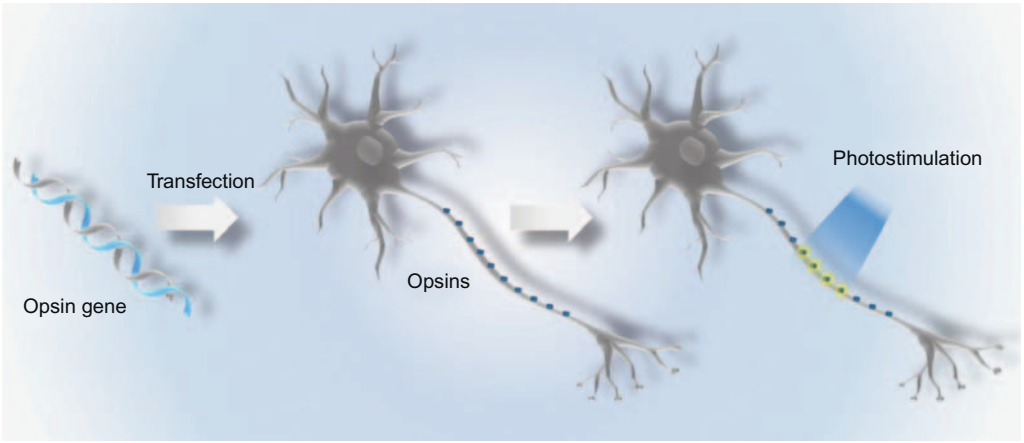

FIGURE 11-1 Principle of optogenetics in neuroscience.

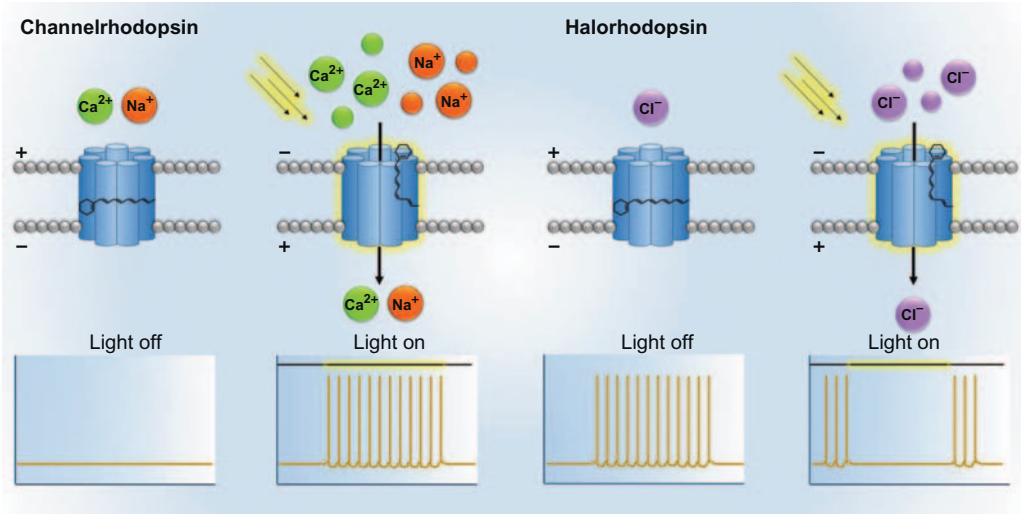

FIGURE 11-2 Targeted photostimulation of channelrhodopsin (depolarization/excitation) and halorhodopsin (hyperpolarization/inhibition) upon irradiation.

moiety ("M"), which is a cysteine-reactive group, to perform the covalent bioconjugation (Fig. 11-3). It is connected to the photoisomerizable azobenzene ("A") and to the neurotransmitter glutamate ("G").[6] Upon irradiation the azobenzene group converts from the *trans*- to the *cis*-form, which changes the conformation of the tether. The neurotransmitter is now able to activate the allosteric site of the ionotropic glutamate receptor (iGluR), which opens

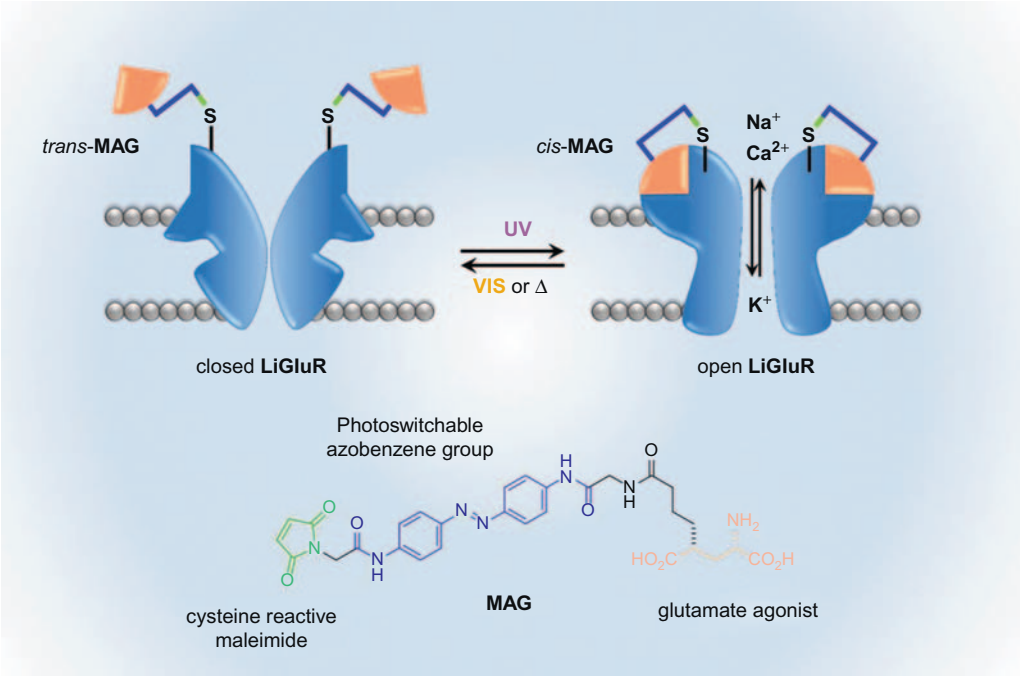

FIGURE 11-3 Maleimide-azobenzene-glutamate (MAG) as photoswitchable tethered ligand for the activation of the light-gated ionotropic glutamate receptor (LiGluR).

the ion channel for sodium and calcium influx and potassium efflux. By this way activation, deactivation, inhibition, and regulation can be addressed individually, providing both reversibility and spatiotemporal resolution. The genetic manipulation that is needed for this approach is advantageous, since it guarantees absolute target specificity but is, of course, very demanding in terms of technical implementation. The necessity for genetic engineering sets these methods, optogenetics, and the PTL approach, as research tools only.

A purely synthetic strategy that does not require any genetical modification employs so-called "caged ligands" (CLs).[7] The term "cage" is not to be taken literally. It simply suggests that the ligand, with it its biological activity, is trapped by a synthetic molecular retainer. Typically this is a photolyzable moiety bound covalently to a pharmacophoric residue with bioactivity.[8] Once the CL is introduced into the organism, the active signaling molecule is released upon irradiation, again providing temporal and spatial accuracy. In a broader sense CLs can be compared to prodrugs that are converted to active drugs by light (instead of metabolism). For example, the ortho-nitrobenzyl derivatives of ATP[9] and cyclic adenosine monophosphate (cAMP)[10] were the first nucleotides with photochemically protecting groups successfully used to photostimulate their targets. Furthermore, glutamate, one of the most prominent neurotransmitters in the brain, has found application in its caged form to map excitatory connections between neurons.[11] For the synthesis of this caged form the

photolabile α-carboxy-2-nitrobenzyl group (αCNB) is used to provide αCNB-glutamate. By doing that, the γ-carboxyl group of the glutamate molecule, responsible for receptor binding, is masked, preventing activation of the glutamate receptor. The neurotransmitter is then liberated after a pulse of UV laser light by cleavage of the αCNB-group (Fig. 11-4). Photolytic release of glutamate was successfully used to map connections between neurons and the distribution of the receptors on the cell surface as well as for kinetic investigation of channel opening and desensitization. However, there are limitations to this approach. First, dynamic control of biological functions is not feasible as the photodeprotection is irreversible. Once the active drug is liberated control over it is lost. Second, total inertness of the caged compound is not given in all cases causing off-target effects and/or lowered spatiotemporal resolution.[4]

Molecular hybridization represents a powerful tool to utilize existing drugs (parent drugs) and optimize their physiochemical properties, with regards to the desired product.[12] For medicinal chemical purposes, this is probably the most promising approach combining pharmacophores and photoswitchable chemical structures. For example, the compound GluAzo, also reported by the Trauner group, represents a hybrid of the neurotransmitter glutamate with the photochromic azobenzene moiety able to reversibly manipulate channel activation of iGluR.[13] Binding of the *trans*-form leads to increased inward currents compared

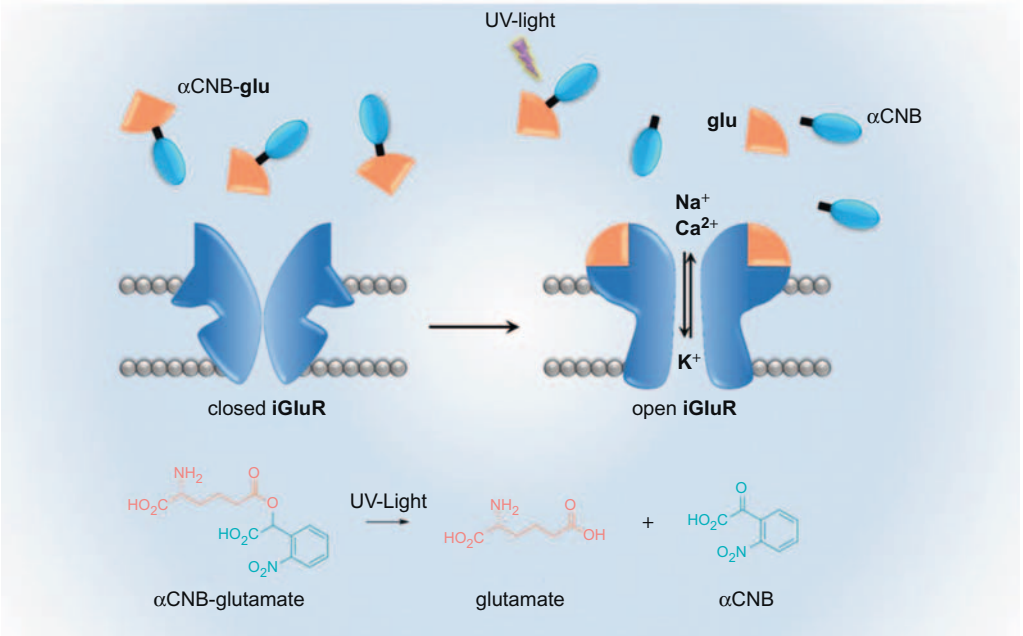

FIGURE 11-4 Photolytic release of glutamate for the light-dependent activation of ionotropic glutamate receptor (iGluR).

to the *cis*-form, which was obtained by UV irradiation (Fig. 11-5). Irradiation with light of the visible spectrum turns *cis*-GluAzo again to *trans*-GluAzo enabling AP firing. GluAzo was one of the first photochromic agonists developed and is also called reversibly cage glutamate since likewise caged glutamate the binding site is masked to prevent binding to the receptor. In contrast to caged glutamate, in the case of GluAzo, masking is reversible upon photoswitching.

Photochromism occurs when a chemical species undergoes a reversible phototransformation between two forms having not only different absorption spectra but also different physicochemical properties, such as refractive indices, dielectric constants, oxidation/reduction potentials, and geometrical structures, upon light exposure.[14] Through the adequate combination of different bioactive structures, new ligands with high therapeutic interest can be designed, as they can show increased affinity and efficacy compared to their parent drugs. The approach of photochromic hybridization adds a new dimension to this design process and gives rise to the emerging field of photopharmacology, which aims to control biological functions by light.[4,15,16] Dynamic control of drug activity is essential as it allows the regulation of biological processes precisely and in a reversible fashion (Fig. 11-5).

The properties of these hybrids are particularly interesting since they are directly related with the structure, which can be modified spatially and temporally upon irradiation. This

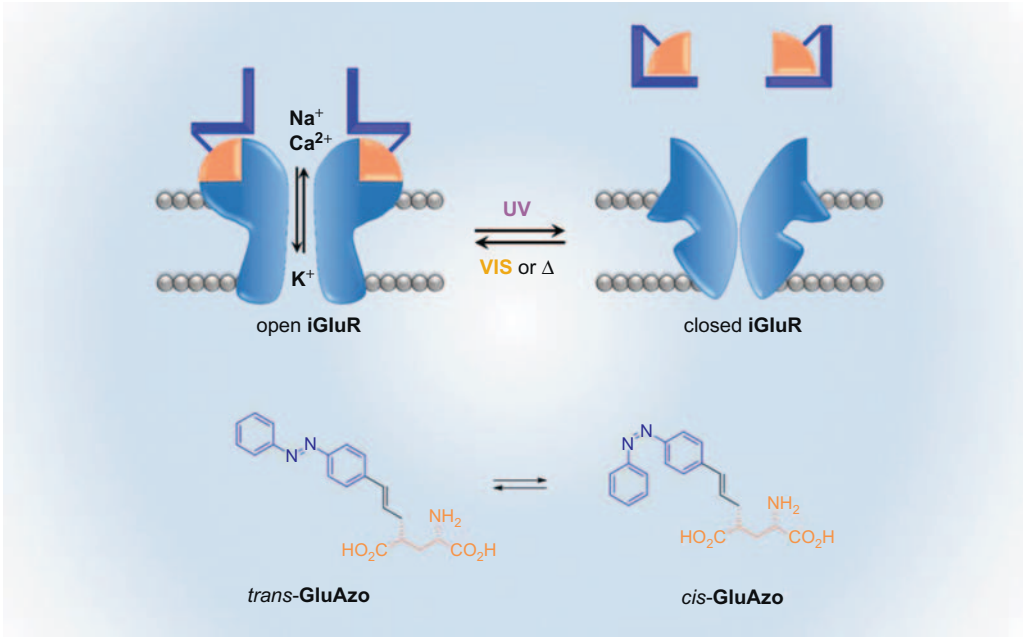

FIGURE 11-5 Remote control of iGluR activity and neuronal firing with GluAzo as photochromic agonist.

allows the use of light as a dynamic remote control for biological and pharmacological activity due to the locally defined mode of action of the photochromic hybrid, enhancing drug selectivity and thereby reducing systemic side effects.

The focus of this chapter is on photochromic ligands (PCL) with azobenzenes as photoswitchable moiety and the application to ion channels, enzyme inhibitors, and GPCR ligands. Synthetic strategies for the design and construction of drug-like photoresponsive hybrids with varied morphologies and functionalities are presented using distinct connection and bioisosterism approaches. The pros and cons of the various approaches will be discussed using specific examples to enable the reader to apply respective techniques for novel purposes.

11.2 Light as an External Stimulus

Most interactions between cells, tissues, and living organisms rely on chemical communication by which biomolecules such as neurotransmitters, hormones, or small molecules interact with receptors, enzymes, and ion channels, causing a biological response related to the input signal. In this context, optical stimuli are particularly interesting, since they can be adjusted in terms of intensity, focus, and wavelength, allowing precise spatial and temporal dosage. Due to the ever-expanding progress in laser technology very small areas can be focused on and biological processes can be monitored with high temporal resolution on a femtosecond scale. In addition, light shows a high degree of orthogonality. That means that light does not interfere with biological processes, which is a prerequisite for photoregulated biochemical communication.

Generally irradiation occurs remotely, which guarantees noninvasiveness and no contamination of the tissue.

As a provider of energy and information light is able to trigger reactions such as isomerization or cleaving reactions depending on the wavelength that is used.[17] In this regard it is important to choose the right wavelength to prevent damage to the living tissue, which is sensitive to high-energy irradiation. It should be short enough to evoke the desired reaction but long enough to avoid harming the tissue. This is a serious restriction to the development of photosensitive systems as most reactions of interest need at least UV-light irradiation. Accordingly, the development of systems that can be addressed in the visible (and harmless) region of the optical spectrum is still challenging researchers that want to utilize the exceptional advantages of light.[18] A more technical problem is the interference of the control of the photoswitch with the biochemical/pharmacological assay applied for the evaluation of compound activity when the assay itself is based on optical/photochemical methods.[14]

However, with light as a regulating stimulus, unparalleled experimental possibilities can be achieved to manipulate the activity of drugs, provided light-absorbing molecular machines (photoswitches) are integrated.

11.3 Molecular Photoswitches

11.3.1 Natural Photoswitches

Living organisms have learned, in the course of evolution, to generate specialized proteins to respond to light and to use its energy. These photoreceptors are responsible, for example, for the development and growth of plants and for the vision of higher organisms, by transformation of light energy into an electrical signal. For this purpose nature generated chromophores that are bound to these proteins. Such small organic molecules can be excited upon irradiation by light of a certain wavelength causing structural transformation and thereby a change in conformation of the protein. As a result, a change in its bioactivity is induced. The most important chromophore for the visual transduction is 11-*cis* retinal, which is covalently bound to the photoreceptor rhodopsin.[19] When hit by a photon 11-*cis* retinal undergoes photoisomerization, changing the conformation of rhodopsin and releasing the transducin G-protein. Subsequently, the GTP-bound G_α subunit activates cGMP phosphodiesterase, which hydrolyzes cyclic GMP and lowers its concentration. This leads to the closure of cyclic GMP-gated cation channel and hyperpolarization of the photoreceptor cell (Fig. 11-6).

Plants, in contrast, do not carry rhodopsin receptors for light detection but react on light by chromophores connected to other proteins. One of the most important is the phytochrome protein expressed by the majority of plants, as well as by some bacteria and fungi.[20] Phytochrome bares a linear tetrapyrrole pigment, which is covalently bound to the protein through a cysteine group. The tetrapyrrole moiety, also called the "bilin" group, is a natural

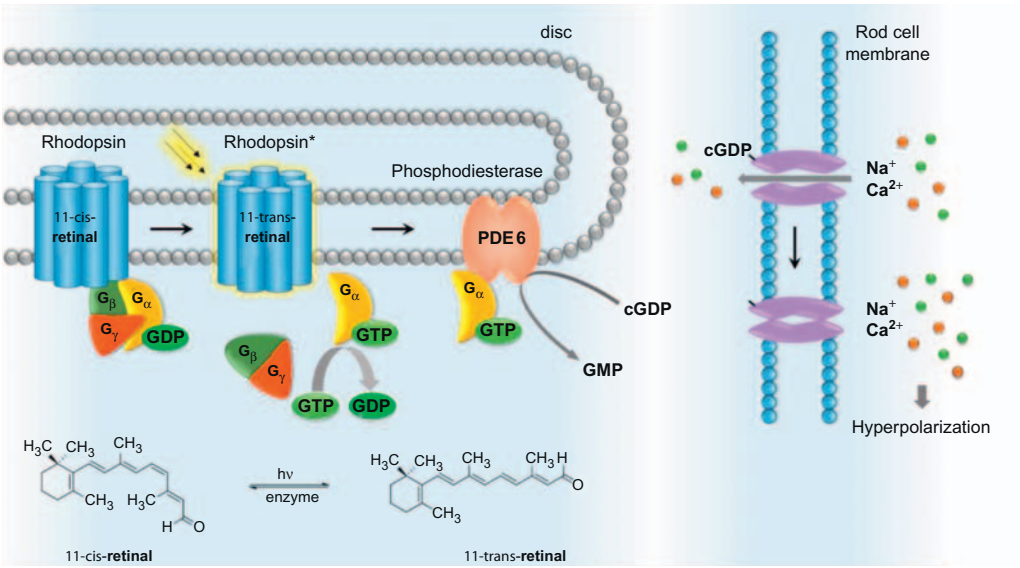

FIGURE 11-6 Signal transduction cascade of light-activated rhodopsin.

photoswitch that changes its conformation upon irradiation and thereby changes the conformation of the attached protein. Accordingly the chromophore exists in two interconvertible forms, namely, phytochrome red (P_r) and phytochrome far red (P_{fr}), based on the wavelength of light they maximally absorb (Fig. 11-7). P_r is the *blue* form absorbing *red light* (660 nm) while P_{fr} is the *green* form absorbing far *red light* (730 nm).

Along with phytochrome proteins, phototropins or more specifically, flavoproteins, are responsible for the regulation of photoperiodism and photomorphogenesis.[21] The flavin chromophore is embedded in the LOV (light-oxygen-voltage) domain of the protein but is not covalently bound. Upon irradiation with blue light a covalent bond between the cysteine residue of the LOV domain and the C(4)a position on the flavin isoalloxazine ring is formed. This leads to a conformational change in the protein and to increased phototropin kinase activity. In the dark, the flavin-C(4)a-adduct is not stable and dissociates from the unbound form.[22]

All these light-activated processes share a common characteristic: the involved chromophore switches between two distinct states that differ in their structure and polarity, in a reversible fashion. In this context one conformation the photoreceptor is active and in the other inactive. This represents the main principle of a photoswitch that nature employed very successfully for light sensitization.

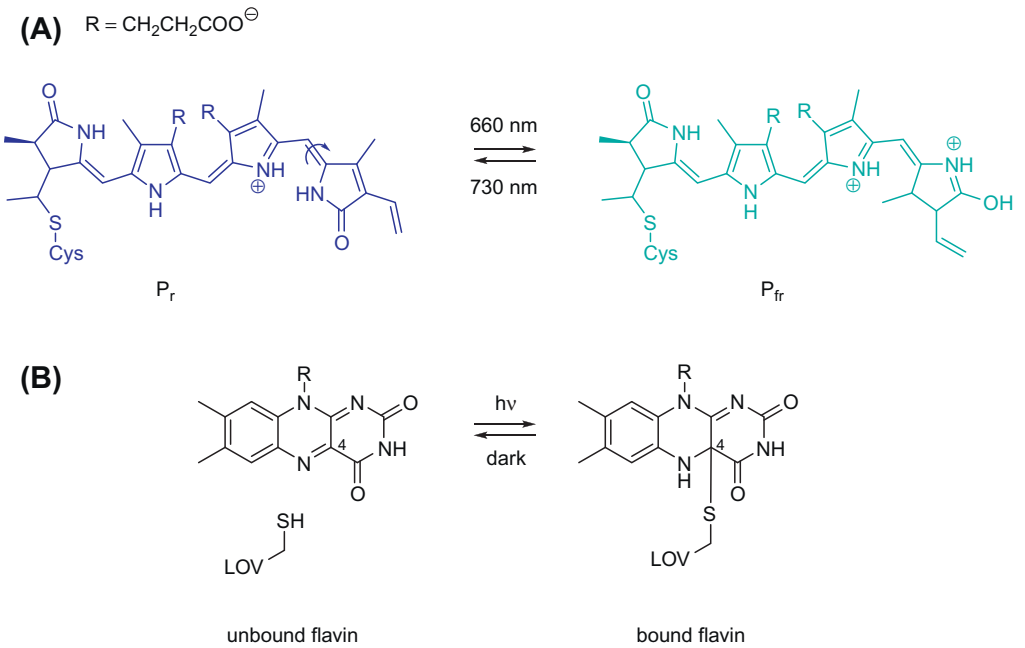

FIGURE 11-7 (A) Phytochrome red (P_r) and far red (P_{fr}) photoswitch. (B) Flavin in its unbound and LOV (light-oxygen-voltage) domain-bound form.

11.3.2 Synthetic Photoswitches

There are only few chromophores that have evolved in nature for light-dependent biological activity. In contrast, chemists are able to synthesize a large number of photoswitches, based on different structures and switching mechanisms. A photoswitchable system must comply with a number of requirements at the same time, which also means that the characteristics of a chemical photoswitch can be chosen to fit the desired biological purpose to be influenced. The photoswitch should respond effectively to light. This means that it undergoes a fast and significant structural or polarity change upon irradiation with wavelengths orthogonal to biological processes.[23] Such molecules usually show broad extinction coefficients and high quantum yields. All these parameters are described by the photostationary state (PSS), which is the ratio between the switched and the unswitched molecule and is usually specified as a percentage. A photoswitch that converts completely to its isomeric form during irradiation represents a PSS of 100%. Needless to say this represents an ideal case that is rarely realized. A selection of the most important synthetic photoswitches, classified into T-type (thermally reversible) and P-type (photochemically reversible) photochromic molecules, is shown in Fig. 11-8.[24]

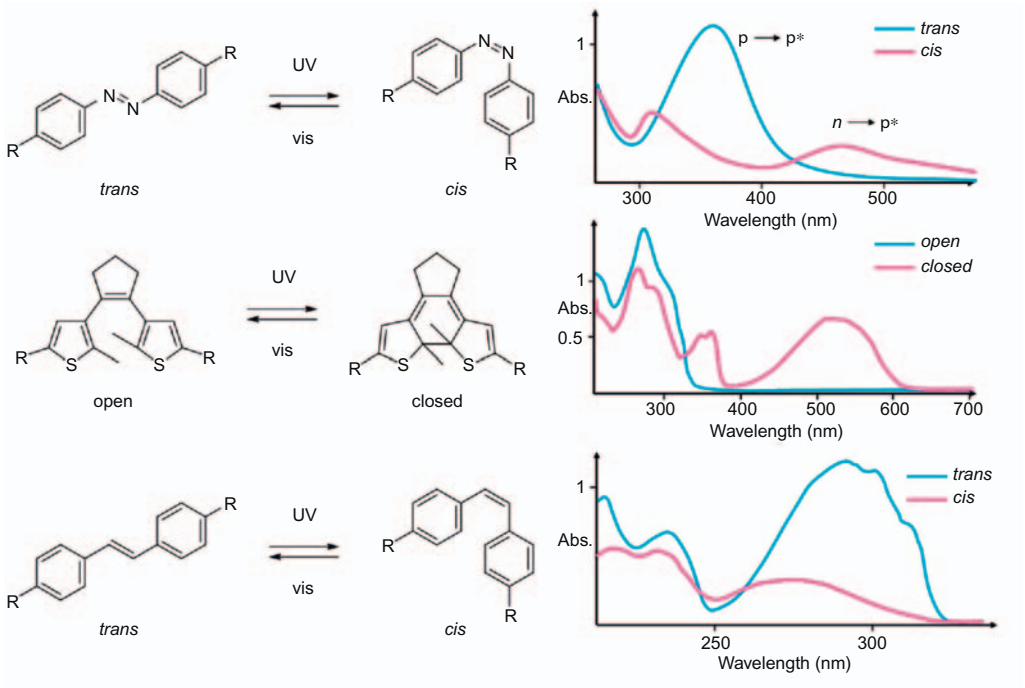

FIGURE 11-8 Photochemical reactions and absorption spectra of azobenzene, dithienylethene, and stilbene photoswitches.

11.3.2.1 Azobenzene

The oldest and best-studied class of synthetic molecular photoswitches are azobenzenes,[25] which consist of two benzene rings connected to each other by an azo group. Due to this structure azobenzene can exist in two stereoisomeric states, namely *cis*-azobenzene and *trans*-azobenzene.[26] The planar and unpolar conformation of the *trans*-state is thermally more stable than the *cis*-state, which is helically chiral. Irradiation with light of 320 nm switches the molecule, causes a rotation around the N=N bond forming the less stable *cis*-form, and causes a dramatic change in geometry and polarity ($\Delta\mu = -3$ D). The reverse process is triggered either thermally (T-Type) or by irradiation with a wavelength of 430 nm. These processes go along with the UV-vis spectra of azobenzenes, which show two different absorption maxima at the respective wavelengths. In the spectrum of *trans*-azobenzene the absorption maximum is at 320 nm resulting from the $\pi - \pi^*$ transition, whereas in the spectrum of the *cis*-form a weak maximum at 430 nm is visible, related to the $n-\pi^*$ transition. As such it is possible to target the less stable *cis*-conformation upon irradiation until the molecule reaches the highest PSS and vice versa. This process is also called photoisomerization and can be repeated over many switching cycles.

Additionally, azobenzenes can reach high extinction coefficients and quantum yields. This renders the switching process highly efficient and allows the use of low-intensity light for photoisomerization. Once in the exited state, azobenzenes perform isomerization very fast, within picoseconds. These properties can be highly advantageous because they avoid the generation of triplet diradicals that would lead to reactive and cytotoxic species, strongly decreasing biocompatibility.

Synthetically, azobenzenes are easily accessible, as they are widely used in the chemical industry. Azobenzenes find application as organic dyes, indicators, and radical reaction initiators and in areas of electronics, nonlinear optics, and optical storage media.[27] Moreover, they are key compounds in chemosensors and liquid crystals.[28] Therefore syntheses of aromatic azo compounds have been the subject of intensive research and versatile and effective methods have been developed (Fig. 11-9). A common strategy to access azobenzenes in good yields is based on the coupling of aryl diazonium salts with an electron-rich aromatic nucleophile (A).[29] This method requires initial in situ formation of a diazonium salt by oxidation of an aromatic primary amine at low temperature (B).[30] Diazonium salts are weak electrophiles that react solely with electron-rich arenes, such as phenols and anilines, often with electron-donating groups EDG (methyl, methoxy, etc.). The Mills reaction (C),[27,31] in contrast, is a synthesis method that works mostly irrespective of the electronic situation. It employs anilines and nitrosoarenes in glacial acetic acid to form the azobenzene moiety. The aromatic nitroso derivatives can be prepared either by oxidation of anilines (D) or by partial reduction of nitroarenes (E). Typical oxidation reagents are ferric chloride,[32] sodium or potassium dichromate and sulfuric acid,[33] acetic acid/ hydrogen peroxide,[34] *m*-chloroperbenzoic acid,[35] and potassium permanganate[36] as well as the two-phase heterogeneous system Oxone.[37] Reductively, nitroso derivatives can be obtained from nitroarenes by zinc-assisted reaction in aqueous ammonium chloride providing the respective hydroxylamine as an intermediate. With ferric chloride the reduction is then stopped at the nitroso

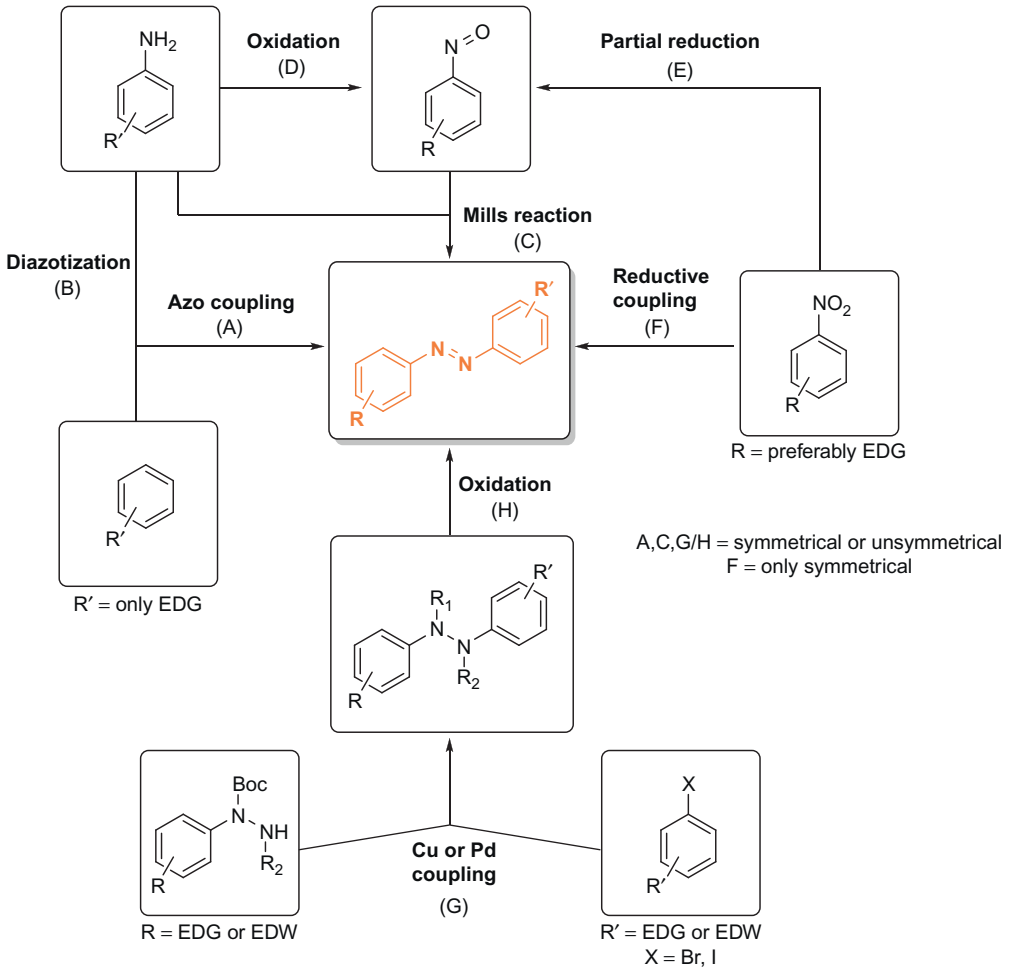

FIGURE 11-9 Azobenzene synthesis routes.

stage, which is used in the Mills reaction. Both strategies are suitable for both symmetric and asymmetric synthesis of the photoswitch.[38] Starting from the nitroarene, azobenzene can be synthesized in a zinc-catalyzed one-pot reductive coupling reaction (F), which provides symmetrical azobenzenes only.[39]

Milder synthesis strategies that extend the scope for more substituents employ fine-tuned transition metal catalysis. *N*-Phenyl hydrazine is converted in a palladium-catalyzed reaction with aryl halides to diaryl hydrazines (G) and subsequently oxidized with NBS/pyridine (H) to give symmetrical and unsymmetrical azobenzenes.[40]

The diverse and versatile access to azobenzenes allow incorporation of a high number of substituents, which is an important factor as the properties of azobenzenes can therefore be

fine-tuned by the nature and location of substituents. For example, azobenzene photoswitches addressed by the visible region of the optical spectrum (avoiding the need for high-energy photons) are more favorable. Changing the substitution pattern offers the possibility to redshift the exiting wavelength for photoisomerization by introduction of electron-donating groups on the aromatic residue, lowering the energy of irradiation and improving biocompatibility. Solubility problems due to the lipophilic nature of azobenzenes can be solved by substitution with hydrophilic or charged functional groups as well. Finally, the thermal stability of each isomer can be influenced by adequate substituents.[41]

Taken together, the unique features of azobenzenes explain their enormous popularity for incorporation into drug-like molecules for light-dependent control over biological function. Being the most important and widely applied synthetic photoswitch, researchers spare no efforts to overcome points of concern as potential long-term toxicity, metabolic instability as well as the problem of delivering light into the body and photo-induced cell damage.

11.3.2.2 Stilbene

A synthetic variation of an azobenzene photoswitch, isoelectronic to azobenzene, is stilbene. It is comprised of two benzene rings, but instead of being connected by an azo group, an ethylene group links the aromatic systems. Analogously, it can perform an *E*/*Z* isomerization upon photoirradiation, toggling between two states different in terms of polarity and geometry. As such it shows thermally bistable behavior in both forms. The structure of the thermodynamically stable *E*-form is nearly planar compared to the *Z*-isomer, which is twisted by 43°. Both isomers show high absorption in the UV/Vis spectra.[23]

Upon irradiation of 313 nm (UV light) photoconversion from the *E* to the *Z* form through a rotation around the C-C double bond takes place. Once excited and "pushed" into the *Z* configuration, stilbene undergoes, as a side reaction, a cyclization via a 6-π electrocyclic reaction to the *trans*-dihydrophenanthrene (DHP). In the absence of oxygen and in the dark DHP returns to *Z*-stilbene, due to its short lifetime (9 s). However, if oxygen is present DHP has a tendency to irreversibly eliminate hydrogen and oxidize to phenanthrene, detracting the photoswitch ability from the molecule (Fig. 11-10). This represents the main challenge of stilbene and renders it unsuitable for biological application, since oxygen is ubiquitous.[24]

To avoid this reaction, methylation of the carbon atoms involved in the cyclization reaction was successfully employed, stopping the reaction at the dihydro-stage and suppressing the formation of phenanthrene. As a result the new compound was found to perform a reversible cyclization reaction even in an oxidizing environment. However, the photochromic

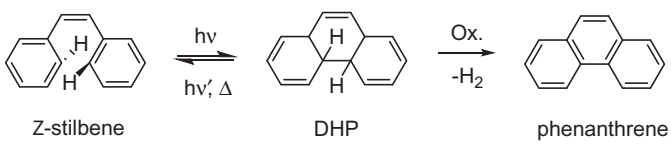

FIGURE 11-10 Cyclization and oxidation reaction after photoconversion of stilbene.

property is achieved at the expense of the lifetime of the dihydro-form, which is too short ($t_{1/2} = 1.5$ min at 20°C) for most practical biological applications.[42]

11.3.2.3 Diarylethene[43]

Replacing the benzene rings with five-membered heterocyclic aromatic moieties counteracts the above drawback of methylated stilbenes with regard to their short halflife. In doing so, the resulting compound becomes thermally stable, not only in the open form but also in the closed dihydro-construct, which is stable in the dark for months even up to 100°C. The dramatic change in thermal stability is due to the low aromatic stabilization energy of the heterocyclic aryl groups. Employing heterocycles gave access to a new class of photoswitches, the diarylethenes, which exhibit a photochromic cyclization reaction upon irradiation, with extremely highly quantum yields (close to 100%), high sensitivity, and rapid response (in the range of picoseconds). Diarylethenes are characterized by their unparalleled fatigue resistance, meaning that cyclization can be repeated many times without losing switching performance (photobleaching). As such, diarylethenes can be applied in optic and optoelectronic technologies as well as in biological systems.[24,41]

Other synthetic photoswitches[23] including spiropyrans, thiophenefulgides, hemithioindigos, and overcrowded alkenes are not further discussed in this context, since they have not yet been applied as drug-like molecules (with one exception, reported in Section 6.3.1).

11.4 Design and Synthesis[15]

Considering that photochromic compounds have to be incorporated into drugs, they have to be suitable for and applicable to biological systems. For this purpose their pharmacokinetic properties, such as metabolic stability, solubility, and toxicity, have to be taken into account. Beside these features, the success of a hybrid compound for photopharmacological research is mainly determined by the compatibility of biological assays with irradiation. The most commonly used bioassays employ optical detection methods in order to determine and quantify biological activity. The switching wavelength should ideally be orthogonal to the wavelength used in the bioassay, which is the case when the respective wavelengths are far enough apart. If not, the wavelength emitted in the measurement process might interfere with the photostimulation of the hybrid, resulting in potentially falsified data. To prevent that, functional assays that don't use light for exaltation/detection such as electrophysiology methods are more convenient. From a synthetic point of view, the hybrid should be designed in a way in which structural diversification is rendered possible, preferably at a late synthetic stage, enabling fine-tuning of the properties related to permeability and receptor binding.

To enable photochromic hybridization, one could just take a drug of interest and covalently attach it to a photoswitch, according to the "trial and error" principle. In many cases, the resulting drug is indeed a photochromic compound, but often suffers from a significant loss of activity. Possible causes might be on the one hand the steric hindrance of the receptor binding process with the "enlarged" drug, decreasing the receptor affinity, and on the other,

the photoswitch might be introduced on a position of a drug, which is essential for binding. Thus a more rational design is preferable, where the 3D structure of the respective protein is taken into account or where the synthesis is related to an already known lead structure.

In the following, two main synthetic strategies to provide light sensitivity into drug molecule, the "azologization" and the "azo-extension" approaches, both are obviously based on azobenzenes, will be discussed.

11.4.1 Azologization

The rational introduction of the azobenzene group into the structure of drugs is called azologization (derived from "azobenzene" combined with "analogization"). Based on the commonly applied bioisosterism approach, azologization searches for suitable substituents that can be exchanged with azobenzenes, the so-called "azosteres," without evoking a significant change in the structure of the parent drug. Azosteres should resemble azobenzenes in size and shape and be sterically and electronically comparable. They include stilbenes, (heterocyclic) *N*-aryl benzamides, benzyl anilines, benzyl phenyl ethers and thioesters, diary esters, 1,2-diphenyl hydrazine, and 1,2-diarylethanes (Fig. 11-11). A wide number of drugs registered in the protein database (PDB) as ligands contain these structural motifs, offering the possibility for light sensitization and light-dependent control of respective biological functions.

The morpholine derivative fomocaine depicts the azologization principle vividly.[44] It is used as a local anesthetic and incorporates in its structure a benzyl phenyl ether, representing an azoster. By replacing it with azobenzene, a new compound was obtained, named fotocaine by Trauner and coworkers (Fig. 11-12). It shows characteristic absorption spectra suggesting photochromic behavior. Isomerization is performed irradiating with 350 nm for *cis* to *trans*-conversion and 450 nm for back-relaxation.

Fomocaine functions as a channel blocker for voltage-gated sodium channels (Na_V) inhibiting APs firing in hippocampal neurons. Investigation into the ability of fotocaine to manipulate neuronal function in a light-dependent manner were performed in mouse brain slices using patch clamp electrophysiology. The results show that AP firing was inhibited when the irradiation wavelength was set to 450 nm at the neurons exposed to fotocaine. In this setting the *trans*-isomer is the predominant form. Upon irradiation with 330 nm and switching to the *cis*-configuration AP firing was enabled. This example vividly demonstrates the benefit of using the azologization approach. Other specific examples are described in the following.

11.4.2 Azo-extension

Analysis of structure-activity data commonly enables the determination of chemical group in a certain lead structure responsible for biological activity and which can be then varied without changing the biological effect. This is important for drug optimization with respect to bioavailability, solubility, and toxicity retaining bioactivity. Therefore it is possible to replace or to extend such variable groups with a photoswitchable motif in a rational manner, in this

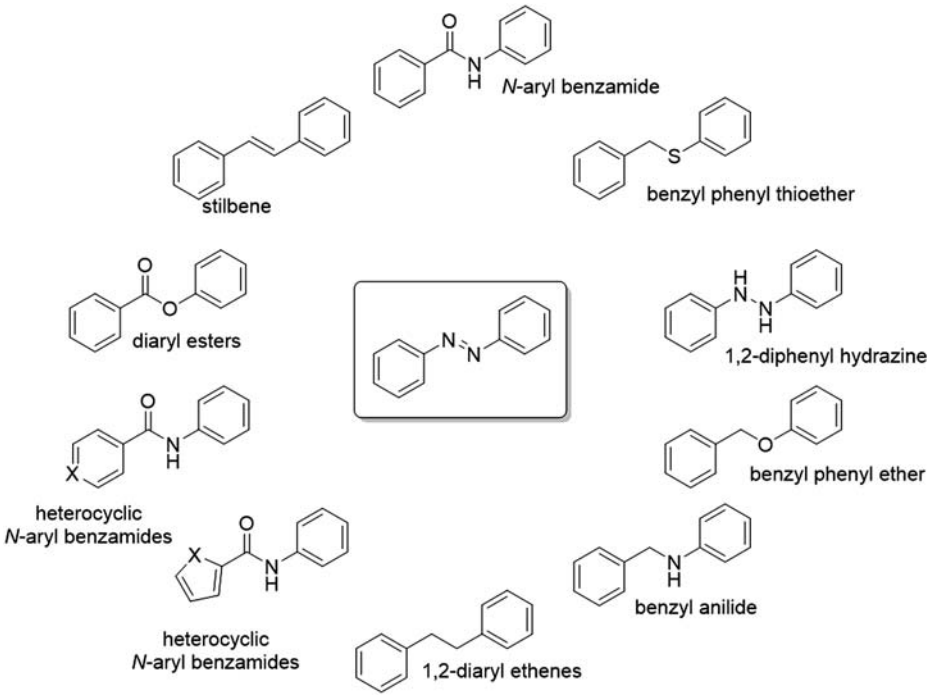

FIGURE 11-11 Structures resembling azobenzene in size and shape ("azosteres").

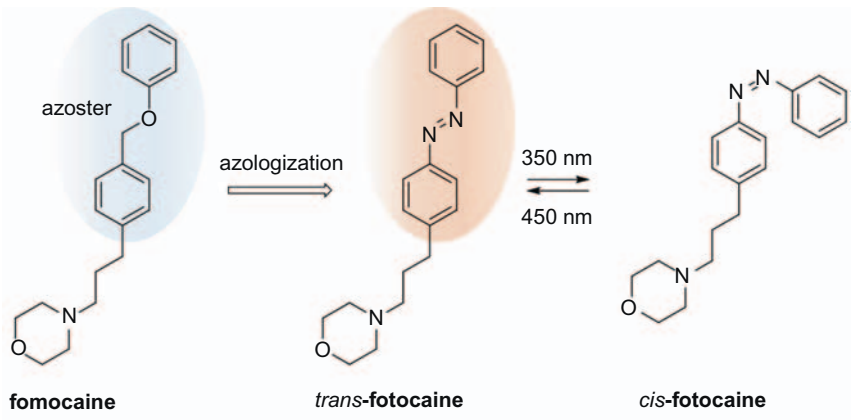

FIGURE 11-12 Application of the azologization principle to **fomocaine**.

case with azobenzene ("azo-extension"). Fig. 11-13 shows two among many compounds where this concept was successfully realized.

A photoswitchable version of the anesthetic propofol (AP-2) was developed by extending the benzene ring to azobenzene.[45] The *trans*-AP-2 showed potentiating effects on the $GABA_A$

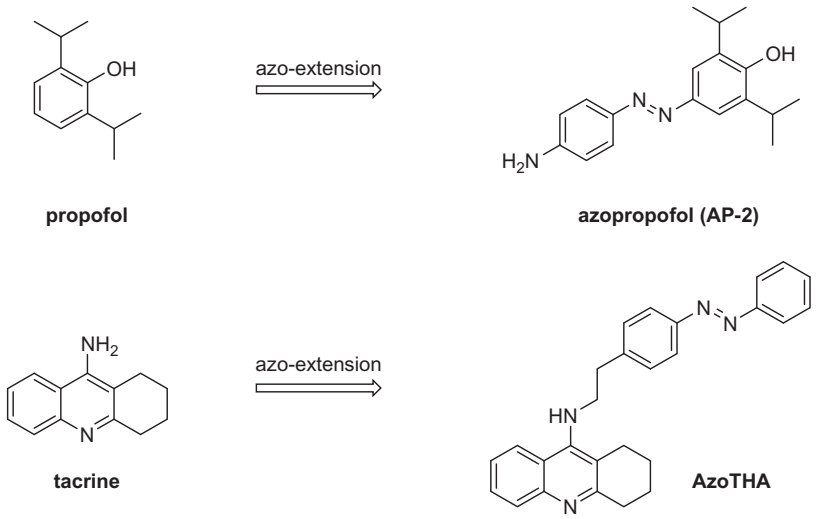

FIGURE 11-13 Azo-extension as a tool for optical control of bioactivity.

receptor, which decreases upon irradiation with violet light as it switches to the *cis*-form. Tacrine (tetrahydroaminoacridine (THA)) represents a centrally acting acetylcholinesterase (AChE) inhibitor used to counteract the effects of muscle relaxants, as a respiratory stimulant, and in the treatment of Alzheimer's disease (AD).[46] Extending tacrine with the photoswitchable unit azobenzene provides AzoTHA, which shows AChE inhibition in the *cis*-state, whereas it becomes less active in the dark-adapted *trans*-state.

11.5 Targets[47]

By applying ligands major breakthroughs have been achieved in neurology,[48] diabetes therapy,[49] vision restoration,[50] cancer chemotherapy,[51,52] and there will likely be many more in the near future. To be able to successfully apply novel photochromic ligands to novel targets, the challenges to be faced are the "photodruggability" of bioactive compounds and the capabilities of medicinal chemists to synthesize and analyze the respective photochromic entities. Obviously, the targets should be responsive to the light-induced changes in the structure and physicochemical properties of the photoswitchable hybrid compound. For this purpose the target is supposed to be accessible for irradiation. To this end it is more favorable when a target is related to a disease that is either exposed and/or locally confined (e.g., skin, eyes).[53] In this section the most important photoswitchable hybrid compounds are listed—with no claim to be exhaustive—based on the species of targets they are acting on. The synthesis strategy used and the pharmacological activity will be presented shortly.

11.5.1 Ion Channels

Ion channels are transmembrane proteins that allow ions to pass the membrane into or out of a cell. They can be classified in many different ways but for the purpose of this section they are classified by their gating, i.e., what opens or closes the channels. Voltage-gated ion channels (VGICs) react in response to changes in membrane potential whereas ligand-gated ion channels (LGICs) open when a chemical ligand, as a small molecule or a neurotransmitter, binds to the protein. Other gating includes stimulation through light, as reported previously by means of opsins, pressure, and displacement or temperature.[54] Photoregulation of ion channels using PCLs provides light sensitivity on the intrinsic excitability of neurons within short timescales.[3,55]

11.5.1.1 Voltage-gated Ion Channels

Kramer and Trauner synthesized and reported on a family of amphiphilic azobenzene molecules targeting VGICs (Fig. 11-14).[56,57] They are designed as charged quaternary ammonium salts (QA), inspired by the anesthetic lidocaine and its QX-314 derivative, extended with the azobenzene moiety and followed by a hydrophobic tail. For instance, acrylamide-azobenzene-quaternary ammonium (AAQ) salts is known to function as *trans*-blockers for the voltage-gated K^+ channel (K_V) acting on the intracellular tetraethylammonium (TEA) binding site. Due to the lipophilic unit it is also able to cross the cell membrane while the alkyl ammonium ion part is responsible for binding to the internal vestibule. In its

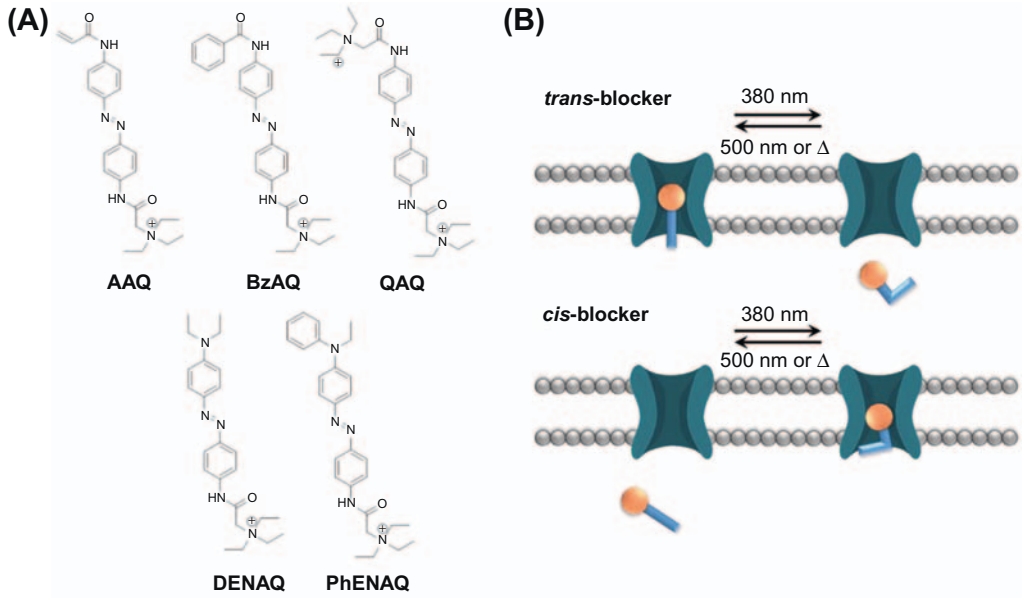

FIGURE 11-14 (A) Family of photoswitchable ion-channel blockers and (B) the principle of isomer-dependent blocking.

trans-form it binds to the channel, where it inhibits K^+ conduction. Irradiation with 380 nm light causes *cis*-transformation, relieves the blockade, and restores K^+ currents. Remarkably, intraocular injection of AAQ in mutant mice lacking retinal photoreceptors led to restoration of light responses without the need for genetic modification or surgical intervention. However, any in vivo use is not trivial. The high-energy UV light can severely damage biological tissues and the possible toxic properties of the acrylamide unit have to be taken into account.

Azobenzene-extended potassium channel blockers can be easily modified by organic chemists to incorporate beneficial characteristics. Enhanced membrane permeation is achieved by replacement of the acrylamide tail with the more hydrophobic benzylamide group (BzAQ).[58] In contrast, QAQ is unlikely to cross the cell membrane because of its double charge. Even though it is membrane impermeant, it modulates TPRV1 ion channels, which are activated by noxious stimuli, and it is responsive to pain-sensing. UV damage is drastically reduced by introduction of an electron-donating diethylamine group at the tail of the quaternary ammonium head (DENAQ). The alkylamino group increases the electron density on one side. As for that, the absorption maximum is shifted into the bathochromic direction to 470 nm, fully operating in the visible region of the electromagnetic spectrum and rendering the in vivo use more accessible. DENAQ is active in the *trans*-configuration and consequently a *trans*-blocker. On the other hand, PhENAQ, a phenyl-substituted variant, works as a *cis*-blocker.

11.5.1.2 Ligand-gated Ion Channels

LGICs are regulated by small molecules. In order to provide light sensitivity, the simplest and most intuitive way is to look at those endogenous ligands. Among different LGICs iGluRs are outstanding, mediating the majority of excitatory synaptic transmission in the central nervous system (CNS). They are key receptors in synaptic plasticity, substantial for memory and learning. Glutamate represents the endogenous ligand of iGluRs and the most abundant neurotransmitter. Its importance and application as photochromic compound was already shown before. IGluRs are subdivided into different classes. The AMPA receptors, responsible for the fast synaptic transmission, are named after the synthetic glutamate analogue α-amino-3-hydroxy-5-methyl-4-isoxazolepropionic acid (Fig. 11-15), which can, as an agonist, selectively activate these receptors. In 2012 Trauner and coworkers developed a photochromic hybrid for the AMPA receptor.[59] The design was based on the potent and highly selective BnTetAMPA (benzyl-tertazolyl-AMPA). Using the azo-extension approach the azobenzene moiety was merged with the AMPA structure providing azobenzene-tetrazolyl-AMPA (ATA). Investigations employing cortical mouse neurons showed reversible generation of APs. In the dark, neuronal firing is triggered effectively, whereas during illumination with green-blue light quickly deactivates firing. In a follow-up study in 2016, ATA found application in restoring light sensitivity in blind retinae, such as AAQ and DENAQ, not as channel blocker but rather as the first photochromic agonist.[60]

N-methyl-*D*-aspartate (NMDA) receptors, also belonging to the family of iGluRs, are expressed throughout the brain in nerve cells and are important for synaptic plasticity

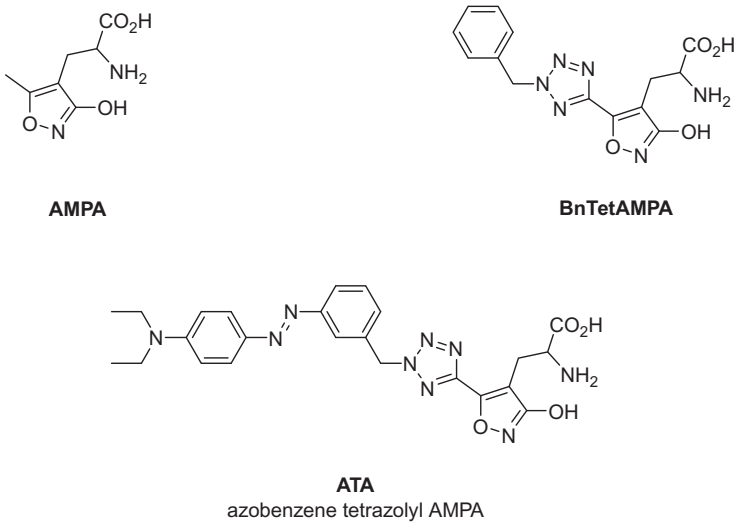

FIGURE 11-15 AMPA and a (photoswitchable) derivative.

control, memory, and learning. As such, selective agonists might play a significant clinical role in the treatment of neurological dysfunction as Alzheimer's, Parkinson's, and Huntington's diseases. DiGregorio, Trauner, and coworkers synthesized a photochromic glutamate analogue selectively activating NMDARs.[61] Following the experience gained with GluAzo and ATA the new compound was designed as an azobenzene-triazole conjugated glutamate (ATG). In contrast to ATA, ATG is inactive in the dark-adapted *trans*-form. Irradiation with 370 nm quickly converts it into the active *cis*-form, representing the first *cis*-agonist. Therefore the activity of ATG can be precisely regulated upon illumination on a millisecond scale. This behavior is highly advantageous because nerve cell damage that stems from excessive stimulation is prevented. Fig. 11-16 illustrates light-controlled AP firing in cortical neurons. Another example of controlling LGICs in a light-dependent manner is AzoCholine.[62] It was designed to resemble MG624, a α7 nicotinic acetylcholine receptor (nAChR) antagonist, using the azologization approach and replacing the stilbene group with azobenzene. Binding of *trans*-AzoCholine on the neuronal-type pentameric ion channel resulted in currents twice as large compared to acetylcholine, detected by patch-clamp electrophysiology (Fig. 11-16). However, 360 nm irradiation reversed this process and deactivated α7 nACh receptors. Finally, AzoCholine showed light-dependent perturbation of behavior in nematodes (Fig. 11-17).

Among numerous pioneering research works, Trauner and coworkers were the first to apply photopharmacology to ATP-sensitive potassium channels (K_{ATP}).[49] These are hetero-octameric proteins comprised of four sulfonylurea receptor subunits (SUR1) along with four $K_{ir}6$ components, creating a channel that allows potassium ion efflux. The SUR1 units monitor the energy balance within the cell by sensing intracellular levels of ATP and in response

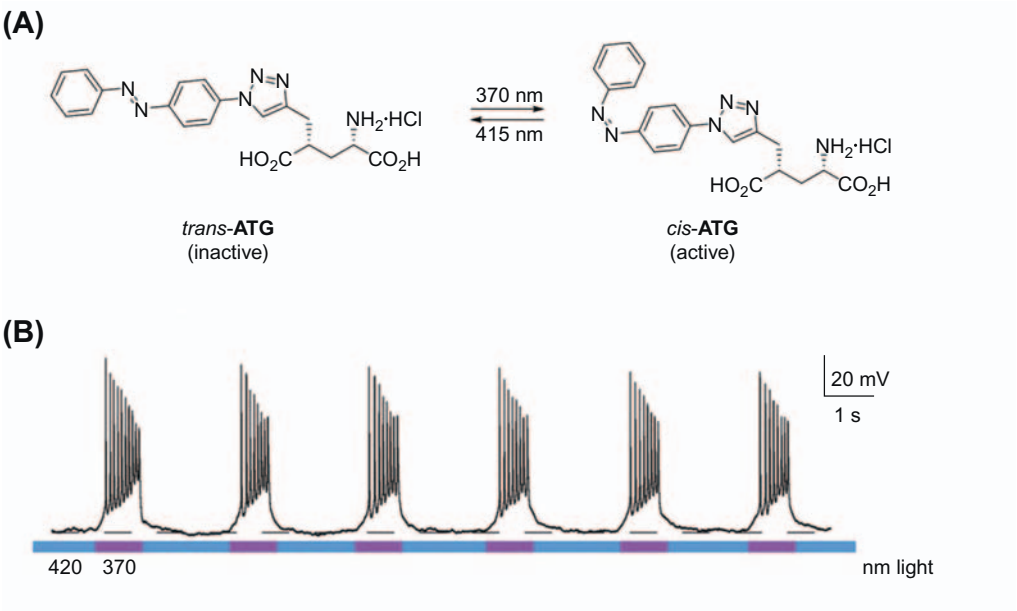

FIGURE 11-16 (A) Photochemical reaction of ATG. (B) Light-dependent AP firing in cortical neuron.

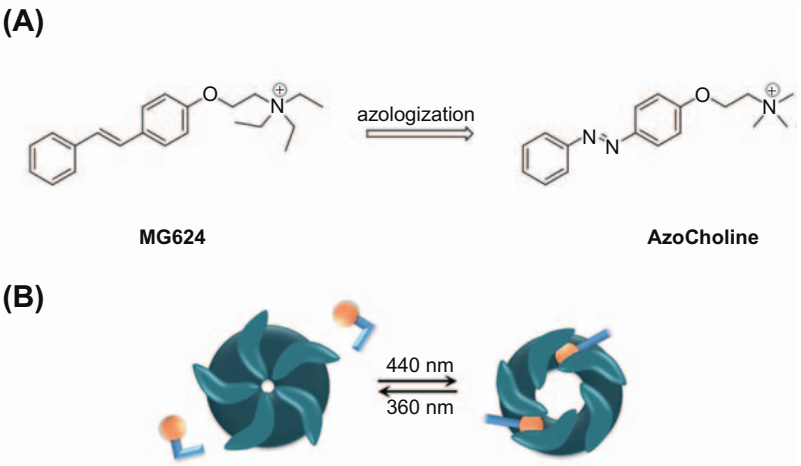

FIGURE 11-17 (A) Azologization of MG624 leading to the design of AzoCholine. (B) Light-controlled activation of nAChR with a photochromic ligand.

opening or closing the inward rectifying potassium channel. In pancreatic beta cells, high levels of glucose leads to increased production of ATP, which in turns binds to the K_{ATP} channel. This results in K_{ATP} closure causing depolarization of the membrane and opening of calcium channels, which trigger insulin secretion. Hence, light activation of K_{ATP} channel may offer a useful research tool for diabetes. Glimepiride, as a sulfonylurea binding to the SUR1 component, is approved for the treatment of type 2 diabetes mellitus (T2DM). It was used as a template for the design and synthesis of JB253 and a redshifted derivative JB558, both photoswitchable glimepiride analogues, by extending its aromatic core to a (heterocyclic) azobenzene (Fig. 11-18). With incorporation of the chromophore, JB253 was readily converted to the *cis*-state applying *blue* light, while the *trans*-state occurred rapidly in the dark through thermal relaxation. JB558 possesses bathochromic-shifted absorption maximum and is *cis*-converted with *yellow-green light* ($\lambda = 520$ nm).[63] It was reported that pancreatic beta cell function and insulin release can be regulated upon illumination using these photochromic sulfonylureas.

Recently, the family of G-protein coupled inwardly rectifying potassium channels (GIRK) channels have emerged as a potential target for photopharmacology. GIRK channels are downstream effectors of G-GPCRs and are activated upon binging of $G_{\beta\gamma}$ subunit becoming permeable for potassium ions. This results in hyperpolarization of the cell membrane,

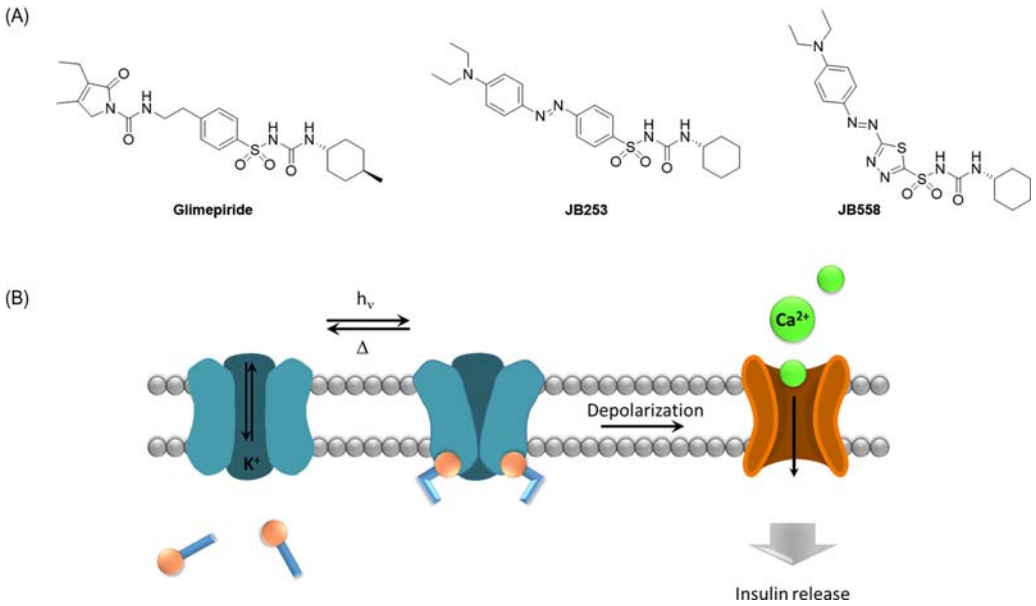

FIGURE 11-18 (A) Glimepiride and photoswitchable variations. (B) Light-induced binding of photoswitchable sulfonylureas on SUR1 causing insulin release.

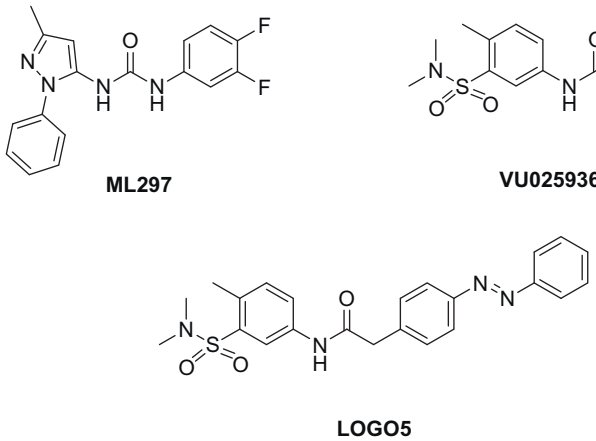

FIGURE 11-19 Light-operated GIRK channel opener 5 (LOGO5) inspired by ML297 and VU259369 activators.

reducing the activity of excitable cells. They are expressed in the pancreas, heart, and brain and play a significant role in cardiac output, coordination of movement, and cognition. With the discovery of the first potent and selective activators of GIRK channels ML297 and VU0259369, the necessary foundation was laid for the design and synthesis of light-operated GIRK channel opener (LOGO) by employing the azo-extension approach. As the first photochromic potassium channel opener, LOGO5 was found to enable the optical control of GIRK channels in the *trans*-configuration and is inactivated with UV light, causing isomerization to *cis*-LOGO5. The potency of *trans*-LOGO5 is comparable to VU0259369 (Fig. 11-19). In vitro, this phenomenon is used for silencing AP firing in dissociated hippocampal neurons. In vivo, the motility of zebrafish larvae can be controlled in a light-dependent fashion.[64]

Lastly, a methodology was found in 2013 to stimulate transient receptor potential (TRP) channels with light.[65] TRP channels are found throughout the body of mammals in almost every cell type and are mainly localized in the cell membrane. They mediate the perception of pain, temperature, pressure, and noxious and pungent chemicals. The study focused on the vanilloid receptor 1 (TRPV1) activated by a variety of chemical stimuli such as capsaicin (CAP), spider toxins, allicin, and physical triggers such as voltage, heat, and low pH but not by light. It acts as an intracellular calcium channel but is also permeable for sodium and potassium to a small extent. The pungent component of hot chili peppers, CAP, is known as an agonist while capsazepine (CPZ), BCTC, and thio-BCTC are specific antagonists with analgesic effects (Fig. 11-20). Bearing aromatic rings extendable to azobenzene, these small molecules represented the basis for the design of photoswitchable derivatives, namely, azo-capsazepine (AC) and azo-BCTC (ABCTC). In the course of in vitro investigations of their light-controlled activity, AC-4 was found to be *trans*-antagonist upon voltage activation of TRPV1, while *cis*-AC-4 inhibits CAP-induced TRPV1 current. ABCTC showed antagonist behavior only as *cis*-isomer.

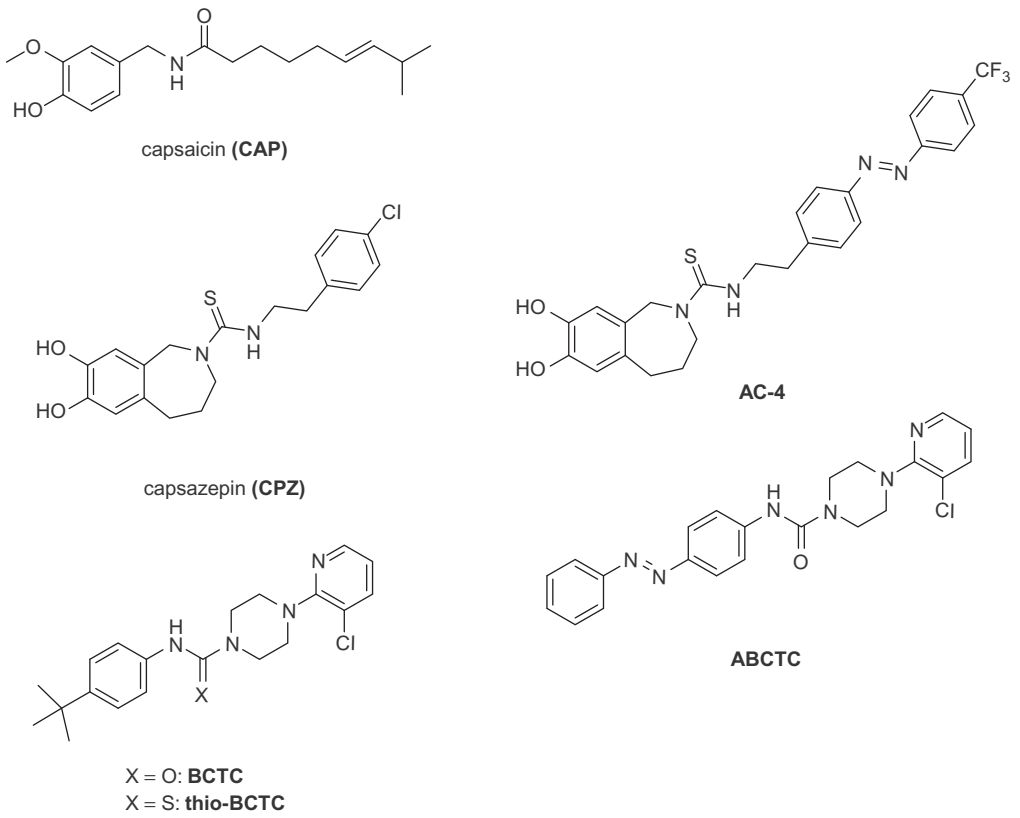

FIGURE 11-20 Ligands for TRPV1 channel and photoswitchable derivatives.

11.5.2 G-Protein Coupled Receptors[66,67]

GPCRs constitute the largest family of transmembrane proteins that perceive a plethora of extracellular signals transducing them to heterotrimeric GTP-binding proteins (shortly G-proteins), which leads to the modulation of downstream effectors. Characteristic for all GPCRs are the seven transmembrane (7-TM) α-helices connected by three intracellular loops (IL-1 to IL-3) and three extracellular loops (EL-1 to EL-3) alternating each other. They are involved in many diseases and as such represent the targets for approximately 40% of all modern medicinal drugs. With the exception of rhodopsin receptors that are responsible for vision, and were described before, none of the GPCRs inherently respond to light stimulation. However, they are activated by various extracellular ligands including hormones, neurotransmitters, and small molecules. This offers the possibility to apply the principles of photopharmacology to GPCRs by hybridization of specific ligands with photochromic

components, thus providing photocontrolled drugs. Therefore photopharmacology holds promise for deeper understanding of GPCR function and dynamics.

While application of photopharmacology to the GPCR family is still in its infancy, it was investigated in 2014−2016, as discussed in the next section.

11.5.2.1 Metabotropic Glutamate Receptors

The first contributions made in this field were in 2014 by the group of Llebaria and Gorostiza, focusing on allosteric modulators of metabotropic glutamate (mGlu) receptors, which belong to the class C subfamily of GPCRs.[68] As the name suggests, they respond to the neurotransmitter glutamate, binding to the orthosteric side of the receptor. But unlike iGluRs, mGluRs are not channels permeant for ions, instead they initialize biochemical cascades, leading to modifications of subordinated proteins that in turn can influence ion channels. In addition to the orthosteric binding site, mGluRs possess allosteric binding sites, which can be selectively targeted by ligands with subtype selectivity (mGluR1-mGluR8). This renders allosteric ligands attractive, since they increase pharmacological selectivity, enabling highly localized therapeutic effects. In this context, VU0415374, a positive allosteric modulator (PAM) of mGluR4, was used as a suitable compound for introducing light sensitivity as it contains two aryl amide groups in the molecular structure, representing azosteres. Replacing synthetically each of them with the azobenzene moiety provided two derivatives, one of them identified as a nanomolar potent negative allosteric modulator (NAM) of mGluR5, alloswitch-1 (Fig. 11-21). Pharmacological activity was investigated in vitro and in vivo demonstrating light-dependent manipulation of mGluR5, even though off-target effects in other receptors could not be excluded. Application of quisqualate (agonist)-induced increase in calcium concentration indicates receptor activation, which is blocked by alloswitch-1. Upon irradiation, receptor activity was restored proving its photocontrolled antagonistic action.

Very recently, a photoswitchable NAM for mGluR4 was published. OptoGluNAM4.1 allows reversible photocontrol of receptor activity in transparent zebrafish larvae.[69] In the dark, treatment with the photochromic agent led to increased motility compared to untreated control animals. Locomotion investigation with alloswitch-1, in contrast, resulted in freezing behavior upon treatment. The different effects found complement each other, as they are consistent with the opposing effects of mGluR4 and mGluR5. While mGluR4 has an inhibitory effect on synaptic glutamate release, mGluR5 enhances neuronal activity. This is an outstanding example of photopharmacological research useful for dissection of physiological roles of mGluRs.

11.5.2.2 Adenosine Receptors

Adenosine receptors, differentiated into four subtypes (A_1, A_{2A}, A_{2B}, A_3), play an important role in the CNS, and in the regulation of the circulatory and immune systems. Agonists and antagonists of adenosine receptors bear the potential for treatment of cerebral and cardiac ischemic diseases, sleep disorders, immune and inflammatory disorders, Parkinson's disease, epilepsy, and cancer. However, the lack of selectivity toward the receptor subtypes is often a

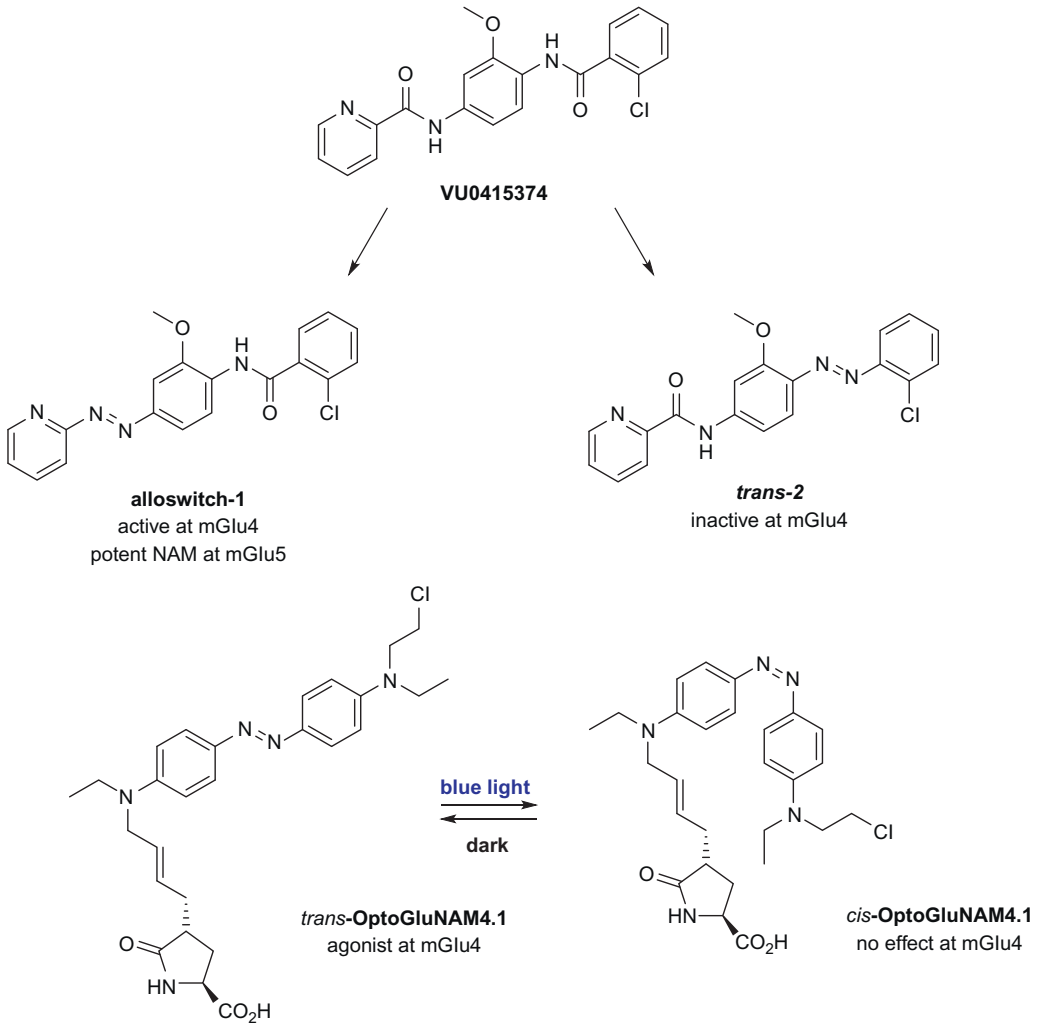

FIGURE 11-21 Light-sensitive allosteric ligands for metabotropic glutamate receptors.

problem and not trivial. Accordingly, Ciruela and coworkers reported the synthesis and analysis of a new photoswitchable adenosine-based compound, the intrinsic activity of which can be modulated in a light-dependent manner.[70] It was obtained by extending the potent but nonselective adenosine receptor agonist N^6-2-(4-aminophenyl)ethyladenosine (APNEA) with the azobenzene chromophore. In the dark, MRS5543 (*trans*) exerts full agonistic effects on the adenosine A_3 receptor and partial agonistic effects on the A_{2A} receptor. In contrast, the *cis*-isomer, induced with blue light (460 nm), still behaved as a full A_3R agonist but became an antagonist of A_{2A}R (Fig. 11-22).

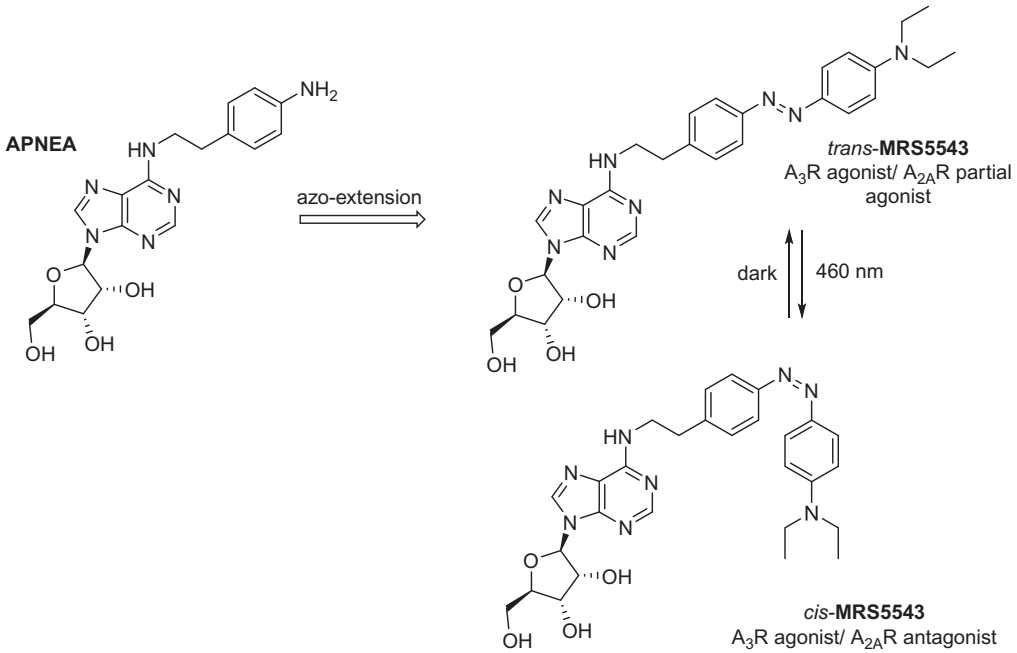

FIGURE 11-22 Azo-extension of APNEA and light-dependent change of intrinsic activity of its photoswitchable derivative.

11.5.2.3 μ-Opioid Receptor

Even though μ-opioid receptors (MOR) belong to the family of rhodopsin-like GPCRs, they are not inherently light responsive. Trauner and coworkers achieved their optical control by extending the phenyl ring of the potent OR agonist fentanyl to azobenzene in order to generate a photochromic variation, termed photofentanyl-2 (PF2), which was found to be an excellent μ-OR agonist (Fig. 11-23).[71] For functional characterization cells were transiently transfected with human MOR together with GIRK, which are natively expressed with MORs in the *locus coeruleus*. This setting is fundamental for analysis by electrophysiological assays, as binding of an agonist to MOR results in dissociation of the $G_{\beta\gamma}$-protein subunit from the G_{α} subunit, activating the GIRK channels and causing measurable currents. Upon testing, PF2 performed light-induced activation of the MOR as a *trans*-agonist, whereas *cis*-PF2, the predominant form of UV light (360 nm) led to significantly decreased activation rates. PF2 and future photochromic MOR effectors could be useful for the study of this receptor, which plays an important role in nociception and is expressed in the spinal cord, brain, and digestive tract.

11.5.3 Enzymes

Serving a huge variety of important biological functions enzymes are essential for living organisms. Nearly every biochemical reaction sequence is catalyzed or controlled by these

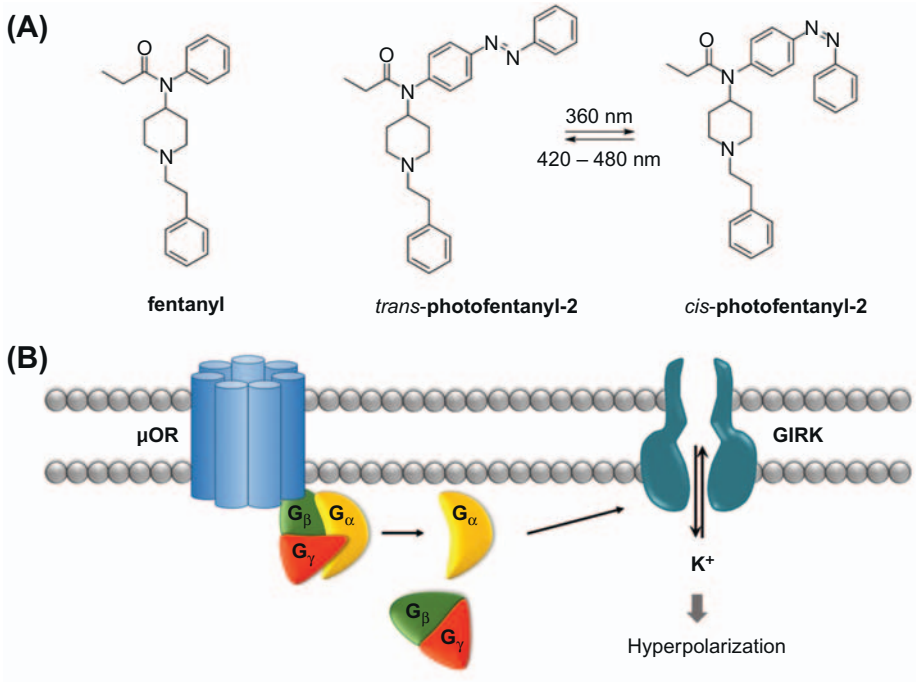

FIGURE 11-23 (A) Photoisomerization of photofentanyl-2 and (B) schematic illustration of GIRK channel activation mediated through μ-opioid receptor (μOR).

proteins by providing reaction pathways with low activation energy under physiological conditions.[72] They are the working machines for the metabolic pathways glycolysis, citric acid cycle, respiratory chain, photosynthesis, transcription and translation, and DNA replication. Phosphatases and kinases are indispensably involved in signal transduction and cell regulation. Muscular movement is exerted by ATPases and proteases and amylases play a significant role in the digestive system. These are only few examples of the myriad of enzymes controlling biological functions. Under this aspect, deficiency and/or malfunction of a single enzyme is often related to vicious and serious diseases, such as cancer, genetic disorders, and intellectual disability, among many others.

Often enzymes are subjected to regulators, generally small molecules, which control their activity by negative feedback mechanisms. As an example, enzymes can work together in consecutive order, forming a metabolic pathway. The end product of an enzyme-catalyzed reaction cascade is usually an inhibitor of the first involved enzyme adjusting the rate of product synthesis according to the demands of the cell. Therefore enzyme inhibitors play a key role in the control of enzyme activity and regulation. Being receptive to small molecules, enzymes can be targeted by researchers, thus expanding the photopharmacological toolbox. The incorporation of photochromic molecular switches into enzyme effectors offers the possibility to alter enzyme activity in a reversible and photocontrolled manner. With this aim,

recently light sensitivity has been introduced to enzymes, such as in phosphoribosyl isomerase A, ribonucleotide reductase, and protease using photoswitchable inhibitors.[73,74] In the further course several illustrative examples of enzyme targets for the photopharmacological approach are discussed.

11.5.3.1 DNA-topoisomerases

Both type II DNA-topoisomerase (also called gyrase) and DNA-topoisomerase IV enzymes are required for unfolding and separation of bacterial DNA and enable cell division and growth of bacteria.[75] To prevent this fluoroquinolone antibiotics, such as ciprofloxacin, are used to inhibit both enzymes simultaneously and therefore cause bacterial cell death. They find application in the treatment of bacterial infections including bone and joint infections, skin infections, and urinary and respiratory tract infections, among others. The research group of Feringa and Szymanski developed a photoswitchable version, which was designed by merging the ciprofloxacin structure with the azobenzene moiety (Fig. 11-24). Indeed, the antibacterial activity of Feringa's quinolone-2 against *Escherichia coli* and *Micrococcus luteus* increased significantly upon irradiation with 365 nm of light compared to the dark-adapted *trans*-isomer. As a temporally activated *cis*-antibiotic it counteracts the possible problem of UV-light tissue damage because it can be "switched on" from outside before administration, whereas it deactivates itself on the scale of hours. From this point of view, contamination of the environment with antibiotics and hence eventually resulting resistance might be avoided.

The same group developed the synthesis of ciprofloxacin-based photoswitches in a later study and demonstrated that light sensitivity can be synthetically introduced in a single step from the already available drug.[76] Two different chromophores were incorporated into the

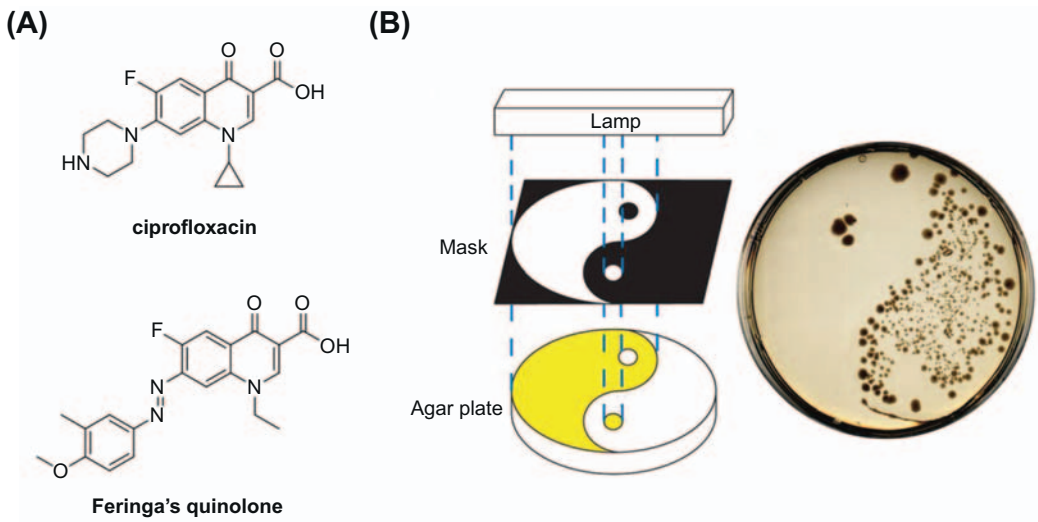

FIGURE 11-24 (A) Antibacterial agent ciprofloxacin and Feringa's quinolone (B) bacterial patterning study.

ciprofloxacin structure, the known azobenzene group and the photochromic spiropyran moiety, which consist of two connected heterocyclic rings orthogonal to each other and can toggle between a neutral closed form and a charged open form. The microbial activity of the resulting photoswitch-modified antibiotics (azofloxacin and spirofloxacin) was shown to be spatiotemporally controlled by light. Interestingly azofloxacin showed antibacterial activity on *M. luteus* almost 50-fold higher than ciprofloxacin.

11.5.3.2 Acetylcholinesterase

AD represents a major public health concern but the cause of this neurodegenerative illness is still poorly understood. (See Chapters 2, 6, 8 and 10 for a detailed discussion of the application of hybrid molecules for neurodegenerative diseases.) AChE operates mainly in the central and autonomous nervous systems and on muscular junctions where it catalyzes the hydrolysis of the neurotransmitter acetylcholine (ACh). Inhibition of this enzyme counteracts the decreased ACh concentration that causes cognitive deficits. Hence, tacrine (THA) is an AChE inhibitor and was approved for the treatment of AD.

A photochromic inhibitor of AChE, which can reversibly switch enzymatic activity upon irradiation with UV light (see structure in Section 4.2) was developed by the research group of Trauner.[46] Additionally, Decker, König, and coworkers developed a dithienylene-based bivalent photoswitchable THA inhibitor that enables the photocontrol of β-amyloid aggregation related to AD (Fig. 11-25).[77] The IC_{50} values of both photoisomers are comparable and in the nanomolar range. AChE hydrolysis is catalyzed by the catalytic active site (CAS) of AChE. It has been shown that a peripheral anionic site (PAS)—not responsible for AChE hydrolysis—mediates the pathophysiological highly relevant aggregation of β-amyloid[78,79]. It could be shown by aggregation and inhibition studies that only the open flexible tacrine photoswitch exerts 100% inhibition of β-amyloid aggregation mediated by AChE (actually the PAS of AChE) whereas the ring-closed rigid isomer showed maximum 43% inhibition. Molecular dynamic simulations indicate that the formation of a network of water molecules within the enzyme might mediate a specific interaction of one tacrine unit of the ring-open form with the PAS. This photoswitch represents a valuable tool for further investigation of the physiological function of AChE that could have an impact on the study of AD (Fig. 11-26).

11.5.3.3 Histone Deacetylase

DNA wraps itself around histone proteins to form a condensed structure that is transcriptionally silent. In order for genes to be expressed and transcription to occur, the histones have to be removed from the DNA to make it freely accessible for transcriptional enzymes. To this end histone transferase (HT) introduces acetyl groups to neutralize the positive charge of the superficial lysine amino acids releasing negatively charged DNA. After transcription of the gene the reversed process is catalyzed by histone deacetylase (HDAC) enzymes restoring the positive charge of the histones and the interaction with DNA. Altered expressions and mutations of genes encoding for HDAC are related to disruption of cell homeostasis and tumor development. Inhibition of HDAC enzymes showed pronounced antitumor activity,

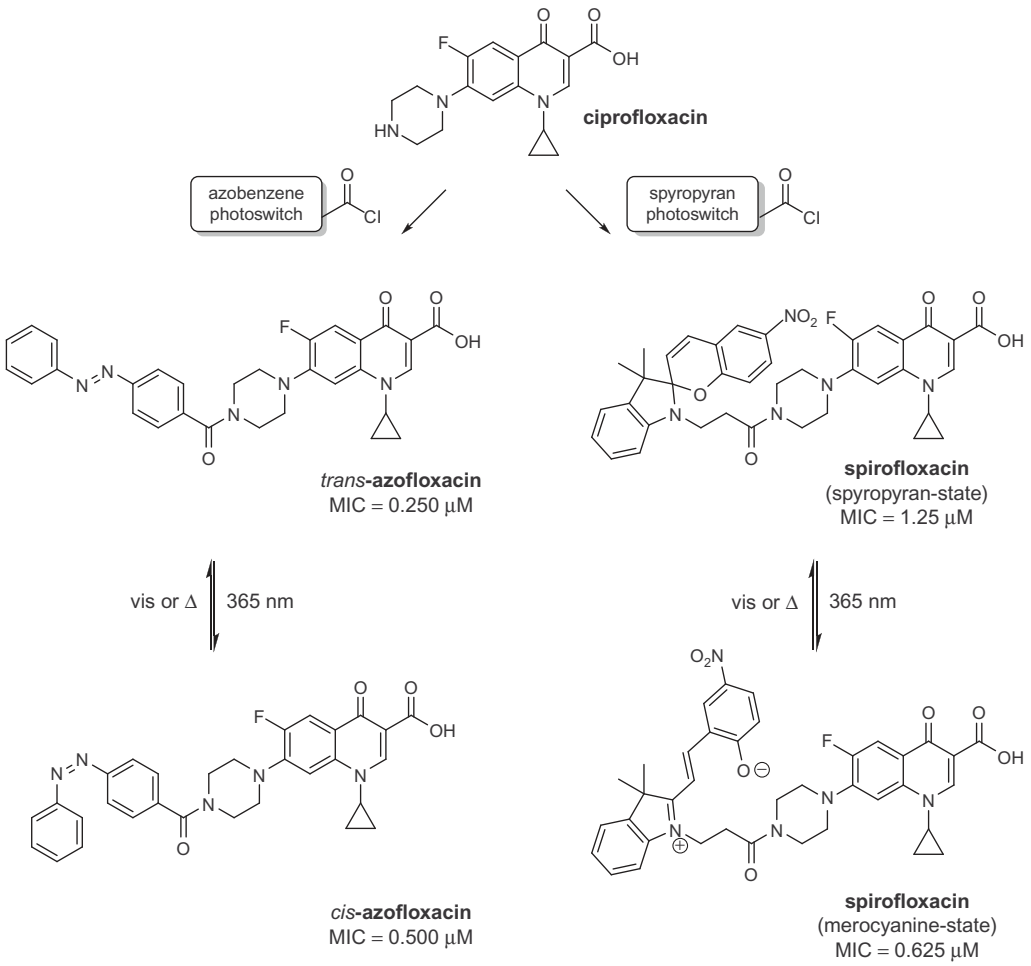

FIGURE 11-25 Single-step synthesis of azofloxacin and spirofloxacin from commercially available antibacterial fluoroquinolones. Both azofloxacin and spirofloxacin show light-dependent changes in minimum inhibitory concentration (MIC).

which renders HDAC inhibitors attractive as anticancer agents.[80] Inspired by the clinically approved drug vorinostat (suberoylanilide hydroxamic acid, SAHA) Feringa and coworkers developed a potential chemotherapeutical agent activated by light.[81] The photoswitchable molecule was designed by replacing the aliphatic linker between the cap moiety and the hydroxamic acid of SAHA. In this case, the aliphatic chain is not necessarily a bioisoster for azobenzene but the lipophilic properties are comparable and as a result the azobenzene moiety did not comprise HDAC inhibitory activity. The compound demonstrated high potency and marked difference between the isomers. Notably, the inhibitory effect is achieved with the thermally less stable *cis*-inhibitor, which enables local activation of the drug without systemic side effects.

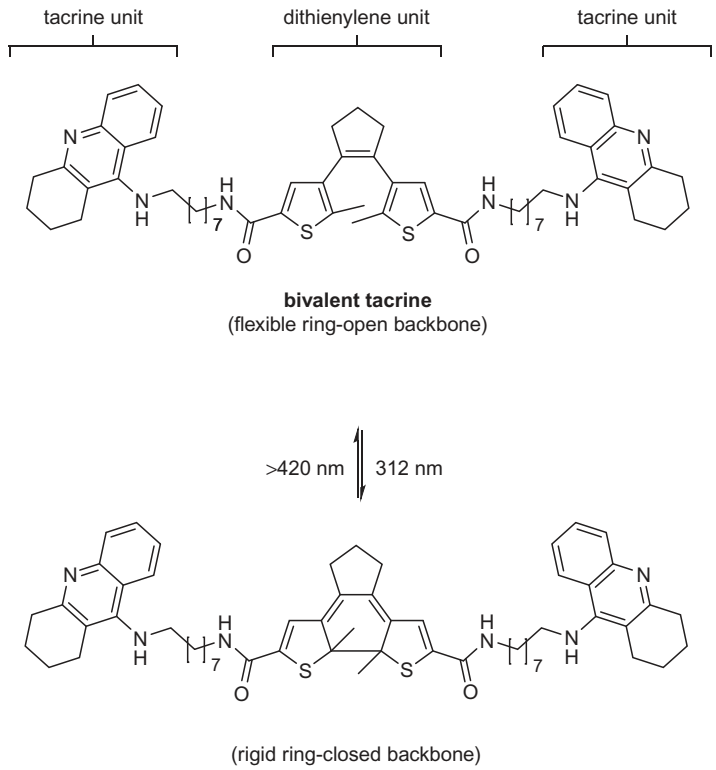

FIGURE 11-26 Light-induced ring closure of the dithienylene-based bivalent tacrine photoswitch.

11.5.3.4 RET Kinase

So-called "rearranged during transfection" (RET) kinases are transmembrane tyrosine kinases and play a pivotal role in the regular development and maintenance of neurons of the central and peripheral nervous system. Thyroid cancer is related to deregulation of RET and hyperactivity of RET kinases. As such they are appealing therapeutic targets for photopharmacology. Photoswitchable RET kinase inhibitors could also be a research tool for resolving quantitative and dynamic aspects of kinase signal transduction. In 2014 Grøtli and coworkers reported the first photoswitchable RET kinase inhibitor with excellent switching properties, stability, and significant difference in inhibitory effect for distinct isomers in live-cell assays (Fig. 11-27).[82] Based on the pyrazolo-pyrimidine RET kinase inhibitor, which displayed good kinase inhibition and selectivity in vitro, the photochromic variation was synthesized. Remarkably, the compound was extended to arylazopyrazole, instead of the usual azobenzene, inspired by the pyrazole group of the parent inhibitor. Arylazopyrazoles, a novel class of five-membered azo-photoswitches, are known to offer quantitative photoswitching and a high percentage of PSS for the isomers.[83] For the new

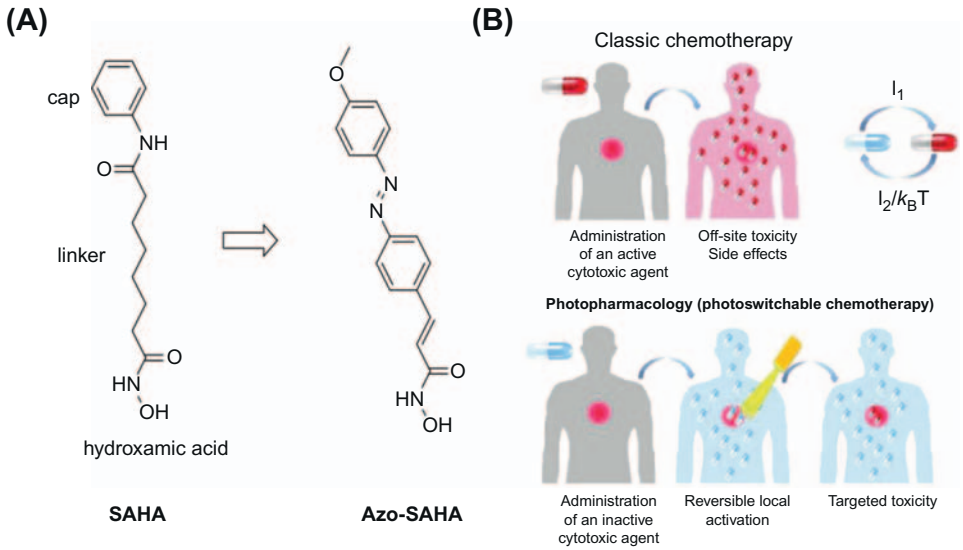

FIGURE 11-27 (A) Compound designed from SAHA anticancer agent. (B) Principle of photoswitchable chemotherapy.

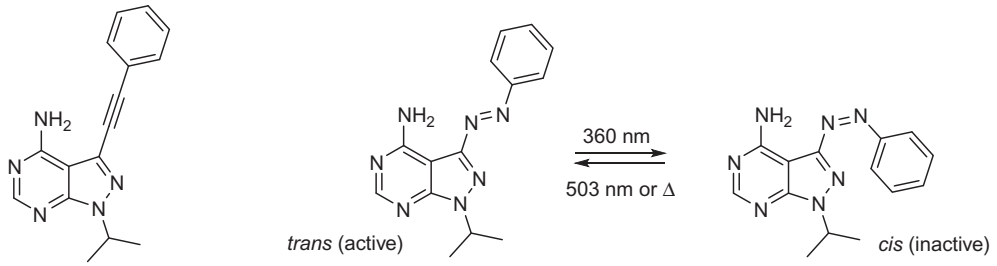

FIGURE 11-28 Arylazopyrazole RET kinase inhibitor based on the potent pyrazole-pyrimidine RET kinase inhibitor.

photoswitch a PSS of 87% for the *cis*-isomer was reached using 365 nm light (determined by HPLC analysis) (Fig. 11-28).

11.6 Conclusion

Light is a fascinating phenomenon that determines life on earth and is responsible for environmental interactions through photochemical reactions such as in vision, photosynthesis, and plant growth. Its bioorthogonality and spatiotemporal resolution are two major advantages that render it suitable to trigger biological functions. Photochromic hybrid compounds make it possible to control and regulate biological processes related to a large number of

diseases with light. This emerging field, often called photopharmacology, attracts the attention of the research community and is far from being overexploited.

Photoswitches, such as azobenzenes, dithienylethenes, and spyropyrans, are the key elements, as they reversibly change their structure upon irradiation resulting in a change of the physicochemical properties (polarity, geometry). Hence, molecular hybridization of photoswitches with pharmacophores provides photochromic hybrid compounds that can toggle between two distinct states depending on the wavelength of light. This photo-induced isomerization may be translated into a change in efficacy and/or activity of drugs, enabling remote control of the respective biological function.

However, photopharmacology is still confined by significant factors. To date, with a few exceptions, high-energy UV light is required for isomerization, which can cause severe damage to tissue and penetrate only partially through most media, which limits therapeutic application as well. Preferably molecular photoswitches are needed that may exhibit photoisomerization in a visible region of the electromagnetical spectrum and that increase the thermal stability of the less stable photoisomer. Obviously, photoisomerization should not be associated with toxicity.

Another major concern is light delivery. Therapeutic targets, such as ion channels, receptors, and enzymes, can only be addressed with photoswitchable ligands if they are accessible by light. In contrast to exposed regions, i.e., skin and eyes, deeper organs are only accessible through more or less invasive incisions and operations.

The design and development of novel light-sensitive compounds is limited by the ability to render them photoresponsive, which is also called photodruggability. Based on a rational approach two main strategies have been developed. The “azologization approach” employs bioisosteres of the azobenzene chromophore (azosteres) and enables rational replacement of sterically and electronically similar moieties. On the other hand, azobenzenes can be attached to certain substituents of the drug, i.e., phenyl rings and other aromatic systems without abrogating the pharmacological activity giving rise to the “azo-extension approach.”

Currently, this field is rapidly expanding and is already featuring valuable breakthroughs in CNS research, cancer chemotherapy, diabetes, antimicrobial agents, and vision restoration in the first step, and other applications will likely follow in the near future. It has to be kept in mind that in vitro studies in suitable assays can easily provide a proof-of-concept, but high affinity and selectivity plus easy switching with high spatiotemporal resolution in an in vivo setting is far more difficult to achieve. Now that the foundations has been laid, researchers will need persistence in the evaluation of the right targets and the design of novel PCLs, but in the end photoswitchable hybrid compounds might find their way in clinical application.

References

1. Deisseroth, K. Optogenetics. *Nat. Methods* **2011**, *8*, 26−29.
2. Dugué, G. P.; Akemann, W.; Knöpfel, T. A Comprehensive Concept of Optogenetics. *Prog. Brain Res.* **2012**, *196*, 1−28.

3. Song, C.; Knöpfel, T. Optogenetics Enlightens Neuroscience Drug Discovery. *Nat. Rev. Drug Discov.* **2016**, *15*, 97−109.
4. Peron, S.; Svoboda, K. From Cudgel to Scalpel: Toward Precise Neural Control with Optogenetics. *Nat. Methods* **2011**, *8*, 30−34.
5. Fehrentz, T.; Schönberger, M.; Trauner, D. Optochemical Genetics. *Angew. Chem. Int. Ed.* **2011**, *50*, 12156−12182.
6. Gorostiza, P.; Volgraf, M.; Numano, R.; Szobota, S.; Trauner, D.; Isacoff, E. Y. Mechanisms of Photoswitch Conjugation and Light Activation of an Ionotropic Glutamate Receptor. *Proc. Natl. Acad. Sci. U.S.A.* **2007**, *104*, 10865−10870.
7. Ellis-Davies, Graham C R Caged Compounds: Photorelease Technology for Control of Cellular Chemistry and Physiology. *Nat. Methods* **2007**, *4*, 619−628.
8. Lee, H.-M.; Larson, D. R.; Lawrence, D. S. Illuminating the Chemistry of Life: Design, Synthesis, and Applications of "caged" and Related Photoresponsive Compounds. *ACS Chem. Biol.* **2009**, *4*, 409−427.
9. Kaplan, J. H.; Forbush, B.; Hoffman, J. F. Rapid Photolytic Release of Adenosine 5'-Triphosphate from a Protected Analog: Utilization by the Sodium: Potassium Pump of Human Red Blood Cell Ghosts. *Biochemistry* **1978**, *17*, 1929−1935.
10. Engels, J.; Schlaeger, E. Juergen Synthesis, Structure, and Reactivity of Adenosine Cyclic 3',5'-phosphate-benzyltriesters. *J. Med. Chem.* **1977**, *20*, 907−911.
11. Wieboldt, R.; Gee, K. R.; Niu, L.; Ramesh, D.; Carpenter, B. K.; Hess, G. P. Photolabile Precursors of Glutamate: Synthesis, Photochemical Properties, and Activation of Glutamate Receptors on a Microsecond Time Scale. *Proc. Natl. Acad. Sci. U.S.A.* **1994**, *91*, 8752−8756.
12. Bérubé, G. An Overview of Molecular Hybrids in Drug Discovery. *Expert Opin. Drug Discov.* **2016**, *11*, 281−305.
13. Volgraf, M.; Gorostiza, P.; Szobota, S.; Helix, M. R.; Isacoff, E. Y.; Trauner, D. Reversibly Caged Glutamate: A Photochromic Agonist of Ionotropic Glutamate Receptors. *J. Am. Chem. Soc.* **2007**, *129*, 260−261.
14. Bouas-Laurent, H.; Dürr, H. Organic Photochromism (IUPAC Technical Report). *Pure Appl. Chem.* **2001**, *73*, 639−665.
15. Broichhagen, J.; Frank, J. A.; Trauner, D. A Roadmap to Success in Photopharmacology. *Acc. Chem. Res.* **2015**, *48*, 1947−1960.
16. Velema, W. A.; Szymanski, W.; Feringa, B. L. Photopharmacology: Beyond Proof of Principle. *J. Am. Chem. Soc.* **2014**, *136*, 2178−2191.
17. Natali, M.; Giordani, S. Molecular Switches as Photocontrollable "smart" Receptors. *Chem. Soc. Rev.* **2012**, *41*, 4010−4029.
18. Bléger, D.; Hecht, S. Visible-light-activated Molecular Switches. *Angew. Chem. Int. Ed.* **2015**, *54*, 11338−11349.
19. Okada, T.; Sugihara, M.; Bondar, A.-N.; Elstner, M.; Entel, P.; Buss, V. The Retinal Conformation and its Environment in Rhodopsin in Light of a New 2.2 A Crystal Structure. *J. Mol. Biol.* **2004**, *342*, 571−583.
20. Britz, S. J.; Galston, A. W. Physiology of Movements in the Stems of Seedling Pisum Sativum L. cv Alaska. *Plant Physiol.* **1983**, *71*, 313−318.
21. Briggs, W. R.; Christie, J. M.; Salomon, M. Phototropins: A New Family of Flavin-binding Blue Light Receptors in Plants. *Antioxid. Redox Signal.* **2001**, *3*, 775−788.
22. Ko, W.-H.; Nash, A. I.; Gardner, K. H. A Lovely View of Blue Light Photosensing. *Nat. Chem. Biol.* **2007**, *3*, 372−374.
23. Szymański, W.; Beierle, J. M.; Kistemaker. Hans, A. V.; Velema, W. A.; Feringa, B. L. Reversible Photocontrol of Biological Systems by the Incorporation of Molecular Photoswitches. *Chem. Rev.* **2013**, *113*, 6114−6178.

24. Irie, M.; Fukaminato, T.; Matsuda, K.; Kobatake, S. Photochromism of Diarylethene Molecules and Crystals: Memories, Switches, and Actuators. *Chem. Rev.* **2014**, *114*, 12174−12277.
25. Hamon, F.; Djedaini-Pilard, F.; Barbot, F.; Len, C. Azobenzenes—Synthesis and Carbohydrate Applications. *Tetrahedron Lett.* **2009**, *65*, 10105−10123.
26. Hartly, G. S. The Cis-form of Azobenzene. *Nature* **1937**, *140*, 281.
27. Merino, E. Synthesis of Azobenzenes: The Coloured Pieces of Molecular Materials. *Chem. Soc. Rev.* **2011**, *40*, 3835−3853.
28. Zhao, R.; Tan, C.; Xie, Y.; Gao, C.; Liu, H.; Jiang, Y. One Step Synthesis of Azo Compounds from Nitroaromatics and Anilines. *Tetrahedron Lett.* **2011**, *52*, 3805−3809.
29. Haghbeen, K.; Tan, E. Wui Facile Synthesis of Catechol Azo Dyes. *J. Org. Chem.* **1998**, *63*, 4503−4505.
30. Wang, M.; Funabiki, K.; Matsui, M. Synthesis and Properties of bis(hetaryl)azo Dyes. *Dyes Pigm.* **2003**, *57*, 77−86.
31. Davey, M. H.; Lee, V. Y.; Miller, R. D.; Marks, T. J. Synthesis of Aryl Nitroso Derivatives by Tert-butyl Hypochlorite Oxidation in Homogeneous Media. Intermediates for the Preparation of High-hyperpolarizability Chromophore Skeletons. *J. Org. Chem.* **1999**, *64*, 4976−4979.
32. Entwistle, I. D.; Gilkerson, T.; Johnstone, R. A. W.; Telford, R. P. Rapid Catalytic Transfer Reduction of Aromatic Nitro Compounds to Hydroxylamines. *Tetrahedron Lett.* **1978**, *34*, 213−215.
33. Haworth, R. Downs. Lapworth, A. LXXXV.—Reduction of Emulsified Nitro-Compounds. Part II. Some Extensions of the Method. *J. Chem. Soc. Trans.* **1921**, *119*, 768−777.
34. Ibne-Rasa, K. M.; Lauro, C. G.; Edwards, J. O. Mechanism of the Oxidation of Nitrosobenzenes by Peroxoacetic Acid. *J. Am. Chem. Soc.* **1963**, *85*, 1165−1167.
35. Bleasdale, C.; Ellis, M. K.; Farmer, P. B.; Golding, B. T.; Handley, K. F.; Jones, P., et al. Synthesis and Spectroscopic Characterisation of 3-chloroperbenzoic Acid-17O,18O, Nitrosobenzene-17O,18O and Nitrosobenzene-15N. *J. Labelled Comp. Radiopharm.* **1993**, *33*, 739−746.
36. Gowenlock, B. G.; Richter-Addo, G. B. Preparations of C-nitroso Compounds. *Chem. Rev.* **2004**, *104*, 3315−3340.
37. Yu, B.-C.; Shirai, Y.; Tour, J. M. Syntheses of New Functionalized Azobenzenes for Potential Molecular Electronic Devices. *Tetrahedron Lett.* **2006**, *62*, 10303−10310.
38. Namiki, K.; Sakamoto, A.; Murata, M.; Kume, S.; Nishihara, H. Reversible Photochromism of a Ferrocenylazobenzene Monolayer Controllable by a Single Green Light Source. *Chem. Commun.* **2007,** 4650−4652.
39. Mori, Y.; Niwa, T.; Toyoshi, K. Carcinogenic Azo Dyes. XVIII. Syntheses of Azo Dyes Related to 3′-hydroxymethyl-4-(dimethylamino) Azobenzene, a New Potent Pepatocarcinogen. *Chem. Pharm. Bull.* **1981**, *5*, 1439−1442.
40. Lim, Y.-K.; Lee, K.-S.; Cho, C.-G. Novel Route to Azobenzenes via Pd-catalyzed Coupling Reactions of Aryl Hydrazides with Aryl Halides, Followed by Direct Oxidations. *Org. Lett.* **2003**, *5*, 979−982.
41. Dong, M.; Babalhavaeji, A.; Samanta, S.; Beharry, A. A.; Woolley, G. Red-shifting Azobenzene Photoswitches for In Vivo Use. *Acc. Chem. Res.* **2015**, *48*, 2662−2670.
42. Irie, M. Diarylethenes for Memories and Switches. *Chem. Rev.* **2000**, *100*, 1685−1716.
43. Warford, C. Chad; Carling, C?-J.; Branda, N. R. From Slow to Fast−The User Controls the Rate of the Release of Molecules from Masked forms Using a Photoswitch and Different Types of Light. *Chem. Commun.* **2015**, *51*, 7039−7042.
44. Schoenberger, M.; Damijonaitis, A.; Zhang, Z.; Nagel, D.; Trauner, D. Development of a New Photochromic Ion Channel Blocker via Azologization of Fomocaine. *ACS Chem. Neurosci.* **2014**, *5*, 514−518.
45. Stein, M.; Middendorp, S. J.; Carta, V.; Pejo, E.; Raines, D. E.; Forman, S. A., et al. Azo-propofols: Photochromic Potentiators of GABA(A) Receptors. *Angew. Chem. Int. Ed.* **2012**, *51*, 10500−10504.

46. Broichhagen, J.; Jurastow, I.; Iwan, K.; Kummer, W.; Trauner, D. Optical Control of Acetylcholinesterase with a Tacrine Switch. *Angew. Chem. Int. Ed.* **2014**, *53*, 7657−7660.
47. Overington, J. P.; Al-Lazikani, B.; Hopkins, A. L. How Many Drug Targets are there? *Nat. Rev. Drug Discov.* **2006**, *5*, 993−996.
48. Banghart, M.; Borges, K.; Isacoff, E.; Trauner, D.; Kramer, R. H. Light-Activated Ion Channels for Remote Control of Neuronal Firing. *Nat. Neurosci.* **2004**, *7*, 1381−1386.
49. Broichhagen, J.; Schönberger, M.; Cork, S. C.; Frank, J. A.; Marchetti, P.; Bugliani, M., et al. Optical Control of Insulin Release Using a Photoswitchable Sulfonylurea. *Nat. Commun.* **2014**, *5*, 1−11.
50. Polosukhina, A.; Litt, J.; Tochitsky, I.; Nemargut, J.; Sychev, Y.; Kouchkovsky, I., et al. Photochemical Restoration of Visual Responses in Blind Mice. *Neuron* **2012**, *75*, 271−282.
51. Hansen, M. J.; Velema, W. A.; Bruin, G. de; Overkleeft, H. S.; Szymanski, W.; Feringa, B. L. Proteasome Inhibitors with Photocontrolled Activity. *ChemBioChem* **2014**, *15*, 2053−2057.
52. Borowiak, M.; Nahaboo, W.; Reynders, M.; Nekolla, K.; Jalinot, P.; Hasserodt, J., et al. Photoswitchable Inhibitors of Microtubule Dynamics Optically Control Mitosis and Cell Death. *Cell* **2015**, *162*, 403−411.
53. Lerch, M. M.; Hansen, M. J.; van Dam. Gooitzen, M.; Szymanski, W.; Feringa, B. L. Emerging Targets in Photopharmacology. *Angew. Chem. Int. Ed.* **2016**, *55*, 10978−10999.
54. Camerino, D. Conte. Tricarico, D.; Desaphy, J.-F. Ion Channel Pharmacology. *Neurotherapeutics* **2007**, *4*, 184−198.
55. Kramer, R. H.; Mourot, A.; Adesnik, H. Optogenetic Pharmacology for Control of Native Neuronal Signaling Proteins. *Nat. Neurosci.* **2013**, *16*, 816−823.
56. Mourot, A.; Tochitsky, I.; Kramer, R. H. Light at the End of the Channel: Optical Manipulation of Intrinsic Neuronal Excitability with Chemical Photoswitches. *Front. Mol. Neurosci.* **2013**, *6*, 1−15.
57. Banghart, M. R.; Mourot, A.; Fortin, D. L.; Yao, J. Z.; Kramer, R. H.; Trauner, D. Photochromic Blockers of Voltage-Gated Potassium Channels. *Angew. Chem. Int. Ed.* **2009**, *48*, 9097−9101.
58. Mourot, A.; Kienzler, M. A.; Banghart, M. R.; Fehrentz, T.; Huber, Florian M. E.; Stein, M., et al. Tuning Photochromic Ion Channel Blockers. *ACS Chem. Neurosci.* **2011**, *2*, 536−543.
59. Stawski, P.; Sumser, M.; Trauner, D. A Photochromic Agonist of AMPA Receptors. *Angew. Chem. Int. Ed.* **2012**, *51*, 5748−5751.
60. Laprell, L.; Hüll, K.; Stawski, P.; Schön, C.; Michalakis, S.; Biel, M., et al. Restoring Light Sensitivity in Blind Retinae Using a Photochromic AMPA Receptor Agonist. *ACS Chem. Neurosci.* **2016**, *7*, 15−20.
61. Laprell, L.; Repak, E.; Franckevicius, V.; Hartrampf, F.; Terhag, J.; Hollmann, M., et al. Optical Control of NMDA Receptors with a Diffusible Photoswitch. *Nat. Commun.* **2015**, *6*, 1−11.
62. Damijonaitis, A.; Broichhagen, J.; Urushima, T.; Hüll, K.; Nagpal, J.; Laprell, L., et al. AzoCholine Enables Optical Control of Alpha 7 Nicotinic Acetylcholine Receptors in Neural Networks. *ACS Chem. Neurosci.* **2015**, *6*, 701−707.
63. Broichhagen, J.; Frank, J. A.; Johnston, N. R.; Mitchell, R. K.; Šmid, K.; Marchetti, P., et al. A Red-shifted Photochromic Sulfonylurea for the Remote Control of Pancreatic Beta Cell Function. *Chem. Commun.* **2015**, *51*, 6018−6021.
64. Barber, D. M.; Schönberger, M.; Burgstaller, J.; Levitz, J.; Weaver, C. D.; Isacoff, E. Y., et al. Optical Control of Neuronal Activity Using a Light-Operated GIRK Channel Opener (LOGO). *Chem. Sci.* **2016**, *7*, 2347−2352.
65. Stein, M.; Breit, A.; Fehrentz, T.; Gudermann, T.; Trauner, D. Optical Control of TRPV1 Channels. *Angew. Chem. Int. Ed.* **2013**, *52*, 9845−9848.
66. Syrovatkina, V.; Alegre, K. O.; Dey, R.; Huang, X.-Y. Regulation, Signalling, and Physiological Functions of G-proteins. *J. Mol. Biol.* **2016,** 1−19.
67. Oldham, W. M.; Hamm, H. E. Heterotrimeric G Protein Activation by G-protein-coupled Receptors. *Nat. Rev. Mol. Cell Biol.* **2008**, *9*, 60−71.

68. Pittolo, S.; Gómez-Santacana, X.; Eckelt, K.; Rovira, X.; Dalton, J.; Goudet, C., et al. An Allosteric Modulator to Control Endogenous G Protein-coupled Receptors with Light. *Nat. Chem. Biol.* **2014**, *10*, 813−815.
69. Rovira, X.; Trapero, A.; Pittolo, S.; Zussy, C.; Faucherre, A.; Jopling, C., et al. OptoGluNAM4.1, a Photoswitchable Allosteric Antagonist for Real-time Control of mGlu4 Receptor Activity. *Cell Chem. Biol.* **2016**, *23*, 929−934.
70. Bahamonde, M. I.; Taura, J.; Paoletta, S.; Gakh, A. A.; Chakraborty, S.; Hernando, J., et al. Photomodulation of G Protein-coupled Adenosine Receptors by a Novel Light-switchable Ligand. *Bioconjugate Chem.* **2014**, *25*, 1847−1854.
71. Schönberger, M.; Trauner, D. A Photochromic Agonist for μ-opioid Receptors. *Angew. Chem. Int. Ed.* **2014**, *53*, 3264−3267.
72. Schomburg, I.; Chang, A.; Placzek, S.; Söhngen, C.; Rother, M.; Lang, M., et al. BRENDA in 2013: Integrated Reactions, Kinetic Data, Enzyme Function Data, Improved Disease Classification: New Options and Contents in BRENDA. *Nucleic Acids Res.* **2013**, *41*, 764−772.
73. Reisinger, B.; Kuzmanovic, N.; Löffler, P.; Merkl, R.; König, B.; Sterner, R. Exploiting Protein. Symmetry to Design Light-Controllable Enzyme Inhibitors. *Angew. Chem. Int. Ed.* **2014**, *53*, 595−598.
74. Karlsson, C.; Blom, M.; Johansson, M.; Jansson, A. M.; Scifo, E.; Karlén, A., et al. Phototriggerable Peptidomimetics for the Inhibition of Mycobacterium Tuberculosis Ribonucleotide Reductase by Targeting Protein-protein Binding. *Org. Biomol. Chem.* **2015**, *13*, 2612−2621.
75. Velema, W. A.; van der Berg, J. P.; Hansen, M. J.; Szymanski, W.; Driessen, Arnold J. M.; Feringa, B. L. Optical Control of Antibacterial Activity. *Nat. Chem.* **2013**, *5*, 924−928.
76. Velema, W. A.; Hansen, M. J.; Lerch, M. M.; Driessen, Arnold, J. M.; Szymanski, W.; Feringa, B. L. Ciprofloxacin-photoswitch Conjugates: A Facile Strategy for Photopharmacology. *Bioconjugate Chem.* **2015**, *26*, 2592−2597.
77. Chen, X.; Wehle, S.; Kuzmanovic, N.; Merget, B.; Holzgrabe, U.; König, B., et al. Acetylcholinesterase Inhibitors with Photoswitchable Inhibition of β-amyloid Aggregation. *ACS Chem. Neurosci.* **2014**, *5*, 377−389.
78. Bartolini, M.; Bertucci, C.; Cavrini, V.; Andrisano, V. β-Amyloid Aggregation Induced by Human Acetylcholinesterase: Inhibition Studies. *Biochem. Pharmacol.* **2003**, *65*, 407−416.
79. García-Ayllón, M.-S.; Small, D. H.; Avila, J.; Sáez-Valero, J. Revisiting the Role of Acetylcholinesterase in Alzheimer's Disease: Cross-Talk with P-tau and β-Amyloid. *Front. Mol. Neurosci.* **2011**, *4*, 1−9.
80. Ropero, S.; Esteller, M. The Role of Histone Deacetylases (HDACs) in Human Cancer. *Mol. Oncol.* **2007**, *1*, 19−25.
81. Szymanski, W.; Ourailidou, M. E.; Velema, W. A.; Dekker, F. J.; Feringa, B. L. Light-controlled Histone Deacetylase (HDAC) Inhibitors: Towards Photopharmacological Chemotherapy. *Chemistry* **2015**, *21*, 16517−16524.
82. Ferreira, R.; Nilsson, J. R.; Solano, C.; Andréasson, J.; Grøtli, M. Design, Synthesis and Inhibitory Activity of Photoswitchable RET Kinase Inhibitors. *Sci. Rep.* **2015**, *5*, 1−8.
83. Weston, C. E.; Richardson, R. D.; Haycock, P. R.; White, Andrew, J. P.; Fuchter, M. J. Arylazopyrazoles: Azoheteroarene Photoswitches Offering Quantitative Isomerization and Long Thermal Half-lives. *J. Am. Chem. Soc.* **2014**, *136*, 11878−11881.

Appendix II:

Agnetta, L.; Kauk, M.; Canizal, M. C. A.; Messerer, R.; Holzgrabe, U.; Hoffmann, C.; Decker, M., A Photoswitchable Dualsteric Ligand Controlling Receptor Efficacy. *Angew. Chem. Int. Ed.* **2017,** *56*, 7282-7287.

https://onlinelibrary.wiley.com/doi/abs/10.1002/anie.201701524

Photopharmacology

International Edition: DOI: 10.1002/anie.201701524
German Edition: DOI: 10.1002/ange.201701524

A Photoswitchable Dualsteric Ligand Controlling Receptor Efficacy

Luca Agnetta[+], Michael Kauk[+], Maria Consuelo Alonso Canizal, Regina Messerer, Ulrike Holzgrabe, Carsten Hoffmann,* and Michael Decker**

Abstract: *The investigation of the mode and time course of the activation of G-protein-coupled receptors (GPCRs), in particular muscarinic acetylcholine (mACh or M) receptors, is still in its infancy despite the tremendous therapeutic relevance of M receptors and GPCRs in general. We herein made use of a dualsteric ligand that can concomitantly interact with the orthosteric, that is, the neurotransmitter, binding site and an allosteric one. We synthetically incorporated a photoswitchable (photochromic) azobenzene moiety. We characterized the photophysical properties of this ligand called BQCAAI and investigated its applicability as a pharmacological tool compound with a set of FRET techniques at the M_1 receptor. BQCAAI proved to be an unprecedented molecular tool; it is the first photoswitchable dualsteric ligand, and its activity can be regulated by light. We also applied BQCCAI to investigate the time course of several receptor activation processes.*

The activity of numerous nervous processes in the human body, such as smooth-muscle contraction, the cardiac rate and force, and glandular secretion, is regulated by the peripheral nervous system, and its parasympathetic nerves are regulated by muscarinic acetylcholine receptors (mAChRs) through the metabotropic action of acetylcholine (ACh).[1] Hence, these receptors have been identified and utilized as therapeutic targets for the treatment of a broad spectrum of diseases.[2]

mAChRs belong to the class A family of G-protein-coupled receptors (GPCRs) and comprise five distinct subtypes.[3] M_1 receptors are abundantly expressed in the cortex, hippocampus, and striatum and play a key role in learning and memory processes. Agonists have been suggested for the treatment of cognitive impairment such as that associated with schizophrenia and Alzheimer's disease (AD).[4] Unfortunately, the tremendous efforts to develop therapeutically applicable selective M_1 ligands have not been successful owing to the high sequence homology of the orthosteric binding sites, that is, the binding sites of ACh. Owing to the plethora of very diverse physiological roles associated with the five mAChR subtypes, the lack of selectivity led to numerous side effects for the experimental therapeutics. As numerous details of the molecular basis of receptor function remain to be elucidated, suitable molecular tools are necessary.

The less conserved allosteric binding sites of the M receptors, including M_1, led to intensive efforts to develop selective allosteric modulators, that is, compounds that affect the binding of an orthosteric ligand or the endogenous neurotransmitter ACh either positively, neutrally, or negatively (Figure 1).[5] Such ligands are able to overcome the problem of subtype selectivity for the M_1 subtype by making use of cooperativity in the selective binding and activation of the receptor.[6]

To take this concept one step further, dualsteric (or bitopic) ligands are developed herein that covalently connect a high-affinity/low-selectivity orthosteric moiety to highly selective allosteric building blocks for concomitant interac-

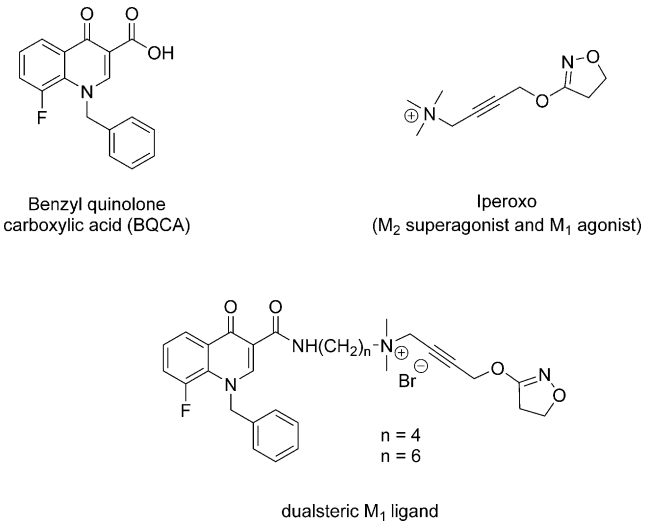

Figure 1. Structures of the non-selective M_1 agonist iperoxo, the positive allosteric modulator (PAM) benzyl quinolone carboxylic acid (BQCA), and a representative dualsteric M_1 ligand consisting of the two building blocks.

[*] L. Agnetta,[+] R. Messerer, Prof. Dr. U. Holzgrabe, Prof. Dr. M. Decker
Pharmaceutical and Medicinal Chemistry
Institute of Pharmacy and Food Chemistry
Julius Maximilian University of Würzburg
Am Hubland, 97074 Würzburg (Germany)
E-mail: ulrike.holzgrabe@uni-wuerzburg.de
michael.decker@uni-wuerzburg.de

M. Kauk,[+] M. C. A. Canizal, Prof. Dr. C. Hoffmann
Department of Pharmacology and Toxicology
Julius Maximilian University of Würzburg
Versbacher Strasse 9, 97078 Würzburg (Germany)
E-mail: c.hoffmann@toxi.uni-wuerzburg.de

M. Kauk,[+] M. C. A. Canizal, Prof. Dr. C. Hoffmann
Rudolf Virchow Center for Experimental Biomedicine
Julius Maximilian University of Würzburg
Josef Schneider Strasse 2, 97080 Würzburg (Germany)

Prof. Dr. C. Hoffmann
Current address: Institute for Molecular Cell Biology
CMB—Center for Molecular Biomedicine
University Hospital Jena, Friedrich Schiller University Jena
Hans-Knöll-Strasse 2, 07745 Jena (Germany)

[+] These authors contributed equally to this work.

Supporting information and the ORCID identification number(s) for the author(s) of this article can be found under: https://doi.org/10.1002/anie.201701524.

tion with both binding sites. Recently, our groups have reported several sets of dualsteric M_1 and M_2 agonists for which dynamic ligand binding is assumed, leading to partial agonism for the M_1 receptor (Figure 1)[7] as well as for the M_2 receptor.[8]

Based on these findings, dualsteric ligands hold great potential both as future therapeutics and as pharmacological tools owing to their unprecedented selectivity at M receptor subtypes, their specificity for signaling pathways ("biased signaling"), their capability for partial agonism, and their potential for studying the process of receptor activation at the molecular level.[6,9] We have now made use of a photopharmacological approach by incorporating a photoswitchable (or photochromic) azobenzene as a linker into the dualsteric ligands described to specifically design dualsteric ligands for investigating spatiotemporal receptor activation processes with high precision.

The rapidly expanding field of photopharmacology aims to introduce light sensitivity into experimental therapeutics or drugs to control and/or investigate biological processes.[10] In this regard, molecular photoswitches that reversibly change their structure and physicochemical properties upon irradiation with light play an important role. The light-induced isomerization of the azobenzene photoswitch from the *trans* form to the thermodynamically less stable *cis* form is associated with significant changes in geometry and polarity.[11] When an azobenzene unit is incorporated into a bioactive compound, this change can be translated into an alteration in the biological activity towards the respective target.[12]

Following the design strategy for the dualsteric iperoxo/BQCA-type hybrids, we connected the superagonist iperoxo to a positive allosteric modulator with an *N*-benzyl quinolone carboxylic acid type structure. To directly investigate the effect of the spacer on the intrinsic activity of these hybrids at the M_1 receptor, we replaced the aliphatic carbon chain (polymethylene linker) with an azobenzene linker. Introducing the photoswitch into this part of the molecule should significantly change the relative position of the two pharmacophores, namely from a linear to a rectangular arrangement (Figure 2), and thus lead to a different binding mode.

Fluorescence detection and fluorescence resonance energy transfer (FRET) techniques are now well-established in pharmacological research for characterizing various processes,[13] such as receptor activation,[14] G-protein activation,[15] and arrestin signaling,[16] or further downstream detection of calcium, diacylglycerol (DAG), or cyclic AMP.[17] The advantage of such approaches compared to other methods is that they can be performed in living cells under almost physiological conditions.

Herein, we report the synthesis, characterization, and pharmacological testing of a benzyl quinolone carboxylic acid–azobenzene–iperoxo (**BQCAAI**) hybrid compound (Figure 2 and Scheme 1), which represents the first photoswitchable dualsteric ligand described to date. For comparison, we also synthesized a derivative with a benzene-containing alkyne linker (**18**; see the Supporting Information, Scheme S3) and photoiperoxo (Scheme S1), a photochromic iperoxo derivative, in which a hydrogen atom of a methyl

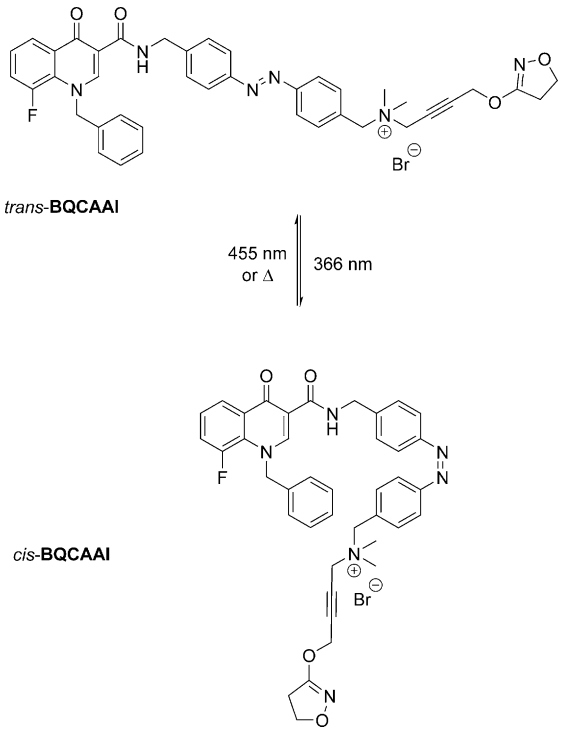

Figure 2. Structure of the photoswitchable dualsteric M_1 ligand **BQCAAI** in the *trans* and *cis* form.

group of the quaternary iperoxo ammonium salt has been replaced by an azobenzene moiety.

The synthesis of **BQCAAI** began with the construction of the quinolone skeleton through a microwave-assisted Gould–Jacobs reaction.[18] Benzylation and subsequent hydrolysis gave acid **4**, which reacted with 4-aminobenzylamine to form amide **5**. To introduce the azobenzene moiety into the target molecule, a Mills reaction was performed. The hydroxy function of the azobenzene compound was replaced by a bromine atom in an Appel reaction to give compound **6**. Finally, iperoxo, which had been synthesized using a convergent synthetic pathway,[19] was connected to the azobenzene group in a microwave-assisted reaction to afford the photoswitchable dualsteric ligand **BQCAAI** (Scheme 1).

As a prerequisite for the light-dependent control of the intrinsic activity (efficacy) at the human M_1 (hM_1) receptor, the photoswitchable compound needs to effectively respond to light. To this end, the structural change between the two photoisomers should be fast and significant, and a high degree of photoconversion (the *trans*/*cis* ratios should differ significantly) is necessary. Furthermore, the stability towards thermal isomerization as well as the intended pharmacological/biological applications have to be taken into account. First, **BQCAAI** was characterized by UV/Vis spectroscopy, which revealed clear photoswitchability (photochromic behavior) and the typical absorption bands of azobenzenes. The absorption maxima at around 325 nm and 430 nm are due to the π–π* and n–π* transitions, respectively, which allows for distinct photoswitching between the *trans* and *cis* forms. This process is reversible as switching can be repeated over many cycles without loss of photochromic behavior (Figures 3

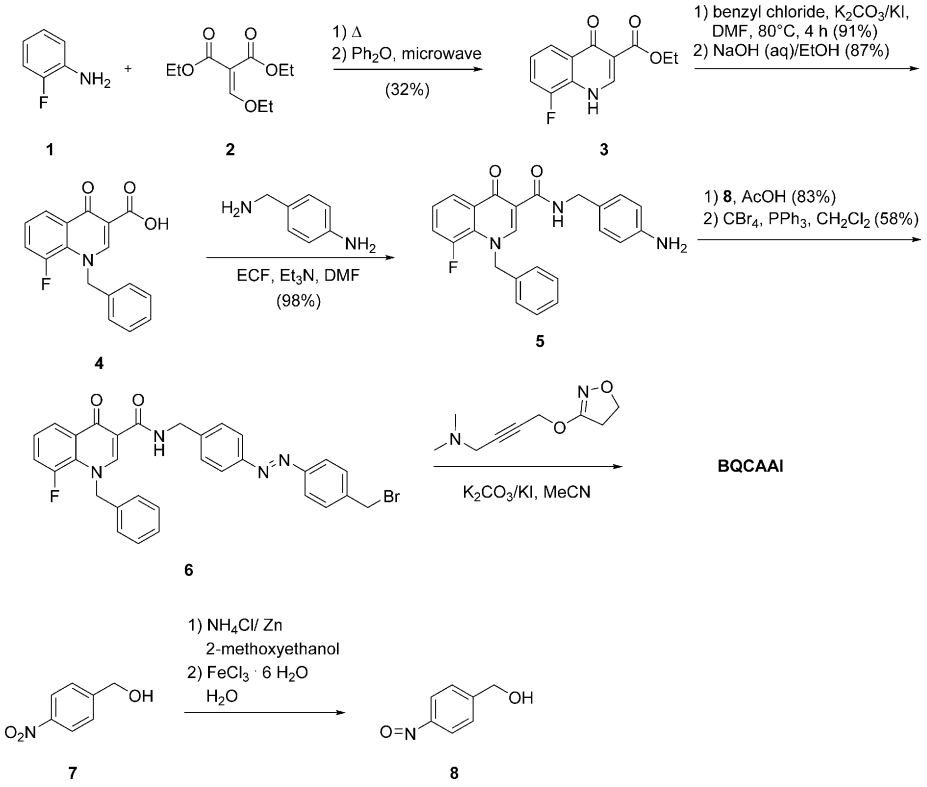

Scheme 1. Synthesis of the benzyl quinolone carboxylic acid–azobenzene–iperoxo hybrid **BQCAAI**.

and 4). Second, the photostationary distribution of **BQCAAI** in the dark was determined by HPLC analysis to be 80% in favor of the *trans* form (20% of the *cis* form). Upon irradiation with UV light ($\lambda = 365$ nm), the ratio changed to 52% in favor of the thermodynamically less stable *cis* isomer (Figure 4). Finally, **BQCAAI** shows excellent thermal stability. When the compound is kept in the dark, the photostationary state is stable for several hours after UV light irradiation (Figure S1).

For pharmacological characterization of **BQCAAI** and its individual building blocks, a range of different fluorescence or FRET methods were applied. The orthosteric building block iperoxo, a synthetic agonist for all mAChR subtypes,[20] was used as a reference for all experiments and showed full agonism ($EC_{50} = 0.57$ μM). In contrast, the azobenzene-modified iperoxo derivative (photoiperoxo) **12** was unable to induce conformational changes at the M_1 receptor, both in the *trans* and in the *cis* form (Figure S2a), which is in agreement with previous findings for the M_1 receptor, namely that increasing the linker length of iperoxo derivatives leads to antagonism at this receptor.[21] To evaluate the affinity of compound **12** to the receptor, a competition experiment was performed (Figure S2b). Iperoxo (10 μM solution) induced a 70% receptor response, and compound **12**, when applied alone, did not induce any conformational changes. When iperoxo and compound **12** were applied together, a signal reduction of on average 50% was observed, indicating that both ligands compete for binding at the receptor. From this experimental setting (see Ref. [21a]), we conclude that photoiperoxo must have a distinct affinity for the receptor and can be regarded as an antagonist. This was confirmed by studying the calcium release upon ligand binding (Figure S2c) with a calcium- and DAG-sensitive fluorescent probe. Whereas iperoxo induced a rapid calcium response, no calcium release was observed for compound **12**, even more than 250 s after application (Figure S2d). When compound **12** was first applied for 20 s followed by addition of iperoxo, an immediate calcium response was detectable for iperoxo (Figure S2e), clearly indicating that compound **12** does not exhibit agonism although binding to the receptor has been indirectly shown (Figure S2b).

The same setting was used for investigations with **BQCAAI**, which showed that both isomers interact with the M_1 receptor (Figure 4a). A receptor response of 25% for the *trans* form and a significantly reduced signal of 14% for the *cis* form were detected. Interestingly, the activation is slower than with iperoxo. Comparable results were obtained for derivative **18** (RM405) with a linear alkynylbenzene linker (Figure 4f),[21a] but the process was significantly slower than for related dualsteric ligands bearing a polymethylene linker. This finding suggests that the receptor activation kinetics of a dualsteric ligand and the structure of the linker moiety are closely related.

To gain further insight into the characteristic properties of *trans*- and *cis*-**BQCAAI** with respect to receptor agonism, G-protein activation was investigated using G-protein FRET sensors. As shown in Figure 4b, both isomers were able to induce a G-protein response. With regard to iperoxo, the *trans* isomer induced a more pronounced signal than the *cis* isomer.

However, both of these FRET sensors are excited at 436 nm, a wavelength that induces isomerization of the azobenzene moiety favoring the *trans* isomer. Given the rapid isomerization from the *cis* to the *trans* isomer (Figure 3b), we wanted to investigate if our detection system interferes with the true efficacy of the two ligand configurations owing to the slower kinetics of the G protein response compared to receptor activation. Repeating the experiment with a lower data sampling frequency (1 Hz, taking 1 data point every second, instead of 10 Hz, with taking data points every 100 ms) reduces the light exposure by 90% and should hence influence the *cis*-to-*trans* isomerization (Figure 4c). When the light exposure was reduced, Gq activation by the *trans* isomer was not affected, whereas the signal of the *cis* isomer was significantly reduced by more than 30%.

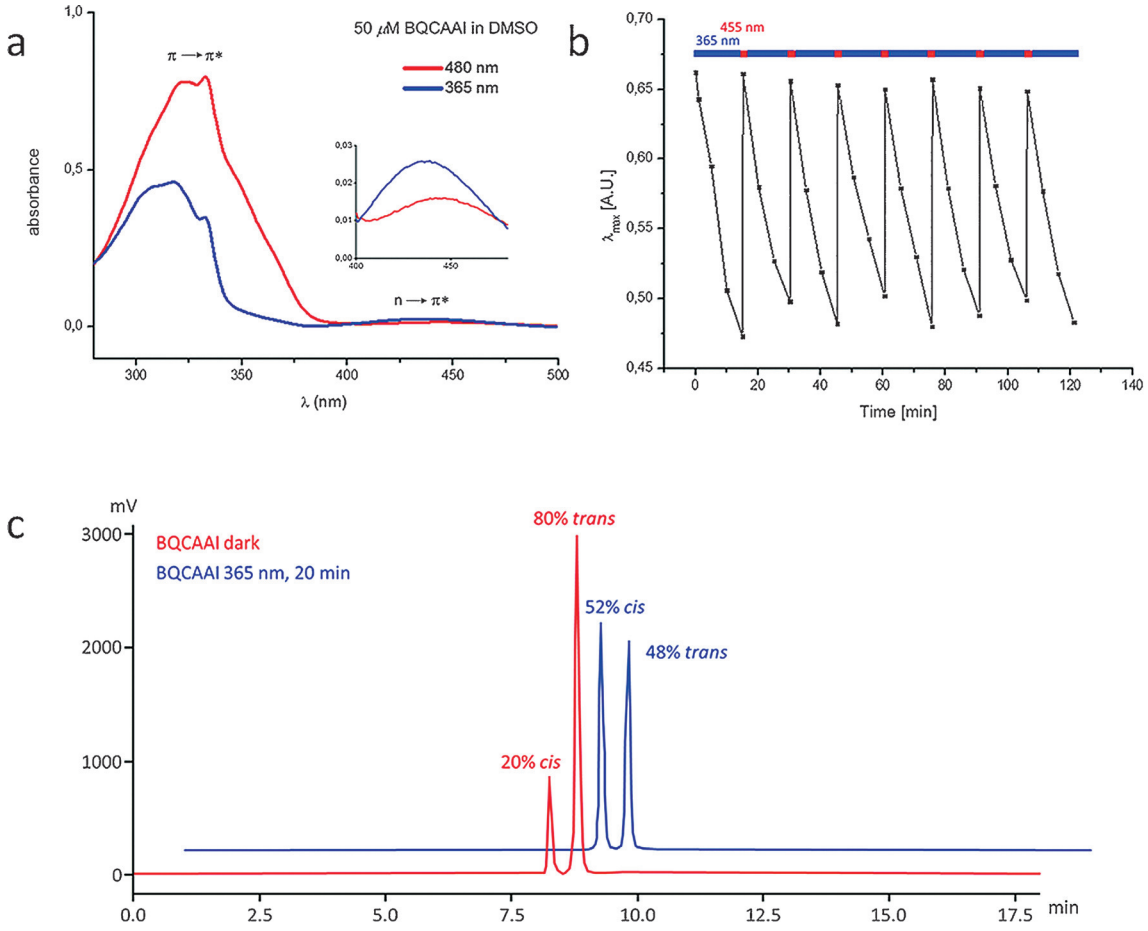

Figure 3. Photochemical characterization. a) Absorption spectra of **BQCAAI**, show distinct photochromic behavior. b) The photoswitching process can be repeated over many cycles without noticeable photofatigue. c) HPLC chromatogram of **BQCAAI** showing the photostationary states in the dark (red) and after irradiation with UV light (blue).

Subsequently, we used a dual Ca^{2+}/DAG fluorescent probe with 488 nm and 562 nm excitation wavelengths,[21a] which can be used simultaneously or separately, with the benefit that one excitation signal lies within the absorption spectrum of **BQCAAI** and the other one does not (Figure 3a). Monitoring calcium only without DAG for **BQCAAI** shows a fast signal for the *trans* isomer (Figure 4d, red trace) whereas the *cis* isomer does not induce a signal over more than 200 s (Figure 4e, red). Exciting both fluorescent probes simultaneously results in the same observation for the *trans* isomer (Figure 4d, green) but in an opposite result for the *cis* isomer (Figure S3), which induces both a calcium and a DAG response, but with a rather long time delay of 45 s. This behavior is likely due to an induced switching process by the light used for detection, which would allow for a certain proportion of the *cis*-**BQCAAI** to switch back to *trans*-**BQCAAI**. This assumption is strengthened by the absence of a calcium signal evoked by *cis*-**BQCAAI** when only the calcium signal is monitored without DAG detection (Figure 4e).

Taken together, we have clear evidence that **BQCAAI** is not only the first reported photoswitchable dualsteric ligand for GPCRs, but also the first "dimmable" one, in the sense that *cis*-**BQCAAI** acts as an antagonist while *trans*-**BQCAAI** is an agonist. We have shown that a direct detection system based on receptor conformational changes has an influence itself because of the current need for an excitation wavelength of 436 nm. The use of a dual Ca^{2+}/DAG sensor helped to overcome this problem. The receptor subtype selectivity of these ligands and the possible application of **BQCAAI** to investigate the receptor activation of other M subtypes are currently unclear and are subject to ongoing research.

Acknowledgements

L.A. and M.K. were supported by the International Doctoral Program "Receptor Dynamics: Emerging Paradigms for Novel Drugs" funded within the framework of the Elite Network of Bavaria. M.C.A.C. was supported by the Marie Curie Initial Training Network (ITN) "WntsApp" (Grant 608180). We thank Montana Molecular and in particular Dr. Anne Marie Quinn for technical support and help with the use of the dual sensor.

Conflict of interest

The authors declare no conflict of interest.

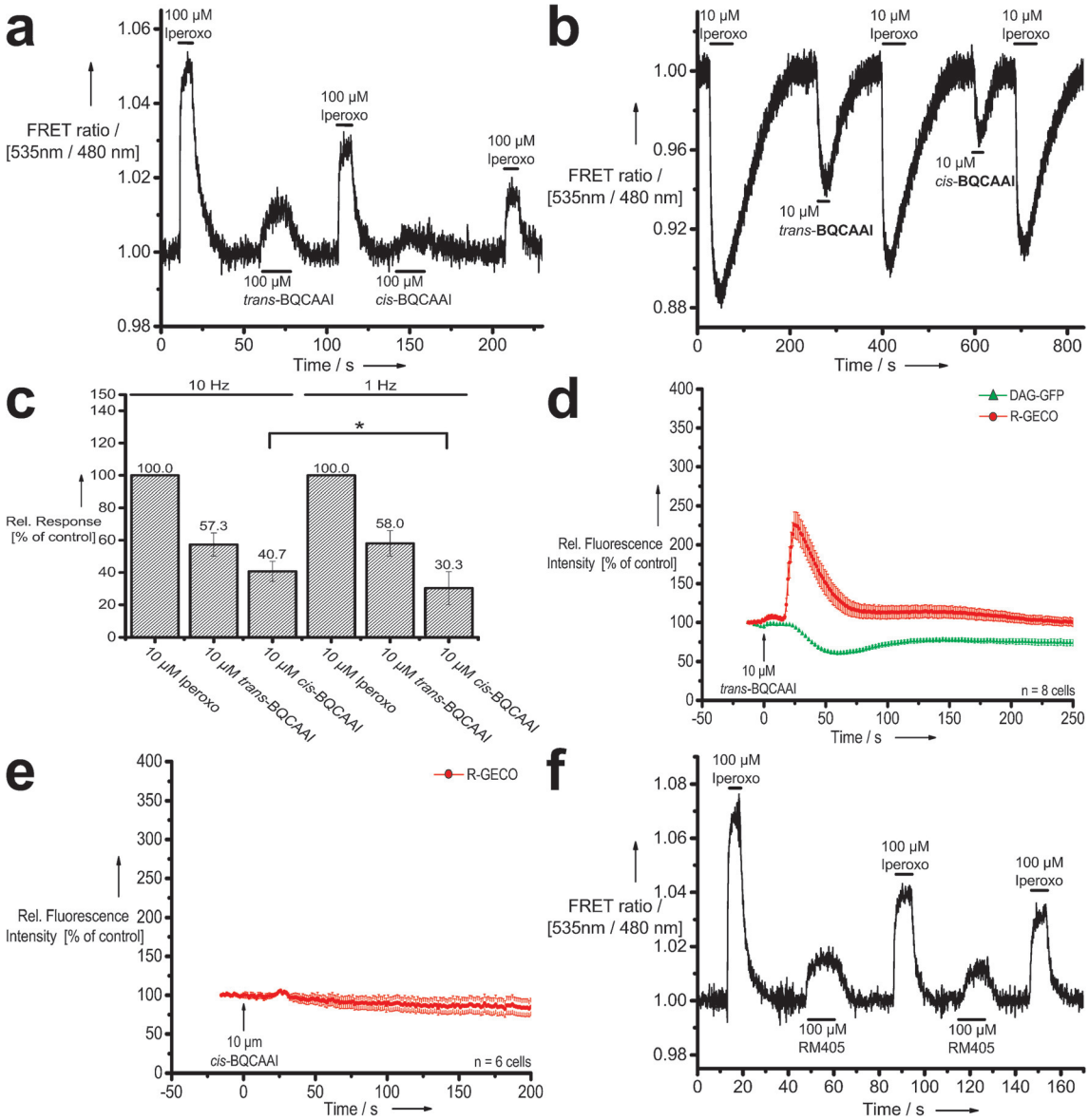

Figure 4. Characterization of the dualsteric **BQCAAI** hybrid compound at the receptor level and its effect on downstream signaling. a) A representative single-cell recording of HEK293 cells stably expressing the M1-IN3-CFP receptor sensor. A solution of 100 µM iperoxo was used as the reference. b) Representative FRET trace of HEK293 cells expressing a Gq sensor. c) Schematic comparison of the Gq activation of both isomers at different irradiation frequencies. d) *trans*-**BQCAAI** induced a detectable Ca^{2+} and DAG response that is significantly lower than the response to iperoxo. e) *cis*-**BQCAAI** was not able to induce a Ca^{2+} response over more than 200 s. f) The *trans*-**BQCAAI** isomer showed reduced activation kinetics at the receptor level compared to a dualsteric ligand with a polymethylene linker. Replacing the polymethylene linker with a benzene-containing linker resulted in comparable activation kinetics.

Keywords: acetylcholine receptors · azobenzenes · dualsteric ligands · G-protein-coupled receptors · photopharmacology

How to cite: *Angew. Chem. Int. Ed.* **2017**, *56*, 7282–7287
Angew. Chem. **2017**, *129*, 7388–7393

[1] J. Wess, R. M. Eglen, D. Gautam, *Nat. Rev. Drug Discov.* **2007**, *6*, 721–733.
[2] a) K. Haga, A. C. Kruse, H. Asada, T. Yurugi-Kobayashi, M. Shiroishi, C. Zhang, W. I. Weis, T. Okada, B. K. Kobilka, T. Haga, T. Kobayashi, *Nature* **2012**, *482*, 547–551; b) C. J. van Koppen, B. Kaiser, *Pharmacol. Ther.* **2003**, *98*, 197–220.
[3] R. M. Eglen, *Auton. Autacoid Pharmacol.* **2006**, *26*, 219–233.
[4] A. Fisher, Z. Pittel, R. Haring, N. Bar-Ner, M. Kliger-Spatz, N. Natan, I. Egozi, H. Sonego, I. Marcovitch, R. Brandeis, *J. Mol. Neurosci.* **2003**, *20*, 349–356.
[5] J. R. Lane, P. M. Sexton, A. Christopoulos, *Trends Pharmacol. Sci.* **2013**, *34*, 59–66.
[6] M. Decker, U. Holzgrabe, *MedChemComm* **2012**, *3*, 752–762.
[7] a) A. Bock, M. Bermudez, F. Krebs, C. Matera, B. Chirinda, D. Sydow, C. Dallanoce, U. Holzgrabe, M. De Amici, M. J. Lohse, G. Wolber, K. Mohr, *J. Biol. Chem.* **2016**, *291*, 16375–16389; b) X. Chen, J. Klöckner, J. Holze, C. Zimmermann, W. K.

Seemann, R. Schrage, A. Bock, K. Mohr, C. Tränkle, U. Holzgrabe, M. Decker, *J. Med. Chem.* **2015**, *58*, 560 – 576.
[8] a) K. Mohr, J. Schmitz, R. Schrage, C. Tränkle, U. Holzgrabe, *Angew. Chem. Int. Ed.* **2013**, *52*, 508 – 516; *Angew. Chem.* **2013**, *125*, 530 – 538; b) A. Bock, N. Merten, R. Schrage, C. Dallanoce, J. Bätz, J. Klöckner, J. Schmitz, C. Matera, K. Simon, A. Kebig, L. Peters, A. Müller, J. Schrobang-Ley, C. Tränkle, C. Hoffmann, M. De Amici, U. Holzgrabe, E. Kostenis, K. Mohr, *Nat. Commun.* **2012**, *3*, 1044; c) A. Bock, B. Chirinda, F. Krebs, R. Messerer, J. Bätz, M. Muth, C. Dallanoce, D. Klingenthal, C. Tränkle, C. Hoffmann, M. De Amici, U. Holzgrabe, E. Kostenis, K. Mohr, *Nat. Chem. Biol.* **2014**, *10*, 18 – 20.
[9] a) B. J. Davie, A. Christopoulos, P. J. Scammells, *ACS Chem. Neurosci.* **2013**, *4*, 1026 – 1048; b) P. Keov, L. Lopez, S. M. Devine, C. Valant, J. R. Lane, P. J. Scammells, P. M. Sexton, A. Christopoulos, *J. Biol. Chem.* **2014**, *289*, 23817 – 23837; c) C. Valant, K. J. Gregory, N. E. Hall, P. J. Scammells, M. J. Lew, P. M. Sexton, A. Christopoulos, *J. Biol. Chem.* **2008**, *283*, 29312 – 29321.
[10] J. Broichhagen, J. A. Frank, D. Trauner, *Acc. Chem. Res.* **2015**, *48*, 1947 – 1960.
[11] W. A. Velema, W. Szymanski, B. L. Feringa, *J. Am. Chem. Soc.* **2014**, *136*, 2178 – 2191.
[12] M. M. Lerch, M. J. Hansen, G. M. van Dam, W. Szymanski, B. L. Feringa, *Angew. Chem. Int. Ed.* **2016**, *55*, 10978 – 10999; *Angew. Chem.* **2016**, *128*, 11140 – 11163.
[13] M. J. Lohse, S. Nuber, C. Hoffmann, *Pharmacol. Rev.* **2012**, *64*, 299 – 336.
[14] a) C. Hoffmann, G. Gaietta, M. Bünemann, S. R. Adams, S. Oberdorff-Maass, B. Behr, J. P. Vilardaga, R. Y. Tsien, M. H. Ellisman, M. J. Lohse, *Nat. Methods* **2005**, *2*, 171 – 176; b) A. D. Stumpf, C. Hoffmann, *Br. J. Pharmacol.* **2016**, *173*, 255 – 266.
[15] a) M. J. Adjobo-Hermans, J. Goedhart, L. van Weeren, S. Nijmeijer, E. M. Manders, S. Offermanns, T. W. Gadella, Jr., *BMC Biol.* **2011**, *9*, 32; b) M. Bünemann, M. Frank, M. J. Lohse, *Proc. Natl. Acad. Sci. USA* **2003**, *100*, 16077 – 16082; c) C. Janetopoulos, T. Jin, P. Devreotes, *Science* **2001**, *291*, 2408 – 2411.
[16] S. Nuber, U. Zabel, K. Lorenz, A. Nuber, G. Milligan, A. B. Tobin, M. J. Lohse, C. Hoffmann, *Nature* **2016**, *531*, 661 – 664.
[17] a) V. O. Nikolaev, M. Bünemann, L. Hein, A. Hannawacker, M. J. Lohse, *J. Biol. Chem.* **2004**, *279*, 37215 – 37218; b) P. Tewson, M. Westenberg, Y. Zhao, R. E. Campbell, A. M. Quinn, T. E. Hughes, *PLoS One* **2012**, *7*, e42791.
[18] E. Leyva, E. Monreal, A. Hernández, *J. Fluorine Chem.* **1999**, *94*, 7 – 10.
[19] J. Kloeckner, J. Schmitz, U. Holzgrabe, *Tetrahedron Lett.* **2010**, *51*, 3470 – 3472.
[20] R. Schrage, A. De Min, K. Hochheiser, E. Kostenis, K. Mohr, *Br. J. Pharmacol.* **2016**, *173*, 3018 – 3027.
[21] a) R. Messerer, M. Kauk, D. Volpato, M. C. Alonso Canizal, J. Klockner, U. Zabel, S. Nuber, C. Hoffmann, U. Holzgrabe, *ACS Chem. Biol.* **2017**, *12*, 833 – 843; b) D. M. Thal, B. Sun, D. Feng, V. Nawaratne, K. Leach, C. C. Felder, M. G. Bures, D. A. Evans, W. I. Weis, P. Bachhawat, T. S. Kobilka, P. M. Sexton, B. K. Kobilka, A. Christopoulos, *Nature* **2016**, *531*, 335 – 340.

Manuscript received: February 11, 2017
Revised manuscript received: March 30, 2017
Version of record online: May 16, 2017

Angewandte Chemie
Eine Zeitschrift der Gesellschaft Deutscher Chemiker

Supporting Information

A Photoswitchable Dualsteric Ligand Controlling Receptor Efficacy

Luca Agnetta[+], Michael Kauk[+], Maria Consuelo Alonso Canizal, Regina Messerer, Ulrike Holzgrabe, Carsten Hoffmann,* and Michael Decker**

anie_201701524_sm_miscellaneous_information.pdf

Supporting Information

1 Synthesis

1.1 General

Common reagents and solvents were obtained from commercial suppliers (Aldrich, Steinheim, Germany; Merck, Darmstadt, Germany) and were used without any further purification. Tetrahydrofuran (THF) was distilled from sodium/benzophenone under an argon atmosphere. Microwave assisted reactions were carried out on a MLS-rotaPREP instrument (Milestone, Leutkirch, Germany) using 8-10 weflon disks. Melting points were determined on a Stuart melting point apparatus SMP3 (Bibby Scientific, UK). Thin-layer chromatography (TLC) was performed on silica gel 60 F_{254} plates (Macherey-Nagel, Düren, Germany) and spots were detected under UV light (λ=254 nm) or by staining with iodine. Merck silica gel 60 (Merck, Darmstadt, Germany) was used for chromatography (230-400 mesh) columns or performed on an Interchim Puri Flash 430 (Ultra Performance Flash Purification) instrument (Montluçon, France) connected to an Interchim Flash ELSD. Used columns are: Silica 25 g – 30 µm, Alox-B 40 g – 32/63 µm, Alox-B 25 g – 32/63 µm (Interchim, Montluçon, France). Nuclear magnetic resonance spectra were recorded with a Bruker AV-400 NMR instrument (Bruker, Karlsruhe, Germany) in [d_6]DMSO, $CDCl_3$, $(CD_3)_2CO$. As internal standard, the signals of the deuterated solvents were used (DMSO-d_6: ^{1}H 2.50 ppm, ^{13}C 39.52 ppm; $CDCl_3$: ^{1}H 7.26 ppm, ^{13}C 77.16 ppm; $(CD_3)_2CO$: ^{1}H 2.05 ppm, ^{13}C 39.52 ppm). Abbreviation for data quoted are: s, singlet; d, doublet; t, triplet; q, quartet; m, multiplet; br, broad; dd, doublet of doublets; dt, doublet of triplets; tt, triplet of triplets; tq, triplet of quartets. Coupling constants (*J*) are given in Hz. For purity and reaction monitoring, analytical HPLC analysis was performed with a system from Shimadzu equipped with a DGU-20A3R controller, LC20AB liquid chromatograph, and a SPD-20A UV/Vis detector. Stationary phase was a Synergi 4 µm fusion-RP (150×4.6 mm) column (Phenomenex, Aschaffenburg, Germany). As mobile phase, H_2O (phase A) and MeOH (phase B) were used with 1 mL min^{-1} (conc. B: 5→90% from 0 to 8 min; 90% from 8 to 13 min; 90→5% from 13 to 15 min; 5% from 15 to 18 min). The purity of all new compounds was found to be ≥95%. ESI mass spectral data were acquired with a Shimadzu LCMS-2020 or on an Agilent LC/MSD Trap G2445D instrument (Waldbronn, Germany). Data are reported as mass-to-charge ratio (*m/z*) of the corresponding positively charged molecular ions. UV/Vis spectra and experiments were

recorded on a Varian Cary 50 Bio UV/Vis Spectrophotometer using Hellma (Type 100-QS) cuvettes (10 mm light path).

1.2 Photoiperoxo

The synthesis of **photoiperoxo** started with condensation of commercially available nitrosobenzene (**9**) with 4-amino benzyl alcohol (**10**) by Mills reaction followed by an Appel bromination resulting in compound **11**. The photochromic iperoxo derivative is then obtained by a microwave assisted reaction (Suppl. Scheme 1).

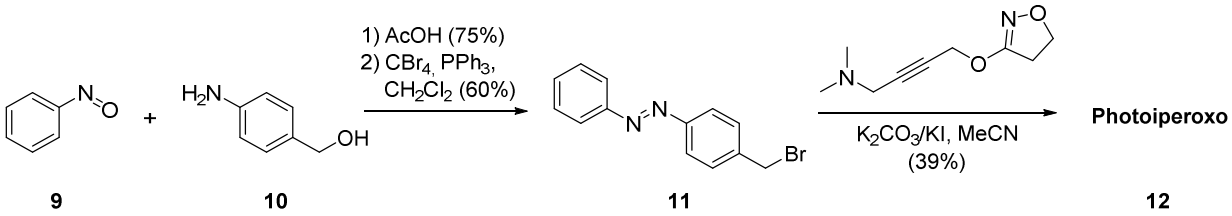

Supporting Scheme 1. Three-step synthesis of photoiperoxo (**12**).

1.2.1 Synthesis of azobenzyl alcohol (13)

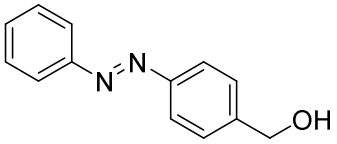

Nitrosobenzene (1.28 g, 11.9 mmol, 3 equiv.) was dissolved in ethanol (10 mL). To this solution (4-aminophenyl)methanol **10** (491 mg, 4.00 mmol, 1 equiv.) and acetic acid (20 mL) were added. The reaction mixture was stirred for 4 h at room temperature. Subsequently, the reaction mixture was poured into 30 mL of ice-cold water and the precipitate was collected by filtration. Column chromatography (CH_2Cl_2:MeOH = 50:1) provided compound **13** (659 mg, 2.99 mmol, 75%) as bright orange needles.

^{1}H NMR (400 MHz, DMSO-d_6): δ [ppm] = 7.88 (m, *J* = 6.9, 1.8 Hz, 4H), 7.65 – 7.50 (m, 5H), 5.40 (t, *J* = 5.7 Hz, 1H), 4.61 (d, *J* = 5.6 Hz, 2H).

^{13}C NMR (101 MHz, DMSO-d_6): δ [ppm] = 152.4, 151.3, 146.9, 131.8, 129.93, 127.6, 122.9, 62.9.

ESI-MS: *m/z* calc. for $C_{13}H_{12}N_2O^+$ $[M+H]^+$: 212.9, found: 213.1.

m.p.: 139°C

1.2.2 Synthesis of azobenzyl bromide (14)

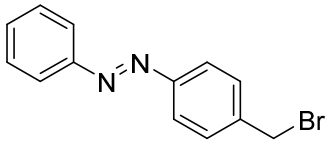

Azobenzyl alcohol **13** (300 mg, 1.41 mmol, 1 equiv.) was dissolved in dry THF (15 mL) under argon atmosphere, tetrabromomethane (703 mg, 2.12 mmol, 1.5 equiv.) and triphenylphosphine (556 mg, 2.12 mmol, 1.5 equiv.) were added and the reaction mixture was stirred for 4 h. The reaction mixture was filtered and the filtrate was evaporated to dryness and purified by column chromatography (EtOAc:Hexane = 1:10) giving yield to compound **14** as orange needles (232 mg, 0.84 mmol, 60%).

^{1}H NMR (400 MHz, DMSO-d_6): δ [ppm] = 7.89 (tt, *J* = 7.7, 2.0 Hz, 4H), 7.69 – 7.57 (m, 5H), 4.80 (s, 2H).

^{13}C NMR (101 MHz, DMSO-d_6): δ [ppm] = 151.9, 151.5, 141.5, 131.7, 130.5, 129.5, 122.9, 122.6, 33.6.

ESI-MS: *m/z* calc. for $C_{13}H_{11}BrN_2^+$ $[M+H]^+$: 275.0, 277.0, found: 274.9, 276.9.

m.p.: 114°C

1.2.3 Synthesis of photo-Iperoxo (15)

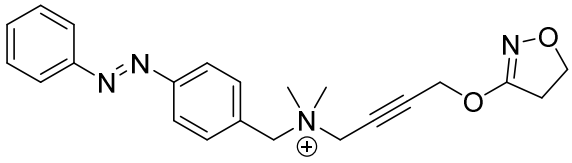

In a microwave reactor azobenzyl bromide **14** (100 mg, 0.36 mmol, 1 equiv.) and the base of iperoxo (132 mg, 0.73 mmol, 2 equiv.) were dissolved in acetonitrile (10 mL) and a catalytic amount (spatula tip) of a 1:1 mixture of potassium iodide and potassium carbonate was added and heated to 80 °C for 4 h (3 min heating from 0 to 80 °C, keep 237 min at 80 °C, 10 min cooling, 700 Watt). Reaction was monitored by LC-MS. The precipitate was filtered off and the solvent was removed under reduced pressure. The crude product was purified by column chromatography (CH_2Cl_2:MeOH:NH_3 = 20:1:0.1) yielding compound **15** as a dark red oil (54 mg, 0.14 mmol, 39%).

^{1}H NMR (400 MHz, $CDCl_3$): δ [ppm] = 7.99 – 7.86 (m, 6H), 7.56 – 7.46 (m, 3H), 5.24 (s, 2H), 4.88 (d, *J* = 7.9 Hz, 4H), 4.42 (t, *J* = 9.6 Hz, 2H), 3.53 – 3.40 (m, 6H), 3.02 (t, *J* = 9.6 Hz, 2H).

^{13}C NMR (101 MHz, $CDCl_3$): δ [ppm] = 166.9, 154.1, 152.6, 134.3, 131.9, 129.3, 129.0, 123.7, 123.3, 87.8, 75.9, 70.2, 66.2, 57.5, 54.8, 50.0, 33.1.

ESI-MS: *m/z* calc. for $C_{22}H_{25}BrN_4O_2^+$ $[M+H]^+$: 377.2, found: 377.2.

1.3 BQCAAI

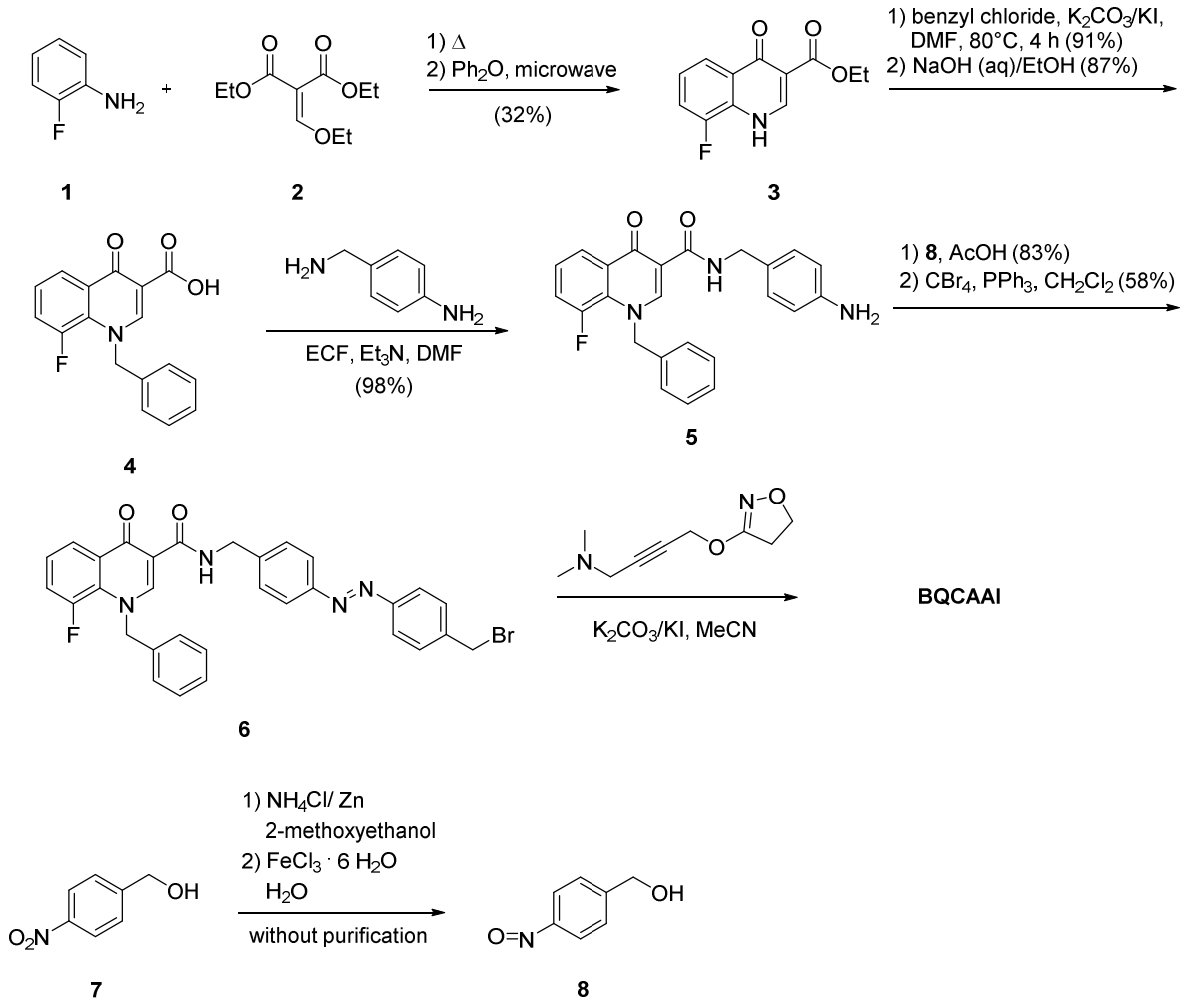

Supporting Scheme 2. Synthesis of **BQCAAI**

1.3.1 Synthesis of (4-nitrosophenyl)methanol (8)

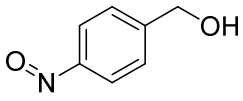

4-Nitrobenzyl alcohol **7** (1.86 g, 12.1 mmol, 1 eq.) and ammonium chloride (0.82 g, 15.3 mmol, 1.26 eq.) were dissolved in 40 mL of 2-methoxyethanol/water (10:1) under nitrogen

atmosphere. To this solution zinc powder (1.95 g, 29.8 mmol, 2.46 eq.) was added at room temperature. The suspension was stirred for 30 minutes and the insoluble matter was filtered off. The pale yellow filtrate was poured into 200 mL of an aqueous solution of ferric chloride hexahydrate (3.31 g, 12.2 mmol, 1.01 eq.) at 0 °C and the solution turned green. The solution was extracted three times with CH_2Cl_2 (50 mL) and was concentrated to 10 mL under reduced pressure. This solution was used without further purification for reaction 1.3.7.

1.3.2 Synthesis of 2-fluoroanilinmethylenmalonate diethylester (2a)

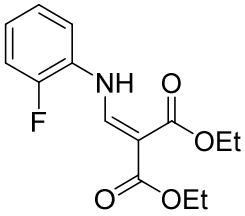

o-Fluoroaniline **1** (4.45 g, 40.0 mmol, 1 eq.) and diethyl ethoxymethylenemalonate **2** (10.4 g, 48.0 mmol, 1.2 eq.) were heated solvent free to 160 °C for 2 h. The mixture was allowed to cool to room temperature. The solid is filtered and washed with pentane (50 mL). Drying under reduced pressure gave the desired product as a white-beige solid (10.1 g, 35.9 mmol, 90%).

^{1}H-NMR (400 MHz, DMSO-d_6): δ [ppm] = 11.06 (d, *J* = 13.4 Hz, 1H), 8.51 (d, *J* = 13.6 Hz, 1H), 7.33 – 7.26 (m, 1H), 7.17 (s, 3H), 4.29 (dd, *J* = 28.8, 7.1 Hz, 4H), 1.36 (dt, *J* = 19.5, 7.1 Hz, 6H).

^{13}C-NMR (101 MHz, DMSO-d_6): δ [ppm] = 168.7, 165.7, 154.2, 151.8, 151.1, 128.1, 125.1, 116.4, 95.3, 60.7, 14.5.

m.p.: 89°C

1.3.3 Synthesis of ethyl-8-fluoro-4-oxo-1,4-dihydrochinoline-3-carboxylate (3)

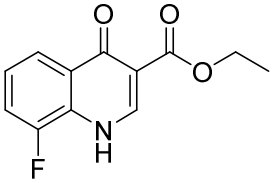

o-Fluoroanilinmethylenemalonate diethyl ester **2a** (9.00 g, 32.0 mmol) and diphenyl ether (25 mL) were charged into a microwave reactor and heated to 210 °C for 1 h (3 min heating

from 0 to 210 °C, keep 47 min at 210 °C, 10 min cooling, 700 watt). After the mixture was cooled down petrol ether was added and the precipitate filtered off and washed again with petrol ether which to give the desired product as a greyish powder (1.90 g, 8.08 mmol, 25%).

^{1}H-NMR (400 MHz, DMSO-d_6): δ [ppm] = 12.44 (s, 1H), 8.38 (s, 1H), 7.95 (d, *J* = 8.0 Hz, 1H), 7.63 (dd, *J* = 9.8, 8.0 Hz, 1H), 7.39 (dd, *J* = 13.1, 8.1 Hz, 1H), 4.21 (d, *J* = 21.3 Hz, 2H), 1.26 (s, 3H).

^{13}C-NMR (101 MHz, DMSO-d_6): δ [ppm] = 173.0, 164.9, 145.1, 129.6, 124.9, 121.8, 117.8, 111.0, 60.3, 14.7.

ESI-MS: *m/z* calc. for $C_{12}H_{10}FN_4O_3^+$ $[M+H]^+$: 236.1, found: 236.1.

m.p.: 175°C

1.3.4 Synthesis of ethyl-1-benzyl-8-fluoro-4-oxo-1,4-dihydrochinoline-3-carboxylate (3a)

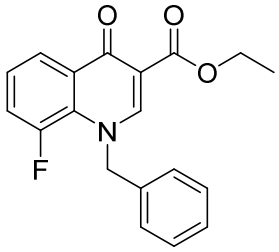

Ethyl-8-fluoro-4-oxo-1,4-dihydrochinoline-3-carboxylate **3** (1.18 g, 5.00 mmol, 1 eq.) was suspended in DMF (75 mL) and potassium carbonate (1.66 g, 12.0 mmol, 2.2 eq.), potassium iodide (0.17 g, 1.00 mmol, 0.2 eq.) and benzyl chloride (3.16 g, 25.0 mmol, 5 eq.) were added to the mixture and heated to 80 °C and stirred for 20 h. After cooling the excess potassium carbonate was filtered off and the solvent removed under reduced pressure. The residue was recrystallized from ethanol, filtered and dried under reduced pressure yielding the desired product as a white powder (1.54 g, 4.72 mmol, 94%).

^{1}H-NMR (400 MHz, DMSO-d_6): δ [ppm] = 8.82 (s, 1H), 8.11 (m, *J* = 8.0, 1.2 Hz, 1H), 7.62 – 7.22 (m, 5H), 7.12 (d, *J* = 7.3 Hz, 2H), 5.72 (d, *J* = 3.3 Hz, 2H), 4.25 (q, *J* = 7.1 Hz, 2H), 1.29 (t, *J* = 7.1 Hz, 3H).

^{13}C-NMR (101 MHz, DMSO-d_6): δ [ppm] = 171.7, 164.2, 152.0, 137.1, 131.0, 128.8, 127.6, 125.6, 122.7, 120.1, 119.8, 110.56, 60.0, 14.3.

ESI-MS: *m/z* calc. for $C_{19}H_{16}FNO_3^+$ $[M+H]^+$: 326.1, found: 326.0.

m.p.: 193°C

1.3.5 Synthesis of *N*-benzyl-8-Fluoro-4-oxo-1,4-dihydroquinoline-3-carboxylic acid (4)

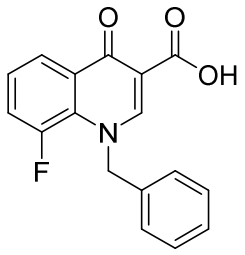

1-Benzyl-ethyl-8-fluoro-4-oxo-1,4-dihydroquinoline-3-carboxylate **3a** (0.30 g, 0.91 mmol) was dissolved in a mixture (4 mL) of equal amounts of sodium hydroxide solution (3N) and ethanol and heated at 90 °C for 1.5 h under stirring. After cooling to room temperature aqueous conc. hydrochloric acid was added until pH = 2. The precipitate was filtered, washed with water and pentane and dried *in vacuo* to yield the desired product as a white powder (0.258 g, 0.87 mmol, 95%).

^{1}H-NMR (400 MHz, DMSO-d_6): δ [ppm] = 14.72 (s, 1H), 9.20 (s, 1H), 8.27 (m, 1H), 7.76 (m, 1H), 7.63 (m, 1H), 7.33 (m, 3H), 7.17 (m, 2H), 5.92 (d, *J* = 3.3 Hz, 2H).

^{13}C-NMR (101 MHz, DMSO-d_6): δ [ppm] = 177.3, 166.0, 153.3, 152.6, 150.8, 137.1, 129.3, 128.2, 127.5, 126.2, 122.8, 121.6, 60.8.

ESI-MS: *m/z* calc. for $C_{17}H_{12}FNO_3^+$ $[M+H]^+$: 298.1, found: 298.0.

m.p.: 176°C

1.3.6 Synthesis of *N*-(4-aminobenzyl)-1-benzyl-8-fluoro-4-oxo-1,4-dihydroquinoline-3-carboxamide (5)

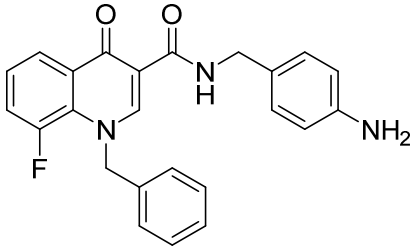

N-Benzyl-8-fluoro-4-oxo-1,4-dihydroquinoline-3-carboxylic acid **4** (0.258 g, 0.87 mmol, 1 eq.) and triethylamine (0.185 g, 0.25 mL, 1.83 mmol, 2.1 eq.) were dissolved in 10 mL of abs. DMF and ethyl chloroformate (0.194 g, 0.17 mL, 1.78 mmol, 2.05 eq.) was added under stirring at 0 °C for 2 h. To this reaction mixture 4-amino benzylamine (0.255 g, 0.24 mL, 2.09 mmol, 2.4 eq.) was added and stirred again for 1 h at 0 °C and subsequently at room temperature overnight. After the reaction had completed the reaction mixture was poured into ice-water. The precipitate was filtered and washed with water and petroleum ether to afford the desired product as white crystals (0.346 g, 0.86 mmol, 98%).

^{1}H-NMR (400 MHz, DMSO-d_6): δ [ppm] = 10.01 (s, 1H), 9.02 (s, 1H), 8.20 (d, J = 8.1 Hz, 1 H), 7.63 (m, 1H), 7.52 (m, 1H), 7.39 – 7.33 (m, 2H), 7.33 – 7.27 (m, 1H), 7.13 (m, 2H), 7.05 (m, 2H), 6.62 – 6.48 (m, 2H), 5.85 (d, *J* = 3.0 Hz, 2H), 5.77 (s, 1H), 5.01 (s, 2H), 4.39 (d, *J* = 5.6 Hz, 2H).

^{13}C-NMR (101 MHz, DMSO-d_6): δ [ppm] = 175.0, 163.7, 156.6, 151.6, 150.8, 148.2, 137.5, 130.5, 129.3, 129.0, 128.1, 126.3, 123.0, 120.7, 120.5, 114.3, 111.9, 60.4, 55.4, 42.6.

ESI: *m/z* calcd. for $C_{24}H_{20}FN_3O_2$ $[M+H]^+$: 402.2; found: 402.1.

m.p.: 204°C

1.3.7 Synthesis of 1-benzyl-8-fluoro-*N*-(4-((4-(hydroxymethyl)phenyl)diazenyl)benzyl)-4-oxo-1,4-dihydroquinoline-3-carboxamide (7)

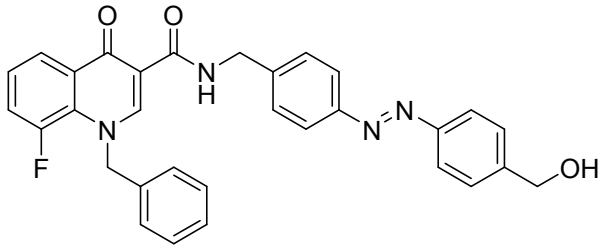

N-(4-Aminobenzyl)-1-benzyl-8-fluoro-4-oxo-1,4-dihydroquinoline-3-carboxamide **5** (0.68 g, 3.00 mmol) was dissolved in acetic acid and nitrosobenzyl alcohol **8** was added in portions. The reaction mixture was stirred at room temperature overnight. The mixture was poured into ice water and methanol was added. The precipitate was filtered off and after drying under reduced pressure the product was obtained as an orange solid (0.64 g, 1.23 mmol, 62%).

^{1}H-NMR (400 MHz, DMSO-d_6): δ [ppm] = 10.29 (t, 1H), 9.02 (s, 1H), 8.23 (m, 1H), 7.88 (m, 4H), 7.70 – 7.48 (m, 6H), 7.39 – 7.22 (m, 3.5 H), 7.14 (m, 2H), 6.84 (m, 0.5 H), 5.89 – 5.74 (s, 2H), 5.28 (t, 1H), 4.57 (dd, 4H).

ESI: *m/z* calcd. for $C_{31}H_{25}FN_4O_3$ $[M+H]^+$: 521.2; found: 521.1.

m.p.: 197°C

1.3.8 Synthesis of 1-Benzyl-*N*-(4-((4-(bromomethyl)phenyl)diazenyl)benzyl)-8-fluoro-4-oxo-1,4-dihydroquinoline-3-carboxamide (8)

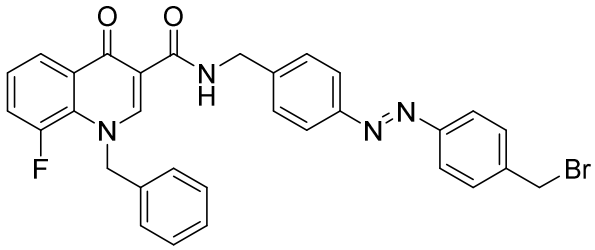

Compound **7** (98.0 mg, 0.19 mmol) and tetrabromomethane (0.18 g, 0.54 mmol) were dissolved in dry DCM. Triphenylphosphine (0.14 g, 0.54 mmol) was added at 0 °C and the mixture was stirred at room temperature overnight. After the solvent was evaporated ethanol was added. The precipitate was filtered off and dried under reduced pressure. The product was obtained as an orange solid (64.0 mg, 0.11 mmol, 58%), which was directly employed in the next reaction due to its instability.

ESI-MS: calc. for $C_{31}H_{24}BrN_4O_2^+$ $[M+H]^+$: 583.1, found: 583.0.

1.3.9 Synthesis of *(E)*-*N*-(4-((4-((1-Benzyl-8-fluoro-4-oxo-1,4-dihydroquinoline-3-carboxamido)methyl)phenyl)diazenyl)benzyl)-4-((4,5-dihydroisoxazol-3-yl)oxy)-*N,N*-dimethylbut-2-yn-1-aminium bromide (BQCAAI)

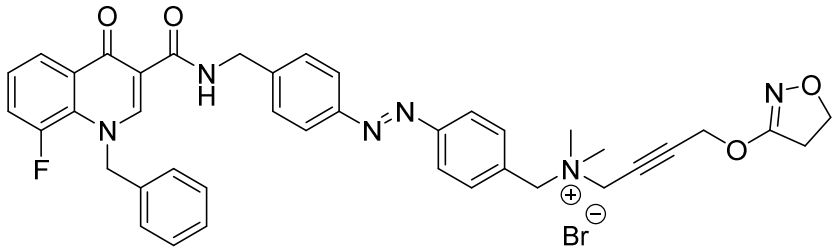

Iperoxo base was synthesized according to a literature procedure.[1] Iperoxo base (123 mg, 0.60 mmol) and compound **8** (200 mg, 0.34 mmol) were dissolved in acetonitrile. A catalytic amount of a mixture of potassium iodide and potassium carbonate (1:1) was added. The

mixture was treated in microwave at 80 °C for 4 h (3 min heating from 0 to 80 °C, keep 237 min at 80 °C, 10 min cooling, 700 watt). After the microwave reactor was cooled to room temperature, the precipitate was filtered off and the solvent was evaporated *in vacuo* down to 5 mL of acetonitrile. After the addition of diethyl ether the precipitate was filtered off. The product was obtained as an orange solid (260 mg, 0.34 mmol, quant. yield).

^{1}H NMR (400 MHz, DMSO-d_6): δ [ppm] = 10.32 (t, *J* = 6.1 Hz, 1H), 8.22 (m, 1H), 9.03 (s, 1H), 8.00 (d, *J* = 8.5 Hz, 2H), 7.92 (d, *J* = 8.4 Hz, 2H), 7.78 (d, *J* = 8.5 Hz, 2H), 7.56 – 7.68 (m, 3H), 7.32 (m, 3H), 7.51 (m, 1H), 7.13 (d, *J* = 7.2 Hz, 2H), 5.84 (d, *J* = 2.8 Hz, 2H), 4.99 (s, 2H), 4.70 (m, 4H), 4.40 (s, 2H), 4.33 (t, *J* = 9.6 Hz, 2H), 3.10 (s, 6H), 3.04 (t, *J* = 9.6 Hz, 2H).

^{13}C-NMR (101 MHz, DMSO-d_6): δ [ppm] = 181.7, 167.3, 164.4, 160.6, 153.4, 151.7, 144.4, 137.4, 134.6, 130.8, 130.5, 129.3, 129.0, 128.2, 126.6 – 126.0, 123.4, 123.0, 111.7, 87.4, 76.7, 75.3, 70.1, 65.7, 60.6, 57.8, 50.0, 42.5, 32.7.

ESI-MS: calc. for $C_{40}H_{38}N_6O_4^+$ $[M+H]^+$: 686.3, found: 686.1.

m.p.: 168°C

Stability towards thermal isomerization

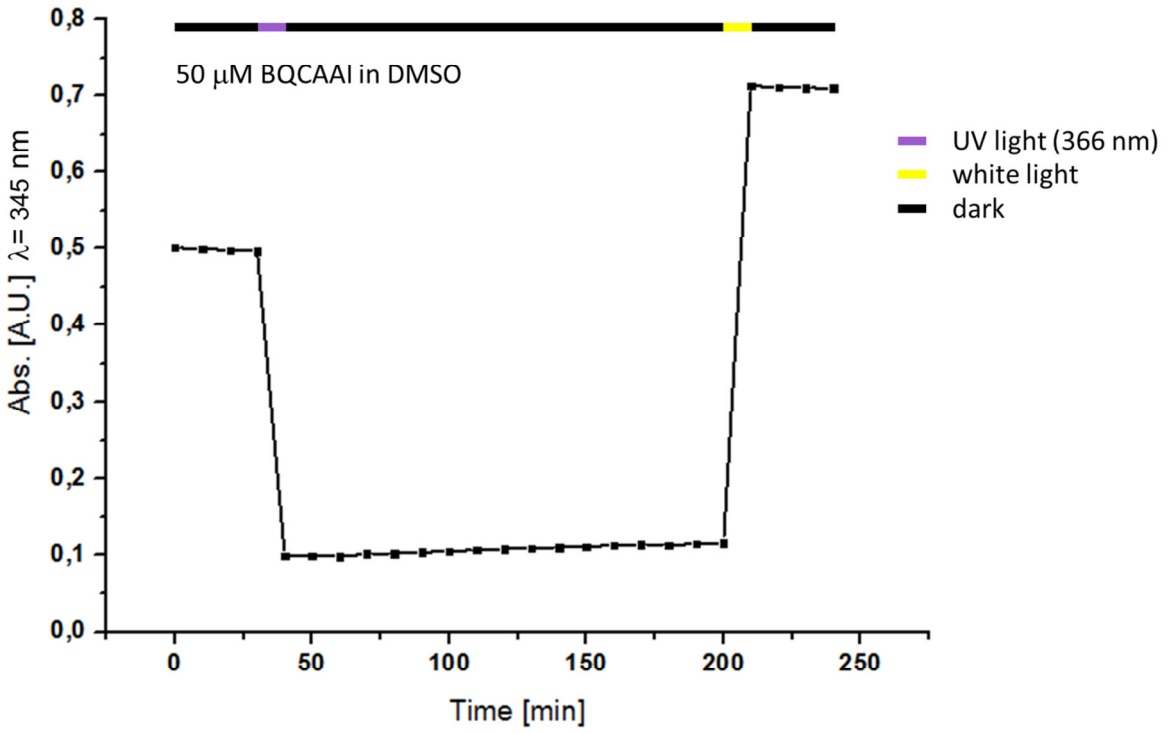

Supporting Figure 1. Thermal stability of the photoswitchable dualsteric M1 ligand **BQCAAI**. Once switched to the *cis*-isomer, the achieved photostationary state (PSS) is stable in the dark for more than 2.5 h. Upon irradiation with white light a photostationary state in favor of the *trans*-isomer is regained. This excellent thermal stability allows the investigation of **BQCAAI** on an hours timescale, clearly distinguishing between the two PSSs.

1.4 *N*-(3-(4-(3-(1-Benzyl-6-fluoro-4-oxo-1,4-dihydroquinoline-3-carboxamido)prop-1-yn-1-yl)phenyl)prop-2-yn-1-yl)-4-((4,5-dihydroisoxazol-3-yl)oxy)-*N*,*N*-dimethylbut-2-yn-1-aminium bromide RM405

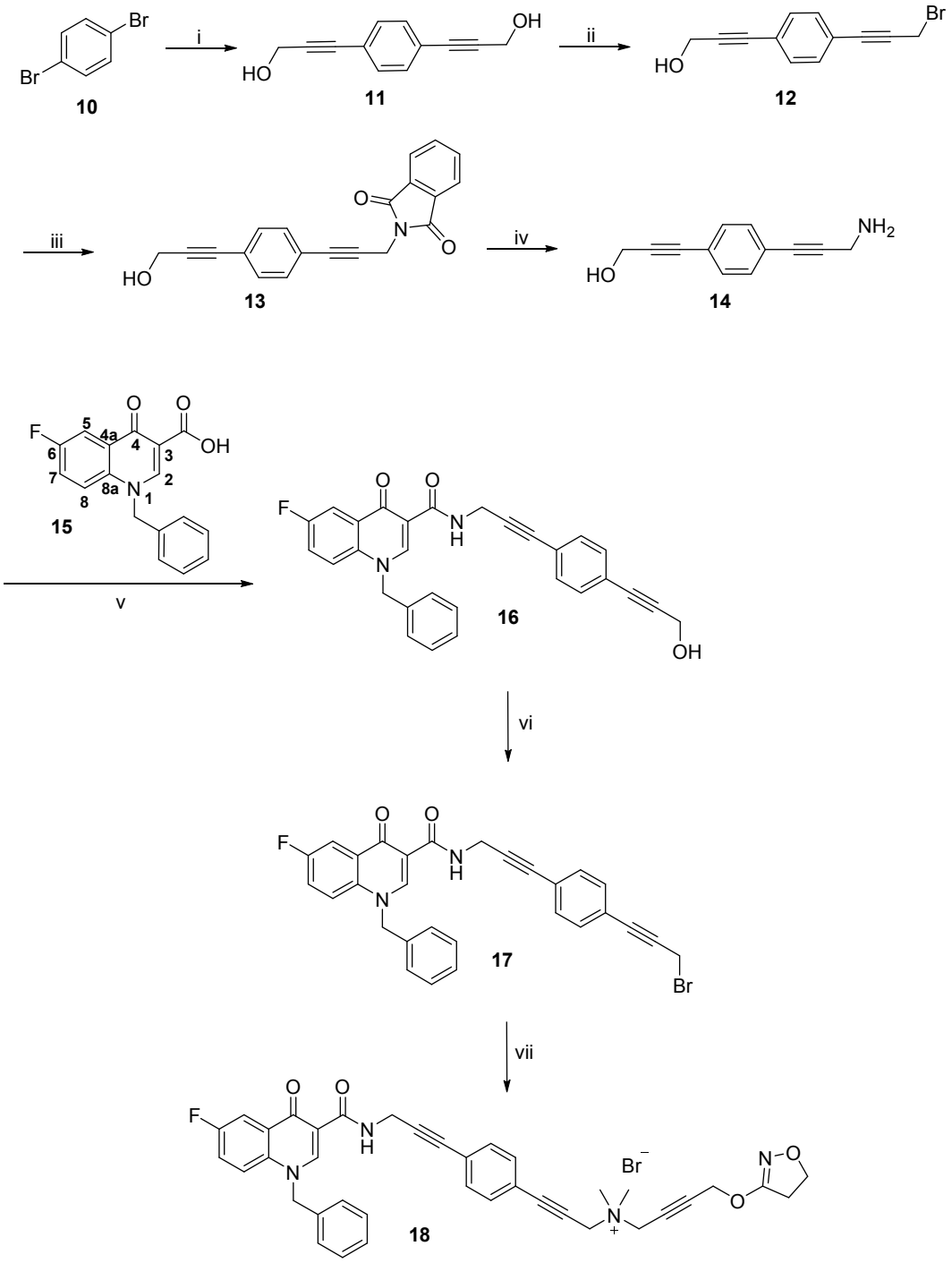

Supporting scheme 3. Reagents and conditions: (i) propargyl alcohol, $Pd(PPh_3)_4$, propylamine, 60 °C; (ii) CBr_4, PPh_3, CH_2Cl_2, 0 °C, rt.; (iii) potassium phthalimide, CH_3CN, 90 °C, rt.; (iv) hydrazine monohydrate, EtOH, 90 °C, rt.; (v) benzyl chloride, K_2CO_3, DMF, 80 °C; (vi) 6 N HCl, MeOH, reflux; (vii) ethyl chlorofomate, NMe_3, DMF, 0 °C, rt.; (viii) CBr_4, PPh_3, CH_2Cl_2, 0 °C, rt.; (ix) iperoxo base, KI/K_2CO_3, CH_3CN, 80 °C (microwave).

For the synthesis of hybrid **18** the two pharmacophores, the base of iperoxo and the fluoro-4-oxo-quinolone skeleton **15**,[1-2] were connected via the rigid spacer **14**. Compound **14** was synthesized by coupling of 1,4-dibromobenzene **10** and propargylic alcohol in a Sonogashira-

like reaction,[3] followed by Appel reaction and Gabriel synthesis. Further reaction with potassium phthalimide and hydrazine monohydrate led to the rigid spacer **14**.

1.4.1 Synthesis of 3,3'-(1,4-phenylene)bis(prop-2-yn-1-ol) (11)

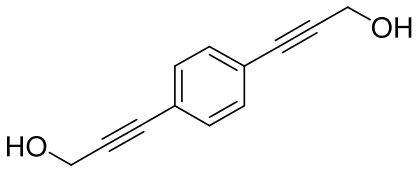

1,4-Dibromobenzene **10** (4.00 g, 17.0 mmol) and $Pd(PPh_3)_4$ (510 mg, 0.44 mmol) were dissolved in 60 mL of propylamine. After addition of 2-propyn-1-ol (5.60 g, 99.9 mmol), the reaction mixture was heated at 60 °C under nitrogen. The reaction was monitored via silica gel TLC (cyclohexane:ethyl acetate = 4:6, R_f = 0.50). After completion of the reaction (2.5 days), the mixture was quenched with 40 mL of conc. HCl. The aqueous layer was extracted three times with diethyl ether. The combined organic layers were dried over Na_2SO_4 and the solvent was removed *in vacuo*. The product was purified using column chromatography (cyclohexane:EtOAc = 7:3 to 4:6). The product was obtained as yellow solid (3.00 g, 16.1 mmol, 95%).

^{1}H NMR ($CDCl_3$, 400 MHz): δ [ppm] = 4.50 (s, 4H), 7.36 (s, 4H).

m.p.: 122°C

1.4.2 Synthesis of 3-(4-(3-bromoprop-1-yn-1-yl)phenyl)prop-2-yn-1-ol (12)

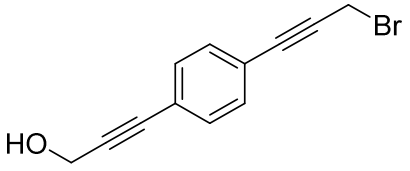

3,3'-(1,4-Phenylene)bis(prop-2-yn-1-ol) **11** (0.63 g, 3.40 mmol) and tetrabromomethane (1.13 g, 3.40 mmol) were dissolved in 20 mL dichloromethane dry under argon. Triphenylphosphine (0.89 g, 3.40 mmol) was added at 0 °C. The reaction mixture was then allowed to warm up to room temperature, stirred overnight and monitored by means of silica gel TLC (cyclohexane/ethyl acetate = 4:6, R_f = 0.72). The solvent was removed *in vacuo* and the product was purified using column chromatography (cyclohexane/EtOAc = 4:6) to yield a yellow solid (0.14 g, 0.57 mmol, 17%).

^{1}H NMR ($CDCl_3$, 400 MHz): δ [ppm] = 4.16 (s, 2H), 4.50 (s, 2H), 7.38 (s, 4H).

^{13}C-NMR ($CDCl_3$, 101 MHz): δ [ppm] = 15.0, 51.7, 85.2, 86.0, 86.1, 89.3, 122.3, 123.1, 131.6, 131.8.

m.p.: 85°C

1.4.3 Synthesis of 2-(3-(4-(3-Hydroxyprop-1-yn-1-yl)phenyl)prop-2-yn-1-yl)isoindoline-1,3-dione (13)

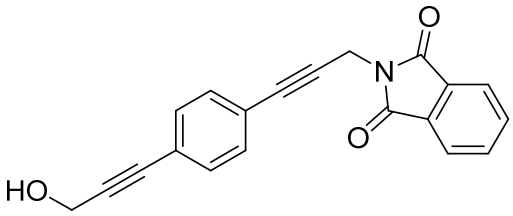

3-(4-(3-Bromoprop-1-yn-1-yl)phenyl)prop-2-yn-1-ol **12** (364 mg, 1.46 mmol) was dissolved in dry acetonitrile (10 mL). Potassium phthalimide (811 mg, 4.38 mmol) was added, and the reaction mixture was stirred at 90 °C for 7.5 h and at room temperature overnight. The reaction was monitored by TLC (cyclohexane:EtOAc = 4:6, R_f = 0.72). The obtained solid was filtered off and the solvent was removed *in vacuo* to yield a beige solid (0.46 g, 1.46 mmol, 100%)

^{1}H NMR ($CDCl_3$, 400 MHz): δ [ppm] = 4.48 (s, 2H), 4.68 (s, 2H), 7.31 - 7.37 (m, 4H), 7.74 (dd, *J* = 3.0, *J* = 5.5 Hz, 2H), 7.90 (dd, *J* = 3.0, *J* = 5.5 Hz, 2H).

^{13}C-NMR ($CDCl_3$, 101 MHz): δ [ppm] = 27.9, 51.6, 82.5, 84.5, 85.2, 89.0, 122.5, 122.7, 123.6, 131.5, 131.8, 132.1, 134.2, 167.1.

m.p.: 143°C

1.4.4 Synthesis of 3-(4-(3-aminoprop-1-yn-1-yl)phenyl)prop-2-yn-1-ol (14)

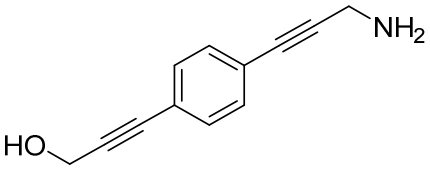

2-(3-(4-(3-Hydroxyprop-1-yn-1-yl)phenyl)prop-2-yn-1-yl)isoindoline-1,3-dione **13** (782 mg, 2.48 mmol) was suspended in 10 mL of ethanol. After addition of hydrazine monohydrate

(0.48 mL, 9.92 mmol) a clear solution was obtained. While the reaction mixture was heated at 90 °C a solid precipitated. Another 3 mL of ethanol were added. The reaction was monitored by TLC (CH_2Cl_2:MeOH = 8:2, R_f = 0.44). The suspension was stirred at 90 °C for 7.0 h and at room temperature overnight. The precipitate was filtered off and washed with ethanol. The solvent was evaporated off and the crude product purified by column chromatography (CH_2Cl_2:MeOH = 9:1 to 7:3) to yield a yellow solid (0.36 g, 1.92 mmol, 77%).

^{1}H NMR (MeOD, 400 MHz): δ [ppm] = 3.60 (s, 2H), 4.39 (s, 2H), 7.36 (s, 4H).

^{13}C-NMR (MeOD, 101 MHz): δ [ppm] = 32.1, 51.2, 83.0, 85.0, 90.7, 92.1, 124.2, 124.7, 132.6.

m.p.: 149°C

1.4.5 Synthesis of 1-benzyl-6-fluoro-*N*-(3-(4-(3-hydroxyprop-1-yn-1-yl)phenyl)prop-2-yn-1-yl)-4-oxo-1,4-dihydroquinoline-3-carboxamide (16)

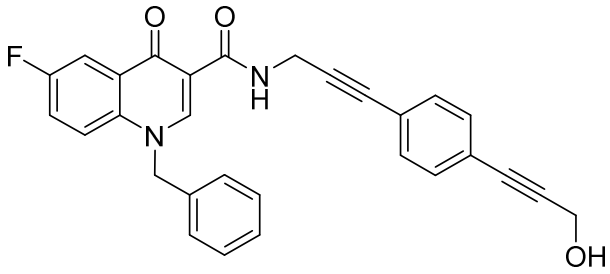

3-(4-(3-Aminoprop-1-yn-1-yl)phenyl)prop-2-yn-1-ol **14** (257 mg, 0.87 mmol) and trimethylamine (0.25 mL, 1.83 mmol) were dissolved in dry DMF (12 mL). Ethyl chloroformate (0.17 mL, 1.78 mmol) was slowly added under stirring at 0 °C for 1.5 h. After addition of **15** (258 mg, 1.39 mmol), the reaction mixture was stirred at 0 °C for 2.5 h and subsequently at room temperature for 64 h. The reaction mixture was poured into ice-water, filtered off, and the solid washed with water and petroleum ether. The white solid was dried *in vacuo* (367 mg, 0.79 mmol, 91%).

^{1}H NMR ($CDCl_3$, 400 MHz): δ [ppm] = 4.42 - 4.52 (m, 4H), 5.47 (s, 2H,), 7.13 - 7.44 (m, 11H), 8.17 (dd, *J* = 2.7, *J* = 8.7 Hz, 1H), 8.93 (s, 1H), 10.22 (br, 1H).

^{13}C-NMR ($CDCl_3$, 101 MHz): δ [ppm] = 29.6, 51.6, 58.1, 82.3, 85.3, 87.4, 88.8, 111.3, 112.3, 119.1, 121.5, 122.3, 123.2, 126.0, 128.8, 129.5, 131.5, 131.7, 133.8, 135.8, 148.5, 159.9, 164.5, 175.9.

m.p.: 206°C

1.4.6 Synthesis of 1-benzyl-*N*-(3-(4-(3-bromoprop-1-yn-1-yl)phenyl)prop-2-yn-1-yl)-6-fluoro-4-oxo-1,4-dihydroquinoline-3-carboxamide (17)

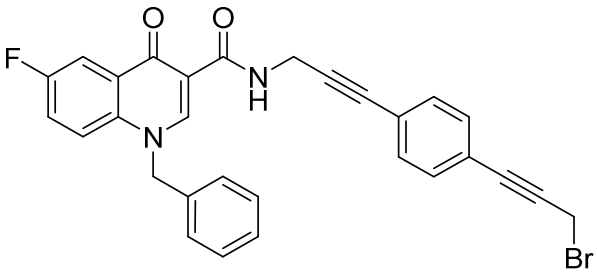

1-Benzyl-6-fluoro-*N*-(3-(4-(3-hydroxyprop-1-yn-1-yl)phenyl)prop-2-yn-1-yl)-4-oxo-1,4-dihydroquinoline-3-carboxamide **16** (300 mg, 0.65 mmol) and tetrabromomethane (0.43 g, 1.29 mmol) were dissolved in dry dichloromethane (15 mL) under argon. Triphenylphosphine (0.34 g, 1.29 mmol) was added at 0 °C. The reaction mixture was then allowed to warm to room temperature and stirred for further 2 days. The solvent was evaporated and the residue crystallized in ethanol and recrystallized in methanol to afford a beige solid (0.19 g, 0.35 mmol, 54%).

^{1}H NMR ($(CD_3)_2CO$, 400 MHz): δ [ppm] = 4.39 (s, 2H), 4.50 (d, *J* = 5.6 Hz, 2H), 5.85 (s, 2H), 7.33 - 7.57 (m, 10H), 7.86 (dd, *J* = 4.3, *J* = 9.4 Hz, 1H), 8.06 (dd, *J* = 3.1, *J* = 9.1 Hz, 1H), 9.03 (s, 1H), 10.22 (dt, *J* = 1.2, *J* = 5.0 Hz, 1H).

^{13}C-NMR ($(CD_3)_2CO$, 101 MHz): δ [ppm] = 16.9, 31.1, 59.0, 83.1, 87.3, 88.5, 90.8, 112.9, 112.9, 122.6, 123.0, 123.9, 128.5, 130.1, 131.0, 133.6, 137.5, 138.0, 138.3, 150.9, 161.7, 165.9, 177.2.

ESI-MS: *m/z* calcd. for $C_{29}H_{21}BrFN_2O_2^+$ $[M+H]^+$: 527.1, found: 527.2.

m.p.: 198°C

1.4.7 Synthesis of *N*-(3-(4-(3-(1-benzyl-6-fluoro-4-oxo-1,4-dihydroquinoline-3-carboxamido)prop-1-yn-1-yl)phenyl)prop-2-yn-1-yl)-4-((4,5-dihydroisoxazol-3-yl)oxy)-*N*,*N*-dimethylbut-2-yn-1-aminium bromide (18)

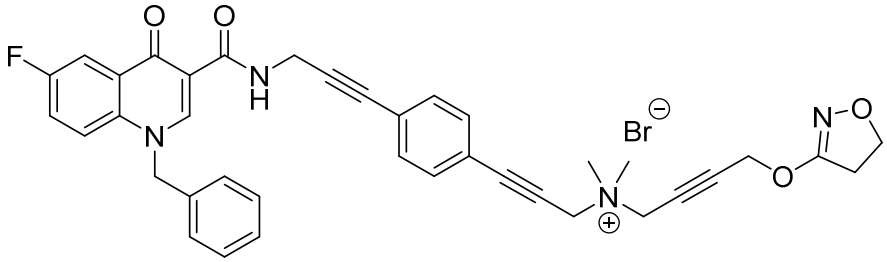

To a solution of iperoxo base[1] (104 mg, 0.57 mmol) in 10 mL acetonitrile, 1-Benzyl-*N*-(3-(4-(3-bromoprop-1-yn-1-yl)phenyl)prop-2-yn-1-yl)-6-fluoro-4-oxo-1,4-dihydroquinoline-3-carboxamide **17** (150 mg, 0.28 mmol) and a catalytic amount of KI/K_2CO_3 (1:1) were added. The reaction mixture was heated in the microwave (500 W, 80 °C) for 6 h. After cooling to room temperature the surplus of KI/K_2CO_3 was filtered off and the solvent was evaporated to half of the volume. Diethyl ether was added and the solution was kept in the fridge overnight. The precipitate obtained was filtered off, washed with Et_2O, and dried *in vacuo* to yield a beige solid (0.12 g, 0.17 mmol, 60%).

^{1}H NMR (DMSO, 400 MHz): δ [ppm] = 3.01 (t, *J* = 9.6 Hz, 2H), 3.22 (s, 6H), 4.32 (t, *J* = 9.6 Hz, 2H) 4.47 (d, *J* = 5.5 Hz, 2H), 4.59 (s, 2H), 4.68 (s, 2H), 4.95 (s, 2H), 5.83 (s, 2H), 7.23 - 7.53 (m, 9H), 7.69 (ddd, *J* = 3.1, *J* = 8.0, *J* = 9.4 Hz, 1H), 7.86 (dd, *J* = 4.3, *J* = 9.4 Hz, 1H), 8.00 (dd, *J* = 3.1, *J* = 9.0 Hz, 1H), 9.13 (s, 1H), 10.19 (t, *J* = 5.6 Hz, 1H).

^{13}C-NMR (DMSO, 101 MHz): δ [ppm] = 28.6, 32.1, 49.8, 53.4, 53.4, 53.9, 56.1, 57.2, 69.5, 75.7, 78.9, 80.9, 86.5, 89.8, 90.0, 110.2, 110.5 (d, J_{CF} = 23.3), 120.1, 121.1 (d, J_{CF} = 7.6), 121.5 (d, J_{CF} = 25.3), 123.5, 126.4, 127.9, 128.9, 128.9, 129.0, 131.6, 132.1, 135.6, 149.0, 159.2 (d, J_{CF} = 245.4), 163.7, 166.6, 174.6 (d, *J* = 1.6).

ESI-MS: *m/z* calcd. for $C_{38}H_{34}FN_4O_4^+$ $[M+H]^+$: 629.3, found: 629.1.

m.p.: 148° C

2 Pharmacology

2.1 Cell culture

All experiments were performed in HEK 293 cells stably expressing the receptor sensor, the Gq sensor or the Ca^{2+}/DAG sensor. Cells were kept at 37 °C in a humidified 7% CO_2 atmosphere and maintained in DMED with 4.5 g l 1, 10% (v/v) FCS, 100 U mL-1 penicillin, 100 µg mL-1 streptomycin sulfate and 2 mM L-glutamine and 200 µg mL 1 G-418. Every two to three days the cell lines were routinely passaged. Untransfected HEK cells were kept in supplemented DMEM without G418.

2.2 Stable cell line generation

Untransfected HEK293 cells were seeded into a culture dish with a confluency of 30 %. 24 hours after seeding, the cells were transfected with the Effectene® Transfection Reagent from Quiagene in accordance with the manufacturer's instructions. 24 hours after transfection, the normal culture medium was replaced by culture medium supplemented with 500 µg/ml G418. The medium was refreshed every two days until the bigger part of the cells were dead. The cells were counted, diluted and applied to 96-well plates resulting in a one cell to well distribution. The resulting monoclonal cell lines were characterized with fluorescence microscopy and investigated concerning their cDNA content.

2.3 Construction of the M1-I3N-CFP receptor FRET sensor

The receptor sensor M1-I3N-CFP used for all experimental approaches has been published and validated previously.[4] An enhanced cyan fluorescent protein (eCFP) was fused to the receptor C-terminus by standard PCR extension overlap technique.[5] Between receptor and fluorescent protein the amino acid sequence SR was inserted as a linker sequence, coding for XbaI restriction site. In the untruncated third intracellular loop (IL3) an amino acid sequence was introduced, thus the novel sequence reads QG227CCPGCCSGS228E. It specifically binds the fluorescein arsenical hairpin binder (FlAsH) and codes for a restriction site. The construct was cloned into pcDNA3 (Invitrogen) and verified by sequencing, done by Eurofins Genomics (Ebersberg, Germany).

2.4 FlAsH labeling

Before each experiment with the receptor FRET sensor a labeling protocol was applied as described previously.[6] Cells were grown on Poly-D-lysine coated glass coverslips to 80 %

confluency. Initially cells were washed with labeling buffer (150 mM NaCl, 10 mM HEPES, 2.5 mM KCl, 4 mM $CaCl_2$, 2 mM $MgCl_2$ supplemented with 10 mM glucose (pH 7.3)). After that cells were incubated with labeling buffer containing 500 nM FlAsH and 12.5 µM 1,2 ethanedithiol (EDT) for 1 h at 37 °C followed by flushing with labeling buffer. To reduce non-specific FlAsH binding, the cells were incubated for 10 min with labeling buffer containing 250 µM EDT. After flushing with labeling buffer the cells were held in cell culture medium. After the labeling protocol was realized FRET experiments were started immediately.

2.5 Construction of the Gq FRET sensor

The Gq FRET sensor used in this study, was published before.[7] The sensor consists of a yellow fluorescent protein (YFP) tagged Gγ subunit and a Gαq subunit with an inserted monomeric Turquoise fluorescent protein (mTurquoise). Due to ligand addition the transiently coexpressed wild type human M1 receptor gets activated and induces a dissociation of the Gq subunits. This results in a decreased FRET efficiency and a reduced FRET ratio. Upon buffer addition the receptor activation starts to decrease, the hetereotrimeric G-protein subunits reassociate and the FRET ration returns to a constant baseline.

2.6 Ligand application

Every probe was freshly prepared, before the experiments were started. Solubilizing the ligands and preparing different ligand concentration was done with a physiological measuring buffer (140 mM NaCl, 10 mM HEPES, 5.4 mM KCl, 2 mM $CaCl_2$, 1 mM $MgCl_2$ (pH 7.3)). Iperoxo was used as a reference ligand, prepared from a 1 mM solution that was stored at -20 °C and that have not been older than one month. Photo-Iperoxo **(12)** has also been prepared from a 1 mM stock that was storded at -20 °C. BQCAAI was stored as a powder at 4°C and was weighed out at the same day the experiments were performed and diluted to 100 µM. After solubilizing, all ligand solutions containing an azobenzene motive were subdivided into two volumes of equal size. One part was treated indistinguishable to normal ligand solutions. The other part was stored at room temperature in the dark under the exposure of 366 nm light (2 x 8 W fluorescent tubes) for at least 20 minutes, until the experiments were started.

2.7 Single cell FRET experiments

FRET experiments were performed at 25 °C in the dark, using HEK293 cells stably expressing the FRET sensors mentioned above. While performing the FRET experiments cells were maintained in measuring buffer. FRET measurements were performed using a Zeiss Axiovert 200 inverted microscope endued with a PLAN-Neoflar oil immersion 100-objective, a dual emission photometric system and a Polychrome IV light source (Till Photonica, Gräfelfig, Germany) as described previously.[6a, 8] Single cells were excited at 436 nm (dichroic 460 nm) with a frequency of 10 Hz. Emitted light was recorded using 535/30 nm and 480/40 nm emission filters and a DCLP 505 nm beam splitter for FlAsH and CFP, respectively. FRET was observed as the ratio of FlAsH/CFP, which was corrected offline for bleed through, direct FlAsH excitation and photo bleaching using the 2015 version of the Origin software. While FRET measurements cells were superfused with measuring buffer or various ligand solutions by using the ALA-VM8 perfusion system (ALA Scientific Instruments).

2.8 Ca^{2+}/DAG experiments

To specifically report the activation of the Gq-signalling pathway we used a dual fluorescence probe from Montana Molecular (downward DAG2/R Geco). This probe consist of two sensor, fused in frame on both sides of a 2A peptide sequence. The DAG sensor has a cpCFP attached to the C1 domain of a protein kinase C (PKC). The calcium sensor R-GECO consist of a red fluorescence protein fused to a Calmodulin domain. Upon receptor activation this dual fluorescence probe respond with an increase in red fluorescence and a decrease in green fluorescence. For each experiment HEK cells stably expressing the dual sensor were transfected with a C-terminal CFP tagged M1AChR. It was reported previously that this receptor construct does not significantly differ from the wild type receptor.

2.9 Confocal microscopy analysis and cell response quantification

Cells were grown on glass coverslips and 48h after transfection placed in an Attofluor holder, maintained in measuring buffer. Analyses were performed with a LeicaSP8 microscope, equipped with four detection channels. CFP was excited at 442 nm (442 Diode) and emission was detected in 460-490 nm range. GFP was excited using the 488 nm line (Ar laser) and detected from 520-575 nm. R-GECO was excited at 562 nm (DPSS 561) and detected from 600-700 nm. For characterizing photoswitchable probes light sources for 442 nm and 488 nm were switched of, in order to prevent enhanced spontaneous ligand isomerization. Time

series were taken using 512*512 resolution and non-sequential scan mode, leading to total image acquisition times of 1.290 sec. Cells were monitored for 200 frames. After 15 seconds cells were stimulated by adding a ligand stock solution. The final ligand concentration in the holder was 10 µM.

3 Supporting figures

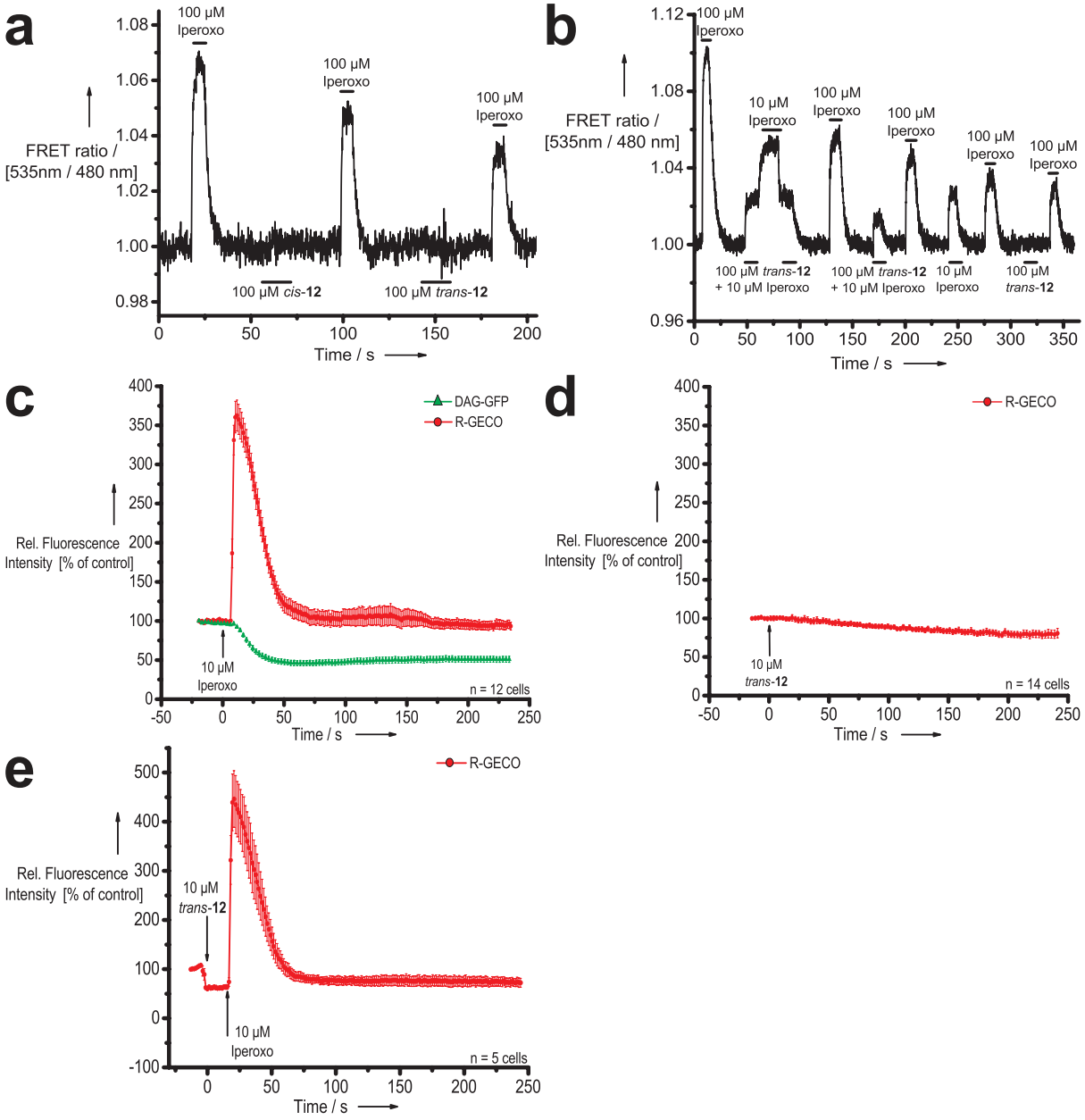

Supporting figure 2 characterization of photoiperoxo **12** in comparison to iperoxo. **(a)** Representative single cell recording of a stable HEK293 cell line expressing the M1-IN3-CFP receptor sensor. Iperoxo in a saturating concentration (100 µM) served as reference. **(b)** Competition experiment with different concentrations of iperoxo and **12** alone or under mixed conditions as indicated. **(c)** DAG und Ca^{2+} sensor characterization upon ligand addition. **(d)** Compound **12** was not able to induce an

increase in Ca^{2+} **(e)** Compound **12** did not induce a Ca^{2+} signal, iperoxo was then added showing Ca^{2+} response.

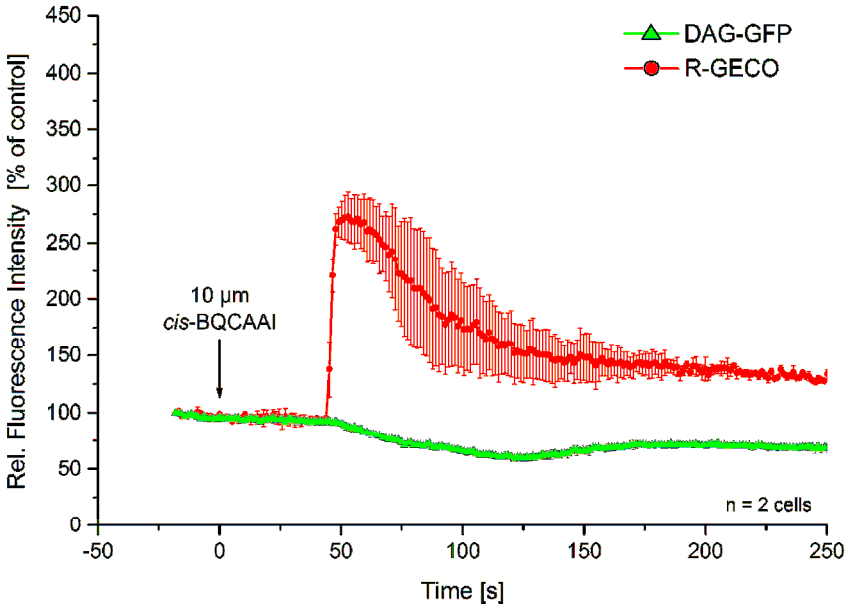

Supporting figure 3 Simultaneous characterization of the *cis* conformer with both fluorescent probes. By using this approach the *cis* conformer induces a 45 seconds delayed DAG and calcium response. This finding indicates, that while recording with the given settings an isomerization of *cis*-BQCAAI to *trans*-BQCAAI occurs.

4 Additional references

[1] J. Kloeckner, J. Schmitz, U. Holzgrabe, *Tetrahedron Lett.* **2010**, *51*, 3470-3472.

[2] Y. Zhi, L. X. Gao, Y. Jin, C. L. Tang, J. Y. Li, J. Li, Y. Q. Long, *Bioorg. Med. Chem.* **2014**, *22*, 3670-3683.

[3] a) C. Werner, H. Hopf, I. Dix, P. Bubenitschek, P. G. Jones, *Chemistry* **2007**, *13*, 9462-9477; b) H. Hopf, P. G. Jones, P. Bubenitschek, C. Werner, *Angew. Chem. Int. Ed.* **1995**, *34*, 2367-2368; *Angew. Chem.* **1995**, *107*, 2592–2594

[4] R. Messerer, M. Kauk, D. Volpato, M. C. Alonso Canizal, J. Klöckner, U. Zabel, S. Nuber, C. Hoffmann, U. Holzgrabe, *ACS Chem. Biol.* **2017**.

[5] S. N. Ho, H. D. Hunt, R. M. Horton, J. K. Pullen, L. R. Pease, *Gene* **1989**, *77*, 51-59.

[6] a) C. Hoffmann, G. Gaietta, M. Bünemann, S. R. Adams, S. Oberdorff-Maass, B. Behr, J. P. Vilardaga, R. Y. Tsien, M. H. Ellisman, M. J. Lohse, *Nat. Methods* **2005**, *2*, 171-176; b) C. Hoffmann, G. Gaietta, A. Zurn, S. R. Adams, S. Terrillon, M. H. Ellisman, R. Y. Tsien, M. J. Lohse, *Nat. Protoc.* **2010**, *5*, 1666-1677; c) A. Zürn, U. Zabel, J. P. Vilardaga, H. Schindelin, M. J. Lohse, C. Hoffmann, *Mol. Pharmacol.* **2009**, *75*, 534-541.

[7] M. J. Adjobo-Hermans, J. Goedhart, L. van Weeren, S. Nijmeijer, E. M. Manders, S. Offermanns, T. W. Gadella, Jr., *BMC Biol.* **2011**, *9*, 32.

[8] J. P. Vilardaga, M. Bünemann, C. Krasel, M. Castro, M. J. Lohse, *Nat. Biotechnol.* **2003**, *21*, 807-812.

Appendix III:

Agnetta, L.; Bermudez, M.; Riefolo, F.; Matera, C.; Claro, E.; Messerer, R.; Littmann, T.; Wolber, G.; Holzgrabe, U.; Decker, M. Fluorination of Photoswitchable Muscarinic Agonists Tunes Receptor Pharmacology and Photochromic Properties. *J. Med. Chem.* **2019**, *62*, 3009-3020.

https://pubs.acs.org/doi/10.1021/acs.jmedchem.8b01822

Journal of Medicinal Chemistry

Article

Cite This: J. Med. Chem. 2019, 62, 3009−3020

pubs.acs.org/jmc

Fluorination of Photoswitchable Muscarinic Agonists Tunes Receptor Pharmacology and Photochromic Properties

Luca Agnetta,[†] Marcel Bermudez,[‡] Fabio Riefolo,[§,∥] Carlo Matera,[§,∥] Enrique Claro,[⊥] Regina Messerer,[†] Timo Littmann,[#] Gerhard Wolber,[‡] Ulrike Holzgrabe,[†] and Michael Decker*[,†]

[†]Pharmaceutical and Medicinal Chemistry, Institute of Pharmacy and Food Chemistry, Julius Maximilian University of Würzburg, Am Hubland, 97074 Würzburg, Germany

[‡]Institute of Pharmacy, Freie Universität Berlin, Königin-Luise-Straße 2 + 4, 14195 Berlin, Germany

[§]Institute for Bioengineering of Catalonia (IBEC), Barcelona Institute for Science and Technology, Carrer Baldiri Reixac 15-21, 08028 Barcelona, Spain

[∥]Network Biomedical Research Center in Bioengineering, Biomaterials, and Nanomedicine (CIBER-BBN), 50018 Zaragoza, Spain

[⊥]Institut de Neurociències (INc) and Departament de Bioquímica i Biologia Molecular, Unitat de Bioquímica de Medicina, Universitat Autònoma de Barcelona (UAB), Bellaterra, 08193 Barcelona, Spain

[#]Institute of Pharmacy, University of Regensburg, Universitätstraße 31, 93053 Regensburg, Germany

Supporting Information

ABSTRACT: Red-shifted azobenzene scaffolds have emerged as useful molecular photoswitches to expand potential applications of photopharmacological tool compounds. As one of them, tetra-*ortho*-fluoro azobenzene is well compatible for the design of visible-light-responsive systems, providing stable and bidirectional photoconversions and tissue-compatible characteristics. Using the unsubstituted azobenzene core and its tetra-*ortho*-fluorinated analogue, we have developed a set of uni- and bivalent photoswitchable toolbox derivatives of the highly potent muscarinic acetylcholine receptor agonist iperoxo. We investigated the impact of the substitution pattern on receptor activity and evaluated the different binding modes. Compounds **9b** and **15b** show excellent photochemical properties and biological activity as fluorination of the azobenzene core alters not only the photochromic behavior but also the pharmacological profile at the muscarinic M_1 receptor. These findings demonstrate that incorporation of fluorinated azobenzenes not just may alter photophysical properties but can exhibit a considerably different biological profile that has to be carefully investigated.

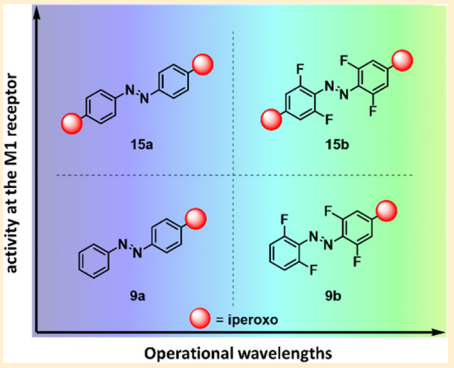

INTRODUCTION

In recent years, many different biochemical targets, including ion channels, enzymes, and lipids, have been effectively modulated in a light-controlled fashion using photoswitchable ligands, expanding the vibrant field of photopharmacology.[1] Now, the potential of the application of photopharmacological tool compounds to G protein-coupled receptors (GPCRs) is being steadily investigated.[2] The rapid light-induced isomerization of photochromic ligands can be directly translated into a change in affinity or activity. This can give important new insights into the binding mode and time course of activation processes, enabling precise spatial and temporal resolution of the complex signaling pathway of GPCRs.[3] The muscarinic acetylcholine (ACh) receptors (mAChRs), which belong to class A GPCRs, have received special attention in this regard due to their role as a prototypic pharmacological system[4] and their therapeutic potential.[5] The muscarinic receptors mediate the excitatory and inhibitory effects of the neurotransmitter acetylcholine (ACh),[6] thus regulating diverse important biological processes. Muscarinic receptors are widely expressed in the human body including the central nervous system (M_1/M_4/M_5) related to neurological processes of memory and learning. In the peripheral nervous system (M_2/M_3), they are related to the so-called "rest and digest" biological functions.[7] In this work, we present an optimized approach for the application of photochromic ligands to GPCRs by using the M_1 receptor as a prototypic model system, outlining the advantages and challenges of using red-shifted molecular photoswitches.

Accordingly, we focused on the highly potent orthosteric agonist iperoxo in the design of bidirectional pharmacological tool compounds with tuned photochemical properties. Iperoxo (iper) is a muscarinic ACh receptor agonist with outstanding potency that is known to tolerate bulky substituents without compromising agonist efficacy.[8] Recently, we reported on photoiperoxo (**9a**), a compound that consists of iperoxo extended with a molecular photoswitch and a dualsteric

Received: November 21, 2018
Published: March 3, 2019

DOI: 10.1021/acs.jmedchem.8b01822
J. Med. Chem. 2019, 62, 3009−3020

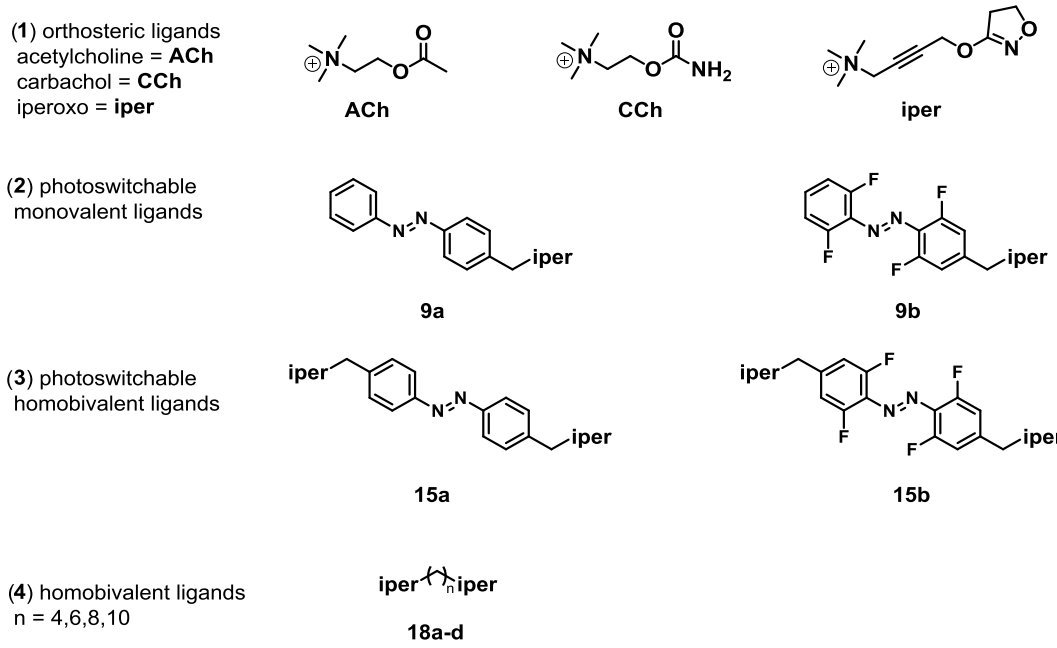

Figure 1. Structures of (1) reference agonists acetylcholine (ACh), carbachol (CCh), and iperoxo (iper); (2) univalent; and (3) homobivalent photoswitchable derivatives with azobenzene- and tetra-*ortho*-fluoro azobenzene scaffolds and homobivalent ligands linked by polymethylene linkers.

photochromic ligand **BQCAAI**.[2c] We made use of azobenzene as a molecular photoswitch to change intrinsically the geometry and polarity of the linking unit and to control its activation by light.[1a,b,d] Upon irradiation with UV- and blue light, and thus triggering a switch from the trans- to the cis-form, we were able to control the efficacy and to investigate the time course of receptor activation processes.[2c]

Despite this remarkable progress in the development of photopharmacological tool compounds, the poor photostationary states (PSSs) of our azobenzene-based systems resulted in an unclear correlation between the ratio of the cis/trans concentration to the actual activity at the receptor. The PSS strongly depends on the electronic environment of the system and the overlap of transitions of the cis/trans photoisomers and can be influenced by changing the substitution pattern of the azobenzene moiety. Additionally, the operational wavelengths to trigger photoisomerization can interfere to a significant degree with the fluorescent readout methods that are commonly used in GPCR research. To investigate the complex nature of M_1 activation, photopharmacological tool compounds should ideally show superior photochemical properties, such as quantitative and stable bidirectional photoswitching, and be responsive to visible rather than high-energy light.[1a,b,d] A convincing approach to optimize the photochemical properties of azobenzenes involving the tetra-ortho-substitution of azobenzene has been described previously by the groups of Woolley[9] and Hecht.[10] By choosing the suitable moieties, tetra-ortho-substitution leads to a separation of the n → π^* transitions of trans and cis isomers and ultimately to almost complete trans/cis photoconversions. Importantly, the desired isomer can be selectively formed with wavelengths in the visible-light window. Despite their promising application in photobiology due to the well-separated n → π^* transitions,[11] ortho-methoxylated azobenzenes are sterically demanding and strongly twisted about the N−N double bond. This makes them unlikely to fit into the narrow receptor binding pocket. Ortho-chlorinated and fluorinated azobenzenes show comparable red-shifted trans n−π^* transitions, albeit somewhat less than ortho-methoxylated, and have been successfully employed in biological applications.[12] However, tetra-ortho-fluoro substituted azobenzenes stand out in their slow thermal cis-to-trans relaxation rate, representing a truly bistable molecular switch on the biological time scale. Moreover, the fluorine substituents are sterically less demanding compared to the chlorine ones.[10a] Based on these results, we further investigated the effect of iperoxo-derived photoswitchable ligands by developing a set of tool compounds, containing the iperoxo motif and the tetra-*ortho*-fluoro azobenzene or unsubstituted azobenzene, separately.

In modern medicinal chemistry, the bivalent strategy has been extensively applied to GPCR ligands.[13] Appropriately designed bivalent ligands can exhibit higher affinity, potency, and selectivity compared with the parent ligand, with potential therapeutic application.[14] Successful examples of the application of this approach to GPCRs include the human cannabinoid receptor 2,[15] opioid receptor,[16] dopamine 2,[17] and muscarinic receptors.[18] To this end, we extended the photoiperoxo structure with another iperoxo moiety, creating a homobivalent ligand, to improve and investigate binding at the M_1 receptor.

RESULTS AND DISCUSSION

We now report the design and synthesis of photoswitchable homobivalent iperoxo (**15a**), tetra-*ortho*-fluoro-photoiperoxo (**9b**), and homobivalent tetra-*ortho*-fluoro-photoiperoxo (**15b**), being the corresponding tetra-ortho-fluorinated analogues of the azobenzene iperoxo derivatives (Figure 1). In addition, we synthesized homobivalent iperoxo derivatives (**18a−d**) connected by aliphatic chains as reference compounds to identify the optimal distance between the two orthosteric moieties for dualsteric binding.

DOI: 10.1021/acs.jmedchem.8b01822
J. Med. Chem. 2019, 62, 3009−3020

Scheme 1. Synthesis of Photoiperoxo and F_4-Photoiperoxo[a]

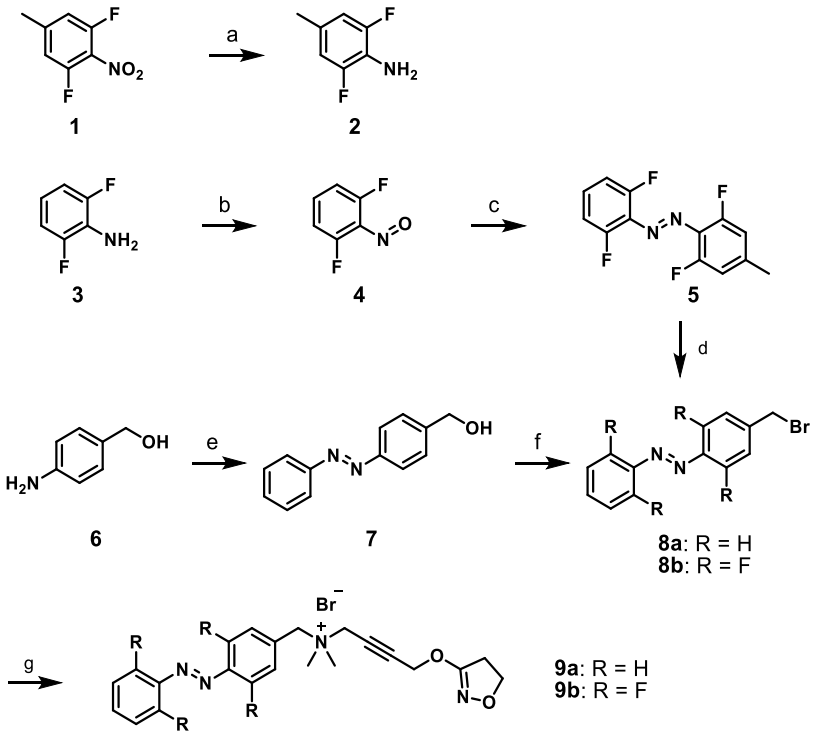

[a]Reagents and conditions: (a) Pd/C, EtOH (87%); (b) oxone, CH_2Cl_2, water; (c) **2**, AcOH/trifluoroacetyl (TFA), toluene (43%); (d) *N*-bromosuccinimide (NBS), azobisisobutyronitrile (AIBN), CCl_4, 80 °C (50%); (e) nitrosobenzene, AcOH (75%); (f) CBr_4, PPh_3, CH_2Cl_2 (60%); (g) 4((4,5-dihydroisoxazol-3-yl)oxy)-*N*,*N*-dimethylbut-2-yn-1-amine **16**, EtOAc/MeCN (39% for **9a**, 92% for **9b**).

Scheme 2. Synthesis of Iper-azo-iper and F_4-Iper-azo-iper[a]

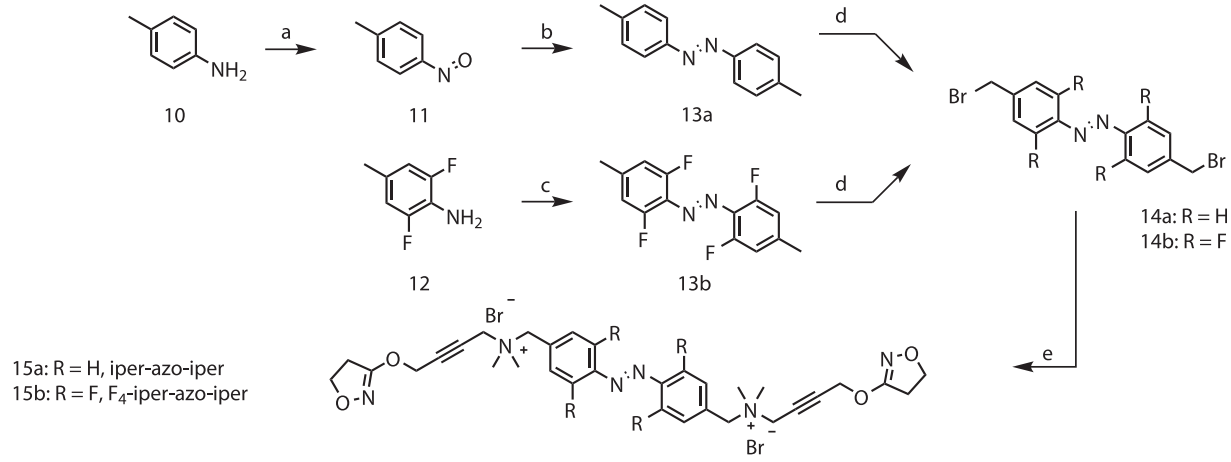

[a]Reagents and conditions: (a) oxone, CH_2Cl_2, water; (b) **10**, AcOH (36%); (c) $KMnO_4$, $FeSO_4{\cdot}7H_2O$, CH_2Cl_2 (29%); (d) NBS, AIBN, CCl_4, 80 °C (76% for **14a**, 24% for **14b**); (e) 4((4,5-dihydroisoxazol-3-yl)oxy)-*N*,*N*-dimethylbut-2-yn-1-amine, EtOAc, 60 °C (83% for **15a**, 32% for **15b**).

Chemistry. The synthetic routes for the uni- and homobivalent ligands are summarized in Schemes 1 and 2, respectively. Azobenzene moieties **5** and **7** were accessed starting from the corresponding anilines **2**, obtained from reduction of 1,3-difluoro-5-methyl-2-nitrobenzene **1**, and commercially available (4-aminophenyl)methanol **6**. Anilines were used in Baeyer–Mills reactions with 1,3-difluoro-2-nitrosobenzene **4** and nitrosobenzene, respectively, to afford precursors for bromination, which took place under either radical (for **8b**) or nucleophilic substitution conditions (for **8a**). Lastly, 4((4,5-dihydroisoxazol-3-yl)oxy)-*N*,*N*-dimethylbut-2-yn-1-amine, prepared using the standard convergent procedure as described previously,[19] was connected to the photoswitches to afford photoiperoxo **9a** and F_4-photoiperoxo **9b**.

The synthesis of the homobivalent ligands started from commercially available *p*-toluidine **10**, which was condensed to compound **13a** by means of a Baeyer–Mills reaction. Tetra-ortho-fluorinated analogue **13b** was obtained by oxidative coupling of **12** with potassium permanganate and iron sulfate heptahydrate as oxidizing reagents. Again, radical bromination and substitution with 4((4,5-dihydroisoxazol-3-yl)oxy)-*N*,*N*-

DOI: 10.1021/acs.jmedchem.8b01822
J. Med. Chem. 2019, 62, 3009–3020

Table 1. UV−Vis Spectroscopic Data of Compounds 9a, 9b, 15a, and 15b[a]

	trans		trans		cis				
cmpd.	λ_{max} ($\pi-\pi^*$)	ε ($\pi-\pi^*$) ($\times10^3$ M^{-1} cm^{-1})	λ_{max} (n−π^*) (nm)	ε (n−π^*) (M^{-1} cm^{-1})	λ_{max} (n−π^*) (nm)	ε (n−π^*) ($\times10^3$ M^{-1} cm^{-1})	$\Delta\lambda$ (n−π^*) (nm)	PSS_{trans} (%)	PSS_{cis} (%)
9a	320	12.2	418	680	418	1.04	<10	90	62
15a	320	22.0	426	920	426	1.42	<10	99	60
9b	307	16.7	443	1440	412	1.80	31	94	86
15b	311	14.8	447	1180	412	1.38	35	93	98

[a] λ_{max} ($\pi-\pi^*$, n−π^*) represents the wavelength at the maximal absorption of the $\pi-\pi^*$ and n−π^* transition bands, respectively. The molar extinction coefficients ε ($\pi-\pi^*$, n−π^*) were calculated according to the Lambert−Beer formula. $\Delta\lambda$ (n−π^*) is the difference between trans and cis regarding λ_{max} of the n−π^* band. PSS percentages after irradiation with operational wavelengths determined by liquid chromatography using the wavelength at the isosbestic point as the detecting wavelength.

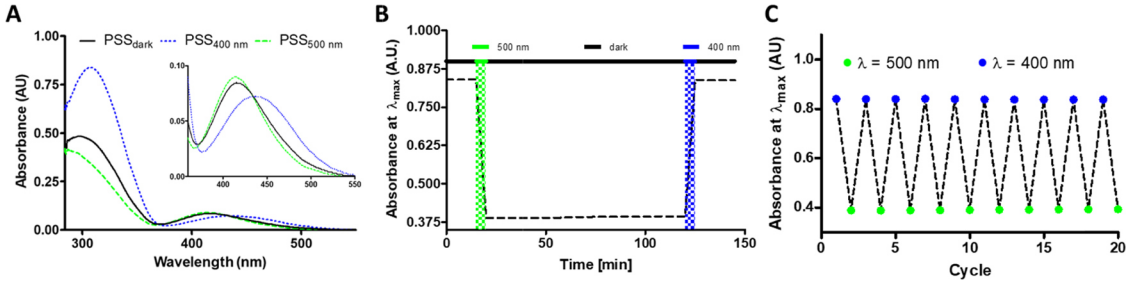

Figure 2. Representative (A) absorption spectra of PSS at the dark-adapted state and after illumination with 400 nm (to trans) and 500 nm (to cis), (B) stability measurement and (C) multiple cis/trans isomerization cycles of compound **9b** in dimethyl sulfoxide at 25 °C. Spectra of compounds **9a**, **15a**, and **15b** are displayed in the Supporting Information section.

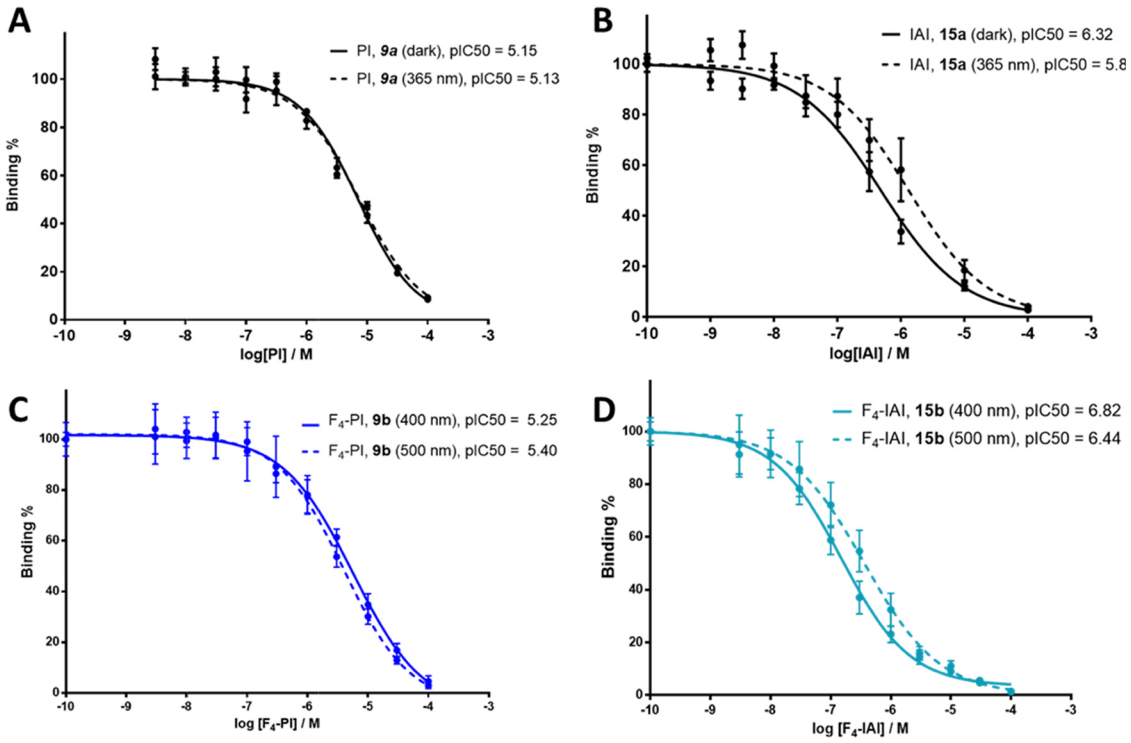

Figure 3. Competition for specific binding of 200 pM [^{3}H]QNB to rat brain membranes containing high density of all the five mAChRs by **9a**, **9b**, **15a**, and **15b**. Data points were fitted using the "log(inhibitor) vs normalized response − variable slope" function in GraphPad Prism 6.

dimethylbut-2-yn-1-amine resulted in formation of target compounds **15a** and **15b**. Aliphatic derivatives (**18a−d**) were synthesized reacting the corresponding double brominated aliphatic chains with 2 equiv of 4((4,5-dihydroisoxazol-3-yl)oxy)-*N*,*N*-dimethylbut-2-yn-1-amine (Suppl. Scheme 5).

UV−Vis Spectroscopic Characterization. The UV−vis absorption spectra of the set of compounds **9a**, **9b**, **15a**, and **15b** were measured at a concentration of 50 μm in dimethyl sulfoxide (DMSO). For compounds **9a** and **15a** (with unsubstituted azobenzene scaffold), we observed a strong $\pi-\pi^*$ transition band at short wavelength ($\lambda_{\pi-\pi^*} \approx 320$ nm)

DOI: 10.1021/acs.jmedchem.8b01822
J. Med. Chem. 2019, 62, 3009−3020

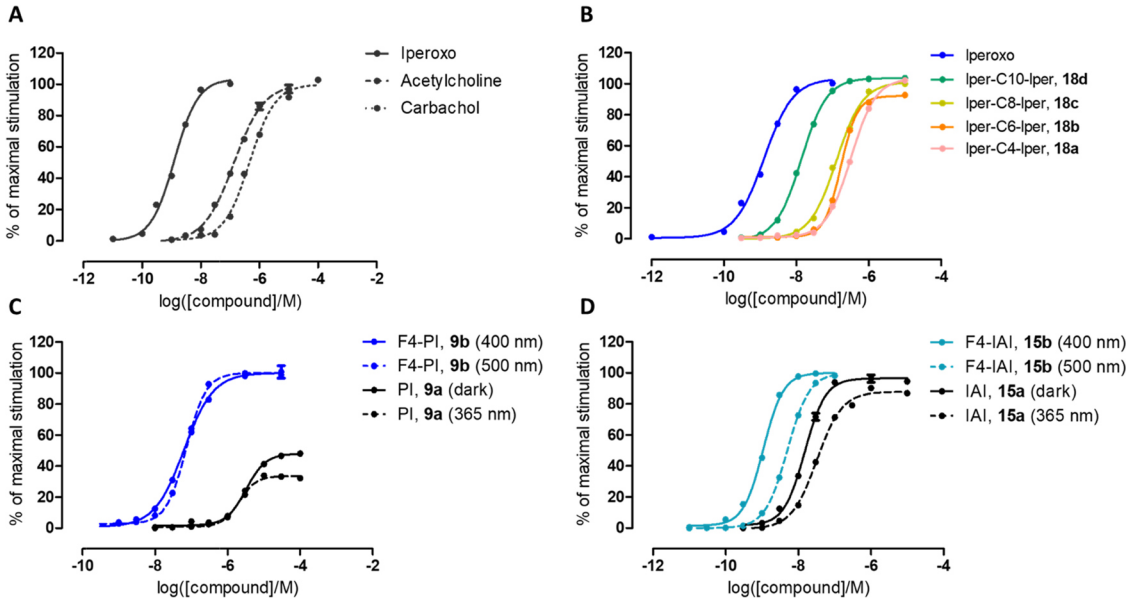

Figure 4. Gα/PLC-β3 split-luciferase interaction assay in HEK 293T cells expressing the human muscarinic M_1 receptors. Concentration−response curves for (A) reference compounds, (B) iper-linker-iper derivatives (**18a−d**), (C) **9a** and **9b**, and (D) **15a** and **15b** at operational wavelengths specific for the respective photoconversion. Data represent means ± standard error of the mean of three to four experiments conducted at least in triplicate.

and a weaker n−π* ($\lambda_{n-\pi^*} \approx 422$ nm) upon irradiation with blue light (400 nm, trans isomer). Irradiation with UV light (365 nm), and thus photoconversion to the cis-isomer, leads to a decrease in absorbance intensity of the $\pi-\pi$* and increase of the n−π* band without affecting the wavelengths of the respective transition bands. Spectra of fluorinated compounds **9b** and **15b** were measured using 400 nm for cis → trans and 500 nm for trans → cis photoconversions. Due to the n-orbital stabilization of electron-withdrawing groups in the cis-state, tetra-ortho-fluoro substitution of the azobenzene core causes a separation of the transitions of the n−π* band, in our case of around 33 nm on average, which makes it possible to address both isomers selectively with light in the visible region (Figure 1A).[20] As a direct consequence, the PSSs (measured by means of liquid chromatography at the isosbestic point wavelength) are substantially higher than for nonfluorinated analogues (Table 1), which is beneficial for the application of photoswitchable ligands in biological systems and allows a clear correlation between the distinct photoisomer and its biological effect. Moreover, multiple cis/trans switching cycles did not cause noticeable degradation, highlighting the reliability and robustness of the photochromic conversion of both the tetra-ortho-fluoro and unsubstituted azobenzene scaffolds. This is confirmed by stability measurements in which the compounds were kept in the dark for at least 120 min after switching to the less stable cis-isomer, without significant changes in absorbance and hence in the PSS. Importantly, this information is required when considering eventual incubation times required in biological assays, making sure that the photoswitchable ligands do not relax to the trans-isoform during the readout (Figure 1B,C). From the physicochemical point of view, this set of compounds shows ideal characteristics for stable and bidirectional photoswitching (Figure 2).

Binding Experiments. First, **9a**, **9b**, **15a**, and **15b** were tested for affinity to the M receptors. This was achieved in competition experiments with the photoswitchable ligands in rat brain membrane preparations. These were conducted as described previously[21] and contained a high density of all the five mAChR subtypes. [^{3}H]Quinuclidinyl benzilate ([^{3}H]QNB) is a nonselective muscarinic ligand, which allows the identification of muscarinic receptors,[22] and displays an equilibrium dissociation constant of about 40 pM,[23] making it suitable for these experiments. Specific binding was defined with test compounds at total nominal concentrations in the range of 1−100 μm and elaborating the raw dpm data from the scintillation counter,[21] representing total radioactivity.

In general, compounds **9a**, **9b**, **15a**, and **15b** were found to show good affinity for the M receptors (Figure 3). In particular, the azobenzene-elongated iperoxo **9a** and **9b** showed a binding affinity in the low-micromolar range, although no significant changes could be observed upon irradiation ($pIC_{50} \simeq 5$ for both photoisomers, Figure 3A,C). The affinity increased significantly for the homobivalent ligands **15a** and **15b**. In good agreement with results from the split-luciferase interaction assay, *trans*-**15a** showed an affinity in the high-nanomolar range, with a significant difference between the two photo isoforms ($pIC_{50} = 6.32$ in the dark vs 5.88 under illumination with 365 nm light, Figure 3B). Thus, we observed that despite the introduction of an azobenzene molecular photoswitch, a good affinity could be preserved. Moreover, the presence of a second moiety of iperoxo, as in the homobivalent ligands **15a** and **15b**, improved binding affinity and created an appreciable difference between trans and cis isomers.

Biological in Vitro Assay. Our goal was to assess the extent to which the pharmacological profiles of these compounds change after fluoro substitution of the azobenzene core. For this purpose, we used a novel split-luciferase complementation technique detecting the interaction between the Gαq subunit and phospholipase C-β3 (PLC-β3) and thus reflecting G protein activation in living HEK 293T cells expressing the human M_1 receptor.[24] The split-luciferase complementation technique is particularly suitable to detect protein−protein interactions and associated signaling in living cells.[25] Since it is

DOI: 10.1021/acs.jmedchem.8b01822
J. Med. Chem. 2019, 62, 3009−3020

not fluorescence-based, no excitement irradiation is needed and, consequently, its readout does not interfere with the operational wavelengths for photoswitching, providing clear-cut and distinguishable concentration−response curves for each photoisomer, which makes it highly suitable for photopharmacological investigations into GPCRs. Technically, HEK 293T cells were engineered to express a fragment of the luciferase at the Gαq subunit of the heterotrimeric G protein and the complementary fragment at the N-terminus of the PLC-β3. Upon binding of the endogenous or synthetic agonists, both fragments are brought in close proximity, leading to a reconstitution of the functional luciferase protein and emission of bioluminescence, in the presence of the substrate luciferin.[24] Also advantageous is the fact that the receptor itself, in this case M_1, remains unengineered in contrast to, for example, fluorescence resonance energy transfer (FRET) sensors, where often large constructs at intracellular loops could act as anchors and may affect changes in conformations. Pharmacological data are depicted in Figure 4 and summarized in Table 2 and show the recorded potencies and efficacies of compounds **9a**, **9b**, **15a**, and **15b**, reflected by the pEC_{50}, and maximal response E_{max} for each isomer. The data are normalized to the maximum response of the synthetic agonist carbachol (CCh) at a concentration of 100 μm. Measurements of the endogenous agonists acetylcholine (ACh) and the synthetic parent compound iperoxo as references were not affected by illumination with operational wavelengths.

Table 2. Pharmacological Data[a]

cmpd.		pEC_{50}		$\%E_{max}$	
iperoxo		8.90 ± 0.02		103.5 ± 1.0	
CCh		6.34 ± 0.02		99.9 ± 0.9	
ACh		6.87 ± 0.03		99.9 ± 1.8	
18a		6.49 ± 0.01		103.6 ± 0.6	
18b		6.77 ± 0.01		92.2 ± 0.6	
18c		6.89 ± 0.01		101.1 ± 0.8	
18d		7.86 ± 0.02		103.7 ± 0.7	
cmpd.	trans	cis	trans	cis	
9a	5.49 ± 0.01	5.68 ± 0.02	48.0 ± 0.4	33.5 ± 0.5	
9b	7.20 ± 0.02	7.14 ± 0.01	98.3 ± 1.2	99.7 ± 0.6	
15a	7.82 ± 0.02	7.49 ± 0.02	96.5 ± 1.1	87.9 ± 0.7	
15b	8.97 ± 0.01	8.30 ± 0.02	99.7 ± 0.3	99.1 ± 0.4	

[a] pEC_{50}, concentration of the indicated compounds inducing a half-maximal effect ($-\log EC_{50}$ values); $\%E_{max}$, maximum effect as a percentage of E_{CCh} (100 μm). Data were obtained by curve fitting to data from individual experiments shown in Figure 4.

First, bivalent alkyl-substituted iperoxo compounds were screened to identify the correlation between the distance of the orthosteric moieties and their corresponding biological activity. For this purpose, homobivalent ligands **18a−d** with different chain lengths were employed. All compounds were characterized as full agonists, and longer spacer proved advantageous for the M_1 affinity, suggesting a dualsteric binding.[26] The C10-spacer, which is comparable to the azobenzene scaffold, shows the highest effect and suggests this distance as optimal for the design of photoswitchable ligands (Suppl. Figure 1).

As investigated in previous studies, photoiperoxo **9a** was unable to induce a conformational change at the M_1 receptor in FRET studies, upon illumination with either UV- or blue light. Instead, it exhibited antagonist behavior in competition experiments.[2c] Using the split-luciferase complementation assay, **9a** shows two distinct curves for each photoisomer, differing in their efficacy. The maximal response E_{max} was 48% for the trans and 34% for the cis photoisomer, indicating partial agonism at the M_1 receptor. Surprisingly, substitution of azobenzene with the tetra-ortho-fluorinated scaffold resulted in full agonist **9b** with a significant potency enhancement and pEC_{50} values almost two log units higher (comparable to endogenous agonist ACh). However, no significant changes in efficacy or affinity could be observed for **9b** upon irradiation.

The potency at the M_1 receptor was modulated effectively by introducing an additional iperoxo moiety, resulting in the homobivalent ligand **15a**. By doing so, considerable improvement in the potency was gained and a difference between the two photoisomers was re-established. Again, replacement of the azo-core with tetra-ortho-fluoro scaffold (**15b**) resulted in a distinctive change toward higher potency, being almost 10-fold more pronounced for the *trans* isomer. Noteworthy, *trans*-**15b** shows a pEC_{50} concentration in the one-digit nanomolar range, which is comparable to the agonist iperoxo itself. This is

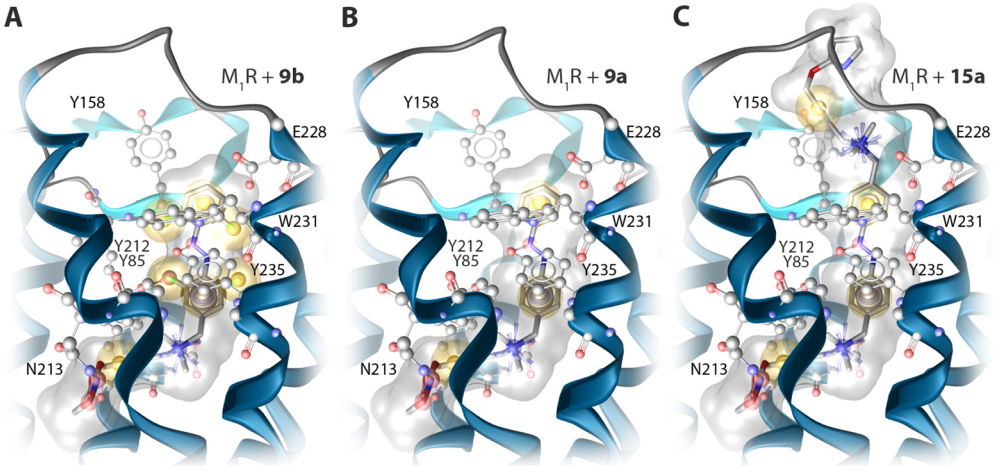

Figure 5. Proposed binding modes and interactions of trans isomers of photoswitchable dualsteric iperoxo derivatives (A) **9b**, (B) **9a**, and (C) **15a** in complex with the M_1 receptor. Positive ionizable centers are shown as blue stars, yellow spheres indicate lipophilic contacts, purple disks show aromatic interactions, and red arrows indicate hydrogen bonds.

DOI: 10.1021/acs.jmedchem.8b01822
J. Med. Chem. 2019, 62, 3009−3020

a remarkable observation, as the introduction of a molecular photoswitch generally causes an overall loss in activity at the receptor. A photoswitch-endowed compound showing an almost identical potency as the reference compound is hard to achieve. Taken together, these findings suggest that binding of trans-form of bivalent derivatives **15a**, **15b**, and **9b** stabilizes the M_1 receptor in the active conformation to a greater extent than **9a**. Additionally, fluoro substitution leads to pronounced differences in biological activity and is beneficial for binding to the M_1 receptor. As such, we developed a set of photopharmacological GPCR tool compounds for a better understanding of M_1 receptor binding modes.

Molecular Modeling. Docking studies using a previously reported homology model of the active M_1 receptor conformation[27] reveal a dualsteric (bitopic) binding mode for all investigated photoswitchable iperoxo derivatives in their trans conformation (Figure 5). We surmise that the photoswitch primarily occurs in solution and that the pharmacological properties are mainly driven by binding of trans isomers. The active M_1 receptor model indicates a narrow channel between the orthosteric and allosteric binding sites, rendering binding of cis conformations to the receptor unlikely due to steric interference with the tyrosine lid. Similar to other iperoxo-based dualsteric ligands,[28] the iperoxo moiety is located in the orthosteric binding pocket showing interactions with D84, N213, and the tyrosine lid consisting of Y85, Y212, and Y235 (Figure 5). For all compounds, a hydrogen bond between the azo group and the hydroxy group of Y235 is formed. The side chain of Y235 shows a reorientation toward the extracellular side, which allows binding of azobenzene scaffolds through $\pi-\pi$ interactions. This side-chain position allows full contraction of the orthosteric binding site without full closure of the tyrosine lid and thereby stabilizes active receptor conformations.

Interestingly, fluorination of the azobenzene scaffold results in a higher potency of **9b** and **15b** compared to the nonfluorinated compounds **9a** and **15a**. This can be rationalized in our model by an optimal geometry of the aromatic ring in the M_1 receptor. Whereas the phenyl ring opposite to Y235 is more flexible in **9a** and **15a**, it is restrained in an orientation optimal for parallel $\pi-\pi$ interaction. This is caused by the spatial requirements of the ortho-fluorine atoms in **9b** and **15b** and an additional hydrogen bond with the hydroxy group of Y85 (Figure 5A). In addition, fluorinated compounds show additional lipophilic contacts with the tyrosine lid as well as W231 (Figure 5A,B). Since the symmetric compounds **15a** and **15b** are larger, they show secondary interactions in the extracellular vestibule compared to **9a** and **9b**. In particular, a charge interaction of the ammonium group in the extracellular receptor domain with E228 can be observed (Figure 5C). Positive charges in the allosteric vestibule recognized by aromatic residues or the EDGE sequence have previously been found to be important for the M_2 receptor.[28b,29]

Interestingly, the M_2 receptor lacks the presence of an acidic residue at the beginning of transmembrane domain 7, suggesting a specific role for E228 in the M_1 receptor. This observation is in accordance with the higher potencies for **15a** and **15b** that can be explained by this specific charge interaction and additional lipophilic contacts with Y158, which were not observed for **9a** and **9b** due to the lack of an allosteric ammonium group (Figure 5). The absence of extensive allosteric interactions and less lipophilic contacts of **9a** compared with **9b** suggests a ligand−receptor complex in which **9a** is not able to fully stabilize the active receptor state. This is supported by previously reported FRET-based measurements indicating the insensitivity of the M_1 receptor upon **9a** binding with regard to conformational changes.[2c] However, the here-applied Gα/PLC-β3 split-luciferase interaction assay unveiled **9a** as a weak partial agonist (E_{max} 34−48%).

At first sight, it may appear conflicting that the cis photoisomers bind to the receptor and induce a receptor response, whereas the docking data predict only the trans photoisomers to bind. On a closer look, even though the fluorinated azobenzene scaffold provides higher PSS, a distinct percentage of trans isomer remains (Table 1), which can still bind and activate the receptor. On a logarithmic scale, as used for the binding and functional studies, even a small trans percentage shows a pronounced effect. An alternative explanation can be rationalized by a second purely allosteric binding mode as shown for several other dualsteric ligands.[26,28a] For such a binding pose, the cis orientation is compulsory, forming $\pi-\pi$ and cation−π interactions, which can, to a certain extent, favor the active state of the receptor. In contrast, the linear nature of the trans photoisomer is not suitable to solely bind to the allosteric binding site. At this stage, this is still a subject of future investigations though.

CONCLUSIONS

We successfully developed a set of photopharmacological tools that allowed detailed investigation of the distinct effects of fluorination and bivalency on binding properties at the M_1 receptor. We designed photoswitchable iperoxo (**9a**) and bivalent iperoxo (**15a**) compounds, as well as the red-shifted congeners (**9b**, **15b**) by introduction of the tetra-ortho-fluoro scaffold. Bivalent compounds (**15a**, **15b**) show much higher affinity compared to the univalent compounds (**9a**, **9b**) due to additional interactions at allosteric binding sites. Remarkably, the fluorine compounds (**9b**, **15b**) not only show improved operational wavelengths as shown in a novel, light-independent luciferase complementation assay, but also increased potency at the M_1 receptor. Bivalent and fluorinated photoiperoxo (**15b**) act as pronounced affinity switches, whereas the univalent photoiperoxo acts as an efficacy switch (**9a**). The work significantly enlarges the photopharmacological toolbox for mAChRs. We strongly recommend detailed pharmacological evaluation for red-shifted compounds since their biological properties might differ significantly from the parent compound. It will be interesting to investigate the potential for in vivo photopharmacological control of this series.

EXPERIMENTAL SECTION

General Information. Common reagents and solvents were obtained from commercial suppliers (Aldrich, Steinheim, Germany; Merck, Darmstadt, Germany) and were used without any further purification. Tetrahydrofuran (THF) was distilled from sodium/benzophenone under an argon atmosphere. Microwave-assisted reactions were carried out on an MLS-rotaPREP instrument (Milestone, Leutkirch, Germany) using 8−10 Weflon disks. Melting points were determined on a Stuart melting point apparatus SMP3 (Bibby Scientific, U.K.). Thin-layer chromatography was performed on silica gel 60 F254 plates (Macherey-Nagel, Düren, Germany), and spots were detected under UV light (λ = 254 nm) or by staining with iodine. Merck silica gel 60 (Merck, Darmstadt, Germany) was used for chromatography (230−400 mesh) columns or performed on an Interchim puriFlash 430 (Ultra Performance Flash Purification)

DOI: 10.1021/acs.jmedchem.8b01822
J. Med. Chem. 2019, 62, 3009−3020

instrument (Montluçon, France). Used columns are silica 25 g, 30 μm, Alox-B 40 g, 32/63 μm, and Alox-B 25 g, 32/63 μm (Interchim, Montluçon, France). Nuclear magnetic resonance spectra were performed with a Bruker AV-400 NMR instrument (Bruker, Karlsruhe, Germany) in DMSO-d_6, $CDCl_3$, $(CD_3)_2CO$. As internal standard, the signals of the deuterated solvents were used (DMSO-d_6: ^1H 2.50 ppm, ^{13}C 39.52 ppm; $CDCl_3$: ^1H 7.26 ppm, ^{13}C 77.16 ppm; $(CD_3)_2CO$: ^1H 2.05 ppm, ^{13}C 39.52 ppm). Abbreviation for data quoted are as follows: s, singlet; d, doublet; t, triplet; q, quartet; m, multiplet; br, broad; dd, doublet of doublets; dt, doublet of triplets; tt, triplet of triplets; and tq, triplet of quartets. Coupling constants (J) are given in hertz. For purity and reaction monitoring, analytical high-performance liquid chromatography (HPLC) analysis was performed with a system from Shimadzu equipped with a DGU-20A3R controller, an LC20AB liquid chromatograph, and an SPD-20A UV−vis detector. Stationary phase was a Synergi 4 μm fusion-RP (150 × 4.6 mm^2) column (Phenomenex, Aschaffenburg, Germany). For the mobile phase, a gradient of MeOH/water with 0.1% formic acid was used. Parameters: A = water, B = MeOH, $V(B)/(V(A) + V(B))$ = from 5 to 90% over 10 min, $V(B)/(V(A) + V(B))$ = 90% for 5 min, $V(B)/(V(A) + V(B))$ = from 90 to 5% over 3 min. The method was performed with a flow rate of 1.0 mL/min. Compounds were only used for biological evaluation if the purity was ≥95%. Electrospray ionization (ESI) mass spectral (MS) data were acquired with Shimadzu LCMS-2020. Data are reported as mass-to-charge ratio (m/z) of the corresponding positively charged molecular ions.

2,6-Difluoro-4-methylaniline (2). 1,3-Difluoro-5-methyl-2-nitrobenzene **1** (1.0 g, 5.78 mmol) and 10% Pd−C (190 mg) in EtOH (20 mL) were hydrogenated under atmospheric pressure for 3 h. The catalyst was filtered off, and the filtrate was evaporated to give **2** as a light reddish oil (0.686 g, 4.80 mmol, 87%). ^1H NMR ($CDCl_3$, 400 MHz): δ (ppm) = 6.63 (m, 2H), 3.49 (s, 2H), 2.23 (s, 3H). ^{13}C NMR ($CDCl_3$, 400 MHz): δ (ppm) = 153.3 (d, J = 8.3 Hz), 151.0 (d, J = 8.3 Hz), 127.4 (t, J = 8.5 Hz), 121.1 (t, J = 16.6 Hz), 111.9−111.3 (m), 20.7 (t, J = 1.7 Hz). ESI-MS: m/z calcd for $C_7H_8F_4N_2^+$ $[M + H]^+$: 144.1, found: 144.1.

1-(2,6-Difluoro-4-methylphenyl)-2-(2,6-difluorophenyl)-diazene (5). 2,6-Difluoraniline **3** (641 mg, 4.96 mmol, 2.00 equiv) was dissolved in dichloromethane (DCM) (30 mL). To this solution, oxone (16.8g, 27.3 mmol, 20.00 equiv) dissolved in water (60 mL) was added. The solution was under argon at room temperature overnight. After separation of the layers, the aqueous layer was extracted with DCM twice. The combined organic layers were washed with 1 N HCl, saturated sodium bicarbonate solution, water, and brine, dried over $MgSO_4$, and evaporated to dryness. Afterward, toluene (10 mL) and 2,6-difluoro-4-metylaniline **2** (357 mg, 2.49 mmol, 1.00 equiv) were added. A mixture of acetic acid (20 mL) and TFA (50 mL) was prepared and added to the solution. The resulting mixture was stirred at room temperature for 24 h. Afterward, it was evaporated to dryness. Purification by column chromatography over silica gel (DCM/petrol ether (PE),1:4, silica gel) yielded the desired product **5** as a deep orange solid (292 mg, 1.09 mmol, 43%). ^1H NMR ($CDCl_3$, 400 MHz): δ (ppm) = 7.40−7.29 (m, 1H), 7.05 (t, J = 8.6 Hz, 2H), 6.87 (d, J = 10.5 Hz, 2H), 2.41 (s, 3H). ESI-MS: m/z calcd for $C_{13}H_9BF_4N_2^+$ $[M + H]^+$: 269.1, found: 269.1.

(4-(Phenyldiazenyl)phenyl)methanol (7). Nitrosobenzene **4a** (1.28 g, 11.9 mmol, 3 equiv) was dissolved in ethanol (10 mL). To this solution, (4-aminophenyl)methanol **6** (491 mg, 4.00 mmol, 1 equiv) and acetic acid (20 mL) were added. The reaction mixture was stirred for 4 h at room temperature. Subsequently, the reaction mixture was poured into 30 mL of ice-cold water, and the precipitate was collected by filtration. Column chromatography (DCM/methanol = 50:1) provided compound **7** (659 mg, 2.99 mmol, 75%) as bright orange needles. ^1H NMR (400 MHz, DMSO-d_6): δ (ppm) = 7.88 (m, J = 6.9, 1.8 Hz, 4H), 7.65−7.50 (m, 5H), 5.40 (t, J = 5.7 Hz, 1H), 4.61 (d, J = 5.6 Hz, 2H). ^{13}C NMR (101 MHz, DMSO-d_6): δ (ppm) = 152.4, 151.3, 146.9, 131.8, 129.93, 127.6, 122.9, 62.9. ESI-MS: m/z calcd for $C_{13}H_{12}N_2O^+$ $[M + H]^+$: 213.1, found: 213.1.

1-(4-(Bromomethyl)phenyl)-2-phenyldiazene (8a). (4-(Phenyldiazenyl)phenyl)methanol **7** (300 mg, 1.41 mmol, 1 equiv) was dissolved in dry THF (15 mL) under argon atmosphere, tetrabromomethane (703 mg, 2.12 mmol, 1.5 equiv) and triphenylphosphine (556 mg, 2.12 mmol, 1.5 equiv) were added, and the reaction mixture was stirred for 4 h. The reaction mixture was filtered, and the filtrate was evaporated to dryness and purified by column chromatography (ethyl acetate (EA)/hex = 1:10) yielding compound **8a** as orange needles (232 mg, 0.84 mmol, 60%). ^1H NMR (400 MHz, DMSO-d_6): δ (ppm) = 7.89 (tt, J = 7.7, 2.0 Hz, 4H), 7.69−7.57 (m, 5H), 4.80 (s, 2H). ^{13}C NMR (101 MHz, DMSO-d_6): δ (ppm) = 151.9, 151.5, 141.5, 131.7, 130.5, 129.5, 122.9, 122.6, 33.6. ESI-MS: m/z calcd for $C_{13}H_{11}BrN_2^+$ $[M + H]^+$: 275.0, 277.0, found: 274.9, 276.9.

1-(4-(Bromomethyl)-2,6-difluorophenyl)-2-(2,6-difluorophenyl)diazene (8b). To a solution of 1,2-bis(2,6-difluoro-4-methylphenyl)diazene **5** (250 mg, 0.93 mmol) in 20 mL of CCl_4 were added NBS (0.332 g, 1.86 mmol) and AIBN (11 mg, 0.076 mmol). The resultant solution was stirred overnight at 80 °C. After evaporation of the solvent, the product was purified by column chromatography over silica gel (DCM/PE,1:4, silica gel) yielding the desired product **8b** (163 mg, 0.47 mmol, 50%). ^1H NMR ($CDCl_3$, 400 MHz): δ (ppm) = 7.38 (t, J = 8.5 Hz, 4H), 7.21 (d, J = 8.5 Hz, 11H), 7.13−7.03 (m, 14H), 6.87 (dt, J = 14.8, 7.3 Hz, 42H), 6.65 (d, J = 8.8 Hz, 4H), 4.44 (s, 6H), 4.33 (s, 19H), 2.41 (s, 2H), 2.29 (s, 6H). ESI-MS: m/z calcd for $C_{13}H_8BrF_4N_2^+$ $[M + H]^+$: 347.0, 349.0 found: 347.0, 349.0.

4-((4,5-Dihydroisoxazol-3-yl)oxy)-*N*,*N*-dimethyl-*N*-(4-(phenyldiazenyl)benzyl)but-2-yn-1-aminium (9a). 1-(4-(Bromomethyl)phenyl)-2-phenyldiazene **8a** (100 mg, 0.36 mmol, 1 equiv) and 4-((4,5-dihydroisoxazol-3-yl)oxy)-*N*,*N*-dimethylbut-2-yn-1-amine **16** (132 mg, 0.73 mmol, 2 equiv) were dissolved in acetonitrile (10 mL) and stirred at room temperature for 12 h. The reaction was monitored by liquid chromatography (LC)−MS. The precipitate was filtered off, and the solvent was removed under reduced pressure. The crude product was purified by column chromatography (DCM/MA/NH_3 = 20:1:0.1) yielding compound **9a** as a dark red oil (54 mg, 0.14 mmol, 39%). ^1H NMR (400 MHz, $CDCl_3$): δ (ppm) = 7.99−7.86 (m, 6H), 7.56−7.46 (m, 3H), 5.24 (s, 2H), 4.88 (d, J = 7.9 Hz, 4H), 4.42 (t, J = 9.6 Hz, 2H), 3.53−3.40 (m, 6H), 3.02 (t, J = 9.6 Hz, 2H). ^{13}C NMR (101 MHz, $CDCl_3$): δ (ppm) = 166.9, 154.1, 152.6, 134.3, 131.9, 129.3, 129.0, 123.7, 123.3, 87.8, 75.9, 70.2, 66.2, 57.5, 54.8, 50.0, 33.1. ESI-MS: m/z calcd for $C_{22}H_{25}BrN_4O_2^+$ $[M + H]^+$: 377.2, found: 377.2.

***N*-(4-((2,6-Difluorophenyl)diazenyl)-3,5-difluorobenzyl)-4-((4,5-dihydroisoxazol-3-yl)oxy)-*N*,*N*-dimethylbut-2-yn-1-aminium Bromide (9b).** 1-(4-(Bromomethyl)-2,6-difluorophenyl)-2-(2,6-difluorophenyl)diazene **8b** (64 mg, 0.184 mmol) and 4-((4,5-dihydroisoxazol-3-yl)oxy)-*N*,*N*-dimethylbut-2-yn-1-amine (34 mg, 0.184 mmol, 1 equiv) in ethyl acetate (10 mL) were charged in a sealed reaction vessel and stirred for 4 h. The precipitate was collected and washed several times with ethyl acetate to afford the desired product **9b** as a bright yellow powder (90 mg, 0.170 mmol, 92%). ^1H NMR (MeOD, 400 MHz): δ (ppm) = 7.63−7.30 (m, 3H), 7.12 (dt, J = 17.0, 8.7 Hz, 2H), 4.97 (d, J = 14.5 Hz, 2H), 4.66 (d, J = 49.0 Hz, 2H), 4.48−4.28 (m, 4H), 3.21 (d, J = 30.4 Hz, 6H), 3.05 (dt, J = 15.1, 9.6 Hz, 2H). ^{13}C NMR (MeOD, 400 MHz): δ (ppm) = 168.82, 154.23 (d, J = 5.1 Hz), 151.71 (d, J = 5.5 Hz), 132.40 (t, J = 9.7 Hz), 131.22 (d, J = 9.0 Hz), 118.4, 118.1, 113.5 (d, J = 19.1 Hz), 89.1, 76.7, 71.2, 66.0, 58.3, 55.3, 51.1, 33.6. ESI-MS: m/z calcd for $C_{22}H_{21}F_4N_4O_2^+$ $[M]^+$: 449.16, found: 449.05.

1-Methyl-4-nitrosobenzene (11). *p*-Toluidine **10** (2.00 g, 18.7 mmol) was dissolved in DCM (60 mL), and a solution of oxone (11.5 g, 18.7 mmol) in water (60 mL) was added. The resulting biphasic mixture was stirred at room temperature for 30 min. The organic layer was separated, and the aqueous layer was extracted twice with DCM. The combined organic layers were washed with 1 M aqueous hydrochloric acid, saturated sodium hydrogen carbonate, and brine and dried over anhydrous sodium sulfate. Mixture **11** was concentrated to 10−15 mL volume, which was further used without purification.

DOI: 10.1021/acs.jmedchem.8b01822
J. Med. Chem. 2019, 62, 3009−3020

4,4′-Dimethylazobenzene (13a). 1-Methyl-4-nitrososbenzene **11** and *p*-toluidine **10** (1.00 g, 9.33 mmol) were dissolved in glacial acetic acid (20 mL) and stirred overnight. The solution was diluted with water and extracted with ethyl acetate. The organic phase was washed four times with water and once with brine and dried over anhydrous sodium sulfate. The crude product was purified by flash chromatography (pentane/diethyl ether, 9:1) to obtain the desired product **13a** as an orange crystalline solid (695 mg, 3.31 mmol, 36%). ^{1}H NMR (400 MHz, $CDCl_3$): δ (ppm) = 7.82 (d, J = 8.3 Hz, 4H), 7.31 (d, J = 8.6 Hz, 4H), 2.44 (s, 6H). ^{13}C NMR (101 MHz, $CDCl_3$): δ (ppm) = 151.0, 141.3, 129.9, 122.9, 21.6. ESI-MS: m/z calcd for $C_{14}H_{14}N_2^+$ $[M + H]^+$: 211.1, found: 211.0.

1,2-Bis(2,6-difluoro-4-methylphenyl)diazene (13b). 2,6-Difluoro-4-methylaniline **12** (397 mg, 2.77 mmol) and a freshly ground mixture of potassium permanganate (1.17 g, 4.21 mmol) and iron(II) sulfate heptahydrate (1.17 g, 7.40 mmol) were dissolved in DCM (10 mL). The solution was refluxed overnight, filtered through celite, dried over anhydrous sodium sulfate, filtered, and concentrated under reduced pressure. The crude residue was purified by column chromatography (DCM/petrol ether 1:1) to give the desired product **13b** (110 mg, 0.39 mmol, 29%). ^{1}H NMR ($CDCl_3$, 400 MHz): δ (ppm) = 6.86 (d, J = 10.3 Hz, 4H, arom. trans), 6.65 (d, J = 8.3 Hz, 0.39H, arom. cis), 2.40 (s, 6 H, $-CH_3$, trans), 2.29 (s, 0.62H, $-CH_3$, cis). ^{13}C NMR ($CDCl_3$, 400 MHz): δ (ppm) = 156.8 (d, J = 5.0 Hz), 154.3 (d, J = 5.2 Hz), 143.2 (t, J = 10.3 Hz), 113.2, 113.0, 21.7.

4,4′-Bis(bromomethyl)azobenzene (14a). To a solution of 4,4′-dimethylazobenzene **13a** (2.17 g, 10.3 mmol) in 20 mL of carbon tetrachloride (40 mL) were added *N*-bromosuccinimide (4.22 g, 23.7 mmol) and azobisisobutyronitrile (127 mg, 0.77 mmol). The resultant solution was stirred overnight at 70 °C, filtered, washed with chloroform and water, and dried under reduced pressure, which yielded **14a** as an orange crystalline powder (2.88 g, 7.81 mmol, 76%). ^{1}H NMR (400 MHz, $CDCl_3$): δ (ppm) = 7.90 (d, J = 8.4 Hz, 4H), 7.54 (d, J = 8.5 Hz, 4H), 4.56 (s, 4H). ^{13}C NMR (101 MHz, $CDCl_3$): δ (ppm) = 152.3, 140.8, 129.9, 32.7. ESI-MS: m/z calcd for $C_{12}H_{13}Br_2N_2^+$ $[M + H]^+$: 368.9, found: 368.8.

1,2-Bis(4-(bromomethyl)-2,6-difluorophenyl)diazene (14b). To a solution of 1,2-bis(2,6-difluoro-4-methylphenyl)diazene **13b** (226 mg, 0.801 mmol) in 17 mL of CCl_4 were added NBS (0.356 g, 2.02 mmol) and AIBN (10 mg, 0.060 mmol). The resultant solution was stirred overnight at 80 °C. After evaporation of the solvent, the product was recrystallized from methanol to afford the desired product **14b** as red needles (86 mg, 0.195 mmol, 24%). ^{1}H NMR ($CDCl_3$, 400 MHz): δ (ppm) = 7.11 (d, J = 9.1 Hz, 4H), 4.43 (s, 4H). ^{13}C NMR ($CDCl_3$, 400 MHz): δ (ppm) = 160.9 (d, J = 7.6 Hz), 158.8 (d, J = 6.7 Hz), 150.4 (t, J = 6.7 Hz), 125.2 (t, J = 27.2 Hz), 114.0 (dd, J = 26.7, 3.7 Hz), 30.6 (t, J = 3.7 Hz). ESI-MS: m/z calcd for $C_{14}H_9Br_2F_4N_2$ + $[M]^+$: 440.9, found: 440.7.

4-((4,5-Dihydroisoxazol-3-yl)oxy)-*N*-(4-((4-(((4-((4,5-dihydroisoxazol-3-yl)oxy)but-2-yn-1-yl)dimethyl-l4-azaneyl)methyl)phenyl)diazenyl)benzyl)-*N*,*N*-dimethylbut-2-yn-1-aminium Bromide (15a). 4,4′-Bis(bromomethyl)azobenzene **14a** (100 mg, 0.272 mmol) and 4-((4,5-dihydroisoxazol-3-yl)oxy)-*N*,*N*-dimethylbut-2-yn-1-amine **16** were dissolved in 30 mL of ethyl acetate and stirred at 60 °C for 16 h. The precipitate was filtered and washed with cold ethyl acetate to afford the desired product **15a** as a yellow powder (166 mg, 0.227 mmol, 83%). ^{1}H NMR (400 MHz, DMSO-d_6): δ (ppm) = 8.03 (d, J = 8.4 Hz, 1H), 7.83 (d, J = 8.4 Hz, 1H), 4.99 (s, 1H), 4.75 (s, 1H), 4.47 (s, 1H), 4.33 (t, J = 9.6 Hz, 1H), 3.13 (s, 3H), 3.05 (t, J = 9.6 Hz, 1H). ^{13}C NMR (101 MHz, DMSO-d_6): δ (ppm) = 166.8, 152.8, 134.2, 131.1, 123.0, 86.8, 76.3, 69.6, 64.9, 57.3, 53.3, 49.5, 32.3. ESI-MS: m/z calcd for $C_{32}H_{40}N_6O_4^{2+}$ $[M]^{2+}$: 286.2, found: 286.1.

***N*,*N*′-((Diazene-1,2-diylbis(3,5-difluoro-4,1-phenylene))bis(methylene))bis(4-((4,5-dihydroisoxazol-3-yl)oxy)-*N*,*N*-dimethylbut-2-yn-1-aminium) Bromide (15b).** 4-((4,5-Dihydroisoxazol-3-yl)oxy)-*N*,*N*-dimethylbut-2-yn-1-amine **16** (24.5 mg, 0.134 mmol) in ethyl acetate (40 mL) was slowly added to a stirred solution of 1,2-bis(4-(bromomethyl)-2,6-difluorophenyl)diazene **14b** (118 mg, 0.269 mmol, 2 equiv) in ethyl acetate (10 mL) at 60 °C. The reaction mixture was stirred for 18 h. The reaction mixture was evaporated to dryness and purified by reverse phase column chromatography (acetonitrile/water) yielding the desired product **15b** as a bright orange powder (35 mg, 0.043 mmol, 32%). ^{1}H NMR (MeOD, 400 MHz): δ (ppm) = 7.55 (dd, J = 60.3, 8.6 Hz, 4H), 5.03 (dd, J = 7.6, 6.1 Hz, 4H), 4.77 (d, J = 38.9 Hz, 4H), 4.51 (s, 2H), 4.44 (s, 2H), 3.29 (d, J = 24.8 Hz, 12H), 3.09 (dt, J = 19.3, 9.7 Hz, 4H). ^{13}C NMR (MeOD, 400 MHz): δ (ppm) = 176.6, 169.90, 168.9 (d, J = 2.4 Hz), 119.0, 118.4, 89.1, 76.7 (d, J = 7.4 Hz), 71.2, 58.4, 55.4 (d, J = 11.4 Hz), 51.2, 33.7. ESI-MS: m/z calcd for $C_{32}H_{36}F_4N_6O_4^{2+}$ $[M]^{2+}$: 322.14, found: 322.25.

General Procedure for the Synthesis of the Homobivalent Quaternary Iperoxo Dimers 18a–d. To a solution of 2 equiv of 4-((4,5-dihydroisoxazol-3-yl)oxy)-*N*,*N*-dimethylbut-2-yn-1-amine **16** in 10 mL of acetonitrile, 1 equiv of the corresponding bromoalkane **17**-C4, **17**-C6, **17**-C8, and **17**-C10 and a catalytic amount of KI/K_2CO_3 (1:1) were added. The reaction mixture was heated in the microwave (500 W, 70 °C) for 2–3 h. After cooling to room temperature, the surplus of KI/K_2CO_3 was filtered off and the solvent was evaporated to half of the volume. The solution was kept in the fridge overnight. The precipitate obtained was filtered, washed with Et_2O, and dried in vacuo.

***N*1,*N*4-Bis(4-((4,5-dihydroisoxazol-3-yl)oxy)but-2-yn-1-yl)-*N*1,*N*1,*N*4,*N*4-tetramethylbutane-1,4-diaminium Bromide (18a).** Light, yellow solid; yield 69%. ^{1}H NMR (400 MHz, DMSO-d_6): δ (ppm) = 2.73–2.77 (m, 4H), 3.03 (t, 4H, J = 9.6 Hz), 3.12 (s, 12H), 3.44–3.48 (m, 4H), 4.33 (t, 4H, J = 9.6 Hz), 4.53 (s, 4H), 4.95 (s, 4H). ^{13}C NMR (101 MHz, DMSO-d_6): δ (ppm) = 19.1, 32.2, 49.7, 53.6, 57.2, 62.2, 69.6, 76.0, 86.1, 166.7. ESI-MS: m/z calcd for $C_{22}H_{36}N_4O_4^{2+}$ $[M]^{2+}$: 210.1, found: 210.1

***N*1,*N*6-Bis(4-((4,5-dihydroisoxazol-3-yl)oxy)but-2-yn-1-yl)-*N*1,*N*1,*N*6,*N*6-tetramethylhexane-1,6-diaminium Bromide (18b).** Light, yellow solid; yield 49%. ^{1}H NMR (400 MHz, DMSO-d_6): δ (ppm) = 1.32–1.37 (m, 4H), 1.69–1.78 (m, 4H), 3.03 (t, 4H, J = 9.6 Hz), 3.11 (s, 12H), 3.36–3.40 (m, 4H), 4.33 (t, 4H, J = 9.6 Hz), 4,50 (s, 4H), 4.94 (s, 4H). ^{13}C NMR (101 MHz, DMSO-d_6): δ (ppm) = 21.6, 25.1, 32.2, 49.7, 53.3, 57.1, 62.9, 69.5, 76.1, 85.9, 166.6. ESI-MS: m/z calcd for $C_{24}H_{40}N_4O_4^{2+}$ $[M]^{2+}$: 224.2, found: 224.1.

***N*1,*N*8-Bis(4-((4,5-dihydroisoxazol-3-yl)oxy)but-2-yn-1-yl)-*N*1,*N*1,*N*8,*N*8-tetramethyloctane-1,8-diaminium Bromide (18c).** Light, yellow solid; yield 15%. ^{1}H NMR (400 MHz, DMSO-d_6): δ (ppm) = 1.29–1.32 (m, 8H), 1.64–1.72 (m, 4H), 3.02 (t, 4H, J = 9.6 Hz), 3.10 (s, 12H), 3.39–3.41 (m, 4H), 4.32 (t, 4H, J = 9.6 Hz), 4,51 (s, 4H), 4.93 (s, 4H). ^{13}C NMR (101 MHz, DMSO-d_6): δ (ppm) = 21.7, 25.5, 28.1, 32.2, 49.7, 53.2, 57.2, 63.0, 69.5, 76.1, 85.9, 166.7. ESI-MS: m/z calcd for $C_{26}H_{44}N_4O_4^{2+}$ $[M]^{2+}$: 238.2, found: 238.1.

***N*1,*N*10-Bis(4-((4,5-dihydroisoxazol-3-yl)oxy)but-2-yn-1-yl)-*N*1,*N*1,*N*10,*N*10-tetramethyldecane-1,10-diaminium Bromide (18d).** Light, yellow solid; yield 36%. ^{1}H NMR (400 MHz, DMSO-d_6): δ (ppm) = 1.30 (s, 12H), 1.62–1.72 (m, 4H), 3.02 (t, 4H, J = 9.2 Hz), 3.09 (s, 12H), 3.36–3.38 (m, 4H), 4.32 (t, 4H, J = 9.2 Hz), 4.51 (s, 4H), 4.93 (s, 4H). ^{13}C NMR (101 MHz, DMSO-d_6): δ (ppm) = 21.7, 25.6, 28.3, 28.6, 32.2, 49.7, 53.2, 57.1, 63.0, 69.5, 76.1, 85.8, 166.6. ESI-MS: m/z calcd for $C_{28}H_{48}N_4O_4^{2+}$ $[M]^{2+}$: 252.2, found: 252.2.

Photochemical Characterization. UV–vis spectra and experiments were recorded on a Varian Cary 50 Bio UV/vis spectrophotometer using Hellma (type 100-QS) cuvettes (10 mm light path). Data were plotted using GraphPad Prism 5.0. For irradiation, high-performance light-emitting diodes (LEDs, Mouser Electronics Inc. or Hartenstein) were used as the light source. A concentration of 50 μm was prepared for each compound and measured in its dark-adapted state. Next, the probe was illuminated with LEDs of different wavelengths (254, 365, 380, 400, 430, 500 nm, and white light) while gradually increasing the irradiation time until no change in the spectrum was detectable. Stability measurements were performed irradiating the probe with the light source, which provided the highest photoconversion to the cis-isomer, and kept in dark for at least 120 min. During this time, the absorbance at λ_{max} was recorded every 5 min. Lastly, the probe was irradiated with the light

DOI: 10.1021/acs.jmedchem.8b01822
J. Med. Chem. 2019, 62, 3009–3020

source, which provided the highest photoconversion to the trans isomer. Photostationary distributions were determined by HPLC analysis using a 50 μm probe in physiological buffer. Absorption was measured at the respective isosbestic point wavelengths. Analysis was carried out with GraphPad Prism software (GraphPad Software Inc., San Diego, CA, www.graphpad.com).

Pharmacology. *Cell Culture.* All experiments were performed with HEK 293T cells stably expressing the novel split-luciferase receptor sensor. Cells were incubated at 37 °C with 5% CO_2 and cultivated in DMEM with 4500 mg/L glucose, 10% (v/v) fetal calf serum, 100 μg/mL penicillin, 100 μg/mL streptomycin sulfate, 2 mM L-glutamine, and 600 μg/mL G-418. Every 2−3 days the cell lines were routinely passaged.

Split-Luciferase Complementation Assay. The assay was performed as described previously,[24] except for the following modifications: a Berthold Mithras LB 940 plate reader was used to quantify the luminescence emitted by the cells, using white, flat-bottomed nunc f96 microwell polystyrene plates.

Molecular Modeling. In brief, all receptor−ligand docking experiments reported in this study were carried out with CCDCs software GOLD version 5.1.[30] The active M_1 receptor homology model used as protein was previously reported.[27] All residues of the extracellular domains and the receptor core region were defined as a potential binding pocket. Default settings were chosen for receptor−ligand docking, and GoldScore was used as the primary scoring function. All obtained docking poses and receptor−ligand interactions were analyzed with LigandScout 4.2 using 3D-pharmacophores.[31]

Binding Experiments. [^{3}H]Quinuclidinyl benzilate ([^{3}H]QNB), ethanol solution, was purchased from Amersham Biosciences (catalog number TRK 604, 42 Ci/mmol, 1 mCi/mL). The experiments were carried out in 10 mM Tris−HCl buffer, pH 7.0, containing 6 mM $MgCl_2$. Rat brain cortices were used as a source of muscarinic receptors in the assay. After cleaning the meninges with buffer-soaked filter paper, cortices were dissected, and white matter was carefully trimmed off. This tissue was homogenized in 40 mL of buffer using a Potter homogenizer with a motor-driven Teflon pestle. The homogenate was centrifuged for 30 min at 50 000*g*, and the resulting pellet was homogenized and centrifuged again. After protein determination by the Bradford assay, the final pellet was resuspended at 1 mg of protein/mL, transferred to 1.5 mL microcentrifuge tubes, and centrifuged once more. After discarding the supernatant, membrane pellets were kept at −80 °C until use.[23] The general procedure consists of the incubation of 20 μg of membrane protein with 200 pM [^{3}H]QNB (200 pM), in a total volume of 2 mL and in the presence of varying concentrations of competing compounds. An excess (2 μm) of the unlabeled muscarinic antagonist atropine was used to define nonspecific binding. After 45 min at 25 °C to reach equilibrium, the reaction mixtures were quickly filtered through glass fiber disks using a semiautomated Brandel harvester allowing the simultaneous filtration of 24 samples.[21] Filters were washed twice with 4 mL of ice-cold Tris−HCl buffer (10 mM, pH 7.0) and counted for radioactivity. The final results were reported as % binding of [^{3}H]QNB in each condition. This analysis was carried out with GraphPad Prism software (GraphPad Software Inc., San Diego, CA, www.graphpad.com).

■ ASSOCIATED CONTENT

Supporting Information

The Supporting Information is available free of charge on the ACS Publications website at DOI: 10.1021/acs.jmedchem.8b01822.

UV−vis spectra, NMR data, HPLC traces, molecular modeling, binding experiments (PDF)

Molecular formula strings (CSV)

Accession Codes

PDB code for the crystal structure of the human M_2 receptor in complex with agonist iperoxo is *4MQS*. This crystal structure was used for the generation of the homology model for computational studies of the human M_1 receptor in complex with compounds **9a**, **9b**, **15a**, **15b**, and **18a−d**.

■ AUTHOR INFORMATION

Corresponding Author

*E-mail: michael.decker@uni-wuerzurg.de.

ORCID

Marcel Bermudez: 0000-0002-7421-3282
Carlo Matera: 0000-0001-6939-3859
Gerhard Wolber: 0000-0002-5344-0048
Ulrike Holzgrabe: 0000-0002-0364-7278
Michael Decker: 0000-0002-6773-6245

Notes

The authors declare no competing financial interest.

■ ACKNOWLEDGMENTS

L.A. and T.L. were supported by the International Doctoral Program "Receptor Dynamics: Emerging Paradigms for Novel Drugs" funded within the framework of the Elite Network of Bavaria (ENB). We kindly thank Prof. Klaus Mohr from the Institute of Pharmacy and Toxicology at Bonn University for fruitful discussions.

■ REFERENCES

(1) (a) Lerch, M. M.; Hansen, M. J.; van Dam, G. M.; Szymanski, W.; Feringa, B. L. Emerging Targets in Photopharmacology. *Angew. Chem., Int. Ed.* **2016**, *55*, 10978−10999. (b) Velema, W. A.; Szymanski, W.; Feringa, B. L. Photopharmacology: Beyond Proof of Principle. *J. Am. Chem. Soc.* **2014**, *136*, 2178−2191. (c) Hüll, K.; Morstein, J.; Trauner, D. In Vivo Photopharmacology. *Chem. Rev.* **2018**, *118*, 10710−10747. (d) Broichhagen, J.; Frank, J. A.; Trauner, D. A Roadmap to Success in Photopharmacology. *Acc. Chem. Res.* **2015**, *48*, 1947−1960.

(2) (a) Pittolo, S.; Gómez-Santacana, X.; Eckelt, K.; Rovira, X.; Dalton, J.; Goudet, C.; Pin, J.-P.; Llobet, A.; Giraldo, J.; Llebaria, A.; Gorostiza, P. An Allosteric Modulator to Control Endogenous G protein-coupled Receptors with Light. *Nat. Chem. Biol.* **2014**, *10*, 813−815. (b) Schönberger, M.; Trauner, D. A Photochromic Agonist for μ-Opioid Receptors. *Angew. Chem., Int. Ed.* **2014**, *53*, 3264−3267. (c) Agnetta, L.; Kauk, M.; Canizal, M. C. A.; Messerer, R.; Holzgrabe, U.; Hoffmann, C.; Decker, M. A Photoswitchable Dualsteric Ligand Controlling Receptor Efficacy. *Angew. Chem., Int. Ed.* **2017**, *56*, 7282−7287. (d) Bahamonde, M. I.; Taura, J.; Paoletta, S.; Gakh, A. A.; Chakraborty, S.; Hernando, J.; Fernández-Dueñas, V.; Jacobson, K. A.; Gorostiza, P.; Ciruela, F. Photomodulation of G Protein-Coupled Adenosine Receptors by a Novel Light-Switchable Ligand. *Bioconjugate Chem.* **2014**, *25*, 1847−1854. (e) Broichhagen, J.; Johnston, N. R.; von Ohlen, Y.; Meyer-Berg, H.; Jones, B. J.; Bloom, S. R.; Rutter, G. A.; Trauner, D.; Hodson, D. J. Allosteric Optical Control of a Class B G-Protein-Coupled Receptor. *Angew. Chem., Int. Ed.* **2016**, *55*, 5865−5868. (f) Hauwert, N. J.; Mocking, T. A. M.; Da Costa Pereira, D.; Kooistra, A. J.; Wijnen, L. M.; Vreeker, G. C. M.; Verweij, E. W. E.; De Boer, A. H.; Smit, M. J.; De Graaf, C.; Vischer, H. F.; de Esch, I. J. P.; Wijtmans, M.; Leurs, R. Synthesis and Characterization of a Bidirectional Photoswitchable Antagonist Toolbox for Real-Time GPCR Photopharmacology. *J. Am. Chem. Soc.* **2018**, *140*, 4232−4243. (g) Westphal, M. V.; Schafroth, M. A.; Sarott, R. C.; Imhof, M. A.; Bold, C. P.; Leippe, P.; Dhopeshwarkar, A.; Grandner, J. M.; Katritch, V.; Mackie, K.; Trauner, D.; Carreira, E. M.; Frank, J. A. Synthesis of Photoswitchable Δ9-Tetrahydrocannabinol Derivatives Enables Optical Control of Cannabinoid Receptor 1 Signaling. *J. Am. Chem. Soc.* **2017**, *139*, 18206−18212. (h) Dolles, D.; Strasser, A.; Wittmann, H.-J.; Marinelli, O.; Nabissi, M.; Pertwee, R. G.; Decker, M. The First

DOI: 10.1021/acs.jmedchem.8b01822
J. Med. Chem. 2019, 62, 3009−3020

Photochromic Affinity Switch for the Human Cannabinoid Receptor 2. *Adv. Ther.* **2018**, *1*, No. 1700032.
(3) Lohse, M. J.; Hofmann, K. P. Spatial and Temporal Aspects of Signaling by G-Protein-Coupled Receptors. *Mol. Pharmacol.* **2015**, *88*, 572−578.
(4) Burger, W. A. C.; Sexton, P. M.; Christopoulos, A.; Thal, D. M. Toward an Understanding of the Structural Basis of Allostery in Muscarinic Acetylcholine Receptors. *J. Gen. Physiol.* **2018**, *150*, 1360−1372.
(5) (a) Kruse, A. C.; Kobilka, B. K.; Gautam, D.; Sexton, P. M.; Christopoulos, A.; Wess, J. Muscarinic Acetylcholine Receptors: Novel Opportunities for Drug Development. *Nat. Rev. Drug Discovery* **2014**, *13*, 549−560. (b) Svoboda, J.; Popelikova, A.; Stuchlik, A. Drugs Interfering with Muscarinic Acetylcholine Receptors and Their Effects on Place Navigation. *Front. Psychiatry* **2017**, *8*, No. 215. (c) van Koppen, C. J.; Kaiser, B. Regulation of Muscarinic Acetylcholine Receptor Signaling. *Pharmacol. Ther.* **2003**, *98*, 197−220. (d) Eglen, R. M. Muscarinic Receptor Subtypes in Neuronal and Non-neuronal Cholinergic Function. *Auton. Autacoid Pharmacol.* **2006**, *26*, 219−233.
(6) Wess, J.; Eglen, R. M.; Gautam, D. Muscarinic Acetylcholine Receptors: Mutant Mice Provide New Insights for Drug Development. *Nat. Rev. Drug Discovery* **2007**, *6*, 721−733.
(7) Caulfield, M. P. Muscarinic Receptors—Characterization, Coupling and Function. *Pharmacol. Ther.* **1993**, *58*, 319−379.
(8) (a) Antony, J.; Kellershohn, K.; Mohr-Andrä, M.; Kebig, A.; Prilla, S.; Muth, M.; Heller, E.; Disingrini, T.; Dallanoce, C.; Bertoni, S.; Schrobang, J.; Tränkle, C.; Kostenis, E.; Christopoulos, A.; Höltje, H. D.; Barocelli, E.; De Amici, M.; Holzgrabe, U.; Mohr, K. Dualsteric GPCR Targeting: A Novel Route to Binding and Signaling Pathway Selectivity. *FASEB J.* **2009**, *23*, 442−450. (b) Disingrini, T.; Muth, M.; Dallanoce, C.; Barocelli, E.; Bertoni, S.; Kellershohn, K.; Mohr, K.; De Amici, M.; Holzgrabe, U. Design, Synthesis, and Action of Oxotremorine-Related Hybrid-Type Allosteric Modulators of Muscarinic Acetylcholine Receptors. *J. Med. Chem.* **2006**, *49*, 366−372.
(9) (a) Beharry, A. A.; Sadovski, O.; Woolley, G. A. Azobenzene Photoswitching without Ultraviolet Light. *J. Am. Chem. Soc.* **2011**, *133*, 19684−19687. (b) Samanta, S.; Beharry, A. A.; Sadovski, O.; McCormick, T. M.; Babalhavaeji, A.; Tropepe, V.; Woolley, G. A. Photoswitching Azo Compounds In Vivo with Red Light. *J. Am. Chem. Soc.* **2013**, *135*, 9777−9784.
(10) (a) Bléger, D.; Hecht, S. Visible-Light-Activated Molecular Switches. *Angew. Chem., Int. Ed.* **2015**, *54*, 11338−11349. (b) Bléger, D.; Schwarz, J.; Brouwer, A. M.; Hecht, S. *o*-Fluoroazobenzenes as Readily Synthesized Photoswitches Offering Nearly Quantitative Two-Way Isomerization with Visible Light. *J. Am. Chem. Soc.* **2012**, *134*, 20597−20600.
(11) Dong, M.; Babalhavaeji, A.; Samanta, S.; Beharry, A. A.; Woolley, G. A. Red-Shifting Azobenzene Photoswitches for in Vivo Use. *Acc. Chem. Res.* **2015**, *48*, 2662−2670.
(12) (a) Rullo, A.; Reiner, A.; Reiter, A.; Trauner, D.; Isacoff, E. Y.; Woolley, G. A. Long Wavelength Optical Control of Glutamate Receptor Ion Channels Using a Tetra-ortho-substituted Azobenzene Derivative. *Chem. Commun.* **2014**, *50*, 14613−14615. (b) Wegener, M.; Hansen, M. J.; Driessen, A. J. M.; Szymanski, W.; Feringa, B. L. Photocontrol of Antibacterial Activity: Shifting from UV to Red Light Activation. *J. Am. Chem. Soc.* **2017**, *139*, 17979−17986. (c) Konrad, D. B.; Frank, J. A.; Trauner, D. Synthesis of Redshifted Azobenzene Photoswitches by Late-Stage Functionalization. *Chem. − Eur. J.* **2016**, *22*, 4364−4368.
(13) Shonberg, J.; Scammells, P. J.; Capuano, B. Design Strategies for Bivalent Ligands Targeting GPCRs. *ChemMedChem* **2011**, *6*, 963−974.
(14) (a) Mohr, K.; Schmitz, J.; Schrage, R.; Tränkle, C.; Holzgrabe, U. Molecular Alliance-From Orthosteric and Allosteric Ligands to Dualsteric/Bitopic Agonists at G Protein Coupled Receptors. *Angew. Chem., Int. Ed.* **2013**, *52*, 508−516. (b) Halazy, S. G Protein-coupled Receptors Bivalent Ligands and Drug Design. *Expert Opin. Ther. Pat.* **1999**, *9*, 431−446.
(15) Nimczick, M.; Pemp, D.; Darras, F. H.; Chen, X.; Heilmann, J.; Decker, M. Synthesis and Biological Evaluation of Bivalent Cannabinoid Receptor Ligands Based on hCB(2)R Selective Benzimidazoles Reveal Unexpected Intrinsic Properties. *Bioorg. Med. Chem.* **2014**, *22*, 3938−3946.
(16) Decker, M.; Si, Y. G.; Knapp, B. I.; Bidlack, J. M.; Neumeyer, J. L. Synthesis and Opioid receptor Binding Affinities of 2-substituted and 3-Aminomorphinans: Ligands for Mu, Kappa, and Delta Opioid Receptors. *J. Med. Chem.* **2010**, *53*, 402−418.
(17) Kühhorn, J.; Hübner, H.; Gmeiner, P. Bivalent Dopamine D2 Receptor Ligands: Synthesis and Binding Properties. *J. Med. Chem.* **2011**, *54*, 4896−4903.
(18) (a) Piergentili, A.; Quaglia, W.; Tayebati, S. K.; Paparelli, F.; Malmusi, L.; Brasili, L. Synthesis and Muscarinic Receptors affinity of a Series of Antagonist Bivalent Ligands. *Farmaco* **1994**, *49*, 83−87. (b) Messer, W. S., Jr. Bivalent Ligands for G Protein-Coupled Receptors. *Curr. Pharm. Des.* **2004**, *10*, 2015−2020.
(19) Kloeckner, J.; Schmitz, J.; Holzgrabe, U. Convergent, Short Synthesis of the Muscarinic Superagonist Iperoxo. *Tetrahedron Lett.* **2010**, *51*, 3470−3472.
(20) Knie, C.; Utecht, M.; Zhao, F.; Kulla, H.; Kovalenko, S.; Brouwer, A. M.; Saalfrank, P.; Hecht, S.; Bléger, D. Ortho-Fluoroazobenzenes: Visible Light Switches with Very Long-Lived *Z* Isomers. *Chem. − Eur. J.* **2014**, *20*, 16492−16501.
(21) Claro, E. Analyzing Ligand Depletion in a Saturation Equilibrium Binding Experiment. *Biochem. Mol. Biol. Educ.* **2006**, *34*, 428−431.
(22) (a) Yamamura, H. I.; Snyder, S. H. Muscarinic Cholinergic Binding in Rat Brain. *Proc. Natl. Acad. Sci. U.S.A.* **1974**, *71*, 1725−1729. (b) Yamamura, H. I.; Kuhar, M. J.; Snyder, S. H. In Vivo Identification of Muscarinic Cholinergic Receptor Binding in Rat brain. *Brain Res.* **1974**, *80*, 170−176.
(23) Sallés, J.; Wallace, M. A.; Fain, J. N. Differential Effects of Alkylating Agents on the Multiple Muscarinic Receptor Subtypes Linked to Activation of Phospholipase C by Carbachol in Rat Brain Cortical Membranes. *J. Pharmacol. Exp. Ther.* **1993**, *264*, 521−529.
(24) Littmann, T.; Ozawa, T.; Hoffmann, C.; Buschauer, A.; Bernhardt, G. A Split Luciferase-based Probe for Quantitative Proximal Determination of Gαq Signalling in Live Cells. *Sci. Rep.* **2018**, *8*, No. 17179.
(25) Hattori, M.; Ozawa, T. Split Luciferase Complementation for Analysis of Intracellular Signaling. *Anal. Sci.* **2014**, *30*, 539−544.
(26) Chen, X.; Klöckner, J.; Holze, J.; Zimmermann, C.; Seemann, W. K.; Schrage, R.; Bock, A.; Mohr, K.; Tränkle, C.; Holzgrabe, U.; Decker, M. Rational Design of Partial Agonists for the Muscarinic M1 Acetylcholine Receptor. *J. Med. Chem.* **2015**, *58*, 560−576.
(27) Bermudez, M.; Rakers, C.; Wolber, G. Structural Characteristics of the Allosteric Binding Site Represent a Key to Subtype Selective Modulators of Muscarinic Acetylcholine Receptors. *Mol. Inf.* **2015**, *34*, 526−530.
(28) (a) Bock, A.; Bermudez, M.; Krebs, F.; Matera, C.; Chirinda, B.; Sydow, D.; Dallanoce, C.; Holzgrabe, U.; De Amici, M.; Lohse, M. J.; Wolber, G.; Mohr, K. Ligand Binding Ensembles Determine Graded Agonist Efficacies at a G Protein-coupled Receptor. *J. Biol. Chem.* **2016**, *291*, 16375−16389. (b) Bermudez, M.; Bock, A.; Krebs, F.; Holzgrabe, U.; Mohr, K.; Lohse, M. J.; Wolber, G. Ligand-Specific Restriction of Extracellular Conformational Dynamics Constrains Signaling of the M2 Muscarinic Receptor. *ACS Chem. Biol.* **2017**, *12*, 1743−1748.
(29) Dror, R. O.; Green, H. F.; Valant, C.; Borhani, D. W.; Valcourt, J. R.; Pan, A. C.; Arlow, D. H.; Canals, M.; Lane, J. R.; Rahmani, R.; Baell, J. B.; Sexton, P. M.; Christopoulos, A.; Shaw, D. E. Structural Basis for Modulation of a G-Protein-coupled Receptor by Allosteric Drugs. *Nature* **2013**, *503*, 295−299.
(30) Jones, G.; Willett, P.; Glen, R. C.; Leach, A. R.; Taylor, R. Development and Validation of a Genetic Algorithm for Flexible Docking. *J. Mol. Biol.* **1997**, *267*, 727−748.

DOI: 10.1021/acs.jmedchem.8b01822
J. Med. Chem. 2019, 62, 3009−3020

(31) Wolber, G.; Seidel, T.; Bendix, F.; Langer, T. Molecule-pharmacophore Superpositioning and Pattern Matching in Computational Drug Design. *Drug Discov. Today* **2008**, *13*, 23−29.

DOI: 10.1021/acs.jmedchem.8b01822
J. Med. Chem. 2019, 62, 3009−3020

Supporting Information

Fluorination of Photoswitchable Muscarinic Agonists Tunes Receptor Pharmacology and Photochromic Properties

Luca Agnetta, Marcel Bermudez, Fabio Riefolo, Carlo Matera, Enrique Claro, Regina Messerer, Timo Littmann, Gerhard Wolber, Ulrike Holzgrabe, Michael Decker

Table of content

1 Synthesis

1.1 Photoiperoxo

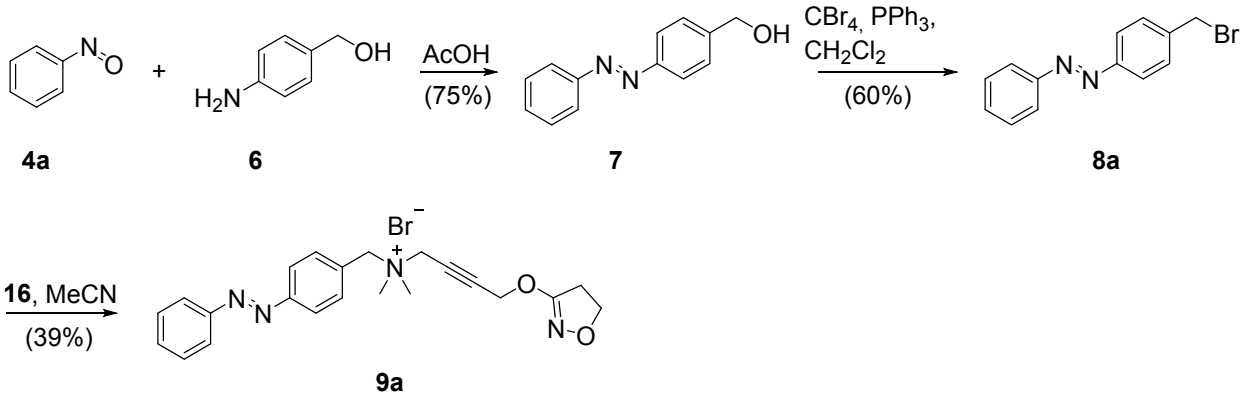

Suppl. Scheme 1 Three-step synthesis of photoiperoxo **9a**.

1.1.1 4-((4,5-dihydroisoxazol-3-yl)oxy)-N,N-dimethyl-N-(4-(phenyldiazenyl)benzyl)but-2-yn-1-aminium (photoiperoxo, 9a)

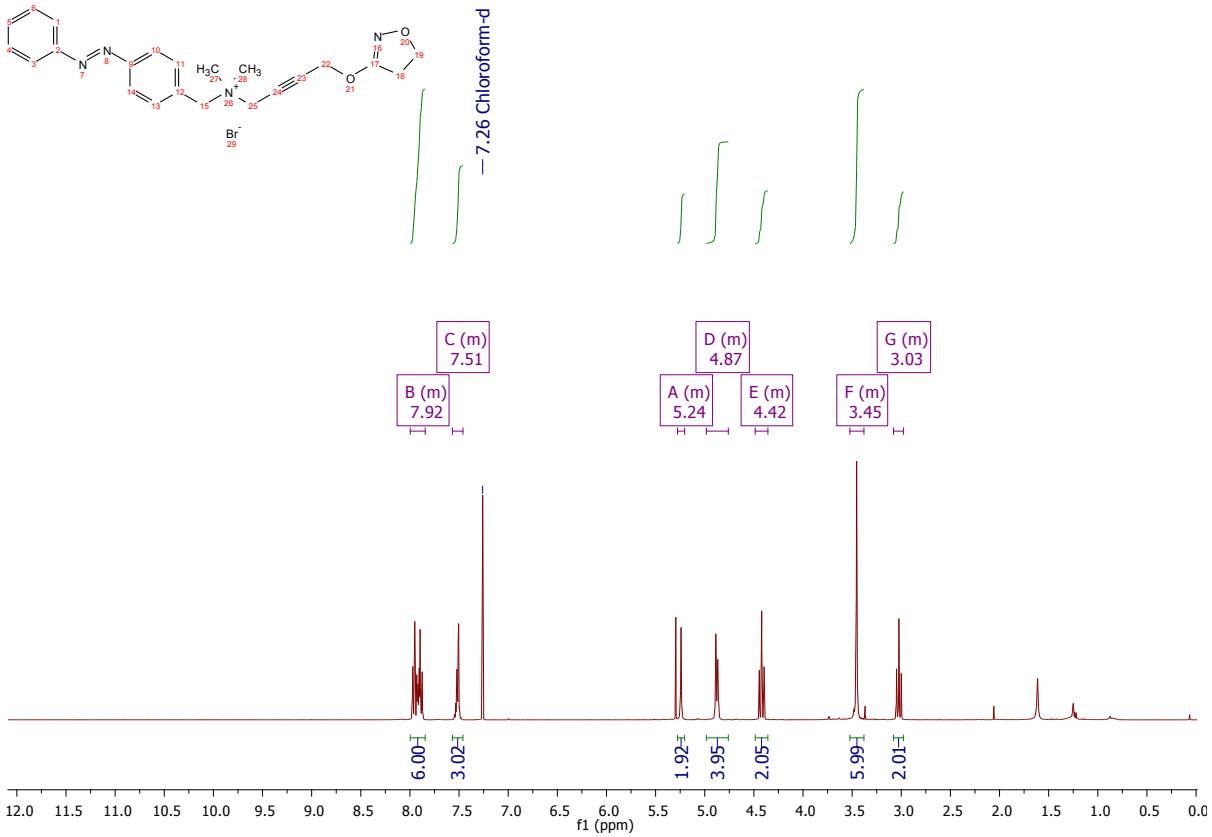

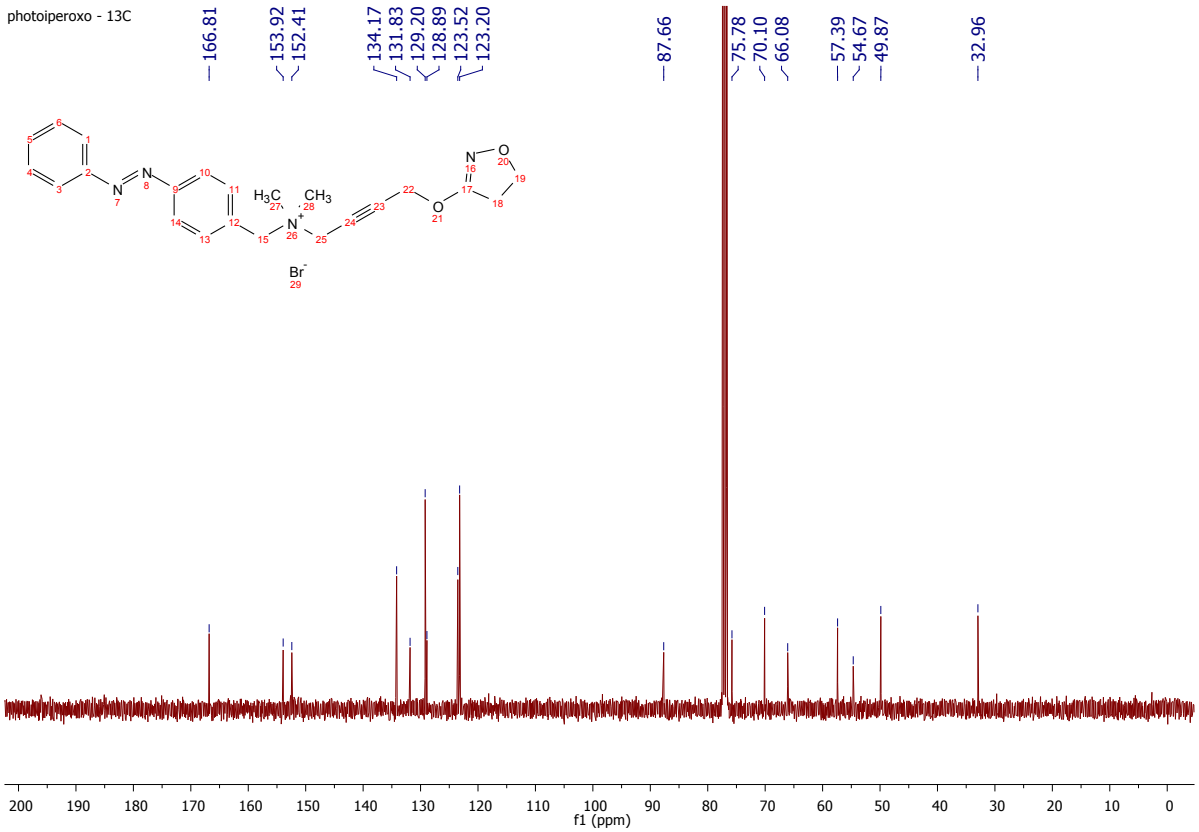
photoiperoxo - 13C
166.81
153.92
152.41
134.17
131.83
129.20
128.89
123.52
123.20
87.66
75.78
70.10
66.08
57.39
54.67
49.87
32.96
200 190 180 170 160 150 140 130 120 110 100 90 80 70 60 50 40 30 20 10 0
f1 (ppm)

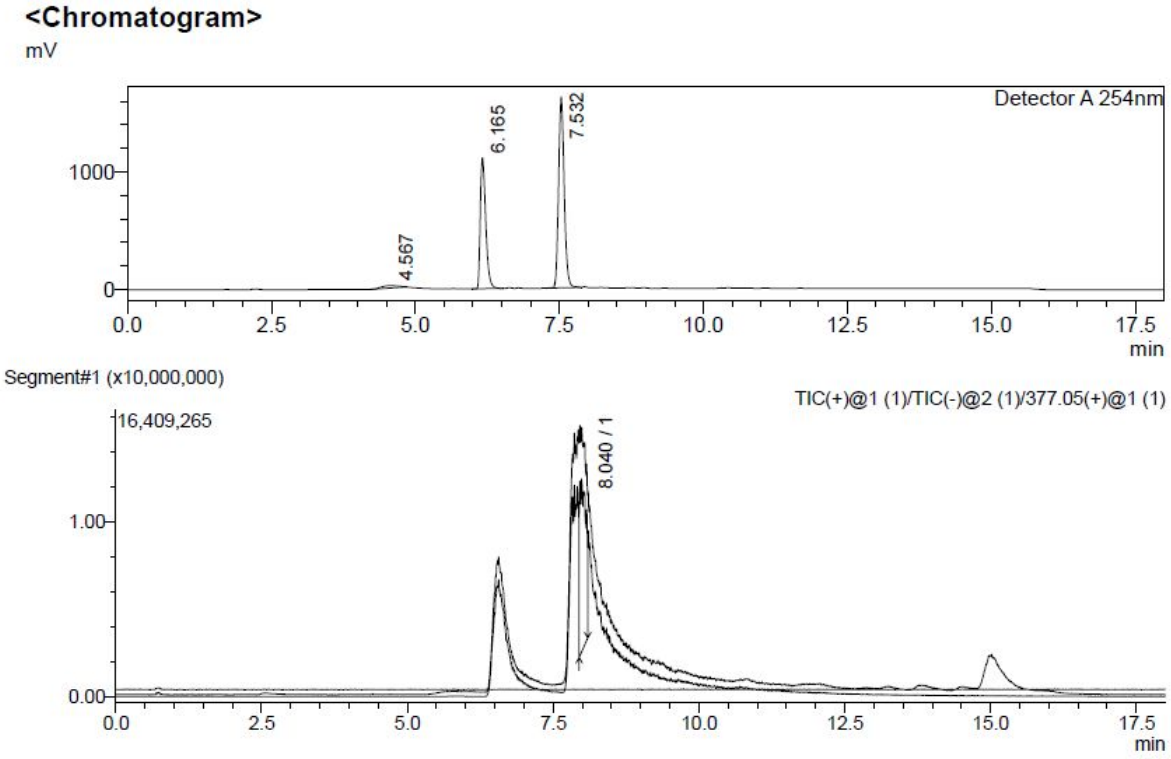
<Chromatogram>
mV
Detector A 254nm
6.165
7.532
4.567
1000
0
0.0 2.5 5.0 7.5 10.0 12.5 15.0 17.5
min
Segment#1 (x10,000,000)
TIC(+)@1 (1)/TIC(-)@2 (1)/377.05(+)@1 (1)
16,409,265
8.040 / 1
1.00
0.00
0.0 2.5 5.0 7.5 10.0 12.5 15.0 17.5
min

Detector A 254nm

Peak#	Ret. Time	Area	Height	Area%
1	4.567	415930	21236	2.218
2	6.165	7316343	1109784	39.014
3	7.532	11020821	1616544	58.768
Total		18753093	2747565	100.000

Line#:1 R.Time:8.040(Scan#:4825)
MassPeaks:406
Spectrum Mode:Averaged 8.037-8.043(4823-4827) Base Peak:377.15(2775140)
BG Mode:Calc Segment 1 - Event 1

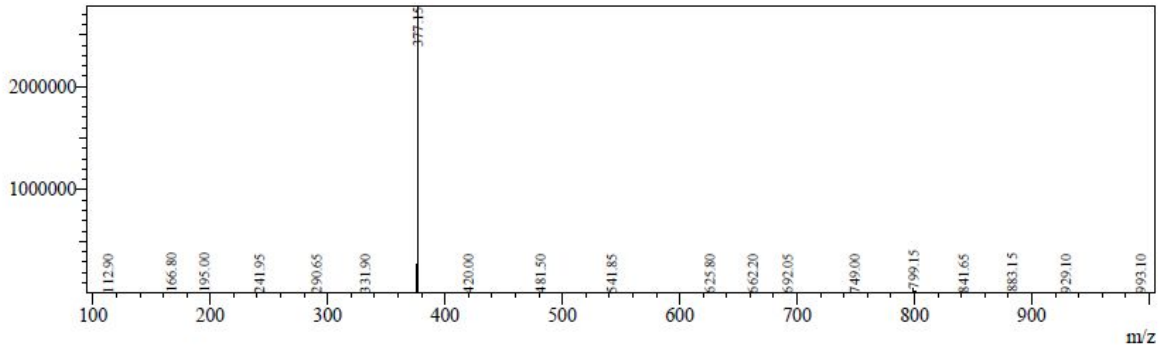

1.2 Iper-Azo-Iper

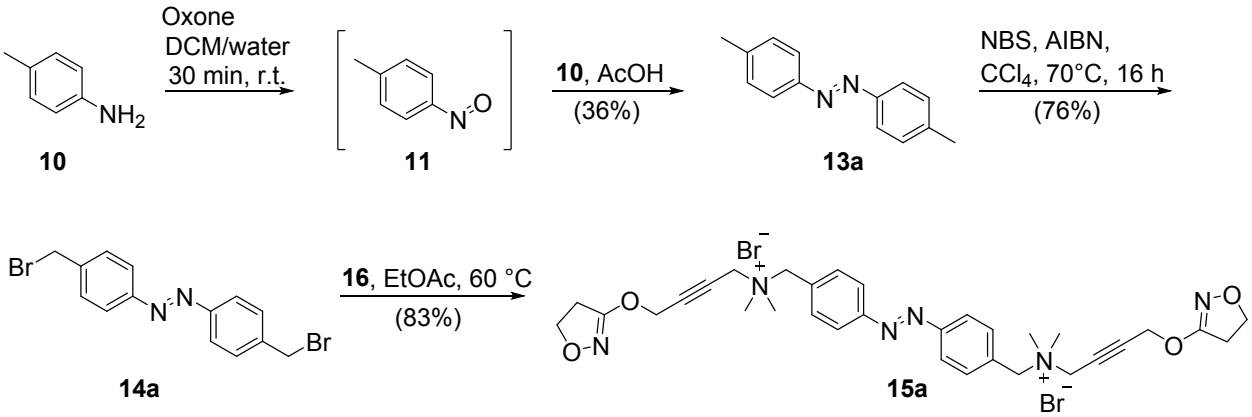

Suppl. Scheme 2 Synthesis of Iper-azo-Iper **15a.**

1.2.1 4-((4,5-dihydroisoxazol-3-yl)oxy)-N-(4-((4-(((4-((4,5-dihydroisoxazol-3-yl)oxy)but-2-yn-1-yl)dimethyl-l4-azaneyl)methyl)phenyl)diazenyl)benzyl)-N,N-dimethylbut-2-yn-1-aminium bromide (iper-azo-iper, 15a)

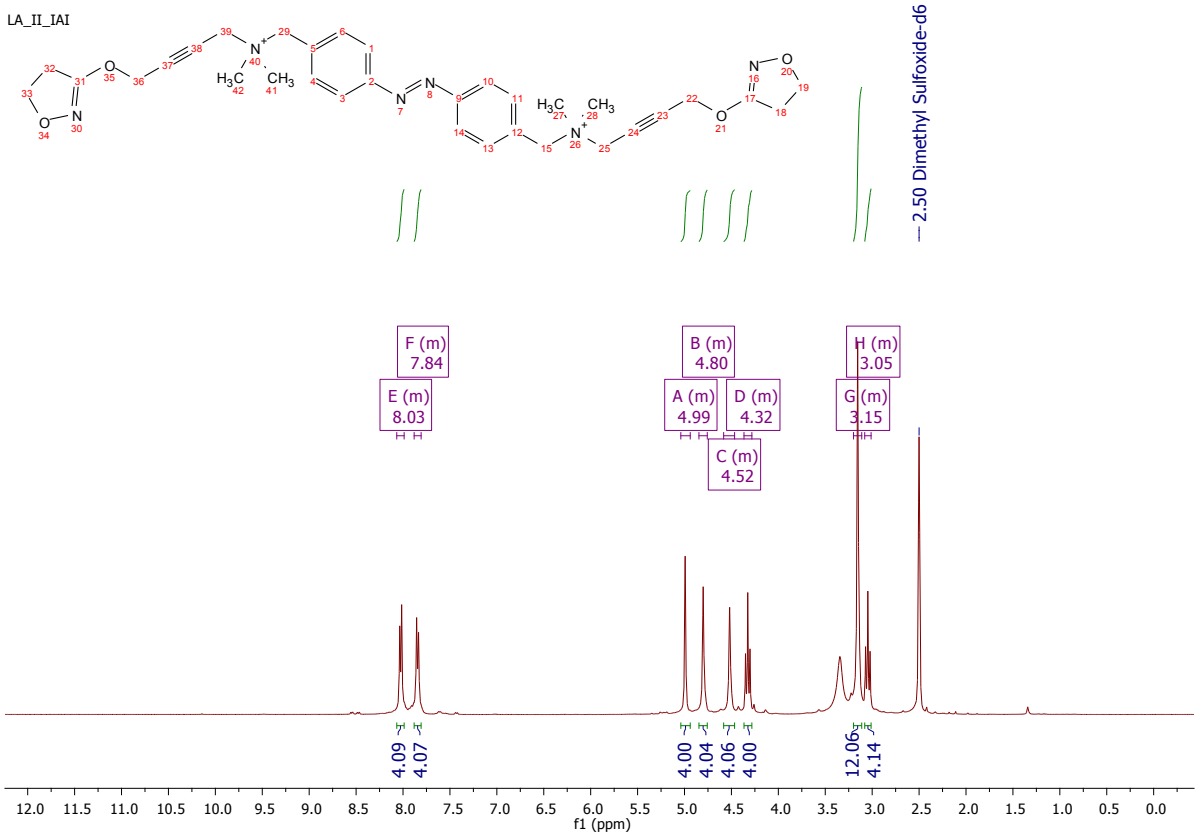

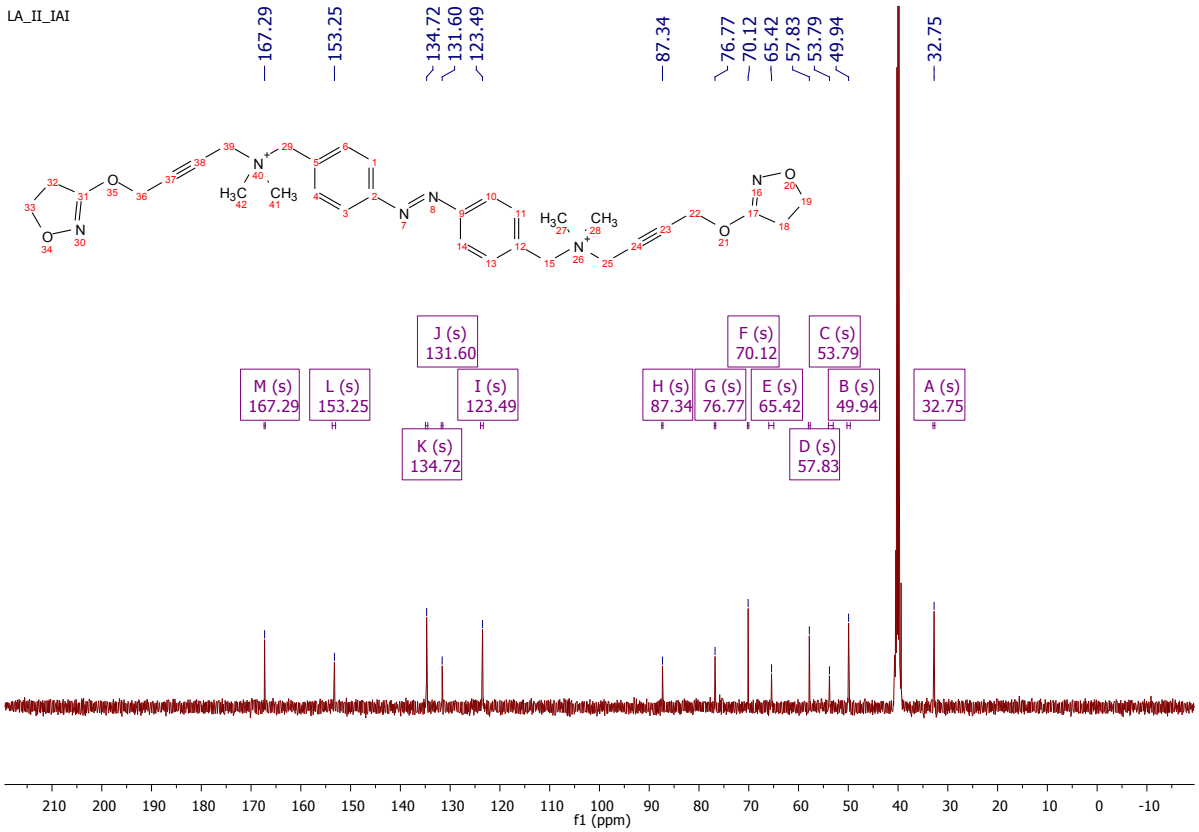
LA_II_IAI
167.29
153.25
134.72
131.60
123.49
87.34
76.77
70.12
65.42
57.83
53.79
49.94
32.75
J (s) 131.60
F (s) 70.12
C (s) 53.79
M (s) 167.29
L (s) 153.25
I (s) 123.49
H (s) 87.34
G (s) 76.77
E (s) 65.42
B (s) 49.94
A (s) 32.75
K (s) 134.72
D (s) 57.83
f1 (ppm)

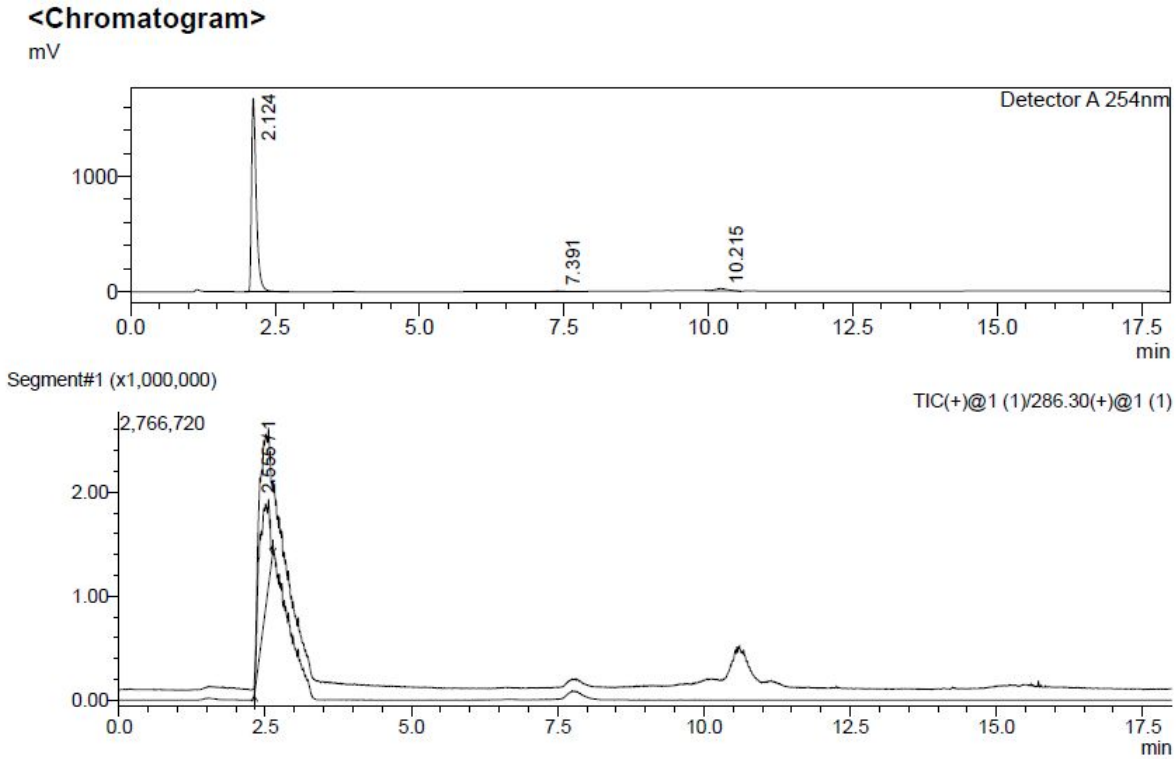
<Chromatogram>
mV
Detector A 254nm
2.124
7.391
10.215
min
Segment#1 (x1,000,000)
TIC(+)@1 (1)/286.30(+)@1 (1)
2,766,720
2.566
min

Detector A 254nm

Peak#	Ret. Time	Area	Height	Area%
1	2.124	9637034	1666813	96.724
2	7.391	38735	4600	0.389
3	10.215	287666	20225	2.887
Total		9963435	1691638	100.000

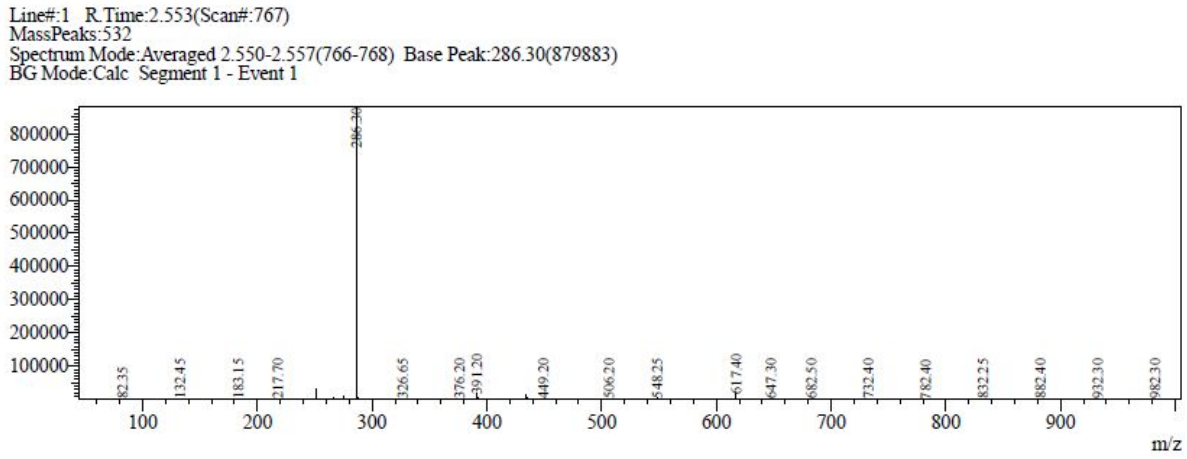

1.3 F4-photoiperoxo

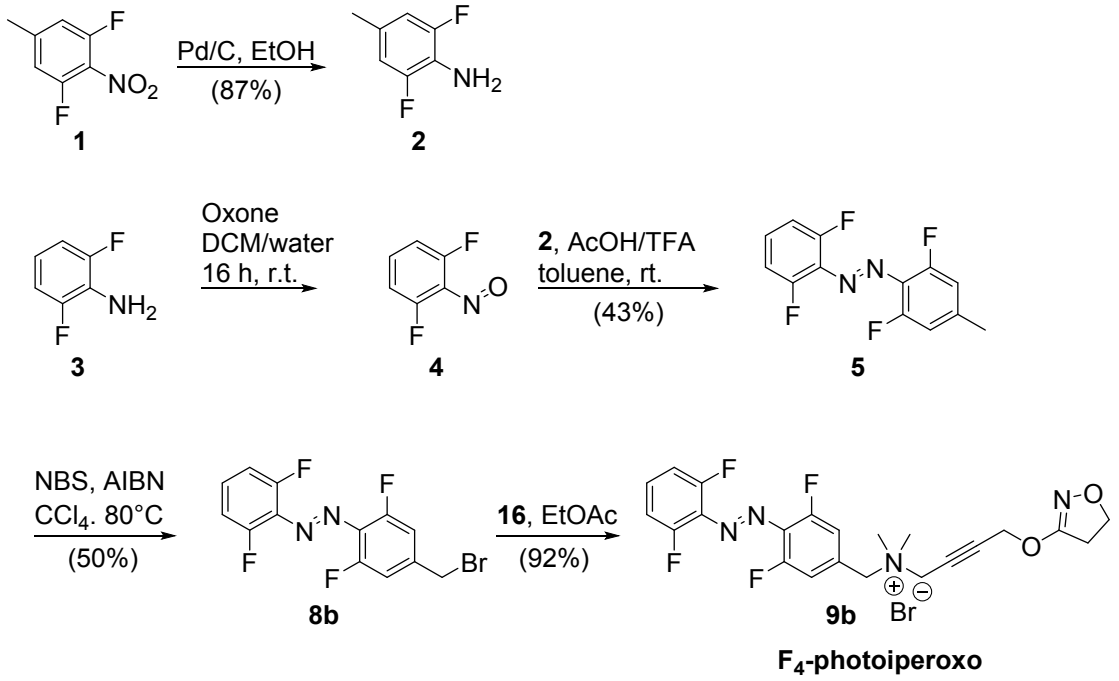

Suppl. Scheme 3 Synthesis of F4-photoiperoxo

1.3.1 *N*-(4-((2,6-difluorophenyl)diazenyl)-3,5-difluorobenzyl)-4-((4,5-dihydroisoxazol-3-yl)oxy)-N,N-dimethylbut-2-yn-1-aminium bromide (F_4-photoiperoxo, 9b)

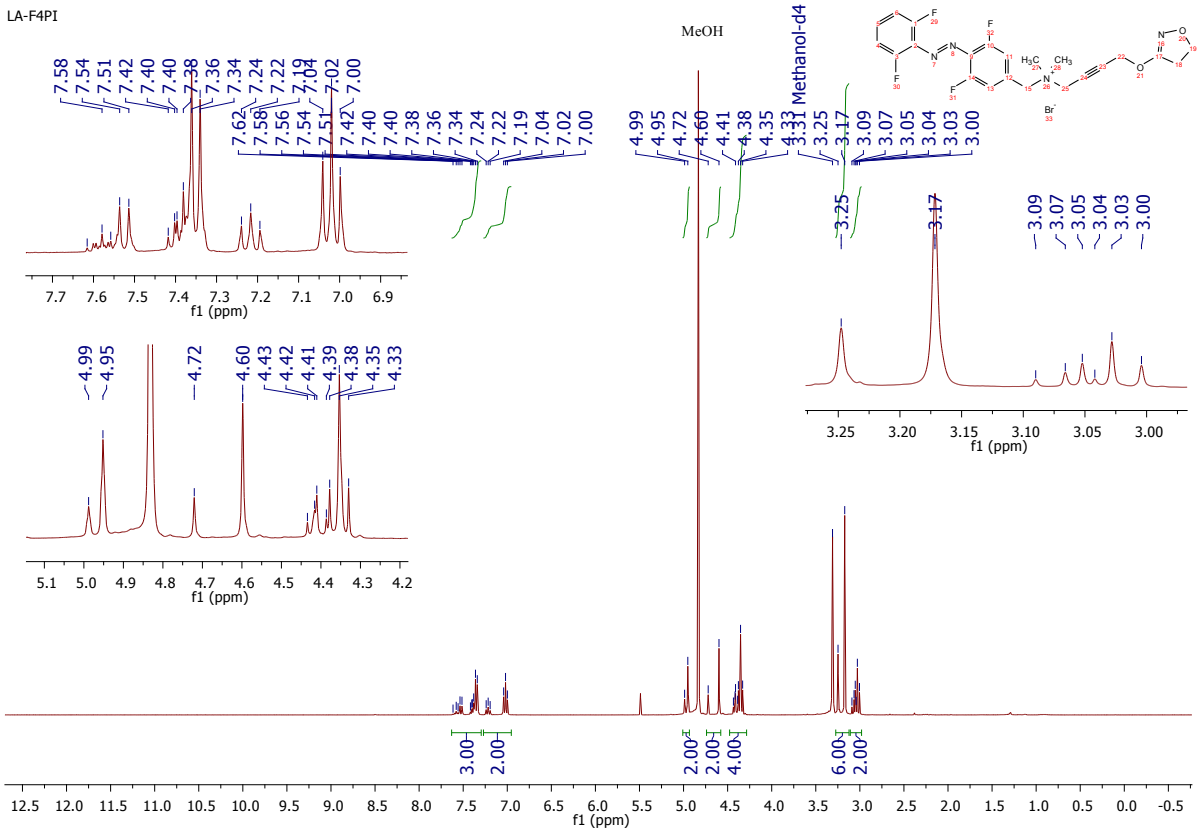

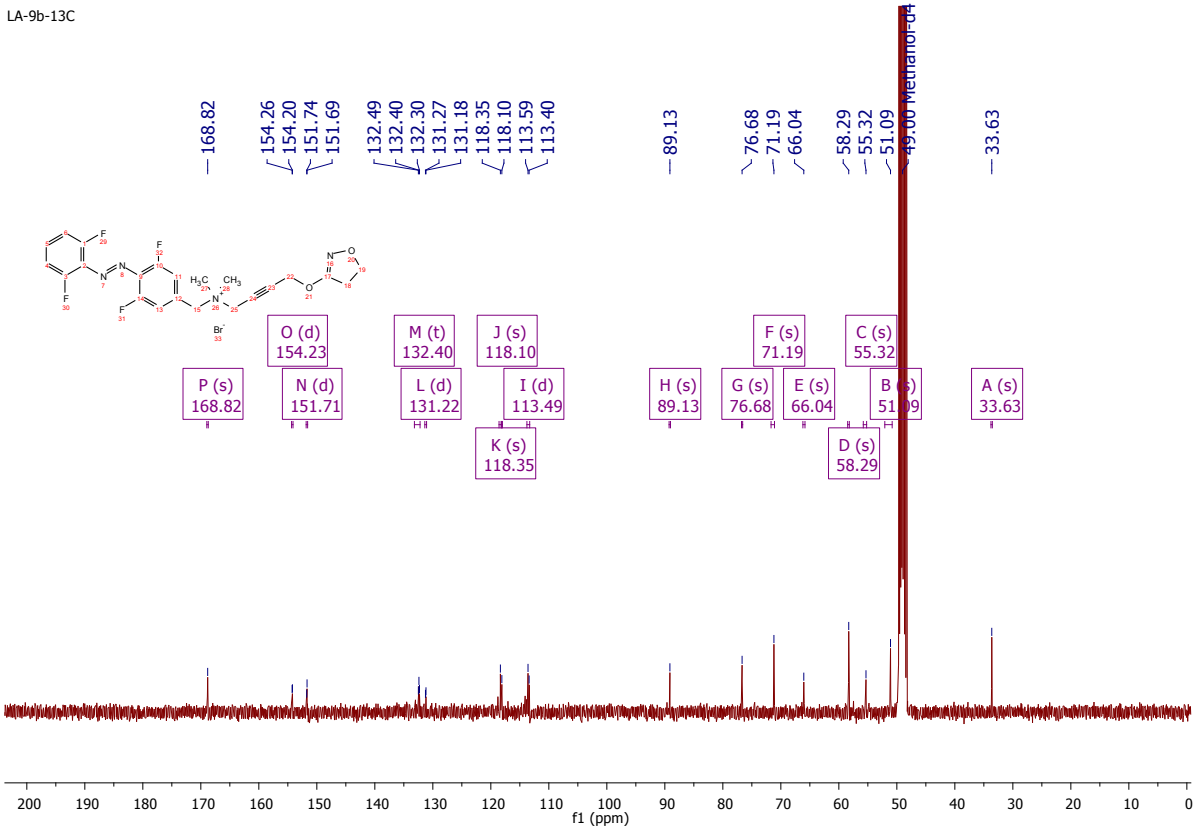
LA-9b-13C
168.82
154.26
154.20
151.74
151.69
132.49
132.40
132.30
131.27
131.18
118.35
118.10
113.59
113.40
89.13
76.68
71.19
66.04
58.29
55.32
51.09
49.00 Methanol-d4
33.63
O (d) 154.23
M (t) 132.40
J (s) 118.10
F (s) 71.19
C (s) 55.32
P (s) 168.82
N (d) 151.71
L (d) 131.22
I (d) 113.49
H (s) 89.13
G (s) 76.68
E (s) 66.04
B (s) 51.09
A (s) 33.63
K (s) 118.35
D (s) 58.29
f1 (ppm)

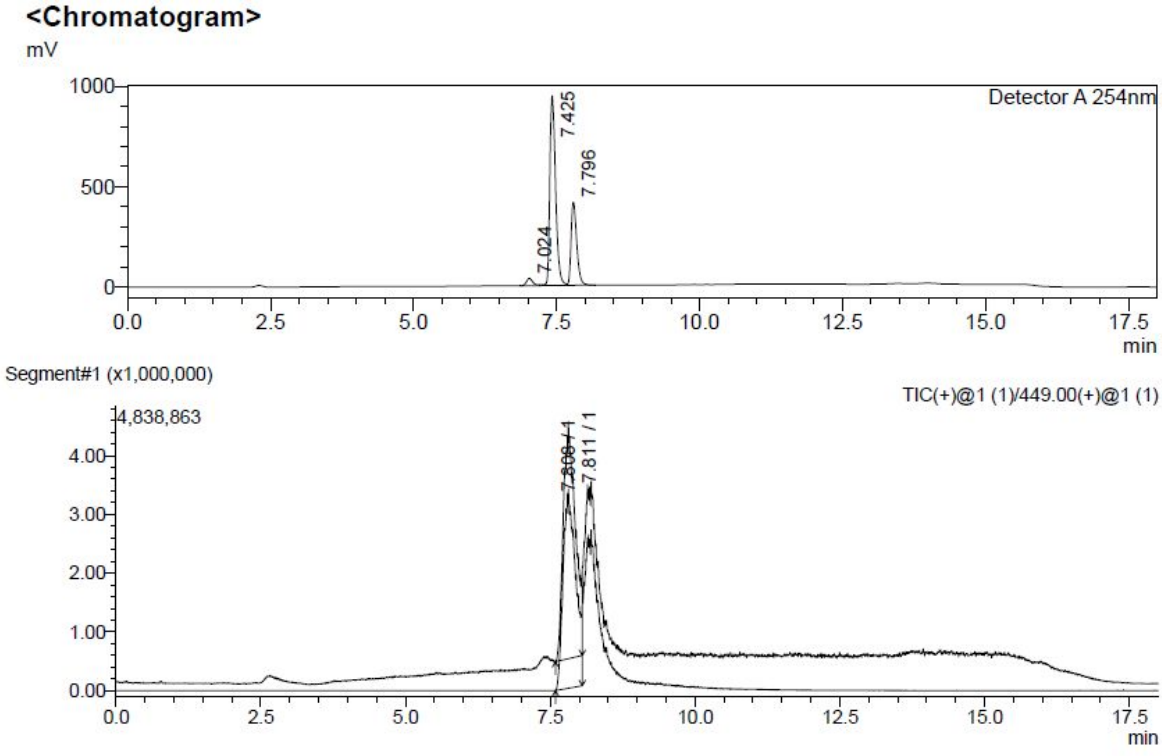
<Chromatogram>
mV
Detector A 254nm
7.425
7.796
7.024
min
Segment#1 (x1,000,000)
TIC(+)@1 (1)/449.00(+)@1 (1)
4,838,863
7.811 / 1
min

Detector A 254nm

Peak#	Ret. Time	Area	Height	Area%
1	7.024	282737	36811	2.889
2	7.425	6654722	941228	67.996
3	7.796	2849446	413148	29.115
Total		9786905	1391187	100.000

Line#:1 R.Time:7.808(Scan#:7809)
MassPeaks:242
Spectrum Mode:Averaged 7.807-7.809(7808-7810) Base Peak:449.00(2387003)
BG Mode:Calc Segment 1 - Event 1

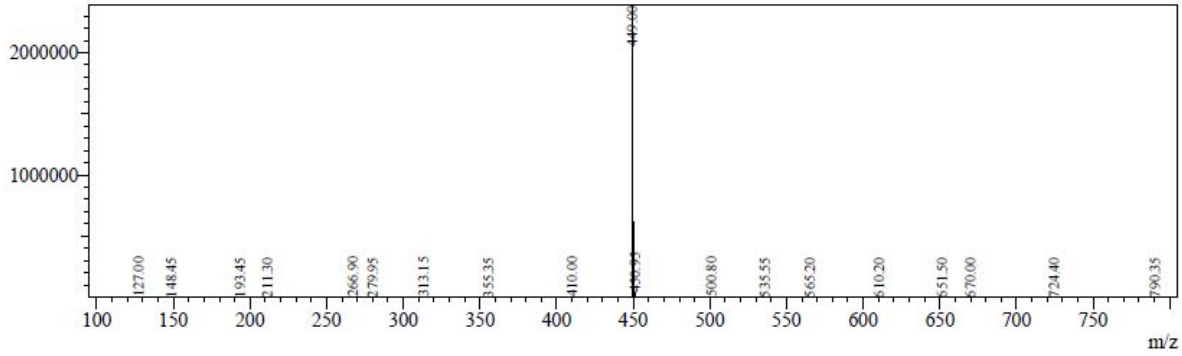

1.4 F_4-iper-azo-iper

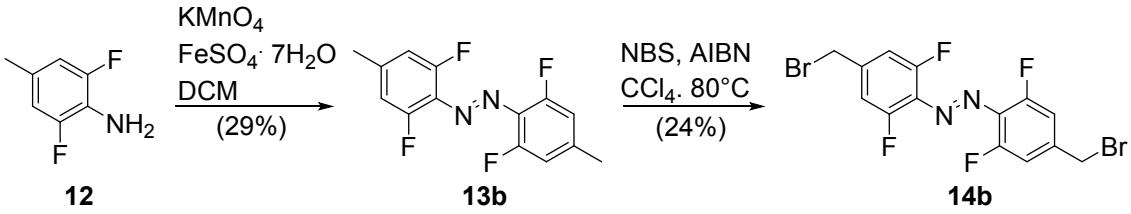

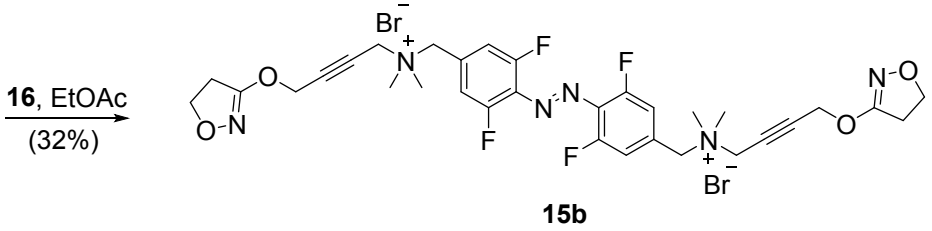

Suppl. Scheme 4 Synthesis of F4-iper-azo-iper

1.4.1 *N,N'*-((diazene-1,2-diylbis(3,5-difluoro-4,1-phenylene))bis(methylene))bis(4-((4,5-dihydroisoxazol-3-yl)oxy)-N,N-dimethylbut-2-yn-1-aminium) bromide (F_4-iper-azo-iper, 15b)

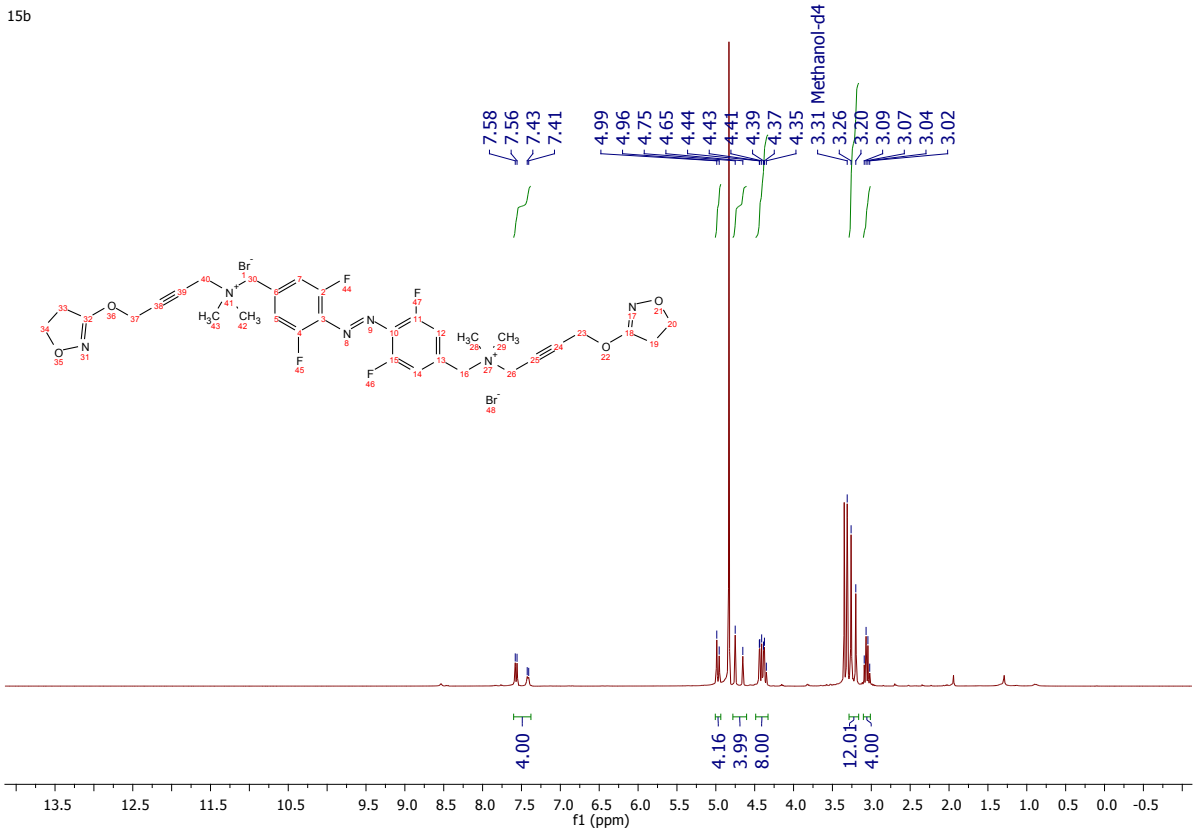

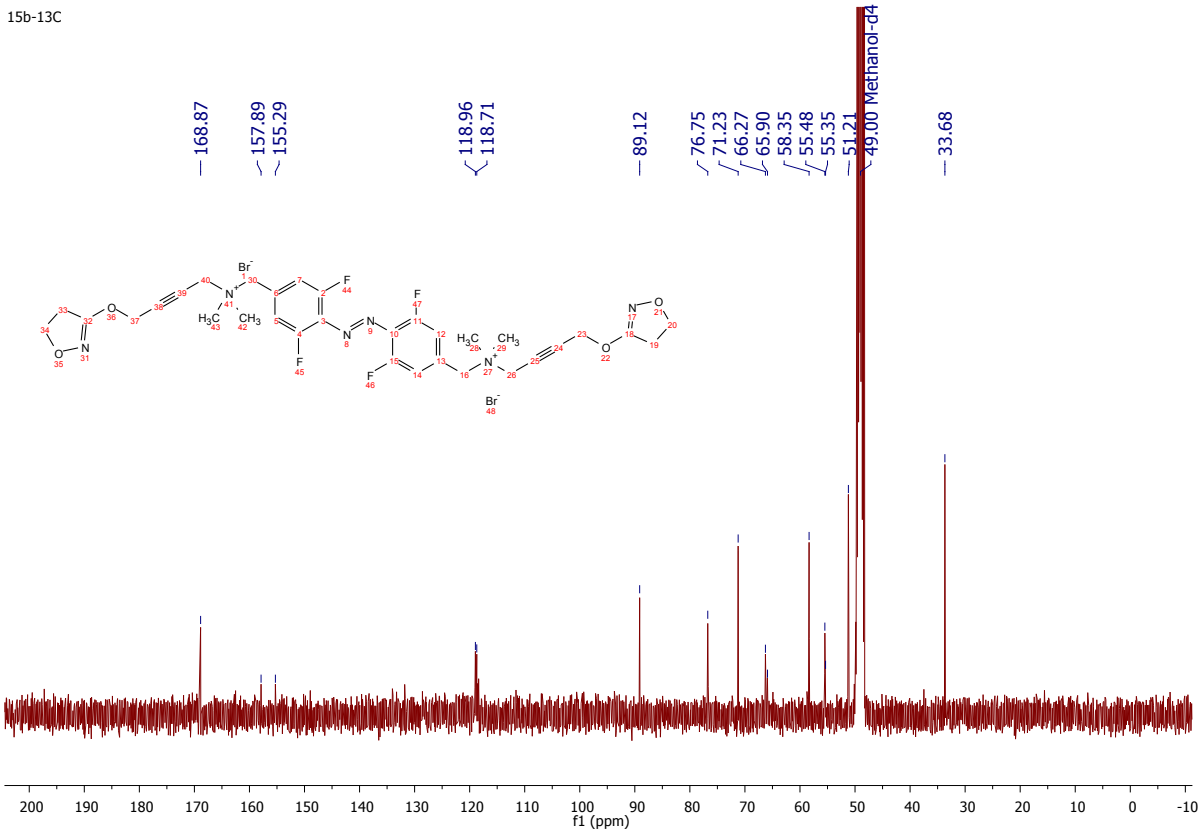
15b-13C
168.87
157.89
155.29
118.96
118.71
89.12
76.75
71.23
66.27
65.90
58.35
55.48
55.35
51.21
49.00 Methanol-d4
33.68
f1 (ppm)

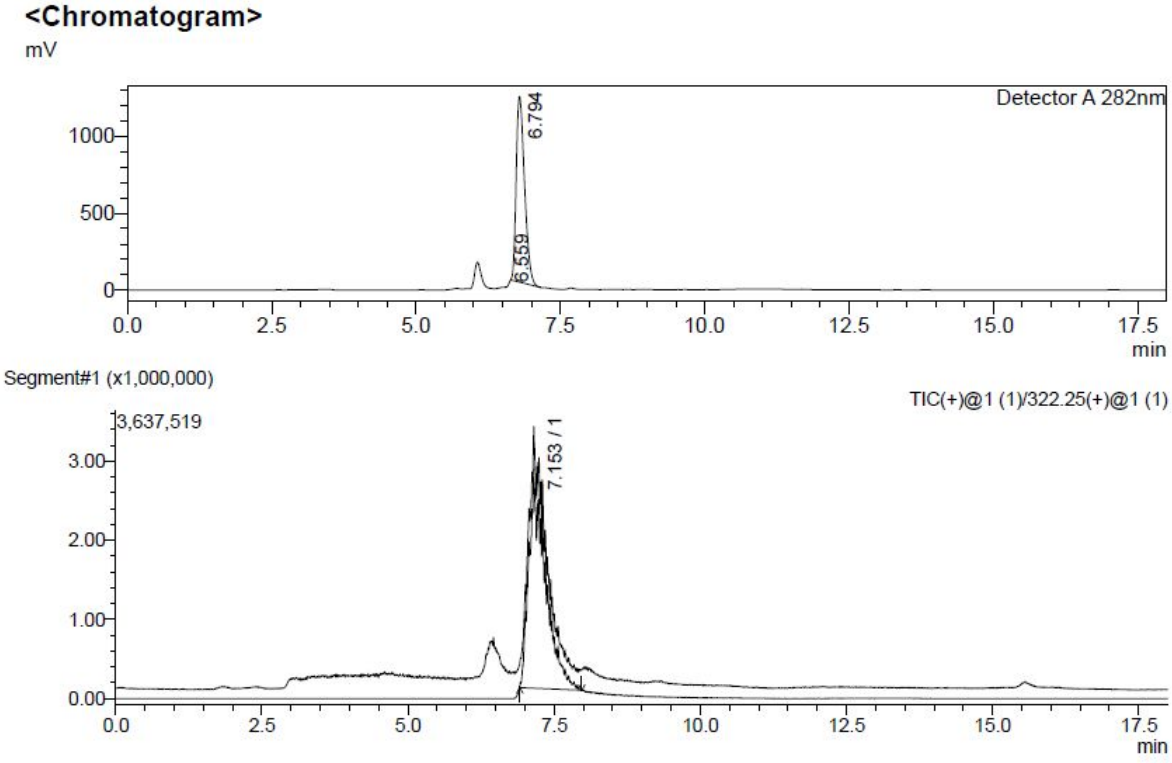
<Chromatogram>
mV
Detector A 282nm
6.794
6.559
min
Segment#1 (x1,000,000)
TIC(+)@1 (1)/322.25(+)@1 (1)
3,637,519
7.153 / 1
min

Detector A 282nm

Peak#	Ret. Time	Area	Height	Area%
1	6.559	238	-335	0.002
2	6.794	12092836	1201775	99.998
Total		12093074	1201440	100.000

Line#:1 R.Time:7.153(Scan#:2147)
MassPeaks:415
Spectrum Mode:Averaged 7.150-7.157(2146-2148) Base Peak:322.25(2800221)
BG Mode:Calc Segment 1 - Event 1

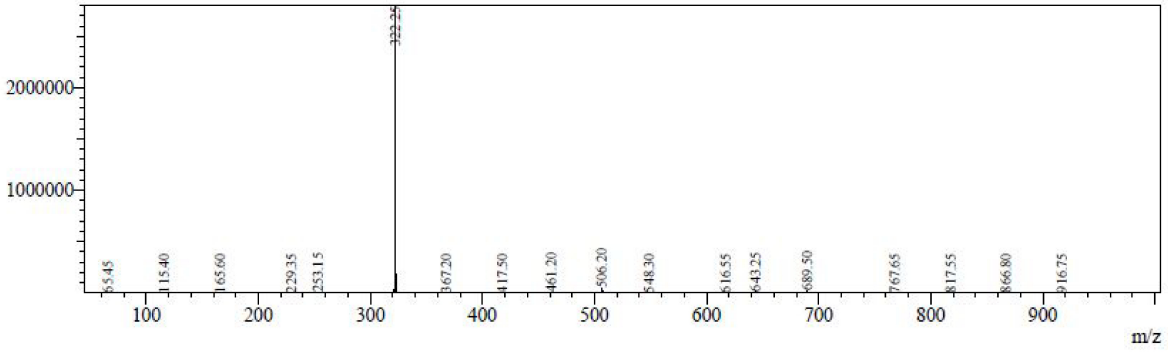

1.5 Iper-Cn-Iper

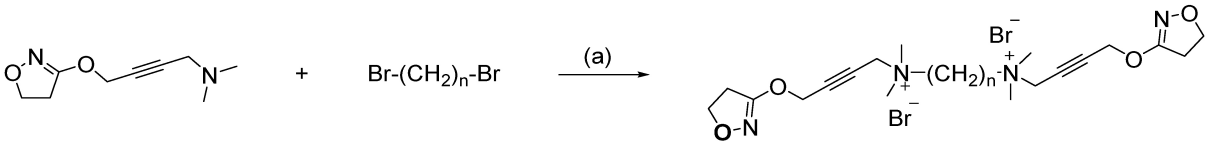

16 **17-Cn** **18-Cn**

Suppl. Scheme 5 Synthesis of 18a-d. (a) KI/K_2CO_3 (1:1), microwave (500 W, 70 °C), 2-3 h.

2 Photochemical characterization

2.1 UV/Vis spectra, stability measurements, multiple switching cycles

2.1.1 Photoiperoxo (PI, 9a)

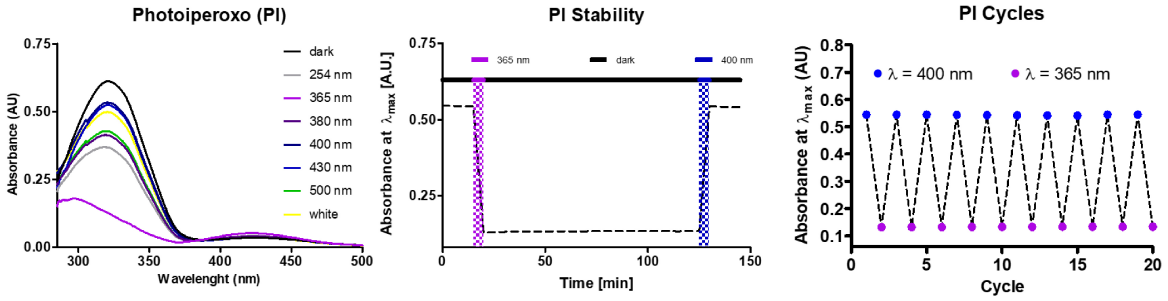

2.1.2 F4-photoiperoxo (F4-PI, 9b)

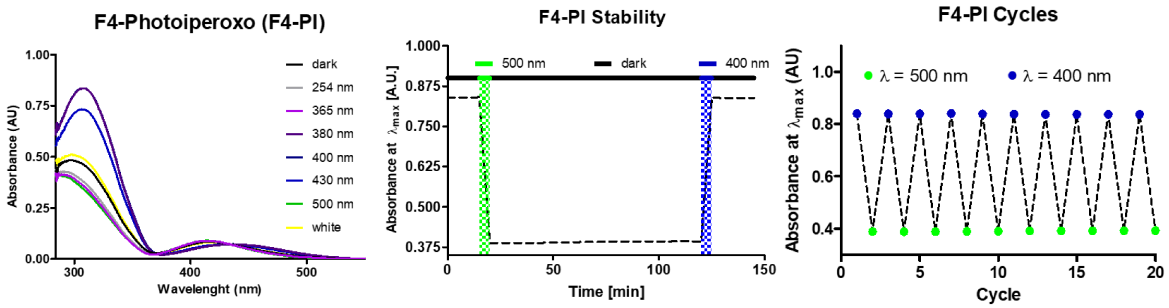

2.1.3 Iper-azo-iper (IAI, 15a)

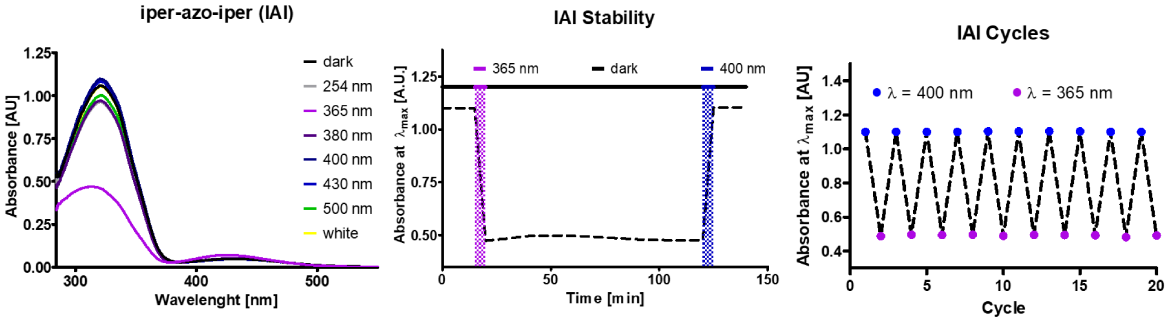

2.1.4 F4-iper-azo-iper (F4-IAI, 15b)

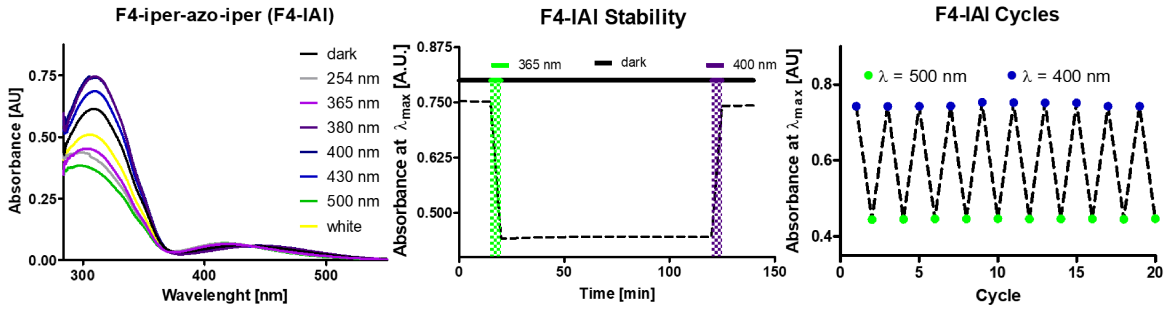

2.2 Photostationary states (PSS)

2.2.1 Photoiperoxo (PI, 9a)

PSS trans

<Chromatogram>

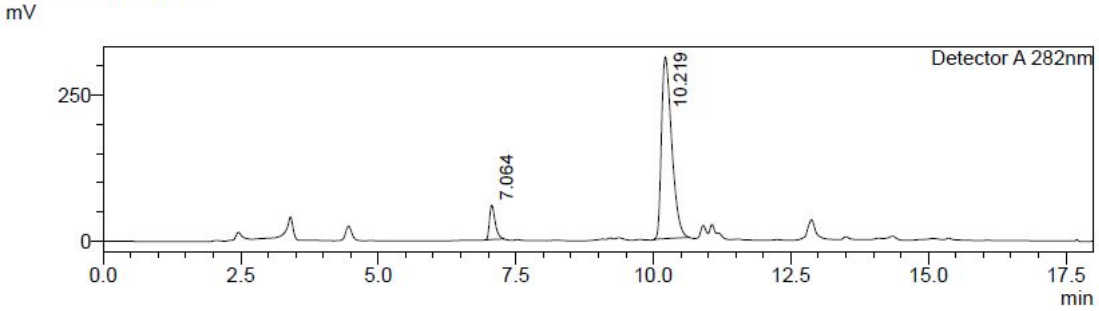

Detector A 282nm

Peak#	Ret. Time	Area	Height	Area%
1	7.064	421894	58784	9.493
2	10.219	4022390	311159	90.507
Total		4444285	369942	100.000

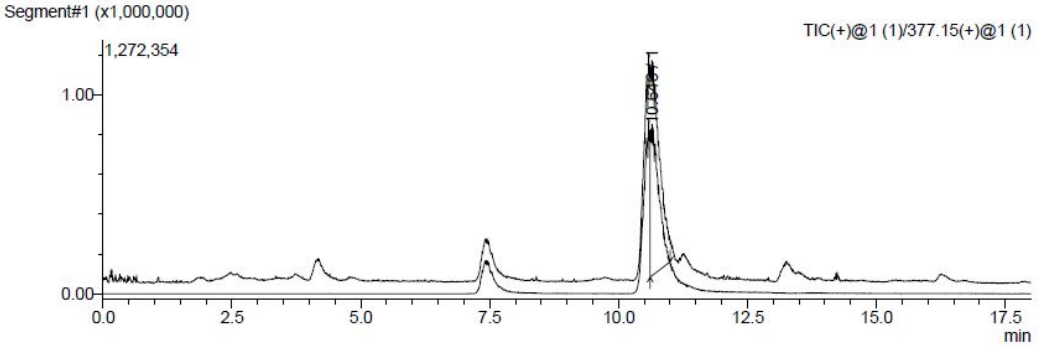

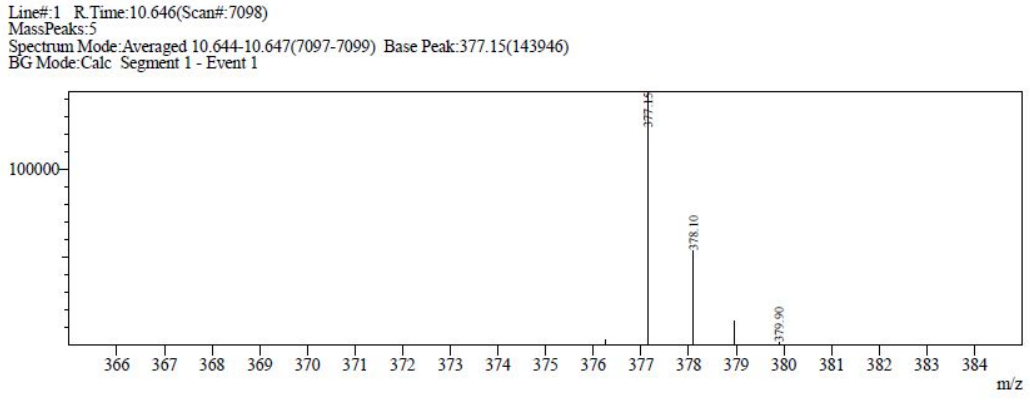

PSS cis

<Chromatogram>

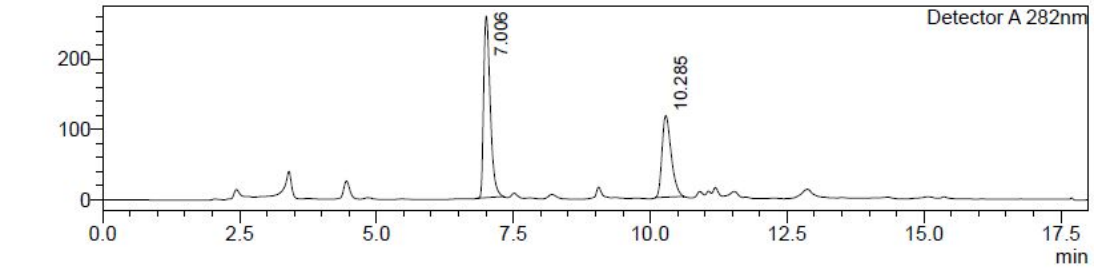

Detector A 282nm

Peak#	Ret. Time	Area	Height	Area%
1	7.006	2160372	257748	61.484
2	10.285	1353319	115789	38.516
Total		3513691	373537	100.000

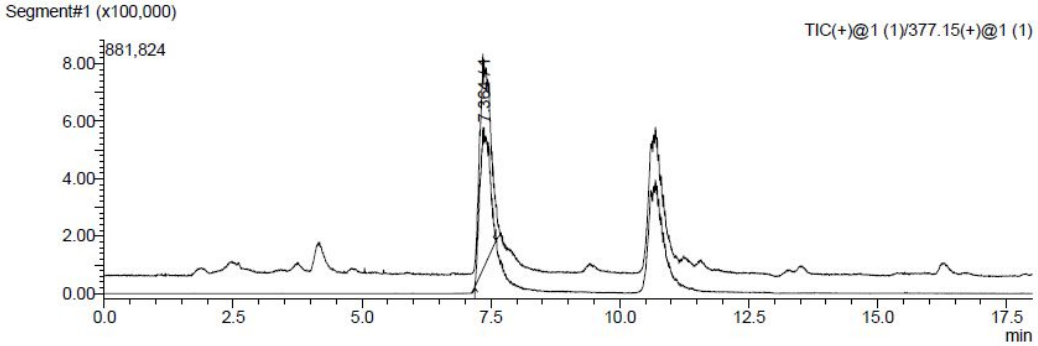

Line#:1 R.Time:7.364(Scan#:4910)
MassPeaks:206
Spectrum Mode:Averaged 7.362-7.365(4909-4911) Base Peak:377.15(484099)
BG Mode:Calc Segment 1 - Event 1

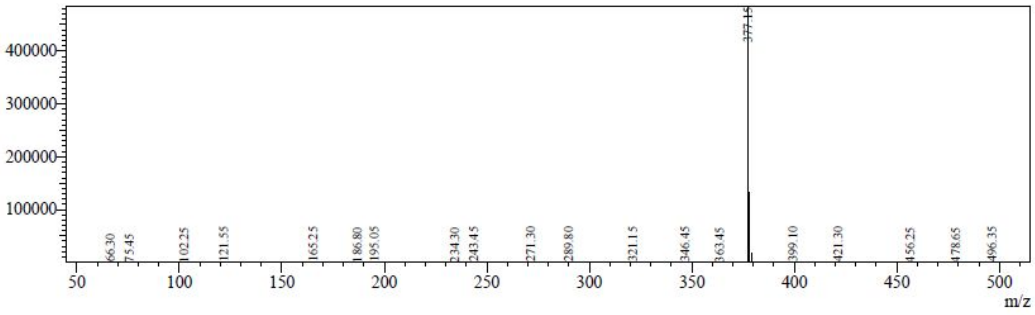

2.2.2 F4-photoiperoxo (F4-PI, 9b)

PSS trans

<Chromatogram>

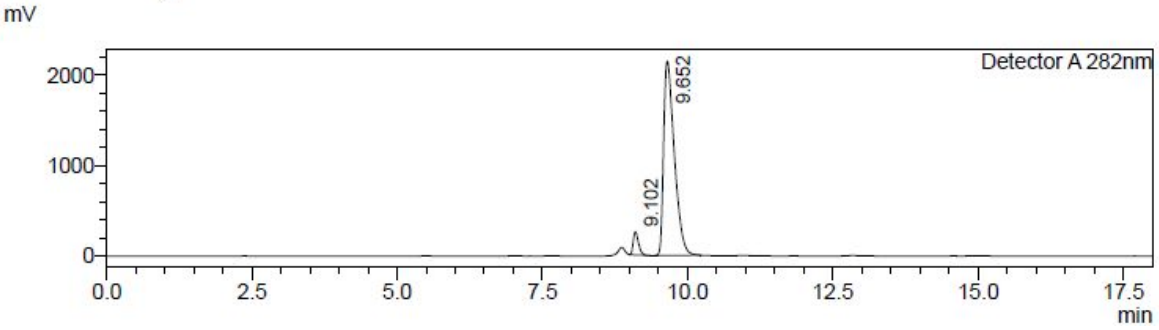

Detector A 282nm

Peak#	Ret. Time	Area	Height	Area%
1	9.102	1621777	255121	5.570
2	9.652	27496596	2143654	94.430
Total		29118373	2398775	100.000

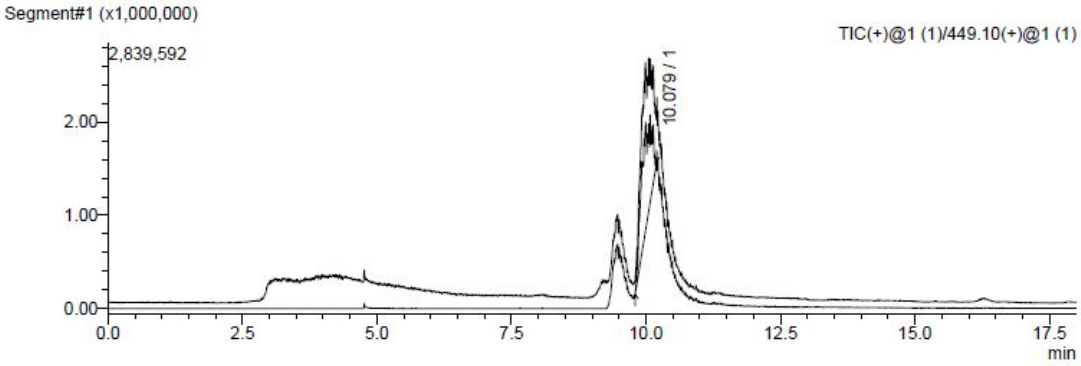

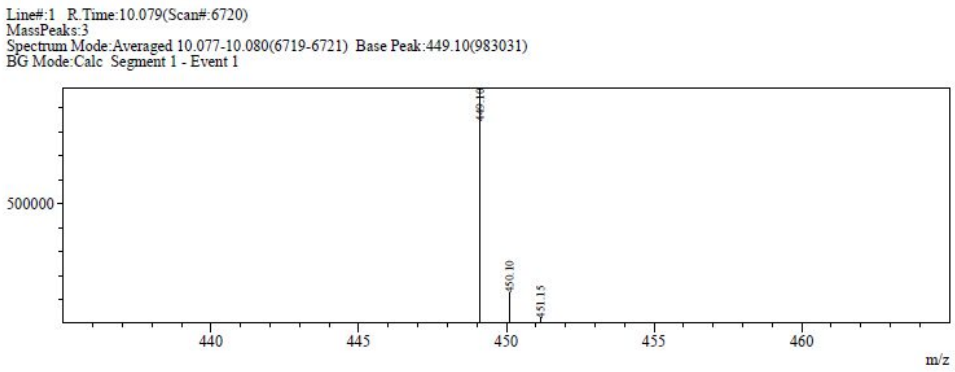

PSS cis

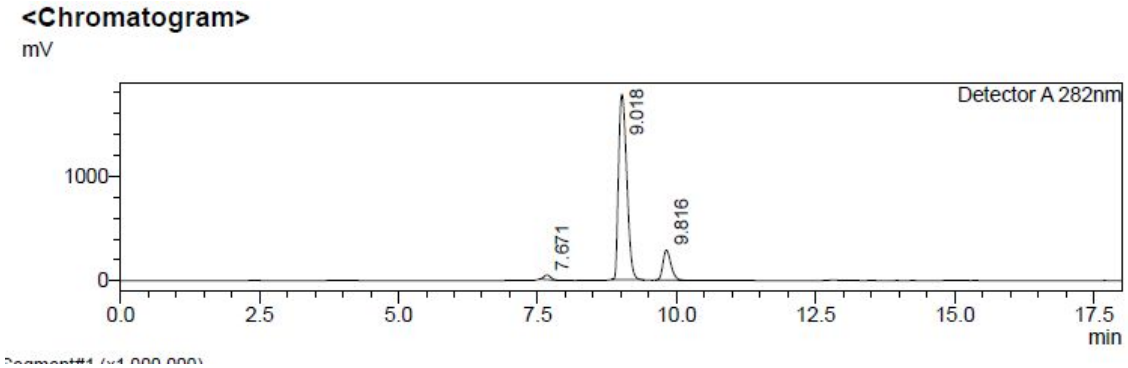

Detector A 282nm

Peak#	Ret. Time	Area	Height	Area%
1	7.671	384052	44993	1.790
2	9.018	18203389	1768753	84.852
3	9.816	2865579	286272	13.357
Total		21453020	2100018	100.000

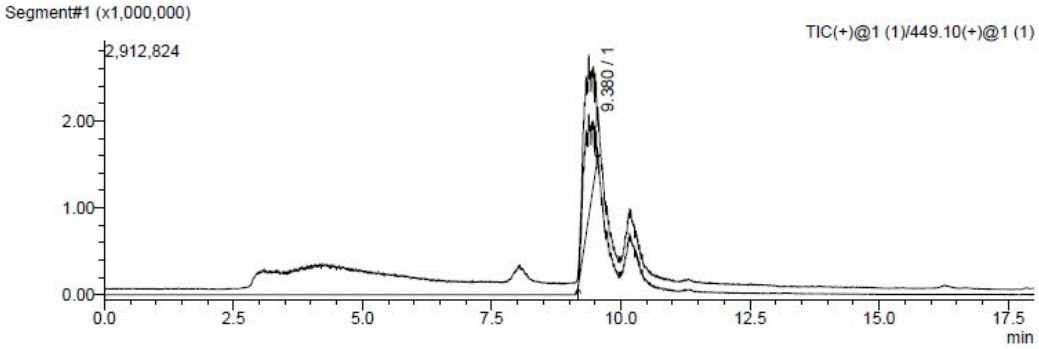

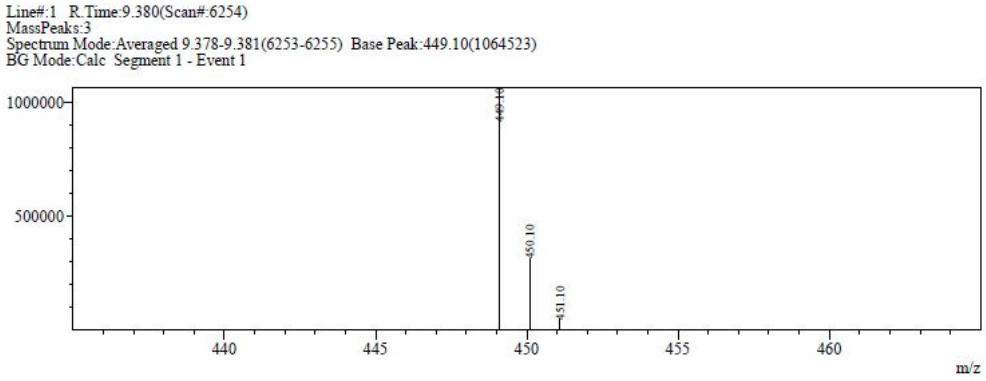

2.2.2.1 Iper-azo-iper (IAI, 15a)

PSS trans

<Chromatogram>

mV

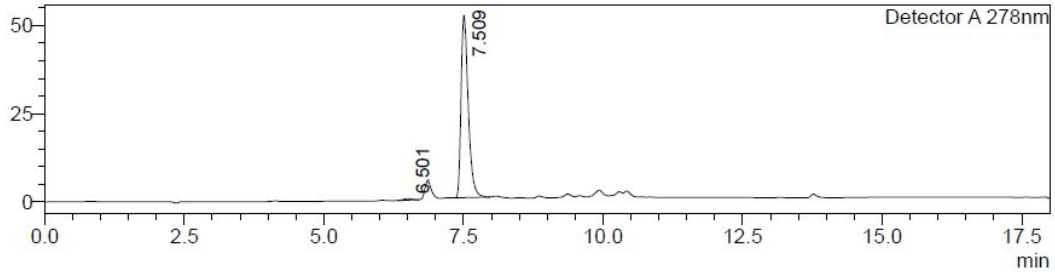

Detector A 278nm

Peak#	Ret. Time	Area	Height	Area%
1	6.501	4524	427	0.969
2	7.509	462176	51581	99.031
Total		466700	52008	100.000

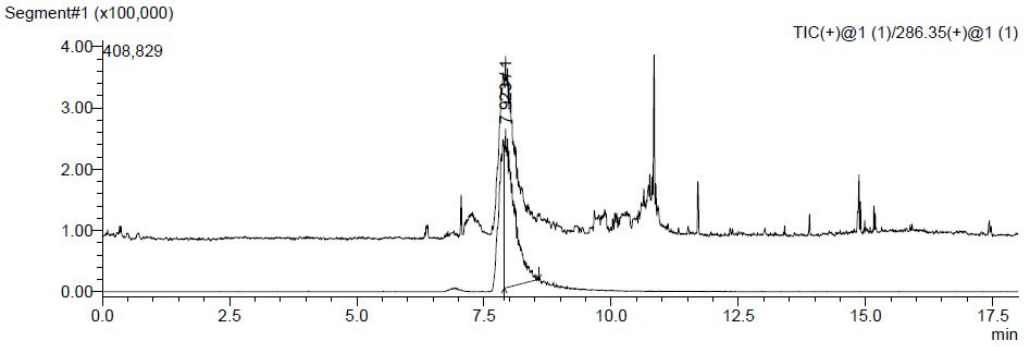

Line#:1 R.Time:7.923(Scan#:2378)
MassPeaks:553
Spectrum Mode:Averaged 7.920-7.927(2377-2379) Base Peak:286.30(64991)
BG Mode:Calc Segment 1 - Event 1

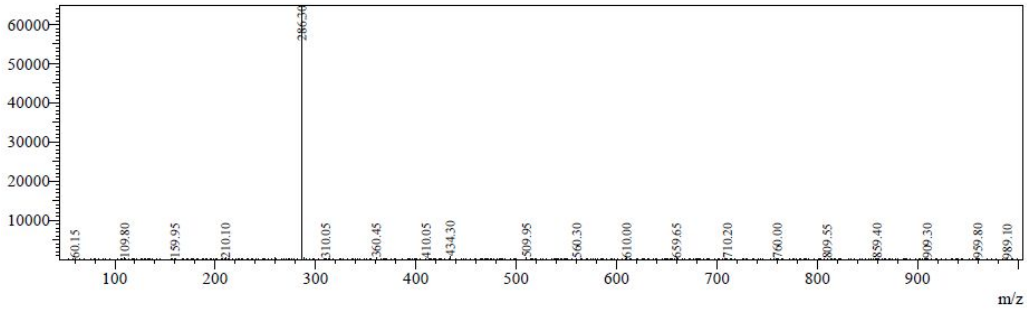

PSS cis

<Chromatogram>

mV

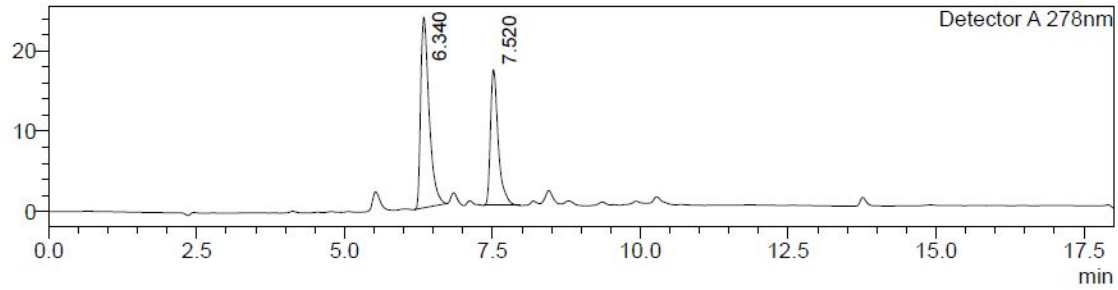

Detector A 278nm

Peak#	Ret. Time	Area	Height	Area%
1	6.340	236211	23707	60.426
2	7.520	154697	16863	39.574
Total		390908	40570	100.000

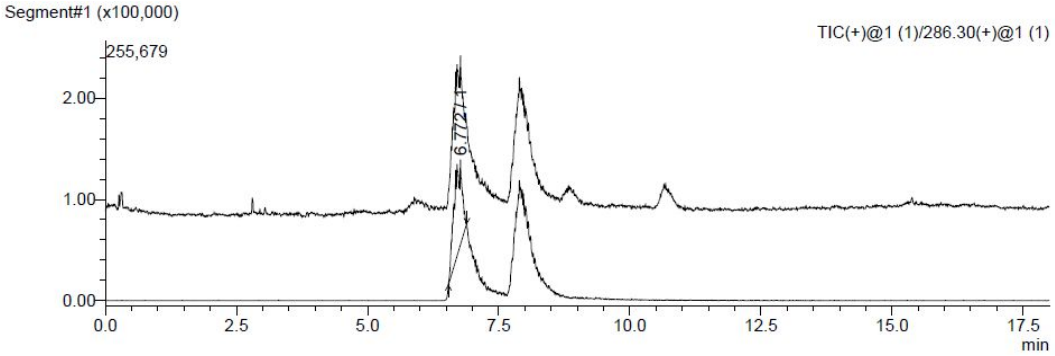

Line#:1 R.Time:6.773(Scan#:2033)
MassPeaks:487
Spectrum Mode:Averaged 6.770-6.777(2032-2034) Base Peak:286.30(78792)
BG Mode:Calc Segment 1 - Event 1

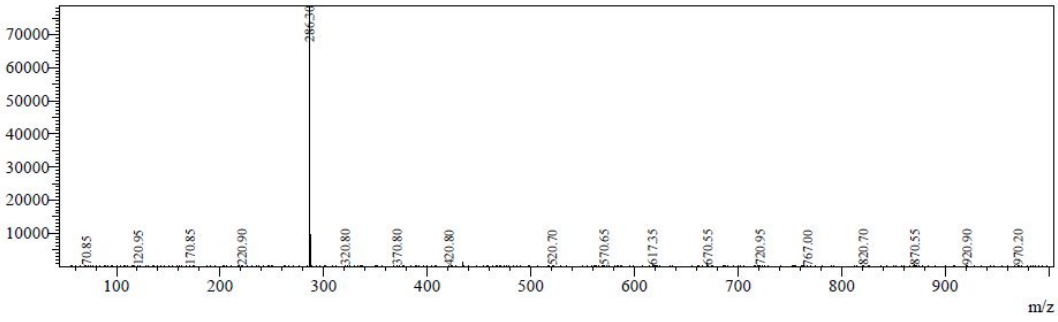

2.2.2.2 F4-iper-azo-iper (F4-IAI, 15b)

PSS trans

<Chromatogram>

mV

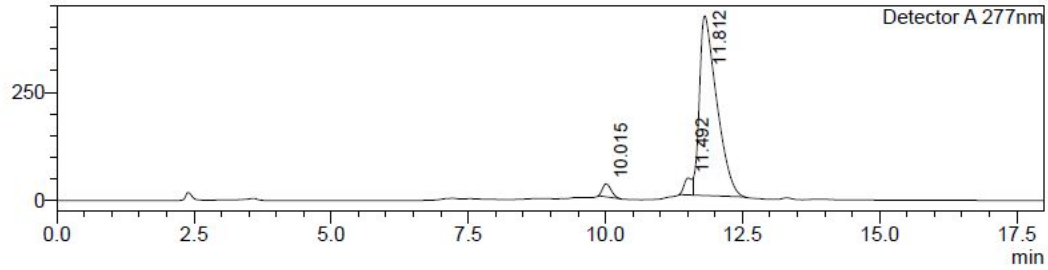

Detector A 277nm

Peak#	Ret. Time	Area	Height	Area%
1	10.015	328834	29981	3.339
2	11.492	399716	37709	4.059
3	11.812	9119981	414604	92.602
Total		9848531	482294	100.000

Segment#1 (x1,000,000)

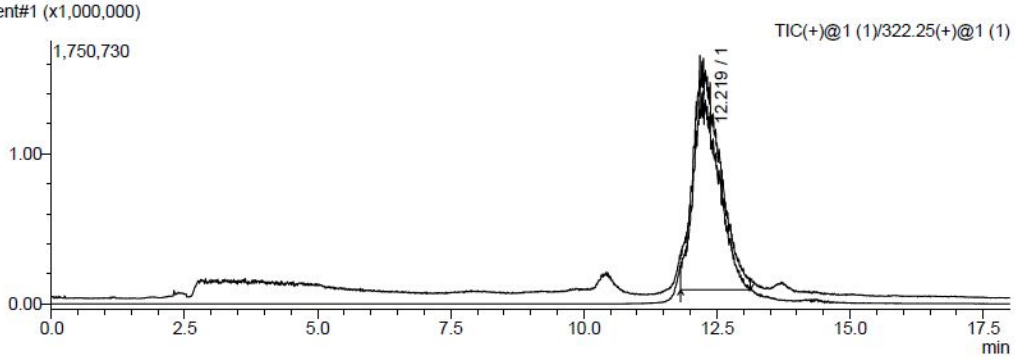

Line#:1 R.Time:12.218(Scan#:7332)
MassPeaks:4
Spectrum Mode:Averaged 12.217-12.220(7331-7333) Base Peak:322.25(1298402)
BG Mode:Calc Segment 1 - Event 1

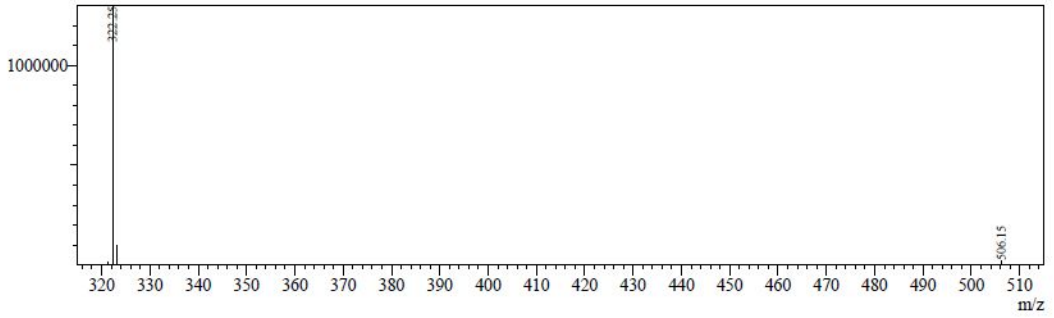

PSS cis

<Chromatogram>

mV

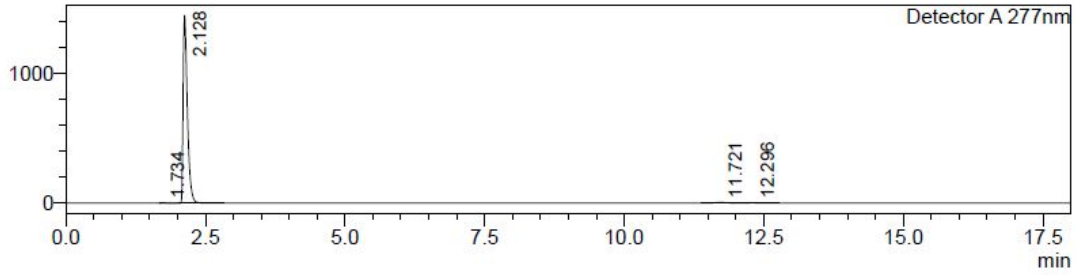

Detector A 277nm

Peak#	Ret. Time	Area	Height	Area%
1	1.734	22033	3342	0.283
2	2.128	7656096	1434599	98.428
3	11.721	70717	4503	0.909
4	12.296	29553	1545	0.380
Total		7778399	1443989	100.000

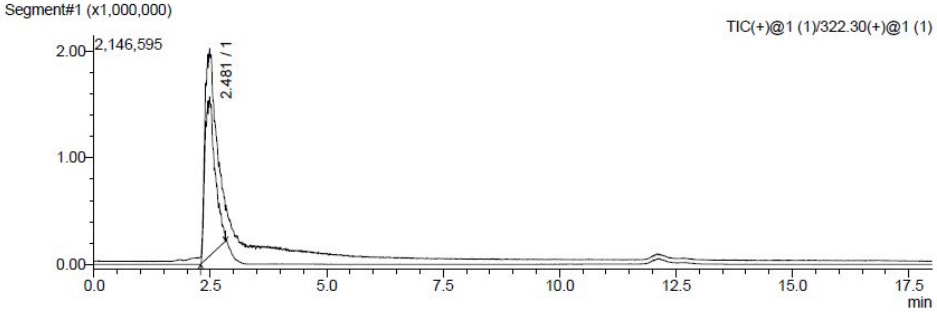

Line#:1 R.Time:2.480(Scan#:1489)
MassPeaks:7
Spectrum Mode:Averaged 2.478-2.482(1488-1490) Base Peak:322.25(1458490)
BG Mode:Calc Segment 1 - Event 1

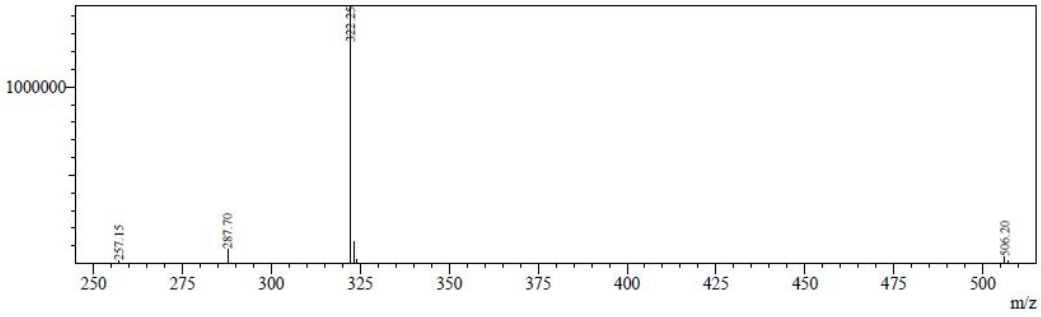

3 Molecular Modeling

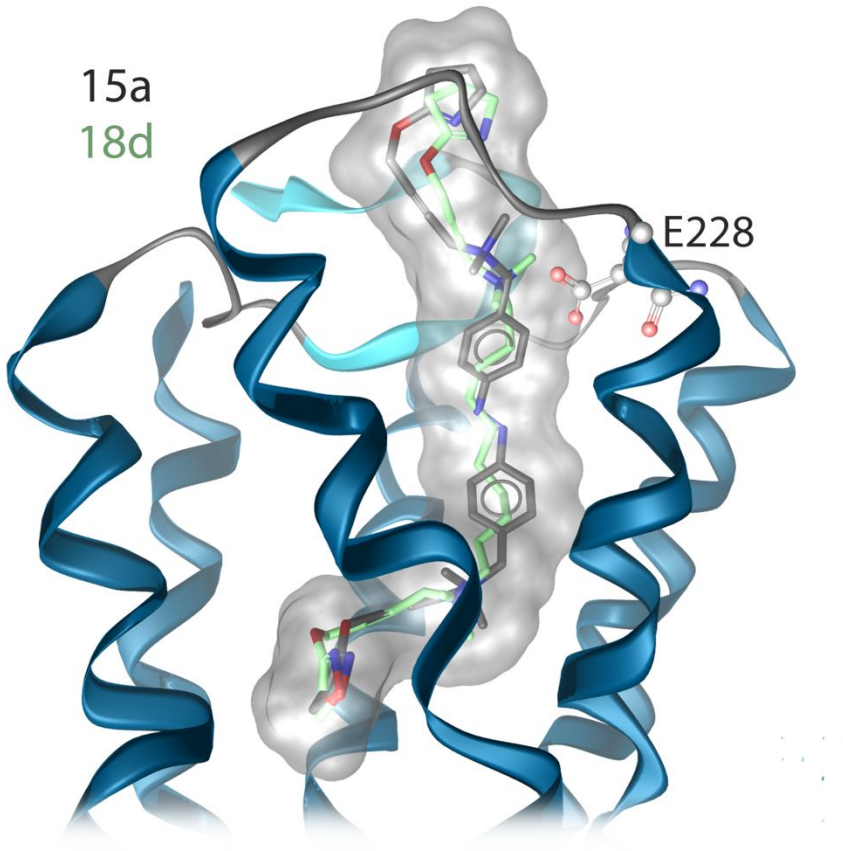

Supp. Figure 1. Comparison of the flexible **18d** and photoswitchable **15a** homobivalent iperoxo dimer bound to the M_1 receptor.

Appendix IV:

Manuscript:

Schramm, S.; **Agnetta, L.**; Bermudez M.; Gerwe, H.; Irmen, M.; Holze, J.; Littmann, T.; Wolber, G; Tränkle, C.; Decker, M. Novel BQCA and TBPB derived M1 Receptor Hybrid-Ligands: Orthosteric Carbachol Differentially Regulates Partial Agonism. *ChemMedChem* **2019**, submitted.

COMMUNICATION

Novel BQCA and TBPB derived M_1 Receptor Hybrid-Ligands: Orthosteric Carbachol Differentially Regulates Partial Agonism

Simon Schramm,[a] Luca Agnetta[a], Marcel Bermudez[b], Hubert Gerwe[a], Matthias Irmen[c], Janine Holze[c], Timo Littmann[d], Gerhard Wolber[b], Christian Tränkle[d] and Michael Decker[a]

[a] Pharmazeutische und Medizinische Chemie
Institut für Pharmazie und Lebensmittelchemie, Julius-Maximilians-Universität Würzburg
Am Hubland, D-97074 Würzburg, Germany
E-mail: michael.decker@uni-wuerzburg.de
[b] Institute of Pharmacy, Freie Universität Berlin, Königin-Luise-Straße 2 + 4, 14195 Berlin, Germany.
[c] Pharmacology and Toxicology, Institute of Pharmacy, University of Bonn, Gerhard-Domagk-Straße 3, 53121 Bonn, Germany.
[d] Institute of Pharmacy, University of Regensburg, 93053 Regensburg, Germany.

To this work have equally contributed S. Schramm (synthesis) and L. Agnetta (pharmacology).

Supporting information for this article is given via a link at the end of the document.

Abstract: Recently, investigations of the complex mechanisms of allostery have led to a deeper understanding of G protein-coupled receptor (GPCR) activation and signaling processes. In this context, muscarinic acetylcholine receptors (mAChRs) are highly relevant according to their exemplary role for the study of allosteric modulation. In this work, we compare and discuss two sets of putatively dualsteric ligands, which were designed to connect carbachol to different types of allosteric ligands. We chose derivatives of TBPB [1-(1'-(2-tolyl)-1,4'-bipiperidin-4-yl)-1H-benzo[*d*]imidazol-2(3*H*)-one] as M_1-selective putatively bitopic, i.e. orthosteric/allosteric agonist, i.e. TBPBds, and a benzyl quinolone carboxylic acid derivative (BQCAd) as an M_1- positive allosteric modulator, varying the distance between the allosteric and orthosteric building blocks. Luciferase protein complementation assays demonstrated that linker length must be carefully chosen to yield agonist or antagonist behavior, respectively. These findings may help to design biased signaling and/or different extents of efficacy.

Muscarinic acetylcholine receptors (mAChRs or M receptors) are involved in the regulation of a variety of physiological functions depending on their localization in both the central and peripheral nervous system.[1] Among them are actions of the central nervous system like cognitive, sensory, motor, behavioral and autonomic processes.[2] In the pathophysiology of schizophrenia, depression, Parkinson's disease and Alzheimer's disease (AD), changes in mAChR activities and levels have been described.[3] In AD, postsynaptic AChRs remain mostly intact during presynaptic cholinergic hypofunction. Hence, depletion of the endogenous neurotransmitter acetylcholine (ACh) may be circumvented by targeting the mAChRs directly.[4]

The M_1 receptor is expressed in brain regions responsible for functions like cognition, learning and memory, which are impaired in AD.[5]It was shown that activation of this subtype has a positive influence on the aggregation of Aβ and neurofibrillary tangles, the key pathophysiological hallmarks of AD.[6-9] By stimulation of the receptor, PKC is activated, and the non-amyloidogenic pathway is favored. An increase in α secretase production suppresses the formation of toxic Aβ plaques. The activation of PKC also regulates the GSK-3β cascade, which leads to stabilization of microtubules and therefore mitigating τ-pathology. Moreover, activation of the M_1 receptor leads to positive influences on decreased cerebral blood flow, caspase activation, DNA damage, oxidative stress and mitochondrial impairment in cells.[10-11] The positive effects that the activation of M_1 can produce were also shown in transgenic mice.[12]

Complex downstream signaling and their interactions complicate elucidation of the physiological roles of individual mAChR subtypes. Furthermore, a lack of subtype selective ligands hampers pharmacological examinations. Subtype-selective targeting is essential for investigations of receptor pharmacology and AD pathology alike.

This is, however, rather difficult, as the orthosteric, i.e. neurotransmitter binding sites of the five M-receptor subtypes show a high degree of homology. This results in major challenges when developing ligands selective for a specific receptor subtype. In contrast, allosteric binding sites at the extracellular vestibule of the receptor are less conserved throughout all five subtypes and show greater topological differences while being conformationally linked to the orthosteric site. Allosteric sites are thus easier to address than the orthosteric binding pockets with regard to selectivity and have been used for the development of selective ligands.[13] Allosteric ligands are divided into allosteric agonists, able to cause a signal by themselves, and allosteric modulators, changing the affinity and/or function and/or signaling preference[14] of an orthosteric ligand.[15-18] Allosteric modulators are, however, dependent on an orthosteric ligand, e.g. an agonist, to transduce signals.

The combination of orthosteric and allosteric moieties connected by a linker moiety has been established as a dualsteric/bitopic ligand approach. Dualsteric/bitopic ligands are designed to selectively target a receptor subtype, by concomitantly addressing both the orthosteric and the allosteric binding site.[19] This approach has the advantage that it is not reliant on the endogenous neurotransmitter and that biased signaling by activation of a specific downstream signal is possible via a single molecule.[16-18]

The design of "dualsteric" ligands can be challenging as they need to meet clear prerequisites to bind simultaneously to the orthosteric and allosteric binding site. For this purpose, the connection points have to be chosen carefully in order to avoid alteration of essential functional groups responsible for receptor binding and function. In addition, the linker length has to be taken into consideration. There is evidence that only an optimal spacer length is able to allow an active hybrid binding, while shorter or longer spacers result in inactive allosteric binding of dualsterically conceptualized hybrid ligands.[20] In earlier studies, a variety of dualsteric M_1 ligands have been developed, including a photoswitchable BQCA-iperoxo hybrid.[21-24]

Since the orthosteric and the allosteric binding pocket of the M_1 receptor are separated by the so-called tyrosine lid formed by three tyrosine residues (Figure 1), dualsteric ligands have to bridge these two sites by a linker. We have chosen three different linker lengths for this study. First, a C_3-alkyl chain linker, because it represents the shortest possible linker length to bypass the tyrosine lid. Second an C_8-alkyl chain, which represents the longest plausible linker length according to our model and previously reported dualsteric ligands for muscarinic receptors.[20, 25-26] Between these two extremes, the C_5-alkyl chain represents the optimal linker length for the M_1 receptor.

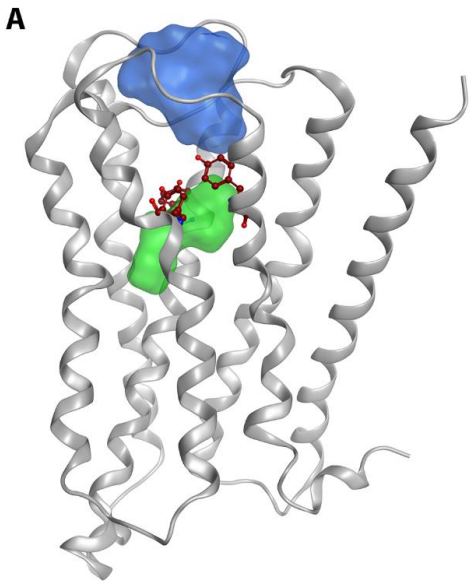

Figure 1. Active M_1 receptor model with the orthosteric and the allosteric binding site shown as green and blue surface, respectively. These two binding sites are separated by tyrosine residues which are forming a lid-like structure (red).

We now have developed two sets of putatively dualsteric ligands as tools for the investigation of M_1 receptor pharmacology. For both sets, carbachol (CCh), a derivative of the endogenous neurotransmitter ACh, was chosen as orthosteric agonist. In contrast to ACh, CCh does not show off-target effects like inhibition of acetylcholinesterase (AChE) and has a reduced rate of hydrolysis.[27]

The allosteric moieties chosen are a truncated 1-(1'-(2-tolyl)-1,4'-bipiperidin-4-yl)-1*H*-benzo[*d*]imidazol-2(3*H*)-one (TBPB), and derivatives of benzyl quinolone carboxylic acid (BQCA). TBPB is an agonist at the M_1 receptor developed at Vanderbilt University, the binding and action of which may occur in a bitopic fashion.[28-30] Remarkably, TBPB showed a shift towards the non-amyloidogenic pathway and reduced aggregation of Aβ *in vitro*.[28] In previous work, TBPB had been connected to AF292, a selective M_1 agonist.[31-32] These putatively dualsteric compounds, however, did not show the agonism intended since AF292 acted as a weak partial agonist only. Therefore, in the current work AF292 was replaced by carbachol. **Figure 1** shows the design of target structures **1** combining a truncated TBPB with carbachol to form hybrid ligands. The benzylated second piperidine moiety had been shown to be dispensable for allosteric agonism.[20, 33]

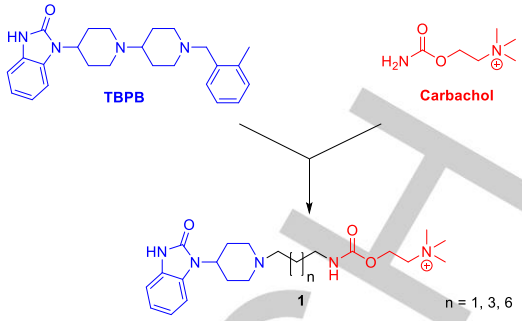

Figure 1. Design of target structures **1** combining the agonist TBPB and the orthosteric carbachol by alkylene linkers of variable lengths.

BQCA (cf. Fig. 2) is described as a positive allosteric modulator and allosteric agonist.[34-35] This compound was shown to be able to reduce the necessary amount of ACh to activate the receptor 129-fold and showed no enhancing activity at other mAChR subtypes.[35-36] We could delineate recently, that the connection of a spacer to a BQCAd canceled the allosteric agonistic action.[20] Structure-activity relationships of BQCA derivatives were conducted thoroughly.[33, 37] We decided to use a derivative as the second allosteric moiety in the current study carrying a fluorine at position 8 of the A-ring and substitute the benzyl ring (B-ring) by naphthalene for an increased M_1 affinity of the resulting ligands,[38] similar to our previously published compounds.[20] **Figure 2** shows the target structures **2** combining carbachol with the BQCA-derived moiety.

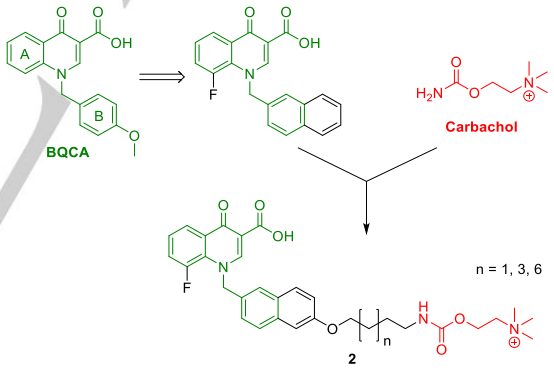

Figure 2. Design of target structures **2** combining derivatives of the allosteric modulator BQCA (BQCAds) and carbachol by alkylene linkers of variable lengths

Synthesis

The dualsteric ligands were accessed by connecting the Boc-protected linkers to the allosteric moieties before introducing the carbachol precursor.

TBPB building block **3** was synthesized following literature protocols (**Scheme 1**).[39-41] Nitroaniline **5** was synthesized by reaction of commercially available 1-fluoro-2-nitrobenzene with a carboxyl protected 4-aminopiperidine. The nitro group was reduced by hydrogenation over palladium on activated charcoal. The diamine **6** was reacted with CDI to form the benzimidazolone **7**. Hydrolysis of the ester protection group led to TBPB-building block **3**.

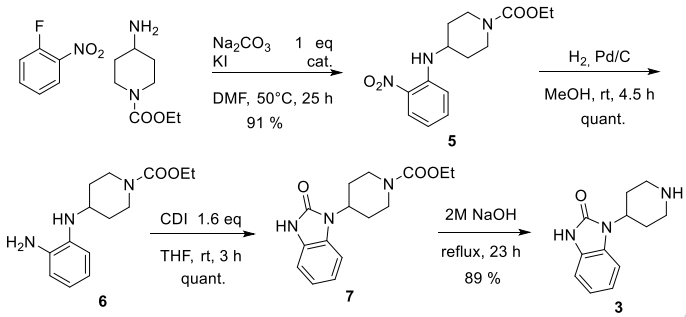

Scheme 1. Synthesis of TBPB-building block **3**.

The C_8-linker **4c** was synthesized from 1,8-octandiol. 1,8-octandiol was mono-tosylated to give compound **8**, which was then substituted with sodium azide in dimethylformamide. Reduction with lithium aluminum hydride yielded 8-aminooctanol **9**. 3-Aminopropanol, 5-aminopentanol and 8-aminooctanol **9** were Boc-protected to give compounds **10a-c**. An Appel reaction to introduce iodine as a leaving group yielded linkers **4a-c** (**Scheme 2**).

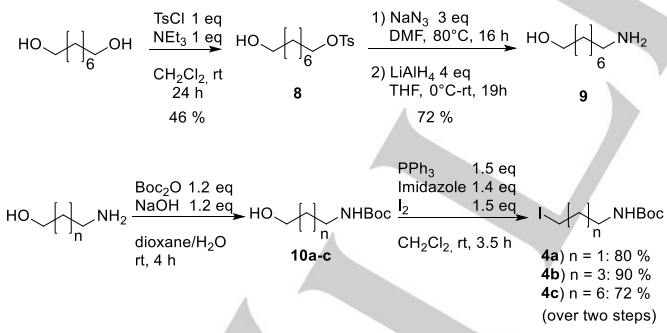

Scheme 2. Synthesis of linkers **4a-c**.

Building blocks **3** and **4a-c** were connected in a substitution reaction to give compounds **11a-c**. Removal of the Boc-protection group was achieved under acidic conditions. 4M HCl in dioxane as solvent gave the free amines **12a-c**. Reaction with 2-chloroethyl chloroformate under basic conditions yielded the carbamates **13a-c**. Compounds **13a** and **13b** were synthesized in dimethylformamide with potassium carbonate as base, but only in low yields. The procedure was changed for compound **13c**, using pyridine as a base in dry dichloromethane. This reaction was finished within 30 min and showed a highly improved yield (**Scheme 3**).

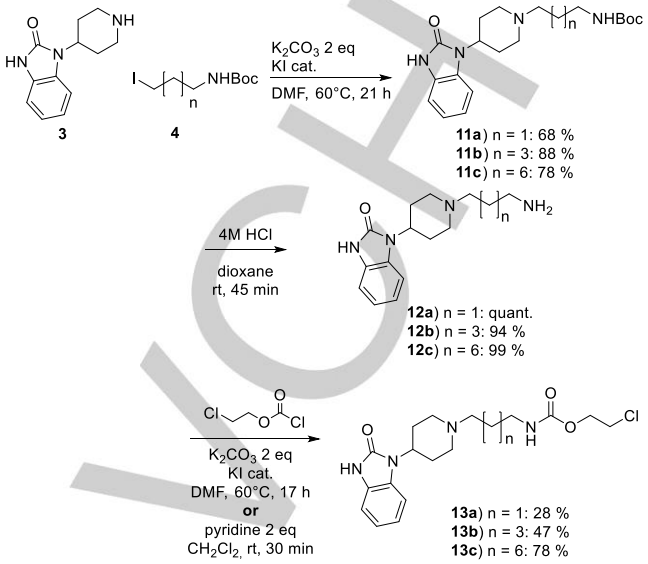

Scheme 3. Synthesis of carbamates **13a-c**.

The final reaction step was the substitution reaction of chloro-compounds **13** with trimethylamine for the formation of the carbachol moiety and target compounds **1a-c** (**Scheme 4**). Due to the large number of byproducts and difficult purification, compounds **1a-c** were obtained in yields of 13% to 20% only (**Scheme 4**).

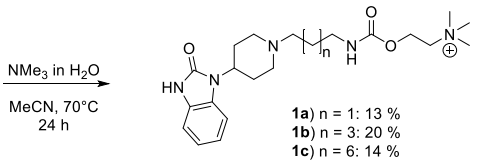

Scheme 4. Last step of the synthesis of dualsteric compounds **1a-c**.

For the BQCA-carbachol hybrids **2**, building block **14** was synthesized by a one-pot Gould-Jacobs synthesis.[37-38] 6-Hydroxy-2-naphthoic acid was esterified with methanol and subsequently reduced to 6-(hydroxymethyl)naphthalen-2-ol **15** (**Scheme 5**).

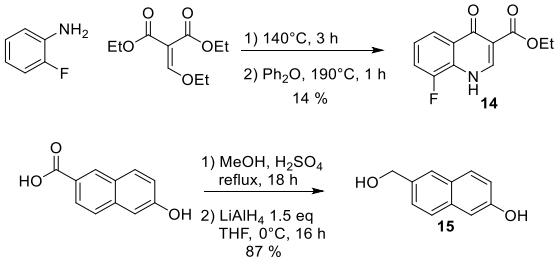

Scheme 5. Synthesis of building blocks **14** and **15**.

Next, the linkers **4a-c** were connected to the naphthyl alcohol **15** in a substitution reaction to yield alcohols **16a-c**. An Appel reaction to introduce iodine as a leaving group gave compounds **17a-c** (**Scheme 6**). The iodine compounds **17a-c**, however, proved to be quite unstable and had to be used for the next reaction step immediately after preparation.

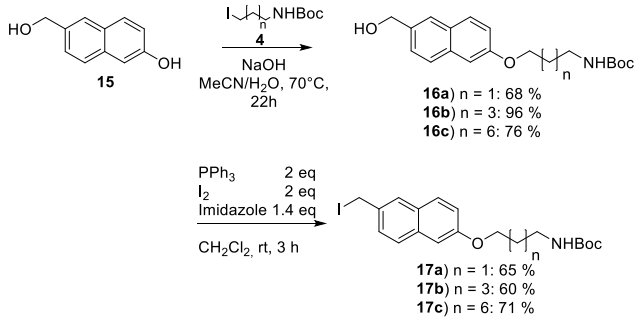

Scheme 6. Synthesis of naphthyl linkers **17**.

Iodine compounds **17a-c** were connected to the quinolone core **14** in dimethylformamide under basic conditions (**Scheme 7**). Boc deprotection of **18** gave the free amines **19a-c**. Carbamate formation was achieved as described above yielding precursors **20a-c**. The last steps were the substitution with trimethylamine and subsequent saponification of the ester using lithium hydroxide. Reaction progression of this step has to be monitored by LCMS. Both the esters and the target compounds **2** showed the same retention on TLC as well as on HPLC. Disappearance of the ester's *m/z* ratio indicated full conversion. The target dualsteric compounds **2** were obtained in yields of 14% to 19% (**Scheme 7**).

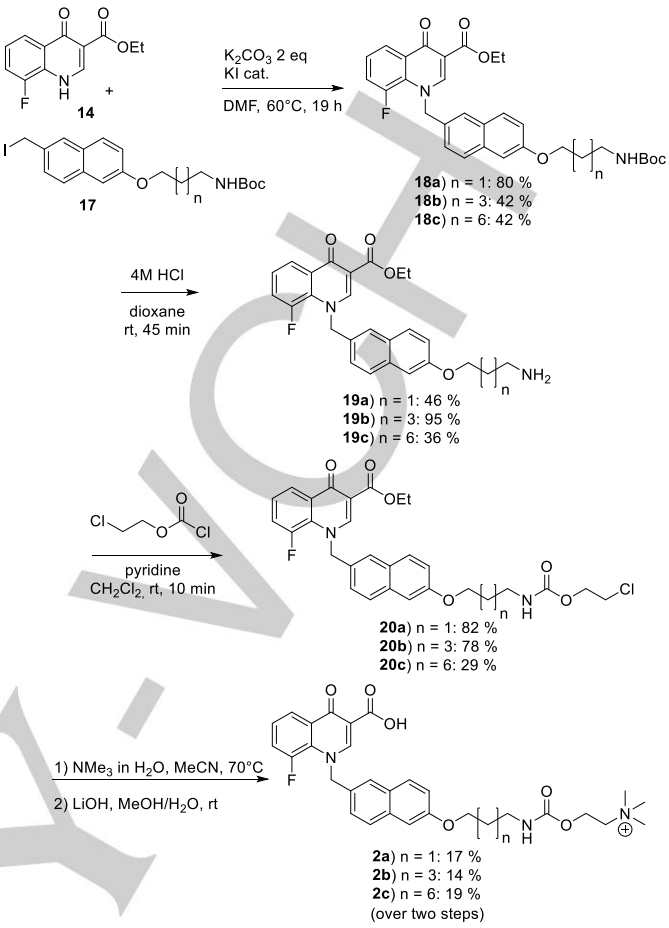

Scheme 7. Synthesis of dualsteric compounds **2a-c**.

For comparison and to investigate binding modes of the designed compounds, reference compounds are required. Thus, the individual allosteric moieties connected to the alkyl linkers were synthesized. Some of these compounds (**21c**, **25c**, **25d**) were previously published.[20] The TBPB reference compounds **21a-c** were synthesized by reaction of the piperidine moiety **3** with the respective halogenated alkane (**Scheme 8**).

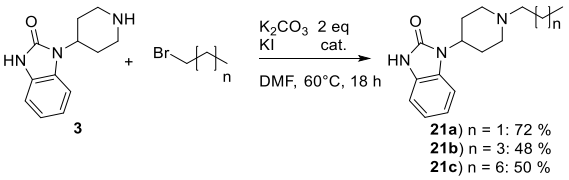

Scheme 8. Synthesis of TBPB reference compounds **21a-c**.

BQCA reference compounds were synthesized analogously to the quinolone compounds described above. Alcohol **15** was reacted with the respective halogenated alkane to give ethers **22a-d**. In an Appel reaction, the alcohols **22a-d** were converted into the respective bromines **23a-d**. The bromo-compounds **23a-d** proved more stable than the respective iodo-compounds **17** (*cf.* above). The bromine was then substituted by quinolone **14** yielding esters **24a-d**. By hydrolysis, BQCA reference compounds **25a-d** were obtained (**Scheme 9**).

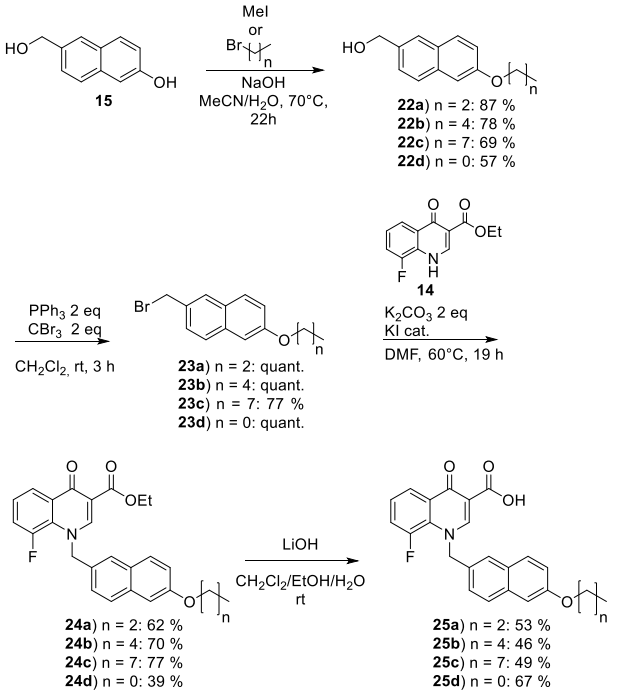

Scheme 9. Synthesis of BQCA reference compounds **25a-d**.

Biological evaluation

The putative dualsteric compounds **1a-c** and **2a-c**, the corresponding reference compounds **21a-c** and **25a-d** as well as the CCh-alkyl reference compounds **28a-c** were evaluated in a novel luciferase protein complementation assay (**Table 1**).[42] The assay was conducted to evaluate receptor response through the $G_{\alpha q}$ protein specific phospholipase C pathway. For each compound, a nine-point concentration-response-curve was recorded and expressed in percent of the maximal cellular response of CCh.

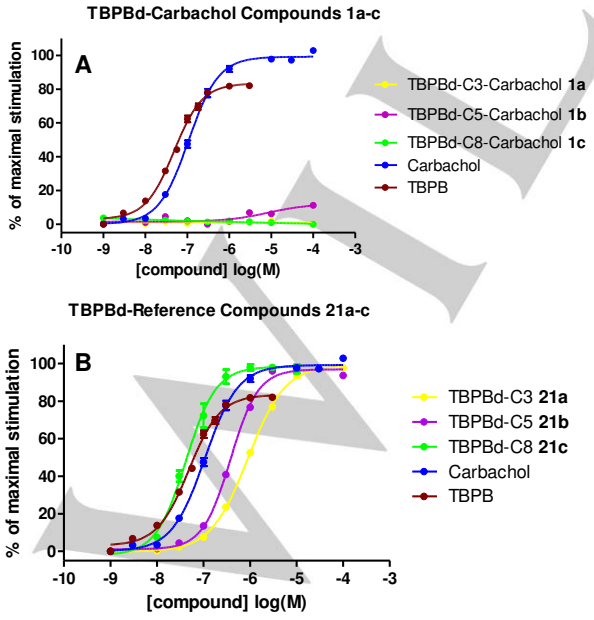

Figure 3. Concentration-response-curves of (A) dualsteric compounds **1a-c** and (B) reference compounds **21a-c** measured in the luciferase complementation *in vitro* assay. Data points represent means ± SEM from three independent experiments, conducted in triplicate.

Figure 3 shows the dose-response curves of the putative dualsteric TBPBd-carbachol compounds **1a-c** and the alkyl reference compounds **21a-c** expressed as a percentage of the maximal cellular response to CCh. No receptor response was caused by the carbachol containing compounds **1a** and **1c.** In contrast, compound **1b** showed weak partial agonism, i.e. its $\%E_{max}$ = 12 ± 2 (cf. **Table 1**) being significantly different from zero (one sample t-test, P>0.05) while the reference compounds **21a, b, c** show full agonism and, depending on their chain lengths, different potencies, with the C8 compound **21c** significantly showing the highest potency of all (One-Way ANOVA with Newman-Keuls post test, P<0.05). Note that the spacers C3, C5 and C8 in compounds **21a**,**b** and **c** enhanced the efficacy of the TBPB (Fig. 3B) and the orthosteric carbachol moiety nearly abolished it in compounds **1a**,**b** and **c** (Fig. 3A).

Table 1. Measures of potency and efficacy induced by muscarinic agonist and hybrids in live HEK 293t cells.[a]

Cmpd.	Cn	pEC_{50}	$\%E_{max}$	Slope
CCh		6.97 ± 0.03	99 ± 1	1.22 ± 0.09
TBPB		7.32 ± 0.02	83 ± 1	1.29 ± 0.07
BQCA		7.20 ± 0.03	90 ± 1	1.60 ± 0.13
1a		n. d.	n. d.	n. d.
1b	3	5.09 ± 0.24	12 ± 2	0.87 ± 0.31
1c	8	n. d.	n. d.	n. d.
2a	3	5.89 ± 0.01	66 ± 0.5	2.02 ± 0.08
2b	5	6.67 ± 0.02	78 ± 1	1.36 ± 0.07
2c	8	6.62 ± 0.03	28 ± 0.5	1.77 ± 0.19
21a	3	6.05 ± 0.01	99 ± 1	1.08 ± 0.03
21b	5	6.42 ± 0.01	97 ± 1	1.46 ± 0.05
21c	8	7.38 ± 0.04	98 ± 2	1.34 ± 0.15
25a	3	5.82 ± 0.02	35 ± 1	2.69 ± 0.23
25b	5	n. d.	n. d.	n. d.
25c	8	n. d.	n. d.	n. d.
25d	1	6.01 ± 0.02	58 ± 1	1.30 ± 0.08
28a	3	4.65 ± 0.18	44 ± 6	0.95 ± 0.21
28b	5	5.27 ± 0.07	28 ± 1	1.24 ± 0.21
28c	8	6.09 ± 0.08	9.4 ± 0.4	1.41 ± 0.37

[a]pEC_{50}, −log EC_{50} value: (-log)concentration of the indicated compounds inducing a half-maximal effect); $\%E_{max}$, maximum effect as a percentage of E_{CCh} (100 µM); Slope factor obtained by curve fitting to data from individual experiments shown in Figures 3-5 using a four-parameter logistic equation. nm: not measurable Data represent means ± SEM from three independent experiments, conducted in triplicate.

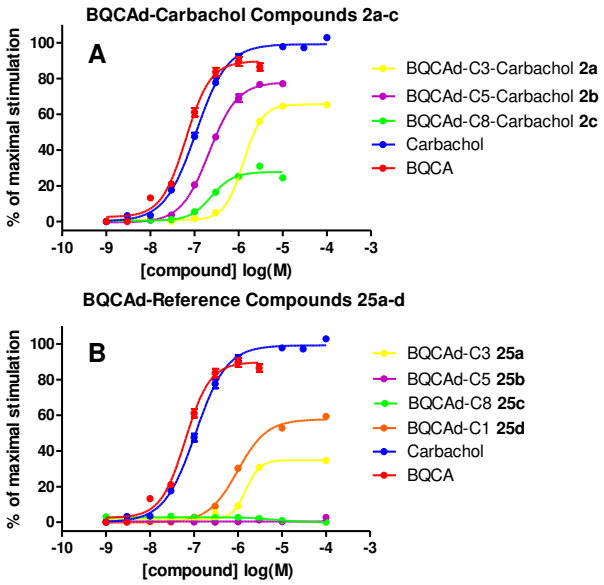

Figure 4. Dose-response curves of (A) dualsteric compounds **2a-c** and (B) reference compounds **25a-d** measured in the Luciferase complementation *in vitro* assay. Data represent means ± SEM from three independent experiments, conducted in triplicate.

Figure 4 shows the dose-response curves of the putative dualsteric BQCAd-carbachol compounds **2a-c** and the corresponding reference compounds **25a-d** in comparison to CCh as the positive control, with its maximum response set to 100%. The reference compounds **25b** and **25c** showed no receptor response as had been expected from a previous study applying deviating assay systems.[20] Interestingly, compounds **25a** and **25d**, however, showed partial agonism suggesting that the minimum spacer length to abolish agonism in the reference compounds is C5 (**25b**) and that C1 (**25d**) and C3 (**25a**) do not suffice. In contrast, all putatively dualsteric compounds **2a-c** showed partial agonism. The C5-linked compound **2b** exhibited the highest efficacy. This finding suggests a putatively dualsteric/bitop ligand binding behavior of **2b** as suggested in Fig. 8 in that its carbachol moiety triggers M_1 receptor activation orthosterically, the efficacy of which decreasing with an increase in spacer-length to C8 as demonstrated by **28c** in Fig. 7. Note that the C5 spacer in compound **2b** abolished efficacy of the allosteric agonist BQCA in compound **25b** (Fig. 4B) and the orthosteric carbachol moiety in **2b** nearly restored it to the level of efficacy of BQCA alone (Fig. 4A). Inactive compounds **1a, 1c, 25b** and **25c** plus the fairly active **1b** were additionally studied which revealed an antagonistic action of **1c** to M_1-receptor activation via the orthosteric carbachol (**Figure 5**). To shed light on the antagonistic properties, the luciferase complementation assay was performed in an antagonist mode, co-incubating the respective test compound with carbachol. BQCAd-reference compounds **25b** and **25c** did not show antagonistic behavior. In contrast, the dualsteric TBPBd compound **1c** revealed clear cut antagonist properties, which were not observed with the shorter ligands **1a** and **b**, indicating that the C8 chain in **1c** is an optimal linker length for compound binding to the receptor without triggering a functional activity. Detailed global data analysis of the functional antagonism between carbachol and **1c** at M_1 receptors was in line with a formally competitive interaction (cf. Fig. 6). Future studies focusing on the binding topography of **1c** will help to elucidate the molecular nature of its antagonistic behavior towards carbachol. Interestingly, the importance for the receptor interaction of the C8 spacer is also confirmed by the corresponding reference compound **21c** which showed the highest potency (**Figure 3**).

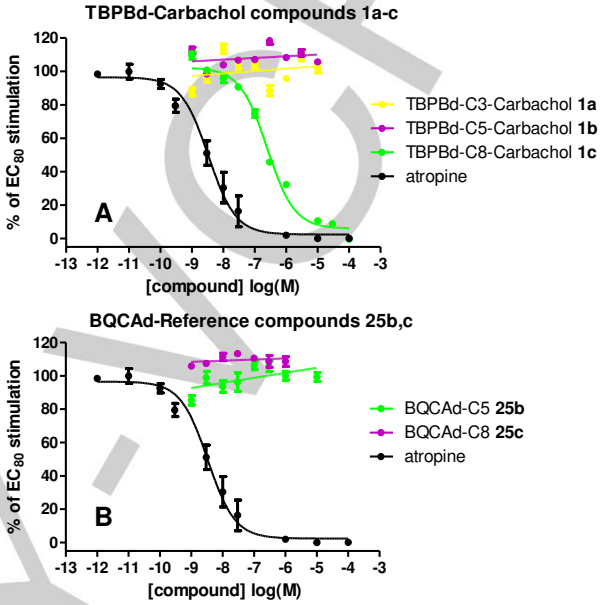

Figure 5. Dose-response curves of (A) putatively dualsteric TBPBd compounds **1a-c** and (B) BQCAd-reference compounds **25b** or **25c** measured in the Luciferase complementation *in vitro* assay in the antagonist mode by co-incubations of EC_{80}-concentration of CCh. Data represent means ± SEM from three independent experiments, conducted in triplicate

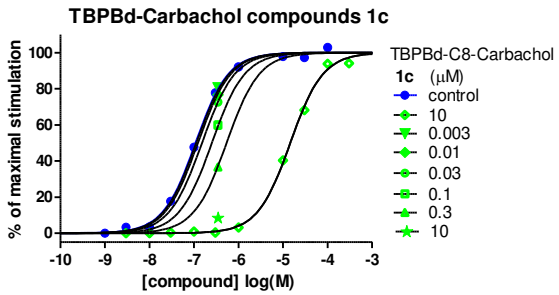

Figure 6 M_1 receptor stimulation by carbachol measured in the Luciferase complementation *in vitro* assay conducted with several concentrations of the dualsteric compound **1c**. Ordinate: response of live HEK296 cells overexpressing the M_1 receptor displayed as a percentage of maximally induced stimulation by CCh. Abscissa: log concentration of CCh. To quantifiy the antagonistic action of **1c**, a control curve with variable concentrations of CCh only (taken from Fig. 3A), a second curve with increasing concentrations of **1c** at one fixed concentration of CCh (taken from Fig. 5A), that induced 80-90% of the maximal receptor response and thirdly, a second full CCh curve shifted by a fixed concentration of **1c** were compiled and fitted by global nonlinear

regression to a model assuming competition of **1c** with CCh at a single site.[43] Data represent means ± SEM from three independent experiments, conducted in triplicate.

Cmpd.	Cn	log K_B
1a	3	n. d.
1b	5	n. d
1c	8	7.12 ± 0.02
25b	5	n. d
25c	8	n. d
Atr	-	9.32 ± 0.12

Table 2. Equilibrium log affinity constants K_B of compound **1c** and atropine (**Atr**) for binding to the M_1-receptor according to the competitive model. Log K_B values were determined with s constrained to unity, if s was not statistically different from s = 1 (F test, P > 0.05), suggesting that **1c** and atropine acted formally competitively with CCh.

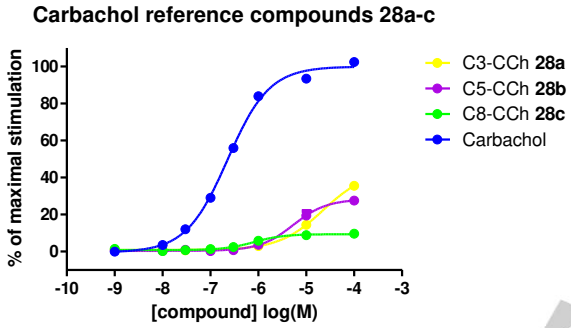

Fig. 7. Dose-response curves of reference compounds **28a-c** and carbachol measured in the Luciferase complementation in vitro assay. Data represent means ± SEM from three independent experiments, conducted in triplicate.

Figure 7 shows the dose-response curves of the CCh-alkyl reference compounds **28a-c** expressed as a percentage of the maximal cellular response to CCh. Compounds **28a-c** showed partial agonism and a decreasing receptor response with increasing chain length of the alkyl rest. Similarly, the potencies of **28a-c** were smaller than that of carbachol (cf. **Table 1**). In contrast to this trend, within this group of carbachol derivatives the potencies increased with chain length, with the C8 compound showing the highest potency (One-Way ANOVA with Newman-Keuls post test, P<0.05). These findings suggest that the CCh-alkyl moieties **28a-c** contribute in part to the agonistic effects of hybrids **1** and **2**, respectively, but do not make up the respective full effects of hybrid efficacy and potency (cf. **Fig. 3** and **4** and **Table 1** for details). This points to the necessity of the allosteric hybrid moieties for a full effect, to a dualsteric/bitopic receptor interaction of the hybrids **1** and **2** and shows that it is productive to develop ligands that bridge between the M_1 orthosteric and allosteric binding sites.

Molecular Modeling

The dualsteric binding mode of **2b** (BQCAd-C5-Carbachol) was analyzed with regard to receptor-ligand interactions by using three-dimensional pharmacophores (**Figure 8**).[44] The shown binding pose was derived by docking to an active receptor model according to a previously published protocol.[25-26] The ammonium group of the carbachol moiety forms a charge interaction with $D105^{3.32}$ and a cation-π interaction with $Y381^{6.51}$, which represents the key interactions for orthosteric ligands. The carbonyl group of the carbamate serves as hydrogen bond acceptor for the hydroxyl group of $Y408^{7.43}$. This represents a remarkable difference compared to the binding mode of carbachol, in which the carbamate structure shows a different orientation (Supporting information). However, orthosteric key interactions (charge interaction with $D105^{3.32}$ and a cation-π interaction with $Y381^{6.51}$) are present in both binding modes and mainly driving agonist activity. The BQCAd moiety is located in the allosteric vestibule at the extracellular loop region and forms lipophilic contacts with $L174^{EL2}$ and $Y179^{EL2}$. Furthermore, the carboxylic acid forms a charge interaction with $K392^{EL3}$.

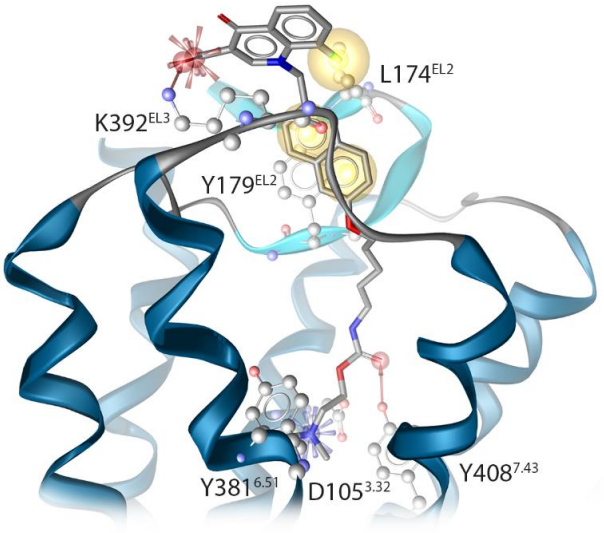

Figure 8. Proposed dualsteric binding mode of **2b** (BQCAd-C5-Carbachol) at the active M_1 receptor model with the carbachol moiety binding at the orthosteric site and the BQCAd building block at the allosteric site. Hydrogen bond acceptors are shown as red arrows, yellow spheres indicate lipophilic contacts, and positive and negative ionizable centers were shown as blue and red stars, respectively.

Conclusion

We have designed and synthesized two sets of novel putative dualsteric hybrid compounds containing the M_1 orthosteric ligand carbachol and either derivatives of BQCA, an allosteric modulator and agonist, or TBPB, a bitopic orthosteric/allosteric agonist. In a first evaluation of their receptor efficacy, agonist activity can be seen for the BQCAd-carbachol-hybrids **2** only, the extent of which is strongly dependent on the spacer length between the moieties. Different to findings published earlier with other non-agonistically active BQCAd building blocks,[20] in the current study spacer lengths smaller than C5 resulted in partially active BQCAd moieties thus contributing to the orthosteric agonistic effect of the carbachol moiety. Nevertheless, the BQCAd moiety **25b** (which includes a C5 spacer) of the BQCAd-carbachol-hybrid **2b**

possessing the highest efficacy (and potency) did not contribute to M_1-receptor activation. This demonstrates that the carbachol moiety pertained part of its agonistic action in this hybrid. Inversely, the orthosteric carbachol massively quenched M_1-receptor activation in the bitopic TBPBd-carbachol-hybrid **1b** to a marginal partial agonism at a high concentration compared to its TBPBd-C5 moiety which behaved as a full agonist. In summary, in the current study, we demonstrate that partial agonism in dualsteric/bitopic compounds can be designed not only by quenching orthosteric receptor activation by an allosteric moiety as in **2b** but also by quenching putative bitopic/dualsteric activation of the receptor protein by an orthosteric moiety such as carbachol in **1b**. These findings practically widen the effect of orthosteric moieties in the concept of putative dualsteric/bitopic ligands. They allow different extents of partial agonism and furthermore enlarge the molecular toolbox of hybrid ligands to investigate mAChR receptor function. More advanced studies with regard to signaling bias and subtype selectivity are ongoing.

Experimental Section

Synthetic procedures and conducted assay procedures are found in the supporting information.

Acknowledgments

Generous support by the Elite Network of Bavaria (ENB) and International Doctoral Program “Receptor Dynamics” for L.A., H. G. and T.L. is gratefully aknowledged.

Keywords: Muscarinic Receptor • GPCR • Dualsteric Ligands • Partial Agonism • Allostery

References

[1] A. C. Kruse; B. K. Kobilka; D. Gautam; P. M. Sexton; A. Christopoulos; J. Wess, *Nat. Rev. Drug Discov.* **2014**, *13*, 549-560.
[2] R. M. Eglen; A. Choppin; N. Watson, *Trends Pharmacol. Sci.* **2001**, *22*, 409-414.
[3] A. Sanabria-Castro; I. Alvarado-Echeverria; C. Monge-Bonilla, *Ann. Neurosci.* **2017**, *24*, 46-54.
[4] R. T. Bartus, *Exp. Neurol.* **2000**, *163*, 495-529.
[5] R. M. Eglen, *Prog. Med. Chem.* **2005**, *43*, 105-136.
[6] A. Fisher, *Neurotherapeutics* **2008**, *5*, 433-442.
[7] A. Fisher, *Neurodegener. Dis.* **2008**, *5*, 237-240.
[8] A. Fisher, *Curr. Alzheimer Res.* **2007**, *4*, 577-580.
[9] A. Fisher, *J. Neurochem.* **2012**, *120*, 22-33.
[10] P. De Sarno; S. A. Shestopal; T. D. King; A. Zmijewska; L. Song; R. S. Jope, *J. Biol. Chem.* **2003**, *278*, 11086-11093.
[11] C. R. Overk; C. C. Felder; Y. Tu; D. A. Schober; K. R. Bales; J. Wuu; E. J. Mufson, *J. Chem. Neuroanat.* **2010**, *40*, 63-70.
[12] E. P. Lebois; J. P. Schroeder; T. J. Esparza; T. M. Bridges; C. W. Lindsley; P. J. Conn; D. L. Brody; J. S. Daniels; A. I. Levey, *ACS Chem. Neurosci.* **2017**, *8*, 1177-1187.
[13] A. Bock; R. Schrage; K. Mohr, *Neuropharmacology* **2018**, *136*, 427-437.
[14] A. E. Davey; K. Leach; C. Valant; A. D. Conigrave; P. M. Sexton; A. Christopoulos, *Endocrinology* **2012**, *153*, 1232-1241.
[15] A. Christopoulos; J. P. Changeux; W. A. Catterall; D. Fabbro; T. P. Burris; J. A. Cidlowski; R. W. Olsen; J. A. Peters; R. R. Neubig; J. P. Pin; P. M. Sexton; T. P. Kenakin; F. J. Ehlert; M. Spedding; C. J. Langmead, *Pharmacol. Rev.* **2014**, *66*, 918-947.
[16] K. Mohr; J. Schmitz; R. Schrage; C. Tränkle; U. Holzgrabe, *Angew. Chem. Int. Ed.* **2013**, *52*, 508-516.
[17] A. Bock; N. Merten; R. Schrage; C. Dallanoce; J. Batz; J. Klöckner; J. Schmitz; C. Matera; K. Simon; A. Kebig; L. Peters; A. Muller; J. Schrobang-Ley; C. Tränkle; C. Hoffmann; M. De Amici; U. Holzgrabe; E. Kostenis; K. Mohr, *Nat. Commun.* **2012**, *3*, 1044.
[18] B. J. Davie; A. Christopoulos; P. J. Scammells, *ACS Chem. Neurosci.* **2013**, *4*, 1026-1048.
[19] J. Antony; K. Kellershohn; M. Mohr-Andrä; A. Kebig; S. Prilla; M. Muth; E. Heller; T. Disingrini; C. Dallanoce; S. Bertoni; J. Schrobang; C. Tränkle; E. Kostenis; A. Christopoulos; H. D. Höltje; E. Barocelli; M. De Amici; U. Holzgrabe; K. Mohr, *FASEB J.* **2009**, *23*, 442-450.
[20] X. Chen; J. Klöckner; J. Holze; C. Zimmermann; W. K. Seemann; R. Schrage; A. Bock; K. Mohr; C. Tränkle; U. Holzgrabe; M. Decker, *J. Med. Chem.* **2015**, *58*, 560-576.
[21] L. Agnetta; M. Bermudez; F. Riefolo; C. Matera; E. Claro; R. Messerer; T. Littmann; G. Wolber; U. Holzgrabe; M. Decker, *J. Med. Chem.* **2019**, *62*, 3009-3020.
[22] L. Agnetta; M. Kauk; M. C. A. Canizal; R. Messerer; U. Holzgrabe; C. Hoffmann; M. Decker, *Angew. Chem. Int. Ed.* **2017**, *56*, 7282-7287.
[23] R. Messerer; C. Dallanoce; C. Matera; S. Wehle; L. Flammini; B. Chirinda; A. Bock; M. Irmen; C. Trankle; E. Barocelli; M. Decker; C. Sotriffer; M. De Amici; U. Holzgrabe, *Med. Chem. Commun.* **2017**, *8*, 1346-1359.
[24] R. Messerer; M. Kauk; D. Volpato; M. C. Alonso Canizal; J. Klockner; U. Zabel; S. Nuber; C. Hoffmann; U. Holzgrabe, *ACS Chem. Biol.* **2017**, *12*, 833-843.
[25] M. Bermudez; C. Rakers; G. Wolber, *Mol. Inform.* **2015**, *34*, 526-530.
[26] M. Bermudez; A. Bock; F. Krebs; U. Holzgrabe; K. Mohr; M. J. Lohse; G. Wolber, *ACS Chem. Biol.* **2017**, *12*, 1743-1748.
[27] K. M. Sanders; M. H. Zhu; F. Britton; S. D. Koh; S. M. Ward, *Exp. Physiol.* **2012**, *97*, 200-206.
[28] C. K. Jones; A. E. Brady; A. A. Davis; Z. Xiang; M. Bubser; M. N. Tantawy; A. S. Kane; T. M. Bridges; J. P. Kennedy; S. R. Bradley; T. E. Peterson; M. S. Ansari; R. M. Baldwin; R. M. Kessler; A. Y. Deutch; J. J. Lah; A. I. Levey; C. W. Lindsley; P. J. Conn, *J. Neurosci.* **2008**, *28*, 10422-10433.
[29] S. J. Bradley; C. Molloy; C. Bundgaard; A. J. Mogg; K. J. Thompson; L. Dwomoh; H. E. Sanger; M. D. Crabtree; S. M. Brooke; P. M. Sexton; C. C. Felder; A. Christopoulos; L. M. Broad; A. B. Tobin; C. J. Langmead, *Mol. Pharmacol.* **2018**, *93*, 645-656.
[30] A. Christopoulos, *Mol. Pharmacol.* **2014**, *86*, 463-478.
[31] A. Fisher, *Jpn. J. Pharmacol.* **2000**, *84*, 101-112.
[32] A. Fisher; R. Brandeis; R. H. N. Bar-Ner; M. Kliger-Spatz; N. Natan; H. Sonego; I. Marcovitch; Z. Pittel, *J. Mol. Neurosci.* **2002**, *19*, 145-153.
[33] M. Decker; U. Holzgrabe, *Med. Chem. Commun.* **2012**, *3*, 752-762.
[34] M. Canals; J. R. Lane; A. Wen; P. J. Scammells; P. M. Sexton; A. Christopoulos, *J. Biol. Chem.* **2012**, *287*, 650-659.
[35] J. K. Shirey; A. E. Brady; P. J. Jones; A. A. Davis; T. M. Bridges; J. P. Kennedy; S. B. Jadhav; U. N. Menon; Z. Xiang; M. L. Watson; E. P. Christian; J. J. Doherty; M. C. Quirk; D. H. Snyder; J. J. Lah; A. I. Levey; M. M. Nicolle; C. W. Lindsley; P. J. Conn, *J. Neurosci.* **2009**, *29*, 14271-14286.
[36] L. Ma; M. A. Seager; M. Wittmann; M. Jacobson; D. Bickel; M. Burno; K. Jones; V. K. Graufelds; G. Xu; M. Pearson; A. McCampbell; R. Gaspar; P. Shughrue; A. Danziger; C. Regan; R. Flick; D. Pascarella; S. Garson; S. Doran; C. Kreatsoulas; L. Veng; C. W. Lindsley; W. Shipe; S. Kuduk; C. Sur; G. Kinney; G. R. Seabrook; W. J. Ray, *Proc. Natl. Acad. Sci. USA* **2009**, *106*, 15950-15955.
[37] S. D. Kuduk; D. C. Beshore, *Curr. Top. Med. Chem.* **2014**, *14*, 1738-1754.
[38] S. D. Kuduk; C. N. Di Marco; V. Cofre; W. J. Ray; L. Ma; M. Wittmann; M. A. Seager; K. A. Koeplinger; C. D. Thompson; G. D. Hartman; M. T. Bilodeau, *Bioorg. Med. Chem. Lett.* **2011**, *21*, 2769-2772.
[39] B. Budzik; V. Garzya; D. Shi; G. Walker; M. Woolley-Roberts; J. Pardoe; A. Lucas; B. Tehan; R. A. Rivero; C. J. Langmead; J. Watson; Z. Wu; I. T. Forbes; J. Jin, *ACS Med. Chem. Lett.* **2010**, *1*, 244-248.
[40] R. Henning; R. Lattrell; H. J. Gerhards; M. Leven, *J. Med. Chem.* **1987**, *30*, 814-819.

[41] N. Xu; C. Yang; X. Gan; S. Wei; Z. Ji, *Int. J. Mol. Sci.* **2013**, *14*, 6790-6804.
[42] T. Littmann; T. Ozawa; C. Hoffmann; A. Buschauer; G. Bernhardt, *Sci. Rep.* **2018**, *8*, 17179.
[43] S. Lazareno; N. J. Birdsall, *Trends Pharmacol. Sci.* **1993**, *14*, 237-239.
[44] T. Seidel; G. Ibis; F. Bendix; G. Wolber, *Drug Discov. Today Technol.* **2010**, *7*, 221-228.

Entry for the Table of Contents

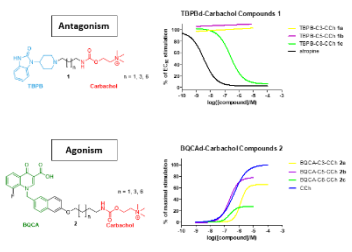

Tailor-made: Dualsteric compounds derived from carbachol as orthosteric moiety can be tailored-made to activate or inactivate the muscarinic M_1 acetylcholine receptor to different extents. BQCA-carbachol derivatives and TBPB-carbachol-derived compounds show partial agonism or a formally competitive antagonism with orthosteric carbachol, respectively. The degree of intrinsic receptor response can be controlled in a wide range by carbachol and the length of the linker.

Supporting Information

Novel BQCA and TBPB derived M_1 Receptor Hybrid-Ligands: Orthosteric Carbachol Differentially Regulates Partial Agonism

Simon Schramm,[a] Luca Agnetta[a], Marcel Bermudez[b], Hubert Gerwe[a], Matthias Irmen[c], Janine Holze[c], Timo Littmann[d], Gerhard Wolber[b], Christian Tränkle[d] and Michael Decker[a]

[a] Pharmazeutische und Medizinische Chemie
Institut für Pharmazie und Lebensmittelchemie, Julius-Maximilians-Universität Würzburg
Am Hubland, D-97074 Würzburg, Germany
E-mail: michael.decker@uni-wuerzburg.de
[b] Institute of Pharmacy, Freie Universität Berlin, Königin-Luise-Straße 2 + 4, 14195 Berlin, Germany.
[c] Pharmacology and Toxicology, Institute of Pharmacy, University of Bonn, Gerhard-Domagk-Straße 3, 53121 Bonn, Germany.
[d] Institute of Pharmacy, University of Regensburg, 93053 Regensburg, Germany.

Table of content

Chemical Synthesis

General

Tetrahydrofuran (THF) was freshly distilled from sodium/benzophenone. Dichloromethane was dried over calcium hydride, distilled and stored over mol sieves. All other common reagents and solvents were purchased from commercial suppliers and used as such. Microwave-assisted reactions were carried out in an MLS-rotaPREP instrument (Milestone, Leutkirch, Germany) using 10 weflon disks. Reaction progress was monitored using analytical thin layer chromatography (TLC) on precoated silica gel GF254 plates (Macherey-Nagel GmbH & Co. KG, Düren, Germany), the spots were detected under UV light (254 nm). Column chromatography was conducted using silica gel (high-purity grade, 0.035-0.070 mm, Merck KGaA, Darmstadt, Germany). Nuclear magnetic resonance spectra were performed with a Bruker AV-400 NMR instrument (Bruker, Karlsruhe, Germany). ESI mass spectral data was acquired on a Shimadzu LCMS 2020. Analytic HPLC was performed on a system from Shimadzu Products equipped with a DGU-20A3R controller, LC20AB liquid chromatograph, and an SPD-20A UV/Vis detector. Stationary phase was a Synergi 4U fusion-RP (150 × 4.6 mm) column. Mobile phase: gradient methanol (0.1% formic acid)/water (0.1% formic acid) (phase A/ phase B) were used. For purity, analytical HPLC a flow rate of 1 mL/min and for preparative HPLC a flow rate of 3 mL/min was used. Compounds were only used for biological evaluation if the purity was ≥ 95%.

Synthesis of Dualsteric TBPB-derived Compounds 1

Synthesis of TBPB-Building Block 3:

Ethyl 4-((2-nitrophenyl)amino)piperidine-1-carboxylate 5[1, 2]

To a stirred suspension of 2-fluoronitrobenzene (5.27 mL, 50.0 mmol, 1.0 eq.), potassium iodide (83 mg, 0.50 mmol, 0.01 eq.) and sodium carbonate (5.30 g, 50 mmol, 1.0 eq.) in dimethylformamide (75 mL), ethyl 4-amino-1-piperidinecarboxylate (8.65 mL, 50 mmol, 1.0 eq.) was added. The reaction mixture was heated at 50 °C for 25 h. After cooling to room temperature, the mixture was diluted with water and extracted with ethyl acetate. The combined organic phases were washed with citric acid solution (10% *w/w*), dried over sodium sulfate and the solvent was removed. The crude product was purified by column chromatography (30 % EtOAc in petroleum ether → 50 %; elute with dichloromethane), which gave 13.4 g (45.7 mmol, 91 %) of the desired product as an orange solid. **^{1}H-NMR (400 MHz, $CDCl_3$)** δ(ppm) = 1.27 (t, *J* = 7.1 Hz, 3 H, CH_3), 1.51 – 1.64 (m, 2 H, *CH_2*-CH), 2.03 – 2.12 (m, 2 H, *CH_2*-CH), 3.06 – 3.17 (m, 2 H, CH_2-N), 3.64 – 3.75 (m, 1 H, CH), 4.01 – 4.12 (m, 2 H, CH_2-N), 4.15 (q, *J* = 7.1 Hz, 2 H, *CH_2*-CH_3), 6.62 – 6.68 (m, 1 H, Ar), 6.87 (d, *J* = 8.3 Hz, 1 H, Ar), 7.40 – 7.46 (m, 1 H, Ar), 8.04 – 8.12 (m, 1 H, NH), 8.16 – 8.21 (m, 1 H, Ar).

Ethyl 4-((2-aminophenyl)amino)piperidine-1-carboxylate 6[1, 2]

A suspension of the nitro-compound **5** (13.4 g, 45.7 mmol, 1.0 eq.) and Pd/C (1.3 g, 10 %) in methanol (250 mL) was stirred at room temperature under H_2-atmosphere for 4.5 h. The reaction mixture was filtered through a pad of celite and the solvent was removed, which gave a dark red oil as the crude product (11.4 g, 43.2 mmol, 95 %).**^{1}H-NMR (400 MHz, MeOD)** δ(ppm) = 1.25 (t, *J* = 7.0 Hz, 3 H, CH_3), 1.32 – 1.46 (m, 2 H, *CH_2*-CH), 1.95 – 2.08 (m, 2 H, *CH_2*-CH), 2.91 – 3.10 (m, 2 H, CH_2-N), 3.42 – 3.54 (m, 1 H, CH), 4.04 – 4.10 (m, 2 H, CH_2-N), 4.11 (q, *J* = 7.1 Hz, 2 H, *CH_2*-CH_3), 6.58 – 6.82 (m, 4 H, Ar).

Ethyl 4-(2-oxo-2,3-dihydro-1*H*-benzo[*d*]imidazol-1-yl)piperidine-1-carboxylate 7[3]

A solution of the diamine **6** (9.38 g, 35.6 mmol, 1.0 eq.) and carbonyldiimidazole (9.24 g, 57 mmol, 1.6 eq.) in tetrahydrofuran (250 mL) was stirred for 3 h at room temperature. The solvent was removed, and the residue was taken up in ethyl acetate (250 mL) and water (75 mL). The phases were separated, and the inorganic phase was extracted with ethyl acetate. The combined organic phases were washed with brine, dried over sodium sulfate and the solvent was removed. The crude product was crystallized from diethyl ether to give the desired product as a light brown solid (11.4 g, 35.6 mmol, quant.). **^{1}H-NMR (400 MHz, MeOD)** δ(ppm) = 1.29 (t, *J* = 7.2 Hz, 3 H, CH_3), 1.76 – 1.85 (m, 2 H, *CH_2*-CH), 2.32 – 2.46 (m, 2 H, *CH_2*-CH), 2.90 – 3.06 (m, 2 H, CH_2-N), 4.17 (q, *J* = 7.3 Hz, 2 H, *CH_2*-CH_3), 4.28 – 4.36 (m, 2 H, CH_2-N), 4.38 – 4.49 (m, 1 H, CH), 7.02 – 7.11 (m, 3 H, Ar), 7.20 – 7.25 (m, 1 H, Ar).

1-(Piperidin-4-yl)-1,3-dihydro-2*H*-benzo[*d*]imidazol-2-one 3[1,2]

A solution of the ester **7** (11.4 g, 35.6 mmol, 1.0 eq.) in a 2M sodium hydroxide solution (250 mL) was heated to 100°C for 23 h. After cooling to 0°C, the mixture was adjusted to pH = 1-2 with concentrated hydrochloric acid and then basified with a 2M sodium hydroxide solution to pH = 13. The basic solution was extracted with ethyl acetate several times. Drying of the organic phases over sodium sulfate and removal of the solvent gave the desired product as a light brown solid (6.9 g, 31.8 mmol, 89 %). **^{1}H-NMR (400 MHz, MeOD)** δ(ppm) = 1.73 – 1.81 (m, 2 H, *CH_2*-CH), 2.39 (qd, *J* = 12.7, 4.3 Hz, 2 H, *CH_2*-CH), 2.76 (td, *J* = 12.7, 2.6 Hz, 2 H, CH_2-N), 3.17 – 3.24 (m, 2 H, CH_2-N), 4.40 (tt, *J* = 12.4, 4.3 Hz, 1 H, CH), 7.01 – 7.10 (m, 3 H, Ar), 7.32 – 7.40 (m, 1 H, Ar).

Syntheses of Linkers 4:

***tert*-Butyl-(3-hydroxypropyl)carbamate 10a**

3-Aminopropanol (0.76 mL, 10 mmol, 1.0 eq.) was dissolved in dioxane/H_2O (2:1) (11 mL). Subsequently a 2M sodium hydroxide solution (6 mL, 1.2 eq.) and Boc_2O (2.62 g, 12 mmol, 1.2 eq.) were added. The reaction mixture was stirred for 4 h at room temperature. Dioxane was removed and the residue was taken up in citric acid solution (10% *w/w*) (40 mL). The mixture was extracted with EtOAc. The combined organic phases were dried over sodium sulfate and the solvents were removed, which gave a colourless oil as the crude product (2.17 g, quant.) which was used in the next reaction without further purification.

***tert*-Butyl-(3-iodopropyl)carbamate 4a**

A solution of imidazole (953 g, 14 mmol, 1.4 eq.) and triphenylphosphine (3.93 g, 15 mmol, 1.5 eq.) in dichloromethane (45 mL) was cooled to 0°C in an ice bath. Iodine (3.81 g, 15 mmol, 1.5 eq.) was added slowly and the mixture was stirred for 45 min at room temperature. A solution of the alcohol **10a** (2.17 g, 10 mmol, 1.0 eq.) in dichloromethane (15 mL) was added to the reaction mixture. The reaction was stirred for 3 h at room temperature. The reaction mixture was then poured into water (50 mL). The phases were separated, and the organic phase was washed with hydrochloric acid (10% *w/w*). The inorganic phases were extracted with dichloromethane. The combined organic phases were dried over sodium sulfate and the solvent was removed. The crude product was purified by column chromatography (petroleum ether 5:1 EtOAc → 3:1; elute with dichloromethane), which gave the desired product as a yellow oil (2.27 g, 7.95 mmol, 80 %). **^{1}H-NMR (400 MHz, $CDCl_3$)** δ(ppm) = 1.43 (s, 9 H, Boc), 1.99 (quin, J = 6.7 Hz, 2 H, CH_2), 3.15 – 3.23 (m, 4 H, 2xCH_2), 4.65 (br. s., 1 H, NH).

***tert*-Butyl-(5-hydroxypentyl)carbamate 10b**

5-Aminopentanol (2.1 mL, 10 mmol, 1.0 eq.) (50% in water) was dissolved in dioxane/H_2O (2:1) (14 mL). Subsequently a 2M sodium hydroxide solution (6 mL, 1.2 eq.) and Boc_2O (2.62 g, 12 mmol, 1.2 eq.) were added. The reaction mixture was stirred for 16 h at room temperature. Dioxane was removed and the residue was taken up in citric acid solution (10% *w/w*). The mixture was extracted with EtOAc. The combined organic phases were dried over sodium sulfate and the solvents were removed, which gave a colourless oil as the crude product (2.42 g, quant.) which was used in the next reaction without further purification.

***tert*-Butyl-(5-iodopentyl)carbamate 4b**

A solution of imidazole (953 mg, 14 mmol, 1.4 eq.) and triphenylphosphine (3.93 g, 15 mmol, 1.5 eq.) in dichloromethane (30 mL) was cooled to 0°C in an ice bath. Iodine (3.81 g, 15 mmol, 1.5 eq.) was added slowly and the mixture was stirred for 1 h at room temperature. A solution of the alcohol **10b** (2.42 g, 10 mmol, 1.0 eq.) in dichloromethane (15 mL) was added to the reaction mixture. The reaction was stirred for 3 h at room temperature. It was then poured into water (50 mL). The phases were separated, and the organic phase was washed with hydrochloric acid (10% *w/w*). The inorganic phases were extracted with dichloromethane. The combined organic phases were dried over sodium sulfate and the solvent was removed. The crude product was purified by column chromatography (petroleum ether 5:1 EtOAc → 3:1; elute with dichloromethane), which gave the desired product as a pale yellow oil (2.82 g, 8.99 mmol, 90 %). **^{1}H-NMR (400 MHz, $CDCl_3$)** δ(ppm) = 1.35 – 1.52 (m, 4 H, 2xCH_2), 1.41 (s, 9 H, Boc), 1.81 (quin, J = 7.2 Hz, 2 H, CH_2), 3.09 (q, J = 6.4 Hz, 2 H, BocN-*CH_2*), 3.16 (t, J = 7.0 Hz, 2 H, CH_2-I), 4.56 (br. s, 1 H, NH). **ESI-MS:** *m/z* calc. for $C_{10}H_{20}INO_2$ $[M+Na]^+$:336.04, found: 336.15.

8-Tosyloctan-1-ol 8

To a suspension of 1,8-Octandiol (3.66 g, 25 mmol, 1.0 eq.) in dichloromethane (100 mL), triethylamine (3.47 mL, 25 mmol, 1.0 eq.), tosylchloride (4.77 g, 25 mmol, 1.0 eq.) and DMAP (31 mg, 0.25 mmol, 0.01) were added. The mixture was stirred at room temperature for 24 h. The mixture was washed twice with water and the organic phase was dried over sodium sulfate and the solvent was removed. Purification by column chromatography (petroleum ether 3:1 EtOAc → 1:1) gave the desired product as a colorless oil (3.74 g, 11.6 mmol, 46 %). **^{1}H-NMR (400 MHz, $CDCl_3$)** δ(ppm) = 1.18 – 1.32 (m, 8 H, 4xCH_2), 1.50 (dt, J = 15.1, 6.5 Hz, 2 H, *CH_2*-CH_2-OH), 1.60 (dt, J = 14.3, 6.5 Hz, 2 H, *CH_2*-CH_2-OTs), 1.78 (br. s., 1 H, OH), 2.41 (s, 3 H, CH_3), 3.57 (t, J = 6.7 Hz, 2 H, *CH_2*-OH), 3.98 (t, J = 6.5 Hz, 2 H, *CH_2*-OTs), 7.29 – 7.34 (m, 2 H, 2xAr-H), 7.73 – 7.77 (m, 2 H, 2xAr-H). **^{13}C-NMR (100 MHz, $CDCl_3$)** δ(ppm) = 21.6 (CH_3), 25.2 (CH_2), 25.6 (CH_2), 28.8 (2xCH_2), 29.1 (CH_2), 32.6 (CH_2), 62.8 (CH_2-OH), 70.7 (CH_2-OTs), 127.8 (2xAr-H), 129.8 (2xAr-H), 133.2 (Ar-C_q), 144.7 (Ar-C_q). **ESI-MS:** *m/z* calc. for $C_{15}H_{24}O_4S$ $[M+Na]^+$:323.13, found: 323.15.

8-Azidooctan-1-ol

Tosylate **8** (3.47 g, 11.6 mmol, 1.0 eq.) was dissolved dimethylformamide (20 mL) and sodium azide (2.25 g, 36.7 mmol, 3.0 eq.) was added. The mixture was heated to 80°C for 17 h. After cooling to room temperature, water and ethyl acetate were added and the phases separated. The organic phase was washed with water several times and dried over sodium sulfate. Removal of the solvent gave the desired product as a golden oil (1.89 g, 11.0 mmol, 95 %). **^{1}H-NMR (400 MHz, $CDCl_3$)** δ(ppm) = 1.26 – 1.39 (m, 8 H, 4xCH_2), 1.48 – 1.60 (m, 4 H, 2xCH_2), 1.91 (s, 1 H, OH), 3.22 (t, J = 6.9 Hz, 2 H, CH_2-N_3), 3.58 (t, J = 6.7 Hz, 2 H, *CH_2*-OH). **^{13}C-NMR (100 MHz, $CDCl_3$)** δ(ppm) = 25.6 (CH_2), 26.6 (CH_2), 28.8 (CH_2), 29.1 (CH_2), 29.2 (CH_2), 32.7 (CH_2), 51.4 (CH_2-N_3), 62.8 (CH_2-OH).

8-Aminooctan-1-ol 9

A solution of 8-azidooctan-1-ol (1.63 g, 9.54 mmol, 1.0 eq.) in tetrahydrofuran was cooled to 0°C. Lithium aluminium hydride (1.45 g, 38.2 mmol, 4.0 eq.) was added in small portions. The mixture was stirred for 20 min at 0°C and 19 h at room temperature. The reaction was quenched with water at 0°C and extracted with ethyl acetate. The combined organic phases were washed with brine and dried over sodium sulfate. Removal of the solvent gave the desired product as a white solid (1.0 g, 6.88 mmol, 72 %). **^{1}H-NMR (400 MHz, $CDCl_3$)** δ(ppm) = 1.20 – 1.34 (m, 8 H, 4xCH_2), 1.40 (quin, J = 6.8 Hz, 2 H, CH_2), 1.51 (quin, J = 7.0 Hz, 2 H, CH_2), 1.82 (br. s., 3 H, NH_2, OH), 2.63 (t, J = 7.0 Hz, 2 H, *CH_2*-NH_2), 3.56 (t, J = 6.7 Hz, 2 H, *CH_2*-OH). **^{13}C-NMR (100 MHz, $CDCl_3$)** δ(ppm) = 25.8 (CH_2), 26.8 (CH_2), 29.4 (2xCH_2), 32.8 (CH_2), 33.6 (CH_2), 42.1 (*CH_2*-NH_2) , 62.5 (*CH_2*-OH). **ESI-MS:** *m/z* calc. for $C_8H_{19}NO$ $[M+H]^+$:146.15, found: 146.25.

***tert*-Butyl(8-hydroxyoctyl)carbamate 10c**

8-Aminooctanol **9** (1.09 g, 7.5 mmol, 1.0 eq.) was dissolved in dioxane/water (2:1) (30 mL), Boc_2O (1.96 g, 9.0 mmol, 1.2 eq.) and sodium hydroxide (360 mg, 9.0 mmol, 1.2 eq.) were added. The mixture was stirred for 5 h at room temperature. Volatiles were removed, and the residue was dissolved in ethyl acetate and citric acid solution (10% *w/w*). The phases were separated, and the inorganic phase was extracted with ethyl acetate. The combined organic phases were washed with brine and dried over sodium sulfate. Removal of the solvent gave the crude product as a yellow solid (1.99 g, 8.11 mmol, quant.) which was used in the next reaction without further purification.

***tert*-Butyl(8-iodooctyl)carbamate 4c**

Triphenylphosphine (3.72 g, 14.2 mmol, 1.5 eq.) and imidazole (900 mg, 13.3 mmol, 1.4 eq.) were dissolved in dichloromethane (50 mL). Iodine (3.60 g, 14.2 mmol, 1.5 eq.) was added. The mixture was stirred for 1 h at room temperature. To this mixture, a solution of Boc-aminooctanol **10c** (2.32 g, 9.46 mmol, 1.0 eq.) in dichloromethane (10 mL) was added. The resulting mixture was stirred for 4 h at room temperature. The reaction was quenched with water and the phases were separated. The organic phase was washed with hydrochloric acid (10% *w/w*) and the combined inorganic phases were extracted with dichloromethane. The combined organic phases were dried over sodium sulfate and the solvent was removed. Column chromatography (petroleum ether 20:1 ethyl acetate) gave the desired product as a colourless oil (2.4 g, 6.8 mmol, 72 %). **^{1}H-NMR (400 MHz, $CDCl_3$)** δ(ppm) = 1.26 – 1.32 (m, 6 H, 3xCH_2), 1.33 – 1.40 (m, 2 H, CH_2), 1.41 – 1.49 (m, 2 H, CH_2), 1.43 (s, 9 H, Boc-CH_3), 1.80 (quin, J = 7.2 Hz, 2 H, CH_2), 3.09 (q, J = 6.4 Hz, 2 H, BocN-CH_2), 3.17 (t, J = 7.0 Hz, 2 H, CH_2-I), 4.51 (br. s, 1 H, NH). **^{13}C-NMR (100 MHz, $CDCl_3$)** δ(ppm) = 7.2 (CH_2-I), 26.7 (CH_2), 28.4 (Boc-CH_3), 28.4 (CH_2), 29.1 (CH_2), 30.0 (CH_2), 30.4 (CH_2), 33.5 (CH_2), 40.6 (BocN-*CH_2*), 79.0 (Boc-C_q), 156.0 (Boc-*C*OO)

Synthesis of Target Compound 1a:

***tert*-Butyl (3-(4-(2-oxo-2,3-dihydro-1*H*-benzo[*d*]imidazol-1-yl)piperidin-1-yl)propyl) carbamate 11a**

The amine **3** (652 mg, 3.00 mmol, 1.0 eq.) and the iodo-compound **4a** (941 mg, 3.30 mmol, 1.1 eq.) were dissolved in dimethylformamide (25 mL), potassium carbonate (829 mg, 6.00 mmol, 2.0 eq.) and potassium iodide (5 mg, 0.03 mmol, 0.01 eq.) were added. The reaction mixture was heated at 60°C for 21 h. The mixture was partitioned between ethyl acetate (100 mL) and water (100 mL). The phases were separated, and the inorganic phase was extracted with ethyl acetate. The combined organic phases were washed with water several times, dried over sodium sulfate and the solvent was removed. Column chromatography (10% methanol in dichloromethane on deactivated silica) gave the desired product as a white foam (768 mg, 2.05 mmol, 68 %). **^{1}H-NMR (400 MHz, $CDCl_3$)** δ(ppm) = 1.43 (s, 9 H, Boc), 1.69 – 1.81 (m, 4 H, *CH_2*-CH, CH_2), 2.29 (t, J = 11.8 Hz, 2 H, CH_2-N), 2.47 – 2.61 (m, 4 H, *CH_2*-CH, CH_2-N), 3.11 (t, J = 6.7 Hz, 2 H, BocN-*CH_2*), 3.18 (d, J = 11.8 Hz, 2 H, CH_2-N), 4.34 (tt, J = 12.4, 4.3 Hz, 1 H, CH), 5.67 (br. s, 1 H, NH), 6.67 – 6.75 (m, 1 H), 6.99 – 7.08 (m, 3 H, Ar), 7.30 – 7.37 (m, 1 H, Ar), 10.50 (br. s, 1 H, NH). **^{13}C-NMR (100 MHz, $CDCl_3$)** δ(ppm) = 26.5 (CH_2), 27.5 (Boc), 27.9 (2xCH-*CH_2*), 38.3 (*CH_2*-N-COO), 50.1 (CH), 52.7 (2xN-CH_2), 55.4 (N-CH_2), 78.6 (Boc-C_q), 109.3 (2xAr-H), 120.9 (Ar-H), 121.2 (Ar-H), 128.3 (Ar-C_q),

128.9 (Ar-C_q), 154.8 (CO), 157.1 (Boc-*C*OO). **ESI-MS:** *m/z* calc. for $C_{20}H_{31}N_4O_3$ $[M+H]^+$: 375.24, found: 375.15.

1-(1-(3-Aminopropyl)piperidin-4-yl)-1,3-dihydro-2*H*-benzo[*d*]imidazol-2-one 12a

The Boc-protected amine **11a** (1.00 g, 2.67 mmol, 1.0 eq.) was dissolved in dichloromethane (25 mL) and trifluoro acetic acid (1.0 mL, 13 mmol, 5.0 eq.) was added. The mixture was stirred at room temperature for 45 min. Water was added and the phases were separated. The inorganic phase was basified to pH ≥ 13 and extracted with ethyl acetate several times. The combined organic phases were washed with brine and dried over sodium sulfate. Removal of the solvent gave the desired product as a white foam (800 mg, 2.92 mmol, quant.). **^{1}H-NMR (400 MHz, $CDCl_3$)** δ(ppm) = 1.71 (quin, J = 6.9 Hz, 2 H, CH_2), 1.78 (dd, J = 12.3, 2.3 Hz, 2 H, CH_2), 2.09 (td, J = 12.0, 2.1 Hz, 2 H, CH_2-N), 2.38 – 2.52 (m, 4 H, , *CH_2*-CH, CH_2-N), 2.86 (t, J = 6.8 Hz, 2 H, *CH_2*-NH_2), 3.09 (d, J = 11.5 Hz, 2 H, CH_2-N), 4.31 (tt, J = 12.5, 4.2 Hz, 1 H, CH), 6.97 – 7.03 (m, 2 H, 2xAr), 7.07 – 7.12 (m, 1 H, Ar), 7.19 – 7.23 (m, 1 H, Ar). **^{13}C-NMR (100 MHz, $CDCl_3$)** δ(ppm) = 29.3 (CH_2), 30.3 (2xCH-*CH_2*), 40.8 (NH_2-CH_2), 50.9 (CH), 53.4 (2xN-CH_2), 56.4 (N-CH_2), 109.7 (2xAr-H), 120.9 (Ar-H), 121.1 (Ar-H), 128.3 (Ar-C_q), 129.1 (Ar-C_q), 155.3 (CO). **ESI-MS:** *m/z* calc. for $C_{15}H_{23}N_4O$ $[M+H]^+$: 275.19, found: 275.00.

2-Chloroethyl (3-(4-(2-oxo-2,3-dihydro-1*H*-benzo[*d*]imidazol-1-yl)piperidin-1-yl)-propyl)carbamate 13a

The amine **12a** (888 mg, 3.24 mmol, 1.0 eq.) was dissolved in dimethylformamide (25 mL). Potassium carbonate (738 mg, 5.34 mmol, 2.0 eq.) and 2-choroethyl chloroformate (276 µL, 2.67 mmol, 1.0 eq.) were added. The mixture was heated to 65°C for 18 h. Water (50 mL) was added, and the mixture extracted twice with ethyl acetate (2x30 mL). The organic phases were washed with water and brine, dried over sodium sulfate and the solvent was removed. Column chromatography (1% methanol in dichloromethane → 3 % → 5 %; on deactivated silica) gave the desired product as a colorless oil (288 mg, 0.76 mmol, 23 %). **^{1}H-NMR (400 MHz, $CDCl_3$)** δ(ppm) = 1.72 (quin, J = 6.2 Hz, 2 H, CH_2), 1.78 – 1.87 (m, 2 H, *CH_2*-CH), 2.07 – 2.19 (m, 2 H, CH_2-N), 2.38 – 2.56 (m, 4 H, *CH_2*-CH, CH_2-N), 3.10 (d, J = 11.8 Hz, 2 H, CH_2-N), 3.27 – 3.35 (m, 2 H, CH_2-N), 3.67 (t, J = 5.6 Hz, 2 H, CH_2-Cl), 4.32 (t, J = 5.6 Hz, 2 H, O-CH_2), 4.35 – 4.45 (m, 1 H, CH), 6.44 (br. s, 1 H, NH), 6.99 – 7.06 (m, 2 H, 2xAr), 7.08 – 7.15 (m, 1 H, Ar), 7.22 – 7.30 (m, 1 H, Ar), 10.58 (br. s., 1 H, NH). **^{13}C-NMR (100 MHz, $CDCl_3$)** δ(ppm) = 26.0 (CH_2), 29.3 (2x*CH_2*-CH), 41.0 (CH_2-N), 42.5 (CH_2-N), 57.0 (CH_2-Cl), 50.5 (CH), 53.2 (2xCH_2-N), 64.4 (O-CH_2), 109.8 (2xAr-H), 121.0 (Ar-H), 121.2 (Ar-H), 128.3 (Ar-C_q), 129.0 (Ar-C_q), 155.3 (C=O), 156.1 (C=O). **ESI-MS:** *m/z* calc. for $C_{18}H_{26}Cl_4N_4O_3$ $[M+H]^+$: 381.17, found: 381.05.

4-(2-Oxo-2,3-dihydro-1*H*-benzo[*d*]imidazol-1-yl)-1-(3-(((2-(trimethylammonio)-ethoxy)carbonyl)amino)propyl)piperidin-1-ium formate 1a

The chloro-compound **13a** (100 mg, 0.26 mmol, 1.0 eq.) was dissolved in acetonitrile (20 mL). Trimethylamine (5 mL) in water (45 v/v%, 60 eq.) were added. The mixture was heated to 80°C for 7d in a sealed vessel. The solvents were removed. Purification by preparative HPLC gave the di-formate salt of the desired product as a colorless oil (17 mg, 0.034 mmol, 13%). **^{1}H-NMR (400 MHz, $CDCl_3$)** δ(ppm) = 1.91 – 2.02 (m, 4 H, CH_2, *CH_2*-CH), 2.78 (q, *J* = 12.1 Hz, 2 H, *CH_2*-CH), 2.93 (t, *J* = 12.0 Hz, 2 H, CH_2-N), 2.98 – 3.06 (m, 2 H, CH_2-N), 3.26 (q, *J* = 7.5 Hz, 2 H, CH_2-NCOO), 3.23 (s, 9 H, NMe_3), 3.57 (br. d, *J* = 10.8 Hz, 2 H, CH_2-N), 3.66 – 3.78 (m, 2 H, *CH_2*-NMe_3), 4.47 – 4.57 (m, 3 H, CH, O-CH_2), 7.05 – 7.10 (m, 3 H, 3xAr), 7.29 – 7.38 (m, 1 H, Ar), 8.50 (s, 2 H, 2x$HCOO^-$). **^{13}C-NMR (100 MHz, $CDCl_3$)** δ(ppm) = 25.1 (CH_2), 26.4 (2x*CH_2*-CH), 38.0 (CH_2-NCOO), 48.5 (CH), 52.0 (2x CH_2-N), 53.07/53.11/53.15 (NMe_3), 54.3 (CH_2-N), 57.9 (O-CH_2), 65.11/65.13/65.17 (*CH_2*-NMe_3), 108.8 (Ar-H), 109.3 (Ar-H), 121.0 (Ar-H), 121.4 (Ar-H), 128.3 (Ar-C_q), 128.8 (Ar-C_q), 154.8 (C=O), 156.2 (HN*C*OO), 167.9 (2x$HCOO^-$). **ESI-MS:** *m/z* calc. for $C_{21}H_{35}N_5O_3$ $[M+H]^{2+}$: 202.64, found: 202.70. *m/z* calc. for $C_{21}H_{35}N_5O_3$ $[M+]^+$: 404.27, found: 404.30.

Synthesis of Target Compound 1b:

tert-Butyl (5-(4-(2-oxo-2,3-dihydro-1_H_-benzo[_d_]imidazol-1-yl)piperidin-1-yl)pentyl) carbamate 11b

The amine **3** (1.96 g, 9 mmol, 1.0 eq.) and the iodo-compound **4b** (2.82 g, 9 mmol, 1.0 eq.) were dissolved in dimethylformamide (60 mL), potassium carbonate (2.49 g, 18 mmol, 2.0 eq.) and potassium iodide (15 mg, 0.09 mmol, 0.01 eq.) were added. The mixture was heated to 60°C for 21 h. The solvent was evaporated to about 20 mL and water (50 mL) and ethyl acetate (50 mL) were added. The phases were separated, and the inorganic phase was extracted with ethyl acetate. The combined organic phases were washed with water several times, dried over sodium sulfate and the solvent was removed. This procedure gave the desired product as a brown solid (3.19 g, 7.93 mmol, 88 %). **^{1}H-NMR (400 MHz, $CDCl_3$)** δ(ppm) = 1.30 – 1.58 (m, 6 H, 3xCH_2), 1.44 (s, 9 H, Boc) 1.74 – 1.86 (m, 2 H, *CH_2*-CH), 2.07 – 2.17 (m, 2 H, CH_2-N), 2.33 – 2.53 (m, 4 H, CH_2-N, *CH_2*-CH), 3.03 – 3.17 (m, 4 H, CH_2-N, BocN-*CH_2*), 4.37 (tt, *J* = 12.5, 4.2 Hz, 1 H, CH), 4.60 (br. s., 1 H, NHBoc), 7.01 – 7.06 (m, 2 H, Ar), 7.08 – 7.12 (m, 1 H, Ar), 7.26 – 7.29 (m, 1 H, Ar), 10.05 (br. s., 1 H, NH). **^{13}C-NMR (100 MHz, $CDCl_3$)** δ(ppm) = 24.8 (CH_2), 26.9 (CH_2), 28.4 (CH_2), 28.5 (Boc-CH_3), 29.3 (2xCH-*CH_2*), 30.0 (CH_2), 40.6 (BocN-*CH_2*), 50.9 (CH), 53.4 (2xN-CH_2), 58.5 (N-CH_2), 79.1 (Boc-C_q), 109.7 (Ar-H), 109.9 (Ar-H), 121.0 (Ar-H), 121.1 (Ar-H), 128.1 (Ar-C_q), 129.2 (Ar-C_q), 155.2 (CO), 156.0 (Boc-*C*OO). **ESI-MS:** *m/z* calc. for $C_{22}H_{34}N_4O_3$ $[M+H]^+$: 403.27, found: 403.30.

1-(1-(5-Aminopentyl)piperidin-4-yl)-1,3-dihydro-2_H_-benzo[_d_]imidazol-2-one 12b

The Boc-protected amine **11b** (985 mg, 2.45 mmol, 1.0 eq.) was dissolved in dichloromethane (15 mL) and trifluoro acetic acid (1.5 mL, 20 mmol, 10 eq.) was added. The mixture was stirred at room temperature for 16 h. Water was added, and the phases were separated. The inorganic phase was basified to pH ≥ 13 and extracted with ethyl acetate several times. The combined organic phases were washed with brine and dried over sodium sulfate. Removal of the solvent gave the desired product as an orange oil (695 mg, 2.30 mmol, 94%). **^{1}H-NMR (400 MHz, $CDCl_3$)** δ(ppm) = 1.29 – 1.40 (m, 2 H, CH_2), 1.45 – 1.58 (m, 4 H, 2xCH_2), 1.79 (br. dd, *J* = 11.9, 2.4 Hz, 2 H, CH-*CH_2*), 2.09 (t, *J* = 11.0 Hz, 2 H, NH_2-CH_2), 2.33 – 2.40 (m, 2 H, N-CH_2), 2.46 (qd, *J* = 12.5, 3.6 Hz, 2 H, CH-*CH_2*), 2.72 (t, *J* = 7.0 Hz, 2 H, N-CH_2), 3.02 – 3.10 (m, 2 H, N-CH_2), 4.34 (tt, *J* = 12.5, 4.0 Hz, 1 H, CH), 6.95 – 7.04 (m, 2 H, 2xAr), 7.06 – 7.11 (m, 1 H, Ar), 7.24 (s, 1 H, Ar). **^{13}C-NMR (100 MHz, $CDCl_3$)** δ(ppm) = 24.8 (CH_2), 26.9 (CH_2), 29.2 (2xCH-*CH_2*), 33.1 (CH_2), 41.8 (NH_2-CH_2), 50.8 (CH), 53.3 (2xN-*CH_2*), 58.4 (N-CH_2), 109.6 (2xAr-CH), 120.7 (Ar-CH), 121.0 (Ar-CH), 128.3 (Ar-C_q), 129.1 (Ar-C_q), 170.1 (CO). **ESI-MS:** *m/z* calc. for $C_{17}H_{26}N_4O$ $[M+H]^+$: 303.22, found: 303.25.

2-Chloroethyl (5-(4-(2-oxo-2,3-dihydro-1*H*-benzo[*d*]imidazol-1-yl)piperidin-1-yl)pentyl)carbamate 13b

The amine **12b** (695 mg, 2.3 mmol, 1.0 eq.) was dissolved in dimethylformamide (10 mL). Potassium carbonate (413 mg, 2.99 mmol, 1.3 eq.) and 2-chloroethyl chloroformate (285 µL, 2.76 mmol, 1.2 eq.) were added. The mixture was heated to 65°C for 16 h. Water was added, and the mixture extracted with ethyl acetate. The organic phases were washed with water and brine, dried over sodium sulfate and the solvent was removed. Column chromatography (1% → 7% methanol in dichloromethane; on deactivated silica) gave the desired product as a colourless oil (435 mg, 1.06 mmol, 47 %). The product was immediately used in the next reaction due to its instability and fast decomposition. **ESI-MS:** *m/z* calc. for $C_{20}H_{31}ClN_4O_3$ $[M+H]^+$: 409.20, found: 409.19.

***N,N,N*-Trimethyl-2-(((5-(4-(2-oxo-2,3-dihydro-1*H*-benzo[*d*]imidazol-1-yl)piperidin-1-yl)pentyl)carbamoyl)oxy)ethan-1-aminium formate 1b**

The chloro-compound **13b** (435 mg, 1.06 mmol, 1.0 eq.) was dissolved in acetonitrile (20 mL). Trimethylamine (10 mL) in tetrahydrofuran (1M, 10 mmol, 10 eq.) was added. The mixture was heated to 80°C for 7d in a sealed vessel. Volatiles were removed. Purification by preparative HPLC gave the formate salt of the desired product as a white solid (84 mg, 0.18 mmol, 20 %). **^{1}H-NMR (400 MHz, $CDCl_3$)** δ(ppm) = 1.39 – 1.48 (m, 2 H, CH_2), 1.59 (quin, J = 7.2 Hz, 2 H, CH_2), 1.77 – 1.87 (m, 2 H, CH_2), 2.02 (dd, J = 12.5, 1.5 Hz, 2 H, 2xN-*CH_2*), 2.88 (ddd, J = 26.6, 13.3, 3.5 Hz, 2 H, 2xN-*CH_2*), 3.08 – 3.19 (m, 4 H, 2xN-*CH_2*), 3.24 (s, 9 H, (NMe_3), 3.71 (dt, J = 4.5, 2.5 Hz, 2 H, *CH_2*-NMe_3), 3.69 (br. d, J = 13.3 Hz, 2 H, 2xCH-*CH_2*), 4.52 (dquin, J = 4.5, 2.5 Hz, 2 H, COO-*CH_2*), 4.60 (tt, J = 12.4, 4.2 Hz, 1 H, CH), 7.05 – 7.11 (m, 3 H, 3xAr), 7.38 – 7.44 (m, 1 H, Ar), 8.55 (s, 1H, $HCOO^-$). **^{13}C-NMR (100 MHz, $CDCl_3$)** δ(ppm) = 23.5 (CH_2), 23.7 (CH_2), 26.0 (2xCH-*CH_2*), 28.9 (CH_2), 40.0 (*CH_2*-N-COO), 48.0 (CH), 51.8 (2xN-*CH_2*), 53.15/53.19/53.23 (NMe_3), 56.4 (N-*CH_2*), 57.8 (COO-*CH_2*), 65.14/65.18/65.21 (*CH_2*-NMe_3), 108.9 (Ar-CH), 109.3 (Ar-CH), 121.0 (Ar-CH), 121.4 (Ar-CH), 128.3 (Ar-C_q), 128.8 (Ar-C_q), 154.7 (CO), 156.1 (CO), 168.3 ($HCOO^-$). **ESI-MS:** *m/z* calc. for $C_{23}H_{39}N_5O_3$ $[M+H]^{2+}$: 216.65, found: 216.75. *m/z* calc. for $C_{23}H_{39}N_5O_3$ $[M+]^+$: 432.30, found: 432.30.

Synthesis of Target Compound 1c:

tert-Butyl (8-(4-(2-oxo-2,3-dihydro-1_H_-benzo[_d_]imidazol-1-yl)piperidin-1-yl)octyl)-carbamate 11c

The amine **3** (1.48 g, 6.8 mmol, 1.0 eq.) and the iodo-compound **4c** (2.40 g, 6.8 mmol, 1.0 eq.) were dissolved in dimethylformamide (75 mL). Potassium carbonate (1.88 mg, 13.6 mmol, 2.0 eq.) and potassium iodide (11.3 mg, 0.07 mmol, 0.01) were added. The reaction mixture was heated to 60°C for 20 h. The mixture was evaporated to 20 mL and partitioned between ethyl acetate (100 mL) and water (100 mL). The phases were separated, and the inorganic phase was extracted with ethyl acetate. The combined organic phases were washed with water several times, dried over sodium sulfate and the solvent was removed. Column chromatography (dichloromethane 25:1 methanol on deactivated silica) gave the desired product as a beige solid (2.34 g, 5.26 mmol, 78 %). **^{1}H-NMR (400 MHz, $CDCl_3$)** δ(ppm) = 1.22 – 1.32 (m, 10 H, 5xCH_2), 1.42 (s, 9 H, Boc-CH_3), 1.47 – 1.57 (m, 2 H, CH_2), 1.80 (dd, J = 12.0, 2.0 Hz, 2 H, CH-*CH_2*), 2.15 (t, J = 11.3 Hz, 2 H, N-CH_2), 2.35 – 2.43 (m, 2 H, N-CH_2), 2.51 (m, 2 H, CH-*CH_2*), 3.03 – 3.16 (m, 4 H, N-CH_2, BocN-*CH_2*), 4.38 (tt, J = 12.4, 4.3 Hz, 1 H, CH), 4.64 (br. s., 1 H, NH), 6.95 – 7.03 (m, 2 H, 2xAr-H), 7.07 – 7.11 (m, 1 H, Ar-H), 7.26 – 7.30 (m, 1 H, Ar-H), 10.72 (br. s., 1 H, NH). **^{13}C-NMR (100 MHz, $CDCl_3$)** δ(ppm) = 26.7 (CH_2), 26.9 (CH_2), 27.5 (CH_2), 28.4 (Boc-CH_3), 29.1 (2x CH-*CH_2*), 29.2 (CH_2), 29.4 (CH_2), 30.1 (CH_2), 40.6 (BocN-*CH_2*), 50.6 (CH), 53.3 (2xN-CH_2), 79.0 (Boc-C_q), 109.7 (Ar-H), 109.9 (Ar-H), 120.1 (Ar-H), 120.9 (Ar-H), 128.3 (Ar-C_q), 129.0 (Ar-C_q), 155.4 (Boc-*C*OO), 156.0 (CO). **ESI-MS:** *m/z* calc. for $C_{20}H_{31}ClN_4O_3$ $[M+H]^+$: 445.32, found: 445.30.

1-(1-(8-Aminooctyl)piperidin-4-yl)-1,3-dihydro-2*H*-benzo[*d*]imidazol-2-one 12c

The Boc-protected amine **11c** (1.00 g, 2.25 mmol, 1.0 eq.) was dissolved in dioxane (40 mL) and 4M hydrochloric acid (40 mL, 160 mmol, 70 eq.) was added. The mixture was stirred at room temperature for 1 h. Volatiles were removed, and the residue dissolved in dichloromethane and water. The phases were separated. The inorganic phase was basified to pH ≥ 13 and extracted with dichloromethane several times. The combined organic phases were dried over sodium sulfate. Removal of the solvent gave the desired product as a brown oil (764 mg, 2.22 mmol, 99%). **^{1}H-NMR (400 MHz, MeOD)** δ(ppm) = 1.30 – 1.40 (m, 8 H, 4xCH_2), 1.42 –1.51 (s, 2 H), 1.53 – 1.62 (m, 2 H), 1.77 (br. dd, J = 14.3, 2.3 Hz, 2 H, CH-*CH_2*), 2.17 (td, J = 12.2, 2.1 Hz, 2 H, N-CH_2), 2.39 – 2.45 (m, 2 H, N-CH_2), 2.53 (qd, J = 12.7, 3.9 Hz, 2 H, CH-*CH_2*), 2.63 (t, J = 7.0 Hz, 2 H, NH_2-*CH_2*), 3.13 (br. d, J = 12.0 Hz, 2 H, N-CH_2), 4.32 (tt, J = 12.5, 4.5 Hz, 1 H, CH), 7.01 – 7.09 (m, 3 H, 3xAr), 7.36 – 7.42 (m, 1 H, Ar). **^{13}C-NMR (100 MHz, MeOD)** δ(ppm) = 26.5 (CH_2), 26.6 (CH_2), 27.3 (CH_2), 28.1 (2xCH-*CH_2*), 29.2 (2xCH_2), 32.4 (CH_2), 41.2 (NH_2-CH_2), 50.5 (CH), 52.9 (2xN-CH_2), 58.3 (N-CH_2), 109.2 (Ar-CH), 109.4 (Ar-CH), 120.8 (Ar-CH), 121.1 (Ar-CH), 128.3 (Ar-C_q), 128.9 (Ar-C_q), 154.9 (CO). **ESI-MS:** *m/z* calc. for $C_{20}H_{32}N_4O$ $[M+H]^+$: 345.26, found: 345.25.

2-Chloroethyl (8-(4-(2-oxo-2,3-dihydro-1*H*-benzo[*d*]imidazol-1-yl)piperidin-1-yl)octyl)carbamate 13c

The amine **12c** (300 mg, 0.87 mmol, 1.0 eq.) was dissolved in dichloromethane (10 mL). Pyridine (148 µL, 1.83 mmol, 2.1 eq.) and 2-chloroethyl chloroformate (108 µL, 1.05 mmol, 1.2 eq.) were added. The mixture was stirred at room temperature for 30 min. Saturated ammonium chloride solution was added and the mixture extracted with dichloromethane. The organic phases were dried over sodium sulfate and the solvent was removed. Column chromatography (2% → 3 % methanol in dichloromethane; on deactivated silica) gave the desired product as a colorless oil (306 mg, 0.68 mmol, 78 %). **^{1}H-NMR (400 MHz, $CDCl_3$)** δ(ppm) = 1.29 – 1.35 (m, 8 H, 4xCH_2), 1.45 – 1.56 (m, 4 H, 2xCH_2), 1.82 (br. dd, J = 12.0, 2.3 Hz, 2 H, CH-CH_2), 2.13 (td, J = 12.0, 1.8 Hz, 2 H, CH-CH_2), 2.35 – 2.42 (m, 2 H, N-CH_2), 2.48 (qd, J = 12.5, 3.8 Hz, 2 H, N-CH_2), 3.10 (br. d, J = 11.5 Hz, 2 H, N-CH_2), 3.18 (q, J = 6.8 Hz, 2 H, N-CH_2), 3.67 (t, J = 5.6 Hz, 2 H, CH_2-Cl), 4.31 (t, J = 5.6 Hz, 2 H, O-CH_2), 4.37 (tt, J = 12.5, 4.3 Hz, 1 H, CH), 4.83 (br. t, J = 4.5 Hz, 1 H, NH), 7.00 – 7.06 (m, 2 H, 2xAr), 7.07 – 7.11 (m, 1 H, Ar), 7.27 – 7.31 (m, 1 H, Ar), 9.70 (br. s., 1 H, NH). **^{13}C-NMR (100 MHz, $CDCl_3$)** δ(ppm) = 26.7 (CH_2), 27.2 (CH_2), 27.6 (CH_2), 29.2 (CH_2), 29.3 (CH_2), 29.5 (2xCH_2), 29.9 (CH_2), 41.1 (N-CH_2), 42.4 (CH_2-Cl), 50.9 (CH), 53.3 (N-CH_2), 53.4 (CH-CH_2), 58.7 (N-CH_2), 64.4 (O-CH_2), 109.6 (Ar-CH), 109.9 (Ar-CH), 121.0 (Ar-CH), 121.1 (Ar-CH), 128.0 (Ar-C_q), 129.2 (Ar-C_q), 155.0 (CO), 155.9 (COO). **ESI-MS:** *m/z* calc. for $C_{23}H_{32}ClN_4O_3$ $[M+H]^+$: 451.25, found: 452.10.

4-(2-Oxo-2,3-dihydro-1*H*-benzo[*d*]imidazol-1-yl)-1-(8-(((2-(trimethylammonio)-ethoxy)carbonyl)amino)octyl)piperidin-1-ium formate 1c

The chloro-compound **13c** (50 mg, 0.22 mmol, 1.0 eq.) was dissolved in tetrahydrofuran (18 mL) and a 1M solution of trimethylamine in tetrahydrofuran (5 mL, 5 mmol, 23 eq.) was added. The mixture was heated to 80°C for 2 d in a sealed vessel. Volatiles were removed. Purification by preparative HPLC gave the di-formate salt of the desired product as a colorless oil (14 mg, 0.03 mmol, 14 %). **^{1}H-NMR (400 MHz, $CDCl_3$)** δ(ppm) = 1.33 – 1.44 (m, 8 H, 4xCH_2), 1.52 (quin, J = 6.5 Hz, 2 H, CH_2), 1.78 (br. s., 2 H, CH_2), 2.03 (br. d, J = 12.8 Hz, 2 H, CH-*CH_2*), 2.77 – 2.91 (m, 2 H, CH-*CH_2*), 3.07 – 3.15 (m, 6 H, 3xN-CH_2), 3.22 (s, 9 H, NMe_3), 3.66 – 3.74 (m, 4 H, N-CH_2, NMe_3-*CH_2*), 4.48 – 4.53 (m, 2 H, COO-*CH_2*), 4.53 – 4.62 (m, 1 H, CH), 7.06 – 7.10 (m, 3 H, 3xAr), 7.31 – 7.36 (m, 1 H, Ar), 8.49 (br. s., 2 H, 2x$HCOO^-$). **^{13}C-NMR (100 MHz, $CDCl_3$)** δ(ppm) = 24.0 (CH_2), 26.0 (2xCH-*CH_2*), 26.3 (2xCH_2), 28.7 (2xCH_2), 29.4 (CH_2), 40.5 (*CH_2*-N-COO), 48.0 (CH), 51.7 (2xN-*CH_2*), 53.07/53.12/53.16 (NMe_3), 56.4 (N-*CH_2*), 57.7 (COO-*CH_2*), 65.16/65.19/65.22 (*CH_2*-NMe_3), 108.7 (Ar-H), 109.3 (Ar-H), 121.0 (Ar-H), 121.4 (Ar-H), 128.3 (Ar-C_q), 128.8 (Ar-C_q), 154.7 (CO), 156.0 (CO), 167.9 ($HCOO^-$). **ESI-MS:** *m/z* calc. for $C_{26}H_{45}N_5O_3$ $[M+H]^{2+}$: 237.68, found: 237.75. *m/z* calc. for $C_{26}H_{45}N_5O_3$ $[M+]^+$: 474.34, found: 474.25.

Synthesis of Dualsteric BQCA-derived Compounds 2

BQCA-Building-Blocks:

Ethyl 8-fluoro-4-oxo-1,4-dihydroquinoline-3-carboxylate 14[4, 5]

A mixture of 2-fluoroaniline (4 mL, 41.4 mmol, 1.0 eq.) and diethyl 2-(ethoxymethylene) malonate (8.4 mL, 41.4 mmol, 1.0 eq.) was heated to 140 °C for 5 h. After cooling, diphenyl ether (20 mL) was added and the mixture was heated to 190 °C for 20 min in a microwave system. After cooling to room temperature diethyl ether was added and the resulting suspension was left stirring overnight. The solid was filtered and washed with diethyl ether, which gave the desired product as a beige solid (1.4 g, 5.95 mmol, 14 %). **^{1}H-NMR (400 MHz, $CDCl_3$)** δ(ppm) = 1.28 (t, J = 7.0 Hz, 3 H, CH_3), 4.22 (q, J = 7.0 Hz, 2 H, *CH_2*-CH_3), 7.40 (td, J = 8.2, 5.0 Hz, 1 H, Ar), 7.65 (ddd, J = 11.0, 8.0, 1.4 Hz, 1 H, Ar), 7.95 – 7.99 (m, 1 H, Ar), 8.39 (s, 1 H, CH), 12.46 (br. s, 1 H, NH). **ESI-MS:** *m/z* calc. for $C_{12}H_{10}FN_4O_3$ $[M+H]^+$: 236.07, found: 236.05.

6-(Hydroxymethyl)naphthalen-2-ol 15[6]

To a solution of 6-hydroxy-2-naphthoic acid (4 g, 21.3 mmol, 1.0 eq.) in methanol (30 mL), 10 drops of concentrated sulfuric acid were added. The mixture was heated to 70°C for 20 h. The mixture was cooled to room temperature and the solvent was removed. The crude methyl ester (4.66 g, 21.3 mmol, 1.0 eq.) was dissolved in dry tetrahydrofuran and the solution was cooled in an ice/salt bath to -20 °C. Lithium aluminium hydride (1.21 g, 32.0 mmol, 1.5 eq.) was added in small portions. The mixture was stirred at 0 °C to room temperature for 16 h. The reaction mixture was cooled to 0 °C and ethyl acetate (50 mL) and water (50 mL) were added slowly. The phases were separated, and the inorganic phase was extracted with ethyl acetate. The combined organic phases were dried over sodium sulfate and the solvent was removed. This procedure gave the desired product as an off-white solid (3.21 g, 18.4 mmol, 87 %). **^{1}H-NMR (400 MHz, $CDCl_3$)** δ(ppm) = 4.70 (s, 2 H, CH_2), 7.06 (dd, J = 8.8, 2.5 Hz, 1 H, Ar), 7.09 (d, J = 2.5 Hz, 1 H, Ar), 7.38 (dd, J = 8.5, 1.8 Hz, 1 H, Ar), 7.62 (d, J = 8.8 Hz, 1 H, Ar), 7.67 – 7.71 (m, 2 H, 2xAr).

Syntheses of Linkers 17:

***tert*-Butyl (3-((6-(hydroxymethyl)naphthalen-2-yl)oxy)propyl)carbamate 16a**

6-(hydroxymethyl)naphthalene-2-ol **15** (1.43 g, 8.22 mmol, 1.0 eq.) and the iodo-compound **4a** (2.34 g, 8.22 mmol, 1.0 eq.) were dissolved in acetonitrile/water (3:1)(100 mL). Sodium hydroxide (360 mg, 9 mmol, 1.1 eq.) was added and the mixture was heated to 70°C for 20 h. Water (50 mL) and ethyl acetate (50 mL) were added. The phases were separated, and the inorganic phase was extracted with ethyl acetate. The combined organic phases were washed with brine, dried over sodium sulfate and the solvent was removed. Purification by column chromatography (petroleum ether 1:2 ethyl acetate) gave the desired product as a pale yellow solid (1.86 g, 5.62 mmol, 68 %). **^{1}H-NMR (400 MHz, MeOD)** δ(ppm) = 1.43 (s, 9 H, Boc), 1.95 – 2.04 (m, 2 H, CH_2), 3.27 (t, J = 6.9 Hz, 2 H, BocNH-*CH_2*), 4.12 (t, J = 6.1 Hz, 2 H, CH_2-O-), 4.72 (s, 2 H, CH_2-OH), 7.12 (dd, J = 8.9, 2.4 Hz, 1 H, Ar), 7.21 (d, J = 2.5 Hz, 1 H, Ar), 7.43 (dd, J = 8.2, 1.6 Hz, 1 H, Ar), 7.70 – 7.74 (m, 3 H, 3xAr). **^{13}C-NMR (100 MHz, MeOD)** δ(ppm) = 27.4 (Boc-CH_3), 29.4 (CH_2), 37.2 (*CH_2*-Boc), 64.0 (CH_2-OH), 65.3 (CH_2-O-), 78.6 (Boc-C_q), 106.3 (Ar-H), 118.6 (Ar-H), 125.0 (Ar-H), 125.6 (Ar-H), 126.6 (Ar-H), 128.9 (Ar-H), 128.9 (Ar-C_q), 134.1 (Ar-C_q), 136.4 (Ar-C_q), 154.9 (Ar-C_q), 157.0 (Boc-*C*OO). **ESI-MS:** *m/z* calc. for $C_{19}H_{25}NO_4$ $[M+Na]^+$: 354.17, found: 354.20.

***tert*-Butyl (3-((6-(iodomethyl)naphthalen-2-yl)oxy)propyl)carbamate 17a**

Triphenylphosphine (2.85 g, 10.88 mmol, 2.0 eq.) and imidazole (519 mg, 7.62 mmol, 1.4 eq.) were dissolved in dry dichloromethane (40 mL) and iodine (2.76 g, 10.88 mmol, 2.0 eq.) was added in portions. The mixture was stirred at room temperature for 1 h. A solution of the alcohol **16a** (1.80 g, 5.44 mmol, 1.0 eq.) in dry dichloromethane (10 mL) was added and the resulting mixture was stirred at room temperature for 3 h. Water (50 mL) was added, and the phases were separated. The organic phase was washed with hydrochloric acid (10% *w/w*). The combined inorganic phases were extracted with ethyl acetate. The combined organic phases were dried over sodium sulfate and the solvent was removed. Purification by column chromatography (petroleum ether 2:1 ethyl acetate) of the crude product gave the desired product as a brown solid (1.56 g, 3.53 mmol, 65 %). Upon evaporation of the solvent, the pure compounds **17a-c** showed partial decomposition and a color change from light yellow to dark orange/brown and were used in the next reaction immediately. Usage of bromine instead of iodine should, however, circumvent these issues. **^{1}H-NMR (400 MHz, $CDCl_3$)** δ(ppm) = 1.44 (s, 9 H, Boc), 1.98 – 2.06 (s, 2 H, CH_2), 3.31 – 3.39 (m, 2 H, CH_2-Boc), 4.07 – 4.14 (m, 2 H, CH_2-O-), 4.61 (s, 2 H, CH_2-I), 7.07 – 7.09 (m, 1 H, Ar), 7.10 – 7.14 (m, 1 H, Ar), 7.40 – 7.44 (m, 1 H, Ar), 7.63 – 7.67 (m, 2 H, 2xAr), 7.71 – 7.74 (m, 1 H, Ar). **^{13}C-NMR (100 MHz, $CDCl_3$)** δ(ppm) = 7.1 (CH_2-I), 28.4 (Boc-CH_3), 29.6 (CH_2), 38.0 (*CH_2*-Boc), 65.8 (CH_2-O-), 79.2 (Boc-C_q), 106.8 (Ar-H), 119.4 (Ar-H), 126.9 (Ar-H), 127.5 (Ar-H), 127.6 (Ar-H), 128.8 (Ar-C_q), 129.3 (Ar-H), 134.0 (Ar-C_q), 134.3 (Ar-C_q), 156.1 (Ar-C_q), 157.3 (Boc-*C*OO). **ESI-MS:** *m/z* calc. for $C_{19}H_{24}INO_3$ $[M+Na]^+$: 464.07, found: 464.10.

***tert*-Butyl (5-((6-(hydroxymethyl)naphthalen-2-yl)oxy)pentyl)carbamate 16b**

6-(hydroxymethyl)naphthalene-2-ol **15** (895 mg, 5.14 mmol, 1.0 eq.) and the iodo-compound **4b** (2.25 g, 7.16 mmol, 1.4 eq.) were dissolved in acetonitrile/water (3:1) (75 mL). Sodium hydroxide (250 mg, 9 mmol, 1.1 eq.) was added and the mixture was heated to 70°C for 22 h. Water (50 mL) and ethyl acetate (50 mL) were added. The phases were separated, and the inorganic phase was extracted with ethyl acetate. The combined organic phases were washed with brine, dried over sodium sulfate and the solvent was removed. Purification by column chromatography (40% → 60% ethyl acetate in petroleum ether) gave the desired product as a white solid (1.78 g, 4.95 mmol, 96 %). **^{1}H-NMR (400 MHz, $CDCl_3$)** δ(ppm) = 1.44 (s, 9 H, Boc), 1.46 – 1.57 (m, 4 H, 2xCH_2), 1.82 (quin, J = 6.8 Hz, 2 H, CH_2), 3.05 – 3.16 (m, 2 H, CH_2), 4.02 (t, J = 6.5 Hz, 2 H, CH_2), 4.78 (s, 2 H, CH_2-OH), 7.07 – 7.15 (m, 2 H, 2xAr), 7.42 (dd, J = 8.5, 1.8 Hz, 1 H, Ar), 7.66 – 7.71 (m, 3 H, 3xAr). **^{13}C-NMR (100 MHz, $CDCl_3$)** δ(ppm) = 23.4 (CH_2),

28.5 (Boc-CH_3), 28.9 (2xCH_2), 29.9 (CH_2), 40.5 (CH_2), 65.4 (CH_2-OH), 67.8 (O-CH_2), 79.2 (Boc-C_q), 106.6 (Ar-H), 119.2 (Ar-H), 125.5 (Ar-H), 125.9 (Ar-H), 127.1 (Ar-H), 128.8 (Ar-C_q), 129.2 (Ar-H), 134.1 (Ar-C_q), 136.2 (Ar-C_q), 157.1 (Ar-*C*O-). **ESI-MS:** *m/z* calc. for $C_{21}H_{29}NO_4$ $[M+Na]^+$: 382.20, found: 382.10.

tert-Butyl (5-((6-(iodomethyl)naphthalen-2-yl)oxy)pentyl)carbamate 17b

Triphenylphosphine (2.60 g, 9.90 mmol, 2.0 eq.) and imidazole (472 mg, 6.93 mmol, 1.4 eq.) were dissolved in dry dichloromethane (50 mL) and iodine (2.51 g, 9.90 mmol, 2.0 eq.) was added in portions. The mixture was stirred at room temperature for 1 h. A solution of the alcohol **16b** (1.78 g, 4.95 mmol, 1.0 eq.) in dry dichloromethane (25 mL) was added and the resulting mixture was stirred at room temperature for 6 h. Water (50 mL) was added, and the phases were separated. The organic phase was washed with hydrochloric acid (10% *w/w*). The combined inorganic phases were extracted with ethyl acetate. The combined organic phases were dried over sodium sulfate and the solvent was removed. Column chromatography (petroleum ether 2:1 ethyl acetate) gave the desired product as a yellow solid (1.37 g, 2.9 mmol, 60 %). Upon evaporation of the solvent, the pure compounds **17a-c** showed partial decomposition and a color change from light yellow to dark orange/brown and were used in the next reaction immediately. Usage of bromine instead of iodine should, however, circumvent these issues. **^{1}H-NMR (400 MHz, $CDCl_3$)** δ(ppm) = 1.45 (s, 9 H, Boc-CH_3), 1.50 – 1.61 (m, 4 H, 2xCH_2), 1.81 – 1.90 (m, 2 H, CH_2), 3.17 (m, 2 H, CH_2), 4.06 (t, *J* = 6.4 Hz, 2 H, CH_2), 4.62 (s, 2 H, I-CH_2), 7.08 (d, *J* = 2.5 Hz, 1 H, Ar-H), 7.13 (dd, *J* = 8.8, 2.5 Hz, 1 H, Ar-H), 7.43 (dd, *J* = 8.5, 2.0 Hz, 1 H, Ar-H), 7.66 (dd, *J* = 8.5, 4.5 Hz, 2 H, 2xAr-H), 7.74 (d, *J* = 1.5 Hz, 1 H, Ar-H). **^{13}C-NMR (100 MHz, $CDCl_3$)** δ(ppm) = 7.2 (CH_2-I), 23.4 (CH_2), 28.5 (Boc-CH_3), 28.9 (CH_2), 29.9 (CH_2), 40.5 (*CH_2*-Boc), 67.8 (CH_2-O-), 79.1 (Boc-C_q), 106.7 (Ar-H), 119.5 (Ar-H), 127.0 (Ar-H), 127.4 (Ar-H), 127.6 (Ar-H), 128.7 (Ar-C_q), 129.3 (Ar-H), 134.1 (Ar-C_q), 134.2 (Ar-C_q), 157.6 (Ar-C_q), 158.8 (Boc-C=O). **ESI-MS:** *m/z* calc. for $C_{21}H_{28}INO_3$ $[M+Na]^+$: 492.10, found: 492.10.

tert-Butyl (8-((6-(hydroxymethyl)naphthalen-2-yl)oxy)octyl)carbamate 16c

The alcohol **15** (1.02 g, 5.87 mmol, 1.0 eq.) and sodium hydroxide (282 mg, 7.04 mmol, 1.2 eq.) were dissolved in acetonitrile/water (3:1)(75 mL) and the iodo-compound **4c** (2.5 g, 7.04 mmol, 1.0 eq.) was added. The mixture was heated to 70 °C for 36 h. The mixture was concentrated and diluted with water. The mixture was extracted with ethyl acetate. The organic phases were washed with brine, dried over sodium sulfate and the solvent was removed.

Column chromatography (40% → 45% ethyl acetate in petroleum ether) gave the desired product as a white solid (1.79 g, 4.45 mmol, 76%). **^{1}H-NMR (400 MHz, $CDCl_3$)** δ(ppm) = 1.24 – 1.39 (m, 8 H, 4xCH_2), 1.43 (s, 9 H, Boc), 1.39 – 1.52 (m, 4 H, 2xCH_2), 1.76 – 1.86 (m, 2 H, CH_2), 2.50 – 2.60 (m, 1 H, OH), 3.02 – 3.11 (m, 2 H, BocNH-*CH_2*), 4.03 (t, *J* = 6.5 Hz, 2 H, -O-CH_2), 4.76 (s, 2 H, OH-CH_2), 7.09 – 7.15 (m, 2 H, 2xAr), 7.41 (dd, *J* = 8.4, 1.6 Hz, 1 H, Ar), 7.68 (dd, *J* = 7.0, 2.0 Hz, 3 H, 3xAr). **^{13}C-NMR (100 MHz, $CDCl_3$)** δ(ppm) = 26.0 (2xCH_2), 26.7 (CH_2), 28.4 (Boc-CH_3), 29.2 (CH_2), 29.3 (CH_2), 30.0 (CH_2), 40.6 (BocNH-*CH_2*), 65.3 (OH-CH_2), 68.0 (-O-CH_2), 79.1 (Boc-C_q), 106.6 (Ar-H), 119.2 (Ar-H), 125.5 (Ar-H), 125.8 (Ar-H), 127.0 (Ar-H), 128.7 (Ar-C_q), 129.3 (Ar-H), 134.1 (Ar-C_q), 136.2 (Ar-C_q), 156.1 (Boc-*C*OO), 157.2 (Ar-*C*O-). **ESI-MS:** *m/z* calc. for $C_{24}H_{35}NO_4$ $[M+Na]^+$: 424.25, found: 424.20.

***tert*-Butyl (8-((6-(iodomethyl)naphthalen-2-yl)oxy)octyl)carbamate 17c**

Triphenylphosphine (2.29 g, 8.72 mmol, 2.0 eq.) and imidazole (415 mg, 6.10 mmol, 1.4 eq.) were dissolved in dichloromethane (50 mL) and iodine (2.21 g, 8.72 mmol, 2.0 eq.) was added slowly. The mixture was stirred for 1 h at room temperature and the alcohol **16c** (1.75 g, 4.36 mmol, 1.0 eq.) was added as a solution in dichloromethane (20 mL). The mixture was stirred at room temperature for 3 h and quenched with water. The phases were separated, and the organic phase was washed with hydrochloric acid (10% *w/w*). The inorganic phases were extracted with dichloromethane. The organic phases were dried over sodium sulfate and the solvent was removed. Purification by column chromatography (petroleum ether 8:1 ethyl acetate) gave the desired product as a yellow oil (1.58 g, 3.09 mmol, 71%). Upon evaporation of the solvent, the pure compounds **17a-c** showed partial decomposition and a color change from light yellow to dark orange/brown and were used in the next reaction immediately. Usage of bromine instead of iodine should, however, circumvent these issues. **^{1}H-NMR (400 MHz, $CDCl_3$)** δ(ppm) = 1.27 – 1.41 (m, 8 H, 4xCH_2), 1.45 (s, 9 H, Boc), 1.42 – 1.53 (m, 4 H, 2xCH_2), 1.79 – 1.88 (m, 2 H, CH_2), 3.11 (q, *J* = 6.3 Hz, 2 H, BocNH-*CH_2*), 4.05 (t, *J* = 6.5 Hz, 2 H, -O-CH_2), 4.63 (s, 2 H, I-CH_2), 7.09 (d, *J* = 2.3 Hz, 1 H, Ar), 7.13 (dd, *J* = 9.0, 2.5 Hz, 1 H, Ar), 7.43 (dd, *J* = 8.4, 1.9 Hz, 1 H, Ar), 7.67 (dd, *J* = 8.8, 4.3 Hz, 2 H, 2xAr), 7.74 (d, *J* = 1.5 Hz, 1 H, Ar). **^{13}C-NMR (100 MHz, $CDCl_3$)** δ(ppm) = 7.2 (I-CH_2), 26.0 (CH_2), 26.8 (CH_2), 28.5 (Boc-CH_3), 29.1 (CH_2), 29.2 (2xCH_2), 29.3 (CH_2), 30.1 (CH_2), 41.4 (BocNH-*CH_2*), 68.0 (-O-CH_2), 79.1 (Boc-C_q), 106.7 (Ar-H), 119.6 (Ar-H), 127.0 (Ar-H), 127.4 (Ar-H), 127.6 (Ar-H), 128.6 (Ar-C_q), 129.2 (Ar-H), 133.0 (Ar-C_q), 134.1 (2xAr-C_q), 154.8 (Boc-*C*OO), 157.5 (Ar-*C*O-). **ESI-MS:** *m/z* calc. for $C_{24}H_{34}INO_3$ $[M+Na]^+$: 534.15, found: 534.10.

Synthesis of Target Compound 2a:

Ethyl 1-((6-(3-((*tert*-butoxycarbonyl)amino)propoxy)naphthalen-2-yl)methyl)-8-fluoro-4-oxo-1,4-dihydroquinoline-3-carboxylate 18a

The iodo-compound **17a** (1.3 g, 2.95 mmol, 1.0 eq.) and the quinolone **14** (694 mg, 2.95 mmol, 1.0 eq.) were dissolved in dimethylformamide (30 mL). Potassium carbonate (815 mg, 5.9 mmol, 2.0 eq.) and potassium iodide (4.9 mg, 0.03 mmol, 0.01 eq.) were added. The mixture was heated to 60°C for 19 h. Water (100 mL) and ethyl acetate (100 mL) were added. The phases were separated, and the inorganic phase was extracted with ethyl acetate. The combined organic phases were washed with water several times, dried over sodium sulfate and the solvent was removed, to give the desired product as a brown solid (1.3 g, 2.37 mmol, 80%). **^{1}H-NMR (400 MHz, $CDCl_3$)** δ(ppm) = 1.42 (t, J = 7.0 Hz, 3 H, CH_3), 1.43 (s, 9 H, Boc), 2.03 (quin, J = 6.1 Hz, 2 H, CH_2), 3.35 (q, J = 6.4 Hz, 2 H, BocNH-*CH_2*), 4.11 (t, J = 6.0 Hz, 2 H, CH_2-O-), 4.41 (q, J = 7.2 Hz, 2 H, *CH_2*-CH_3), 5.66 (s, 2 H, CH_2-N), 7.08 – 7.15 (m, 2 H, 2xAr), 7.21 – 7.35 (m, 4 H, 4xAr), 7.45 (s, 1 H, Ar), 7.64 (d, J = 8.8 Hz, 1 H, Ar), 7.70 (d, J = 8.5 Hz, 1 H, Ar), 8.34 – 8.38 (m, 1 H, Ar), 8.58 (s, 1 H, CH). **^{13}C-NMR (100 MHz, $CDCl_3$)** δ(ppm) = 14.4 (CH_3), 28.4 (Boc-CH_3), 29.6 (CH_2), 38.0 (BocNH-*CH_2*), 60.9 (CH_2-N), 61.1 (*CH_2*-CH_3), 65.9 (CH_2-O-), 79.3 (Boc-C_q), 106.6 (Ar-H), 111.4 (*C*=CH), 119.7 (Ar-H), 119.8 (d, J = 22.7 Hz, Ar-H), 123.9 (d, J = 2.9 Hz, Ar-H), 124.3 (Ar-H), 125.0 (Ar-H), 125.5 (d, J = 8.8 Hz, Ar-H), 127.9 (Ar-H), 128.54 (d, J = 6.6 Hz, Ar-C_q), 128.7 (Ar-C_q), 129.4 (Ar-H), 130.6 (d, J = 1.5 Hz, Ar-C_q), 132.0 (Ar-C_q), 134.3 (Ar-C_q), 151.6 (CH), 151.88 (d, J = 250.9 Hz, Ar-C_q), 156.0 (Boc-*C*OO), 157.3 (Ar-*C*O-), 165.5 (*C*OOEt), 173.2 (CO). **ESI-MS:** *m/z* calc. for $C_{31}H_{33}FN_2O_6$ $[M+Na]^+$: 571.22, found: 571.20.

Ethyl 1-((6-(3-aminopropoxy)naphthalen-2-yl)methyl)-8-fluoro-4-oxo-1,4-dihydroquinoline-3-carboxylate 19a

The Boc-protected amine **18a** (539 mg, 0.98 mmol, 1.0 eq.) was dissolved in dioxane (60 mL) and 4M hydrochloric acid (40 mL, 160 mmol, 160 eq.) was added. The mixture was stirred at room temperature for 4 h. Volatiles were removed, and the residue dissolved in dichloromethane and water. The phases were separated. The inorganic phase was basified to pH ≥ 13 and extracted with dichloromethane several times. The combined organic phases were dried over sodium sulfate. Removal of the solvent gave the desired product as a brown oil (200 mg, 0.45 mmol, 46 %). **^{1}H-NMR (400 MHz, $CDCl_3$)** δ(ppm) = 1.40 (t, J = 7.2 Hz, 3 H, CH_3), 1.96 (quin, J = 6.5 Hz, 2 H, CH_2), 2.92 (t, J = 6.8 Hz, 2 H, NH_2-*CH_2*), 4.13 (t, J = 6.1 Hz, 2 H, O-CH_2), 4.39 (q, J = 7.2 Hz, 2 H, *CH_2*-CH_3), 5.62 (br. d, J = 2.0 Hz, 2 H, N-CH_2), 7.08 –

7.15 (m, 2 H, 2xAr), 7.18 – 7.32 (m, 3 H, 3xAr), 7.42 (br. s, 1 H, Ar), 7.61 (d, *J* = 9.0 Hz, 1 H, Ar), 7.67 (d, *J* = 8.8 Hz, 1 H, Ar), 8.31 – 8.36 (m, 1 H, Ar), 8.56 (s, 1 H, CH). **^{13}C-NMR (100 MHz, $CDCl_3$)** δ(ppm) = 14.4 (CH_3), 32.9 (CH_2), 39.2 (NH_2-*CH_2*), 60.89/61.05 (N-CH_2), 61.1 (*CH_2*-CH_3), 66.0 (O-CH_2), 106.5 (Ar-H), 111.3 (*C*=CH), 119.78 (Ar-H), 119.82 (d, *J* = 22.7 Hz, Ar-H), 123.83 (d, *J* = 3.7 Hz, Ar-H), 124.3 (Ar-H), 125.0 (Ar-H), 125.49 (d, J = 8.1 Hz, Ar-H), 127.9 (Ar-H), 128.51 (d, *J* = 6.6 Hz, Ar-C_q), 128.60 (Ar-C_q), 129.4 (Ar-H), 130.51 (d, *J* = 1.5 Hz, Ar-C_q), 131.9 (Ar-C_q), 134.3 (Ar-C_q), 151.61 (CH), 151.86 (d, *J* = 250.9 Hz, Ar-CF), 157.5 (Ar-*C*O-), 165.4 (*C*OOEt), 173.2 (CO). **ESI-MS:** *m/z* calc. for $C_{26}H_{25}FN_2O_4$ $[M+H]^+$: 449.19, found: 449.10.

Ethyl 1-((6-(3-(((2-chloroethoxy)carbonyl)amino)propoxy)naphthalen-2-yl)methyl)-8-fluoro-4-oxo-1,4-dihydroquinoline-3-carboxylate 20a

The amine **19a** (100 mg, 0.22 mmol, 1.0 eq.) was dissolved in dichloromethane (40 mL). Pyridine (26.6 µL, 0.33 mmol, 1.5 eq.) and 2-chloroethyl chloroformate (27.3 µL, 0.26 mmol, 1.2 eq.) were added. The mixture was stirred for 30 min at room temperature. Saturated ammonium chloride solution was added, and the mixture extracted with dichloromethane. The organic phases were dried, and the solvent was removed. Purification by column chromatography (1% methanol in dichloromethane; on deactivated silica) gave the desired product as a colourless oil (100 mg, 0.18 mmol, 82 %). **^{1}H-NMR (400 MHz, $CDCl_3$)** δ(ppm) = 1.40 (t, *J* = 7.2 Hz, 3 H, CH_3), 2.05 (quin, *J* = 6.3 Hz, 2 H, CH_2), 3.42 (q, *J* = 6.5 Hz, 2 H, NH-*CH_2*), 3.62 – 3.66 (m, 2 H, O-CH_2), 4.11 (t, *J* = 5.9 Hz, 2 H, CH_2-Cl), 4.29 (t, *J* = 5.5 Hz, 2 H, O-CH_2), 4.40 (q, *J* = 7.1 Hz, 2 H, *CH_2*CH_3), 5.16 (br. s., 1 H, NH), 5.64 (d, *J* = 2.0 Hz, 2 H, N-CH_2), 7.08 (d, *J* = 2.3 Hz, 1 H, Ar), 7.12 (dd, *J* = 8.9, 2.4 Hz, 1 H, Ar), 7.19 – 7.33 (m, 3 H, 3xAr), 7.43 (br. s, 1 H, Ar), 7.62 (d, *J* = 9.0 Hz, 1 H, Ar), 7.68 (d, *J* = 8.5 Hz, 1 H, Ar), 8.32 – 8.36 (m, 1 H, Ar), 8.57 (s, 1 H, CH). **^{13}C-NMR (100 MHz, $CDCl_3$)** δ(ppm) = 14.4 (CH_3), 29.3 (CH_2), 38.6 (NH-CH_2), 42.3 (O-CH_2), 60.89/61.05 (N-CH_2), 61.12 (*CH_2*-CH_3), 64.5 (O-CH_2), 65.8 (CH_2-Cl), 106.6 (Ar-H), 111.4 (*C*=CH), 119.64 (Ar-H), 119.83 (d, *J* = 22.7 Hz, Ar-H), 123.85 (d, *J* = 2.9 Hz, Ar-H), 124.4 (Ar-H), 125.0 (Ar-H), 125.51 (d, *J* = 8.1 Hz, Ar-H), 127.9 (Ar-H), 128.52 (d, *J* = 7.3 Hz, Ar-C_q), 128.7 (Ar-C_q), 129.5 (Ar-H), 130.67 (d, *J* = 1.5 Hz, Ar-C_q), 131.9 (Ar-C_q), 134.2 (Ar-C_q), 151.62 (CH), 151.78 (d, *J* = 253.1 Hz, Ar-CF), 156.0 (NH*C*OO), 157.2 (Ar-*C*O-), 165.4 (*C*OOEt), 173.2 (CO). **ESI-MS:** *m/z* calc. for $C_{29}H_{28}ClFN_2O_6$ $[M+H]^+$: 555.17, found: 555.10.

3-Carboxy-8-fluoro-4-oxo-1-((6-(3-(((2-(trimethylammonio)ethoxy)carbonyl)amino)-propoxy)naphthalen-2-yl)methyl)-1,4-dihydroquinolin-1-ium formate 2a

The chloro-compound **20a** (64 mg, 0.12 mmol, 1.0 eq.) was dissolved in acetonitrile (12 mL) and trimethylamine in water (45w%) (10 mL) was added. The mixture was heated to 75 °C for 1 d in a sealed vessel. Volatiles were removed. The residue was dissolved in methanol and lithium hydroxide (17 mg, 6.9 mmol, 6 eq.) in water was added. The mixture was stirred at room temperature until LCMS showed disappearance of the ester. The mixture was neutralized with 2M hydrochloric acid. Volatiles were removed, and the residue was purified by preparative HPLC to give the formate salt of the product as a colorless oil (13 mg, 0.02 mmol, 17 %). **^{1}H-NMR (400 MHz, $CDCl_3$)** δ(ppm) = 2.03 (br. t, J = 5.0 Hz, 2 H, CH_2), 3.17 (s, 9 H, NMe_3), 3.33 – 3.38 (m, 2 H, NH-CH_2), 3.64 (br. s., 2 H, CH_2-NMe_3), 4.11 (br. s., 2 H, O-CH_2), 4.49 (br. s., 2 H, O-CH_2), 5.92 (br. s., 2 H, N-CH_2), 7.10 (d, J = 7.5 Hz, 1 H, Ar), 7.19 (br. s., 1 H, Ar), 7.28 (d, J = 5.0 Hz, 1 H, Ar), 7.51 – 7.62 (m, 3 H, 3xAr), 7.66 (d, J = 7.8 Hz, 1 H, Ar), 7.75 (br. d, J = 5.5 Hz, 1 H, Ar), 8.33 (d, J = 7.0 Hz, 1 H, Ar), 8.40 (s, 2 H, $HCOO^-$), 9.04 (br. s., 1 H, CH). **^{13}C-NMR (100 MHz, $CDCl_3$)** δ(ppm) = 29.1 (CH_2), 37.6 (NH-CH_2), 53.03/53.07/53.10 (NMe_3), 57.8 (O-CH_2), 61.3 (N-CH_2), 65.0 (O-CH_2), 65.12/65.15/65.19 (CH_2-NMe_3), 106.2 (Ar-H), 111.3 (*C*=CH), 119.2 (Ar-H), 121.0 (d, J = 23.5 Hz, Ar-H), 122.5 (d, J = 2.9 Hz, Ar-H), 124.3 (Ar-H), 124.9 (Ar-H), 126.8 (d, J = 8.8 Hz, Ar-H), 127.5 (Ar-H), 128.8 (Ar-C_q), 128.9 (Ar-C_q), 129.1 (Ar-H), 130.7 (d, J = 1.5 Hz, Ar-C_q), 132.3 (Ar-C_q), 134.4 (Ar-C_q), 151.8 (CH), 152.1 (d, J = 254.6 Hz, Ar-CF), 156.1 (NH*C*OO), 157.5 (Ar-*C*O-), 166.9 (*C*OOH), 167.5 ($HCOO^-$), 173.5 (CO). **ESI-MS:** *m/z* calc. for $C_{30}H_{33}FN_3O_6$ $[M+H]^{2+}$: 275.63, found: 275.70.

Synthesis of Target Compound 2b:

Ethyl 1-((6-(5-((*tert*-butoxycarbonyl)amino)pentoxy)naphthalen-2-yl)methyl)-8-fluoro-4-oxo-1,4-dihydroquinoline-3-carboxylate 18b

The iodo-compound **17b** (1.37 g, 2.93 mmol, 1.0 eq.) and the quinolone **14** (689 mg, 2.93 mmol, 1.0 eq.) were dissolved in dimethylformamide (30 mL). Potassium carbonate (850 mg, 6.15 mmol, 2.1 eq.) and a catalytic amount of potassium iodide were added. The mixture was heated to 60°C for 23 h. Water (100 mL) and ethyl acetate (100 mL) were added. The phases were separated, and the inorganic phase was extracted with ethyl acetate. The combined organic phases were washed with water several times, dried over sodium sulfate and the solvent was removed. Purification by column chromatography (petroleum ether : ethyl acetate 1:1 → 1:3) gave the desired product as a white solid (708 mg, 1.25 mmol, 42 %). **^{1}H-NMR (400 MHz, $CDCl_3$)** δ(ppm) = 1.39 (t, J = 7.2 Hz, 3 H, CH_3), 1.42 (s, 9 H, Boc), 1.46 – 1.60 (m, 4 H, 2xCH_2), 1.83 (quin, J = 6.8 Hz, 2 H, CH_2), 3.13 (q, J = 5.8 Hz, 2 H, BocN-CH_2), 4.02 (t, J = 6.5 Hz, 2 H, O-CH_2), 4.39 (q, J = 7.1 Hz, 2 H, *CH_2*-CH_3), 5.62 (d, J = 2.0 Hz, 2 H, N-CH_2), 7.06 (d, J = 2.5 Hz, 1 H, Ar), 7.11 (dd, J = 9.0, 2.5 Hz, 1 H, Ar), 7.17 – 7.37 (m, 3 H, 3xAr), 7.42 (br. s, 1 H, Ar), 7.60 (d, J = 9.0 Hz, 1 H, Ar), 7.67 (d, J = 8.8 Hz, 1 H, Ar), 8.31 – 8.36 (m, 1 H, Ar), 8.56 (s, 1 H, CH). **^{13}C-NMR (100 MHz, $CDCl_3$)** δ(ppm) = 14.4 (CH_3), 23.4 (CH_2), 28.4 (Boc-CH_3), 28.8 (CH_2), 29.9 (CH_2), 40.5 (BocN-*CH_2*), 60.90/61.05 (N-CH_2), 61.09 (O-CH_2), 67.8 (*CH_2*-CH_3), 79.1 (Boc-C_q), 106.5 (Ar-H), 111.3 (*C*=CH), 119.80 (Ar-H), 119.81 (d, J = 22.7 Hz, Ar-H), 123.82 (d, J = 3.7 Hz, Ar-H), 124.3 (Ar-H), 125.0 (Ar-H), 125.48 (d, J = 8.8 Hz, Ar-H), 127.8 (Ar-H), 128.48 (Ar-C_q), 128.51 (d, J = 11 Hz, Ar-C_q), 129.3 (Ar-H), 130.47 (d, J = 1.5 Hz, Ar-C_q), 131.9 (Ar-C_q), 134.3 (Ar-C_q), 151.62 (CH), 151.86 (d, J = 250.2 Hz, Ar-CF), 156.0 (Ar-*C*O-), 157.6 (Boc-*C*OO), 165.4 (*C*OOEt), 173.2 (CO). **ESI-MS:** *m/z* calc. for $C_{33}H_{37}FN_2O_6$ $[M+Na]^+$: 599.25, found: 599.25.

Ethyl 1-((6-((5-aminopentyl)oxy)naphthalen-2-yl)methyl)-8-fluoro-4-oxo-1,4-dihydroquinoline-3-carboxylate 19b

The Boc-protected amine **18b** (586 mg, 1.0 mmol, 1.0 eq.) was dissolved in dichloromethane (25 mL) and trifluoro acetic acid (1.0 mL, 10 mmol, 10 eq.) was added. The mixture was stirred at room temperature for 4 h. Water was added, and the phases were separated. The inorganic phase was basified to pH ≥ 13 and extracted with ethyl acetate several times. The combined organic phases were washed with brine and dried over sodium sulfate. Removal of the solvent gave the desired product as a colorless oil (215 mg, 0.45 mmol, 45 %). **^{1}H-NMR (400 MHz, $CDCl_3$)** δ(ppm) = 1.34 (t, J = 7.2 Hz, 3 H, CH_3), 1.43 – 1.52 (m, 4 H, 2xCH_2), 1.75 – 1.84 (m, 2 H, CH_2), 2.61 – 2.69 (m, 1 H, NH_2-*CH_2*), 3.95 – 4.01 (m, 2 H, O-CH_2), 4.33 (q, J = 7.0 Hz, 2 H, *CH_2*CH_3), 5.57 (d, J = 2.3 Hz, 2 H, N-CH_2), 7.01 (d, J = 2.5 Hz, 1 H, Ar), 7.06 (dd, J = 8.9, 2.4 Hz, 1 H, Ar), 7.14 (dd, J = 8.5, 1.5 Hz, 1 H, Ar), 7.16 – 7.26 (m, 2 H, 2xAr), 7.36 (br. s, 1 H, Ar), 7.55 (dd, J = 9.0, 1.8 Hz, 1 H, Ar), 7.61 (d, J = 8.5 Hz, 1 H, Ar), 8.26 – 8.30 (m, 1 H, Ar), 8.51 (s, 1 H, CH). **^{13}C-NMR (100 MHz, $CDCl_3$)** δ(ppm) = 14.4 (CH_3), 23.5 (CH_2), 29.1 (CH_2), 33.6 (CH_2), 42.2 (NH_2-*CH_2*), 60.9 (N-CH_2), 61.1 (*CH_2*CH_3), 67.9 (O-CH_2), 106.5 (Ar-H), 111.4 (*C*=CH), 119.82 (d, J = 22.7 Hz, Ar-H), 119.84 (Ar-H), 123.9 (d, J = 2.9 Hz, Ar-H), 124.3 (Ar-H), 125.0 (Ar-H), 125.5 (d, J = 8.1 Hz, Ar-H), 127.8 (Ar-H), 128.52 (d, J = 4.4 Hz, Ar-C_q), 128.56 (Ar-C_q), 129.3 (Ar-H), 130.4 (d, J = 1.5 Hz, Ar-C_q), 131.9 (Ar-C_q), 134.3 (Ar-C_q), 151.62 (CH), 151.88 (d, J = 250.9 Hz, Ar-CF), 157.6 (Ar-*C*O-), 165.4 (*C*OOEt), 173.2 (CO). **ESI-MS:** *m/z* calc. for $C_{28}H_{29}FN_2O_6$ $[M+H]^+$: 476.21, found: 476.55.

Ethyl 1-((6-((5-(((2-chloroethoxy)carbonyl)amino)pentyl)oxy)naphthalen-2-yl)methyl)-8-fluoro-4-oxo-1,4-dihydroquinoline-3-carboxylate 20b

The amine **19b** (215 mg, 0.45 mmol, 1.0 eq.) was dissolved in dichloromethane (20 mL). Pyridine (55 µL, 0.68 mmol, 1.5 eq.) and 2-chloroethyl chloroformate (56 µL, 0.54 mmol, 1.2 eq.) were added. The mixture was stirred at room temperature for 30 min. Saturated ammonium chloride solution was added and the mixture extracted with dichloromethane. The organic phases were dried over sodium sulfate and the solvent was removed. Purification by column chromatography (ethyl acetate 5:1 petroleum ether; on deactivated silica) gave the desired product as a colorless oil (202 mg, 0.35 mmol, 78 %). **^{1}H-NMR (400 MHz, $CDCl_3$)** δ(ppm) = 1.32 (t, J = 7.2 Hz, 3 H, CH_3), 1.38 – 1.55 (m, 4 H, 2xCH_2), 1.75 (quin, J = 6.8 Hz, 2 H, CH_2), 3.13 (q, J = 6.5 Hz, 2 H, NH-*CH_2*), 3.56 (t, J = 5.6 Hz, 2 H, CH_2-Cl), 3.94 (t, J = 6.4 Hz, 2 H, O-CH_2), 4.20 (t, J = 5.6 Hz, 2 H, O-CH_2), 4.31 (q, J = 7.3 Hz, 2 H, *CH_2*-CH_3), 4.94 (br. s., 1 H, NH), 5.54 (d, J = 2.0 Hz, 2 H, N-CH_2), 6.98 (d, J = 2.3 Hz, 1 H, Ar), 7.03 (dd, J = 9.0, 2.5 Hz, 1 H, Ar), 7.10 – 7.24 (m, 3 H, 3xAr), 7.34 (br. s, 1 H, Ar), 7.53 (d, J = 9.0 Hz, 1 H, Ar), 7.59 (d, J = 8.5 Hz, 1 H, Ar), 8.23 – 8.28 (m, 1 H, Ar), 8.49 (s, 1 H, CH). **^{13}C-NMR (100 MHz, $CDCl_3$)** δ(ppm) = 14.4 (CH_3), 23.3 (CH_2), 28.8 (CH_2), 29.7 (CH_2), 40.9 (NH-CH_2), 42.3 (CH_2-Cl), 60.87/61.03 (N-CH_2), 61.07 (*CH_2*-CH_3), 64.4 (O-CH_2), 67.7 (O-CH_2), 106.5 (Ar-H), 111.3 (*C*=CH), 119.78 (Ar-H), 119.81 (d, J = 22.7 Hz, Ar-H), 123.79 (d, J = 2.9 Hz, Ar-H), 124.3 (Ar-H), 125.0 (Ar-H), 125.48 (d, J = 8.1 Hz, Ar-H), 127.8 (Ar-H), 128.52 (d, J = 8.8 Hz, Ar-C_q), 128.6 (Ar-C_q), 129.4 (Ar-H), 130.52 (d, J = 1.5 Hz, Ar-C_q), 131.9 (Ar-C_q), 134.3 (Ar-C_q), 151.62 (CH), 151.85 (d, J = 251.6 Hz, Ar-CF), 156.0 (NH*C*OO), 157.5 (Ar-*C*O-), 165.4 (*C*OOEt), 173.2 (CO). **ESI-MS:** *m/z* calc. for $C_{31}H_{32}ClFN_2O_6$ $[M+H]^+$: 583.20, found: 583.10.

2-(((5-((6-((3-Carboxy-8-fluoro-4-oxoquinolin-1(4*H*)-yl)methyl)naphthalen-2-yl)oxy)pentyl)carbamoyl)oxy)-*N,N,N*-trimethylethan-1-aminium formate 2b

The chloro-compound **20b** (100 mg, 0.17 mmol, 1.0 eq.) was dissolved in acetonitrile (15 mL) and trimethylamine in water (45w%)(10 mL) was added. The mixture was heated to 80 °C for 1 d in a sealed vessel. Volatiles were removed. The residue was suspended in methanol and lithium hydroxide was added to adjust the pH ≥ 12. The mixture was stirred at room temperature until LCMS showed disappearance of the ester. To neutralize the mixture 2M hydrochloric acid was added. Volatiles were removed, and the residue was purified by reversed phase column chromatography to give the formate salt of the product as a colorless oil (15 mg, 0.024 mmol, 14%). **^{1}H-NMR (400 MHz, $CDCl_3$)** δ(ppm) = 1.52 – 1.62 (m, 4 H, 2xCH_2), 1.82 (quin, *J* = 6.7 Hz, 2 H, CH_2), 3.15 (t, *J* = 6.8 Hz, 2 H, NH-*CH_2*), 3.20 (m, 9 H, NMe_3), 3.64 – 3.69 (m, 2 H, *CH_2*-NMe_3), 4.06 (t, *J* = 6.3 Hz, 2 H, O-CH_2), 4.46 – 4.53 (m, 2 H, O-CH_2), 5.92 (br. s., 2 H, N-CH_2), 7.09 (dd, *J* = 8.8, 2.0 Hz, 1 H, Ar), 7.15 – 7.20 (m, 1 H, Ar), 7.27 (br. d., 1 H, Ar), 7.50 – 7.63 (m, 3 H, 3xAr), 7.65 (d, *J* = 9.0 Hz, 1 H, Ar), 7.75 (d, *J* = 8.3 Hz, 1 H, Ar), 8.30 – 8.36 (m, 1 H, Ar), 9.05 (s, 1 H, CH). **^{13}C-NMR (100 MHz, $CDCl_3$)** δ(ppm) = 23.1 (CH_2), 28.6 (CH_2), 29.2 (CH_2), 40.4 (NH-CH_2), 53.08/53.12/53.16 (NMe_3), 57.7 (O-CH_2), 61.16/61.32 (N-CH_2), 65.15/65.18/65.21 (CH_2-NMe_3), 67.5 (O-CH_2), 106.1 (Ar-H), 107.9 (*C*=CH), 119.3 (Ar-H), 121.02 (d, *J* = 22.7 Hz, Ar-H), 122.45 (d, J = 3.7 Hz, Ar-H), 124.2 (Ar-H), 124.9 (Ar-H), 126.86 (d, *J* = 8.8 Hz, Ar-H), 127.5 (Ar-H), 128.7 (Ar-C_q), 128.95 (d, *J* = 8.8 Hz, Ar-C_q), 129.0 (Ar-H), 130.5 (Ar-C_q), 130.58 (d, *J* = 2.2 Hz, Ar-C_q), 134.5 (Ar-C_q), 151.8 (CH), 152.25 (d, *J* = 250.2 Hz, Ar-CF), 156.0 (NH*C*OO), 157.6 (Ar-*C*O-), 167.5 (*C*OOEt), 177.7 (CO). **ESI-MS:** *m/z* calc. for $C_{32}H_{37}FN_3O_6$ $[M+H]^{2+}$: 289.64, found: 289.75. *m/z* calc. for $C_{32}H_{37}FN_3O_6$ $[M+]^{+}$: 578.27, found: 578.20.

Synthesis of Target Compound 2c:

Ethyl 1-((6-((8-((*tert*-butoxycarbonyl)amino)octyl)oxy)naphthalen-2-yl)methyl)-8-fluoro-4-oxo-1,4-dihydroquinoline-3-carboxylate 18c

The quinolone **14** (726 mg, 3.09 mmol, 1.0 eq.) and the iodo-compound **17c** (1.58 g, 3.09 mmol, 1.0 eq.) were dissolved in dimethylformamide (30 mL). Potassium carbonate (854 mg, 6.18 mmol, 2.0 eq.) and a catalytic amount of potassium iodide were added. The mixture was heated to 60°C for 24 h. The mixture was concentrated, diluted with water and extracted with ethyl acetate. The organic phases were washed with water several times, washed with brine, dried over sodium sulfate and the solvent was removed. Purification by column chromatography (petroleum ether : ethyl acetate 1:1 → 1:3) gave the desired product as an oily white solid (803 mg, 1.30 mmol, 42 %). **^{1}H-NMR (400 MHz, $CDCl_3$)** δ(ppm) = 1.26 – 1.37 (m, 8 H, 4xCH_2), 1.38 – 1.51 (m, 4 H, 2xCH_2), 1.39 (t, J = 7.5 Hz, 3 H, CH_3), 1.43 (s, 9 H, Boc), 1.81 (quin, J = 7.0 Hz, 2 H, CH_2), 3.09 (q, J = 6.0 Hz, 2 H, BocNH-*CH_2*), 4.02 (t, J = 6.4 Hz, 2 H, -O-CH_2), 4.40 (q, J = 6.8 Hz, 2 H, *CH_2*-CH_3), 5.63 (br. s., 2 H, N-CH_2), 7.07 (br. s, 1 H, Ar), 7.12 (br. d, J = 8.8 Hz, 1 H, Ar), 7.18 – 7.33 (m, 3 H, 3xAr), 7.43 (br. s, 1 H, Ar), 7.61 (d, J = 8.8 Hz, 1 H, Ar), 7.68 (d, J = 8.3 Hz, 1 H, Ar), 8.34 (d, J = 7.5 Hz, 1 H, Ar), 8.57 (s, 1 H, CH). **^{13}C-NMR (100 MHz, $CDCl_3$)** δ(ppm) = 14.4 (CH_3), 26.0 (CH_2), 26.7 (CH_2), 28.4 (Boc-CH_3), 29.1 (CH_2), 29.2 (CH_2), 29.3 (CH_2), 30.1 (CH_2), 40.6 (BocNH-*CH_2*), 60.91/61.06 (N-CH_2), 61.09 (*CH_2*-CH_3), 68.0 (O-CH_2), 79.0 (Boc-C_q), 106.5 (Ar-H), 111.3 (*C*=CH), 119.80 (d, J = 22.7 Hz, Ar-H), 119.87 (Ar-H), 123.84 (d, J = 2.9 Hz, Ar-H), 124.2 (Ar-H), 125.00 (d, J = 1.5 Hz, Ar-H), 125.47 (d, J = 8.1 Hz, Ar-H), 127.8 (Ar-H), 128.53 (d, J = 7.3 Hz, Ar-C_q), 128.54 (Ar-C_q), 129.3 (Ar-H), 130.4 (Ar-C_q), 131.9 (Ar-C_q), 134.3 (Ar-C_q), 151.62 (CH), 151.88 (d, J = 249.4 Hz, Ar-CF), 156.0 (Boc-*C*OO), 157.7 (Ar-*C*O-), 165.4 (*C*OOEt), 173.2 (CO). **ESI-MS:** *m/z* calc. for $C_{36}H_{33}FN_2O_6$ $[M+Na]^+$: 641.30, found: 641.30.

Ethyl 1-((6-((8-aminooctyl)oxy)naphthalen-2-yl)methyl)-8-fluoro-4-oxo-1,4-dihydroquinoline-3-carboxylate 19c

The Boc-protected amine **18c** (762 mg, 1.23 mmol, 1.0 eq.) was dissolved in dioxane/ethyl acetate (1:1)(30 mL) and 4M hydrochloric acid (43 mL, 120 mmol, 100 eq.) was added. The mixture was stirred at room temperature for 4 h. Volatiles were removed, and the residue dissolved in dichloromethane and water. The phases were separated. The inorganic phase was basified to pH ≥ 13 and extracted with dichloromethane several times. The combined organic phases were dried over sodium sulfate. Removal of the solvent gave the desired product as a brown oil (250 mg, 0.44 mmol, 36 %). **^{1}H-NMR (400 MHz, $CDCl_3$)** δ(ppm) = 1.29 – 1.52 (m, 8 H, 4xCH_2), 1.41 (t, 3 H, CH_3), 1.77 – 1.87 (m, 4 H, 2xCH_2), 2.67 (t, J = 6.9 Hz, 2 H, NH_2-*CH_2*), 4.04 (t, J = 6.5 Hz, 2 H, O-CH_2), 4.41 (q, J = 7.2 Hz, 2 H, *CH_2*-CH_3), 5.64 (d, J =

2.0 Hz, 2 H, N-CH_2), 7.08 (d, *J* = 2.5 Hz, 1 H, Ar), 7.13 (dd, *J* = 8.8, 2.5 Hz, 1 H, Ar), 7.19 – 7.34 (m, 3 H, 3xAr), 7.44 (br. s, 1 H, Ar), 7.62 (d, *J* = 9.0 Hz, 1 H, Ar), 7.69 (d, *J* = 8.5 Hz, 2 H, 2xAr), 8.34 – 8.37 (m, 1 H, Ar), 8.58 (s, 1 H, CH). **^{13}C-NMR (100 MHz, $CDCl_3$)** *δ*(ppm) = 14.4 (CH_3), 26.0 (CH_2), 26.8 (CH_2), 29.1 (CH_2), 29.3 (CH_2), 33.4 (CH_2), 42.1 (CH_2), 51.5 (NH_2-CH_2), 60.84/61.00 (N-CH_2), 61.02 (*CH_2*-CH_3), 68.03 (O-CH_2), 105.4 (Ar-H), 110.2 (*C*=CH), 118.78 (d, *J* = 22.7 Hz, Ar-H), 118.81 (Ar-H), 122.74 (d, *J* = 2.9 Hz, Ar-H), 123.2 (Ar-H), 123.9 (Ar-H), 124.2 (d, *J* = 8.1 Hz, Ar-H), 126.8 (Ar-H), 127.48 (d, *J* = 6.6 Hz, Ar-C_q), 127.49 (Ar-C_q), 128.3 (Ar-H), 129.4 (Ar-C_q), 130.8 (Ar-C_q), 133.3 (Ar-C_q), 150.58 (CH), 150.74 (d, *J* = 251.6 Hz, Ar-CF), 156.6 (Ar-*C*O-), 164.3 (*C*OOEt), 172.1 (CO). **ESI-MS:** *m/z* calc. for $C_{31}H_{35}FN_2O_4$ $[M+H]^+$: 519.27, found: 519.15.

Ethyl 1-((6-((8-(((2-chloroethoxy)carbonyl)amino)octyl)oxy)naphthalen-2-yl)methyl)-8-fluoro-4-oxo-1,4-dihydroquinoline-3-carboxylate 20c

The amine **19c** (125 mg, 0.22 mmol, 1.0 eq.) was dissolved in dichloromethane (20 mL). Pyridine (27 µL, 0.33 mmol, 1.5 eq.) and 2-chloroethyl chloroformate (27 µL, 0.26 mmol, 1.2 eq.) were added. The mixture was stirred at room temperature for 1 h. Saturated ammonium chloride solution was added, and the mixture extracted with dichloromethane. The organic phases were dried over sodium sulfate and the solvent was removed. Column chromatography (ethyl acetate 5:1 petroleum ether) gave the desired product as a colorless oil (40 mg, 0.064 mmol, 29 %). **^{1}H-NMR (400 MHz, $CDCl_3$)** *δ*(ppm) = 1.29 – 1.38 (m, 8 H, 4xCH_2), 1.41 (t, *J* = 7.2 Hz, 3 H, CH_3), 1.44 – 1.54 (m, 4 H, 2xCH_2), 1.77 – 1.86 (m, 2 H, CH_2), 3.17 (q, *J* = 6.6 Hz, 2 H, CH_2), 3.66 (t, *J* = 5.6 Hz, 2 H, CH_2-Cl), 4.03 (t, *J* = 6.5 Hz, 2 H, -O-CH_2), 4.29 (t, *J* = 5.6 Hz, 2 H, -O-CH_2), 4.41 (q, *J* = 7.0 Hz, 2 H, *CH_2*-CH_3), 5.65 (d, *J* = 2.0 Hz, 2 H, N-CH_2), 7.08 (d, *J* = 2.5 Hz, 1 H, Ar), 7.13 (dd, *J* = 8.8, 2.5 Hz, 1 H, Ar), 7.21 (dd, *J* = 8.5, 1.5 Hz, 1 H, Ar), 7.23 – 7.35 (m, 2 H, 2xAr), 7.44 (br. s, 1 H, Ar), 7.63 (d, *J* = 9.0 Hz, 1 H, Ar), 7.69 (d, *J* = 8.8 Hz, 1 H, Ar), 8.34 – 8.37 (m, 1 H, Ar), 8.58 (s, 1 H, CH). **^{13}C-NMR (100 MHz, $CDCl_3$)** *δ*(ppm) = 14.4 (CH_3), 26.0 (CH_2), 26.6 (CH_2), 29.1 (CH_2), 29.2 (CH_2), 29.3 (CH_2), 29.9 (CH_2), 41.1 (CH_2), 42.4 (CH_2-Cl), 60.94/61.10 (N-CH_2), 61.13 (*CH_2*-CH_3), 64.4 (-O-CH_2), 68.0 (-O-CH_2), 106.5 (Ar-H), 111.4 (*C*=CH), 119.84 (d, *J* = 23.5 Hz, Ar-H), 119.88 (Ar-H), 123.88 (d, J = 2.9 Hz, Ar-H), 124.3 (Ar-H), 125.01 (d, J = 1.5 Hz, Ar-H), 125.50 (d, J = 8.8 Hz, Ar-H), 127.8 (Ar-H), 128.55 (Ar-C_q), 128.57 (d, J = 2.2 Hz, Ar-C_q), 129.3 (Ar-H), 130.38 (d, J = 1.5 Hz, Ar-C_q), 132.0 (Ar-C_q), 134.4 (Ar-C_q), 151.64 (CH), 151.81 (d, J = 247.2 Hz, Ar-CF), 155.9 (NH*C*OO), 157.7 (Ar-*C*O-), 165.5 (*C*OOEt), 173.2 (CO). **ESI-MS:** *m/z* calc. for $C_{34}H_{38}ClFN_2O_6$ $[M+H]^+$: 625.25, found: 625.15.

3-Carboxy-8-fluoro-4-oxo-1-((6-((8-(((2-(trimethylammonio)ethoxy)carbonyl)amino)-octyl)oxy)naphthalen-2-yl)methyl)-1,4-dihydroquinolin-1-ium formate 2c

The chloro-compound **20c** (46 mg, 0.074 mmol, 1.0 eq.) was dissolved in acetonitrile (12 mL) and trimethylamine in water (45%)(10 mL) was added. The mixture was heated to 75 °C for 1 d in a sealed vessel. Volatiles were removed. The residue was dissolved in methanol and lithium hydroxide (10 mg, 0.44 mmol, 6 eq.) in water was added. The mixture was stirred at room temperature until LCMS showed disappearance of the ester. To neutralize the mixture 2M hydrochloric acid was added. Volatiles were removed, and the residue was purified by preparative HPLC to give the formate salt of the product as a colorless oil (10 mg, 0.014 mmol, 19 %). **^{1}H-NMR (400 MHz, $CDCl_3$)** δ(ppm) = 1.33 – 1.41 (m, 6 H, 3xCH_2), 1.47 – 1.53 (m, 4 H, 2xCH_2), 1.77 – 1.85 (m, 2 H, CH_2), 3.10 (t, *J* = 7.0 Hz, 2 H, N-CH_2), 3.19 (s, 9 H, NMe_3), 3.63 – 3.68 (m, 2 H, *CH_2*-NMe_3), 4.05 (t, *J* = 6.3 Hz, 2 H, O-CH_2), 4.46 – 4.52 (m, 2 H, O-CH_2), 5.93 (br. s., 2 H, N-CH_2), 7.09 (dd, *J* = 9.0, 2.3 Hz, 1 H, Ar), 7.18 (d, *J* = 2.0 Hz, 1 H, Ar), 7.28 (d, *J* = 8.3 Hz, 1 H, Ar), 7.51 – 7.61 (m, 3 H, 3xAr), 7.66 (d, *J* = 9.0 Hz, 1 H, Ar), 7.75 (d, *J* = 8.3 Hz, 1 H, Ar), 8.34 (dd, *J* = 7.0, 2.3 Hz, 1 H, Ar), 8.38 (s, 1 H, $HCOO^-$), 9.06 (s, 1 H, CH). **^{13}C-NMR (100 MHz, $CDCl_3$)** δ(ppm) = 25.7 (CH_2), 26.4 (CH_2), 28.9 (2xCH_2), 29.0 (CH_2), 29.4 (CH_2), 40.5 (N-CH_2), 53.04/53.07/53.11 (NMe_3), 57.7 (O-CH_2), 61.15/61.30 (N-CH_2), 65.15/65.19/65.21 (*CH_2*-NMe_3), 67.6 (O-CH_2), 106.1 (Ar-H), 113.1 (*C*=CH), 119.3 (Ar-H), 121.00 (d, J = 23.5 Hz, Ar-H), 122.47 (d, J = 2.9 Hz, Ar-H), 124.2 (Ar-H), 124.9 (Ar-H), 126.82 (d, J = 8.8 Hz, Ar-H), 127.5 (Ar-H), 128.7 (Ar-C_q), 129.0 (Ar-H, Ar-C_q), 130.6 (Ar-C_q), 134.0 (Ar-C_q), 134.5 (Ar-C_q), 152.12 (d, J = 251.6 Hz, Ar-CF), 151.8 (CH), 156.0 (NH*C*OO), 157.7 (Ar-*C*O-), 166.7 ($HCOO^-$), 167.6 (COOH), 177.7 (CO). **ESI-MS:** *m/z* calc. for $C_{35}H_{43}FN_3O_6$ $[M+H]^{2+}$: 310.80, found: 310.66. *m/z* calc. for $C_{35}H_{43}FN_3O_6$ $[M+]^+$: 620.31, found: 620.30.

Synthesis of Reference Compounds 21 and 35

Syntheses of Reference Compounds 21:

General Procedure A: The amine **3** (1.0 eq.) and the alkyl halide (1.0 eq.) were dissolved in dimethylformamide. Potassium carbonate (2.0 eq.) and potassium iodide (0.01 eq.) were added. The reaction mixture was heated to 60 °C overnight. The mixture was diluted with ethyl acetate and water. The phases were separated, and the inorganic phase was extracted with ethyl acetate. The combined organic phases were washed with water several times, dried over sodium sulfate and the solvent was removed. Purification by column chromatography yielded the desired product.

1-(1-Propylpiperidin-4-yl)-1,3-dihydro-2*H*-benzo[*d*]imidazol-2-one 21a

According to general procedure **A** amine **3** (149 mg, 0.69 mmol, 1.0 eq.), 1-bromopropane (84.9 mg, 0.69 mmol, 1.0 eq.), potassium carbonate (191 mg, 1.38 mmol, 2.0 eq), potassium iodide (1.15 mg, 6.9 μmol, 0.01 eq.) and dimethylformamide (10 mL) were used. Purification by column chromatography (dichloromethane 10:1 methanol on deactivated silica) gave the desired product as a colorless oil (130 mg, 0.50 mmol, 73%). **^{1}H-NMR (400 MHz, $CDCl_3$)** δ(ppm) = 0.92 (t, J = 7.3 Hz, 3 H, CH_3), 1.50 – 1.62 (m, 2 H, CH_2), 1.77 – 1.87 (m, 2 H, *CH_2*-CH), 2.10 – 2.19 (m, 2 H, *CH_2*-CH), 2.34 – 2.41 (m, 2 H, CH_2-N), 2.51 (qd, J = 12.5, 3.9 Hz, 2 H, CH_2-N), 3.12 (d, J = 11.8 Hz, 2 H, CH_2-N), 4.39 (tt, J = 12.5, 4.3 Hz, 1 H, CH), 6.99 (quind, J = 7.5, 1.5 Hz, 2 H, Ar), 7.09 – 7.14 (m, 1 H, Ar), 7.24 – 7.29 (m, 1 H, Ar), 10.98 (br. s., 1 H, NH). **^{13}C-NMR (100 MHz, $CDCl_3$)** δ(ppm) = 12.0 (CH_3), 20.2 (CH_2), 29.2 (2x CH-*CH_2*), 50.8 (CH), 53.3 (2xN-CH_2), 60.5 (N-CH_2), 109.8 (2xAr-H), 120.9 (Ar-H), 121.1 (Ar-H), 128.4 (Ar-C_q), 129.1 (Ar-C_q), 155.5 (CO). **ESI-MS:** *m/z* calc. for $C_{15}H_{21}N_3O$ $[M+H]^+$: 260.18, found: 260.15.

1-(1-Pentylpiperidin-4-yl)-1,3-dihydro-2*H*-benzo[*d*]imidazol-2-one 21b

According to general procedure **A** amine **3** (159 mg, 0.73 mmol, 1.0 eq.), 1-bromopentane (110 mg, 0.73 mmol, 1.0 eq.), potassium carbonate (202 mg, 1.46 mmol, 2.0 eq.), potassium iodide (1.21 mg, 7.3 μmol, 0.01 eq.) and dimethylformamide (10 mL) were used. Purification by column chromatography (dichloromethane 15:1 methanol on deactivated silica) gave the desired product as a white solid (100 mg, 0.35 mmol, 48%). **^{1}H-NMR (400 MHz, $CDCl_3$)** δ(ppm) = 0.92 (t, J = 7.3 Hz, 3 H, CH_3), 1.27 – 1.40 (m, 4 H, 2xCH_2), 1.56 (dt, J = 15.1, 7.5 Hz, 2 H, CH_2), 1.80 – 1.89 (m, 2 H, *CH_2*-CH), 2.11 – 2.22 (m, 2 H, *CH_2*-CH), 2.38 – 2.46 (m, 2 H, CH_2-N), 2.53 (qd, J = 12.5, 3.8 Hz, 2 H, CH_2-N), 3.15 (br. d, J = 11.8 Hz, 2 H, CH_2-N), 4.42 (tt, J = 12.5, 4.2 Hz, 1 H, CH), 7.02 (quind, J = 7.3, 1.4 Hz, 2 H, 2xAr-H), 7.11 – 7.16 (m, 1 H, Ar-H), 7.26 – 7.31 (m, 1 H, Ar-H), 11.01 (br. s., 1 H, NH). **^{13}C-NMR (100 MHz, $CDCl_3$)** δ(ppm) = 14.7 (CH_3), 22.6 (CH_2), 26.8 (2x CH-*CH_2*), 29.2 (CH_2), 29.9 (CH_2), 50.8 (CH), 53.3 (2xN-CH_2), 58.7 (N-CH_2), 109.8 (2xAr-H), 120.9 (Ar-H), 121.1 (Ar-H), 128.4 (Ar-C_q), 129.1 (Ar-C_q), 155.5 (CO). **ESI-MS:** *m/z* calc. for $C_{17}H_{25}N_3O$ $[M+H]^+$: 288.21, found: 288.15.

1-(1-Octylpiperidin-4-yl)-1,3-dihydro-2*H*-benzo[*d*]imidazol-2-one 21c

According to general procedure **A** amine **3** (180 mg, 0.83 mmol, 1.0 eq.), 1-bromooctane (160 mg, 0.83 mmol, 1.0 eq.), potassium carbonate (229 mg, 1.66 mmol, 2.0 eq.), potassium iodide (1.38 mg, 8.3 μmol, 0.01 eq.) and dimethylformamide (10 mL) were used. Purification by column chromatography (dichloromethane 15:1 methanol on deactivated silica) gave the desired product as a white solid (134 mg, 0.41 mmol, 50%). **^{1}H-NMR (400 MHz, $CDCl_3$)** δ(ppm) = 0.87 (t, J = 7.0 Hz, 3 H, CH_3), 1.20 – 1.36 (m, 10 H, 5xCH_2), 1.48 – 1.59 (m, 2 H. CH_2), 1.82

(dd, *J* = 11.9, 2.1 Hz, 2 H, *CH*$_2$-CH), 2.14 (t, *J* = 11.3 Hz, 2 H, *CH*$_2$-CH), 2.35 – 2.44 (m, 2 H, CH$_2$-N), 2.51 (qd, *J* = 12.4, 3.4 Hz, 2 H, CH$_2$-N), 3.12 (br. d, *J* = 11.5 Hz, 2 H, CH$_2$-N), 4.40 (tt, *J* = 12.5, 4.2 Hz, 1 H, CH), 6.99 (quind, *J* = 7.3, 1.4 Hz, 2 H, 2xAr-H), 7.09 – 7.14 (m, 1 H, Ar-H), 7.24 – 7.29 (m, 1 H, Ar-H), 11.01 (br. s., 1 H, NH). **^{13}C-NMR (100 MHz, CDCl$_3$)** δ(ppm) = 14.1 (CH$_3$), 22.7 (CH$_2$), 27.1 (CH-*CH*$_2$), 27.7 (CH-*CH*$_2$), 29.2 (2xCH$_2$), 29.9 (2xCH$_2$), 31.6 (CH$_2$), 50.8 (CH), 53.3 (2xN-CH$_2$), 58.7 (N-CH$_2$), 109.8 (2xAr-H), 120.8 (Ar-H), 121.1 (Ar-H), 128.4 (Ar-C$_q$), 129.1 (Ar-C$_q$), 155.5 (CO). **ESI-MS:** *m/z* calc. for $C_{20}H_{31}N_3O$ $[M+H]^+$: 330.25, found: 330.30.

Syntheses of Reference Compounds 25:

General Procedure B: The alcohol **15** (1.0 eq.), the alkyl halide (1.3 - 1.5 eq.) and sodium hydroxide (1.5 eq.) were dissolved in a mixture of acetonitrile and water (3:1). The mixture was heated to 70 °C overnight. The mixture was diluted with water and extracted with ethyl acetate. The organic phases were washed with brine, dried over sodium sulfate and the solvent was removed. Purification by column chromatography yielded the desired product.

(6-Propoxynaphthalen-2-yl)methanol 22a

According to general procedure **B** alcohol **15** (505 mg, 2.9 mmol, 1.0 eq.), 1-bromopropane (396 µL, 535 mg, 4.35 mmol, 1.5 eq.), sodium hydroxide (174 mg, 4.35 mmol, 1.5 eq.) and acetonitrile/water (3:1)(20 mL) were used. Purification by column chromatography (petroleum ether 2:1 ethyl acetate) gave the desired product as a white solid (550 mg, 2.5 mmol, 87%). **^{1}H-NMR (400 MHz, $CDCl_3$)** δ(ppm) = 1.10 (t, J = 7.4 Hz, 3 H, CH_3), 1.83 – 1.94 (m, 2 H, CH_2), 4.04 (t, J = 6.7 Hz, 2 H, CH_2), 4.78 (s, 2 H, CH_2-OH), 7.11 – 7.19 (m, 2 H, 2xAr), 7.42 (dd, J = 8.4, 1.9 Hz, 1 H, Ar), 7.67 – 7.72 (m, 3 H, 3xAr). **^{13}C-NMR (100 MHz, $CDCl_3$)** δ(ppm) = 10.6 (CH_3), 22.6 (CH_2), 65.5 (CH_2-OH), 69.6 (CH_2), 106.6 (Ar-H), 119.3 (Ar-H), 125.6 (Ar-H), 125.8 (Ar-H), 127.2 (Ar-H), 128.7 (Ar-C_q), 129.3 (Ar-H), 134.2 (Ar-C_q), 136.0 (Ar-C_q), 157.3 (Ar-*C*O-).

(6-(Pentyloxy)naphthalen-2-yl)methanol 22b

According to general procedure **B** alcohol **15** (505 mg, 2.9 mmol, 1.0 eq.), 1-bromopentane (539 µL, 657 mg, 4.35 mmol, 1.5 eq.), sodium hydroxide (174 mg, 4.35 mmol, 1.5 eq.) and acetonitrile/water (3:1)(20 mL) were used. Purification by column chromatography (petroleum ether 2:1 ethyl acetate) gave the desired product as a white solid (550 mg, 2.25 mmol, 78%). **^{1}H-NMR (400 MHz, $CDCl_3$)** δ(ppm) = 0.99 (t, J = 7.0 Hz, 3 H, CH_3), 1.38 – 1.56 (m, 4 H, 2xCH_2), 1.82 – 1.92 (m, 2 H, CH_2), 4.06 (t, J = 6.7 Hz, 2 H, CH_2), 4.75 (s, 2 H, CH_2-OH), 7.10 – 7.19 (m, 2 H, 2xAr), 7.41 (dd, J = 8.5, 1.8 Hz, 1 H, Ar), 7.64 – 7.72 (m, 3 H, 3xAr). **^{13}C-NMR (100 MHz, $CDCl_3$)** δ(ppm) = 14.1 (CH_3), 22.6 (CH_2), 28.3 (CH_2), 29.0 (CH_2), 65.4 (CH_2-OH), 68.1 (CH_2), 106.6 (Ar-H), 119.3 (Ar-H), 125.6 (Ar-H), 125.9 (Ar-H), 127.1 (Ar-H), 128.7 (Ar-C_q), 129.3 (Ar-H), 134.2 (Ar-C_q), 136.0 (Ar-C_q), 157.3 (Ar-*C*O-).

(6-(Octyloxy)naphthalen-2-yl)methanol 22c

According to general procedure **B** alcohol **15** (505 mg, 2.9 mmol, 1.0 eq.), 1-bromooctane (757 µL, 840 mg, 4.35 mmol, 1.5 eq.), sodium hydroxide (174 mg, 4.35 mmol, 1.5 eq.) and acetonitrile/water (3:1)(20 mL) were used. Purification by column chromatography (petroleum ether 2:1 ethyl acetate) gave the desired product as a white solid (580 mg, 2.02 mmol, 69%). **^{1}H-NMR (400 MHz, $CDCl_3$)** δ(ppm) = 0.93 (t, J = 7.0 Hz, 3 H, CH_3), 1.27 – 1.45 (m, 8 H, 4xCH_2), 1.47 – 1.57 (m, 2 H, CH_2), 1.81 – 1.91 (m, 2 H, CH_2), 4.06 (t, J = 6.7 Hz, 2 H, CH_2), 4.75 (s, 2 H, CH_2-OH), 7.10 – 7.19 (m, 2 H, 2xAr), 7.41 (dd, J = 8.4, 1.6 Hz, 1 H, Ar), 7.65 – 7.72 (m, 3 H, 3xAr). **^{13}C-NMR (100 MHz, $CDCl_3$)** δ(ppm) = 14.2 (CH_3), 22.7 (CH_2), 26.2 (CH_2), 29.3 (2xCH_2), 29.5 (CH_2), 31.9 (CH_2), 65.4 (CH_2-OH), 68.1 (CH_2), 106.6 (Ar-H), 119.3 (Ar-H), 125.6 (Ar-H), 125.8 (Ar-H), 127.1 (Ar-H), 128.7 (Ar-C_q), 129.3 (Ar-H), 134.2 (Ar-C_q), 136.0 (Ar-C_q), 157.3 (Ar-*C*O-).

(6-Methoxynaphthalen-2-yl)methanol 22d

According to general procedure **B** alcohol **15** (505 mg, 2.9 mmol, 1.0 eq.), iodomethane (235 µL, 535 mg, 3.77 mmol, 1.3 eq.), sodium hydroxide (4.35 mmol) and acetonitrile/water (3:1)(20 mL) were used. Purification by column chromatography (petroleum ether 2:1 ethyl acetate) gave the desired product as a white solid (309 mg, 1.64 mmol, 57%). **^{1}H-NMR (400 MHz, MeOD)** δ(ppm) = 3.86 (s, 3 H, CH_3), 4.70 (s, 2 H, CH_2-OH), 7.10 (dd, J = 8.9, 2.6 Hz, 1 H, Ar), 7.18 (d, J = 2.5 Hz, 1 H, Ar), 7.42 (dd, J = 8.3, 1.8 Hz, 1 H, Ar), 7.67 – 7.73 (m, 3 H, 3xAr). **^{13}C-NMR (100 MHz, MeOD)** δ(ppm) = 54.3 (CH_3), 64.0 (CH_2-OH), 105.4 (Ar-H), 118.4 (Ar-H), 125.0 (Ar-H), 125.6 (Ar-H), 126.7 (Ar-H), 128.9 (Ar-H, Ar-C_q), 134.2 (Ar-C_q), 136.4 (Ar-C_q), 157.7 (Ar-*C*O-).

General Procedure C: triphenylphosphine (2.0 eq.) and tetrabromomethane (2.0 eq.) were dissolved in dichloromethane. The mixture was cooled to 0 °C and a solution of the alcohol (1.0 eq.) in dichloromethane was added. The mixture was stirred for 3 h at room temperature. Water was added and the mixture extracted with dichloromethane. The organic phases were dried over sodium sulfate and the solvent was removed. Purification by column chromatography yielded the desired product.

2-(Bromomethyl)-6-propoxynaphthalene 23a

According to general procedure **C** alcohol **22a** (229 mg, 1.06 mmol, 1.0 eq.), triphenylphosphine (556 mg, 2.12 mmol, 2.0 eq.), tetrabromomethane (703 mg, 2.12 mmol, 2.0 eq.) and dichloromethane (20 mL) were used. Purification by column chromatography (petroleum ether 20:1 ethyl acetate) gave the desired product as a light yellow oil (300 mg, 1.07 mmol, quant.). **^{1}H-NMR (400 MHz, $CDCl_3$)** δ(ppm) = 1.11 (t, J = 7.4 Hz, 3 H, CH_3), 1.84 – 1.95 (m, 2 H, CH_2), 4.05 (t, J = 6.7 Hz, 2 H, CH_2), 4.67 (s, 2 H, CH_2-Br), 7.13 (d, J = 2.5 Hz, 1 H, Ar), 7.19 (dd, J = 8.8, 2.5 Hz, 1 H, Ar), 7.47 (dd, J = 8.4, 1.9 Hz, 1 H, Ar), 7.69 – 7.76 (m, 3 H, 3xAr)**. ^{13}C-NMR (100 MHz, $CDCl_3$)** δ(ppm) = 10.7 (CH_3), 22.6 (CH_2), 34.6 (CH_2-Br), 69.6 (CH_2), 106.6 (Ar-H), 119.6 (Ar-H), 127.3 (Ar-H), 127.6 (Ar-H), 127.8 (Ar- H), 128.6 (Ar-C_q), 129.4 (Ar-H), 132.7 (Ar-C_q), 134.5 (Ar-C_q), 157.8 (Ar-*C*O-).

2-(Bromomethyl)-6-(pentyloxy)naphthalene 23b

According to general procedure **C** alcohol **22b** (200 mg, 0.82 mmol, 1.0 eq.), triphenylphosphine (4.30 mg, 1.64 mmol, 2.0 eq.), tetrabromomethane (544 mg, 1.64 mmol, 2.0 eq.) and dichloromethane (20 mL) were used. Purification by column chromatography (petroleum ether 15:1 ethyl acetate) gave the desired product as a light brown oil (385 mg, 0.93 mmol, quant.). **^{1}H-NMR (400 MHz, $CDCl_3$)** δ(ppm) = 0.98 (t, J = 7.3 Hz, 3 H, CH_3), 1.39 - 1.55 (m, 4 H, 2xCH_2), 1.83 – 1.91 (m, 2 H, CH_2), 4.08 (t, J = 6.7 Hz, 2 H, CH_2), 4.74 (s, 2 H, CH_2-Br), 7.13 (d, J = 2.5 Hz, 1 H, Ar), 7.18 (dd, J = 8.8, 2.5 Hz, 1 H, Ar), 7.47 (dd, J = 8.5, 1.8 Hz, 1 H, Ar), 7.70 – 7.76 (m, 3 H, 3xAr)**. ^{13}C-NMR (100 MHz, $CDCl_3$)** δ(ppm) = 14.1 (CH_3), 22.5 (CH_2), 28.3 (CH_2), 29.0 (CH_2), 46.9 (CH_2-Br), 68.1 (CH_2), 106.6 (Ar-H), 119.6 (Ar-H), 126.8 (Ar-H), 127.5 (Ar-H), 128.5 (Ar- H), 128.6 (Ar-C_q), 129.4 (Ar-H), 132.4 (Ar-C_q), 134.5 (Ar-C_q), 157.8 (Ar-*C*O-).

2-(Bromomethyl)-6-(octyloxy)naphthalene 23c

According to general procedure **C** alcohol **22c** (286 mg, 1.00 mmol, 1.0 eq.), triphenylphosphine (525 mg, 2.00 mmol, 2.0 eq.), tetrabromomethane (663 mg, 2.00 mmol, 2.0 eq.) and dichloromethane (20 mL) were used. Purification by column chromatography (petroleum ether 20:1 ethyl acetate) gave the desired product as a light yellow oil (286 mg, 0.77 mmol, 77%). **^{1}H-NMR (400 MHz, $CDCl_3$)** δ(ppm) = 0.95 (t, J = 6.8 Hz, 3 H, CH_3), 1.28 – 1.45 (m, 8 H, 4xCH_2), 1.49 – 1.58 (m, 2 H, CH_2), 1.83 – 1.92 (m, 2 H, CH_2), 4.08 (t, J = 6.7 Hz, 2 H, CH_2), 4.66 (s, 2 H, CH_2-Br), 7.13 (d, J = 2.5 Hz, 1 H, Ar), 7.19 (dd, J = 9.0, 2.5 Hz, 1 H, Ar), 7.47 (dd, J = 8.4, 1.9 Hz, 1 H, Ar), 7.69 – 7.76 (m, 3 H, 3xAr)**. ^{13}C-NMR (100 MHz, $CDCl_3$)** δ(ppm) = 14.2 (CH_3), 22.7 (CH_2), 26.2 (CH_2), 29.3 (CH_2), 29.4 (CH_2), 29.5 (CH_2), 31.9 (CH_2), 46.8 (CH_2-Br), 68.0 (CH_2), 106.6 (Ar-H), 119.4 (Ar-H), 125.6 (Ar-H), 125.8 (Ar-H), 127.2 (Ar-H), 128.7 (Ar-C_q), 129.3 (Ar-H), 134.2 (Ar-C_q), 136.1 (Ar-C_q), 157.3 (Ar-*C*O-).

2-(Iodomethyl)-6-methoxynaphthalene 23d

Triphenylphosphine (860 mg, 3.28 mmol, 2.0 eq.) and imidazole (157 mg, 2.30 mmol, 1.4 eq.) were dissolved in dichloromethane (30 mL) and iodine (833 mg, 3.28 mmol, 2.0 eq.) was added slowly. The mixture was stirred for 1 h at room temperature and the alcohol **22d** (309 mg, 1.64 mmol, 1.0 eq.) was added as a solution in dichloromethane (10 mL). The mixture was stirred at room temperature for 3 h and quenched with water. The phases were separated, and the organic phase was washed with hydrochloric acid (10% *w/w*). The inorganic phases were extracted with dichloromethane. The organic phases were dried over sodium sulfate and the solvent was removed. Purification by column chromatography (petroleum ether 15:1 ethyl acetate) gave the desired product as a brown solid (486 mg, 1.63 mmol, 99 %). The product was used in the next reaction immediately. **^{1}H-NMR (400 MHz, $CDCl_3$)** δ(ppm) = 3.86 (s, 3 H, CH_3), 4.33 (s, 2 H, CH_2-I), 7.12 (d, J = 2.5 Hz, 1 H, Ar), 7.19 (dd, J = 8.8, 2.5 Hz, 1 H, Ar), 7.45 (dd, J = 8.4, 1.9 Hz, 1 H, Ar), 7.65 – 7.71 (m, 3 H, 3xAr). **^{13}C-NMR (100 MHz, $CDCl_3$)** δ(ppm) = 6.2 (CH_2-I), 54.3 (CH_3), 106.0 (Ar-H), 118.9 (Ar-H), 125.2 (Ar-H), 125.3 (Ar-H), 126.8 (Ar-H), 128.8 (Ar-H), 128.9 (Ar-C_q), 134.4 (Ar-C_q), 136.4 (Ar-C_q), 157.9 (Ar-*C*O-).

General Procedure D: alkyl halide **23** (1.0 eq.) and the quinolone **14** (1.0 eq.) were dissolved in dimethylformamide. Potassium carbonate (2.0 eq.) was added. The mixture was heated to 60 °C overnight. Water and ethyl acetate were added. The phases were separated, and the inorganic phase was extracted with ethyl acetate. The combined organic phases were washed with water several times, dried over sodium sulfate and the solvent was removed.

Ethyl 8-fluoro-4-oxo-1-((6-propoxynaphthalen-2-yl)methyl)-1,4-dihydroquinoline-3-carboxylate 24a

According to general procedure **D** the bromo-compound **23a** (296 mg, 1.06 mmol, 1.0 eq.), the quinolone **14** (249 mg, 1.06 mmol, 1.0 eq,), potassium carbonate (293 mg, 2.12 mmol, 2.0 eq.) and dimethylformamide (15 mL) were used. Removal of the solvent after workup gave (286 mg, 0.66 mmol, 62%) of the desired product as an orange solid. **^{1}H-NMR (400 MHz, $CDCl_3$)** δ(ppm) = 1.04 (t, J = 7.4 Hz, 3 H, CH_3), 1.39 (t, J = 7.2 Hz, 3 H, CH_3), 1.84 (sxt, J = 7.1 Hz, 2 H, CH_2), 3.99 (t, J = 6.7 Hz, 2 H, CH_2), 4.39 (q, J = 7.3 Hz, 2 H, CH_2), 5.63 (d, J = 2.3 Hz, 2 H, CH_2), 7.07 (d, J = 2.5 Hz, 1 H, Ar), 7.12 (dd, J = 9.0, 2.5 Hz, 1 H, Ar), 7.17 – 7.32 (m, 3 H, 3xAr), 7.42 (s, 1 H, Ar), 7.61 (d, J = 9.0 Hz, 1 H, Ar), 7.67 (d, J = 8.5 Hz, 1 H, Ar), 8.31 – 8.35 (m, 1 H, Ar), 8.57 (s, 1 H, CH). **^{13}C-NMR (100 MHz, $CDCl_3$)** δ(ppm) = 10.6 (CH_3), 14.4 (CH_3), 22.5 (CH_2), 60.9 (CH_2), 61.1 (CH_2), 69.6 (CH_2), 106.5 (Ar-H), 111.3 (*C*=CH), 119.84 (d, J = 22.7 Hz, Ar-H), 119.87 (Ar-H), 123.81 (d, J = 3.7 Hz, Ar-H), 124.3 (Ar-H), 125.0 (Ar-H), 125.51 (d, J = 8.1 Hz, Ar-H), 127.8 (Ar-H), 128.5 (Ar-C_q), 128.7 (Ar-C_q), 129.3 (Ar-H), 130.4 (Ar-C_q), 131.9 (Ar-C_q), 134.3 (Ar-C_q), 151.6 (CH), 151.79 (d, J = 250.9 Hz, Ar-CF), 157.7 (Ar-*C*O-), 165.4 (*C*OOEt), 173.3 (CO). **ESI-MS:** *m/z* calc. for $C_{26}H_{24}FNO_4$ $[M+H]^+$: 434.18, found: 434.25.

Ethyl 8-fluoro-4-oxo-1-((6-(pentyloxy)naphthalen-2-yl)methyl)-1,4-dihydroquinoline-3-carboxylate 24b

According to general procedure **D** the bromo-compound **23b** (252 mg, 0.82 mmol, 1.0 eq.), the quinolone **14** (193 mg, 0.82 mmol, 1.0 eq.), potassium carbonate (227 mg, 1.64 mmol, 2.0 eq.) and dimethylformamide (15 mL) were used. Removal of the solvent after workup gave the desired product as an orange solid (265 mg, 0.57 mmol, 70%). **^{1}H-NMR (400 MHz, $CDCl_3$)** δ(ppm) = 0.93 (t, *J* = 7.5 Hz, 3 H, CH_3), 1.33 – 1.51 (m, 4 H, CH_2), 1.40 (t, *J* = 7.2 Hz, 3 H, CH_3), 1.82 (quin, *J* = 7.5 Hz, 2 H, CH_2), 4.03 (t, *J* = 6.5 Hz, 2 H, CH_2), 4.40 (q, *J* = 7.1 Hz, 2 H, CH_2), 5.62 (s, 2 H, CH_2), 7.08 (d, *J* = 2.3 Hz, 1 H, Ar), 7.13 (dd, *J* = 8.9, 2.4 Hz, 1 H, Ar), 7.17 – 7.32 (m, 3 H, 3xAr), 7.42 (s, 1 H, Ar), 7.61 (d, *J* = 9.0 Hz, 1 H, Ar), 7.67 (d, *J* = 8.3 Hz, 1 H, Ar), 8.32 – 8.36 (m, 1 H, Ar), 8.57 (s, 1 H, CH). **^{13}C-NMR (100 MHz, $CDCl_3$)** δ(ppm) = 14.0 (CH_3), 14.4 (CH_3), 22.5 (CH_2), 28.3 (CH_2), 28.9 (CH_2), 60.9 (CH_2), 61.1 (CH_2), 68.1 (CH_2), 106.5 (Ar-H), 111.3 (*C*=CH), 119.82 (d, *J* = 22.7 Hz, Ar-H), 119.88 (Ar-H), 123.82 (d, *J* = 3.7 Hz, Ar-H), 124.3 (Ar-H), 124.99 (d, *J* = 1.5 Hz, Ar-H), 125.49 (d, *J* = 8.1 Hz, Ar-H), 127.8 (Ar-H), 128.5 (Ar-C_q), 128.7 (Ar-C_q), 129.3 (Ar-H), 130.39 (d, *J* = 1.5 Hz, Ar-C_q), 131.9 (Ar-C_q), 134.4 (Ar-C_q), 151.6 (CH), 151.79 (d, *J* = 250.9 Hz, Ar-CF), 157.7 (Ar-*C*O-), 165.4 (*C*OOEt), 173.3 (CO). **ESI-MS:** *m/z* calc. for $C_{28}H_{28}FNO_4$ $[M+H]^+$: 462.21, found: 462.25.

Ethyl 8-fluoro-1-((6-(octyloxy)naphthalen-2-yl)methyl)-4-oxo-1,4-dihydroquinoline-3-carboxylate 24c

According to general procedure **D** the bromo-compound **23c** (269 mg, 0.77 mmol, 1.0 eq.), the quinolone **14** (181 mg, 0.77 mmol, 1.0 eq.), potassium carbonate (213 mg, 1.54 mmol, 2.0 eq.) and dimethylformamide (15 mL) were used. Removal of the solvent after workup gave the desired product as an orange solid (284 mg, 0.56 mmol, 72%). **^{1}H-NMR (400 MHz, $CDCl_3$)** δ(ppm) = 0.87 (t, *J* = 7.3 Hz, 3 H, CH_3), 1.23 – 1.37 (m, 8 H, 4xCH_2), 1.39 (t, *J* = 7.0 Hz, 3 H, CH_3), 1.43 – 1.51 (m, 2 H, CH_2), 1.81 (quin, *J* = 6.5 Hz, 2 H, CH_2), 4.02 (t, *J* = 6.7 Hz, 2 H, CH_2), 4.35 – 4.42 (m, 2 H, CH_2), 5.63 (d, *J* = 2.0 Hz, 2 H, CH_2), 7.07 (d, *J* = 2.5 Hz, 1 H, Ar), 7.12 (dd, *J* = 9.0, 2.5 Hz, 1 H, Ar), 7.17 – 7.32 (m, 3 H, 3xAr), 7.42 (s, 1 H, Ar), 7.61 (d, *J* = 9.0 Hz, 1 H, Ar), 7.67 (d, *J* = 8.5 Hz, 1 H, Ar), 8.31 – 8.36 (m, 1 H, Ar), 8.57 (s, 1 H, CH). **^{13}C-NMR (100 MHz, $CDCl_3$)** δ(ppm) = 14.1 (CH_3), 14.4 (CH_3), 22.7 (CH_2), 26.1 (CH_2), 29.2 (2xCH_2), 29.4 (CH_2), 31.8 (CH_2), 60.9 (CH_2), 61.1 (CH_2), 68.1 (CH_2), 106.5 (Ar-H), 111.3 (*C*=CH), 119.83 (d, *J* = 23.5 Hz, Ar-H), 119.88 (Ar-H), 123.81 (d, *J* = 3.7 Hz, Ar-H), 124.2 (Ar-H), 124.99 (d, *J* = 1.5 Hz, Ar-H), 125.49 (d, *J* = 8.1 Hz, Ar-H), 127.8 (Ar-H), 128.53 (d, *J* = 6.6 Hz, Ar-C_q), 128.53 (Ar-C_q), 129.3 (Ar-H), 130.4 (Ar-C_q), 131.9 (Ar-C_q), 134.4 (Ar-C_q), 151.6 (CH), 151.79 (d, *J* = 250.2 Hz, Ar-CF), 157.7 (Ar-*C*O-), 165.3 (*C*OOEt), 173.2 (CO). **ESI-MS:** *m/z* calc. for $C_{31}H_{34}FNO_4$ $[M+H]^+$: 504.25, found: 504.25.

Ethyl 8-fluoro-1-((6-methoxynaphthalen-2-yl)methyl)-4-oxo-1,4-dihydroquinoline-3-carboxylate 24d

According to general procedure **D** the iodo-compound **23d** (477 mg, 1.60 mmol, 1.0 eq.), the quinolone **14** (376 mg, 1.60 mmol, 1.0 eq.), potassium carbonate (442 mg, 3.20 mmol, 1.0 eq.) and dimethylformamide (20 mL) were used. Purification by column chromatography (petroleum ether 1:3 ethyl acetate) gave the desired product as a white solid (260 mg, 0.64 mmol, 40%). **^{1}H-NMR (400 MHz, $CDCl_3$)** δ(ppm) = 1.41 (t, *J* = 7.2 Hz, 3 H, CH_3), 3.89 (s, 3 H, OCH_3), 4.41 (q, *J* = 7.1 Hz, 2 H, CH_2), 5.65 (d, *J* = 2.0 Hz, 2 H, CH_2), 7.09 (d, *J* = 2.3 Hz, 1 H, Ar), 7.13 (dd, *J* = 8.9, 2.4 Hz, 1 H, Ar), 7.19 – 7.35 (m, 3 H, 3xAr), 7.45 (s, 1 H, Ar), 7.63 (d, *J* = 8.8 Hz, 1 H, Ar), 7.71 (d, *J* = 8.5 Hz, 1 H, Ar), 8.36 (dd, *J* = 7.9, 1.4 Hz, 1 H, Ar), 8.58 (s, 1 H, CH). **^{13}C-NMR (100 MHz, $CDCl_3$)** δ(ppm) = 14.4 (CH_3), 53.4 (CH_2), 55.4 (CH_3), 61.1 (CH_2), 105.7 (Ar-H), 111.4 (*C*=CH), 119.6 (Ar-H), 119.82 (d, *J* = 22.7 Hz, Ar-H), 123.87 (d, *J* = 3.7 Hz, Ar-H), 124.3 (Ar-H), 125.0 (Ar-H), 125.50 (d, *J* = 8.1 Hz, Ar-H), 127.9 (Ar-H), 128.5 (Ar-C_q), 128.7 (Ar-C_q), 129.4 (Ar-H), 130.54 (d, *J* = 1.5 Hz, Ar-C_q), 131.9 (Ar-C_q), 134.3 (Ar-C_q), 151.6 (CH), 151.75 (d, *J* = 251.0 Hz, Ar-CF), 158.2 (Ar-*C*O-), 165.4 (*C*OOEt), 173.2 (CO). **ESI-MS:** *m/z* calc. for $C_{24}H_{20}FNO_4$ $[M+H]^+$: 406.14, found: 406.10.

General Procedure E: the ester **24** (1.0 eq.) and LiOH (2.2 eq. - 6.0 eq.) were dissolved in a mixture of tetrahydrofuran and water. The clear solution was stirred at room temperature until LCMS showed full conversion. The mixture was acidified to pH=1-2 with 2M hydrochloric acid and extracted with ethyl acetate. The combined organic phases were washed with water several times, dried over sodium sulfate and the solvent was removed to give the crude product.

8-Fluoro-4-oxo-1-((6-propoxynaphthalen-2-yl)methyl)-1,4-dihydroquinoline-3-carboxylic acid 25a

According to general procedure **E** the ester **24a** (286 mg, 0.66 mmol, 1.0 eq) and LiOH (96 mg, 4.0 mmol, 6.0 eq.) were used. The dry crude product was taken up in methanol and filtered. The solid was washed with petroleum ether and diethyl ether to give the desired product as an off-white solid (142 mg, 0.35 mmol, 53%). **^{1}H-NMR (400 MHz, $CDCl_3$)** δ(ppm) = 1.06 (t, J = 7.4 Hz, 3 H, CH_3), 1.81 – 1.91 (m, 2 H), 4.01 (t, J = 6.5 Hz, 2 H, CH_2), 5.77 (d, J = 2.3 Hz, 2 H, CH_2), 7.09 (d, J = 2.5 Hz, 1 H, Ar), 7.15 (dd, J = 8.8, 2.5 Hz, 1 H, Ar), 7.20 (dd, J = 8.5, 1.5 Hz, 1 H, Ar), 7.40 – 7.50 (m, 3 H, 3xAr), 7.64 (d, J = 9.0 Hz, 1 H, Ar), 7.69 (d, J = 8.8 Hz, 1 H, Ar), 8.35 – 8.39 (m, 1 H, Ar), 8.89 (s, 1 H, CH), 14.61 (br. s., 1 H, COOH). **^{13}C-NMR (100 MHz, $CDCl_3$)** δ(ppm) = 10.6 (CH_3), 22.5 (CH_2), 62.0 (CH_2), 69.6 (CH_2), 106.5 (Ar-H), 109.1 (*C*=CH), 120.1 (Ar-H), 121.21 (d, J = 22.7 Hz, Ar-H), 123.29 (d, J = 3.7 Hz, Ar-H), 124.2 (Ar-H), 125.4 (Ar-H), 126.77 (d, J = 8.1 Hz, Ar-H), 128.0 (Ar-H), 128.5 (Ar-C_q), 129.3 (2xAr-C_q), 129.4 (Ar-H, Ar-C_q), 134.6 (Ar-C_q), 151.2 (CH), 152.40 (d, J = 251.8 Hz, Ar-CF), 157.9 (Ar-*C*O-), 166.4 (*C*OOH), 177.7 (CO). **ESI-MS:** *m/z* calc. for $C_{24}H_{20}FNO_4$ $[M+H]^+$: 406.14, found: 406.15.

8-Fluoro-4-oxo-1-((6-(pentyloxy)naphthalen-2-yl)methyl)-1,4-dihydroquinoline-3-carboxylic acid 25b

According to general procedure **E** the ester **24b** (237 mg, 0.57 mmol, 1.0 eq.) and LiOH (31 mg, 1.30 mmol, 2.3 eq.) were used. The dry crude product was taken up in methanol and filtered. The solid was washed with petroleum ether and diethyl ether to give the desired product as a light pink solid (113 mg, 0.26 mmol, 46%). **^{1}H-NMR (400 MHz, $CDCl_3$)** δ(ppm) = 0.94 (t, J = 7.0 Hz, 3 H, CH_3), 1.35 – 1.51 (m, 4 H, 2x CH_2), 1.80 – 1.88 (m, 2 H, CH_2), 4.05 (t, J = 6.5 Hz, 2 H, CH_2), 5.78 (d, J = 2.3 Hz, 2 H, CH_2), 7.09 (d, J =2.5 Hz, 1 H, Ar), 7.15 (dd, J = 8.8, 2.5 Hz, 1 H, Ar), 7.21 (dd, J = 8.5, 1.3 Hz, 1 H, Ar), 7.41 – 7.51 (m, 3 H, 3xAr), 7.64 (d, J = 9.0 Hz, 1 H, Ar), 7.70 (d, J = 8.5 Hz, 1 H, Ar), 8.36 – 8.39 (m, 1 H, Ar), 8.89 (s, 1 H, CH), 14.60 (br. s., 1 H, COOH). **^{13}C-NMR (100 MHz, $CDCl_3$)** δ(ppm) = 14.0 (CH_3), 22.5 (CH_2), 28.2 (CH_2), 28.9 (CH_2), 62.0 (CH_2), 68.1 (CH_2), 106.5 (Ar-H), 109.2 (*C*=CH), 120.1 (Ar-H), 121.21 (d, J = 22.7 Hz, Ar-H), 123.32 (d, J = 3.7 Hz, Ar-H), 124.2 (Ar-H), 125.4 (Ar-H), 126.77 (d, J = 8.1 Hz, Ar-H), 128.1 (Ar-H), 128.5 (Ar-C_q), 129.3 (2xAr-C_q), 129.4 (Ar-H, Ar-C_q), 134.6 (Ar-C_q),

151.2 (CH), 151.77 (d, *J* = 252.4 Hz, Ar-CF), 157.9 (Ar-*C*O-), 166.4 (*C*OOH), 177.8 (CO). **ESI-MS:** *m/z* calc. for $C_{26}H_{24}FNO_4$ $[M+H]^+$: 434.18, found: 434.25.

8-Fluoro-1-((6-(octyloxy)naphthalen-2-yl)methyl)-4-oxo-1,4-dihydroquinoline-3-carboxylic acid 25c

According to general procedure **E** the ester **24c** (282 mg, 0.56 mmol, 1.0 eq) and LiOH (80 mg, 3.36 mmol, 6.0 eq.) were used. The dry crude product was taken up in methanol and filtered. The solid was washed with petroleum ether and diethyl ether to give the desired product as a white solid (130 mg, 0.27 mmol, 49%). **^{1}H-NMR (400 MHz, $CDCl_3$)** δ(ppm) = 0.88 (t, *J* = 6.8 Hz, 3 H, CH_3), 1.23 – 1.41 (m, 8 H, 4xCH_2), 1.43 – 1.53 (m, 2 H, CH_2), 1.78 – 1.87 (m, 2 H, CH_2), 4.04 (t, *J* = 6.7 Hz, 2 H, CH_2), 5.78 (d, *J* = 2.3 Hz, 2 H, CH_2), 7.09 (d, *J* = 2.5 Hz, 1 H, Ar), 7.15 (dd, *J* = 8.8, 2.5 Hz, 1 H, Ar), 7.21 (dd, *J* = 8.5, 1.5 Hz, 1 H, Ar), 7.41 – 7.51 (m, 3 H, 3xAr), 7.64 (d, *J* = 8.8 Hz, 1 H, Ar), 7.70 (d, *J* = 8.8 Hz, 1 H, Ar), 8.35 – 8.40 (m, 1 H, Ar), 8.89 (s, 1 H, CH), 14.61 (s, 1 H, COOH). **^{13}C-NMR (100 MHz, $CDCl_3$)** δ(ppm) = 14.1 (CH_3), 22.7 (CH_2), 26.1 (CH_2), 29.2 (2xCH_2), 29.4 (CH_2), 31.8 (CH_2), 61.9 (CH_2), 68.2 (CH_2), 106.5 (Ar-H), 109.2 (*C*=CH), 120.1 (Ar-H), 121.21 (d, *J* = 23.5 Hz, Ar-H), 123.31 (d, *J* = 3.7 Hz, Ar-H), 124.1 (Ar-H), 125.4 (Ar-H), 126.77 (d, *J* = 8.8 Hz, Ar-H), 128.1 (Ar-H), 128.5 (Ar-C_q), 129.3 (2xAr-C_q), 129.4 (Ar-H, Ar-C_q), 134.6 (Ar-C_q), 151.2 (CH), 151.56 (d, *J* = 250.8 Hz, Ar-CF), 157.9 (Ar-*C*O-), 166.4 (*C*OOH), 177.7 (CO). **ESI-MS:** *m/z* calc. for $C_{29}H_{30}FNO_4$ $[M+H]^+$: 476.22, found: 476.35.

8-Fluoro-1-((6-methoxynaphthalen-2-yl)methyl)-4-oxo-1,4-dihydroquinoline-3-carboxylic acid 25d

According to general procedure **E** the ester **24d** (259 mg, 0.64 mmol, 1.0 eq.) and LiOH (34 mg, 1.41 mmol, 2.2 eq.) were used. The dry crude product was taken up in ethyl acetate and filtered. The solid was washed with water and petroleum ether to give the desired product as an off-white solid (161 mg, 0.43 mmol, 67%). **^{1}H-NMR (400 MHz, DMSO-d_6)** δ(ppm) = 3.84 (s, 3 H, CH_3), 6.01 (d, *J* = 3.3 Hz, 2 H, CH_2), 7.12 (dd, *J* = 9.0, 2.5 Hz, 1 H, Ar), 7.29 (d, *J* = 2.5 Hz, 1 H, Ar), 7.32 (dd, *J* = 8.7, 1.6 Hz, 1 H, Ar), 7.54 (s, 1 H, Ar), 7.61 (td, *J* = 8.0, 4.3 Hz, 1 H, Ar), 7.67 – 7.77 (m, 2 H, 2x Ar), 7.81 (d, *J* = 8.8 Hz, 1 H, Ar), 8.26 (dd, *J* = 8.0, 1.3 Hz, 1 H, Ar), 9.24 (s, 1 H, CH), 14.85 (s, 1 H, COOH). **^{13}C-NMR (100 MHz, DMSO-d_6)** δ(ppm) = 55.7 (CH_3), 61.3 (CH_2), 106.3 (Ar-H), 108.8 (*C*=CH), 119.5 (Ar-H), 121.82 (d, *J* = 22.7 Hz, Ar-H), 122.83 (d, *J* = 3.7 Hz, Ar-H), 124.6 (Ar-H), 125.1 (Ar-H), 127.6 (Ar-H), 127.7 (Ar-H), 127.9 (Ar-H), 128.7 (Ar-C_q), 128.7 (Ar-C_q), 129.0 (Ar-C_q), 129.5 (d, *J* = 7.3 Hz, Ar-C_q), 129.8 (Ar-H), 132.1 (Ar-C_q), 134.2 (Ar-C_q), 152.8 (CH), 152.35 (d, *J* = 252.4 Hz, Ar-CF), 158.0 (Ar-*C*O-), 166.1 (*C*OOH), 177.6 (CO). **ESI-MS:** *m/z* calc. for $C_{22}H_{16}FNO_4$ $[M+H]^+$: 378.11, found: 378.15.

Synthesis of Reference compounds 28a-c

General Procedure F: The respective amine (2.5 eq.) was dissolved in hexane (16 mL) and the solution was cooled down to 0 °C. Subsequently a solution of 2-chloroethyl carbonochloridate (1.0 eq.) in hexane (5 mL) was added dropwise within 30 minutes. The reaction was then allowed to warm up to room temperature and stirring was continued for one hour. It was then quenched with water and extracted with diethyl ether. Organic layers were combined and washed with 1N hydrochloric acid and brine then dried over sodium sulfate. Evaporation of the solvent under reduced pressure gave the desired carbamate as a colorless oil.

2-chloroethyl propylcarbamate 26a

According to general procedure **F** propylamine (3.55 g, 4.94 mL, 60 mmol, 2.5. eq.) and 2-chloroethyl carbonochloridate (3.43 g, 2.48 mL, 24 mmol, 1.0 eq.) were used. Evaporation of the solvent under reduced pressure gave the desired carbamate **26a** as a colorless oil (3.45 g, 20.8 mmol, 87%) which was used without further purification. **^{1}H-NMR (400 MHz, $CDCl_3$)** δ(ppm) = 0.88 (td, J = 7.4, 2.0 Hz, 3H), 1.58 – 1.41 (m, 2H), 3.19 – 3.01 (m, 2H), 3.63 (dd, J = 7.6, 3.1 Hz, 2H), 4.26 (d, J = 4.9 Hz, 2H), 4.97 (s, 1H). **^{13}C-NMR (100 MHz, $CDCl_3$)** δ(ppm) = 11.18 (s), 23.11 (s), 42.37 (s), 42.80 (s), 64.37 (s), 156.02 (s). **ESI-MS:** *m/z* calc. for $C_6H_{12}ClNO_2$ $[M+H]^+$: 166.06, found: 166.05.

2-chloroethyl pentylcarbamate 26b

According to general procedure **F** amylamine (5.23 g, 6.96 mL, 60 mmol, 2.5 eq.) and 2-chloroethyl carbonochloridate (3.43 g, 2.48 mL, 24 mmol, 1.0 eq.) were used. Evaporation of the solvent under reduced pressure gave the desired carbamate **26b** as a colorless oil (4.62 g, 23.9 mmol, 99%) which was used without further purification. **^{1}H-NMR (400 MHz, $CDCl_3$)** δ(ppm) = 0.86 (t, J = 6.8 Hz, 3H), 1.37 – 1.20 (m, 4H), 1.64 – 1.39 (m, 2H), 3.13 (dd, J = 13.3, 6.7 Hz, 2H), 3.63 (t, J = 5.5 Hz, 2H), 4.27 (t, J = 5.5 Hz, 2H), 4.92 (s, 1H). **^{13}C-NMR (100 MHz, $CDCl_3$)** δ(ppm) = 13.99 (s), 22.36 (s), 28.91 (s), 29.60 (s), 41.13 (s), 42.39 (s), 64.41 (s), 155.98 (s). **ESI-MS:** *m/z* calc. for $C_8H_{16}ClNO_2$ $[M+H]^+$: 194.09, found: 194.10.

2-chloroethyl octylcarbamate 26c

According to general procedure **F** octylamine (7.76 g, 9.94 mL, 60 mmol, 2.5 eq.) and 2-chloroethyl carbonochloridate (3.43 g, 2.48 mL, 24 mmol, 1.0 eq.) were used. Evaporation of the solvent under reduced pressure gave desired carbamate **26c** as a colorless oil (5.53 g, 23.5 mmol, 98%). **^{1}H-NMR (400 MHz, $CDCl_3$)** δ(ppm) = 0.95 – 0.77 (m, 3H), 1.23 (dd, J = 13.9, 7.0 Hz, 10H), 1.61 – 1.37 (m, 2H), 3.14 (dd, J = 12.2, 5.7 Hz, 2H), 3.64 (t, J = 4.6 Hz, 2H), 4.27 (t, J = 4.5 Hz, 2H), 4.91 (s, 1H). **^{13}C-NMR (100 MHz, $CDCl_3$)** δ(ppm) = 14.09 (s), 22.66 (s),

26.77 (s), 29.23 (s), 29.26 (s), 29.91 (s), 31.81 (s), 41.15 (s), 42.37 (s), 64.40 (s), 155.97 (s). **ESI-MS:** *m/z* calc. for $C_{11}H_{22}ClNO_2$ $[M+H]^+$: 236.13, found: 236.15.

General Procedure G: Carbamate **26** (1.0 eq.) was dissolved in dry acetone (45 mL) and sodium iodide (2.0 eq.) was added. The reaction mixture was refluxed 24-72 hours and the resulting precipitate was filtered off. The solvent was concentrated under reduced pressure and the residue was dissolved in diethyl ether. The resulting suspension was filtered again and washed with water. It was then dried over sodium sulfate and the solvent was removed to yield the desired Iodo-compound as a yellow solid which was used without further purification.

2-iodoethyl propylcarbamate 27a

According to general procedure **G** 2-iodoethyl propylcarbamate was prepared from compound **26a** (3.33 g, 20.1 mmol, 1.0 eq.) and sodium iodide (6.02 g, 40.2 mmol, 2.0 eq.). The obtained crude product **27a** was used in the next step without further purification as a yellow solid (4.07 g, 15.8 mmol, 79%). **ESI-MS:** *m/z* calc. for $C_6H_{12}INO_2$ $[M+H]^+$: 257.99, found: 258.00.

2-iodoethyl pentylcarbamate 27b

According to general procedure **G** 2-iodoethyl pentylcarbamate was prepared from compound **26b** (4.60 g, 23.8 mmol, 1.0 eq.) and sodium iodide (10.7 g, 71.3 mmol, 2.0 eq). The obtained crude product **27b** was used in the next step without further purification as a yellow solid (6.39 g, 22.4 mmol, 94%). **^{1}H-NMR (400 MHz, $CDCl_3$)** δ(ppm) = 0.87 (t, J = 6.9 Hz, 3H), 1.38 – 1.19 (m, 4H), 1.60 – 1.38 (m, 2H), 3.13 (dd, J = 13.4, 6.8 Hz, 2H), 3.26 (t, J = 6.7 Hz, 2H), 4.26 (t, J = 6.7 Hz, 2H), 4.86 (s, 1H). **^{13}C-NMR (100 MHz, $CDCl_3$)** δ(ppm) = 1.77 (s), 14.04 (s), 22.38 (s), 28.92 (s), 29.62 (s), 41.13 (s), 64.86 (s), 155.78 (s). **ESI-MS:** *m/z* calc. for $C_8H_{16}INO_2$ $[M+H]^+$: 286.02, found: 286.05.

2-iodoethyl octylcarbamate 27c

According to general procedure **G** 2-iodoethyl pentylcarbamate was prepared from compound **26c** (5.50 g, 23.3 mmol, 1.0 eq) and sodium iodide (7.00 g, 46.6 mmol, 2.0 eq). The obtained crude product **27c** was used in the next step without further purification as a yellow solid (7.16 g, 21.9 mmol, 94%).**^{1}H-NMR (400 MHz, $CDCl_3$)** δ(ppm) = 0.87 (t, J = 6.8 Hz, 3H), 1.38 – 1.18 (m, 10H), 1.47 (dt, J = 20.6, 10.2 Hz, 2H), 3.16 (dd, J = 13.4, 6.7 Hz, 2H), 3.38 – 3.23 (m, 2H), 4.34 (dt, J = 41.6, 6.9 Hz, 2H), 4.76 (s, 1H). **^{13}C-NMR (100 MHz, $CDCl_3$)** δ(ppm) = 1.78 (s), 14.20 (s), 22.75 (s), 26.84 (s), 29.31 (s), 29.34 (s), 30.02 (s), 31.90 (s), 41.23 (s), 64.93 (s), 155.82 (s). **ESI-MS:** *m/z* calc. for $C_{11}H_{22}INO_2$ $[M+H]^+$: 328.07, found: 328.10.

General Procedure H: iodo-compound **27** (1.0 eq.) was dissolved in acetone (60 mL) and trimethylamine (50 wt%) (1.2 eq.) was added. The reaction mixture was stirred at room temperature overnight. The solvent was removed under reduced pressure and the crude product was purified by column chromatography (dichloromethane 10:1 methanol).

N,N,N-trimethyl-2-((propylcarbamoyl)oxy)ethan-1-aminium 28a

According to general procedure **H** N,N,N-trimethyl-2-((propylcarbamoyl)oxy)ethan-1-aminium was prepared from compound **27a** (3.35 g, 13.0 mmol, 1.0 eq.) and a 50 wt% aqueous solution of trimethylamine (2.14 mL, 15.6 mmol, 1.2 eq.). The crude product was purified by column chromatography (dichloromethane 10:1 methanol). The product **28a** was obtained as a yellow foam (1.61 g, 5.10 mmol, 40%). **^{1}H-NMR (400 MHz, DMSO-d$_6$)** δ(ppm) = 0.83 (t, J = 7.4 Hz, 3H), 1.41 (dd, J = 14.4, 7.2 Hz, 2H), 2.95 (dd, J = 13.2, 6.6 Hz, 2H), 3.15 (d, J = 6.9 Hz, 9H), 3.71 – 3.55 (m, 2H), 4.37 (s, 2H), 7.31 (t, J = 5.5 Hz, 1H). **^{13}C-NMR (100 MHz, DMSO-d$_6$)** δ(ppm) = 11.20 (s), 22.50 (s), 42.04 (s), 53.04 (s), 57.37 (s), 64.19 (s), 155.20 (s). **ESI-MS:** *m/z* calc. for $C_9H_{21}N_2O_2^+$ $[M]^+$: 189.16, found: 189.20.

N,N,N-trimethyl-2-((pentylcarbamoyl)oxy)ethan-1-aminium 28b

According to general procedure **H** N,N,N-trimethyl-2-((pentylcarbamoyl)oxy)ethan-1-aminium was prepared from compound **27b** (5.07 g, 17.8 mmol, 1.0 eq.) and a 50 wt% aqueous solution of trimethylamine (3.15 mL, 21.3 mmol, 1.2 eq.). The crude product was purified by column chromatography (dichloromethane 10:1 methanol). The product **28b** was obtained as a yellow solid (4.37 g, 12.7 mmol, 71%). **^{1}H-NMR (400 MHz, DMSO-d$_6$)** δ(ppm) = 0.84 (t, J = 7.0 Hz, 3H), 1.32 – 1.16 (m, 4H), 1.46 – 1.33 (m, 2H), 2.97 (dd, J = 13.0, 6.8 Hz, 2H), 3.15 (s, 9H), 3.63 (dd, J = 15.1, 10.1 Hz, 2H), 4.36 (s, 2H), 7.29 (t, J = 5.6 Hz, 1H). **^{13}C-NMR (100 MHz, DMSO-d$_6$)** δ(ppm) = 13.83 (s), 21.72 (s), 28.34 (s), 28.89 (s), 53.03 (s), 54.96 (s), 57.35 (s), 64.16 (s), 155.12 (s). **ESI-MS:** *m/z* calc. for $C_{11}H_{25}N_2O_2^+$ $[M]^+$: 217.19, found: 217.20.

N,N,N-trimethyl-2-((octylcarbamoyl)oxy)ethan-1-aminium 28c

According to general procedure **H** N,N,N-trimethyl-2-((octylcarbamoyl)oxy)ethan-1-aminium was prepared from compound **27c** (4.74 g, 14.5 mmol, 1.0 eq.) and a 50 wt% aqueous solution of trimethylamine (2.40 mL, 17.4 mmol, 1.2 eq.). The crude product was purified by column chromatography (dichloromethane 10:1 methanol). The product **28c** was obtained as a light yellow solid (2.60 g, 6.73 mmol, 46%). **^{1}H-NMR (400 MHz, DMSO-d$_6$)** δ(ppm) = 0.99 (t, J = 6.7 Hz, 3H), 1.41 (d, J = 2.0 Hz, 10H), 1.65 – 1.54 (m, 2H), 3.20 (t, J = 7.1 Hz, 2H), 3.36 (s, 9H), 3.94 – 3.78 (m, 2H), 4.69 – 4.56 (m, 2H). **^{13}C-NMR (100 MHz, DMSO-d$_6$)** δ(ppm) = 14.41 (s), 23.66 (s), 27.84 (s), 30.33 (s), 30.36 (s), 30.78 (s), 32.94 (s), 41.91 (s), 54.76 (s), 59.15 (s), 66.60 (s), 157.36 (s). **ESI-MS:** *m/z* calc. for $C_{14}H_{31}N_2O_2^+$ $[M]^+$: 259.24, found: 259.25.

Divergent position of the carbachol moiety.

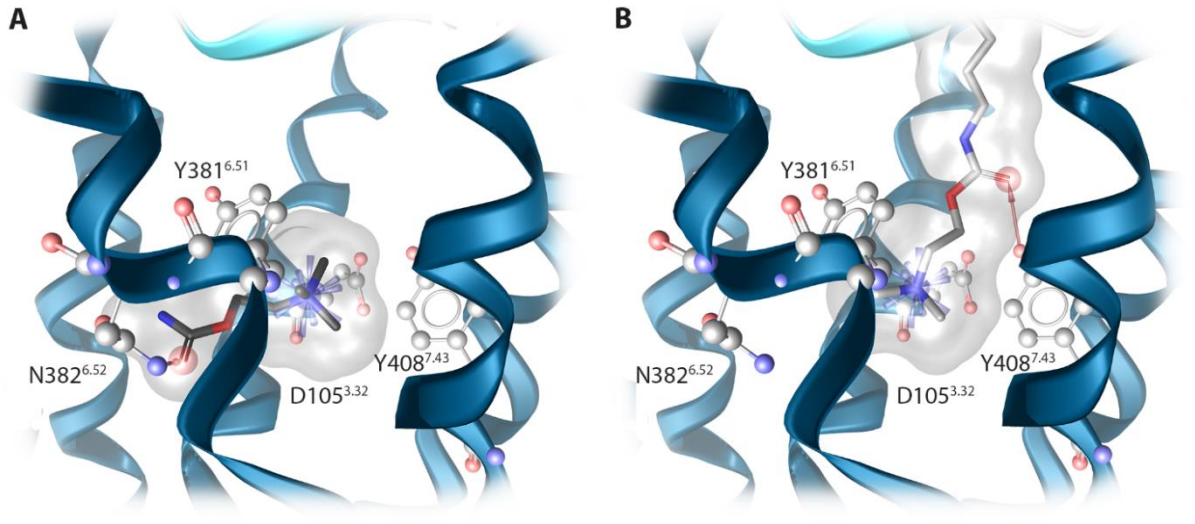

Supporting Figure 1. Carbachol (A) and the carbachol substructure in the hybrid ligands (B) show a different positioning in the orthosteric binding site. The orthosteric key interactions (charge interaction with $D105^{3.32}$ and a cation-π interaction with $Y381^{6.51}$) are present in both binding modes. Due to a spatial limitation of the orthosteric binding site a functionalization at the carbamate strongly reduces agonist activity of carbachol derivatives, because the abovementioned key interactions are disrupted. However, the BQCAd building block of the dualsteric ligand BQCAd-C5-Carbachol serves as an anchor at the allosteric vestibule and allows the ammonium group of the carbachol moiety to form the key interactions necessary for receptor activation.

Gα/PLCβ3 Split Luciferase Complementation Assay

TBPB and BQCA compounds were purchased from Merck KGaA (HPLC >98%). The assay was performed as described previously,[7] except for the following modifications: A Berthold Mithras LB 940 plate reader was used to quantify the luminescence emitted by the cells, using white, flat bottomed nunc™ f96 microwell™ polystyrene plates. Analysis was carried out with GraphPad Prism 5.0 software (GraphPad Software Inc., San Diego CA, www.graphpad.com).

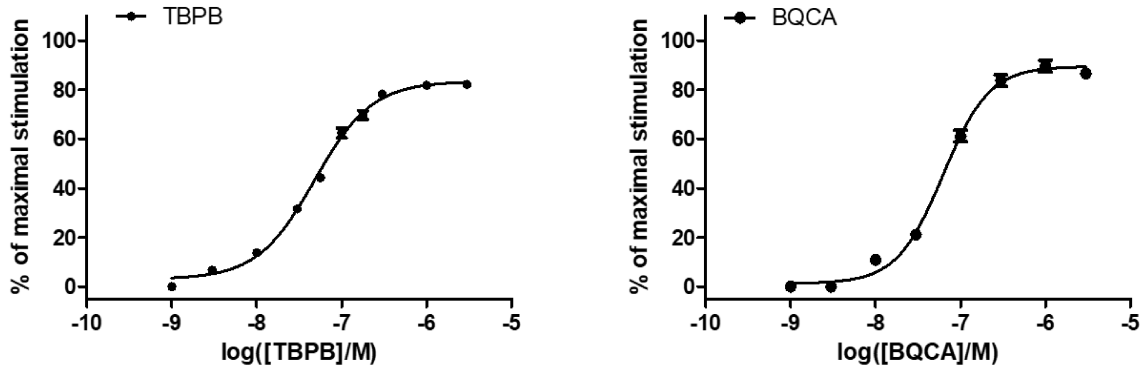

Supporting Figure 2. Dose-response-curves of reference compounds TBPB and BQCA. Data represent mean ± SEM from two independent experiments, conducted in triplicate.

Determination of the Schild Slope Factor *s* and Equilibrium Affinity Constant K_B.

In order to finally characterize the interaction between CCh and bitopic compounds in the above mentioned functional experiments, a modified Schild method[8] was utilized.[9] Since the logistic slope factor of the inhibition curve cannot be regarded isolated from the agonist slope,[9b] a simultaneous analysis of three data sets, meaning I) various concentrations of CCh alone (control curve) and II) several titrations of test compounds in the presence of a fixed concentration of CCh which corresponds to 80 – 90% of its maximum effect (inhibition curve), and thirdly, III) a second full CCh curve shifted by a fixed concentration of the test compound were compiled and fitted to the following equation:[9c]

$$Effect = \frac{(E_{max} - basal)}{\left(1 + \left\{\frac{EC_{0.5,control}}{[A]} \times (1 + [B]^{s} \cdot K_{B})\right\}^{n}\right)} + basal \qquad (II)$$

E_{max} and basal determine the maximum and minimum effects of CCh; *n*: slope factor of the agonist curve (corresponding to the Hill slope factor), $EC_{0.5,control}$ is the concentration of the agonist which is necessary to produce a half-maximal effect, [A] is the concentration of the agonist, [B] is the concentration of the antagonist, K_B indicates the equilibrium affinity constant of B and *s* the Schild slope factor. Finally, we performed a statistical test (F-test) that indicated whether or not s differed from unity. This way we could determine whether the interaction is formally competitive or noncompetitive (Schild slope set to s compared to unconstrained). $P<0.05$ was considered as the level of statistical significance.

[1] B. Budzik, V. Garzya, D. Shi, G. Walker, M. Woolley-Roberts, J. Pardoe, A. Lucas, B. Tehan, R. A. Rivero, C. J. Langmead, J. Watson, Z. Wu, I. T. Forbes, J. Jin, *ACS Med. Chem. Lett.* **2010**, *1*, 244-248.
[2] R. Henning, R. Lattrell, H. J. Gerhards, M. Leven, *J. Med. Chem.* **1987**, *30*, 814-819.
[3] N. Xu, C. Yang, X. Gan, S. Wie, Z. Ji, *Int. J. Mol. Sci.* **2013**, *14*, 6790-6804.
[4] S. D. Kuduk, D. C. Beshore, *Curr. Top. Med. Chem.* **2014**, *14*, 1738-1754.
[5] S. D. Kuduk, C. N. Di Marco, V. Cofre, W. J. Ray, L. Ma, M. Wittmann, M. A. Seager, K. A. Koeplinger, C. D. Thompson, G. D. Hartman, M. T. Bilodeau, *Bioorg. Med. Chem. Lett.* **2011**, *21*, 2769-2772.
[6] X. Chen, J. Klöckner, J. Holze, C. Zimmermann, W. K. Seemann, R. Schrage, A. Bock, K. Mohr, C. Tränkle, U. Holzgrabe, M. Decker, *J. Med. Chem.* **2015**, *58*, 560-576.
[7] T. Littmann, T. Ozawa, C. Hoffmann, A. Buschauer, G. Bernhardt, *Sci Rep.* **2018**, *8*, 17179.
[8] O. Arunlakshana, H. O. Schild, *Br. J Pharmacol. Chemother.* **1959**, *14*, 48-58.
[9] a) D. R. Waud, B. E. Waud, *Am. J. Physiol.* **1975**, *229*, 1632-1634. b) S. Lazareno, N. J. Birdsall, *Trends Pharmacol. Sci.* **1993**, *14*, 237-239. c) C. Tränkle, A. Dittmann, U. Schulz, O. Weyand, S. Buller, K. Johren, E. Heller, N. J. Birdsall, U. Holzgrabe, J. Ellis; H. D. Höltje, K. Mohr, *Mol. Pharmacol.* **2005**, *68*, 1597-1610.

Appendix V:

Curriculum Vitae